# Electrical Resistivity and Temperature of Fresh Cement Paste as Indicators for Setting Time

**Ahmad Shahroodi**

Thesis submitted to the University of Ottawa
in partial Fulfillment of the requirements for the
DOCTOR OF PHILOSOPHY

Ottawa-Carleton Institute for Civil Engineering
Faculty of Engineering
University of Ottawa

## ABSTRACT

The process, rate, and quality of cement hydration (a complex physical-chemical process) affect the properties development of concrete, such as its compressive strength, penetrability, and setting. Among all, setting time is one of the important properties for the concrete industry, as it is the factor in determining the consolidation, finishing, and curing time of a concrete pour. Inadequate determination of concrete setting time will result in improper finishing, formation of cold joints between layers of concrete, and curing time delay. Therefore, short- and long-term performance of concrete, concrete durability, and its life span will be affected. Concrete setting time proceeds from an initial stage (end of concrete pouring and consolidation) to a final stage (end of finishing process and beginning of curing) with the hydration of cement particles in the matrix of concrete. The accurate determination of the setting time in concrete projects has always been a question. Setting time is measured in laboratory setups by the traditional method of the Vicat needle (as standardized in ASTM C191). However, the field condition of a concrete pour is different from a lab set up, so the importance of replacing a lab-based setting time test with a field applicable method is out of question.

This research project studies the feasibility of using a practical and non-destructive technique to detect the actual concrete setting time and its development in a reasonable amount of time. In this research, the electrical properties and internal temperature of cementing-based mixtures are monitored over the first 24 hours of hydration. The electrical properties of concrete and cement-based materials and corresponding internal temperature are influenced by many factors affected by cement hydration, similar to the setting time. The main goal of this research project is to establish a predicting method for the fresh cement paste setting time by monitoring either the electrical properties or the internal temperature of the mixture. To isolate the effect of the specimen geometry, electrical resistivity has been chosen as the electrical properties' representative in this study. It is measured by a novel resistivity-meter setup. However, to develop a time-saving and accurate method, microstructure factors affecting the electrical resistivity development of fresh cement paste need to be studied. These factors are (1) the ionic concentration and ionic variation in the pore solution (in the liquid phase of the

cement paste microstructure), and (2) the hydration products formation and crystallization (or the physical characteristics of the cement paste microstructure). Since formation of hydration products and crystallization are exothermic, the changes in the internal temperature of the materials are also monitored.

Finally, reliable predicting indicators, electrical resistivity and internal temperature values, which are influenced by not only the fresh stage ionic concentration, but also by the development and changes in the physical characteristics of microstructure are proposed to the industry.

***Keywords:*** Electrical resistivity and conductivity, setting time, Vicat needle, cement hydration, fresh concrete resistivity-meter, pore solution, microstructure, ionic concentration, porosity, Limestone cement, cement paste, XRD, ICP, TGA, internal temperature

## ACKNOWLEDGEMENT

A special note of thanks and appreciation are extended to Professor Beatriz Martin-Perez (project main supervisor) for her guidance, inspiration, and kind support throughout my thesis endeavour. Special thanks to Dr. Aali Alizadeh as the thesis co-supervisor for all his encouragement, guidance, and supervision. Sincere appreciation is also due to the Giatec Scientific Inc. (project industrial partner) for financial and instrumental/technical supporting throughout the project. Many thanks to the Natural Sciences and Engineering Research Council and the University of Ottawa for providing a large portion of the research funding.

For their help in performing all of the gruelling laboratory work at the University of Ottawa (uOttawa), the Department of Civil Engineering, Materials Research section, and recognition is also due to Dr. Muslim Majid and UROP students Robert Wang and Chris Al-Jazzar. In addition, the technical advices and work from Dr. Nimal De Silva, manager at the uOttawa Advanced Geochemistry Laboratory, Ms. Rola Mansa, former technical at the uOttawa Centre for Catalysis Research and Innovation, and Mr. Bulat Gabidullin, XRD specialist at the uOttawa X-Ray Core Facility have helped this research. Their kind help in this research project is highly appreciated. Many thanks to Prof. Vanapalli, former Chair at the Department of Civil Engineering, for his support through planning and building of the research facility specialized to the Concrete Technology at the Structural Laboratory site.

And last, but certainly not the least, the author wishes to thank his parents for their vital positive energy, financial assistance, and encouragement. Special thanks to my lovely fiancé and many thanks to my lovely brother and sister. Their love and advice helped me survive and enjoy the lonely life in Canada and the long hours of the doctorate research spent in the laboratory.

# TABLE OF CONTENTS

# LIST OF TABLES

# LIST OF FIGURES

## LIST OF ABBREVIATIONS

| | |
|---|---|
| **ASTM** | American Society for Testing and Materials |
| **$C_3S$** | Alite, $3CAO.SiO_2$, Tricalcium silicate |
| **$C_2S$** | Belite, $2CaO.SiO_2$, Dicalcium silicate |
| **$C_3A$** | Celite, $3CaO.\ Al_20_3$, Tricalcium aluminate |
| **$C_4AF$** | Ferrite, $4CaO.Al_2O_3.\ Fe_2O_3$, |
| **CH** | Calcium Hydroxide, $Ca(OH)_2$ or Portlandite |
| **CSA** | Canadian Standard Association |
| **C-S-H or CSH** | Calcium Silicate Hydrate |
| **DTA** | Derivatives Thermo-Gravimetric Analysis |
| **FW** | Free Water |
| **GU** | General Use (Type 10 Cement) |
| **GUbSF** | General Use blended with Silica Fume |
| **GUL** | General Use with Limestone (>5% replacement) |
| **HE** | High Early (Type 30 Cement) |
| **ICP** | Inductively Coupled Plasma |
| **OPC** | Ordinary Portland Cement |
| **SCMs** | Supplementary Cementitious Materials |
| **TGA** | Thermo-Gravimetric Analysis |
| **XRD** | X-ray Diffraction |

## LIST OF OXIDES ABBREVIATION

| | |
|---|---|
| **A** | Aluminium Oxide or Alumina ($Al_2O_3$) |
| **C** | Calcium Oxide or Lime (CaO) |
| **$\bar{C}$** | Carbon Dioxide ($CO_2$) |
| **F** | Iron Oxide ($Fe_2O_3$) |
| **H** | Water ($H_2O$) |
| **K** | Potassium Oxide ($K_2O$) |
| **M** | Magnesium Oxide or Periclase (MgO) |
| **N** | Sodium Oxide ($Na_2O$) |
| **P** | Phosphorus Hemi-pentoxide ($P_2O_5$) |
| **S** | Silicon Dioxide or Silica ($SiO_2$) |
| **$\bar{S}$** | Sulphur Trioxide ($SO_3$) |
| **T** | Titanium Oxide or Titania ($TiO_2$) |

## LIST OF REPRESENTATIVES

| | |
|---|---|
| **AFm** | Mono-sulphate ($Al_2O_3$-$Fe_2O_3$-mono) |
| **AFt** | Ettringite ($Al_2O_3$-$Fe_2O_3$-tri) |
| **i-PrOH** | Isopropanol alcohol or Dimethyl Carbinol ($C_3H_8O$) |

*If we knew what it was we were doing, it would not be called research, would it?*

*Albert Einstein*

# 1. INTRODUCTION

Concrete is a complex composite material made of cementing (result of cement hydration with water and admixtures) and aggregate phases, whose micro and macro structure properties change over time. The process, rate, and quality of cement hydration (as a complex physical-chemical process) affect the mechanical properties (e.g., compressive strength), the physical properties (e.g., penetrability), the electrical properties (e.g., electrical conductivity), and the chemical properties (e.g., alkalinity of pore solution) of concrete. These properties are important for concrete construction as concrete performance and long-term durability are influenced by them.

Among all properties of concrete, setting is one of the most important ones in the concrete construction industry. The setting time is the only reliable indicator for determining finishing and curing time. Many surface problems (e.g., scaling, spalling, cracking, and delamination) in poured concrete elements are related to inaccurate determination of the finishing and curing time. These problems may result in later age durability problems in the concrete elements. Improper finishing of an already set concrete (due to longer determination of setting time) will result in formation of permanent concrete surface problems. Also, concrete curing (which starts after finishing is completed) will start later, resulting in a less durable concrete surface.

Hence, the importance of determining the actual setting time of concrete is out of question, especially in severe climates where unpredictable extreme cold or heat affects the concrete setting time drastically. In Canada's cold winters, the special precautions recommended by the Canadian Standard Association in CSA A23.1-14 with regard to delivery, pouring, placing, finishing and curing of concrete mixtures in freezing temperatures are extremely important to follow. All the mentioned construction operations depend on the setting time (initial or final) of the concrete, which is affected by the cold/hot temperatures on job sites. However, monitoring the setting time of concrete by the only available standard testing method for cement pastes (ASTM C191) is neither adoptable to concrete (as it is only for cement pastes), nor completely applicable to actual construction conditions. Standard ASTM C191 focuses on the determination of a cement paste setting time similar to the paste used in the concrete. However, actual conditions a concrete element may face in construction (e.g.,

temperature, wind velocity, forms temperature, humidity) are not considered. Construction conditions have significant effects on cement hydration and therefore concrete setting time. In addition, although the cement paste setting time is responsible for concrete setting time, the aggregate temperature, moisture condition, and absorption can influence the setting time of the paste phase as well. None of these are considered when ASTM C191 is employed to study the setting time of a cement paste. Therefore, it can be said that there is not a practical method for field measurement of the initial or final setting times of concrete, so proposing a test method which can measure the setting time of concrete on-site (where job site conditions govern) can benefit the concrete industry.

This research project focuses on a practical and non-destructive technique to detect the actual concrete setting time and its development in a reasonable amount of time. This technique measures changes in another changing property of the concrete over the time concrete sets. The development of this property needs to be influenced by the same factors affecting the setting time, which is the formation of new cementing materials hydration products. This property is the electrical resistivity (representative of electrical properties) of cement products, which is independent from specimen geometry and probes. With a method studied in this research program, the electrical resistivity of concrete can be monitored over time on-site if the electrical electrodes, which are connected to a data logger and an electrical source, are placed in the fresh concrete after pouring into the formwork. Electrical charges transfer within the concrete matrix from a source of energy to the other (electrical poles). However, they tend to pass through mediums with less electrical resistance. Since fresh concrete is a combination of water containing cement paste and solid aggregate phase (higher electrical resistance), electrical charges theoretically pass through the low-resistant cement paste phase. Therefore, it can be said that the electrical properties of the hydrating cement paste represent the electrical properties development of fresh concrete.

Since the factors influencing the electrical properties of cement paste are similar to the factors influencing other properties of the cement matrix of the concrete, it may be theoretically concluded that the electrical resistivity can be used as an indicator for other cement paste properties (e.g., setting time in this project). Therefore, the electrical resistivity measurement

technique is studied in this research for estimating the setting time of cement-based materials. If it is proved that electrical resistivity development of concrete (cement paste of the concrete) can be used as an indicator of concrete setting time (cement paste setting time), this method can be used to estimate the setting time on-site by considering the construction conditions.

During the setting time of cement paste, two states co-exist: the solid phase (hydrated cement paste) and the liquid phase (pore solution which is going to be used by un-hydrated cement particles as they hydrate). Hence, the electrical resistivity of the paste is influenced by the electrical resistivity of both states. Therefore, in this work, the electrical properties of both the solid and liquid phases are studied. However, there are challenges to measure and monitor the resistivity of both states separately. These challenges are discussed and overcome in this research project. Ultimately, the main challenge of this research project is to calibrate the setting time and electrical conductivity with the influencing microstructure (solid and liquid) properties.

## 1.1. Objective and Scope

An initial objective of this research plan is to modify the standard test available for determining the setting time of cement paste of concrete. The setting time determination test (represented in ASTM C191) is a laboratory test which does not consider job site conditions. Also, ASTM C191 relies on the operator visual measurement accuracy, so the test results reported are sometimes not precise. The main objective of this research program is to present and offer an advanced and accurate technology for measuring the setting time of concrete on-site, by considering the site and construction conditions. This technique focuses on monitoring the changes in electrical properties and internal temperature of the mixture over the first 24 hours, the traditional timeframe for formwork removal. The potential of using the changes in the electrical resistivity (independent from electrodes size and geometry of specimens) and temperature of the cement paste over the first 24 hours as indicating factors for determining the setting time of the concrete is the main objective of this research project.

In addition to the main objective of the project, a new construction time frame is going to be proposed to the concrete industry (besides the initial and final setting). This time limit is the time when the shear strength of the cement-based materials starts developing to the level

where workability of the mixture is reduced beyond the construction level. In this part of the project, the yield strength is considered as a factor representing workability (without having segregation and delamination in the paste) of fresh concrete mixtures.

## 1.2. Research Significance

Technically, changes in electrical properties of fresh concrete are not only influenced by the electrical properties of the solid part of the paste matrix (hydrating cement), but also influenced by the electrical properties of the pore solution (filling the pore network). However, it has been stated that when the electrical current passes through a composite medium, electrons choose to travel through the path with the least electrical resistance. By applying this fundamental physics concept to concrete (a matrix of solid aggregates and water containing cement paste), it can be assumed that the electrical current passes through the cement paste medium, if the concrete is placed into an electrical circuit. In other words, the electrical properties of the fresh cement phase of concrete can theoretically represent the electrical properties of the fresh concrete.

On the other hand, due to the exothermic reaction of cement particles during the hydration process, the internal temperature of a mixture increases while hydration products are formed. Cement hydration is responsible for the development of physical, mechanical, and electrical properties of concrete. Hence, changes in internal temperature can theoretically be related to the development of concrete properties.

In this research project, the development of the physical properties (from time 0 until the first 24 hours) of cement pastes is monitored, while the development in the microstructure (hydration crystal formation and changes in pore solution and pore network) is studied at the same time. Then, the setting time of the cement paste is related to the changes in electrical resistivity development and internal temperature of the fresh cement paste over the first 24 hours. Subsequently, these relationships are calibrated with the changes in microstructure of the cement paste, so they relate only to the cement hydration.

## 1.3. Outline of the Thesis

This doctorate research thesis first reviews the literature which contains brief information about the electrical resistivity of concrete at early and later ages, including influencing factors. In the second part of the literature review, the standard testing method for cement paste setting time determination is discussed in detail followed by influencing parameters.

The test plan and methodology are discussed in detail in Chapter 3. In this chapter, other tests and their standard methods are discussed as well. The test results which study the macrostructure and microstructure properties of hydrating cement pastes are presented in Chapter 4. Chapter 5 presents the analysis and discussion of the test results. Finally, a summary and concluding remarks are provided in Chapter 6. Extra information is provided in the Appendices of the thesis after the list of references.

# 2. LITERATURE REVIEW

## 2.1. Introduction

Concrete gradually sets and hardens within the first few hours from mixing (from the time cement particles come in contact with water). Setting is the first and one of the most important properties of concrete developed over the first few hours of hydration. The time of concrete surface initial/final finishing, sealing, curing, and architectural works are dependent on concrete setting time. Some of the durability and structural defects are the results of incorrect determination of this physical property (examples shown in Figure 2-1).

**Figure 2-1: Incorrect concrete setting determination results in permanent cracking (left) and improper surface finishing (right)**

However, the only standard testing method for determining the setting time and consistency of hydraulic cements is the laboratory Vicat needle test (ASTM C191 and C187, respectively).

## 2.2. Cement Paste Setting Time Test (ASTM C191)

The term "setting" refers to the solidification of the plastic cement paste due to ettringite (hydrous calcium aluminum sulphate mineral with formula $Ca_6Al_2(SO_4)_3(OH)_{12}\cdot 26H_2O$) formation in cement hydration. The setting time of 650g of cement paste can be determined by means of a Vicat needle (test apparatus in Figure 2-2) measurement as described in the standard ASTM C191. This test is conducted at room temperature (22-23°C) and relative humidity (around 45-50%).

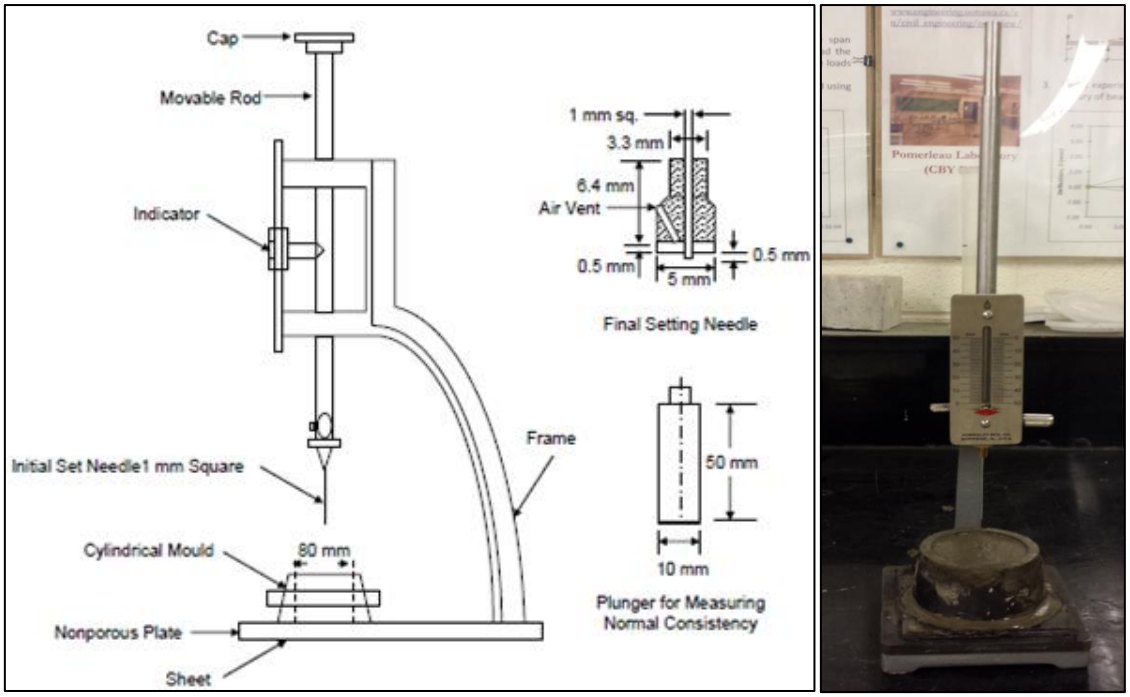


**Figure 2-2: Cement paste setting time test apparatus (ASTM C191)**

In the Vicat needle test, the resistance of the standard cement paste to the penetration of the standard needle, under a total mass of 300 g, is measured. The diameter of the needle is 1.00±0.05 mm. The initial setting time is determined when the Vicat needle penetrates 25 mm into the cement paste sample. However, it is not always possible to record right at the time when the standard needle penetrates 25 mm into the cement paste specimen. Hence, in case the 25 mm record is missed, an interpolation is required. As indicated in ASTM C191, the Vicat time of setting can be calculated also as (to the nearest 1 minute):

$$\left[ \left(\frac{H-E}{C-D}\right) \times (C-25) \right] + E \qquad [2\text{-}1]$$

where:

E= time of last penetration greater than 25mm (in minutes),

H= time of the first penetration less than 25mm (in minutes),

C= penetration reading at time E, and

D= penetration reading at time H.

The initial setting time is the beginning of the cement solidification. At this time, the cement paste becomes unworkable, so concrete placement and consolidation become difficult to perform (Mehta and Monteiro, 2005). Final finishing must be started at the initial setting time, after placement, consolidation and initial finishing are completed.

The final setting time is the time for the first needle penetration measurement that does not mark the specimen surface with a complete circular impression to the nearest 5 minutes. This is the time for completion of the cement paste solidification. Cement curing can start at this stage, since the absorbed moisture cannot contribute to the mix design Water-to-Cementing Material (W/CM) ratio.

The initial and final setting time of Portland cement paste are also used for the purpose of material Quality Control (QC). According to ASTM C150 and CSA A3000, the initial setting time for standard hydraulic Portland cement requires to be not less than 45 minutes and the final setting time require to be not more than 375 minutes.

In addition, similar equipment (with different needle as shown in Figure 2-3) is used for measuring the consistency of the cement mixture, as described in ASTM C187.

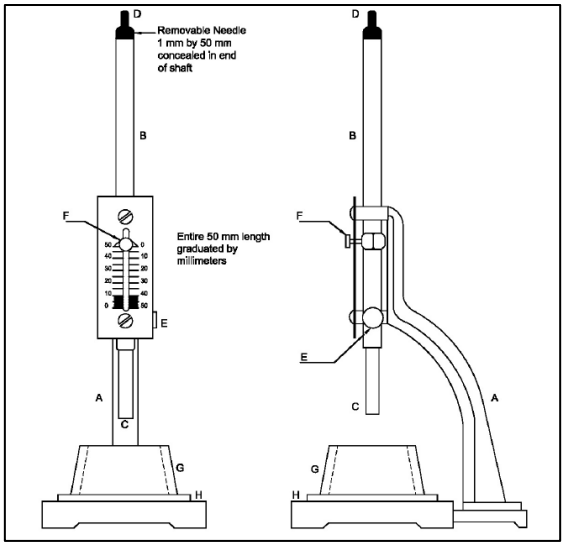


**Figure 2-3: Vicat consistency apparatus (ASTM C187)**

ASTM C187 method is used to study the effect of water or chemical admixtures on the consistency of a cement paste.

Both ASTM C187 and ASTM C191 have several limitations; they do not consider environmental and construction conditions, aggregate effects, and additives influence to the parameters. In addition, their results are inflected by cement paste preparation and laboratory condition. Also, human error is common as all measurements are recorded by the visual reading of the operator. Therefore, replacing them with an in-situ measurement method is beneficial.

## 2.3. Electrical Resistivity (ρ)

Electrical resistance or resistivity is another property of cement-based materials, like cement paste or concrete, which is developed over time. The measurement of the concrete electrical resistivity is popular and widely used primarily because of the easy and fast usage (Coyle et al., 2019). The electrical resistivity of cement-based materials is usually used in quality control. Electrical resistivity can also be used to evaluate a concrete structure health and durability by detecting chloride penetration and crack formation. This property has been studied for nearly a century (Spragg et al., 2013). Electrical resistivity measurement technique doesn't have the limitations of the Rapid Chloride Permeability Test (RCPT) which has been

widely used for permeability and also durability assessment of concrete structures. RCPT measures the charge passed in as saturated sample over time while a constant voltage is applied. However, it has a few shortcomings related to its relatively long sample preparation time (vacuum saturation method), its destructive nature (concrete cores must be taken from the structure), and sample heating during 6 hours of the test, which influences the results (Julio-Betancourt and Hooton, 2004).

In general, the ability of any material (cement paste in this project) to withstand the transfer of the electrical ions (subjected to an electrical field) is called electrical resistance, R, in ohms. This is the simplest electrical measurement that can be made on a cementitious material. Since the applied electrical current (I) and potential difference applied to a cementitious specimen is sufficiently small, a linear relationship exists between the voltage (V) and current (from Ohm's law, V=RI). This electrical property is dependent on the size, shape, and even length of the specimen and electrical probes. However, the electrical resistivity ($\rho$) of a material, which is independent of the volume and shape of the sample and probes, can be calculated from the electrical resistance as:

$$\rho = R\frac{A}{L}, \ \rho = KR \qquad [2\text{-}2]$$

where, $R$ is the electrical resistance ($\Omega$), $A$ is the specimen's cross-section area ($cm^2$), $L$ is the specimen's length (cm), and $K$ (geometry correction factor) is a geometrical factor (depending on specimen size, shape, and the resistivity-meter electrical probes distance). $K$ is a geometry-independent material property that describes the electrical resistance of concrete. This factor can be determined numerically or experimentally (Spragg et al., 2013).

The dimension of resistivity is resistance multiplied by length, so the unit is usually $\Omega$.m or k$\Omega$.cm. To measure the electrical resistivity, a concrete specimen, or a part of a specimen, is placed in between two electrical electrodes connected to an electrical source. Due to the potential difference created by the source in between the electrodes, electrical current pass between the electrodes through the cementitious material medium. Electrical current electrons pass through the pore solution occupied the pore structure of cement paste (as electrical current has the tendency to pass through low resistance mediums). The electrical

resistivity of concrete is a measurement of its ability to resist electron transfer. This electrical property of concrete has become an indicator for assessing the physical properties of the pore structure and microstructure and the chemistry of the pore solution for more than forty years (Monfore, 1968). This physical parameter, which can be measured simply, is different for every material and can be found from electromagnetism tables. For concrete, it is difficult to find a unique number as the electrical resistivity of each concrete component is different.

If electrical circuit is completed (regardless of the electrical current path), electrical resistivity of the medium can be calculated. There are several electrical resistivity measurement setups for determining this electrical property in concrete technology.

### 2.3.1. Electrical Resistivity Measurement Configurations

Three common electrical resistivity-meter setups for measuring electrical resistivity of concrete (or cement paste) have been studied in previous projects. In all configurations, at least two metal electrodes are needed to set up an electric circuit. These electrodes are connected to a source of electrical power and a voltmeter. While electrical current passes through the sample, a drop in the voltage is measured by the voltmeter and therefore the electrical resistivity value is calculated by the meter.

#### 2.3.1.1. Consensor Measurement Technique

In this method, a cement sample is modelled as a combination of a resistor and a capacitor. As a result, a change in the dielectric properties of the cement paste, which is related to the hydration process of the cement, is measured. The dielectric properties of the matrix are the electrical permittivity (dielectric constant) and conductivity. The electrical permittivity (i.e., capacitor) represents the electrical polarization of a material, whereas the electrical conductivity (i.e., resistor) represents the amount of electrical current passing through the sample. This structure is schematically shown in Figure 2-4.

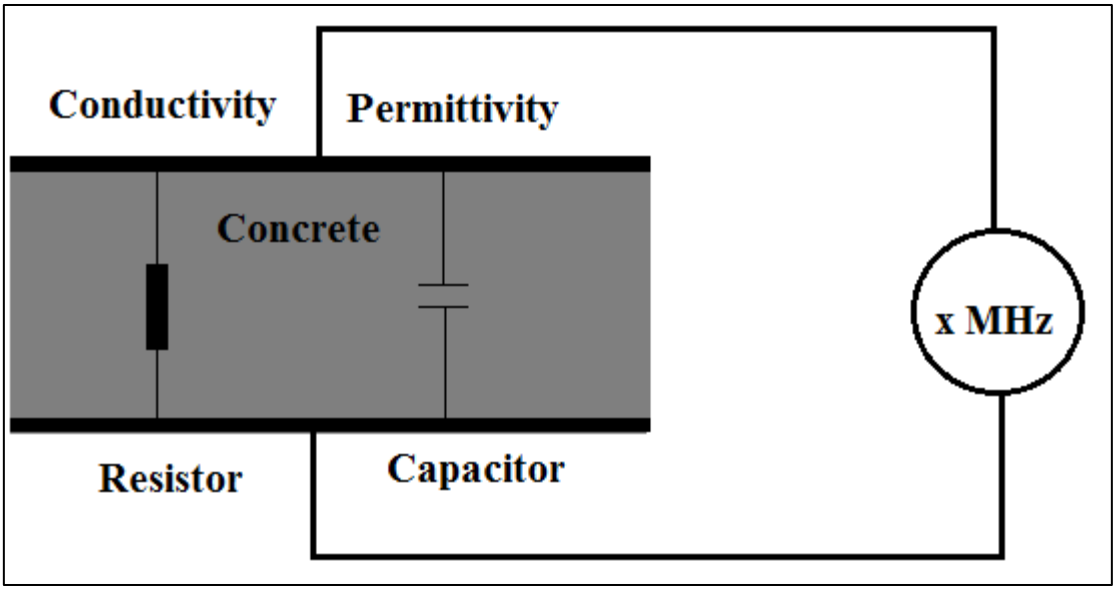


**Figure 2-4: Dielectric properties of concrete represented as resistor and capacitor**

In this resistivity setup, the geometry correction factor (K) is A/L, where A is the specimen cross-section area ($mm^2$) and L is the length of the specimen (mm).

It is stated that the changes in the density of the hydration products from low values to higher ones results in changing in the permittivity of concrete with the degree of hydration. The measured permittivity using the Consensor system could be strongly influenced by the electrode-specimen interface effect at low frequencies, i.e., less than 10MHz (Xiao et al., 2008). In this setup, electrodes can be directly in contact with the cement (or concrete in the hardened stage) specimen's faces by using a conductive gel (to avoid any electrode resistance as possible) or be embedded in the sample right after casting the mixture. The embedded electrodes resistivity setup is the test setup used for fresh cement paste resistivity measurement in this research project. The most important consequence of embedded electrodes in cement samples is the electrodes effects (similar to polarization). It has been concluded from previous researches that a frequency between 5 kHz and 15 kHz (depending on sample resistance) was normally sufficient to reduce the electrode polarization effects (McCarter and Puyrigaud, 1995).

The polarization potential, which depends on the ions present and the materials of the electrodes, is a result from the reactions taking place at the electrodes. During the polarization reactions, thin films of oxygen, hydrogen, or other gases are formed on the electrodes surface. This formation results in a lower electrical potential creation (Monfore, 1968). This stage is called "electrolysis occurring". The electrolysis occurring for building a layer of polarized material in the area, surrounding the electrodes, is patterned as (Hansson et al., 1983):

$$2H_2O + 2e^- \rightarrow H_2 + 2OH^-$$

$$4OH^- \rightarrow O_2 + 2H_2O + 4e^-$$

For electrodes containing iron elements,

$$3Fe + 4H_2O \rightarrow Fe_3O_4 + 8H + 8e^-$$

$$2Fe + 3H_2O \rightarrow Fe_2O_3 + 6H + 6e^-$$

Polarization phenomena occur at the electrode-paste interface, with the reaction initiating an excess of electrical field opposing the applied field from the resistivity-meter. In other words, if the conductor is an electrolyte (e.g., cement paste) the passage of the direct current will cause polarization and the establishment of a potential at the electrodes that opposes the applied potential (Monfore, 1968). As a result, the measured concrete resistivity is overestimated by 50-60% by the DC method (rather than the AC method) due to the electrode polarization potential or back emf at the electrode surfaces (El-Dieb et al., unpublished).

In this case, the polarization potential reduces the past current through the specimen as formulated in Equation 2-3:

$$I = \frac{E_a - E_p}{R} \qquad [2\text{-}3]$$

where, $E_a$ is the applied potential (V) and $E_p$ is the polarization potential (or back emf) (V).

This polarization effect can be avoided at a frequency of 10 kHz or higher, as it was interpreted this to mean that the capacitive reactance of concrete is much larger than its electrical

resistivity (Neville, 1995). Polarization effects can be avoided by using cyclic DC resistivity-meters or AC currents (Monfore, 1968).

In AC resistivity-meters, the electrode/concrete interface polarization and capacitive effects (formation of a thin gas film between the electrodes and the electrolyte) are not observed, resulting in real (and lower than a DC instrument) resistivity values (El- Dieb et al., unpublished). However, the dipoles of ions in the pore solution of concrete subject to AC current can direct the electrical current. Therefore, the AC current can be employed to measure the electrical resistance (R) of concrete, but the non-resistive opposition reactance (X) to the AC current should be considered. The joint opposition of reactance (X) and resistance (R) to the applied current represents the impedance (Z). This complex number can be represented as the vector sum of resistance on the real axis and reactance on the negative imaginary axis, as shown in Figure 2-5.

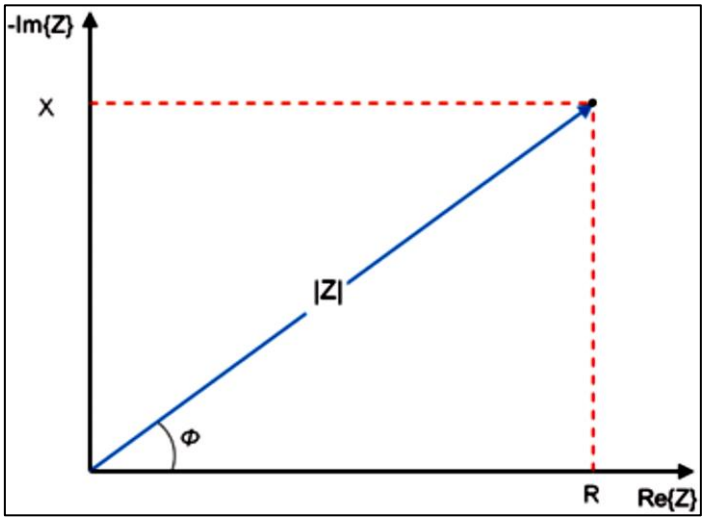


**Figure 2-5: Impedance as a vector sum of resistance and reactance**

The impedance is represented by its magnitude |Z| and phase angle Ø. Both of them vary with the frequency of the applied current (Layssi et al., 2015). Therefore, all these factors should be taken in consideration if AC current is employed for electrical resistivity measurement.

Besides the polarization effect, the physical contact between the resistivity-meter embedded electrodes and the cement paste plays an important role in determining the accuracy of the resistivity measurement.

Another factor that needs to be considered in embedded resistivity-meters is the possibility of corrosion in the electrodes. As cement hydration proceeds, autogenous and thermal shrinkage occur leading to some separation in the electrode-paste boundary. This separation can cause corrosion in the electrodes, so stainless-steel electrodes are suggested. The electrical resistivity of stainless-steel electrodes is near zero, but in case of any resistance in the electrode (or on the electrodes surface as a connection between electrode and specimen), the concrete resistance calculation is modified as (McCarter et al., 2009):

$$R_{paste} = R_{measured} - R_{electrode} \quad [2\text{-}4]$$

where, $R_{electrode}$ is the electrical resistance of the electrode (Ω). To obtain the true resistivity, the use of a high-frequency instrument is necessary, so the potential interface region resistance is "short-circuited" and therefore not considered in measurement (McCarter et al., 2009).

Hence, DC measurements are more appropriate than AC, if the current or potential required to overcome polarization are subtracted from the total value of current or potential, respectively (Monfore, 1968). This potential drop due to polarization effects is the intercept on the voltage axis of the linear portion of the $V_{cell}$ vs. $I_{curve}$ (Hansson et al., 1983). If a sine-wave current source is used, impedance is likely to be measured between the voltage probes (electrode/cement interface problems) rather than a resistance, and this may vary with frequency, so the results are doubtful (Ewins, 1990). In practice, this method is expected to be less accurate and poorly reproducible because the electrode size has an important effect on the measured values (Polder, 2000). Therefore, the size of the interface area between the electrodes and the cement paste should be minimized.

In case AC measurement is used to avoid the electrolysis effects, the Alternating Current Impedance Spectroscopy (ACIS) measurement system is the most representative. This method was first suggested by McCarter et al. in 1990 for studying hardened cement paste over a frequency range of 10 MHz to 15 MHz. As observed in the Nyquist plot (Figure 2-6),

two arcs existed in the electrical response, the first one in the high frequency region (cement paste) and the other one in the relatively low frequency region (stainless steel electrodes).

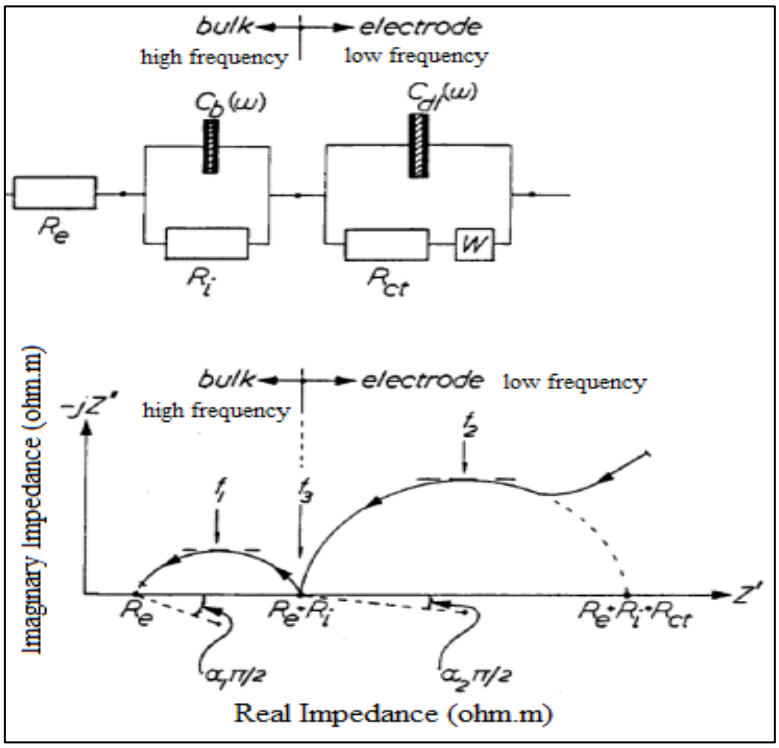


**Figure 2-6: Nyquist plot: Schematic diagram of the complex impedance response for hydrating cement between a pair of electrodes (McCarter el al, 1990)**

The high frequency arc represents the bulk cement paste impedance behaviour and the low frequency region results from the electrode-cement interface effects (right-hand side of the plot). This method has three circuit elements in series:

a) electrodes effects are represented by a parallel combination of resistor and capacitor (frequency-dependant), $R_{ct}$ and $C_{dl}$, respectively.

b) element $R_i$ represents the bulk ionic resistance of the cement paste, which is independent from the applied frequency of the electrical field.

c) element $R_e$ represents the resistance of the matrix, which is dependent to the applied frequency of the electrical field.

It was found that the radii of the complex arcs increased as the cement hydration proceeded (McCarter el al., 1990). However, changes in the microstructure during the cement hydration process resulted in the delayed appearance of the high-frequency arc. This method was used later on for porosity studies of microstructures. It was found that a large high frequency indicated a dense transition area and a highly discontinuous pore structure (Xiao et al., 2008). Torrents et al. (1998) pointed out that the most reliable parameter was the bulk resistivity of the material obtained from ACIS, which was found at the intersection of the two arcs where the imaginary component was practically zero (Xiao et al., 2008).

As finally suggested, at frequencies higher than 10 kHz, electrode effects can be considered eliminated, but the impedance still displays frequency dependence (McCarter et al., 1990). Electrode configurations, test-cell geometry, calibration procedure, and operating voltage are the other factors influencing the ACIS test results.

#### 2.3.1.2. Surface Resistivity (4-probe resistivity)

This method is the most widely used technique to measure surface electrical resistivity for hardened concrete. The method was originally developed by Wenner (1916) for soil (earth) resistivity measurements. In this method, two outer probes apply a low-frequency alternating current (to eliminate capacitive effects) to the sample, while the instrument measures the voltage drop between its two inner probes as shown in Figure 2-7. All electrodes are in a straight line and equally spaced.

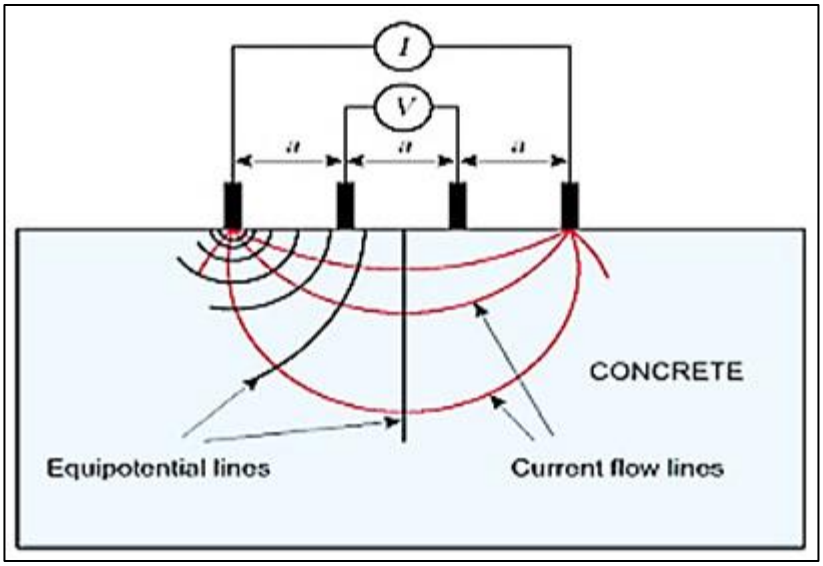


**Figure 2-7: Schematic representation of four-electrode resistivity test-the Wenner method (Polder, 2001)**

In this resistivity setup, the geometry correction factor (K) has been numerically determined as (Spragg et al., 2013):

$$K=\frac{2\pi a}{1.09-\frac{0.527}{\frac{d}{a}}+\frac{7.34}{(\frac{7.34}{\frac{d}{a}})^2}} \quad [2\text{-}5]$$

where, *d* is the thickness of the specimen (mm), *L* is the specimen length (mm) and *a* is the probe spacing (mm).

The probe spacing can be adjusted between 0-100 mm. The spacing between the probes can be influenced by several factors such as the thickness of the concrete element, the location of the probe array from the edges of the concrete specimen, and the thickness of the concrete cover (rebar depth). The surface electrical resistivity for a semi-infinite homogenous is calculated by using Equation 2-6:

$$\rho = 2\pi a \frac{V}{I} \quad [2\text{-}6]$$

where a is the probe spacing (mm), *I* is the electrical current (mA) between 0.01 to 10 kHz, and *V* is the voltage drop (V).

The four-point method is non-destructive, timesaving, simple, and adjustable for concrete site projects. This test is used to compare surface treatments and corrosion resistance analysis of covercrete. However, some source of errors can influence the test results: (1) concrete geometry and edge effects, (2) surface contact, (3) surface non-homogeneity, (4) reinforcing steel bars, (5) environmental conditions, and (6) moisture content of concrete.

#### 2.3.1.3. Non-contact Resistivity Measurement Technique

Polarization and gas release problems can be prevented by using AC current in resistivity-meters, but cracking, resistance, and separation between the electrodes and the cement paste can still affect the resistivity test results. These problems have been solved recently by a method recommended by Li et al. (2003), since there are no electrodes in the test setup (shown in Figure 2-8).

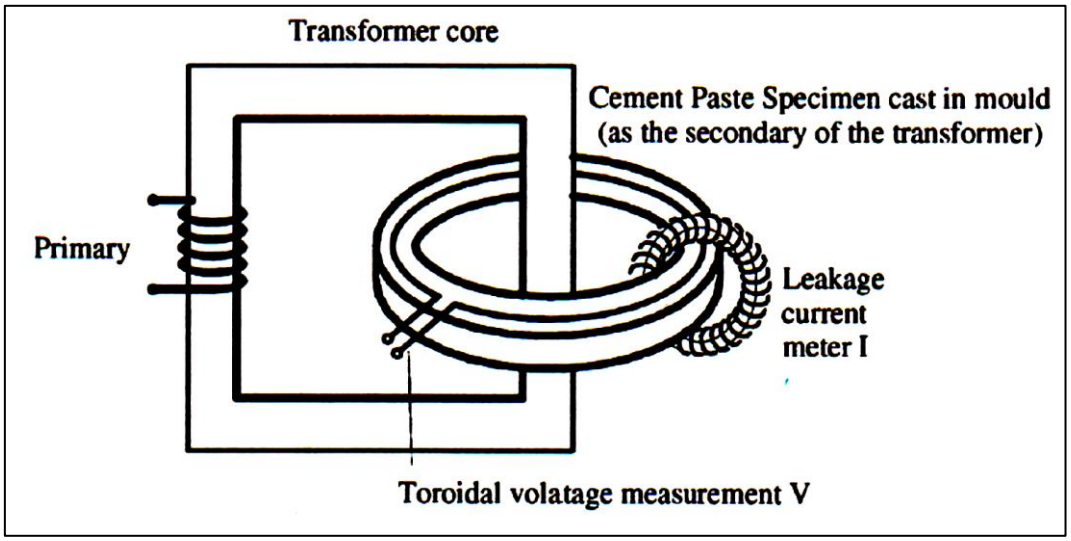


**Figure 2-8: Non-contact electrical resistivity test setup (reproduced from Xiao et al., 2008)**

In this test setup, the cementitious material is cast in a ring sample and a fixed frequency of 1000 Hz is applied to it. The resulting value is the pure electrical resistivity, which is attributed to the ion migration in the pore solution (Xiao et al., 2008). The advantage of this method is

the possibility of building non-destructively a quantitative relationship between resistivity and the hydration process of cement-based materials.

### 2.3.1.4. Embedded electrode Measurement Technique

In this setup, electrodes are embedded in the concrete at the time of pouring and measurement starts as soon as they are connected to the source of electrical energy. The setup is schematically shown in Figure 2-9 . The device then measures the matrix resistance to electrical charges passage.

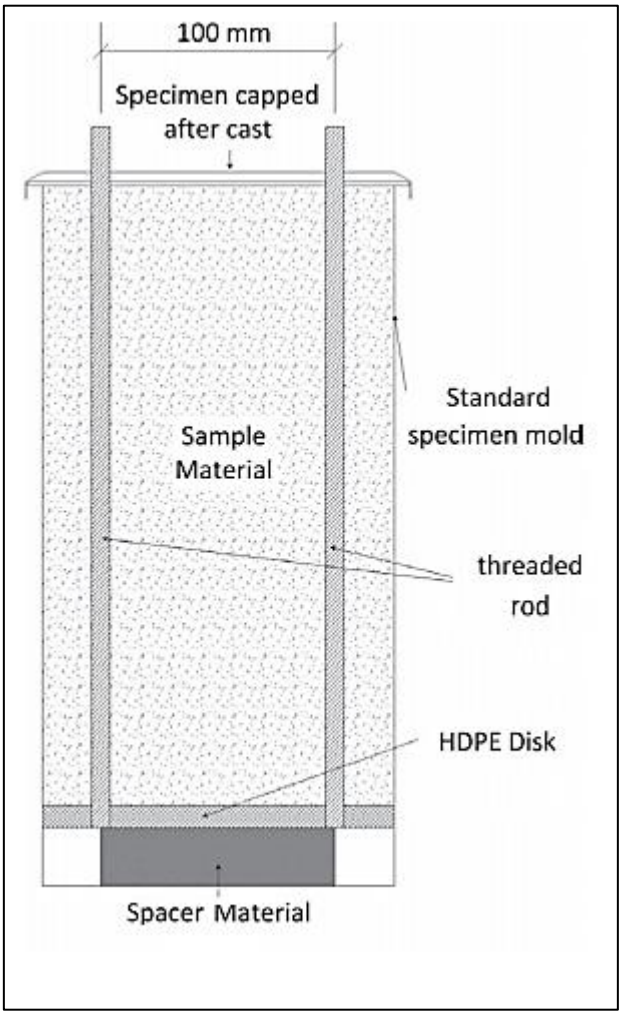


**Figure 2-9: Embedded electrodes resistivity setup (Spragg et al., 2013)**

In this setup, the development of electrical resistivity is measured over the course of cementing materials hydration, so the method can be used in all stages of cement hydration in

concrete. As measured experimentally by Spragg et al., the geometry correction factor (K) for this resistivity setup is 0.2 m.

### 2.3.2. Electrical Resistivity of Concrete Over Time

It has been reported in various literatures that the electrical resistivity of concrete changes over time in a very broad range: in hardened concrete, from $10^{11}$ Ω.cm for oven-dried concretes to less than $10^{3}$ Ω.cm for saturated concretes (Lopez and Gonzalez, 1993), while in fresh concrete (before final setting stage), from $10^{2}$ Ω.cm to $10^{3}$ Ω.cm by the end of the final setting (Xiao et al., 2008), as compared in Figure 2-10.

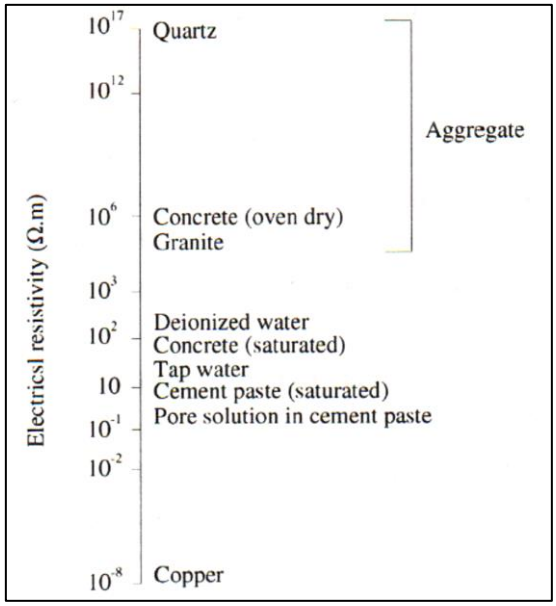


**Figure 2-10: Electrical resistivity variety of materials (Xiao et al., 2008)**

It can be observed that the electrical resistivity of cementing-based materials (e.g., cement paste) changes with time over the course of hydration.

Also, the influencing factors on the electrical conductivity at early and later ages are different from each other. Based on previous studies, the electrical resistivity development of fresh cement paste within the hydration period dynamically records ion dissolution, while the period of decreasing porosity is the dominant factor for later age resistivity (Gu et al., 1993,

in Xiaoshend and Lianzhen, 2014). In other words, the electrical resistivity of concrete at the fresh and the hardened stage must be studied separately.

#### 2.3.2.1. Electrical resistivity of the hardened concrete

The electrical resistivity is mainly used in studying and evaluating concrete at the hardened stage. The application of this electrical property measurement in the concrete industry is for:

1) *Durability assessment:* Since the major types of fluid transportation through concrete (permeability and diffusion) are analogous to the flow of a current under a potential difference (hence, electrical resistance), electrical properties of concrete can serve as a simple and effective assessing indicator of fluid transport processes and so, durability (McCarter et al., 2009).

2) *Corrosion resistance*: During rebar corrosion in concrete (one of the main causes for reinforced concrete deterioration), an electrical circuit is formed as schematically shown in Figure 2-11; the corrosion current passes through the concrete from the cathode to the anode. Therefore, the resistance of concrete to corrosion is related to concrete electrical resistance. Increasing the electrical resistivity of concrete can break the corrosion electrical circuit and it can protect the reinforcing bars.

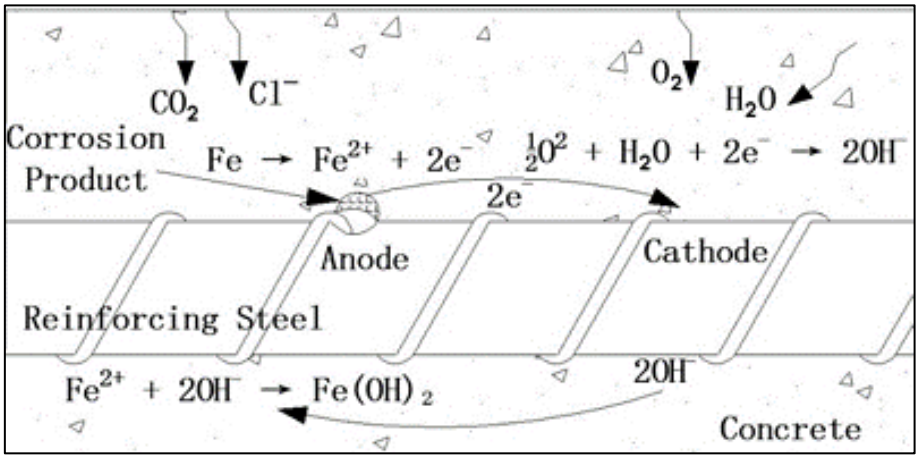


**Figure 2-11: Schematic view of reinforcing bar corrosion in concrete (Zhao et al., 2011)**

Steel corrosion rate is inversely proportional over a wide electrical resistivity range, so an important application for the electrical resistivity values is to indicate the corrosion rate of

steel bars in concrete. There is not a general agreement about the resistivity level above which corrosion risks will be negligible, but a relation between resistivity and rate of steel corrosion has been presented to industry as tabulated in Table 2-1.

**Table 2-1: Electrical resistivity values for rebar corrosion rate (Millard and Gowers, 1991)**

| **Electrical Resistivity** (KΩ. cm) | **Corrosion Rate Risk Level** |
|---|---|
| > 20 | Low |
| 10 - 20 | Moderate |
| 5 -10 | High |
| < 5 | Very High |

In general, a low concrete electrical resistivity is related to a high risk of rebar corrosion.

As noted in previous studies, the electrical resistivity of the hardened concrete is dependent on the degree of pore saturation (humidity), pore structure continuity, ionic concentration in the pore solution, and to a lesser extent, on the degree of paste hydration (Lopez and Gonzalez, 1993). This electrical property can be measured non-destructively using electrodes placed on a concrete surface (or on the side of a hardened concrete unit or specimen) or by embedded electrodes, which are placed in the fresh mixture just after casting. This requires at least two electrodes, one of which may be a reinforcing bar in case of in-situ measurements. A voltage is applied between the electrodes and the resulting current is measured, or vice versa. From Ohm's law, the ratio of voltage to electrical current results in the resistance of the concrete sample (R=V/I). The resistivity is obtained by multiplying the measured resistance by a conversion factor, called the cell constant, *m*. For a given cell arrangement, the cell constant can be obtained from either theoretical considerations or calibration using standard concrete samples or electrolytes of known resistivity (Polder, 2000). In order to have the cell constant, *m*, different cell arrangements must be studied.

### 2.3.2.2. Electrical resistivity of fresh concrete

In hardened concrete, the physical characteristics of the concrete matrix in addition to the moisture content are the main factors for apparent resistivity changes. However, in fresh

concrete, the cement matrix has still not been fully formed, so the physical characteristics of the matrix are not a dominant factor. This is the reason that in opposed to hardened concrete, the electrical resistivity of fresh concrete has not been studied enough.

To understand the electrical properties of a cement-based mixture at the fresh stage, the all mixture components need to be studied, separately:

1- The cement matrix which contains un-hydrated (or partially hydrated) cement particles and the liquid phase, which is the solution containing chemical ions from the cement particles and admixtures,

2- The solid phase from coarse aggregates, fine aggregates, and fillers.

Previous research has shown that the type of aggregate (and filler) does not have any significant effect on the resistivity of the mixtures (fresh) or the pore fluid (McCarter and Puyrigaud, 1995). The reason behind this finding is that the resistance of the solid phase is several orders of magnitude higher than that in the fresh cement paste phase. Therefore, the aggregate phase (the phase makes concrete and paste different) is regarded as electrically inert. Hence, the electrical resistivity of concrete and cement paste is the same at the fresh stage (initial 2 to 3 hours from the mixing). In fresh stage, electrical currents always pass through the medium with higher conductivity (see Figure 2-12), so in cement paste itself, the conductive path for an electrical current is the liquid phase in between cement particles.

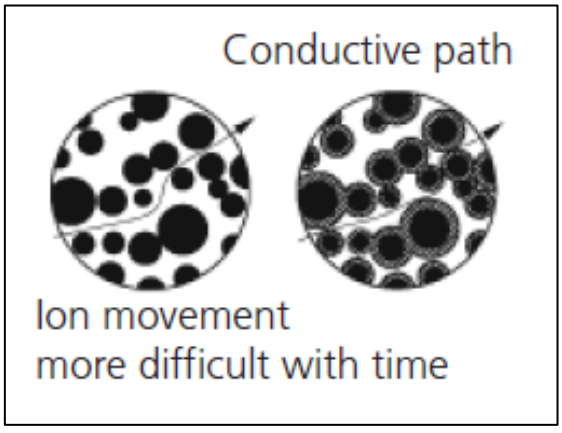


**Figure 2-12: Electrically conductive path in cement paste structures (Wei and Xiao, 2014)**

Therefore, to study concrete electrical resistivity at fresh stage, solid phase effects can be neglected, and only cement paste electrical behaviour must be studied.

As cementing matrix hydrates, not only the ionic concentration, but also the size of the conductive path (electrolyte) is changed. As the result, the trend of electrical resistivity of the conductive path (responsible for the cement paste conductivity) shows different characteristics.

According to previous researches, changes in the electrical resistivity value (and trend) of the cement paste can be divided into four major phases with three boundary points, $P_1$, $P_2$, and $P_3$ (Wei and Xiao, 2014) as illustrated in Figure 2-13 for four types of cement mixes.

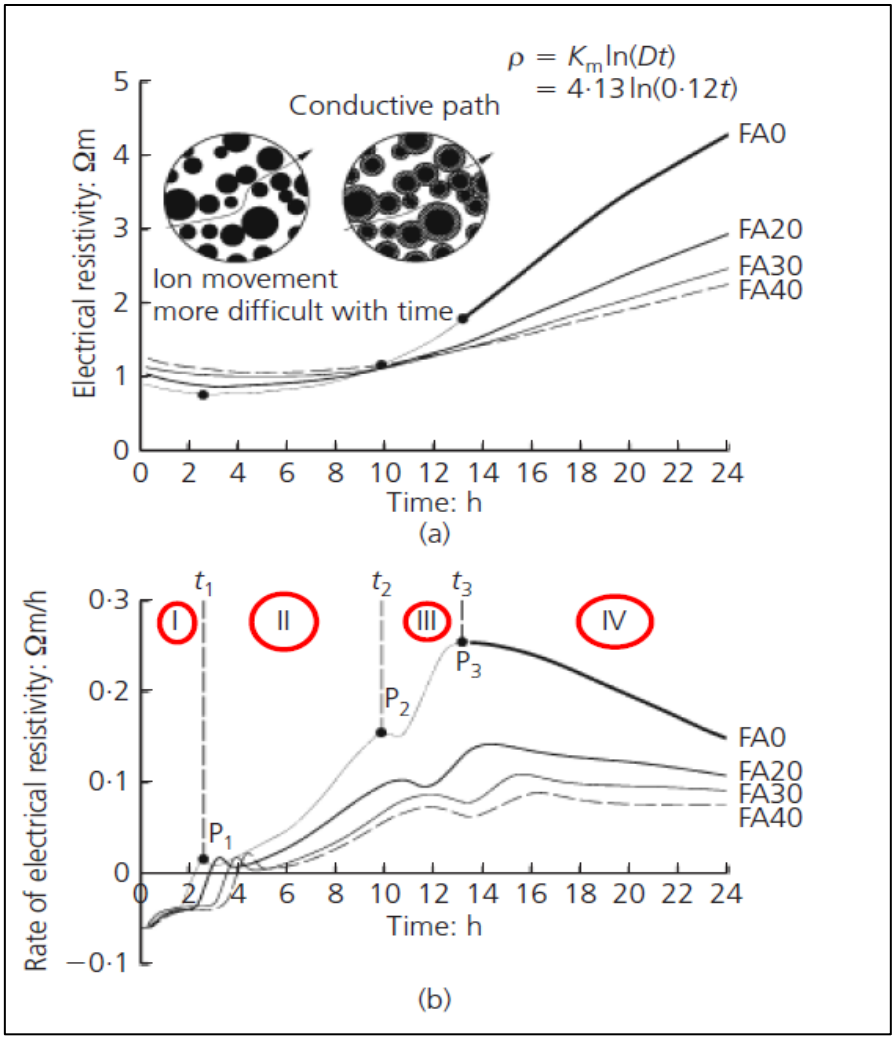


**Figure 2-13: Typical electrical resistivity development (a) and rate of electrical resistivity development (b) of 100% Portland cement paste (FA0), 20% fly ash replacement (FA20), 30% fly ash replacement (FA30), and 40% fly ash replacement (FA40) over 24h (W/CM=0.40)**

***Phase I (dissolution and precipitation):*** As soon as cementing material (pure Portland cement or a percentage replacement with supplementary cementitious materials, SCMs) is in contact with water, a reduction in the bulk electrical resistivity is observed. This reduction, which happens in Phase I after mixing with water, indicates the dissolution of ions (e.g., $Na^{+}$, $K^{+}$, $Ca^{++}$, $OH^{-}$, $SO_4^{2}$) from the cement (Wei and Xiao, 2014). In this stage, the un-hydrated cement particles contribute to the electrical resistance in the cement paste. In phase I, a slight increase in resistivity values at the beginning represents the formed hydration products (such as

ettringite observed from the XRD pattern in Figure 2-14) blocking the ions conductive paths after supersaturation of the solution.

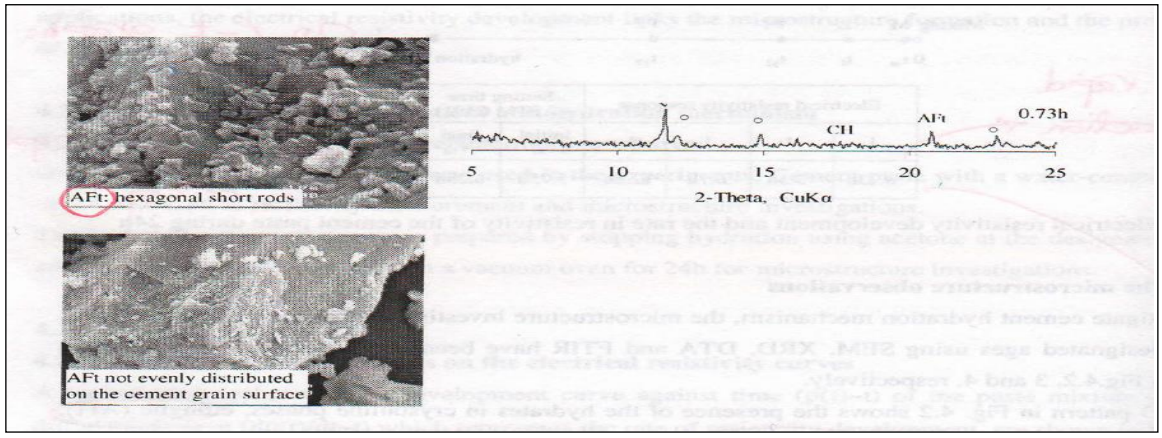


**Figure 2-14: $C_3A$ rapid reaction and ettringite formation from XRD pattern (Xiao et al., 2008)**

After this stage, the electrical resistivity of the fresh cement paste depends on not only the volume of water in the mix, but also the concentration of ionic species within the aqueous phase.

***Phase II (induction and setting):*** When $SO_4^{2-}$ (dissolved from gypsum) is sufficient in the hydration system solution, ettringite forms and remains stable. Therefore, at $P_1$, the electrical resistivity of the cement paste starts to increase. This point is the beginning of the induction period and close to the initial setting of the paste. The setting of cement at this stage is dominated by $C_3S$ hydration and C-S-H formation (Xiao et al., 2008). C-S-H formation leads to significant increase in the electrical resistivity due to percolation of the matrix within the microstructure.

***Phase III (acceleration):*** After $SO_4^{2-}$ is consumed and no more reacts with $C_3A$ and gypsum, the ettringite (AFt) is converted into monosulphate and $C_4AH_{19}$. As a result, alumina, ferric oxide, tri-sulphate is partly transformed to alumina, ferric oxide, mono-sulphate (AFm), as shown in Figure 2-15.

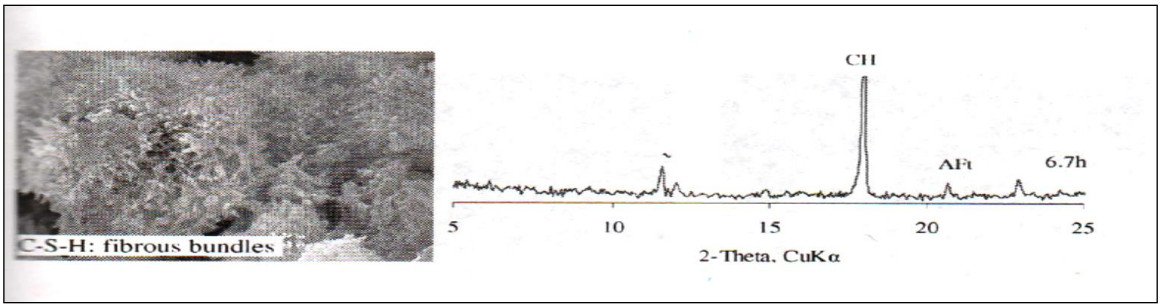


**Figure 2-15: XRD pattern of point $P_2$ close to final setting (Xiao et al., 2008)**

This completes the cement setting phase (final setting is somewhere in between $P_2$ and $P_3$, but more likely close to $P_2$).

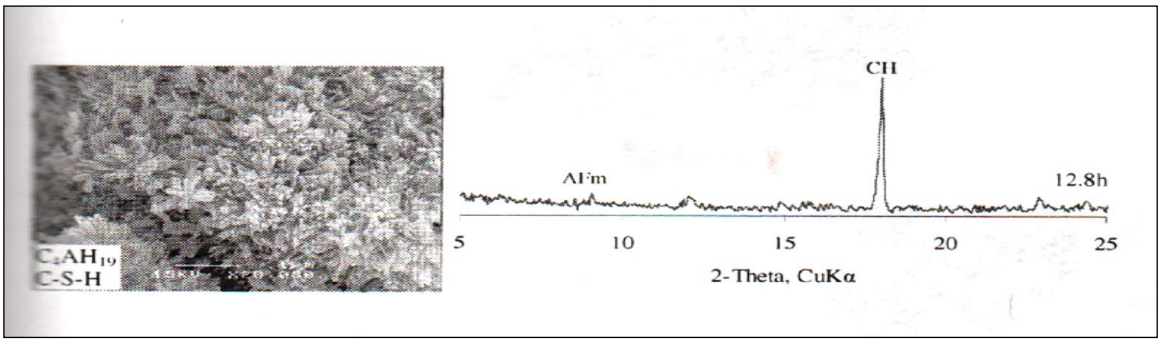


**Figure 2-16: XRD pattern of ettringite transfer to mono-sulphate at point $P_3$ (Xiao et al., 2008)**

By comparing Figure 2-15 and Figure 2-16, it is observed that the intensity of the ettringite (AFt) peaks decreases as a result of the transformation to monosulphate (AFm). Close to the end of this stage, the formation of the C-S-H which was permeable and porous at first (causing the diffusion of ions in the pore solution) is observed (Bentz et al., 2016).

***Phase IV (deceleration and hardening):*** In this phase, the hydration mechanism changes from the phase-boundary reaction to a diffusion-controlled process (Xiao et al., 2008, in Wei and Xiao, 2014). At this stage, a rapid increase in resistivity (followed by a reduction in the rate of increase in resistivity) is observed over the setting period.

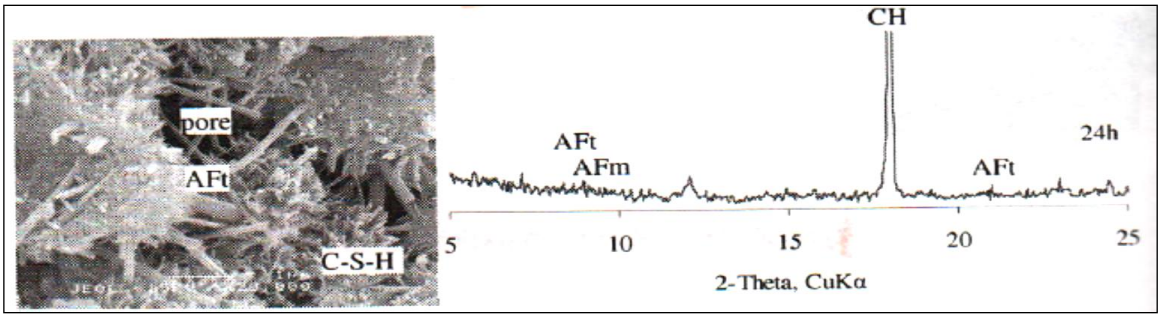


**Figure 2-17: XRD pattern of hydrated cement paste and hydration products at Phase IV**

A second reaction of $C_3A$ is observed in this stage. The hydrated AFt as long rods can be observed in the paste (as noted in Figure 2-17) resulting from the second $C_3A$ hydration. After 24 h, the components in anhydrous cement are largely consumed and the hydration products (C-S-H, CH, AFt, and AFm) are formed in the hardened cement paste. In this stage, the porosity of C-S-H reduces as more C-S-H is produced (due to cement hydration) and penetration of ions.

In summary, the main four stages in cement hydration which affect electrical resistivity values are summarized in Table 2-2.

**Table 2-2: The stages of cement hydration process (Xiao et al., 2008)**

| Hydration Stage | Cement Hydration Result | Chemical Phenomena | Chemical Reaction |
|---|---|---|---|
| **I** | Stiffening and Dynamic Balance | Initial and rapid $C_3A$ reaction<br>CH nucleation | $C_3A+3(\overline{C}\overline{S}H_2)+26H\rightarrow C_6\overline{A}\overline{S}_3H_{32}$<br>$Ca^{2+}+OH^- \rightarrow Ca(OH)_2$ |
| **II** | Setting | Chemical reaction control of $C_3S$ | $C_3S+11H \rightarrow C_3S_2H_8+3CH$ |
| **III** | Hardening | $C_3S$ hydration<br>phase transfer from AFt to AFm | $C_3S+11H \rightarrow C_3S_2H_8+3CH$<br>$2C_2S+9H \rightarrow C_3S_2H_8+CH$<br>$C_6\overline{A}\overline{S}_3H_{32}\rightarrow C_4\overline{A}\overline{S}H_{12}+2CaSO_4$<br>$C_6\overline{A}\overline{S}_3H_{32}+2C_3A+4H\rightarrow$<br>$3C_4\overline{A}\overline{S}H_{12}$ |
| **IV** | Hardening and Deceleration | Second $C_3A$ reaction and other hydration components | $C_3A+3(\overline{C}\overline{S}H_2)+26H\rightarrow C_6\overline{A}\overline{S}_3H_{32}$<br>$C_3S+11H \rightarrow C_3S_2H_8+3CH$<br>$2C_2S+9H \rightarrow C_3S_2H_8+CH$ |

It can be said that the fresh stage electrical resistivity relates to the ions transfer through the paste. Ionic concentration (from the chemical phase of cement hydration) and transferability (from the physical phase of cement hydration) can be factors for the analysis of the hydration process.

Cement hydration has been traditionally studied using the calorimetric method. In this method, the hydration stages are identified by measuring the amount of heat released, and the mechanism of hydration is explained based on heat evolution. However, concrete develops in semi-adiabatic, rather than pseudo-isothermal conditions, so this method does not properly represent the cement hydration process. Also, the liberated heat content is neither simply proportional to the degree of hydration nor to the cement physical structure development (Gartner et al., 2002).

In this research program, the potentials of suggesting the use of electrical resistivity as a reliable indicator for cement hydration and also other properties development related to the hydration process (i.e., setting) is studied.

As explained before, the most dominant factor on electrical properties changes in cementitious mixtures in the fresh stage is the ions in the aqueous phase. This ionic content (for a given water content and cementing type) alters by changing the cement content or the type of cementitious materials in the mixture. In addition, the usage of chemical admixtures can affect the ionic content and concentration in the aqueous phase of a fresh cement paste. Therefore, to consider the ions effect on the electrical properties of a cementitious mixture at the fresh stage, it is recommended that the formation factor (F), which is a function of the saturated specimen resistivity, is considered instead of the cement specimen electrical resistivity only (McCarter and Puyrigaud, 1995).

$$F = \frac{\rho_0}{\rho_S} = \varphi^{-n} \qquad [2\text{-}7]$$

where $\rho_0$ is the resistivity of the saturated cement paste (composite system), $\rho_s$ is the resistivity of saturating water (conductive component), $\phi$ is the fraction of volume of water contained within the paste (i.e., porosity because the specimen is saturated), and exponent *n* depends on the degree of cementation of the paste, which is normally between 2 to 3 for saturated stones (McCarter and Puyrigaud, 1995). Increasing *n* indicates that the rock (cement paste here) has more cement content and therefore a more constricted capillary pore network.

When it comes to concrete rather than cement paste, the formation equation becomes more complicated as more variables are involved.

Fresh cement paste is modelled as a 2-component system containing nonconductive particles (cement grains) dispersed in an ionically conducting liquid phase. If the free water content is denoted by $\phi$, the fractional cross-sectional area available for electrical conduction across the model is numerically equal to $\phi$. Therefore, it can be derived from Equation 2-8 that

$$R_C = \frac{\rho_{water} \times L}{A} \Rightarrow R_C = \frac{\rho_{water} \times 1}{\varphi^n} \qquad [2\text{-}8]$$

where, $R_C$ is the electrical resistance (Ω) of cement paste, $\rho_{water}$ is the water electrical resistivity (Ω.m), $A$ is the cross-section area ($m^2$) and $L$ is the length of the specimen crossed by electrons (m)

On the other hand, for a unit cube of cement mortar,

$$R_C = \rho_C \frac{L}{A} = \rho_C \times \frac{1}{1 \times 1} \Rightarrow R_C = \rho_C \quad [2\text{-}9]$$

where $\rho_C$ is the electrical resistivity of cement paste. Factor $n$ is only applicable after setting of the cement paste when the capillary pore network is assumed to be interconnected, so this value in the fresh concrete is assumed 1. Therefore, Equation 2-3 is modified as

$$\rho_C = \frac{\rho_{water}}{\phi^1} \quad [2\text{-}10]$$

It can be said that $\phi$ is equal to the Free Water (FW) of the paste divided by 1000 (FW/1000) because of the water density, if free water is in $kg/m^3$. Hence,

$$F = \frac{\rho_0}{\rho_s}(\text{eq.1}) \Rightarrow cement(paste) : F = \frac{\rho_p}{\rho_w} = \phi^{-1} = \frac{1000}{FW} \quad [2\text{-}11]$$

where, $\rho_p$ and $\rho_w$ are the resistivity of the cement paste and the interstitial water, respectively, at the time of testing.

Therefore, the electrical resistivity of interstitial water should be measured at the time that the cement paste resistivity is measured. In this case, the interstitial fluid has to be extracted from the same sample immediately after the electrical resistivity measurement. There are many methods recommended for extracting this fluid (such as centrifuging or pressurizing), but among all of them, the vacuum filtration technique is the most practical and timesaving one. In this method, a stainless-steel vacuum probe, connected to a pump with a pressure capacity of $2 \times 10^{-3}$ mbar, is placed into the cement paste sample to extract the fluid. The filtration system contained within the overall design prevents cement particles from contaminating the extracted water. A shaking table can be used to ease penetration of the vacuum probe into the

sample. After extracting the fluid, its resistivity and temperature are measured by the same resistivity-meter instrument.

It was discussed before that the electrical resistivity of the fluid phase has the controlling effect on the bulk resistivity of the fresh cement paste. On the other hand, the solution resistivity is not a dominant factor at a later stage. A two-component model proposed by Wei et al. (2005) has shown that the bulk resistivity of cement paste is mainly influenced by the paste porosity at later ages. The electrical resistivity is modelled with the following logarithmic equation at this stage (Wei et al., 2005):

$$\rho_C(t) = K \ln(\frac{t}{t_0}) \qquad [2\text{-}12]$$

where, K is the rate of cement hydration, which is directly related to rate of decrease in paste porosity, *t* is the time of measurement and $t_0$ is the reference time (S).

Equation 2-12 can predict the resistivity development during the deceleration and steady state period (phase IV in Figure 2-13). However, it is stated in the literature that the electrical resistivity of the paste at the fresh stage (phases I, II, and III in Figure 2-13) is related to the electrical properties of the pore solution.

In summary, the electrical resistivity of fresh cement paste is mainly influenced by the ionic characteristics of the pore solution (concentration and type of ions), whereas the resistivity of hardened cement paste depends on the physical characteristics of the pore network. Those are the primary influencing factors, while secondary factors, such as aggregate size, can affect electrical resistivity measurements as well.

### 2.3.3. Primary Influencing Factors on Electrical Resistivity

Electrical resistance (or resistivity) is the ability of concrete to prevent electron movement through its matrix. Electron movement happens when electrons from one pole or electrode (connected to the source of energy) are taken by ions (in the pore structure) and transferred to the other pole to complete the electrical circuit. Therefore, an electrical circuit can be created in this composite material, which can be linked to the circulation of fluids through the pore

network. Generally, the current flows through the pore liquid in the cement paste, and aggregates can be considered inert (Ferreira and Jalali, 2010).

Concrete is a composite material whose components can be described as: (a) a solid phase purely resistive (aggregates), (b) a solid phase which participates in the conduction through its porous structure (cement matrix) and is the source of ions found in the third phase, (c) the liquid phase, i.e., interstitial solution. Therefore, three electrical paths through the cementitious material are possible, as schematically shown in Figure 2-18: (a) through both aggregate and cement paste, (b) through the particles (aggregate in concrete or un-hydrated cement particles in paste), (c) through the cement paste only.

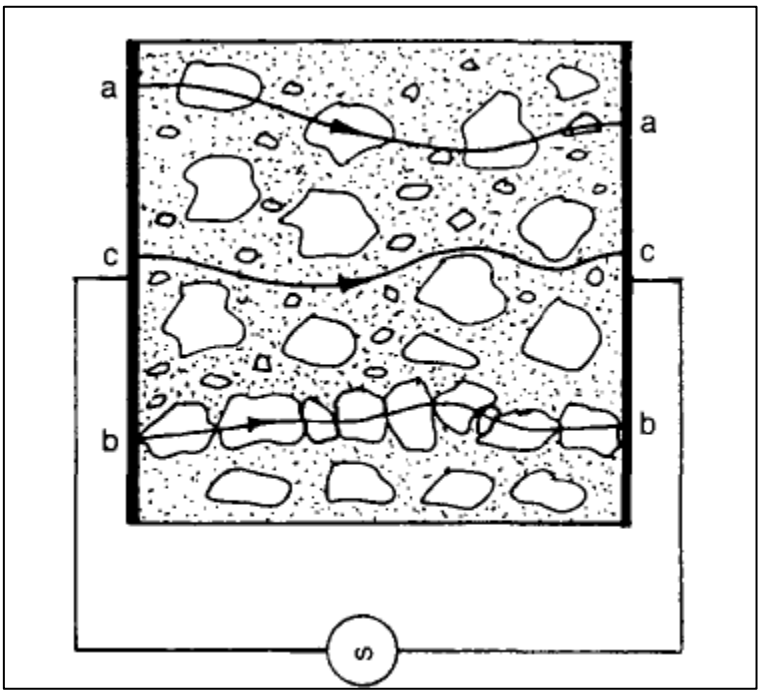


**Figure 2-18: Possible electrical paths between electrodes in concrete (McCarter and Puyriguard, 1995)**

Theoretically, the properties of the paste network and aggregates can affect the electrical resistivity values of concrete. However, it has been shown that the paste composition has a larger effect than aggregate choice with respect to resistivity of hardened concrete, especially in concretes with less than 28 days of age (McCarter and Puyrigaud, 1995). The effect of the paste composition is observed in the properties of the pore network, which is the path of

electrons movement. Therefore, the factors affecting the pore network are the most influencing factors on electrical resistivity values.

#### 2.3.3.1. Pore Network

The ionic content in pore solution, and physical characteristics of the pore network (i.e., connectivity) are important factors in the ability of electrons movement within the matrix, and therefore, electrical resistivity development. In other words, to completely understand the electrical resistivity development of a cement matrix, it must be measured in conjunction to the study of physical/chemical properties development of the pore network. In hardened stage, pore network physical characteristics can be studied by Scanning Electron Microscopy (SEM), X-ray Diffraction (XRD), and Mercury intrusion porosimetry (MIP) while in fresh stage, there is not a solid network to be studied. In fresh stage (main focus of this research program), the characteristics of the medium are evaluated by the cementing material hydration (by XRD, hydration products formations). Also, since the medium contains ions, the ionic concentration and characteristics are important factors.

It has been found from a review of the literature that the ionic concentration, which is a factor of water content, cementitious materials type, content, and ions type at various stages of cement hydration has a significant influence on the electrical resistivity of the fresh cement paste in the early-stages. Therefore, the test variables should focus on those factors affecting the type and concentration of ions within the liquid phase. Since drinkable tap water is used for mixing pastes, the only remaining factors that may affect ionic properties of the pore liquid are the type of cementitious materials and their quantity and chemical admixtures.

Chemical admixtures are used in small dosages, so it is expected not to see their influences on the ionic concentration in the liquid phase as it is swamped out by ions already present from cementitious materials. However, a high dosage of chemicals may have some influence in changing the number of cations in the concrete pore solution. Scanning Electric Microscopy (SEM) results by Xiao et al. (2008) have indicated that at high dosages of superplasticizers, the early cement hydration process of cement paste is influenced. In this case, the microstructure of the cement paste developed at much slower rate than in a control paste without chemical admixtures.

Cementing materials is a combination of ordinary Portland cement (OPC) (with standard chemical composition) and addition of Supplementary Cementitious Materials (SCMs). Theoretically, replacing OPC with any kind of SCM, for durability and economical purposes, would result in higher resistivity value in the fresh paste, since SCMs are unreactive during very early-stages of hydration and act as electrical inert fillers. After their hydration, the cement matrix and the concentration and mobility of the ions in the pore solution is affected by the SCMs pozzolanic properties. In comparing OPC to any supplementary cementitious material, replacing OPC may affect the fresh cement paste resistivity if the ionic concentration in the fluid phase is changed. In most cases, SCMs create a finer pore size distribution and lower ionic concentration and therefore higher electrical resistivity values are measured than in normal OPC (Xiao et al., 2008). The type of Portland cement used in a mixture is important in resistivity studies at the fresh stage, because the ionic properties in the pore fluid are affected. Also, $C_3A$ content, which has some effect on the setting time, is another important factor; it has been observed that sulphate-resistant Portland cement (with lower $C_3A$ content) showed higher electrical resistivity at the fresh stage, as the ionic concentration within the water phase is reduced (McCarter and Puyrigaud, 1995). Also, alkali content will change the resistivity of cement paste at both the fresh and the hardened stages (Monfore, 1968). Finally, electrical resistivity at different ages shows a decrease in value, if the cement content is decreased or W/CM ratio is increased (Xiao et al., 2008). W/CM ratio not only influences the total porosity of the cement paste, but also affects the ionic concentration in the pore solution.

### 2.3.4. Secondary Influencing Factors on Electrical resistivity

The measured electrical resistivity of hardened concrete is affected by the pore size distribution, pore system connectivity, pore fluid electrical properties (i.e., conductivity), degree of saturation of the concrete, and concrete temperature. In addition, concrete-electrode interface conditions, electrical frequency and electrodes configuration can affect the measured resistivity values.

#### 2.3.4.1. Concrete temperature

As described in the studies published in the literature, the cement paste (or concrete) temperature at the time of testing is an important factor on resistivity value changes regardless

of the resistivity test setup. This factor is more influencing in the fresh-stage resistivity studies, as the internal temperature can influence the ionic movement through the liquid medium. Therefore, possible changes in the cement paste temperature should be considered during the measurement of the electrical resistivity.

The electrical current flow in the concrete (at fresh or hardened stages) is carried by the ions ($Na^+$, $K^+$ $Ca^{2+}$, $SO_4^{2-}$, and $OH^-$) in the pore solution (Liu and Presuel-Monreno, 2014). Temperature is one of the factors that can affect the mobility of ions within the pore solution. Therefore, temperature has a significant effect on the concrete electrical resistivity (Polder, 2001). As reported by Layssi et al. (2015), a temperature increase of 1.8°F (1°C) can result in about 3% decrease in the electrical resistivity of concrete.

Hence, the effect of concrete temperature should be considered when the electrical properties of concrete are studied. In that regard, the linear relationship applicable to electrolytic solutions can describe the effect of temperature on concrete resistivity, as shown in Equation 2-13:

$$\Delta\rho = \rho\alpha\Delta T \Rightarrow \rho_T - \rho_{ref.} = \rho_{ref}\alpha(T - T_{ref.}) \Rightarrow \rho_T = \rho_{ref.}[1 + \alpha(T - T_{ref})] \qquad [2\text{-}13]$$

where α (1/°C) is the thermal coefficient of resistivity of fresh cement paste (different from that in the hardened cement paste), T is the temperature (°C), $T_{ref}$ is the datum/reference temperature (20°-23°C), and $\rho$ is the electrical resistivity (kΩ.cm). To find out the thermal coefficient of resistivity, the pore fluid should be extracted from the fresh cement paste mixture over a wide range of temperatures (e.g., 10°C to 50°C) for liquid electrical resistivity measurement. By having the electrical resistivity value at room temperature ($\rho_{ref.}$) and using Equation 2-13, parameter α for fresh cement paste can be determined. As reported in the literature, the value of α is between 0.022 and 0.035/°C (McCarter et al., 2005 in Liu and Presuel-Monreno, 2014).

It was found, however, that Equation 2-13 is only applicable to an interval of ±5°C from the datum/reference temperature (Chrisp et al., 2001). Also, Equation 2-13 does not consider the effect of temperature change in the activation energy. In physical terms, the activation energy $E_a$ quantifies the amount of thermal energy required to promote a mole of ions in the concrete

pore solution (e.g., $Na^+$, $K^+$ $Ca^{2+}$, $SO_4^{2-}$, and $OH^-$) from equilibrium state to activated state, so they can carry a current flow under an electrical field. It can be said that the activation energy of conduction, $E_a$, is a fitted parameter describing how sensitive an electrical measurement is to temperature, so a higher activation energy value corresponds to a higher sensitivity of the electrical resistivity measurement to temperature (Coyle et al., 2019).

The Arrhenius equation has been popularly used to describe the relationship between the electrical resistivity and temperature by considering the effect of the activation energy of conduction, as expressed in Equation 2-14. This equation is used to correct electrical resistivity for temperature effects using an activation energy of conduction:

$$\rho_T = \rho_{ref}.exp[\frac{E_a}{R}\ (\frac{1}{T} - \frac{1}{T_{ref}})] \qquad [2\text{-}14]$$

where $\rho_{ref}$ is the electrical resistivity (Ω.m) at the reference temperature, $\rho_T$ is the resistivity at testing temperature (Ω.m), $R$ is the universal gas constant which is 8.314 $Jmol^{-1}K^{-1}$, $T$ is the testing temperature (K), $T_{ref}$ is the reference temperature, and $E_a$ is the activation energy of conduction (kJ/mol).

It has been shown in previous researches that the change in the electrical resistivity with temperature agrees well with the Arrhenius exponential curve when the temperature of the concrete is above 0˚C (Tomlinson et al., 2017), so Equation 2-14 can be employed to normalize the electrical resistivity values of concretes with temperatures above 0˚C.

To normalize the measured electrical resistivity values, the temperature of the concrete must be measured simultaneously. Then, the activation energy of the concrete must be calculated. By using the relationship described in Equation 2-14, the normalized electrical resistivity values (independent from the effect of concrete temperature) can be calculated.

The activation energy of conduction, $E_a$, for a concrete mixture can be determined by multiplying the slope of the conductivity (1/Ω.cm) versus 1000/(T+273) curve by the gas constant (Tomlinson et al., 2017). However, during the early-stages of hydration, the curve changes, as the conductivity changes. The reason of the changes is the leakage of ions in the

pore solution when cement particles become in contact with the water. By absorption of ions in the hydration product, the conductivity may be changed. Therefore, the slope of the conductivity (1/Ω.cm) versus 1000/(T+273) curve changes during the early-stages of hydration. This is the reason behind a wide range of activation energy values reported in the literature, as summarized in Table 2-3.

**Table 2-3: Reported values of activation energy in various cement-based materials (Coyle et al., 2019)**

| Reference | Ea (kJ/mol) | Cementing Material Type | Condition | W/C Ratio |
|---|---|---|---|---|
| McCarter et al. (1993) | 17.7 | Paste | Saturated | 0.40-0.80 |
| Elkey and Sellevold (1995) | 14.0 | Concrete | Saturated | 0.40-0.60 |
| McCarter (1995) | 19.4 | Mortar | Saturated | 0.40 |
| Chrisp et al. (2001) | 25.7 | Concrete | Saturated | 0.40-0.44 |
| Julio-Bentancourt and Hooton (2004) | 19.7 | Concrete | Saturated | 0.25-0.79 |
| Sant, Rajabipour, and Weiss (2008) | 25.6–27.6 | Paste | Sealed | 0.30 |
| Castro et al. (2010) | 9.7–10.2 | Pore solution | Extracted from sealed paste | 0.36-0.50 |
| Spragg et al. (2013) | 23.4 | Concrete | Sealed | 0.42 |
| | 8.2 | Pore solution | Extracted from sealed paste | 0.42 |

According to Table 2-3, the values of $E_a$ for pore solutions range 8.2-10.2 kJ/mol, while the corresponding range of $E_a$ for concrete is 14.0-25.7 kJ/mol. Therefore, it is important to choose the appropriate $E_a$.

As reported by Coyle et al. (2019), the $E_a$of pore solutions remains relatively constant (an average value of 13.9±1.5 kJ/mol) for typical pore solutions and is slightly lower than the $E_a$ of saturated specimens (an average value of 15.8 kJ/mol). While it is better to directly measure the $E_a$ of a concrete mixture, this is not always feasible or practical. In such cases, for pore

solutions, a value of 13.9 kJ/mol can be used, and for saturated concretes, a value of 15.8 kJ/mol can be used (Coyle et al., 2019).

#### 2.3.4.2. Degree of saturation

Since electrical charges are passing from one electrode to the other through the pore system (in the pore solution), the degree of saturation can affect the measured electrical resistivity. To compare the electrical resistivity values, cementing-based specimens should be at the same degree of saturation. In hardened concrete studies, concrete samples are usually ensured to be at the Saturated Surface Dry (SSD) condition. In fresh concrete studies, the degree of saturation is not a factor as the forming pore system is in 100% moisture content.

It is noted that the concrete moisture content (the degree of saturation of the pores) may exhibit conductive or insulating characteristics. It has been shown that the moisture content affects the activation energy of conduction, $E_a$, by changing the connectivity of the fluid-filled pores, and therefore the ionic mobility in the pore system (Coyle et al., 2019).

#### 2.3.4.3. Frequency of the waves

As Layssi et al. (2015) explained, the general representation of the impedance spectrum consists of two arcs in high (attributed to the microstructure of concrete) and low (influenced by conditions at the electrode-concrete interface) frequency ranges, as shown schematically in Figure 2-19.

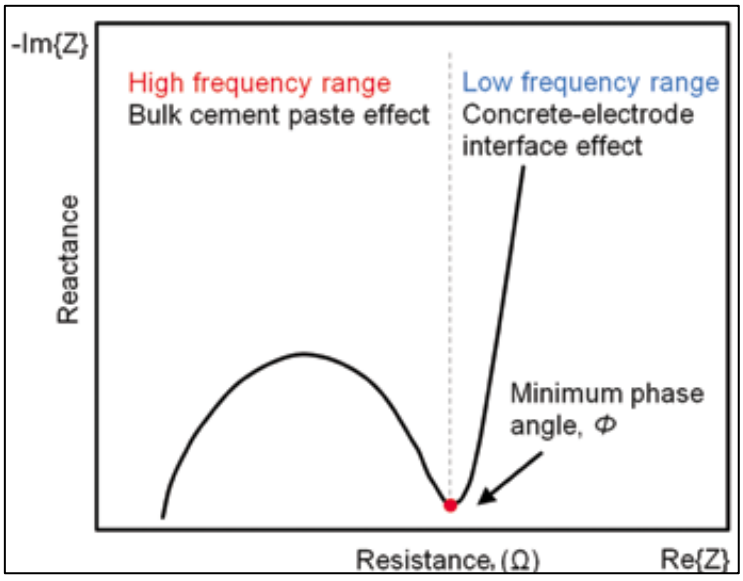

**Figure 2-19: Schematic representation of the AC Impedance response of concrete (reproduced from Layssi et al., 2015)**

Determining the optimum frequency depends on many factors such as the resistivity-meter configuration and the specimen moisture conditions. It has been observed that higher resistivity values are measured when lower signal frequencies are used (9% increase in resistivity as the frequency dropped to 1,000 Hz to 40 Hz), as shown in Figure 2-20.

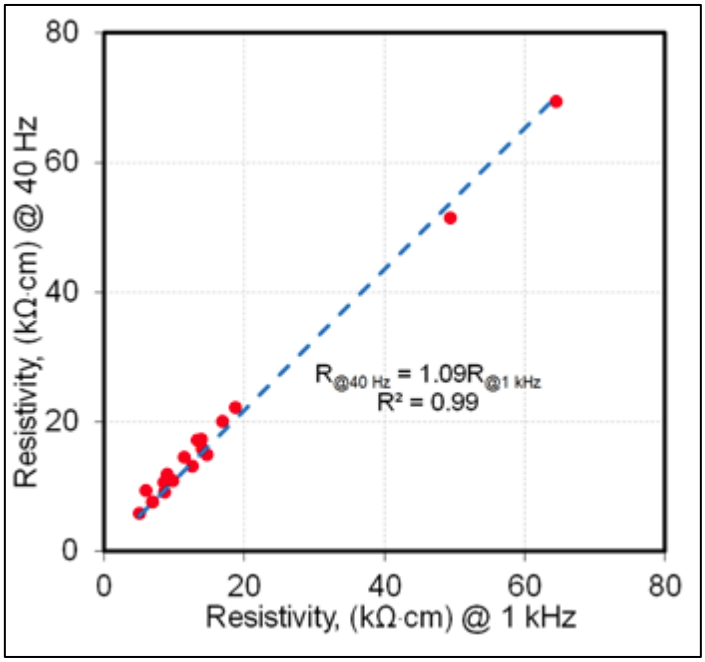


**Figure 2-20: Signal frequency effect on the measured bulk electrical resistivity values (reproduced from Layssi et al., 2015)**

It can be said that in the uniaxial resistivity measurement technique (bulk resistivity), lower frequency generally results in overestimated resistivity measurements, due to electrode concrete contact interface as illustrated in Figure 2-19.

## 2.4. Gaps in the State of the Art

The standard methods described in Section 2.2 for determining the setting time are not applicable to concrete projects sites. Also, the test method described in ASTM C91 is a

laboratory-based method, so the environmental conditions of a concrete site (e.g., temperature) are not considered.

Therefore, to determine the actual setting time of a concrete mixture poured in a structural form, a practical method, which can be applied on-site, is required.

# 3. TEST PLAN AND METHODOLOGY

## 3.1. Introduction

Three main goals are defined for this research project as:

I. Proposing a new, time saving, and more accurate technique for obtaining the setting time of cement paste from changes in electrical properties during the fresh stage,

II. Identifying the hydration stages (and therefore setting behaviour) with the aid of bulk electrical resistivity measurements and corresponding microstructure investigation, and

III. Studying the transition stage from liquid to solid during the cement hydration by electrical resistivity measurements, by considering the changes in the pore network and pore solution.

To fulfill the goals of the project, the mix designs, which represent the most common mixtures in the concrete industry, are first selected. The next part of the chapter focuses on the tests conducted in this research project at both microstructure and macrostructure levels in hydrating cement pastes.

## 3.2. Mix Design Selection

As it was concluded in Section 2.3.2.2, the solid phase does not have a significant effect on the electrical resistivity of a concrete mixture at the fresh stage. In other words, the solid phase can be removed from the matrix and a similar cement paste electrical resistivity can represent that in similar concrete. This is the reason behind studying various cement pastes in this research program.

The electrical properties of a cement paste are significantly influenced by the Water-to-Cementitious (W/CM) ratio and cement type, as described in Section 2.3.3.1. The W/CM ratio not only influences the total porosity of the cement paste, but also affects the ionic concentration in the pore solution. In this research project, three common W/CM ratios of

0.37 (often used in high performance mix designs such as bridge girders and culverts), 0.40 (commonly used in building structures), and 0.43 (widely used in projects with less concrete durability and strength requirements such as slabs-on-grade) are chosen.

In today's concrete construction industry, the use of blended Portland cements has been widely increased. Efficient use of an optimal blended cement offers economic and technical benefits to a concrete infrastructure. However, the performance of blended cements should be investigated, as discussed in Section 2.3.3.1. One of the most important concerns about the blended cements is their setting time. For this reason, two types of blended cements are studied in this research project, general use cement blended with silica fume (labelled as GUbSF) and general use cement containing limestone (labelled as GUL in this project), in addition to general use (GU) and high early (HE) cements.

The cement paste mixtures studied in this project are presented in Table 3-1.

**Table 3-1: Cement paste mixtures properties**

| **Portland Cement Type*** (from Lafarge Cement) | **Supplementary Cementitious Material** (% replacement) | **W/CM ratio** | | |
|---|---|---|---|---|
| | | **0.37 (HPC)** | **0.40 (Structural)** | **0.43 (Non-structural)** |
| **General Use** *(GU-Type 10)* | <%5 Limestone | ✓ | ✓ | ✓ |
| **Limestone Cement** *(GUL)* | 12 - 15 | ✓ | ✓ | ✓ |
| **Silica Fume Blended** *(GUbSF)* | 5.5 - 7.5 | ✓ | ✓ | ✓ |
| **High Early** *(HE-Type 30)* | | ✓ | ✓ | ✓ |

All cements were donated by Lafarge Canada (Ottawa Plant) and kept in capped barrels to limit the possible changes in the composition due to early hydration with air moisture and

carbonation. The chemical and mineralogical composition of the cements, determined by the X-Ray Fluorescence (XRF) technique (according to the method described in CSA A3003) by the supplier, are presented in Table 3-2.

**Table 3-2: Chemical and mineral composition of cements**

| **Cement Type** | **Oxide Composition** (%) | | | | | | | **Potential Mineral Composition** (%)* | | | |
|---|---|---|---|---|---|---|---|---|---|---|---|
| | **$SiO_2$** | **$Al_2O_3$** | **$Fe_2O_3$** | **CaO** | **MgO** | **$SO_3$** | **$Na_2O$**** (eq) | **$C_3S$** | **$C_2S$** | **$C_3A$** | **$C_4AF$** |
| **GU** (reference) | 19.4 | 5.0 | 3.2 | 61.9 | 2.3 | 3.9 | 0.60 | 55 | 14 | 8 | 10 |
| **GUL** | 18.6 | 4.8 | 3.0 | 60.3 | 2.2 | 3.8 | 0.61 | 56 | 11 | 8 | 9 |
| **GUbSF** | 25 | 4.3 | 2.9 | 57.1 | 2.6 | 3.7 | 0.86 | | | | |
| **HE** | 19.7 | 4.8 | 2.2 | 61.8 | 2.7 | 4.2 | 0.86 | 54 | 16 | 9 | 7 |

**The values were checked with the Bogue equations in addition*
*** $Na_2O$(eq %) = $Na_2O$ (%) + 0.658.$K_2O$ (%)*

All cement paste mixtures were prepared in four steps, according to the standard method described in ASTM C305:

*Step 1)* Pouring water and cement (start the time watch, $t_0$) for 30s absorption,

*Step 2)* Mixing at slow speed (140±5 rev/min.) for 30s,

*Step 3)* Resting for 15s (while scraping the edges of the mixer bowl), and

*Step 4)* Final mixing at medium speed (285±10 rev/min.) for 60s.

After mixing is over, experimental measurements are started. To prevent any self-desiccation due to the loss of moisture from diffusion to the surface, the specimens remain capped during the first 24 hours of hydration. Moisture loss can result in air voids formation in the mixtures which affects the electrical resistivity readings.

However, for some experiments, which will be described, the hydration process needs to be stopped at certain times. Hydration stoppage will be done by using isopropanol alcohol at the

designated times and the semi-hydrated specimens are then dried and kept in a vacuum chamber until the experimental measurement time. The first stoppage is scheduled at the initial 2 hours of hydration. Two hours after mixing is selected based on the preliminary studies and tests results of the project (which will be described in Section 4.2.5). The other stoppage times are the critical points from the setting point of view (initial and final setting times). Finally, 24-hour stoppage point is selected as the most common time for concrete forms removal and initial concrete properties measurement in industrial projects.

To achieve the described objectives, two categories of testing are performed in this research project:

1- Macrostructure-level studies, and

2- Microstructure-level studies.

### 3.3. Macrostructure Level Studies

At this level of testing, the physical and electrical properties of each mixture are studied and analyzed as summarized below. The tests performed at this stage have three different purposes:

a) Determination of the consistency and stiffening time of the specimens to establish the time frame for other testing,

b) Quality Control (QC) of the materials and specimens (i.e., vane shear and temperature), and

c) Macrostructure properties analysis (i.e., electrical resistivity, setting time, and compressive strength).

#### 3.3.1. Consistency

Consistency is defined as the relative flowability of a fresh cementitious-based mixture. Based on consistency, a mixture can be defined as dry, plastic, fluid, or wet.

Two types of consistency were measured in this research project: initial consistency (flow test) and construction consistency (penetration test). Consistency was determined to validate the mixing procedure, mix designs, quality, and properties of the mixture components.

### 3.3.1.1. Initial Consistency

Initial consistency is an important factor in determining the quality of the mix design, mixing procedure, and mixture materials. The mini-slump cone (shown in Figure 3-1), technique similar to ASTM WK27311, is a reliable test for determining the initial consistency of cement paste mixtures. The mini-slump cone used for this test was designed and built at the University of Ottawa.

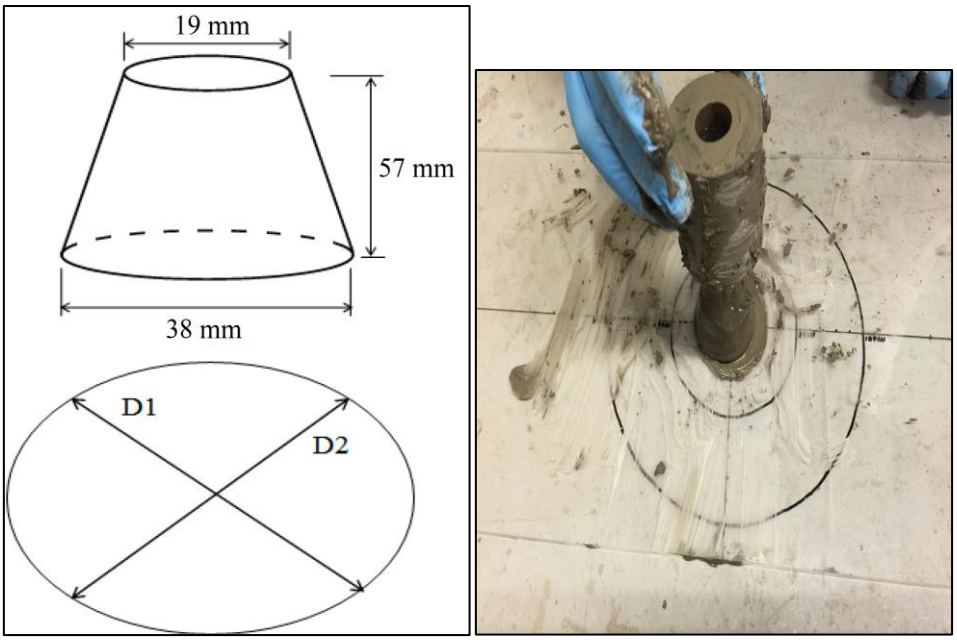


**Figure 3-1: Mini-slump cone initial consistency (slump) test method**

The test is conducted at 10 minutes from the mixing time by pouring fresh cement paste into the acrylic mini-slump cone followed by spatula tapping compaction (laterally and vertically), as described in ASTM WK27311. Rapid cone lifting to ensure the cone clear of the flowing paste (without imparting an upward momentum to the paste) results in spread of the paste. The average of two perpendicular diameters of the paste spread ($D_1$ and $D_2$) is the initial consistency of the mixture.

### 3.3.1.2. Construction Consistency

Consistency of the mixes at the time of pouring is a valuable factor in determining the workability and quality of mixes. Construction consistency of the fresh cement paste mixtures is studied in this research project, at 10 minutes, 60 minutes, and 120 minutes from mixing (2 hours is the latest allowable placement and consolidation time for a fresh concrete load according to CSA A23.1, Concrete Materials and Methods of Concrete Construction/Test Methods and Standard Practices for Concrete). ASTM C187 provides a standard test method for determining the consistency of cement paste mixes at initial stages and the apparatus is shown in Figure 3-2.

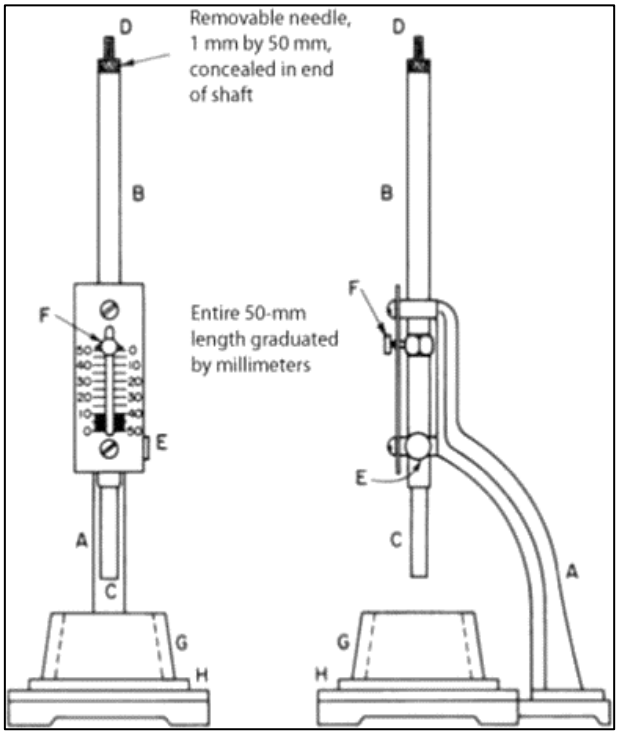


**Figure 3-2: Construction consistency apparatus (ASTM C187, 2011)**

The apparatus used for the construction consistency measurement is that used for the Vicat test (similar to the one used for setting time, but with a different needle of 10 mm), as illustrated. The consistency is the average of three measurements of the rod penetration in the sample within 30s.

### 3.3.2. Setting Time

After mixing water with cement powder, there are two significant stages in the process of setting of the cement paste: initial setting time and final setting time. These are the indicating stages of concrete setting, workability, and finishability, in concrete construction. Initial and final setting times of cement paste are determined by the test method described in ASTM C191 (Standard Test Method for Time of Setting of Hydraulic Cement by Vicat Needle).

**Figure 3-3: ASTM C191 test apparatus**

The initial setting time is the time taken by the cement paste to stiffen enough so that the needle of the Vicat's apparatus (shown in Figure 3-3) penetrates by 5-7 mm from the bottom of the mould. The initial setting time is an indication of the critical stage after which cement paste fresh properties, such as workability, are not available. Therefore, in concrete construction, not only cementing mixtures consolidating, but also the initial surface finishing must be completed before reaching the initial setting time. Final setting happens when the apparatus needle (1-mm diameter) does not form any visible indentation on the test specimen surface. In practice, all final finishing should be completed prior to the final setting time. Surface curing can start after the final setting time.

### 3.3.3. Rheology Vane Shear

A cement paste starts stiffening (losing consistency), even before the initial setting time. This can be observed by visually inspecting a cement paste mixture, but ASTM C191 is not able to determine the stiffening time; it shows 40 mm needle penetration at any time prior to the initial setting. The beginning of the stiffening process is important, as this is the time the solid phase in the cement paste matrix starts forming and the quantity of the pore solution starts reducing. In concrete construction, the beginning of the stiffening time is the point when the mixture starts developing shear strength, so further mixing, pouring, or consolidating is not recommended. Otherwise, a significant plastic deformation or yielding occurs due to an applied shear stress. Thus, this crucial time needs to be determined in this study along with the concurrent microstructure properties of the pastes.

Since there is not a standard test to measure the stiffening start point, the development of yield stress in the fresh cement paste mixture, as a rheological factor, was used as an indication for the increase in viscosity.

Besides stiffening, the workability of concrete and cement pastes can be studied by focusing on the rheological properties of the paste. A modified test procedure described in ASTM D4648 (Standard Test Methods for Laboratory Miniature Vane Shear Test for Saturated Fine-Grained Clay Soil) is used here to determine the development of yield stress of the cement paste mixes. The apparatus of the tests which is called Vane Shear Test is shown in Figure 3-4.

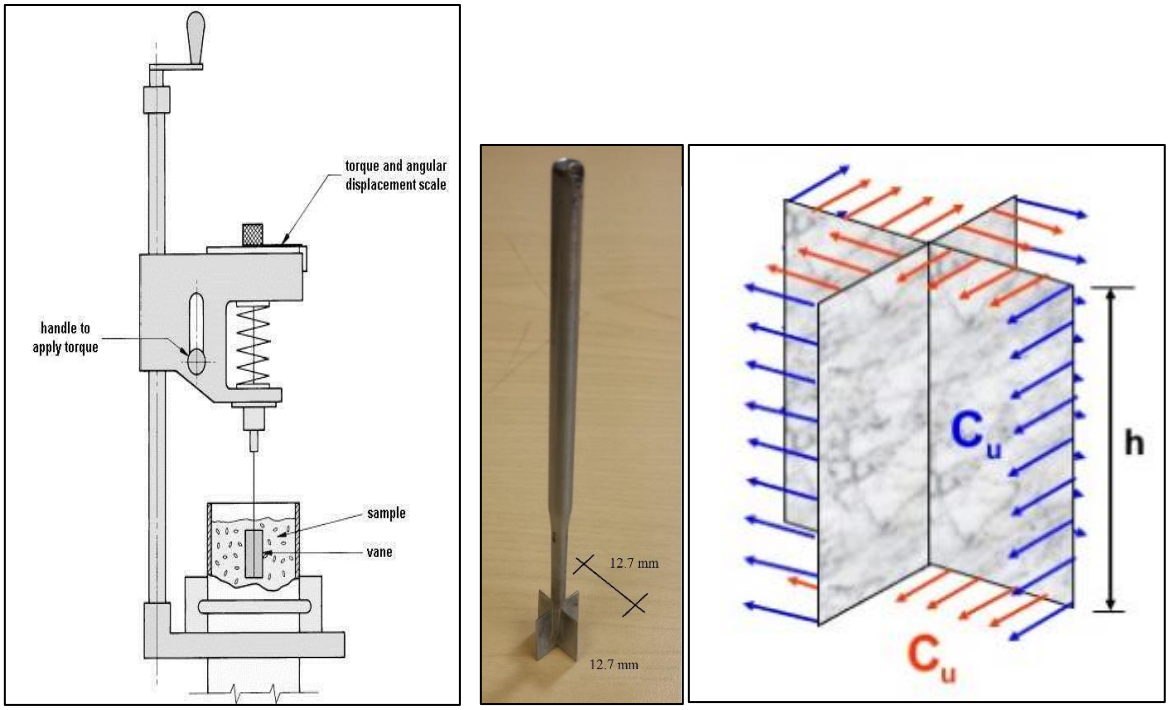


**Figure 3-4: (a) Vane shear test machine (left), (b) 1:1 blade (middle), and (c) uniform shear stress distribution on the Vane shear blades (right)**

A Ø50×100mm cement paste cylinder is cast for each mix design described in Table 3-1, at different testing times for the rheology studies. By placing the blade in the specimen (penetration depth is 50mm), a constant torque which is rotated at a constant rate of 60°/min to 90°/min., is applied by the machine to a stiff shaft and a calibrated torque spring. This rotational rate is chosen to avoid any drainage of moisture from the specimens or any further consolidation in the mixture. When the test is conducted, the top of the spring unit is rotated at a constant rotation rate, while the bottom of the spring remains stationary or nearly stationary until enough energy (torque) is built up in the spring. Prior to the failure of the spring (when it reaches its maximum capacity), the bottom of the spring and the vane begin to rotate slowly. By the time the torque applied by the spring overcomes the yield stress of the cement paste; the vane blade rotates rapidly to bring the paste to the total failure.

As described in ASTM D4648, the calibrated torque spring produces failure that varies somewhere between purely stress-controlled and strain-controlled conditions. Based on the rotational angle difference ($\Delta_f$-$\Delta_i$, where $\Delta_f$ is the final rotational angle, $\Delta_i$ is the initial

rotational angle), the shear strength ($\tau$) is calculated. Assuming the distribution of the shear strength is uniform across the ends of the failed cylinder and along the shear blade (as schematically shown in Figure 3-4), the Vane blade constant *K*, in $m^3$, can be calculated as follows:

$$K = \frac{\prod D^2 H}{2\times10^9}\left[1 + \frac{D}{3H}\right] \ (SI\ Units) \qquad [3\text{-}1]$$

where, *D* is the measured diameter of the vane (mm) and *H* is the measured height of the vane (mm).

The maximum measured torque (*T*) can be calculated from:

$$T = K_{spring}\,(\Delta_f - \Delta_i) \qquad [3\text{-}2]$$

where, $\Delta_f$ is the final rotational angle, $\Delta_i$ is the initial rotational angle, and $K_{spring}$ is the spring constant, which is the inverse of the slope of the calibration curve (°/N.m). The calibration curves are usually provided by the Vane shear equipment manufacturer.

Finally, the undrained shear strength ($\tau$) in Pascals, the point where a significant plastic deformation or yielding occurs due to an applied shear stress, is calculated from:

$$\tau = \frac{T}{K} \qquad [3\text{-}3]$$

where, *K* is the Vane constant ($m^3$), obtained from Equation 3-1, and *T* is the measured torque (N.m).

### 3.3.4. Temperature

An ordinary Portland cement (OPC) starts reacting with water immediately after the first contact. There are two types of reactions observed between OPC and water:

1- **Through-solution hydration:** Dissolution of cement components into their ions, as explained in Chapter 0, Phase I of hydration followed by the formation of the hydration products in the solution, and finally, precipitation of the hydrates, as

described in Chapter 2, Phases I and II. The through-solution hydration is responsible for early-stage property development of the cement matrix.

2- **Solid-state hydration:** Hydration at the surface of the anhydrous cement components which dominates the later stage hydration beyond Phase II of hydration as described in Chapter 0 (Phase III, and IV).

In general, cement hydration is an exothermal process. The generated heat results in an increase in the temperature of the cementitious mixture. It is observed that determining the heat of hydration by calorimetry is not always accurate, especially in mixtures with slow pozzolanic reaction (Langan B. W. and Weng K., 2002). Therefore, the effect of the generated heat, in the form of change in the internal temperature of the mixtures, is monitored in this research project. Change in the temperature of the fresh cement paste over the first 24 hours is an important factor in determining the cementitious materials hydration and setting time of the mixture. Also, it was observed in Section 2.3.4.1 that cementing-based material temperature has significant effect on the electrical properties of the matrix.

To study the thermal properties of all mixtures at different time intervals, all raw materials (water and cement powder) are kept and monitored at room temperature (22-23°C) for 24 hours, prior to mixing. Therefore, the initial temperature of all the mixtures is 22-23°C. Otherwise, measured values must be calibrated with the reference temperature (e.g., 22°C), as described in Equation 2-13.

During the cement hydration, the internal temperature of the testing specimen is monitored by an embedded thermistor with an accuracy of 0.1˚C. The cement paste temperature is monitored over the process of hydration as a quality control measurement. In case unexpected changes in the temperature of the cement paste are observed, the test is redone, and the reason is investigated. In addition, the specimen temperature is used to normalize the measured electrical resistivity by employing the Arrhenius relationship (Equation 2-14).

### 3.3.5. Fresh Stage Electrical Resistivity

The electrical resistivity of fresh cement paste reflects cement hydration information from the ion concentration and microstructure (porosity during the deceleration period). Therefore, this property can be used for quality control of mixtures of OPC or other cementitious materials. However, in this research program, the electrical resistivity measurement of fresh cement-based matrixes is going to be analysed for replacing a mechanical test, setting time determination. In other words, the main goal of this research program is to replace the standard test method for determining the setting time of hydraulic cement pastes (ASTM C191) with the measurement of electrical resistivity changes.

In this research project, the bulk resistivity of fresh cement paste is measured at various ages. The test setup is similar to the embedded measurement technique setup described in Section 2.3.1.4. In this test setup, a cement paste sample is modelled as a combination of a resistor and a capacitor, which is placed in between two stainless-steel electrodes connected to the source of electrical energy (schematically shown in Figure 3-5). The device then measures the matrix resistance to electrical charges passage. This method can be used in all stages of cement hydration. Electrical resistivity development during the fresh stage of cement paste (from the time cement particles are in contact with water unit final setting time) is an important factor in studying early-stage changes in the paste.

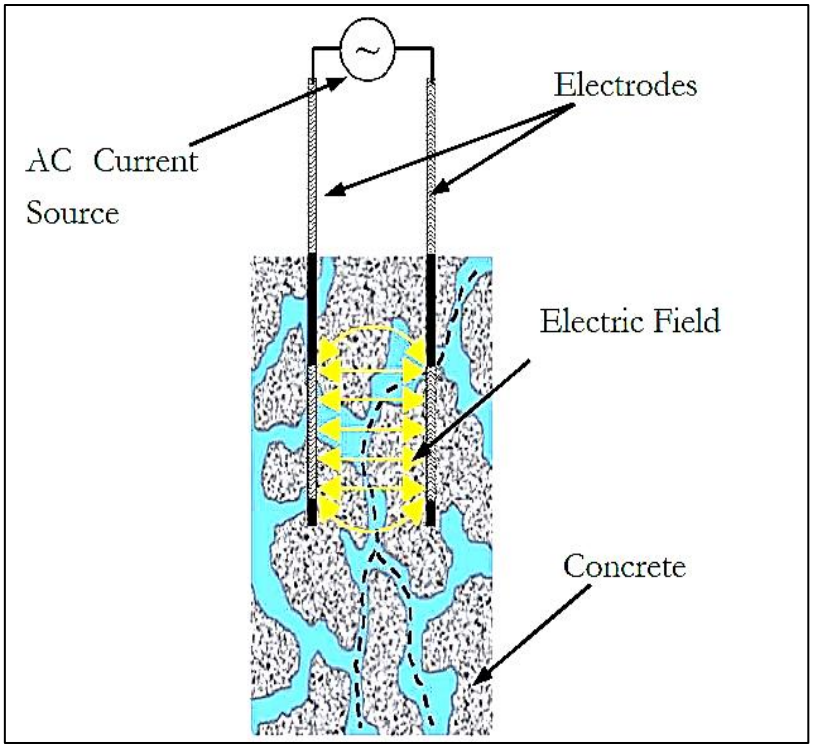


**Figure 3-5: Embedded electrodes electrical resistivity setup in fresh concrete (photo courtesy of Giatec Scientific Inc., 2015)**

In this project test setup, electrodes are in contact with the cement paste and the electrical resistance of the paste in between the electrodes is measured. In this test setup, two steel rods (50-mm apart) are placed in a Ø100×200 mm cylinder, at the time the cement paste is cast. The in-place resistivity electrodes are shown in Figure 3-6.

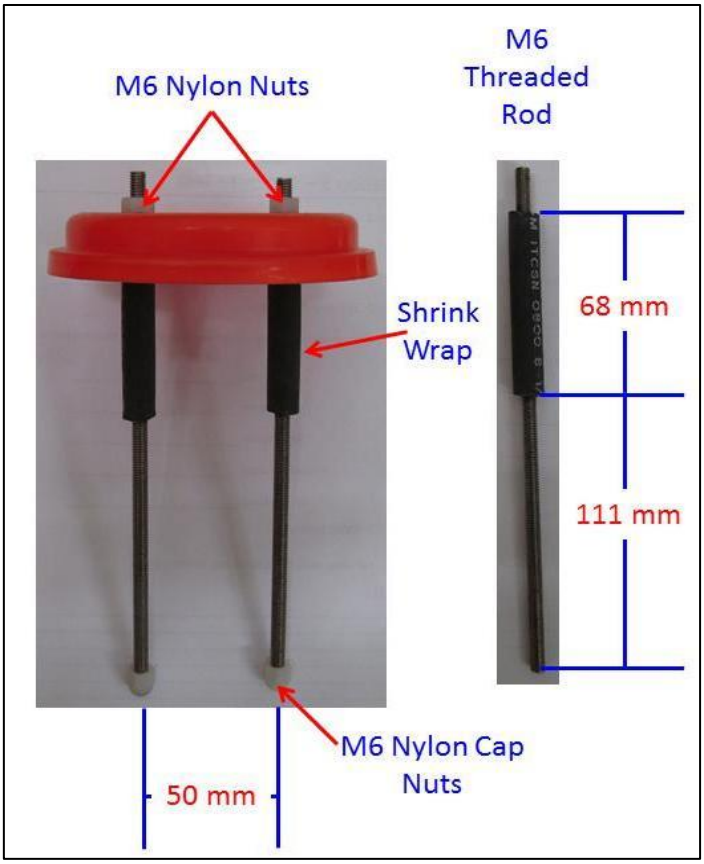


**Figure 3-6: Electrodes setup for fresh cement paste electrical resistivity measurement (photo courtesy of Giatec Scientific Inc., 2015)**

The steel electrodes are connected to a source of electrical power. To avoid polarization effects described in Section 2.3.3, a small alternating sinusoidal current at 10 kHz is applied through the cement paste. The voltage drop between the two ends of the cement paste is then measured. The impedance ($Z$) can then be calculated in Ω from the measured voltage and applied current values. Based on the value of the impedance, the current scale may vary from 10 μA to 1 mA. The impedance can be read on a cellphone application called SmartBox™ which is connected to the meter via Bluetooth.

Finally, the electrical resistance (real impedance) is converted to electrical resistivity, which is independent from the sample geometrical properties. Electrical resistivity, $\rho_c$, is obtained by multiplying the measured resistance, $R_c$, by a geometrical conversion factor, called the cell

constant, *K*. The cell constant is a factor of the probe distance and the geometry of the cement body in between the electrodes. If the cell constant is known,

$$\rho_C = KR_C \qquad [3\text{-}4]$$

where $\rho_c$ is the electrical resistivity of the cement paste (kΩ.cm), and $R_c$ is the electrical resistance (Ω).

As mentioned in Section 2.3.1, for a given cell arrangement, the cell constant can be obtained either from theoretical considerations or from calibration using standard concrete samples or electrolytes of known resistivity. In order to have the cell constant, different cell arrangements must be studied.

However, the following mathematical approach is used for determining the cell constant in this research project, based on the resistivity setup schematically modelled in Figure 3-7.

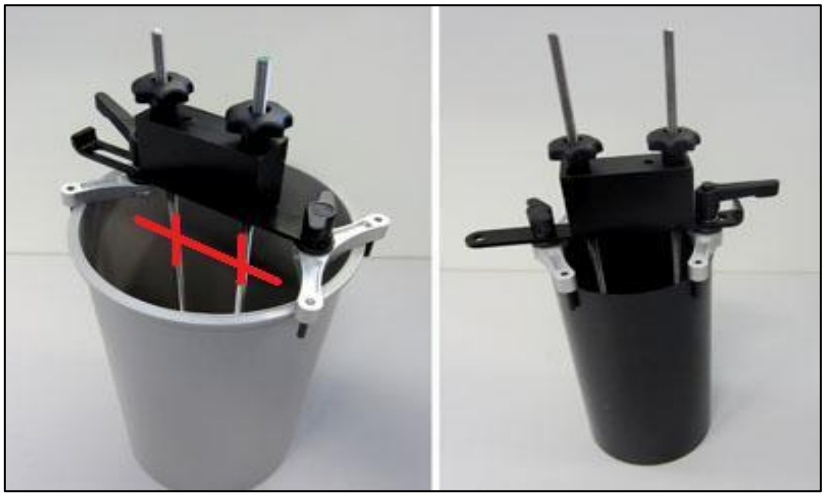

**Figure 3-7: Fresh cement resistivity electrodes setup (photo courtesy of the Giatec Scientific Inc., 2015)**

The electrical current density, *j*, is obtained from the current, *i*, as:

$$j = \lim_{A \to 0} \frac{i}{A} \qquad [3\text{-}5]$$

where *a* is the cross-section of the path the electrical current goes through. In this case, Ohm's law becomes:

$$V = Ri = \rho\frac{L}{A}i \Rightarrow V = \rho r\frac{i}{A} \Rightarrow V = \rho r j \Rightarrow derivative: \frac{dV}{dr} = j\rho \qquad [3\text{-}6]$$

It can be assumed that the current flux, *j*, at distance *r* goes through half of a cylindrical surface [2π(r)*h*/2] around the electrode:

$$j = \lim_{A\to 0}\frac{i}{A} \Rightarrow j = \lim_{r\to 0}\frac{i}{\pi r h} \qquad [3\text{-}7]$$

where *r* is the distance between the electrodes (mm), and *h* is the height of the electrode (mm), as shown in Figure 3-6.

Substituting Equation 3-6 into Equation 3-7 results in:

$$j = \frac{dV}{dr} \times \frac{1}{\rho} \Rightarrow j\rho(dr) = dV \Rightarrow eq.19: \frac{dV}{dr} = \lim_{r\to 0}\frac{i}{\pi r h}\rho \qquad [3\text{-}8]$$

Integrating Equation 3-8 gives:

$$\int \frac{dV}{dh}dr = \int \frac{i}{\pi h r}\rho(dr) \Rightarrow V = \frac{i\rho}{\pi h} ln(r) + C \qquad [3\text{-}9]$$

where *C* is a constant of integration. Equation 3-9 gives the potential around a single current electrode. The potential difference between electrodes can be simplified as (the spacing between electrodes is 50 mm as shown in Figure 3-6):

$$\Delta V = \frac{i\rho}{\pi h} ln(r) \qquad [3\text{-}10]$$

Therefore,

$$R\pi h = \rho\, ln(r) \qquad [3\text{-}11]$$

The resistivity $\rho$ in-between the electrodes, as calculated from Equation 3-11 and along the electrodes height, is graphically represented in Figure 3-8.

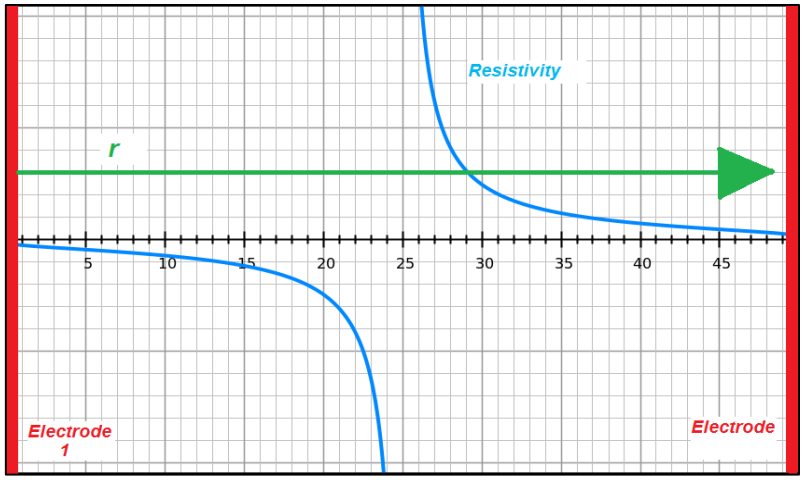


**Figure 3-8: Bulk electrical resistivity distribution trend between embedded electrodes**

The geometrical conversion factor, *K*, can be mathematically calculated from:

$$K = \frac{\pi h}{\ln r} \qquad [3\text{-}12]$$

This mathematical conversion factor should be calibrated with an experimental result, by comparing the electrical resistivity and resistance of a known solution

In this research project, at a preliminary stage, the electrical resistivity setup constant factor is calibrated by an experimental method (which will be described in Section 4.2.2). Then, the electrical resistivity of cement pastes with various mix designs are monitored by the device, over the first 24 hours of hydration.

### 3.3.6. Compressive Strength (24 hours)

Concrete forms are traditionally removed after 24 hours from casting. At this stage, compressive strength is one of the factors determining the development of physical properties and therefore hydration. If concrete has not achieved the certain strength, which is called the stripping strength, demoulding of the concrete element is not accepted. Therefore, strength plays an important role at the first 24 hours of hydration. In this research project, three Ø50×100 mm cement paste cylinders were cast and tested for 1-day compressive strength (and fracture analysis) according to ASTM C109, as illustrated in Figure 3-9.

**Figure 3-9: Compressive strength test sample and setup (left) and fracture pattern (right)**

The compressive strength is determined as the average of three specimens at the time of testing.

Considering the fact that different cement types are used in this research project, different strength values are expected. Cement mixtures containing limestone as the replacement to aggregate (and also cement) or silica fume have shown higher compressive strength at early ages compared to normal cement concrete and mortar mixtures (Bentz et al., 2016). In High Early (HE) mixtures, the finer cement particles result in a significant higher rate of hydration (higher surface area) in addition to higher $C_3S$ and therefore higher early-age (until day 7) compressive strength (Nevile, 2008).

### 3.4. Microstructure Level Studies

The fresh cement paste structure is a combination of the solid phase (partially formed pore structure or un-hydrated cementing particles) and the liquid phase (pore solution). It has been stated in the literature that some scientists claimed that the electrical conductivity of the cement paste is mainly influenced by the electrical properties of the pore solution (Liu and

Shi, 2012). This argument is based on the concept that the electrons are transferred through the pore solution (by the pore solutions ions) from one electrode to the other. In other words, the main factor affecting the electrical properties of the cement paste is the electrical properties of the pore solution. Based on this argument, the physical characteristics of the pore structure in the fresh stage do not have significant effects on the electrical conductivity development of the paste. If this argument is valid, the electrical resistivity cannot be related to properties influenced by the physical structure (e.g., setting time) and the hypothesis of this research project is questionable. To study this argument, both the pore solution and the pore structure properties (electrical, physical, and chemical) are studied, separately.

The microstructure of the cement pastes is studied in this work at various stages of hydration: 2 hours (as it is the maximum allowable time for placing, compacting, and finishing a cement-based mixture, according to CSA A23.1, and it also corresponds to the starting time of cement stiffening, as described in Section 4.2.5), initial setting, final setting, and 24 hours (as the common time for form removal and strength measurement in concrete industry). At each stage, it is assumed that the electrical resistance measured by the resistivity meter (which will be converted to resistivity by the method described in Section 3.3.5) is a factor of the electrical resistance of the pore structure: liquid phase of pore solution and solid phase of semi-hydrated cement. These two states are parallel to each other to form the resistance of the cement paste. Therefore, the electrical properties of each state are measured and studied, separately.

### 3.4.1. Pore Solution Analysis

Hydration of cement is a dissolution-precipitation process. Therefore, analyzing the cement pore solutions from quantitative and qualitative points of view leads to information about the associated nature of hydrated solid phases and therefore developed physical and mechanical properties of the paste (e.g., setting). The pore solution is extracted from the cement paste mixtures by either direct vacuum suction-filtration (Figure 3-10) or centrifuge (Figure 3-12). Both technologies are used in this research project upon need.

**Figure 3-10: Extraction of pore solution from cement paste under direct vacuum suction**

Using the direct vacuum method, the cement paste mixtures are placed under a pressure of negative 20mmHg, until the pore solution is completely extracted, and the cement paste becomes dry. In low water-to-cementitious ratios or rich cement paste mixtures, the direct vacuum suction method is not efficient, so the centrifuge technique is employed to extract the pore solution from the paste mixtures. In this research program, the Legend T+ Centrifuge produced by the Thermo Fisher Scientific Co. with a maximum speed of 10,000rpm is employed (Figure 3-11).

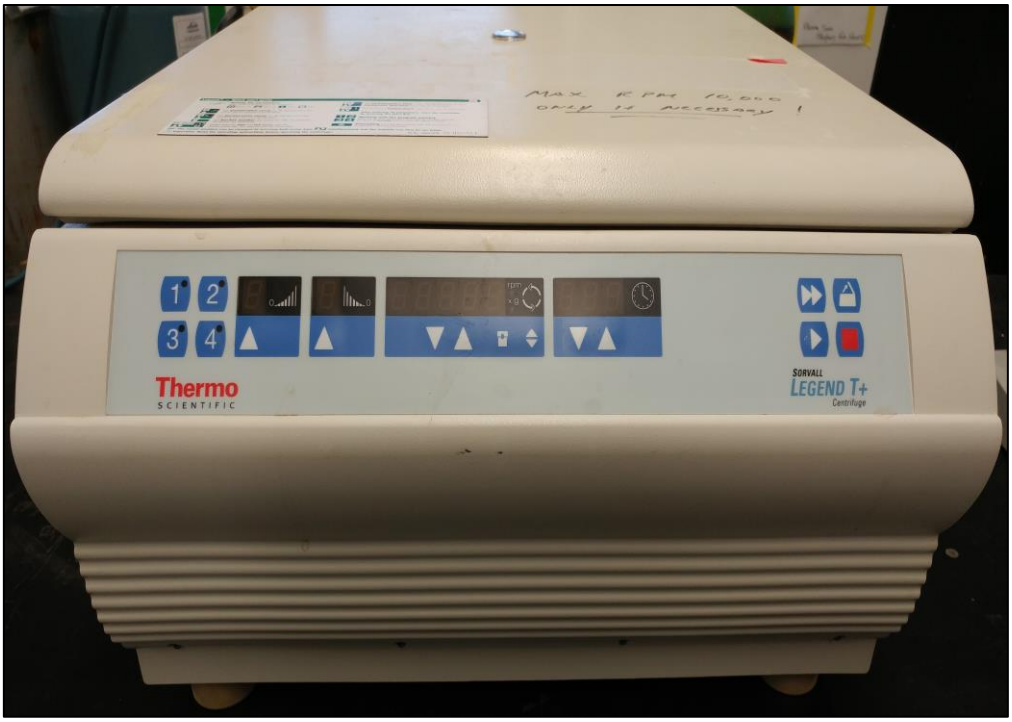


**Figure 3-11: Legend T+ centrifuge for pore solution extraction from cement paste**

In the centrifuge, the specimens must be placed in opposite to keep the machine, balanced, so for every cement paste samples, two standard tubes of samples are prepared, as shown in Figure 3-12.

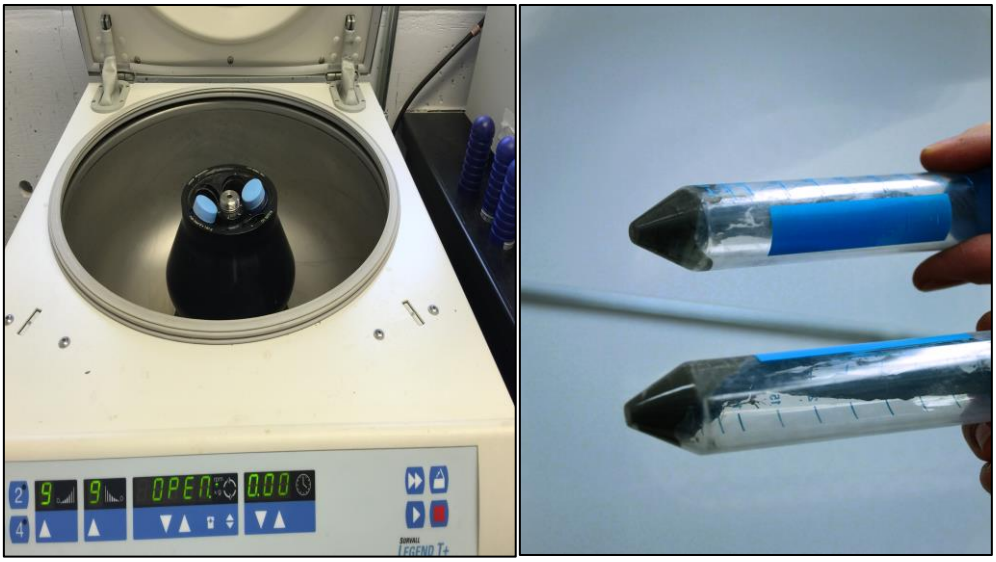


**Figure 3-12: Centrifuge technology for pore solution extraction from low W/CM mixtures**

In using the latter extraction technique, part of the extracted solution sometimes stays in the centrifuge tube as a gas. To maximize the centrifuged solutions, it is necessary to cool the tube down to convert the gas into liquid.

The extracted pore solution is kept in sealed plastic tubes until further analysis, as shown in Figure 3-13. Within the 1-day from extraction, the extracted solutions are tested for density, electrical properties, pH, and ionic concentration.


**Figure 3-13: Pore solution kept in plastic tubs until testing time**

To study and compare the chemical composition and electrical properties of the extracted solutions, all the measurements must be done at room temperature; the composition is restricted to cement pastes without any chemical admixture, ternary blends, and the W/CM ratio needs to be less than 1.0 (Vollpracht et al., 2016). All the conditions recommended in the literature are met in this research project.

### 3.4.1.1. Pore solution chemical composition and pH

The pH of an aqueous solution is the measure of how acidic or basic it is. The pH of an aqueous solution can be determined by measuring the concentration of hydronium ion in the solution. The term pH refers to the "potential of Hydrogen ion", and it is calculated as the negative of the logarithm of the concentration of hydronium.

In this research project, the pH is first measured by the pH-meter after the solution is extracted from the cement paste, as shown in Figure 3-14.

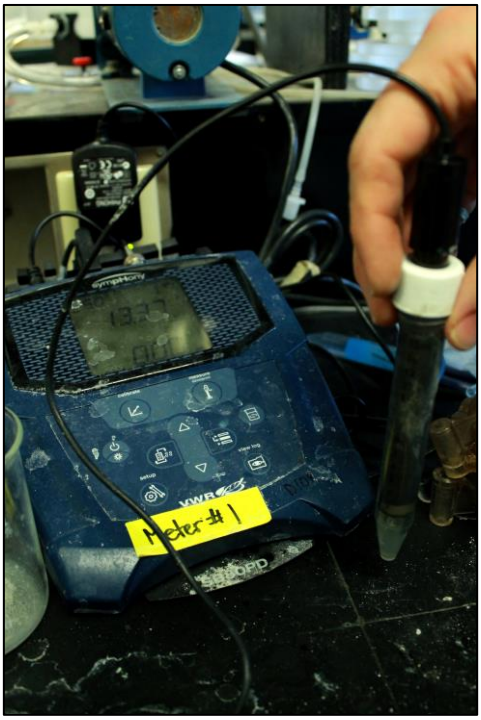

**Figure 3-14: pH determination of extracted pore solution**

To measure $OH^-$, which is an important indicator to analyze the alkalinity of a pore solution, titration according to ASTM D4662 is used. However, the literature has shown that hydroxide concentrations can be estimated from the pH value of the pore solution (Vollpracht et al., 2016), as:

$$pH = (-\log {}^{[OH^-]}) + 14.0 \qquad [3\text{-}13]$$

where, [$OH^-$] is the hydroxide concentration in mol/l (determined via titration). In the pore solution extracted from a semi-hydrated cement paste, the hydroxides ions are present as dissolved complexes such as NaOH, KOH, and CaOH.

In addition to pH determination, analyzing the ions, leached in the pore solution (elemental characterization), is important for gaining insight into the reactivity and hydration process of the cement. One of the most versatile methods of inorganic (cement hydration products) liquids analysis is the Inductively Coupled Plasma (ICP) mass spectrometry.

The ICP was developed for Optical Emission Spectrometry (OES) by Fassel et al. in 1965 at Iowa State University and by Greenfield et al. at Albright & Wilson, Ltd. in the United Kingdom, in the mid-1960s (Hou and Jones, 2000). ICP with OES is based upon the spontaneous emission of photons from ions that have been excited by plasma and it has a very wide range of application in industry. Liquid and gas samples may be injected directly into the ICP, while solid samples require extraction or acid digestion so that the analytes are present in a solution (Hou and Jones, 2000). This technique is used in a wide range of fields, including purity analysis of environmental water and composition analysis of solutions and materials such as ceramics, and plastics (Morishige and Kimura, 2008).

The industrial applications and type of sample for the ICP-OES analysis are summarized in Table 3-3.

**Table 3-3: Survey of elemental application areas of ICP/OES (Boss and Fredeen, 1997)**

| Industrial Categories | Examples of samples |
|---|---|
| Agricultural and Food | Animal tissues, beverages, feeds, fertilizers, garlic, nutrients, pesticides, plant materials, rice flour, soils, vegetables, wheat flour |
| Biological and Clinical | Brain tissue, blood, bone, bovine liver, feces, fishes, milk powder, orchard leaves, pharmaceuticals, pollen, serum, urine |
| Geological | Coal, minerals, fossils, fossil fuel, ore, rocks, sediments, soils, water |
| Environmental and Water | Brines, coal fly ash, drinking water, dust, mineral water, municipal wastewater, plating bath, sewage sludge, slags, seawater, soil |
| Metals | Alloys, aluminum, high-purity metals, iron, precious metals, solders, steel, tin |
| Organic | Adhesives, amino acids, antifreeze, combustion materials, cosmetics, cotton cellulose, dried wood, dyes, elastomers, epoxy, lubricant, organometallic, organophosphates, oils, organic solvent, polymers, sugars |
| Other materials | Acids, carbon, catalytic materials, electronics, fiber, film, packaging materials, paints and coatings, phosphates, semiconductors, superconducting materials |

The wide application of IC-Plasma is due to its impressive characteristics as an analytical atomic emission source, compared to the other emission sources such as Direct Current Plasma (DCP), Laser-Induced Plasma (LIP), and electrical discharge.

In this research project, the ICP-OES is a quantitative method for determining trace elements (i.e., ions leached in this project) in liquid (i.e., extracted pore solution in this project) samples. Therefore, the pore solution, as an inorganic material, is tested for ionic concentration ($Al^{3+}$, $Ca^{2+}$,$K^{+}$, $Mg^{2+}$, $Na^{+}$, and $S^{2}$) by ICP mass spectrometry, with an OES with the Charge Coupled Device (CCD) detector (Figure 3-15). The concentration (and therefore effectiveness on cement properties) of other elements such as iron is very low (µg/L), so they are not analyzed in this test.


**Figure 3-15: ICP-OES machine with CCD detector**

The schematic of a typical ICP-OES equipment is shown in Figure 3-16. The instrument contains two main parts:

***Past I)*** Inductively Coupled Plasma (ICP)

***Part II)*** Optical spectrometer

The instrument contains a sample introduction section, a source for plasma, a detector, a spectrometer, and a data processing system.

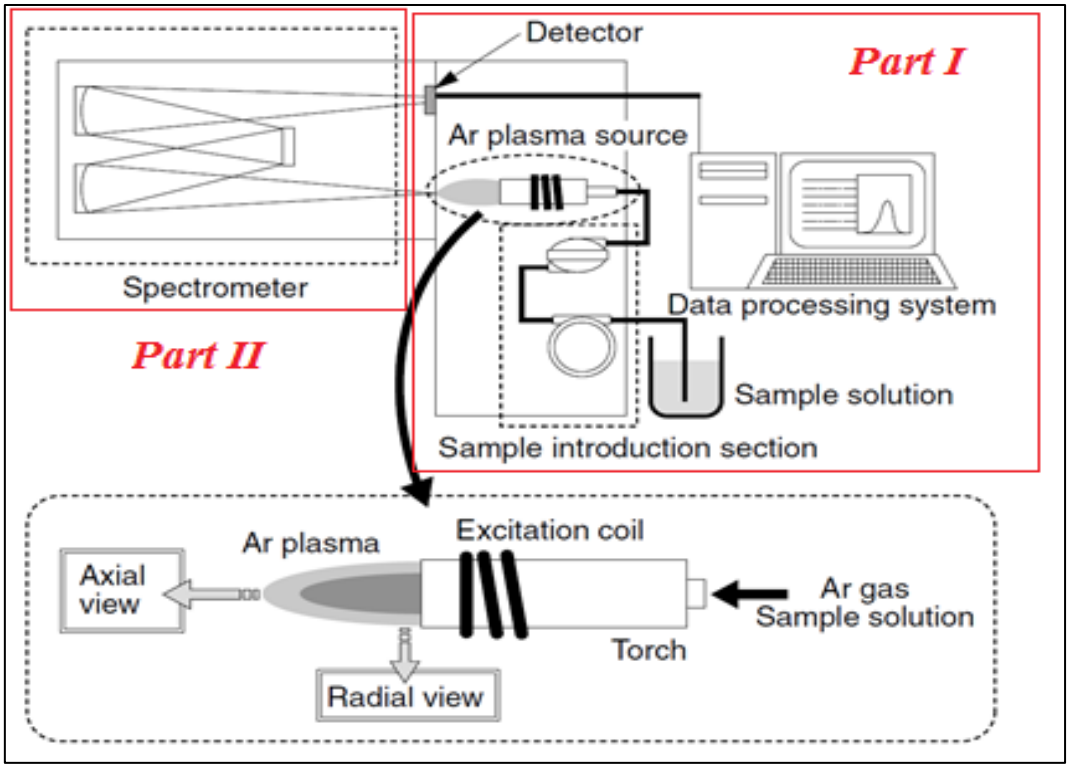


**Figure 3-16: Schematic of an ICP-OES equipment with axial or radial view (modified from Morishige and Kimura, 2008)**

When the ICP-OES is turned on, an intense electromagnetic field is created within the coil by the high-power Radio Frequency (RF) signal flowing in the coil (as explained by Lenz's law in physics). The coil surrounds a quartz glass torch which is a combination of three concentric (outer, intermediate, and inner) glass tubes, shown in Figure 3-17.

**Figure 3-17: ICP-OES sample torch containing three concentric quartz glass tubes**

In this method plasma (very intense, teardrop shape, brilliant white, and super high in temperature) is generated inside the torch by making a contact between the supplied argon gas with the electromagnetic field created by a high-frequency electric current applied to the work coil at the tip of the torch tube. In this procedure, the argon gas is ionized in the intense high frequency oscillated electromagnetic field (created by the RF coil). The power of the RF is 700W to 1500W and an AC current oscillates inside the coil at a rate corresponding to the frequency of the RF generator (27 or 40MHz). The high-power RF adds energy via a procedure called RF-induced collision. This is method is called the inductive coupling and the plasma created is called the Inductive-Coupled Plasma (ICP). A stable, high temperature plasma is then generated as the result of the inelastic collisions created between the neutral argon atoms and the charged particles (Huang and Hieftje, 1989). As explained by Hou and Jones (2000), to prevent the walls of the tube from melting, the argon in the outer glass tube flows (10–15L/min.) into the torch. It sustains the high-temperature plasma and positions the plasma relative to the outer walls and the induction coil. The intermediate glass tube injects argon at a rate of 0-1.5L/min. to lift the plasma.

In this project, a semi-hydrated cement pore solution is sprayed, by a peristaltic pump, into the torch with a high-temperature plasma. The plasma is generated by subjecting argon gas (Ar plasma) to a high frequency field (by the excitation coil). This is called the Flame Technique with a flame temperature in the range from 6000 to 10,000K at its core (Hou and Jones, 2000). The temperature gradient at different heights above the load oil is shown in Figure 3-18.

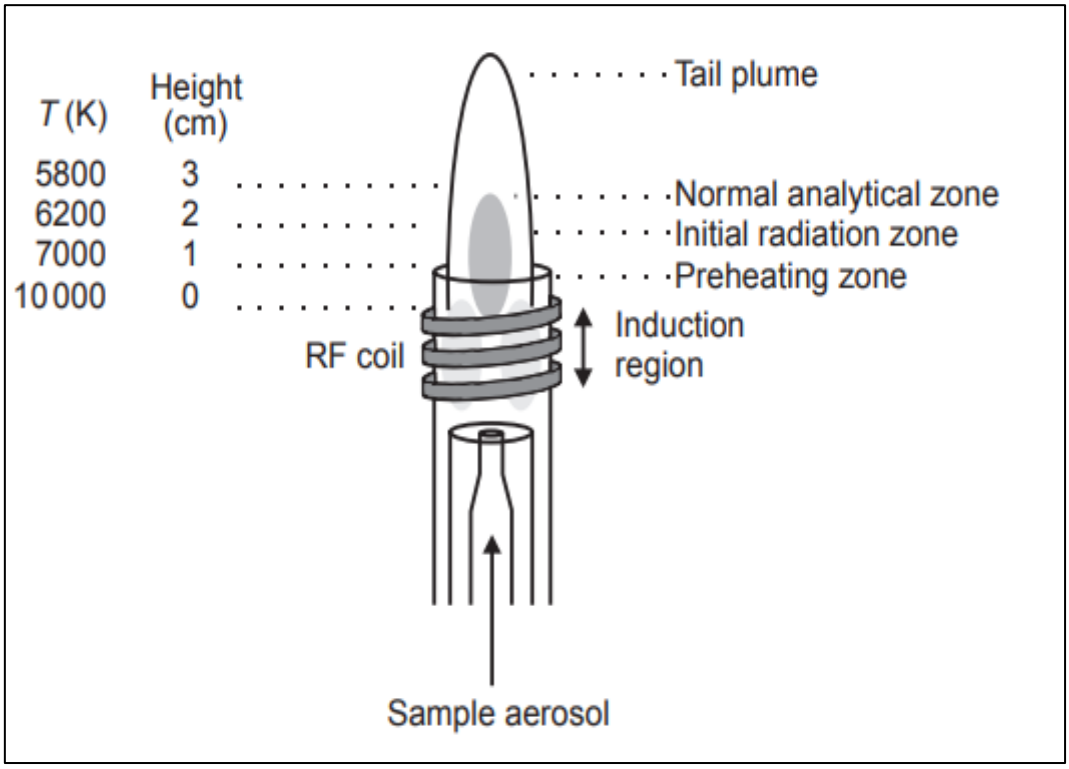


**Figure 3-18: Schematic diagram of an ICP assembly and temperatures above the loading coil (Hou and Jones, 2000)**

It is observed that the in the plasma, the highest temperature is at the Induction Region (IR) characterized by a bright continuum emission. Plasma (i.e., typically argon-based) operates at much higher temperatures than flames and graphite furnaces, the efficiency for the atomization (conversion of atoms to ions) and excitation process, thus ICP-OES has improved detection limits, high precision and an extended linear response range (Caruso et al., 2017).

Inside the glass torch, the solution is prayed into an analytical nebulizer, where it is changed into mist. The procedure of the conversion of the liquid sample into an aerosol and then transported to the plasma is done with a nebulizer. Three types of pneumatic nebulizers are commonly employed in ICP/OES: the concentric nebulizer, the crossflow nebulizer, and the Babington nebulizer, as shown in Figure 3-19.

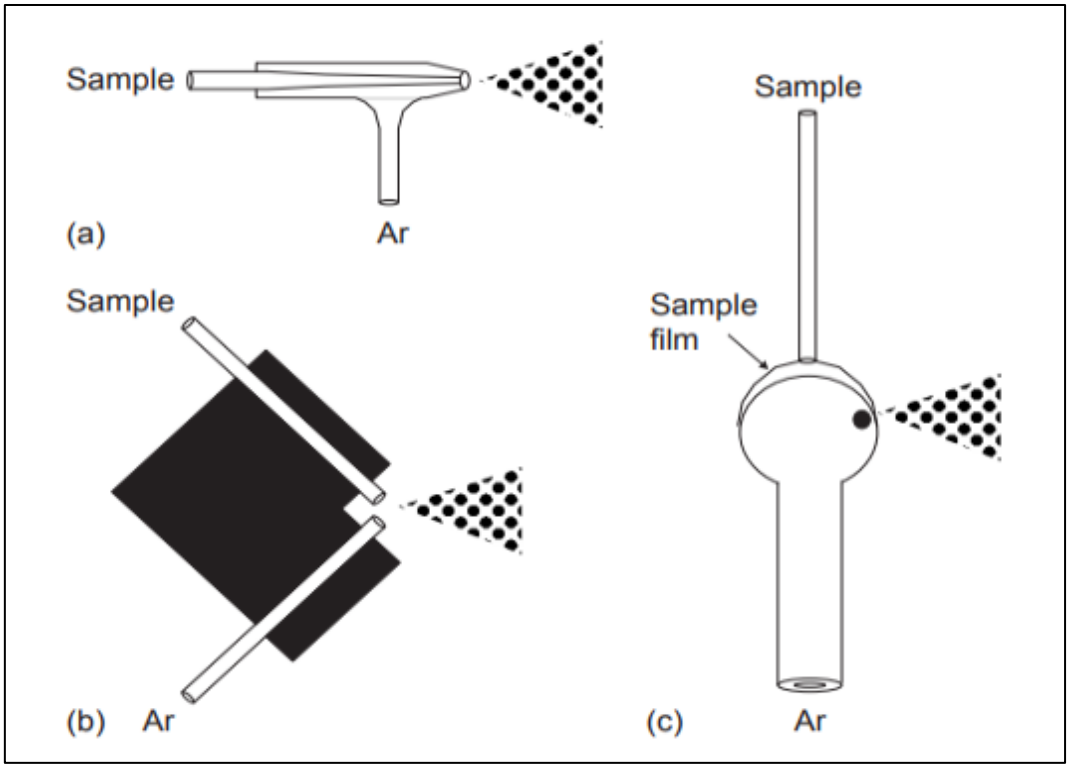


**Figure 3-19: Schematic diagrams of three types of pneumatic nebulizer: (a) the concentric nebulizer, (b) the crossflow nebulizer, and (c) the Babington nebulizer (Hou and Jones, 2000)**

The difference between the nebulizers is in their spraying capacity, reduction in the problem of clogging, and the rate of spaying. However, for small quantity of samples or for samples with possible fused silica, the other types are recommended.

The mist sample is carried and introduced directly inside the centre plasma flame by the argon gas flow through the IR. The solution is carried and sprayed with the inner argon (at the rate of 0.5-1.5L/min.). The mist solution collides with the charged ions in the Ar plasma, dried, vaporized, and then energized through collisional excitation at high temperature. The

vaporized solution is broken down into charged ions (ionization process). As a result, the pore solution is ionized due to radiation is given off at the characteristic wavelengths of the ionized elements. In other words, when plasma energy is given to the sprayed solution sample, the component elements (atoms) of the solution are excited. Due to the excitement and relaxation to the ground state, radiation is created (emission of a photon) and the radiation transfer into the second part of the ICP-OES (the optical spectrometer). The process is schematically shown in Figure 3-20.

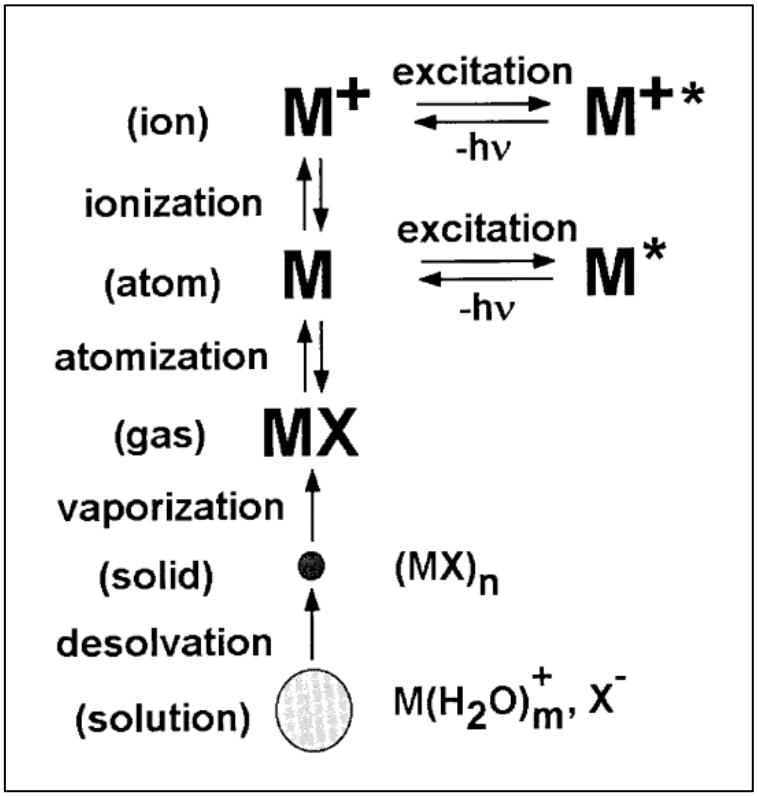


**Figure 3-20: ICP discharge functionality of the introduced solutions droplet (Charles and Kenneth, 2004)**

When the excited atoms return to a low energy position, emission rays (spectrum rays) are released and transferred to the Part II of ICP-OES. Depending on the position where the emission radiation is collected, collimated, filtered and detected, there are two types of view (transfer of emission rays from Part I to Part II): radial view (lateral 90° view of the plasma) and axial view (top view of the plasma plume). As reported in the literature, the radial view

is less affected by coexisting elements, but it has lower sensitivity, whereas the axial view is affected from coexisting elements in the solution, but it provides greater detection sensitivity (Morishige and Kimura, 2008). This may be attributed to the longer viewing path available down the axis of the plasma in the axial view (Hou and Jones, 2000). The optical emission spectrometry part of ICP-OES consists of a light source unit, a lens or a concave mirror to collect emitted photons, a spectrophotometer, a detector and a data processing unit.

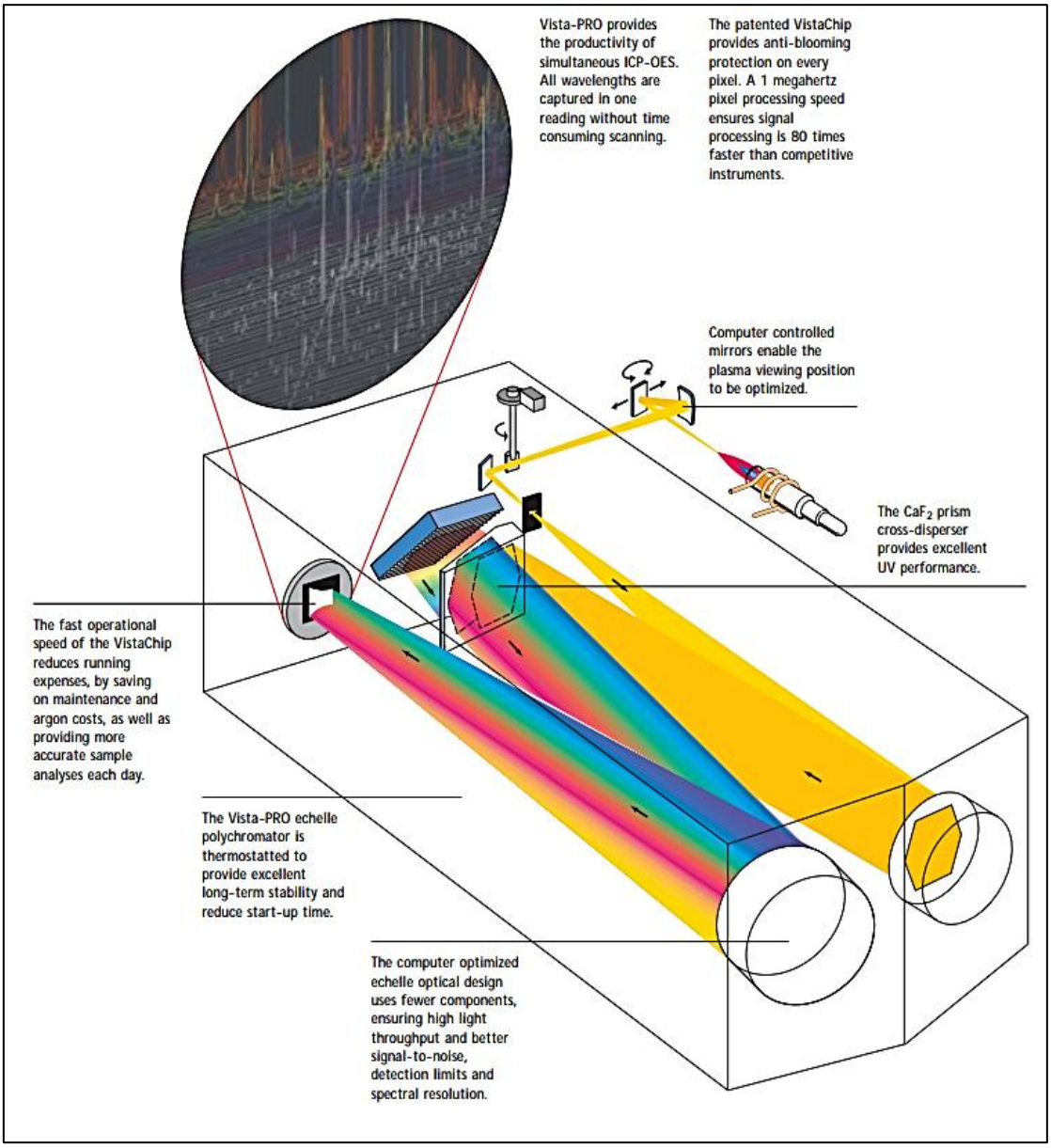


**Figure 3-21: Structure and functionality of the optical spectrometer part in Simultaneous ICP-OES (Manual of Varian Vista-PRO CCD Simultaneous ICP-OES, Varian Inc.)**

In the optical spectrometer part, the emission intensity of the light (indicative of the concentration of the element within the sample) is separated into different wavelengths (colours). Since every element has a unique wavelength (presented in Appendix G), the wavelength analysis of the axial or radial view of the photons emission spectra from the excitement/relaxation of the ions is used to qualitatively and quantitatively determine the elements in the solution. The wavelength is used to identify the elements from which they are originated (a linear correspondence between the signal and the analyte concentration of the resulting signals).

The main challenge with ICP-OES is to calibrate the instrument to utilize the ICP-OES to the concentration of the coexisting elements in the solution. In this research, 2-hour pore solutions are tested for ionic analysis with the ICP-OES, so the contents in the sample are known and the purity of them is low. Therefore, the calibration solution is adjusted to be the same in order to minimize the influence of coexisting elements on the measurements. Since ICP-OES is used in this project for quantitative analysis, a calibration solution adjusted to a known concentration of the pore solution element is prepared. The difference between the intensity of emissions of the pore solution sample with the calibration solution is the source of element determination in the sample.

At the end, it is important to mention that the samples are diluted to 1:10 and then acidified immediately to a pH of about 1, before placing them in the instrument.

Not only the type of ions, but also the total ions in the pore solution are important parameters in studying the electrical conductivity of a cement paste mixture. Since electrons travel through a liquid medium of ions (pore network in cement paste microstructure), more ions result in easier electron movement from one electrode to the other, and therefore higher electrical conductivity.

### 3.4.1.2. Pore Solution Density

The density of the pore solution is an indicator for solids in the solution. Therefore, the density of pore solutions extracted from the various cement paste mixtures is measured and compared. It is expected to have all extracted pore solutions with similar densities. Therefore, the test results are used to validate the samples before starting advance testing on them. In addition, the total molecular mass of the ions in the pore solution should be less than the unit mass of the solution. This is the second validation test for the results obtained by the method described in Section 3.4.1.

### 3.4.1.3. Pore Solution Electrical Properties

The electrical resistivity (or inverse of conductivity) of a cement paste mixture can be influenced by the electrical properties of the solid structure (physical characteristics of the microstructure) and the electrical properties of the pore solution filling the pore network. Therefore, the electrical conductivity of the extracted pore solutions is measured in this research program to analyze the electrical behaviour of the cement paste. An especial conductivity-meter called ECTestr 11+ (maximum measurement range of 20.0mS/cm with ±1% accuracy and resolution of 0.01mS/cm) was used. A small quantity of the pore solution is placed on the sensor of the instrument (shown in Figure 3-22) and the Valox® housing and stainless-steel electrodes offer accurate conductance value of the solution.


**Figure 3-22: Cup-style sensor version of the solution conductivity-meter**

The description of the conductivity-meter is presented in Table 3-4.

**Table 3-4: Description of the pore solution conductivity-meter**

| Description | | Range |
|---|---|---|
| **Range** | Conductivity | 0 to 2000µS, 0 to 20.00mS |
| | Temperature | 0 to 50°C |
| **Resolution** | Conductivity | 10µS, 0.10mS |
| | Temperature | ±0.1°C |
| **Accuracy** | Conductivity | ±1% full scale |
| | Temperature | ±0.5°C |
| **Temperature Compensation** | | Automatic, 0 to 50°C, 2% per °C |
| **Calibration** | | One or two points |
| **Power** | | Four 1.5V alkaline batteries (included), approximately 150 hours of continuous use |

Detailed information about the instrument is presented in Appendix F.

### 3.4.2. Hydration Products Analysis

As described before, the electrical resistance of the liquid phase (pore solution) and solid phase (hydrated cement paste) can make the electrical resistance of the whole cement paste. To study the electrical properties of cementitious materials at early ages (or desired hydration degree at 2 hours, initial setting, final setting and at 24 hours in this research program), the hydration of the cement needs to be stopped. To achieve it, the capillary water in the fresh cement paste samples needs to be removed, which results in a weak and semi-hydrated microstructure. Extracting the pore solution from the fresh cement paste under the direct vacuum suction (as described in Section 3.4.1) is not a reliable method for this purpose, because the capillary and in layer water cannot be extracted with the direct suction. They are many methods (e.g., heat drying) to stop the hydration, but most of them damage the microstructure (Taylor and Tuner, 1987). The only method with no negative influence on the microstructure of a hydrated cement paste is water replacement with an inert solvent. It has

been observed that isopropanol alcohol (or dimethyl Carbinol, $C_3H_8O$ or i-PrOH) chosen as the inert solvent to replace water is the most effective solution (Wang et al., 2016). In this research project, partially dried binder pastes are mixed with isopropanol alcohol, and the mixture is kept under 10 vol. % of aqueous solution of isopropanol for 24 hours (as shown in Figure 3-23).

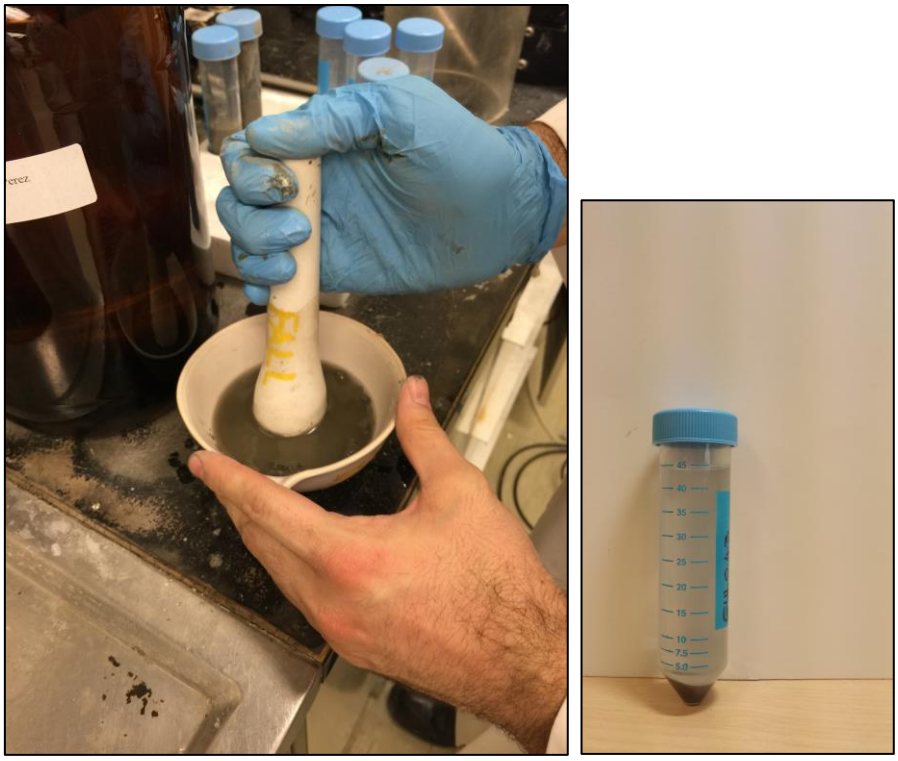

**Figure 3-23: Cement paste mixing with isopropanol to stop the hydration process**

It is an acceptable assumption that by practising water replacement with this alcohol, the cement hydration process is completely stopped (Wang et al., 2016). After 24 hours, alcohol is extracted from the mixture by vacuum suction. The vacuumed cement sample, which is a partially hydrated cement powder, is placed under vacuum with the indicating desiccant Drierite salt, impregnated with cobalt chloride, until the test time of the semi-hydrated cement paste, as illustrated in Figure 3-24.

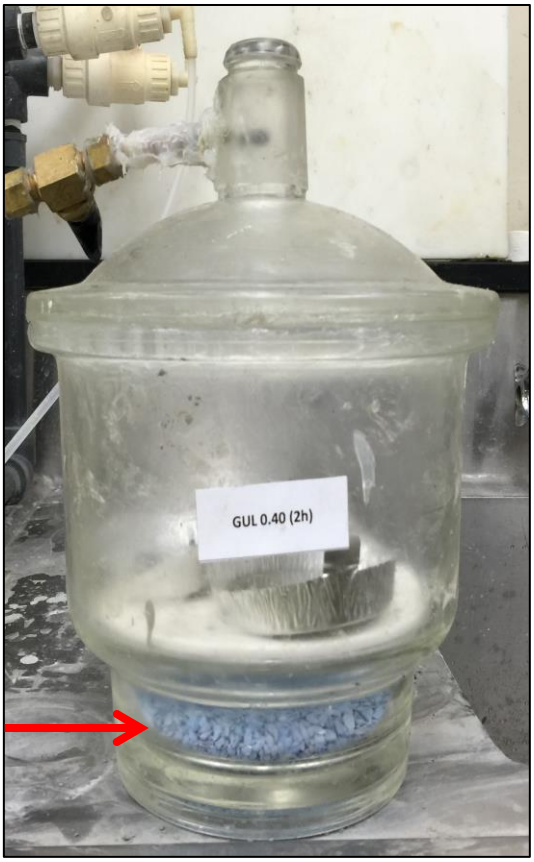


**Figure 3-24: Drying partially hydrated cement powders with the Descant salt in vacuumed chambers**

The Drierite's original colour is light blue which changes to pink (or other colours) upon absorption of moisture (or other gases). If the colour of the salt changes at the time the chamber is open, it is assumed that the cement powder contained some moisture, so its hydration had not been stopped. In this case, the sample is disregarded, and all the process is repeated to get semi-hydrated cement powder samples.

However, preliminary testing showed that measuring the electrical resistivity of semi-hydrated dried powders at different times was scattered and not reliable. Thus, the electrical resistivity measurement of semi-hydrated cement powders is replaced with studying the hydration products development at different times of testing. For this purpose, powders obtained are tested for microstructure properties (TGA and XRD). To predict the expected results of microstructure assessment, cement hydration is needed to be considered. All four main cement minerals (tabulated in Table 3-2) react at different rates and therefore different

times of hydration. As a result, different solid phases are formed. The behaviour of each of these minerals ($C_3S$, $C_2S$, $C_3A$, and $C_4AF$) has been studied by synthesizing and hydrating them in their pure form, under controlled conditions. Crystal shapes of $C_3S$ and $C_2S$ are shown in Figure 3-25.

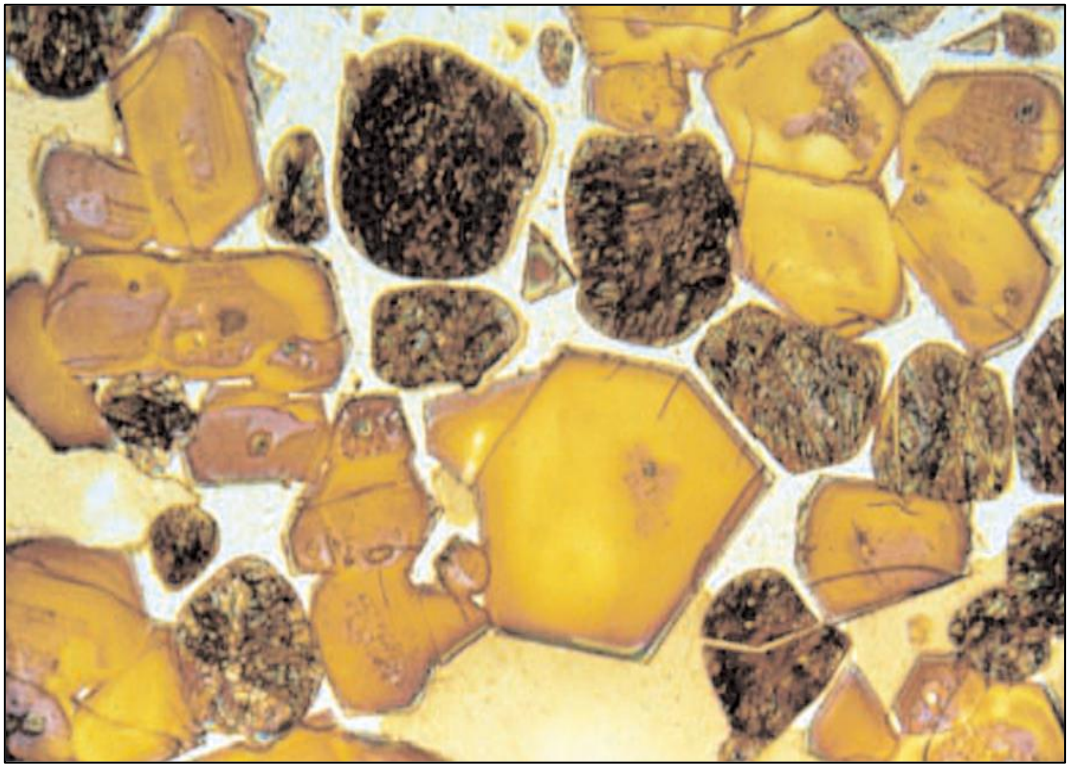

**Figure 3-25: Polished thin-section examination shows Alite ($C_3S$) as light, angular crystals, the darker, rounded crystals are Belite ($C_2S$)-Magnification 400X (Kosmatka et al., 2011)**

Alite (Tricalcium silicate phase - $Ca_3SiO_5$, or $C_3S$) is the most important cement role playing mineral in early-age property development of Portland cements. This mineral is the majority in Portland cement. The reaction of Alite is summarized as

$$C_3S + \text{water} \rightarrow \text{C-S-H} + \text{mCH}$$

where, C-S-H or CSH is the gel phase calcium silicate hydrate or Tobermorite (main product of Portland cement hydration) and CH is the calcium hydroxide (or Portlandite in mineral name), $Ca(OH)_2$, which is the bi-product of cement hydration (shown in Environmental Scanning Electron Microscope image in Figure 3-26). C-S-H is the most abundant reaction

product of Portland cement hydration. C-S-H is responsible for hydrated cement properties because it forms continuous layers binding together the original cement particles and hydrated particles, like glue (Neville, 2008). This is the main difference between C-S-H and other hydration products. Other hydration products are discrete crystals with no connection to the solid phases, so they cannot contribute to mechanical and physical properties of hydrated cement. CH has little contribution to strength and it much more soluble than C-S-H (Nevile, 2008).

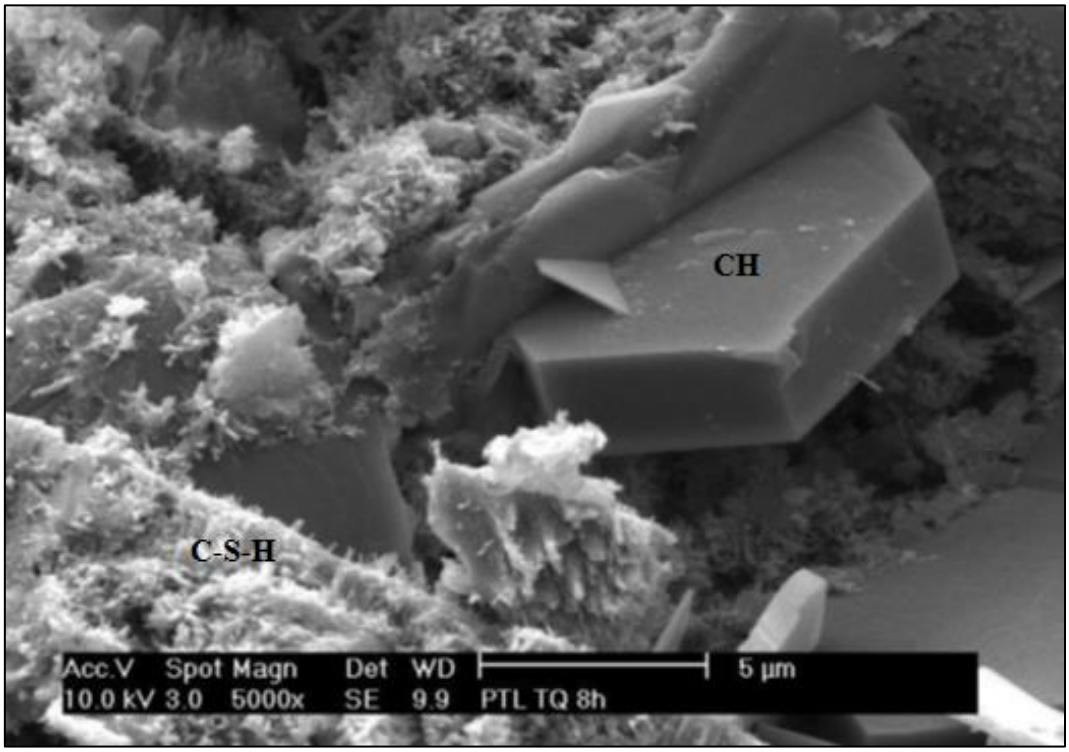


**Figure 3-26: ESEM figure of C-S-H and a well-developed Portlandite crystal growing on the clinker grains (Artioli and Bullard, 2013)**

Belite (Dicalcium silicate phase - $Ca_2SiO_4$ or $C_2S$) is also responsible for strength and other properties development of Portland cement. However, the rate of reaction is slower than Alite, so later-age properties are mainly affected by Belite hydration. The reaction of Belite is summarized as;

$$C_2S + water \rightarrow C\text{-}S\text{-}H + nCH$$

Belite hydration produced similar hydration product as Alite reaction, but with less CH (Mehta and Monteiro, 2006).

The reaction of the other two minerals (Celite or Tricalcium aluminate-$C_3A$ and Tetracalcium Aluminoferrite- $C_4AF$) happens after sulphate ions are present in the pore solution. $C_3A$ is the most reactive mineral of all the four main minerals. Solubility of Celite ($C_3A$) is even higher than that in $C_3S$ under the following sequence:

$$C_3A + \text{water} \rightarrow \text{C-A-H} + \text{water}$$

where, C-A-H is called hydrogarnet or calcium aluminate hydrate. Due to $C_3A$ hydration, heat is generated, and cement paste is set rapidly which is called the flash setting (Neville, 2008). To prevent flash setting, gypsum ($CaSO_4 \cdot 2H_2O$ or $C\bar{S}H_2$) is added to Portland cement. In addition to gypsum, other sulphates are added to the cement clinker in small quantity (e.g., sulphate of sodium, potassium and calcium). When gypsum is added, sulphate is leached into the pore solution (as gypsum is highly soluble) and $C_3A$ reaction with water contacting sulphate and its reaction is not resulted in a flash setting anymore:

$$C_3A + 3C\bar{S}H_2 + 26H \rightarrow C_6A\bar{S}_3H_{32}$$

where, $C_6A\bar{S}_3H_{32}$ is the mineral form of ettringite. Ettringite forms prismatic needles, as shown in Figure 3-27.

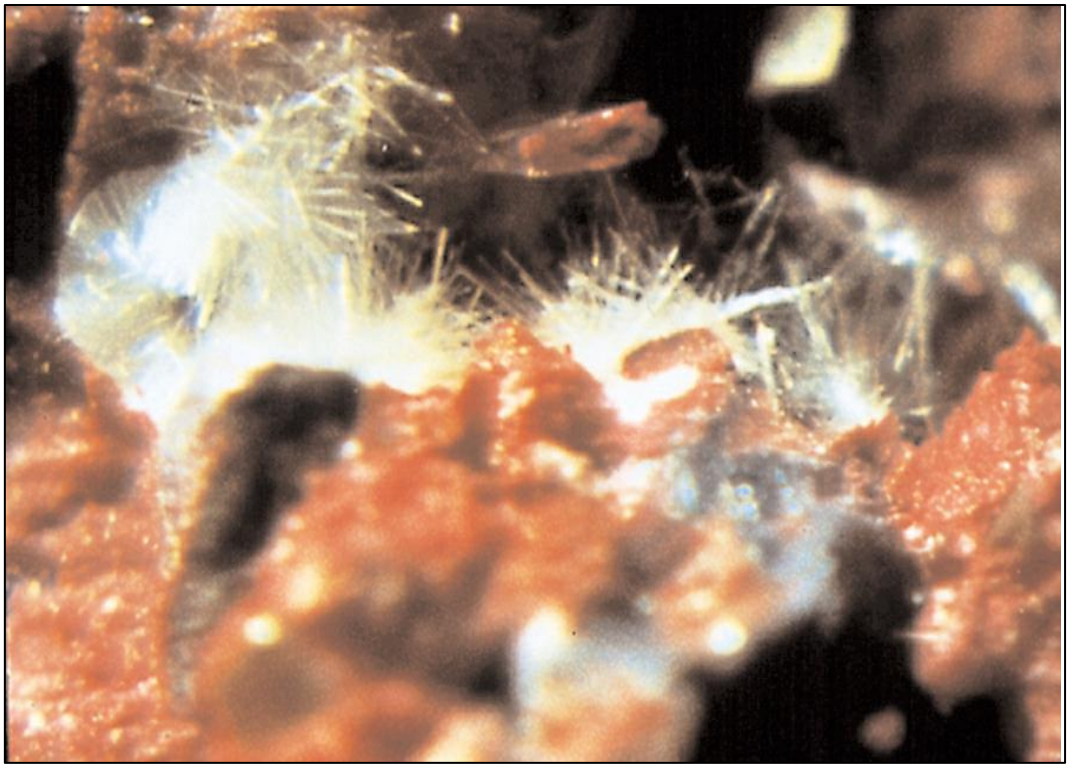

**Figure 3-27: Cluster of large ettringite rod-like crystals in hydrated cement paste (Kosmatka et al., 2011)**

After reduction of sulphate ions in the pore solution, ettringite becomes less stable and it converts to a different solid phase with less sulphate which is called monosulfoaluminate ($C_4A\bar{S}H_{12}$), within the first couple of days of hydration (Neville, 2008) as patterned below:

$$2C_3A + C_6A\bar{S}_3H_{32} + 4H \rightarrow 3\ C_4A\bar{S}H_{12}$$

The formation of mineral ettringite and conversion to monosulfoaluminate are both exothermic, so the internal temperature of the cement-based mixtures is increased. If addition sulphate becomes available, monosulphate will be converted to ettringite again. Scan electron microscopic photos of ettringite formed from $C_3A$ reaction with gypsum and $C_3A$ crystals are shown in Figure 3-28.

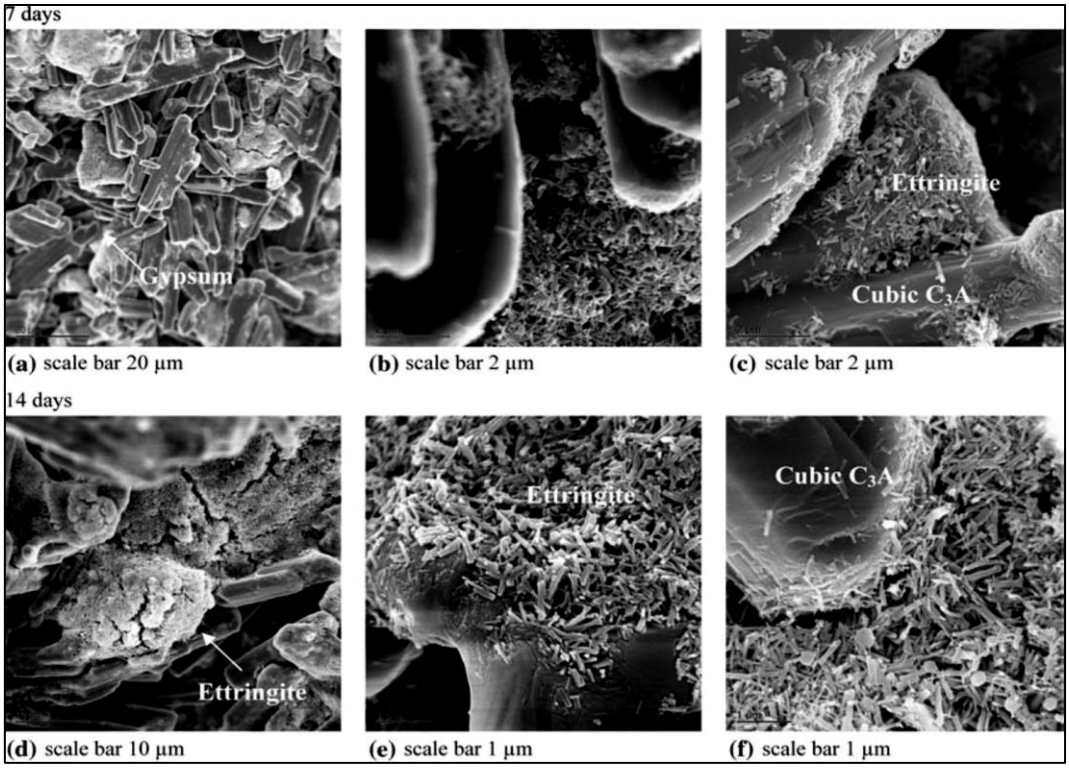


**Figure 3-28: SEM pictures of ettringite formation from a cubic $C_3A$ + gypsum + $H_2O$ mixture, at 7 and 14 days, W/CM = 0.6 (Kirchheim et al., 2009)**

Tetracalcium Aluminoferrite- $C_4AF$ or ferrite phase reacts slower than $C_3A$, but in a similar way (Mehta and Monteiro, 2006). In other words, $C_4AF$ reacts with water and gypsum as patterned below:

$$C_4AF + 3C\bar{S}H_2 + 12H \rightarrow C_{6(}A \text{ or } F)\bar{S}_xH_y + (F \text{ or } A)H_z$$

where, (A or F) indicates the substitution of aluminum with variable s of iron, or vice versa. Because of the described substation, the final product of ferrite phase hydration is not either pure ettringite or pure monosulfoaluminate. In a Portland cement paste where the $C_3A$ and $C_4AF$ are mixed together, it can be safely assumed that the final products of their hydration contain both aluminum and iron. Therefore, the final their final hydration products are called AFt (alumina, ferric oxide, tri-sulphate) and AFm (alumina, ferric oxide, mono-sulphate) in cement chemistry. Ettringite and monosulphate are the most common and important member of the AFt and AFm group, respectively.

#### 3.4.2.1. Hydration Products Quantity

Calcium Hydroxide (CH) is one of the major hydrated products that comprise over 20% of the hydration products in a fully cured cement paste (Jelica et al., 2007). Since the presence of CH is predominantly in the form of well-defined crystals, the estimation of CH content can be used as an indicator for not only the Portland cement hydration characteristics, but also the degree of hydration. In addition to CH, Calcium Silicate Hydrate (C-S-H or CHS) is the other-end product of the reaction of Alite and Belite with water, which is responsible for many of the hydrated cement properties.

Among various techniques, the combination of Thermo-Gravimetric Analysis (TGA) and Derivatives Thermo-Gravimetric Analysis (DTA) are widely employed to determine the characteristics of a material, rate of degradation, absorbed moisture content of the material, the amount of inorganic and organic components in the material, or the kinetics of a reaction based on the weight changes. DTA locates the thermal ranges corresponding to the decomposition of different phases in a hydrated paste. TGA measures the weight loss of the pastes due to decomposition of phases, simultaneously. By the help of TGA results, the CH content can be estimated from the weight loss.

In this research program, TGA/DTA is used to determine the characteristics of cement paste mixtures and the amount of inorganic and organic components in them at different phases of the hydration (2 hours, initial setting, final setting, and 24 hours). For this purpose, the Universal V4.5A TA Instruments (the automated Q5000-IR model) is employed, as shown in Figure 3-29.


**Figure 3-29: TGA universal V4.5A TA Instruments automated Q5000-IR**

Detail information of the TGA instrument is provided in the appendix B.

After placing a small portion of unhydrated or hydrated cement in an aluminum open cement pane (all available pans for TA Q5000-IR are shown in Figure 3-30), it is placed in the instrument 25-sample consul.

**Figure 3-30: TGA Q5000-IR sample pans (photo Courtesy of TA Instrument, Machine Manual)**

The pan selected by the instrument containing the samples is placed in the furnace for testing. During the test, changes in the weight of the sample is measured, as shown in Figure 3-31. As indicated in the manual, the furnace that offers the widest range of linear (0.1 to 500°C/min.) and ballistic (+2000°C/min.) heating rates from ambient to 1200°C.

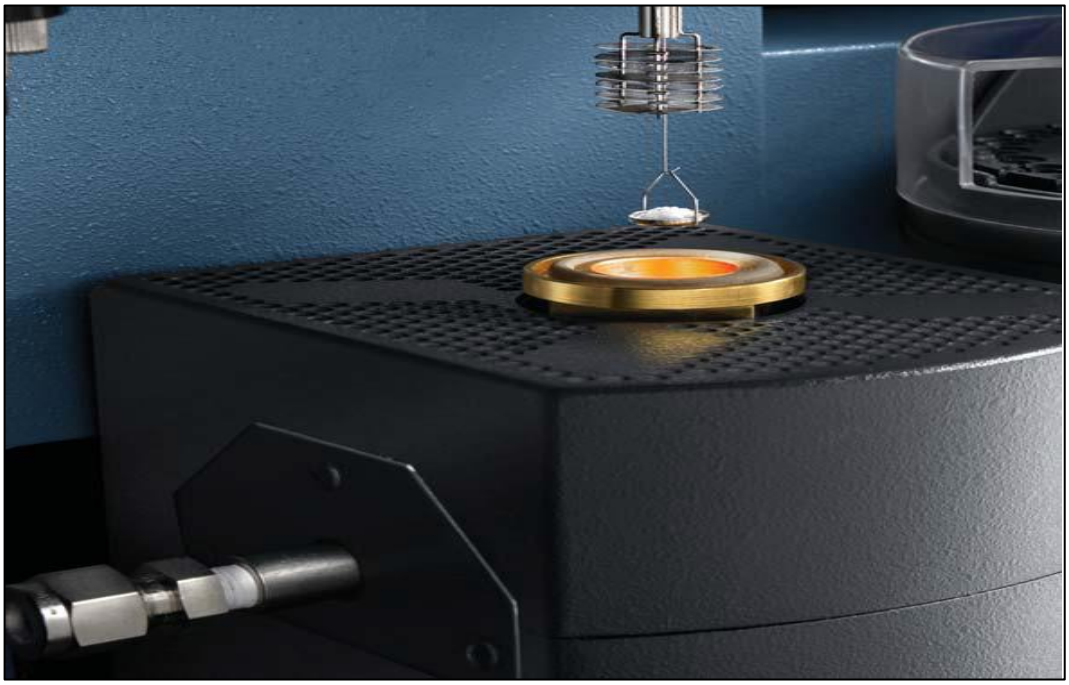

**Figure 3-31: Sample placement in TGA (photo Courtesy of TA Instrument, Machine Manual)**

The autosampler design provides smooth loading and unloading of the sample pan without disturbing the balance.

The atmosphere is nitrogen (to purge the lines of oxygen and stabilize the apparatus) in this project with a heating ramp of 10ºC/min., from room temperature (22-23°C) to a maximum temperature of 1000ºC. All this is done by the quantitative measurements of the mass changes in the cement powder (in a ceramic crucible) associated with thermal degradation.

For the analysis, TGA and DTA of the cement powder are divided into four endothermic effects:

I) **Room temperature – 100ºC:** Removal of any possible free water or isopropanol alcohol.

II) **100–350ºC:** In this stage, the water in the hydration products starts being removed. De-hydration of C–S–H (a gradual decrease in mass loss over a wide range of temperatures, but with no sharp peak) can be studied. However, ettringite, AFt, $C_3A.3CaSO_4.32H_2O$, (the main peak in this stage), mono-sulphate, AFm, $C_3A.CaSO_4.12H_2O$, and calcium aluminate hydrate, CAH, can be detected in this stage. All types of water including inter-layer and capillary pores water are removed at this stage, which is shown by small peaks. However, in some cases, it is difficult to distinguish the dehydration of C-S-H and AFm by monitoring the weight loss, as significant peaks are not detected (limitations of the TGA technique).

III) **350–500ºC:** Quantity of the Portlandite, $Ca(OH)_2$, content is obtained and Dihydroxylation (decomposition) is observed, following the chemical reaction below:

$$Ca(OH)_2 \rightarrow CaO + H_2O$$

IV) **Above 500–600ºC:** De-carbonation of calcium carbonate (Calcite, $CaCO_3$) is detected at this stage. In case of carbonation during sample manipulation, some peaks for Calcite at about 700-800ºC are observed.

$$CaCO_3 \rightarrow CaO + CO_2$$

It can be concluded that the reason behind the mass loss is different in each temperature range; for example, the loss of water is the reason behind the mass loss of Portlandite decomposition, while for Calcite, it is a loss of $CO_2$ (Villain et al., 2007).

Figure 3-32 illustrates the four endothermic stages of TGA result analysis and dehydration of cement hydration products at weight loss peaks.

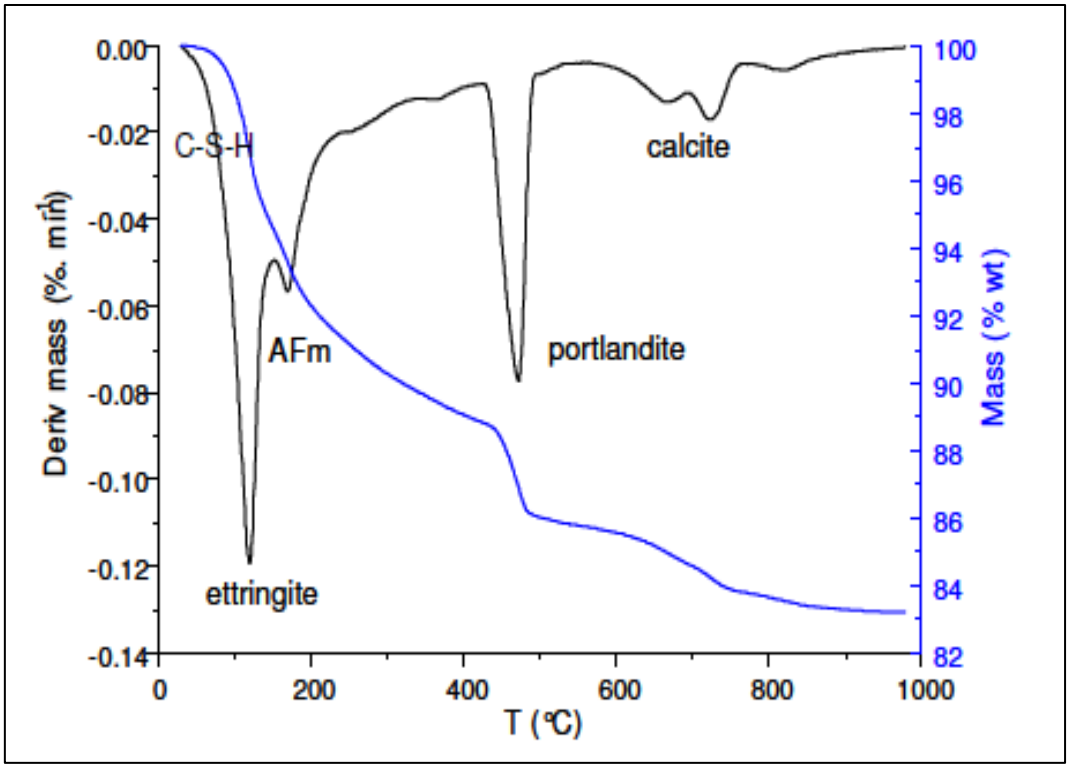


**Figure 3-32: Schematic view of TGA method results and analysis (for cement paste adopted from poster by Dilnesa)**

At the end of the project, the TGA raw data are normalized to residual weight of un-hydrated cements at 1000°C. This procedure returns both the physically- and chemically bound water of the hydrated samples and allows correction for carbonates either already present in the un-hydrated cement or coming from carbonation during manipulation (although samples are vacuumed sealed from carbonation). Also, the percentage of cement hydration indicators (e.g. $Ca(OH)_2$, $CaCO_3$) and total weight loss is determined.

Mass loss of CH can be calculated from the TGA/DTA results by using the formula in Equation 3-14 (Nuruddeen, 2014).

$$\mathbf{CH} = \frac{\mathbf{4.11W_{480}}}{\mathbf{W_{120}}}\mathbf{X100} \qquad [3\text{-}14]$$

where, CH is the Calcium Hydroxide (% mass), $W_{480}$ is the mass loss at 480°C, and $W_{120}$ is the mass loss at 120°C.

### 3.4.2.2. Hydration Products Crystal Formation

The quality of cement hydration, which can be studied by analyzing the hydration phase mineralogy, is used as an indicator for development of cement electrical resistivity. X-ray Diffraction (XRD) of a powder is a rapid analytical technique, primarily used for phase identification of a crystalline material. In physics, X-rays (electromagnetic waves similar to light but with much shorter wavelength around $\lambda$ = 0.2-200 Å) are avoided by obstacles when the obstacles have a size that compares to the wavelength. When the X-ray wave (generated by a cathode ray tube) falls on a crystal, the incident rays emit by the sample's crystal atoms. Because of the interaction between the rays and crystals atomic planes, constructive interference and diffracted ray beams will be reflected. The characteristic of the diffracted X-ray beams received by the XRD machine can provide a unique "fingerprint" of the crystals present in the sample. In a periodic display of atoms (i.e., crystal) with various parallel planes at a distance of "d" (as schematically shown in Figure 3-33), the constructive interference of the waves occurs if the conditions of Bragg's law ($2d\sin\theta=n\lambda$, where "n" is a whole number) are satisfied (Jumate. and Manea, 2011).

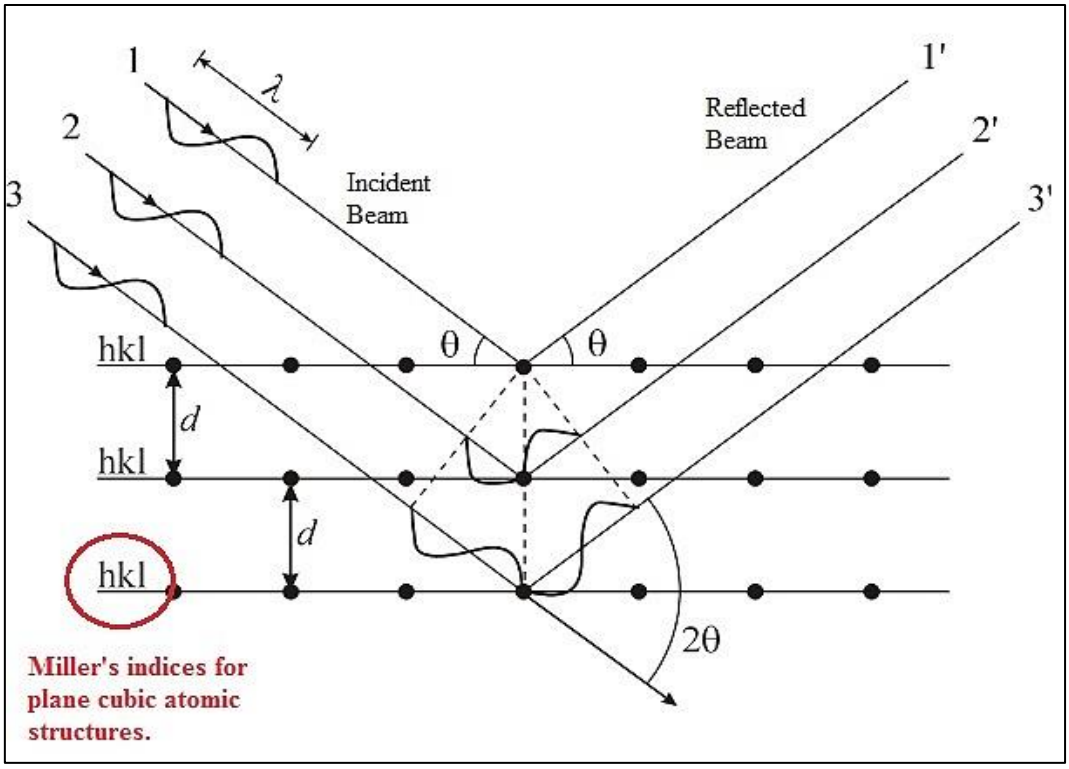


**Figure 3-33: X-ray diffraction for a structure with plane atomic structure (modified from image at https://fys.kuleuven.be/iks/nvsf/images/xrd_figure_1.jpg)**

Angle "θ" is the Bragg's diffraction angle. Each crystalline has its own diffraction image. Finally, the diffraction image, which depends on the crystals structure in the material, is achieved. For XRD analysis, a diffractometer is used in a Bragg-Brentano arrangement. In this arrangement, the specimen (cement powder in this project) is rotated by the diffraction angle of "θ", while the detector is turned by the angle "2θ", as shown in Figure 3-34.

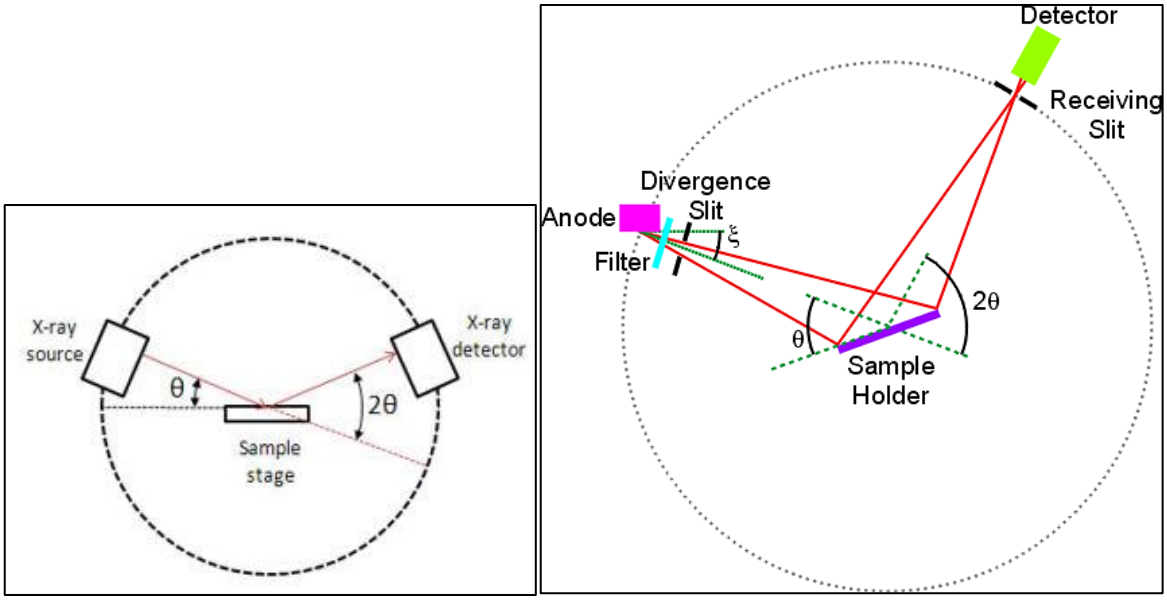


**Figure 3-34: Layout of an X-ray diffractometer (modified from Jumate and Manea, 2011)**

The diffractograms (the result of the XRD test) which depends on the material structure, is formed from a succession of diffraction peaks. The y-axis is the diffracted X-radiation intensity, measured in pulses/second, and the x-axis is the angle "2θ", where "θ" is the Bragg angle, measured in degrees. From the peaks and XRD peak analysis, not only the crystalline structure can be determined, but also the qualitative and quantitative phase analysis can be done.

Hydrated cement pastes are formed of a mixture of many crystalline phases which are defined by a certain system based on their atomic structure (e.g., cubic, hexagonal, trigonal, tetragonal, monoclinic, and etc.), a certain elementary cell geometry (e.g., simple, centred base, etc.), and by the parameters of the elementary cell. The explained physics phenomenon is used to analyze the crystals in the hydrated cement paste if their atomic planes (i.e., obstacles) are at comparable size with the X-rays wavelength.

The powder method of XRD is adopted in the present study with atomic planes size of the formed crystals comparable with the X-ray wavelength.

***XRD Machine and Analyzing Software:*** All samples were tested at room temperature (22-23°C) on Rigaku Ultima IV powder diffractometer (Scintag XDS 2000), shown in Figure 3-35, in Bragg-Brentano geometry, with an X-ray source of Cu Kα radiation (λ = 1.5418Å).


**Figure 3-35: Rigaku Ultima IV powder diffractometer**

First, the samples, semi-hydrated cement powders, are placed in the stainless-steel sample holder (shown in Figure 3-36).

**Figure 3-36: XRD sample holder**

Cement powder sample is consolidated and compacted by vertical pressure, as shown in Figure 3-37. Before applying vertical pressure, sample surface is covered with 100×100mm weighing paper.

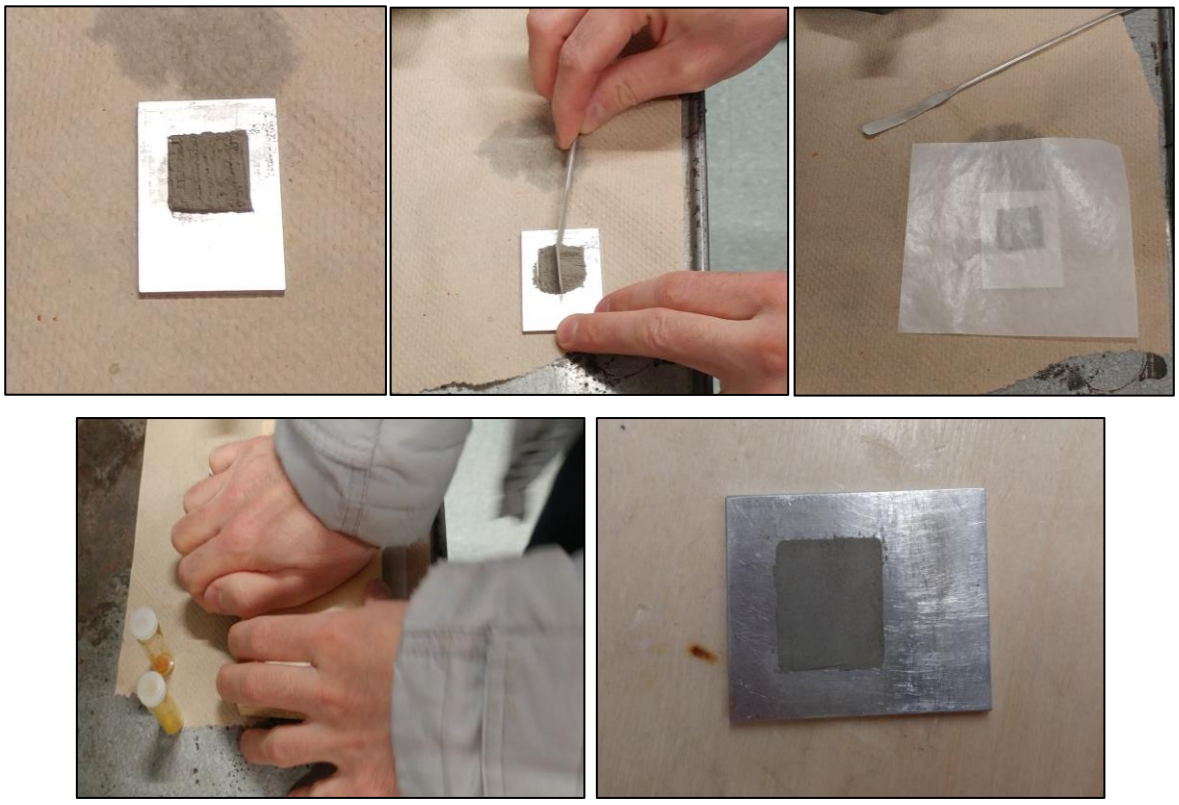

**Figure 3-37: Process of sample preparation for XRD test**

Then, the prepared sample is placed in the machine for testing as shown in Figure 3-38.

**Figure 3-38: Cement sample placement in XRD machine**

The spectra are obtained in the range $4^{\circ} < 2\theta < 85^{\circ}$ using a step size of $0.03^{\circ}$ step widths and 5º/min. scan speed for all specimens. All samples were analyzed with a basic configuration (θ:2θ configuration). The identification is performed by calculating the Bragg's relationship using XpertScore® software and making use of the powder diffraction file database. All phases are identified, and their amount is measured.

In general, solids have three types of atomic positioning as schematically shown in Figure 3-39.

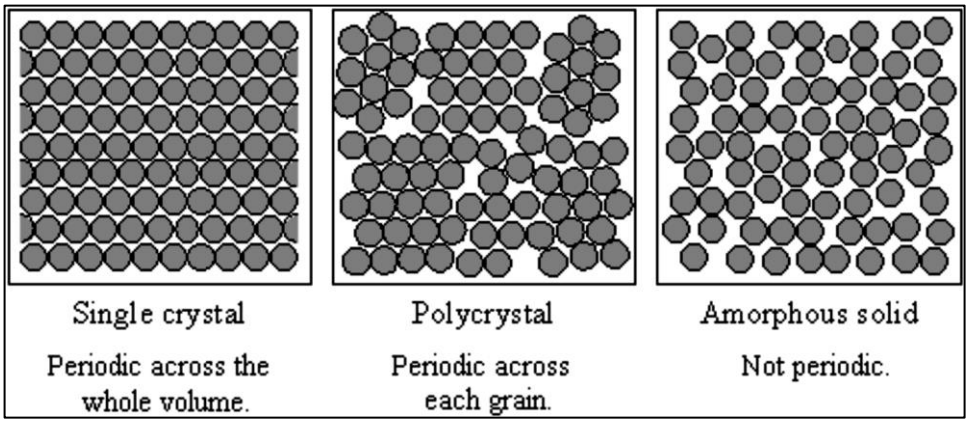


**Figure 3-39: Schematic of a single crystal, polycrystalline and amorphous atomic positions (Sharpley I., 2015)**

As reported in literatures, a crystalline material will show sharp peaks representing X-rays diffracted from the lattice planes, whereas an amorphous (e.g., C-S-H in this project) material exhibits a broad peak due to it not possessing long-range order (Sharpley I., 2015). In this case, C-S-H is identified indirectly, by the presence of a broad "hump" in the background intensity (Sharpley I., 2015).

After collecting the data from the XRD machine, data needs to be analyzed. Analysis can be done by two independent methods: the Reference Intensity Ratio (RIR) method and the Rietveld method. The RIR method is employed in this research project for quantitative analysis of cement powder diffraction results. This method is based on scaling (comparing) the diffraction data with diffraction of standard reference materials. In this method, it is assumed that the factors shown on a quantitative analysis by cement powder diffraction are ratio to a constant, except concentration. Hence, measurement of ratios and peak areas will result in concentration determination. The ratio is measured by Intensity Analyte divided by Intensity Corundum (I/Ic). There are two methods to determine I/Ic:

1- **Experimental:** I/Ic can be determined by adding a known weight fraction of corundum to a pure specimen of the analyte of interest.

2- **Chemical Based Calculation:** If the atomic parameters of analyte is available, I/Ic can be calculated. It is important to mention that in this method; the atomic parameters of corundum are available.

In this project, the Powder Diffraction File (PDF) database of X-ray powder diffraction patterns maintained by the International Center for Diffraction Data (ICDD) is used to determine I/Ic. This database has been prepared by the excremental approach. Then, the vendor program interface to PDF to automatically measure I/Ic and peak area from the quantitative analysis by cement powder diffraction patterns.

As indicated in the literature, X-ray diffractometry is not a reliable technique for quantitative analysis (Ukrainczyk, 2006), but it can help identifying a large variety of crystalline phases formation. Also, in case there are more than one kind of amorphous such as unhydrated

Calcium Silicate Hydrate (C-S-H) or unhydrated Blast Furnace Slag (BFS), XRD cannot distinguish them (Hoshino et al., 2006). This is the reason XRD is used in conjunction with TGA in this research program.

From XRD results, the presence of ettringite, Portlandite $Ca(OH)_2$, calcite $CaCO_3$, Quartz $SiO_2$, and Calcium Carbonate Hydrate $CaCO_3 \cdot XH_2O$ can also be identified.

# 4. EXPERIMENTAL RESULTS

## 4.1. Introduction

This chapter presents the results obtained from the experimental programs laid out in Chapter 3. The experimental results are categorized under macrostructure properties and microstructure test results.

## 4.2. Macrostructure Level Test Results

### 4.2.1. Consistency

Mixture consistency is not only important for workability determination of the mixture, but also for estimating the setting time. Two types of consistency are measured in this research program: the initial consistency at the time of mixing (similar to the time a concrete truck is loaded at a ready-mix plant), and the construction consistency after an hour (similar to the time concrete is poured on a project and construction operations are started).

#### 4.2.1.1. Initial Consistency

As described in Chapter 3, the test is conducted after 10 minutes from mixing by pouring fresh cement paste into the acrylic mini-slump cone. The average of the two perpendicular diameters of the paste spread is the initial consistency of the mixture, as shown in Figure 4-1, for the four mix designs at the three W/CM ratios.

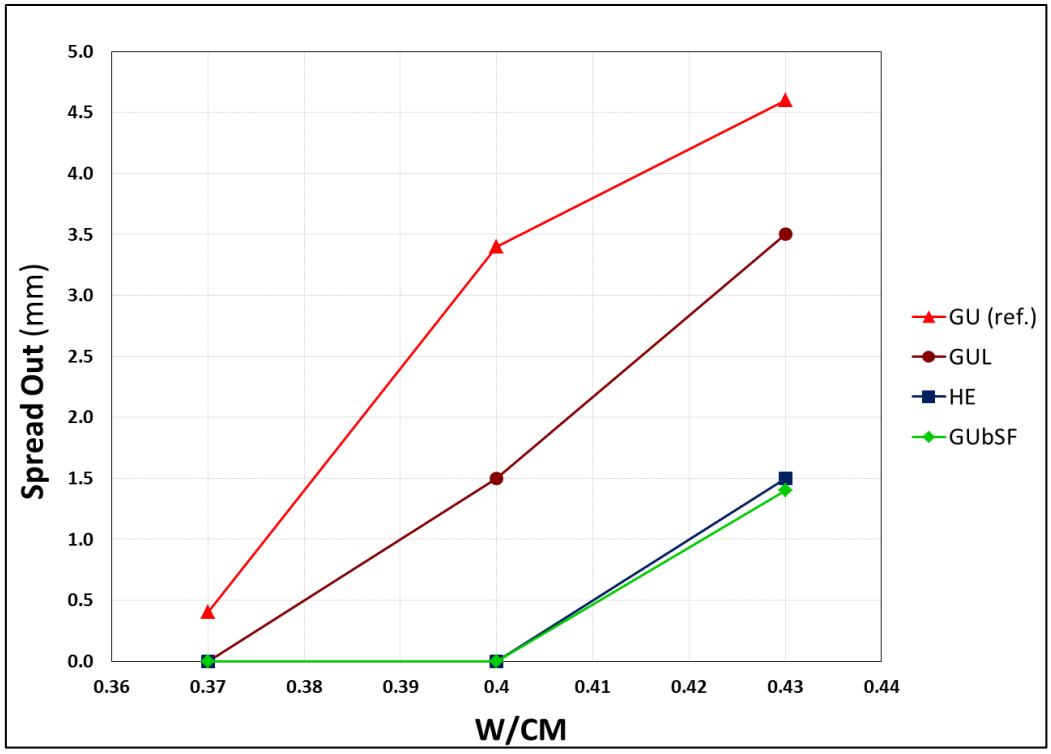


**Figure 4-1: Mini slump cone (initial consistency) test result trend of cement paste mixture**

As the W/CM ratio increased, the consistency of the cement paste mixtures increased from plastic to fluid. This change, which is represented by increase in the flow, was more significant in GU and GUL mixtures compared to HE and GUbSF mixtures. The consistency of both High Early (HE) and blended with silica fume (GUbSF) mixes showed similar trend to the addition of water. In these mixtures, the addition of water does not increase the consistency for W/CM lower than 0.40. An increase in consistency is observed for, W/CM ratios greater than 0.40.

In HE and GUbSF cements, it has been noted that the addition of water in the range of W/CM below 0.4 (range typically used for high performance concrete mixtures) does not result in consistency development. This can be explained by the high reactivity of finer particles in those cement types.

#### 4.2.1.2. Construction Consistency

Besides initial consistency, the construction consistency of the mixtures is measured to validate the mix design and mixing procedure. Construction consistency is measured at 60 minutes and 120 minutes from the mixing time according to the method described in ASTM C187. The consistency values are the average of three measurements of the probe in the cement paste, as shown in Figure 4-2.

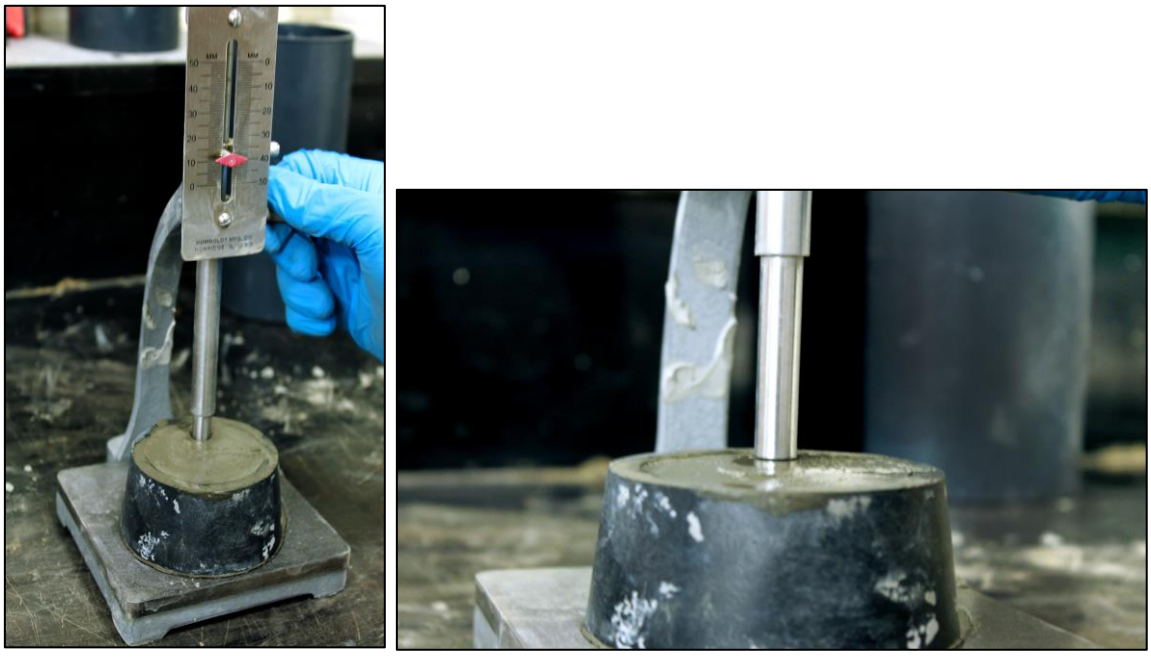

**Figure 4-2: Construction consistency measurement of cement mixtures (ASTM C187)**

The changes in the construction consistency of mixtures during the first 60 minutes were not significant, but it was observed that the initiation of the construction consistency in the mixtures started around 60-90 minutes of hydration as shown in Table 4-1. Lower consistency values represent a drier cement paste mixture.

**Table 4-1: Construction consistency of the mixtures in the first hour of hydration (ASTM C187)**

| **Mix Design** | | **Construction Consistency** (mm) | | **Construction Consistency Development** (min.) |
|---|---|---|---|---|
| **Cement Type** | **W/CM** | **Initial (after mixing)** | **At 1 hour** | |
| **GU** | **0.37** | 40.0 | 38.0 | 60 |
| | **0.40** | 40.0 | 40.0 | 70 |
| | **0.43** | 40.0 | 40.0 | 90 |
| **GUL** | **0.37** | 40.0 | 40.0 | 80 |
| | **0.40** | 40.0 | 40.0 | 100 |
| | **0.43** | 40.0 | 40.0 | 125 |
| **GUbSF** | **0.37** | 40.0 | 40.0 | 65 |
| | **0.40** | 40.0 | 40.0 | 85 |
| | **0.43** | 40.0 | 40.0 | 120 |
| **HE** | **0.37** | 40.0 | 15.5 | 45 |
| | **0.40** | 40.0 | 34.5 | 55 |
| | **0.43** | 40.0 | 38.0 | 60 |

It is observed that the consistency started developing around 1 hour of hydration. From 1 hour of hydration to 2 hours, changes in the construction consistency were observed. Hence, the construction consistency at 120 minutes was analyzed, as a quality control indicator of the mixture. Figure 4-3 illustrates the construction consistency of two mix designs (GU and HE) at 120 minutes.

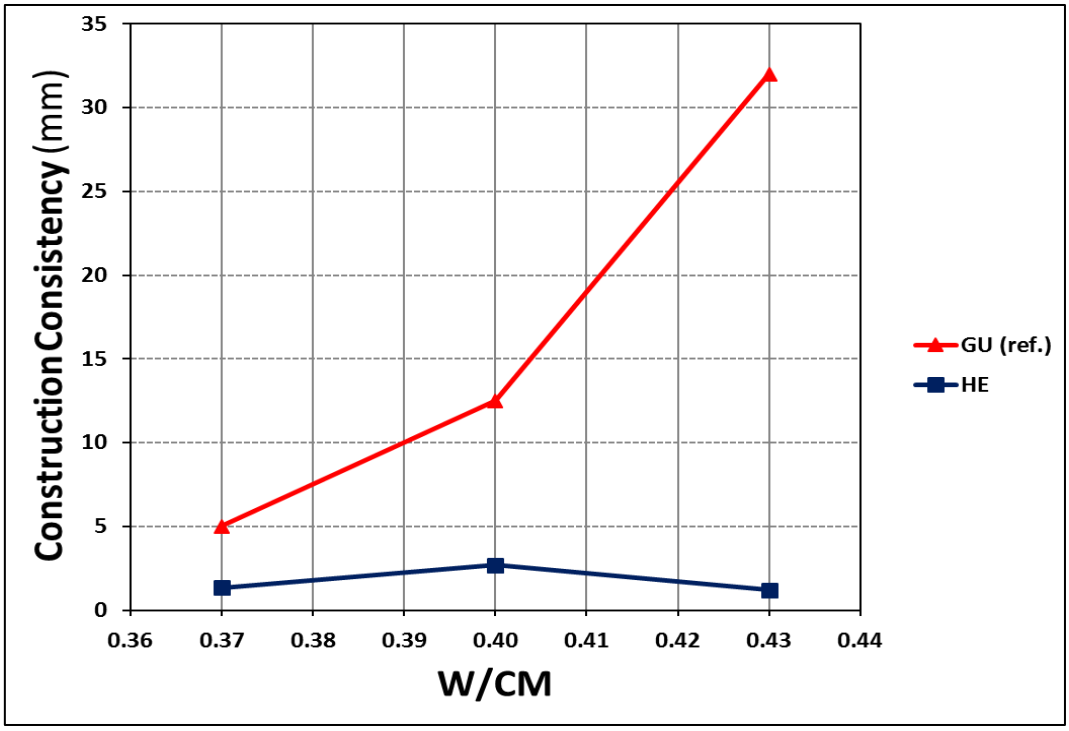


**Figure 4-3: Construction consistency of cement paste mixtures at 120 minutes**

By comparing the trends of the construction consistency with W/CM in Figure 4-3 to those of the initial consistency in Figure 4-1, it is noted that the construction consistency of the HE mixture with a W/CM=0.43 did not follow the expected trend. This was an indicator that mixture HE 0.43 was invalid and that another batch of the same mixture needed to be mixed and tested. Figure 4-4(a) illustrates the results of the construction consistency at 120 minutes for all the mixtures and W/CM ratios (with new HE 0.43 mixture).

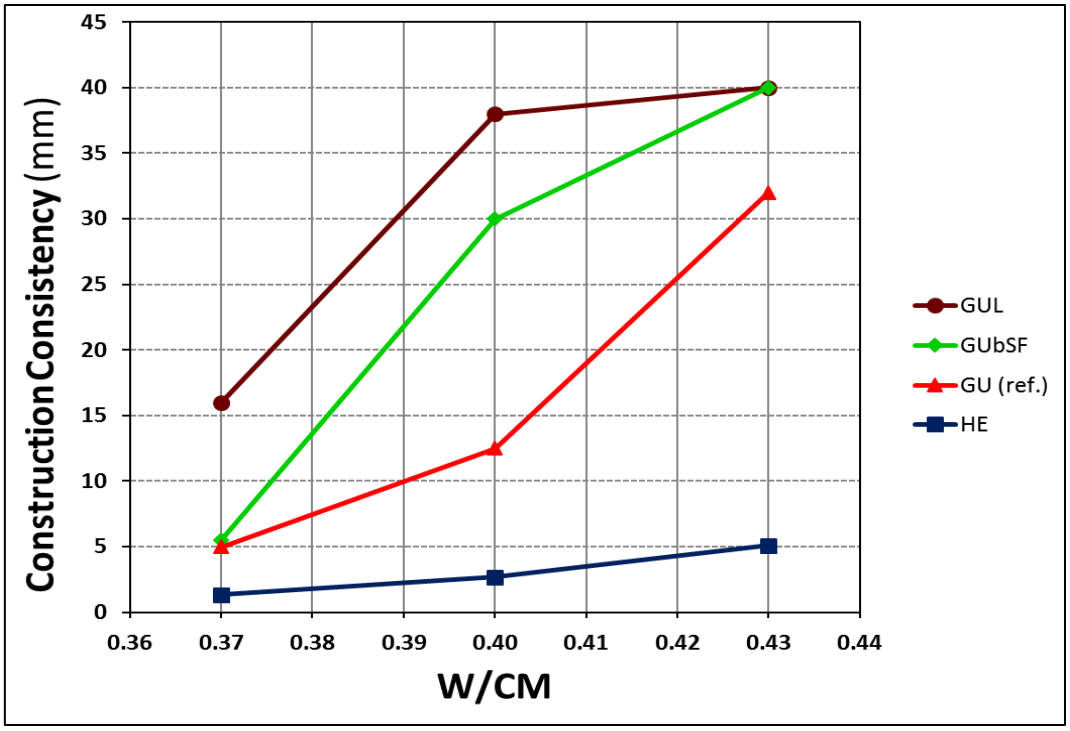


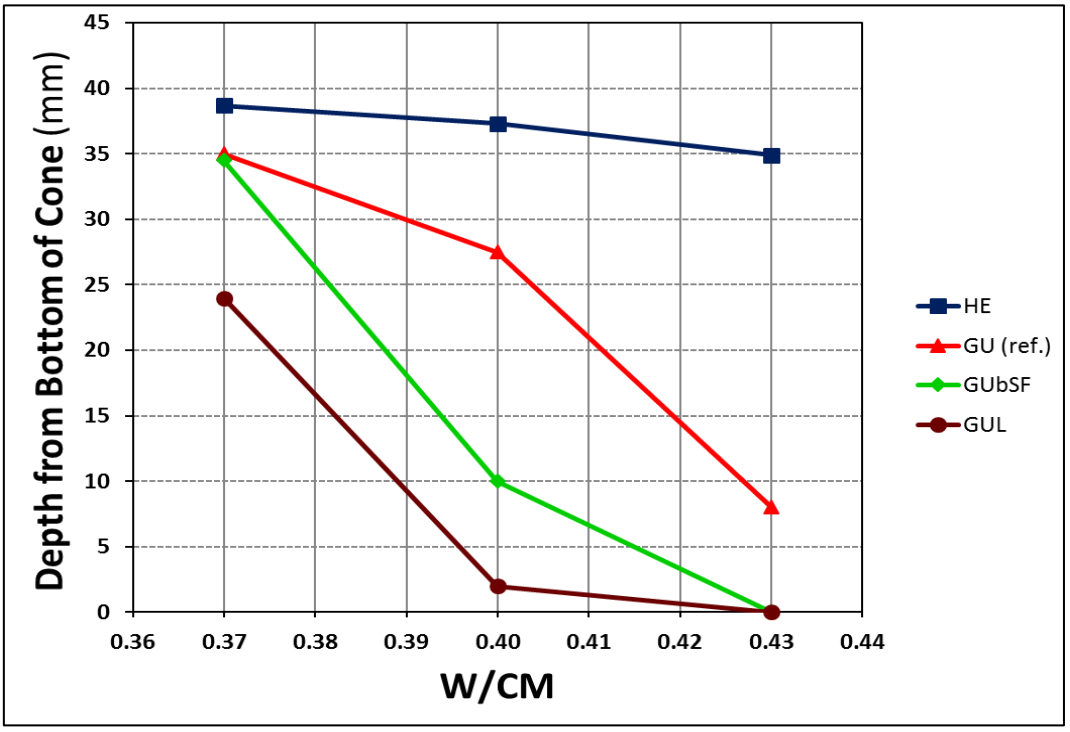


**Figure 4-4: (a) 2-hour construction consistency, (b) depth from bottom of the cone (bottom) of cement paste mixtures**

According to Figure 4-4 (a), it is observed that the consistency of HE cement pastes (Type 30) did not change significantly as the W/CM ratio increased after an hour, while the W/CM ratio had a significant effect on the construction consistency of GU cement paste (Type 10). The consistency of GUbSF and GUL mixtures did not increase significantly when the W/CM ratio was increased from 0.40 to 0.43. However, these results are due to the limitation of the instrument used for measurement, since the maximum penetration depth of the rod is 40 mm. A visual observation revealed that extra water indeed increased the consistency of the mixtures.

In all mixtures, the construction consistency of GU was more sensitive to extra water after 2 hours, while HE showed the least sensitivity to addition of water. Similar behaviour was observed in Figure 4-1 (a), where GU had the highest rate of increase in initial consistency compared to the other mixtures.

Contrary to the initial consistency test results presented in Section 4.2.1.1, the construction consistency of GUbSF and HE mixtures became wetter from a W/CM ratio of 0.37 to 0.40. After two hours, extra water increased the consistency of GUbSF mixtures considerably (from 5 to 30 mm), while it had low effect on the HE mixtures consistency. It shows that the HE mixtures are capable to react with extra water during the early times of hydration, while GUbSF and GUL mixtures react with water beyond 2 hours. Therefore, adding a certain amount of water does not result in similar consistency increase in all mixtures. The higher reactivity of HE mixtures can be due to the finer cement particle size (physical), which is independent from the length of hydration, but in GUbSF and GUL mixtures, the contribution of additives to the reaction (which is chemical) is observed beyond 2 hours.

As expected, GU cements with additives replacement (GUL and GUbSF) showed wetter construction consistency compared to GU cement, as the total amount of GU cement powder in those mixtures is lower and additives do not participate in early hydration before 2 hours. Therefore, extra water remains in the mixture matrix and results in a higher construction consistency.

Based on the results illustrated in Figure 4-1 and Figure 4-4, cement types GU and GUL are considered as normal setting cements, while HE cement is considered as a fast setting cement, for the purpose of this research.

### 4.2.2. Fresh Stage Electrical Resistivity

The electrical resistance of fresh cement paste was measured from time 0 (immediately after mixing) until 24 hours, which is usually the period corresponding to the traditional formwork removal, practised in the concrete construction industry. The techniques used to monitor the changes in the electrical properties of the cement paste during hydration have been described in Section 3.3.5. The resistivity-meter measures the changes in the electrical resistance of the mixtures every 5 minutes. The measured electrical resistance, which is dependent on the specimen geometry, probe size, shape, and probe spacing, must be converted to electrical resistivity, an intrinsic material property. There are two methods for this conversion: application of a conversion geometric factor and usage of a known conductive solution.

**I) Conversion Factor:**

From experimental results reported in the literature, the geometry correction factor (K) for embedded electrodes resistivity-meter is 0.20 m, as discussed in Section 2.3.1.4. The numerical model derived in Section 3.3.5. shows that K can be calculated from Equation 4-1:

$$\boldsymbol{K = \frac{\pi r}{2 \ln h}} \qquad [4\text{-}1]$$

where, *r* is the distance between the electrodes and *h* is the height of the embedded probes. According to the resistivity setup described in Section 3.3.5, r= 5cm and h=11cm, therefore, K= 0.21m.

**II) Conductive Solution:** For this purpose, sodium chloride was used as the standard conductive solution. As reported by the supplier (Ricca Chemical Co.), the conductivity standard of the solution at room temperature (22-23°C) is 20mS/cm. Therefore, the resistivity of the solution is 0.05kΩ.cm. The electrical resistance of the standard known solution was measured as 3Ω at 24°C using the test setup for

the fresh cement paste resistance measurement, as shown in Figure 4-5. It follows then that the geometric correction factor for the electrode setup used is K 0.05×10/3=0.17m.


**Figure 4-5: Measurement of the electrical properties of the standard conductivity solution**

The geometry correction factor determined by the numerical and experimental methods are both approximately equal to 0.2m. In this research program, all resistance values measured by the resistivity meter were converted to electrical resistivity by multiplying in the geometry correction factor determined by the conductive solution method. Figure 4-6 to Figure 4-17 illustrate the electrical resistivity evolution a long time for all the cement pastes over the first 24 hours of hydration.

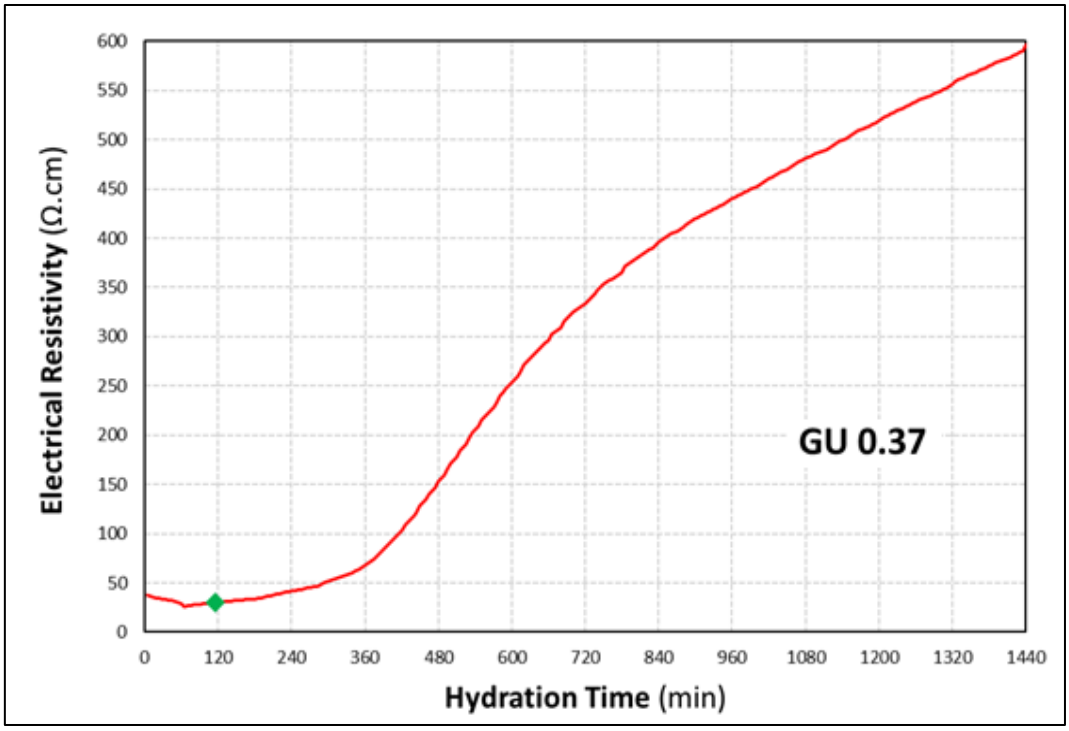


**Figure 4-6: Electrical resistivity development of GU 0.37 mixtures over the first 24 hours of hydration**

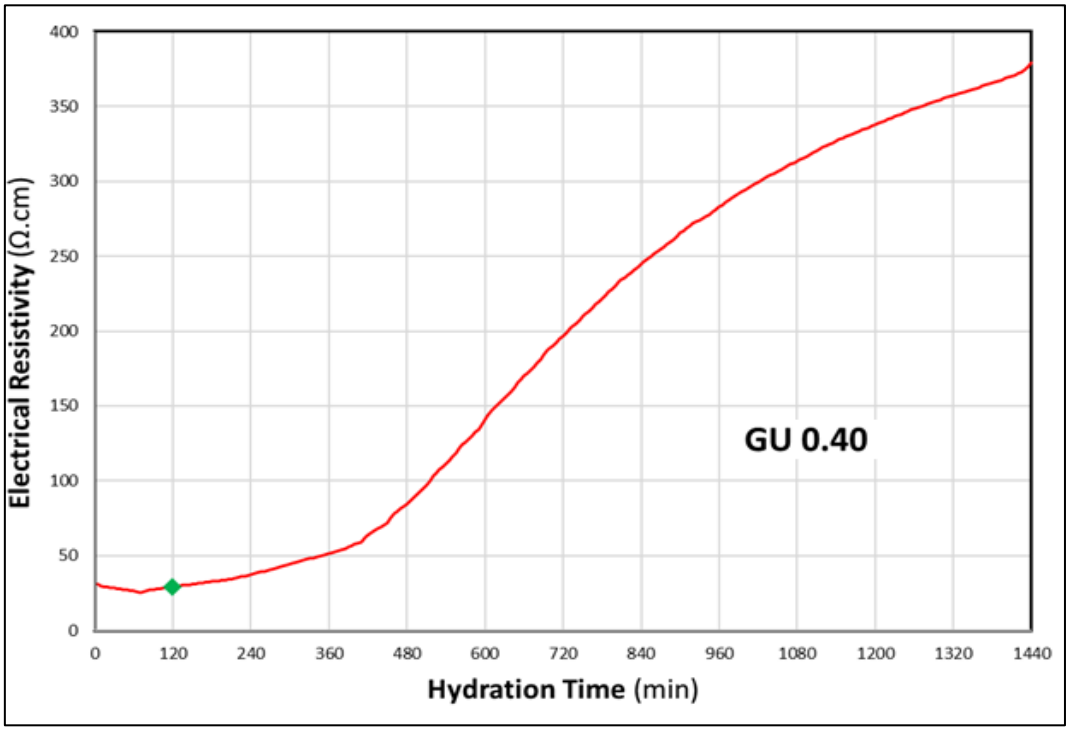


**Figure 4-7: Electrical resistivity development of GU 0.40 mixtures over the first 24 hours of hydration**

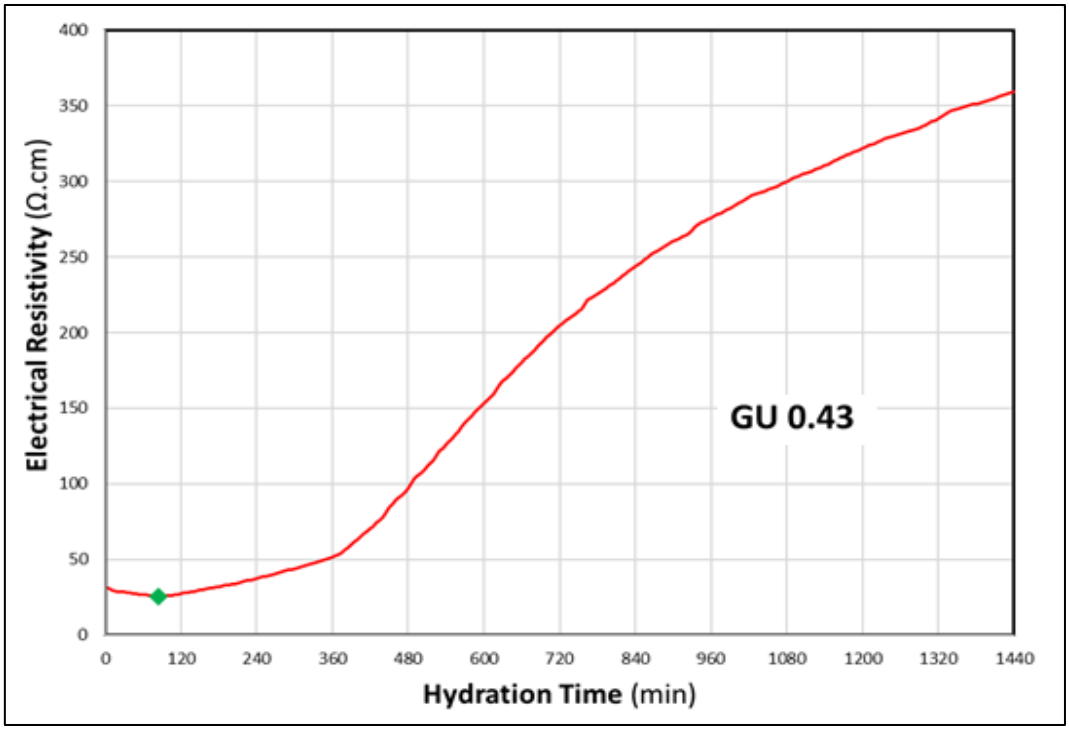


**Figure 4-8: Electrical resistivity development of GU 0.43 mixtures over the first 24 hours of hydration**

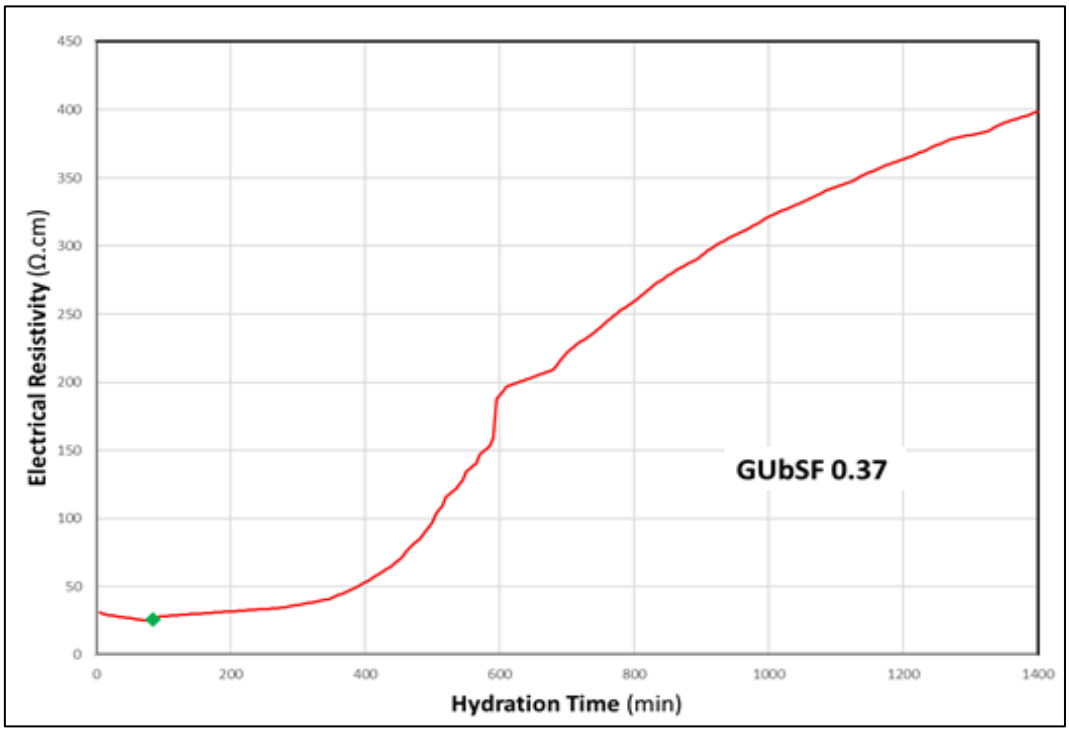


**Figure 4-9: Electrical resistivity development of GUbSF 0.37 mixtures over the first 24 hours of hydration**

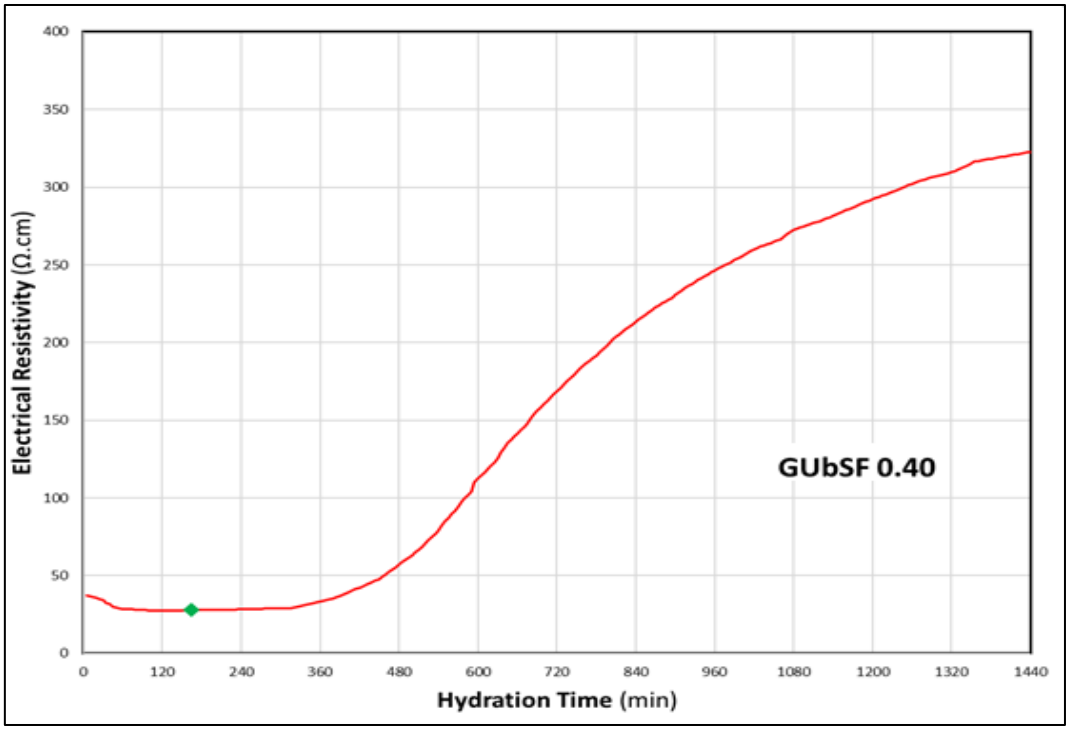


**Figure 4-10: Electrical resistivity development of GUbSF 0.40 mixtures over the first day of hydration**

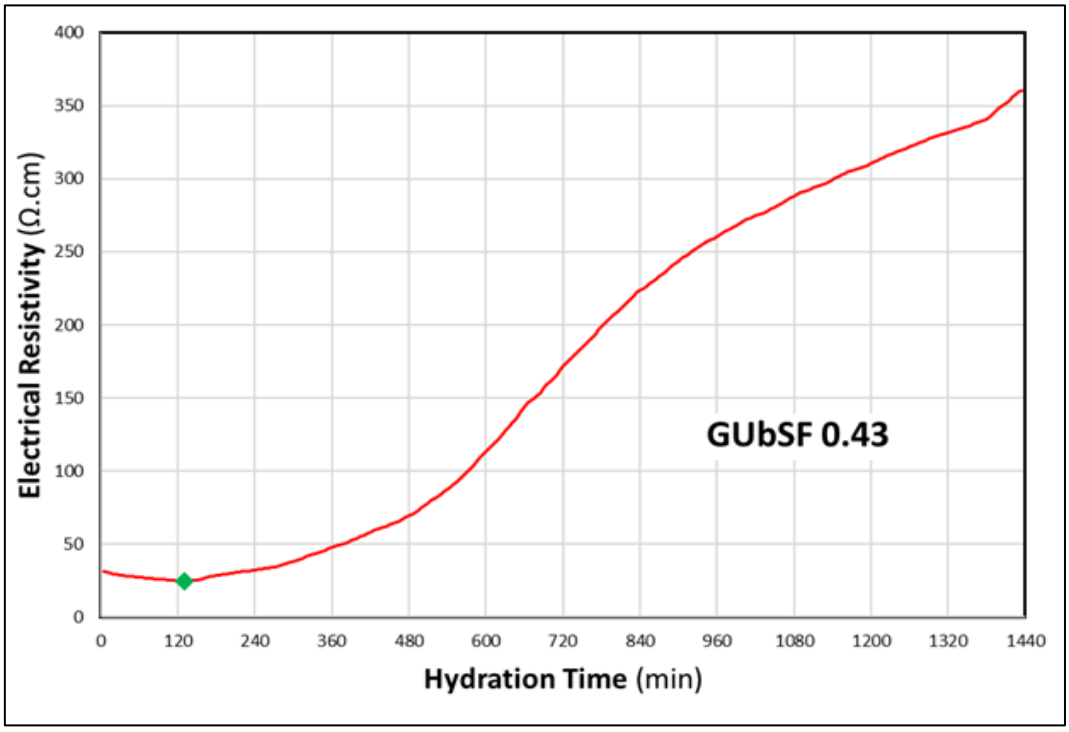


**Figure 4-11: Electrical resistivity development of GUbSF 0.43 mixtures over the first day of hydration**

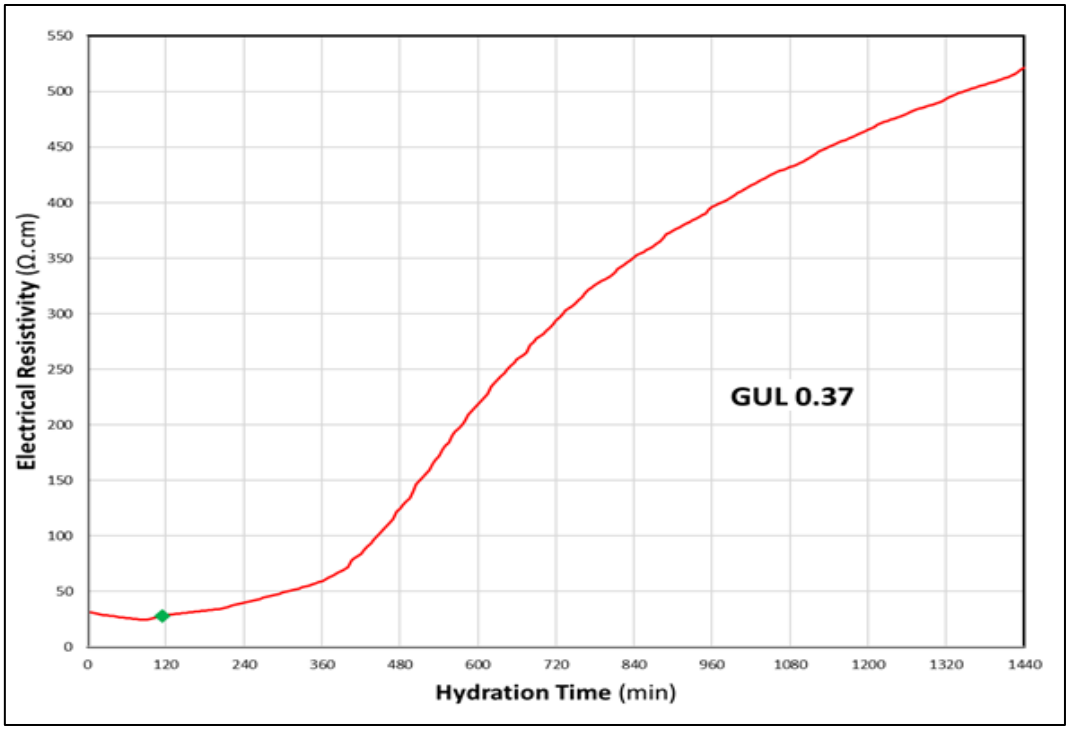


**Figure 4-12: Electrical resistivity development of GUL 0.37 mixtures over the first day of hydration**

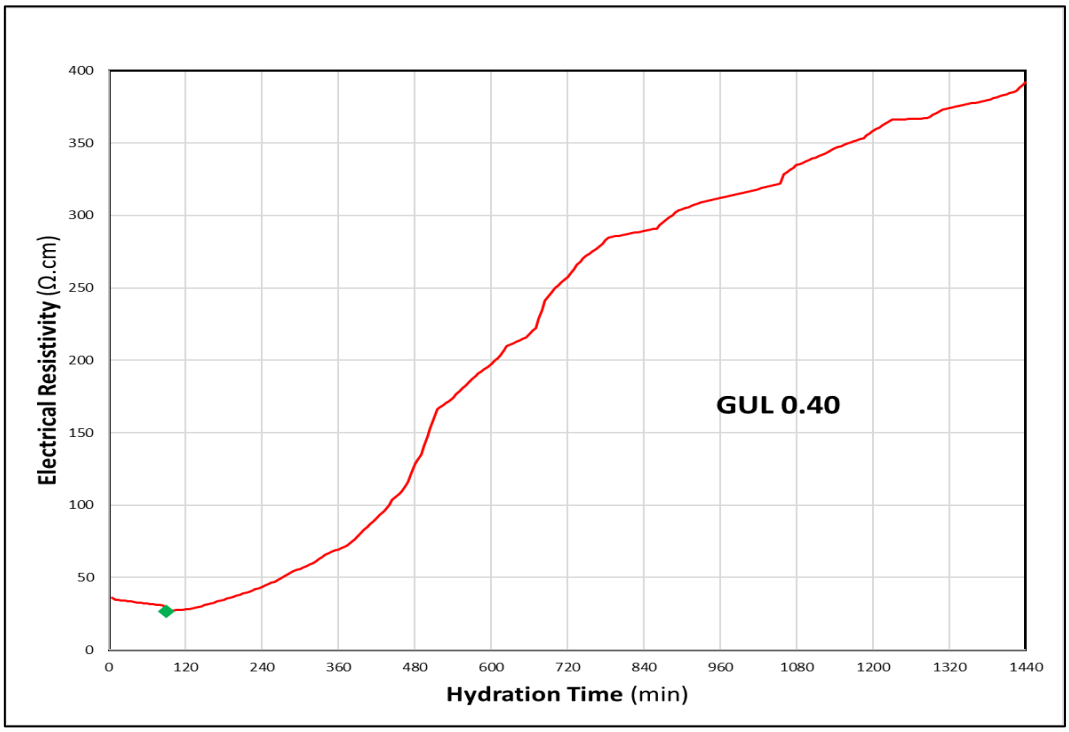


**Figure 4-13: Electrical resistivity development of GUL 0.40 mixtures over the first day of hydration**

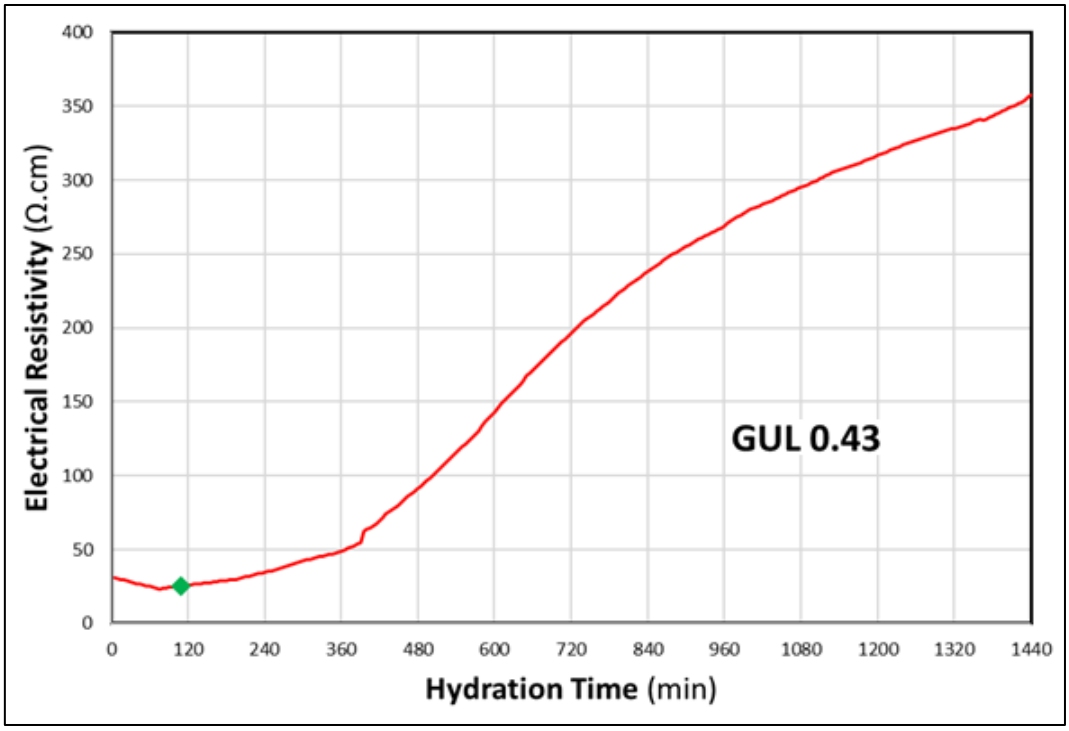


**Figure 4-14: Electrical resistivity development of GUL 0.43 mixtures over the first day of hydration**

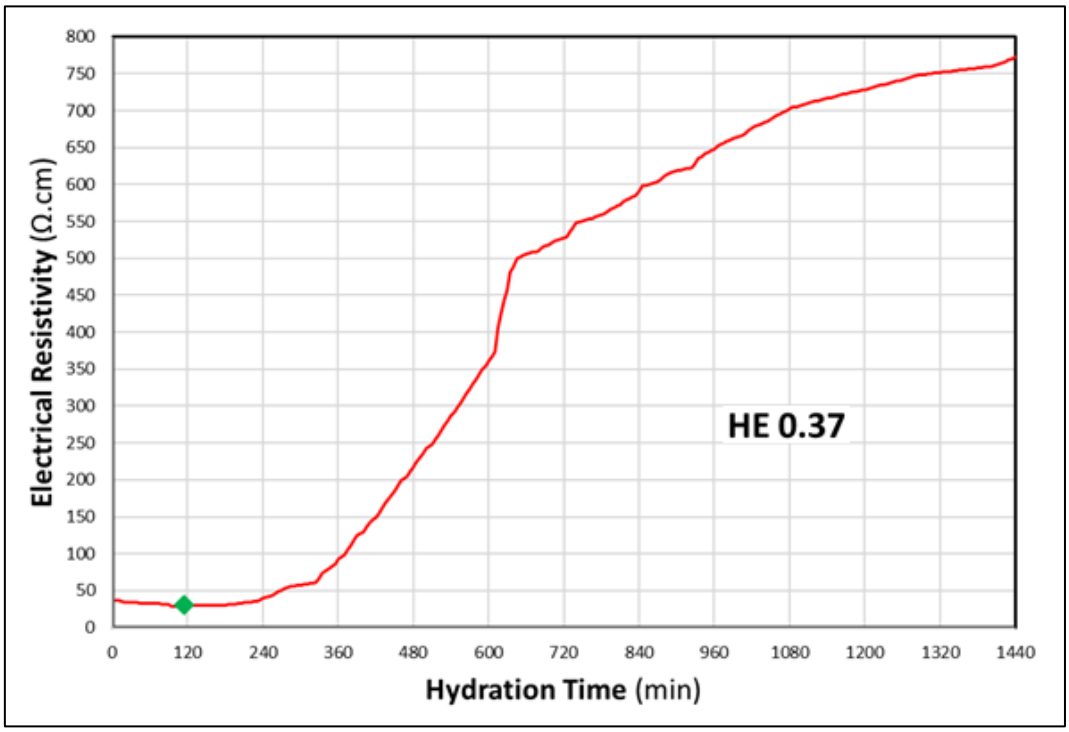


**Figure 4-15: Electrical resistivity development of HE 0.37 mixtures over the first day of hydration**

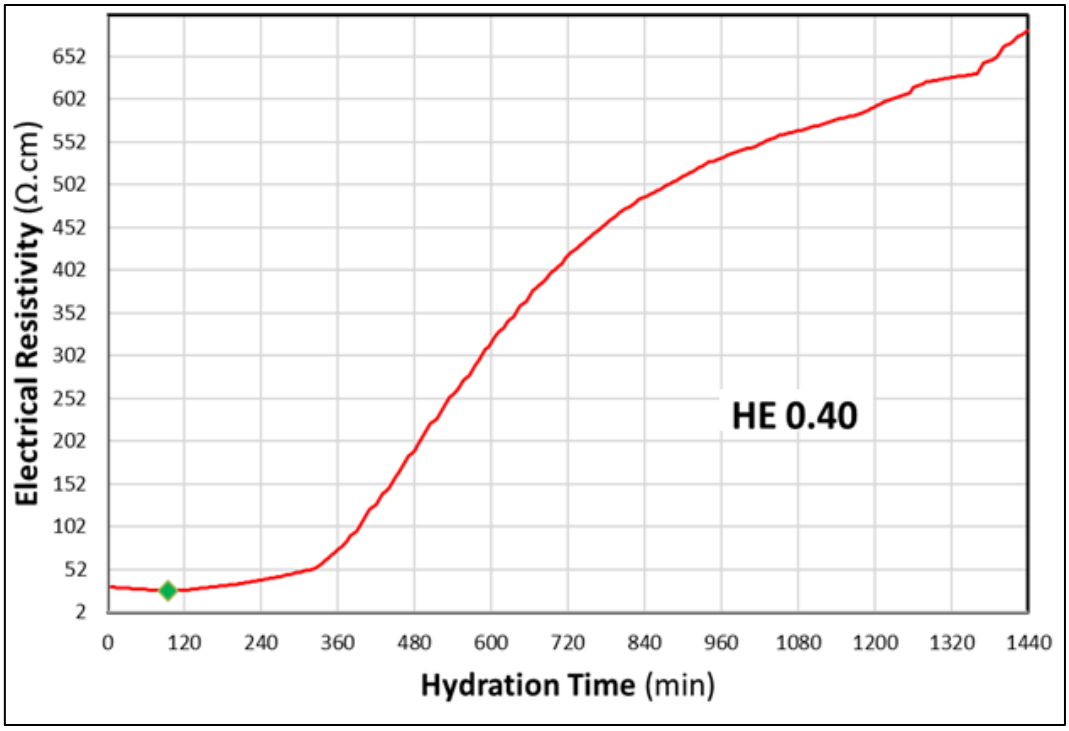


**Figure 4-16: Electrical resistivity development of HE 0.40 mixtures over the first day of hydration**

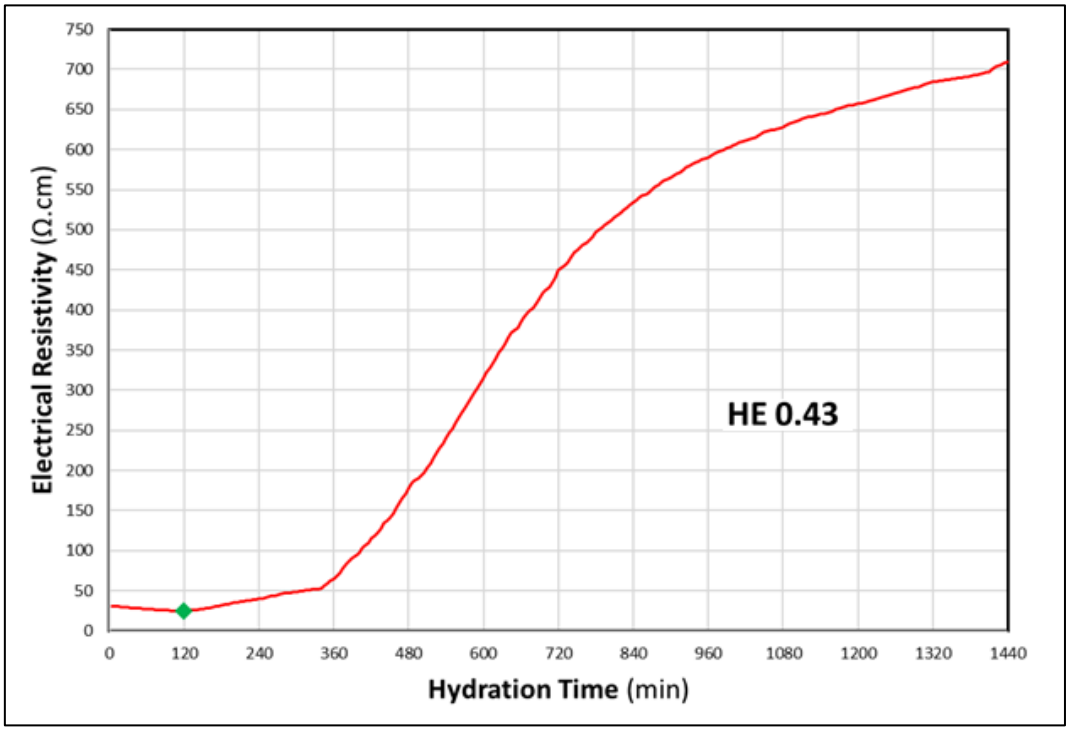


**Figure 4-17: Electrical resistivity development of HE 0.43 mixtures over the first day of hydration**

From the figures, it is noted that the electrical resistivity of cement pastes develops over time. At the beginning of cement hydration, a reduction in the electrical resistivity is observed, which translates into an increase in the conductivity of the cement paste mixture. As explained in the literature, this reduction, which happens in Phase I after mixing with water, indicates the dissolution of ions ($Na^{+}$, $K^{+}$, $Ca^{++}$, $OH^{-}$, $SO_4^{2-}$) from the cement into the pore solution (Wei and Xiao, 2014). In this stage, the un-hydrated cement particles contribute to the electrical resistance in the cement paste. This reduction continues until the time that the leached ions start contributing into the formation of some cement hydration crystals. The green diamond on the graphs highlights the critical tuning point at which the electrical resistivity measured by the instrument described in Section 3.3.5 shows a change in trend. Theoretically, this is the point where ion concentration content (ions leached from cement into the pore solution) starts reducing. This will be further corroborated by experimental data from the microstructure analysis presented in Chapter 5.

#### 4.2.2.1. Cement type effect on electrical properties development

The effect of cement type on the development of electrical properties of the cement paste can be observed in Figure 4-18, Figure 4-19, and Figure 4-20, which show the time evolution of the electrical resistivity of four cement paste mixtures at W/CM ratios of 0.37, 0.40, and 0.43, respectively.

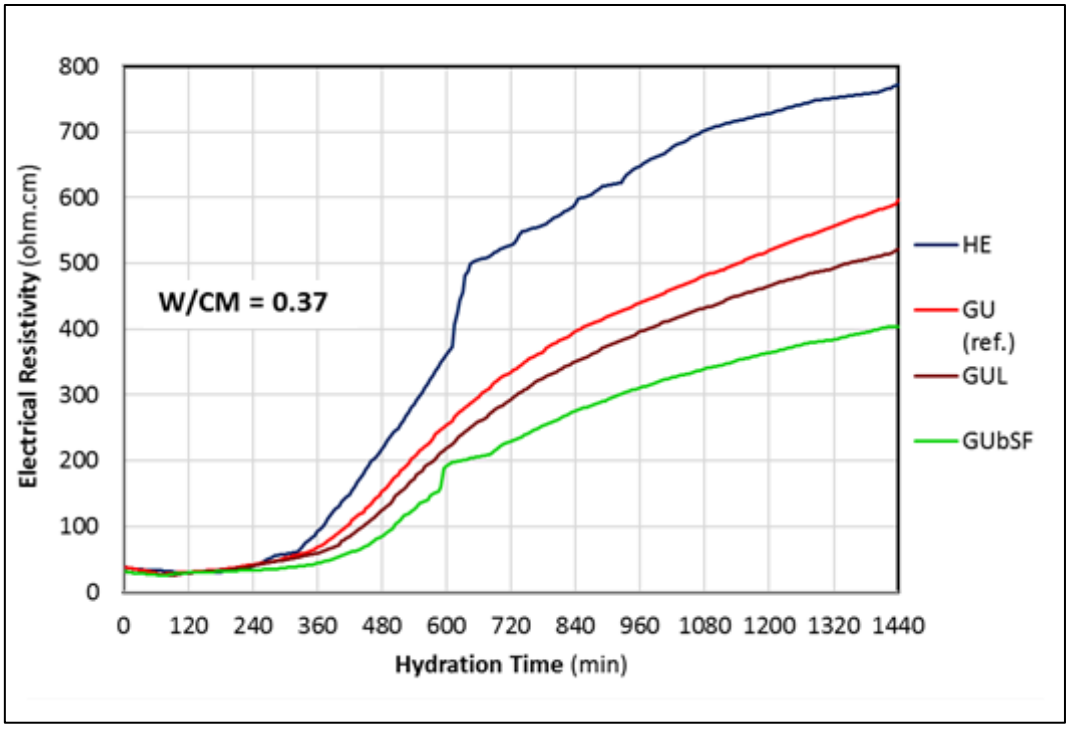


**Figure 4-18: Cement type effect on the first 24-h electrical resistivity of paste with W/CM= 0.37**

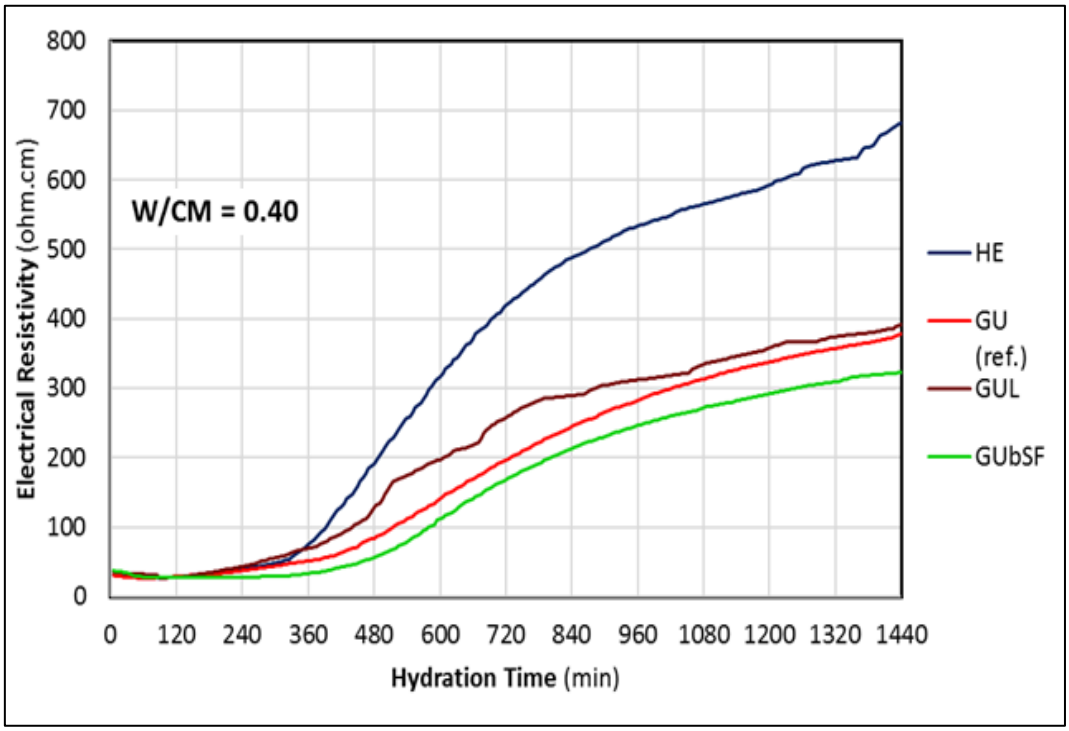


**Figure 4-19: Cement type effect on the first 24-h electrical resistivity of paste with W/CM= 0.40**

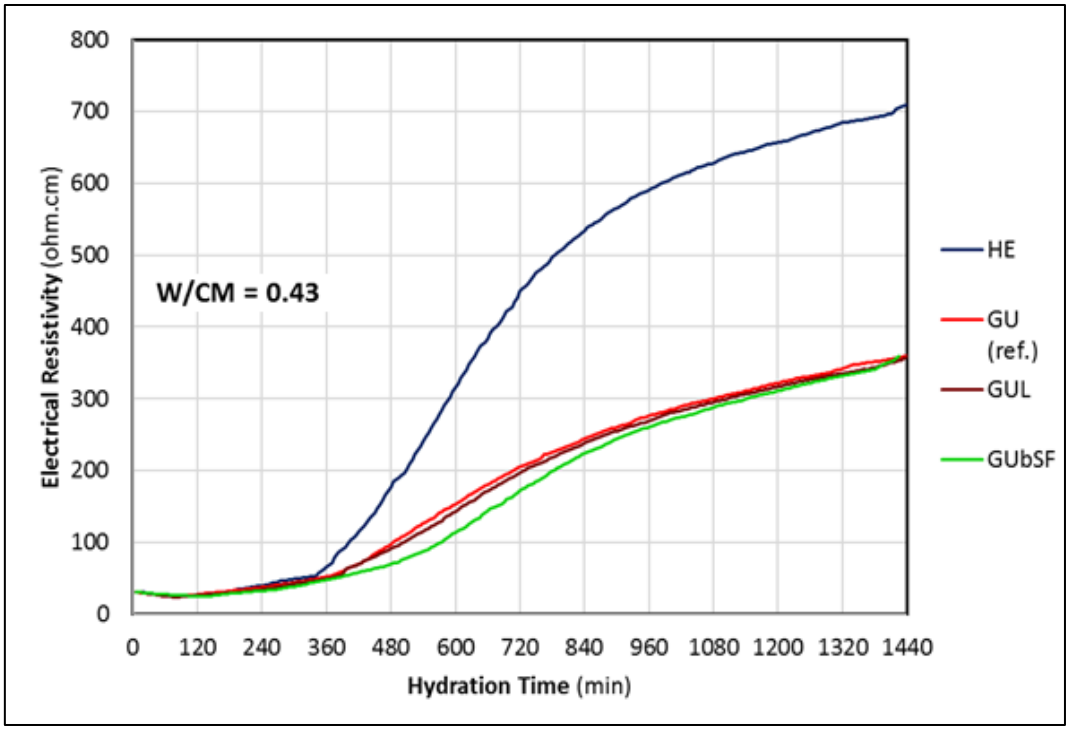


**Figure 4-20: Cement type effect on the first 24-h electrical resistivity of paste with W/CM= 0.43**

In all cement paste mixtures, the HE cement paste showed the highest resistivity development over the first 24 hours of hydration. HE cement quickly reacts with water over the course of hydration, and as a result of that, cement hydration products start forming fast, which results in earlier stiffening and earlier higher resistivity. Theoretically, the presence of silica fume particles in the fresh paste matrix should result in higher electrical resistance than similar mixtures without it, because silica fume does not contribute into the secondary hydration in the early-stages of hydration (Neville, 2008). However, it is stated that as the mixtures become hydrated, the effect of silica fume particles in blocking the path of electrical charges is less significant. In higher stages of hydration, the formation of hydration products has more effect on the electrical resistivity development than the presence of physical particles in the pore solution or pore structure. As the W/CM ratio increases, the unit concentration of silica fume in the pore solution is reduced and therefore, the presence of silica fume in the form of physical particles has less effect on the resistivity development. Similar behaviour can be noted when the electrical properties development of GU mixtures is compared with those of GUL mixtures. GUL mixtures have as at least 12% replacement of GU cement by limestone,

therefore, less hydration products are formed during the first 24 hours of hydration, and the electrical resistivity is expected to be lower in GUL mixtures. As the W/CM ratio is increased to 0.43, the effect of having less cement product on the electrical resistivity development becomes less dominant, and all three GU, GUL, and GUbSF mixtures showed similar electrical resistivity values for a W/CM of 0.43 (Figure 4-20).

#### 4.2.2.2. W/CM ratio effect on electrical properties development

The water-to-cementitious materials (W/CM) ratio is one of the most important factors in determining the durability and performance of a cement-based mixture. The effect of the W/CM ratio is compared for each cement type paste mixture in Figure 4-21 to Figure 4-24.

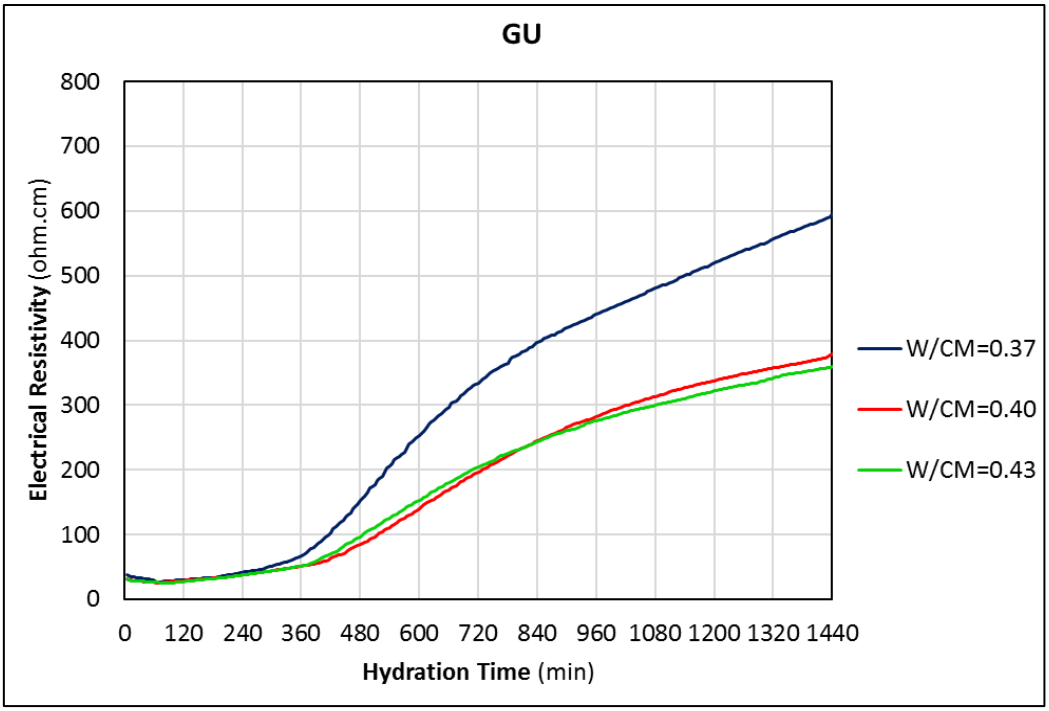


**Figure 4-21: W/CM ratio effect on GU cement pastes electrical resistivity over the first 24-h of hydration**

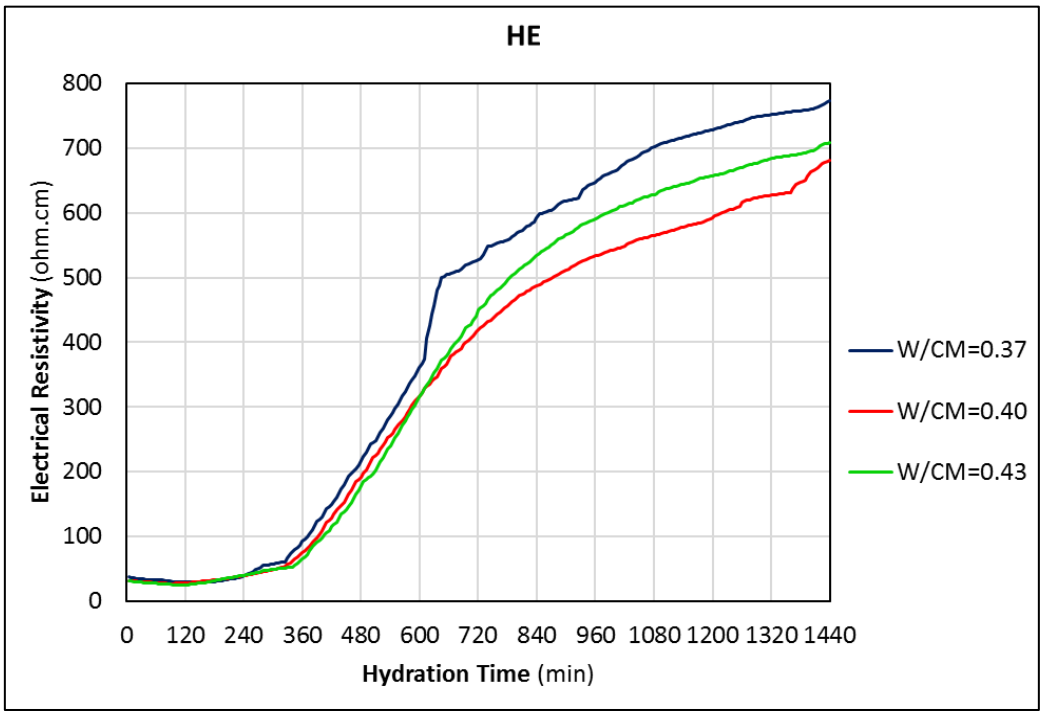


**Figure 4-22: W/CM ratio effect on HE cement pastes electrical resistivity over the first 24-h of hydration**

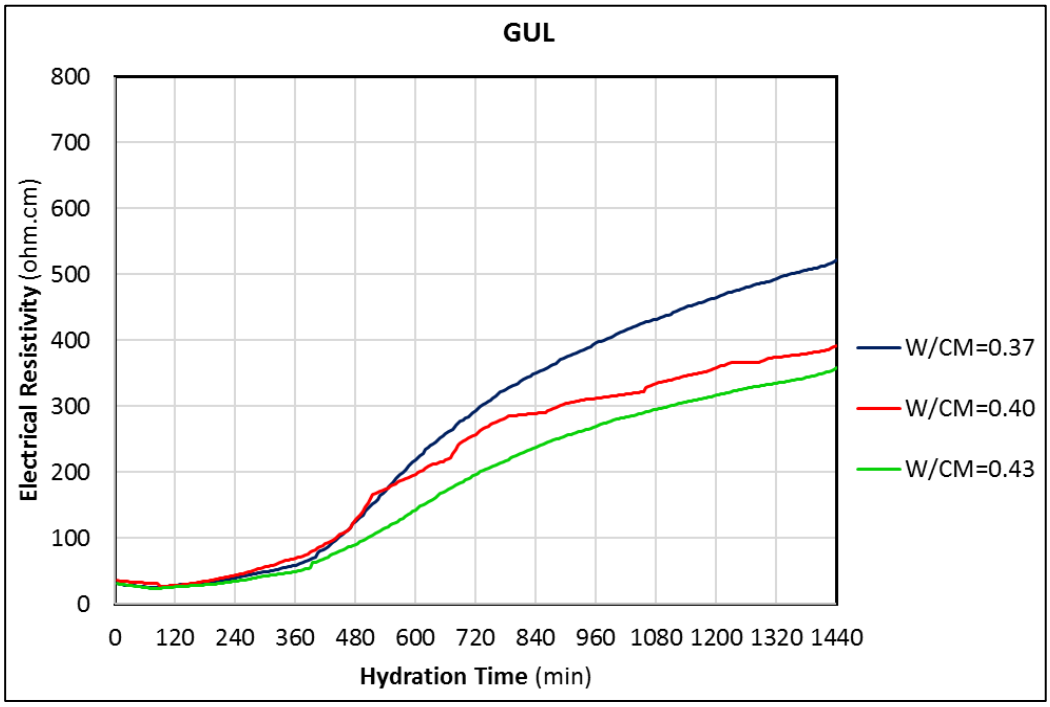


**Figure 4-23: W/CM ratio effect on GUL cement pastes electrical resistivity over the first 24-h of hydration**

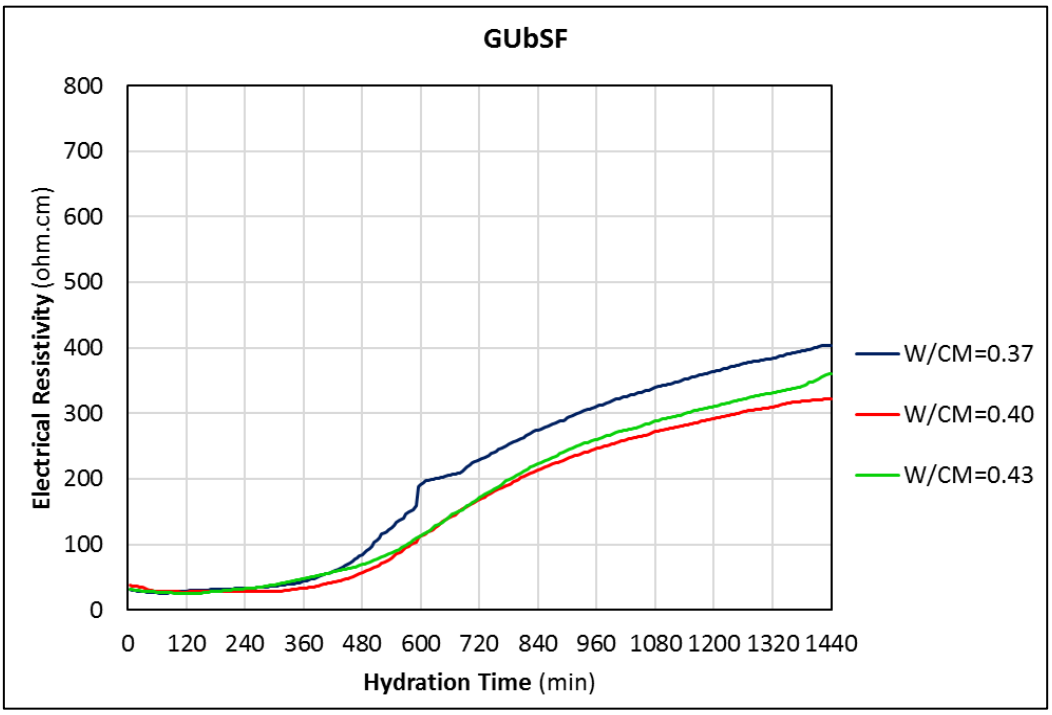


**Figure 4-24: W/CM ratio effect on GUbSF cement pastes electrical resistivity over the first 24-h of hydration**

It is observed that in all cement pastes, as the W/CM ratio increases, the electrical resistivity of the cement paste decreases. The highest resistivity was observed in cement pastes with a W/CM ratio of 0.37. The effect of the W/CM ratio was not significant at early ages for the first 6 hours, while the effect of water content in the mix design started influencing the electrical properties of the cement paste around the initial setting time (will be discussed more in Section 4.2.2). However, in HE and GUbSF mixtures, the effect of higher W/CM ratio on electrical resistivity reduction was not significant in higher water values. It can be due to the higher rate of hydration in those mixes; the presence of free water in HE and GUbSF are reduced, as the water is used during the hydration process.

#### 4.2.2.3. Rate of Change (ROC) in Electrical Resistivity

The development of electrical properties was further studied by plotting the Rate of Change (ROC) in electrical resistivity against time. The ROC is the speed at which the electrical resistivity of cement paste changes over the time (i.e., momentum of the electrical resistivity). The ROC is an extremely important factor, as it shows the positive and negative momentum

of resistivity and turning points. All those can be used to study the hydration rhythm of the cement paste over the first 24 hours of hydration.

The comparison between the electrical resistivity values of cement pastes and its ROC over the first day of hydration is shown in Figure 4-25 to Figure 4-36. In all the figures, the ROC, presented in green in Figure 4-25 to Figure 4-36, is calculated and plotted from the first derivative of the relationship that defines the electrical resistivity development over time; the corresponding equation of electrical resistivity is shown in the figures.

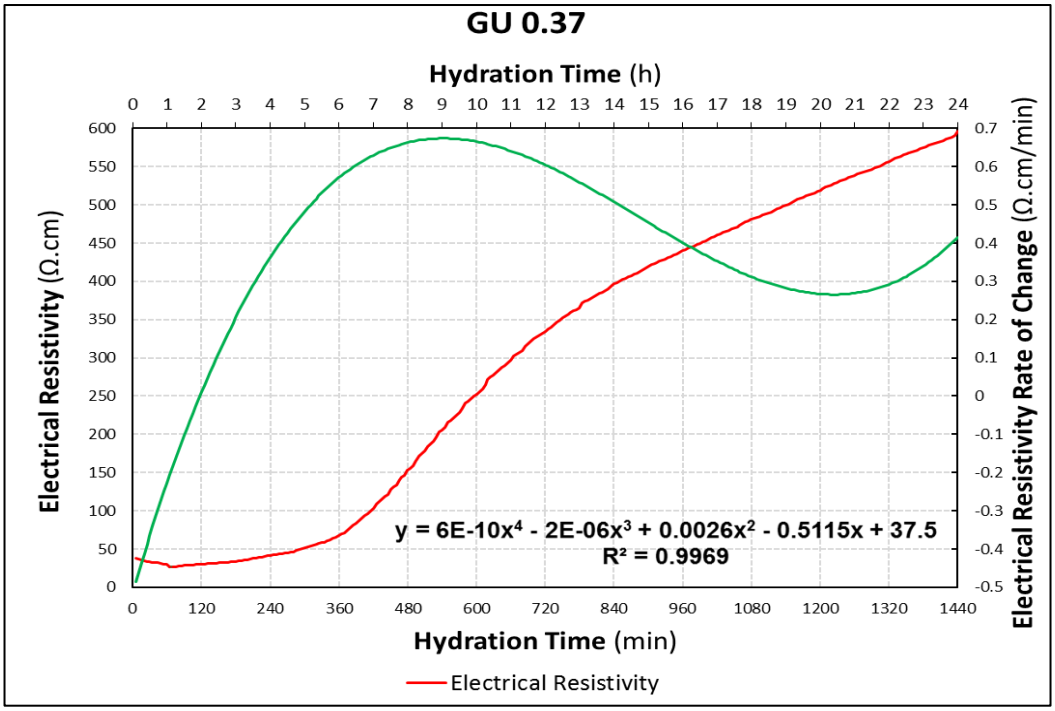


**Figure 4-25: Electrical resistivity and its ROC of GU 0.37 cement paste over the first 24 h of hydration**

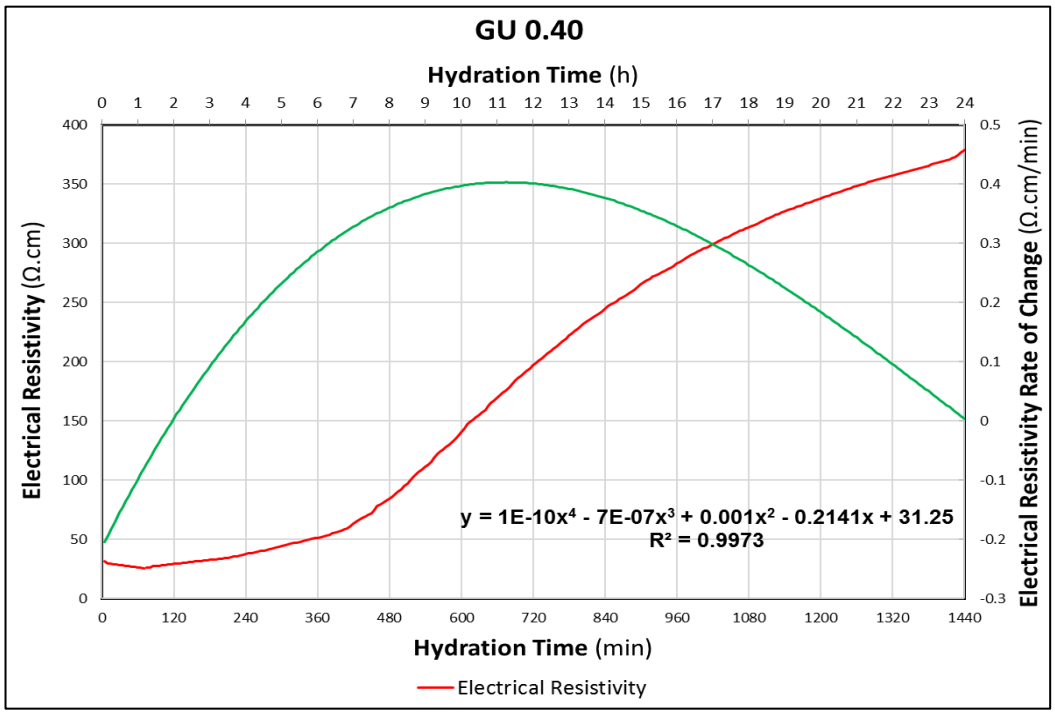


**Figure 4-26: Electrical resistivity and its ROC of GU 0.40 cement paste over the first 24 h of hydration**

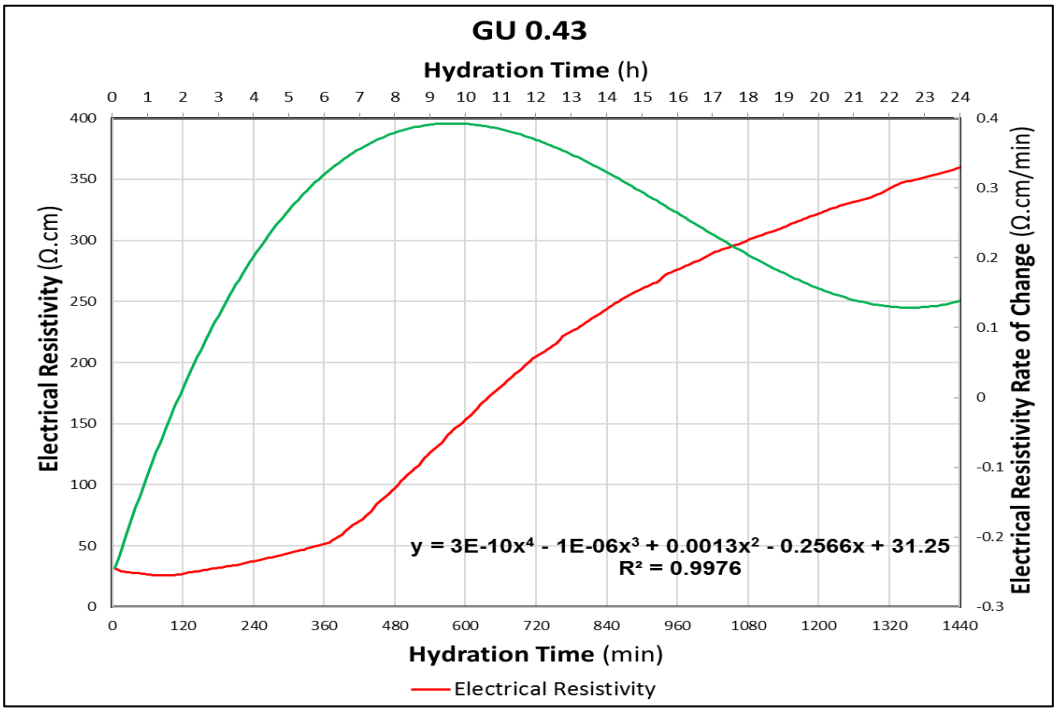


**Figure 4-27: Electrical resistivity and its ROC of GU 0.43 cement paste over the first 24 h of hydration**

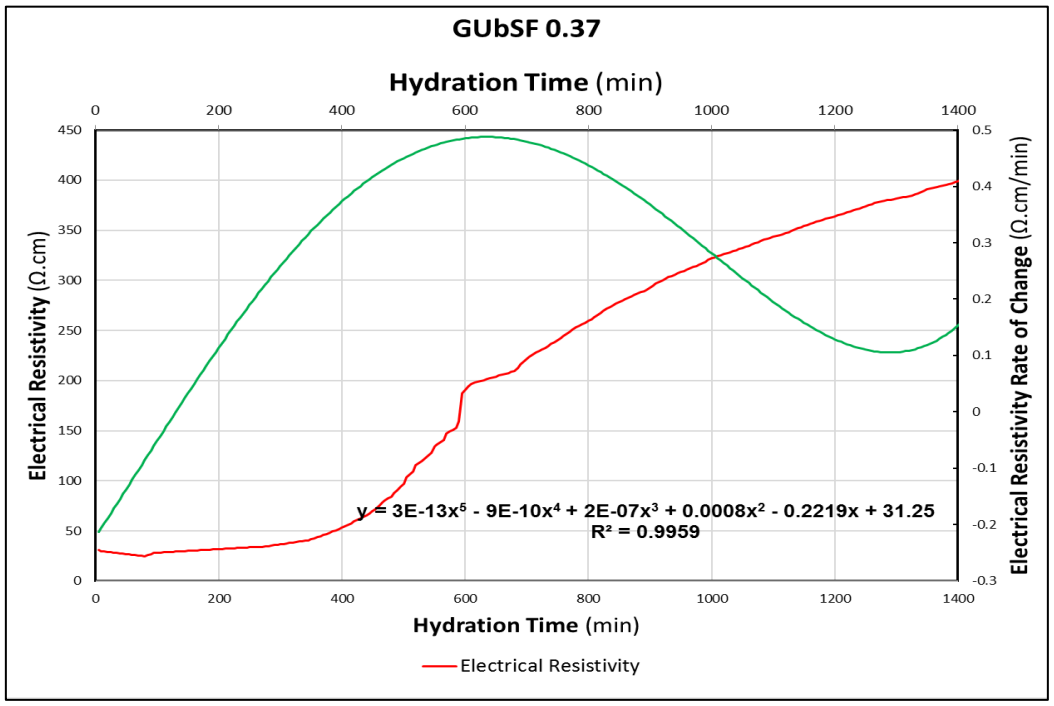


**Figure 4-28: Electrical resistivity and its ROC of GUbSF 0.37 cement paste over the first 24 h of hydration**

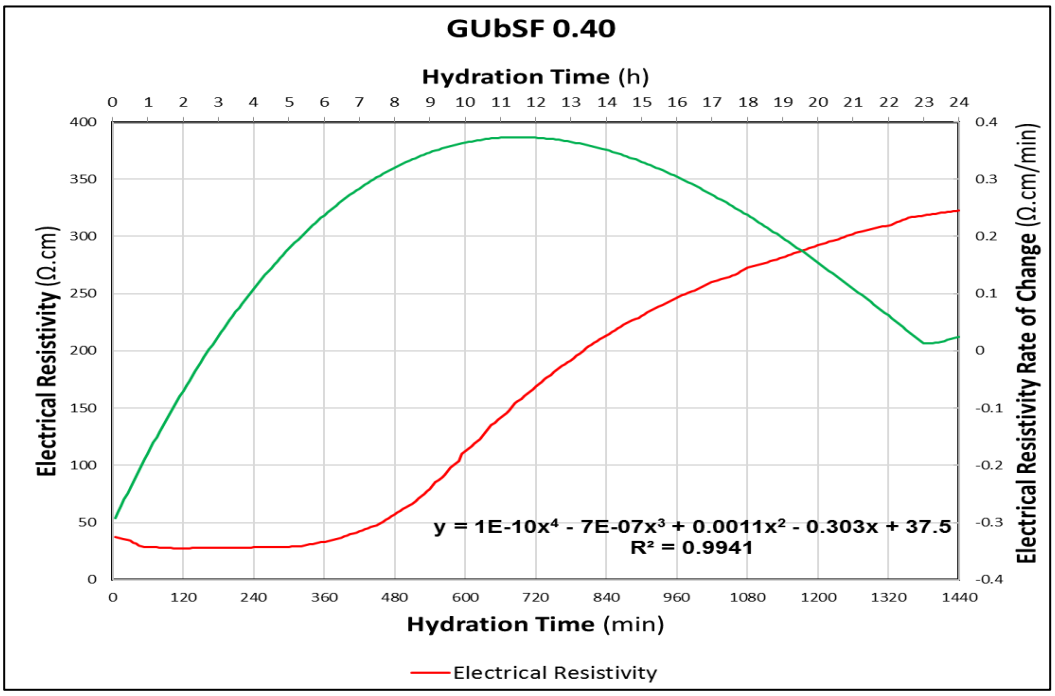


**Figure 4-29: Electrical resistivity and its ROC of GUbSF 0.40 cement paste over the first 24 h of hydration**

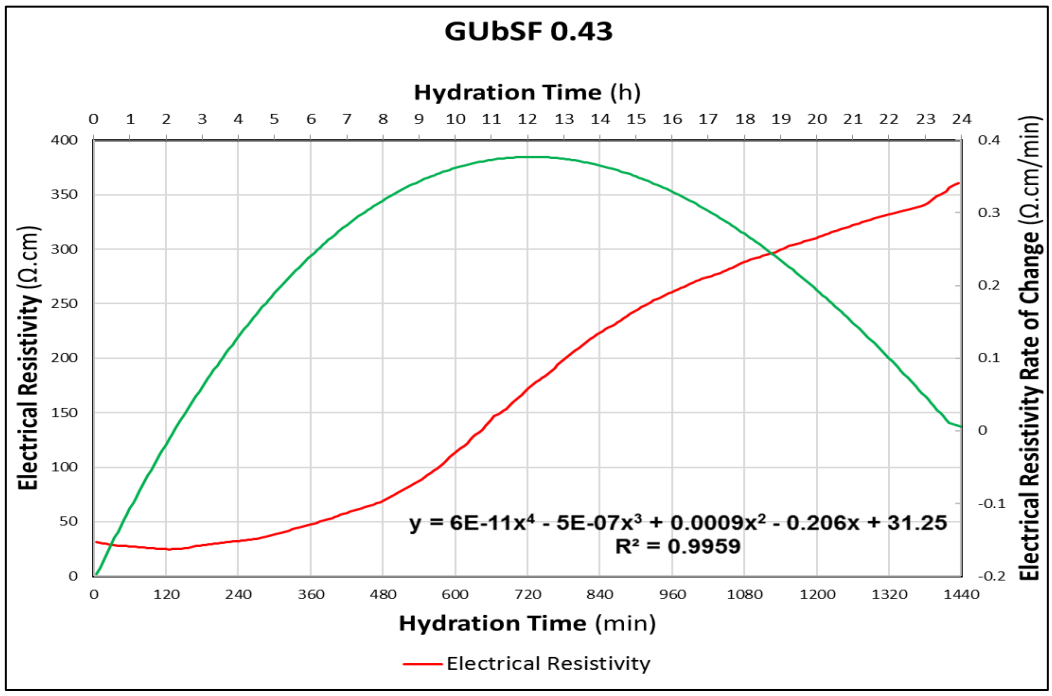


**Figure 4-30: Electrical resistivity and its ROC of GUbSF 0.43 cement paste over the first 24 h of hydration**

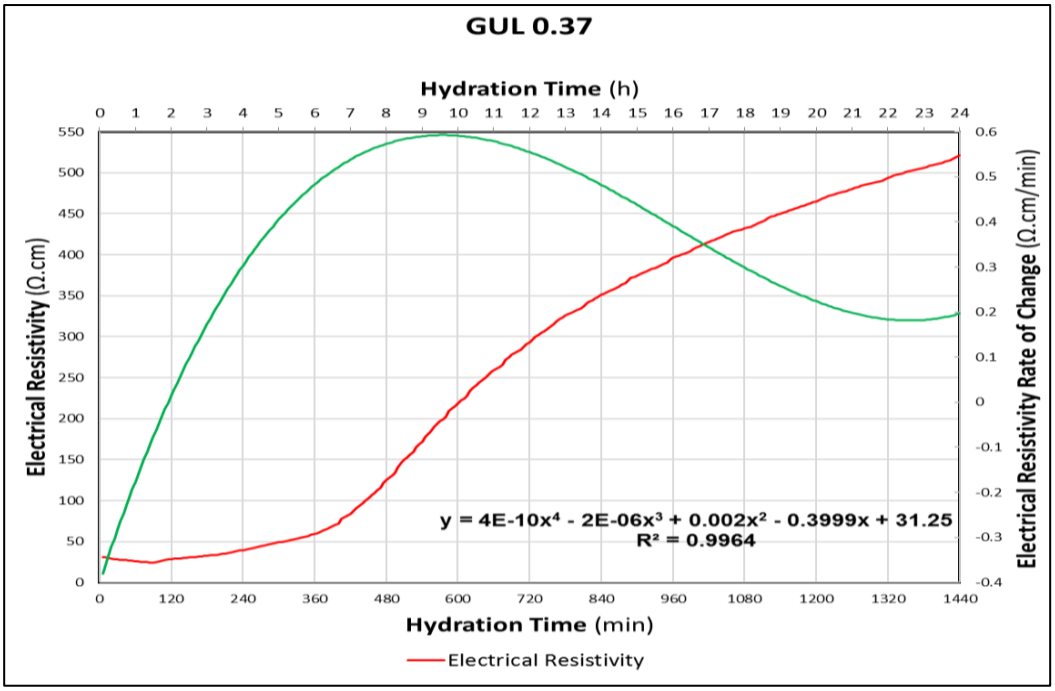


**Figure 4-31: Electrical resistivity and its ROC of GUL 0.37 cement paste over the first 24 h of hydration**

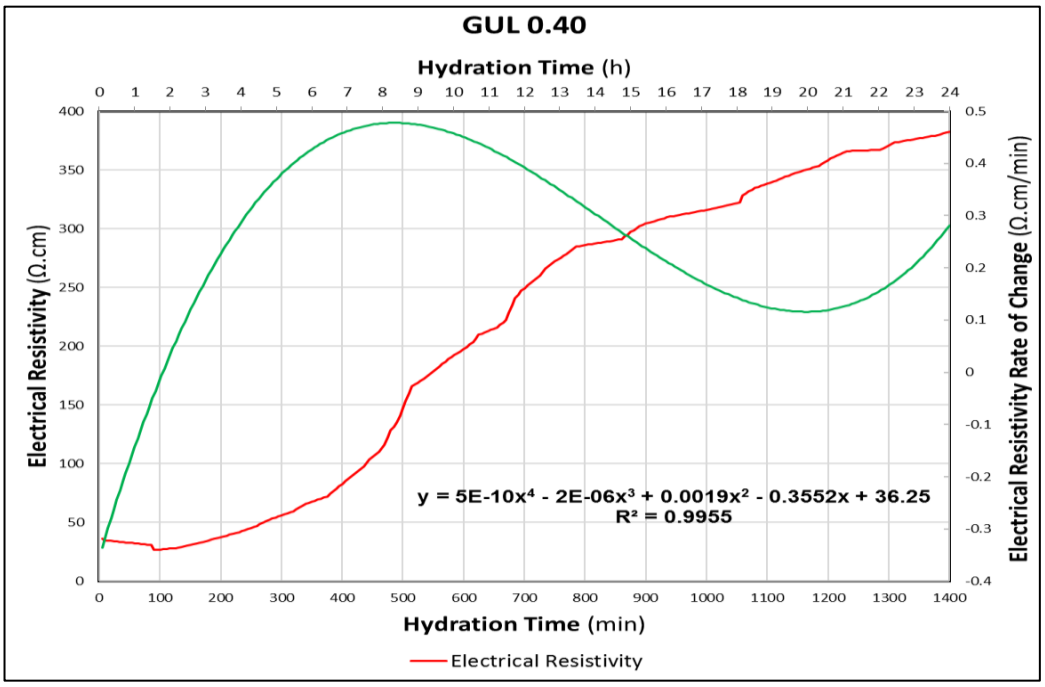


**Figure 4-32: Electrical resistivity and its ROC of GUL 0.40 cement paste over the first 24 h of hydration**

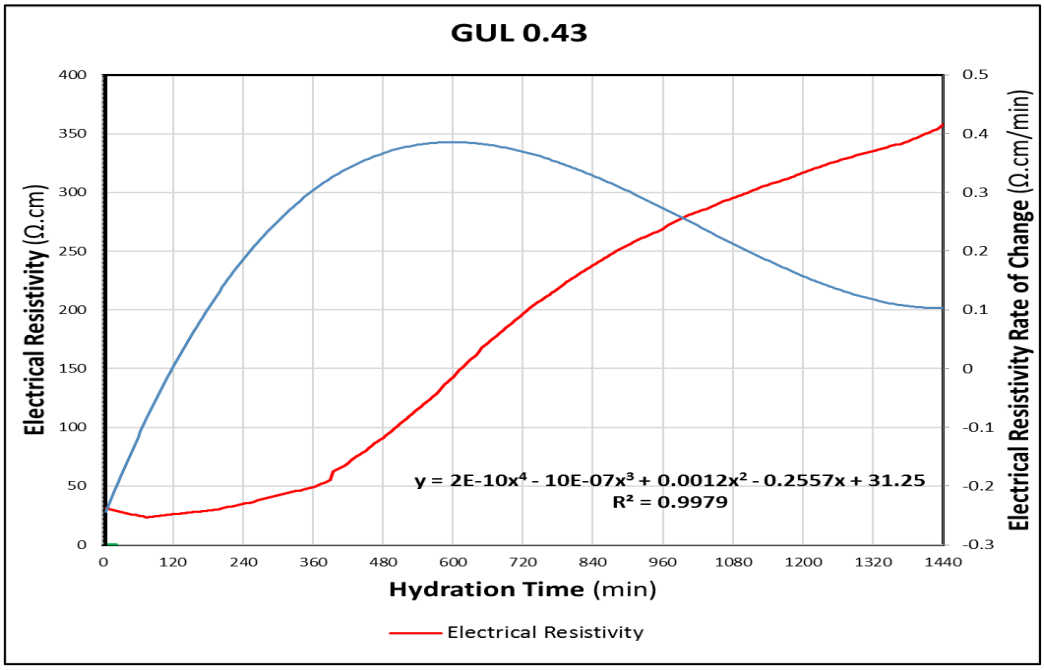


**Figure 4-33: Electrical resistivity and its ROC of GUL 0.43 cement paste over the first 24 h of hydration**

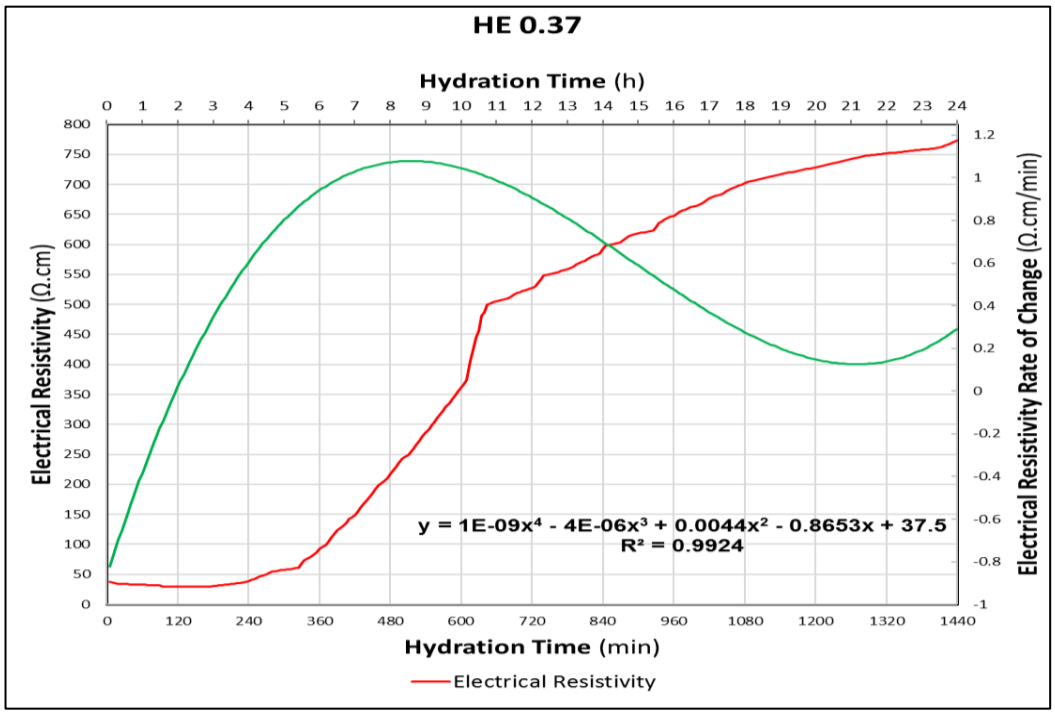


**Figure 4-34: Electrical resistivity and its ROC of HE 0.37 cement paste over the first 24 h of hydration**

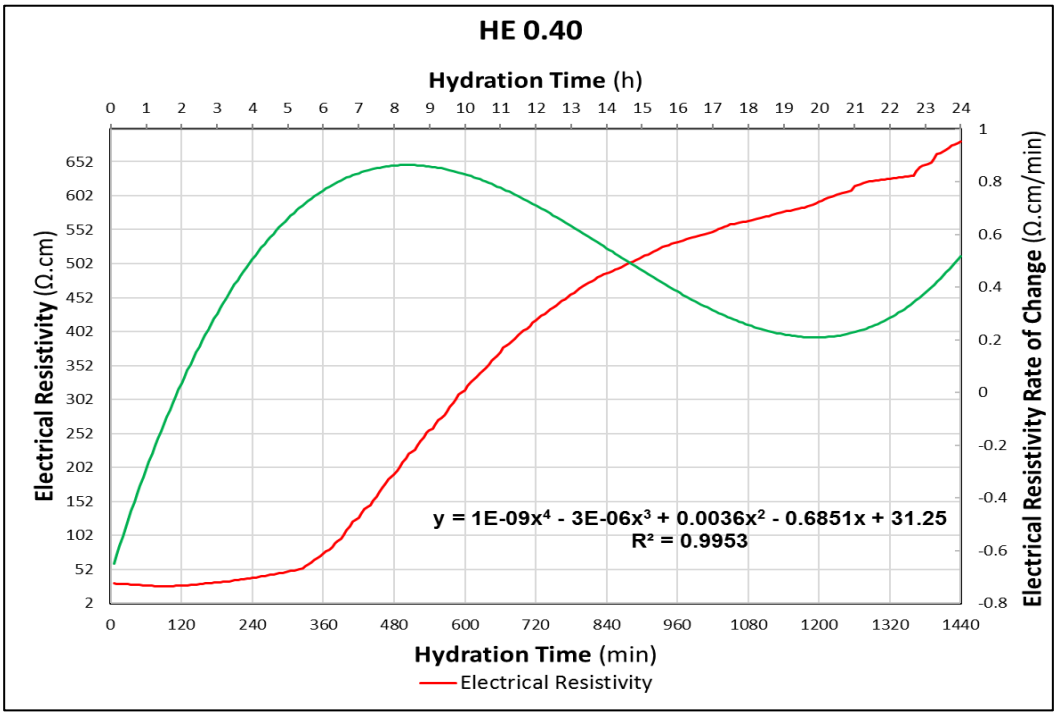


**Figure 4-35: Electrical resistivity and its ROC of HE 0.40 cement paste over the first 24 h of hydration**

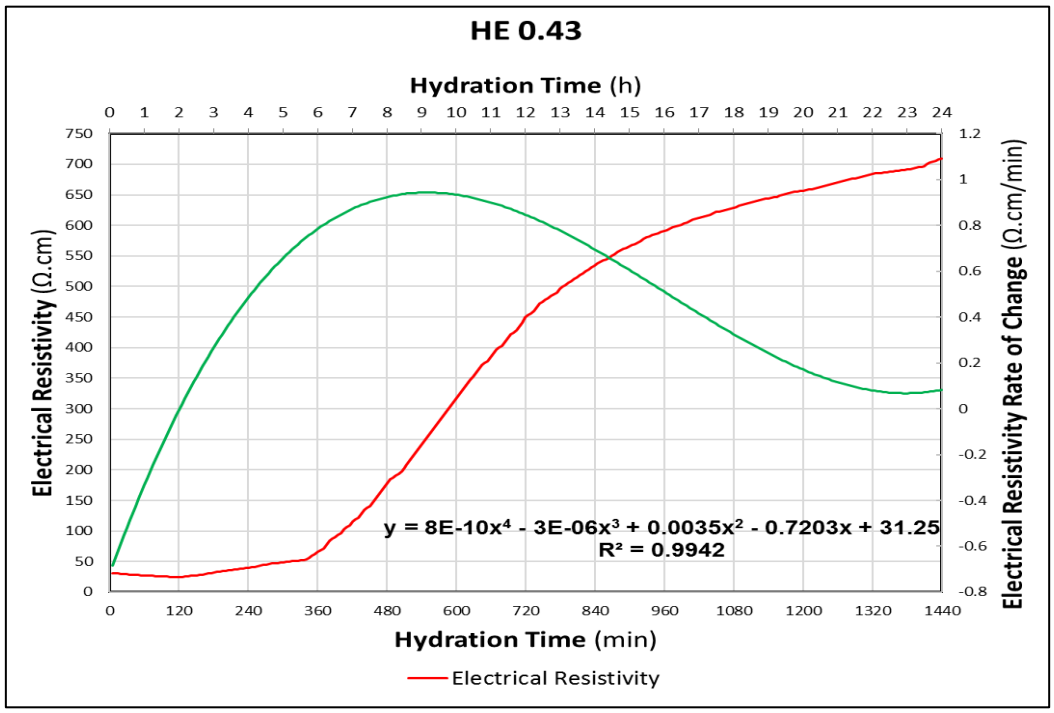


**Figure 4-36: Electrical resistivity and its ROC of HE 0.43 cement paste over the first 24 h of hydration**

From the figures, it is observed that the Rate of Change (ROC) in the electrical resistivity development of cement paste rapidly increases from mixing to a time beyond the final setting (between 8 and 10 hours of hydration). After the turning point, a negative momentum of resistivity is observed until 20-24 hours of hydration. Beyond that, the electrical resistivity increases again with a positive momentum. It is observed that before the turning point (stages of setting), the formation of cement hydration products are the influencing factors in the resistivity development, while beyond that, the development of hydration products is slower. As a result, the electrical resistivity does not increase as fast as before the turning point. Around 20-24 hours of hydration, further formation of cement hydration products results in a positive momentum in electrical resistivity development. Further analysis of the microstructure of the hydrated cement paste can provide more insight for the changes in the ROC of the electrical resistivity.

### 4.2.3. Compressive Strength (24 hours)

The compressive strength of the cement paste at 1 day is an important factor in determining the curing effects and concrete mixture quality. The 24-hour compressive strength of three Ø50×100 mm cement paste cylinders was measured according to ASTM C109. Figure 4-37 illustrates the average of three measurements for all pastes with W/CM of 0.37, 0.40, and 0.43. Detail test results and specimens' properties are presented in Appendix H.

As shown in Figure 4-37, the compressive strength decreases as the W/CM ratio increases, and it is higher for the cement paste made of HE cement.

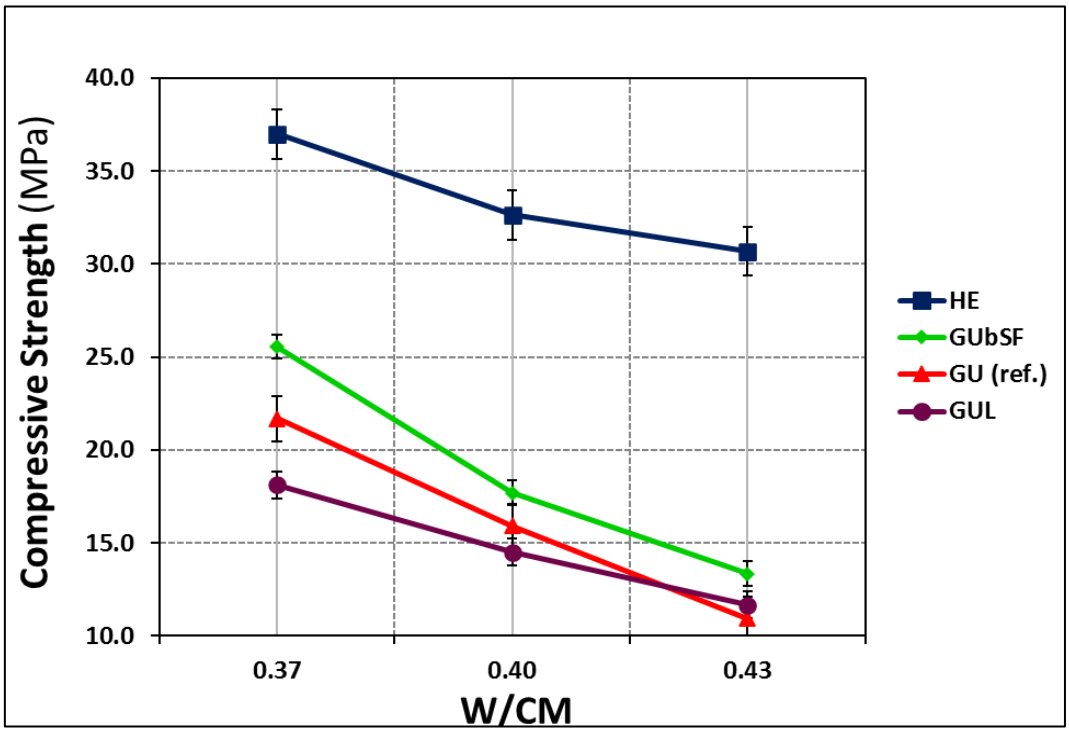


**Figure 4-37: Compressive strength at 24 hours after casting (average of 3 cylinders)**

The highest 1-day strength in HE cement paste mixture is expected due to its very fine cement particle size. However, the effect of limestone in the 24-hour strength of cement mixtures, observed in Figure 4-37 is interesting.

The fractured shape of the cement paste cylinders was acceptable according to CSA A23.2-9C, as shown in Figure 4-38. The standard refers to fracture types of concrete cylinders tested

for compressive strength, but the acceptable fracture types can be used in cement paste cylinders fracture analysis. In case the type of failure was not acceptable according to the standard, the measured compressive strength of that specimen was eliminated from the calculations.

**Figure 4-38: Comparison of fractured shapes resulting from compressive strength test (acceptable columnar fracture on right)**

As expected from the quality control test results from the cement supplier, the highest compressive strength at 24 hours was for the HE cement paste (see Figure 4-37). However, the compressive strength of GU cement paste at 24 hours was lower than that of GUbSF and GUL mixtures, even though the latter had partial replacement of Portland cement with supplementary cementitious materials (limestone and silica fume). It can be concluded that at 24 hours of hydration, the effect of supplementary cementitious materials reaction with biproducts of Portland cement hydration resulted in slightly higher compressive strength. This conclusion needs to be confirmed with the analysis of the microstructure of cement hydration products at 24 hours of hydration.

### 4.2.4. Setting Time

The initial setting time and final setting time of all cement paste mixtures were measured according to the method described in Section 3.3.2. For the initial setting time, the penetration was calculated as the average of 10 measurements in a 35×35mm area as shown in Figure 4-39. The conical ring (a mould) of the testing apparatus is 40±1mm in height, 70±3mm in bottom diameter, and 60±3mm in top diameter. Both diameters are measured from the inside.

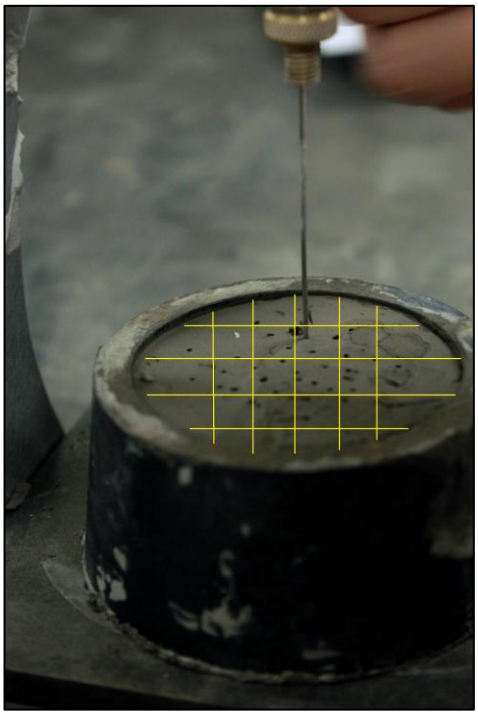

**Figure 4-39: Vicat testing area for the setting time of cement paste**

The initial and final setting times of the mix designs studied are shown in Figure 4-40 and Figure 4-41, respectively.

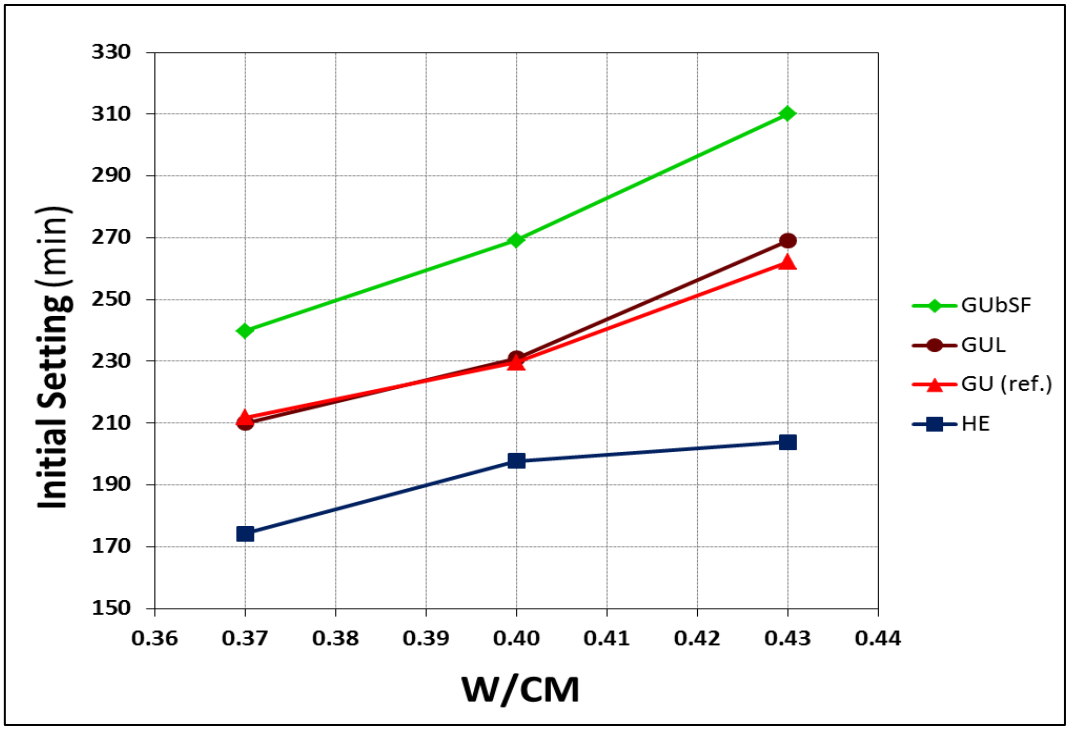


**Figure 4-40: Initial setting time of cement paste mixtures**

From Figure 4-40, it is noted that the initial setting time is increased as the water content of the mixture (represented by the W/CM ratio) is increased. However, the rate of the increase in the reference mixture (GU cement) is more than 30% than that in the HE mixtures.

It is observed that the mixture containing silica fume showed longer initial setting time, which can be related to the later contribution of silica fume to the setting properties of the mixtures.

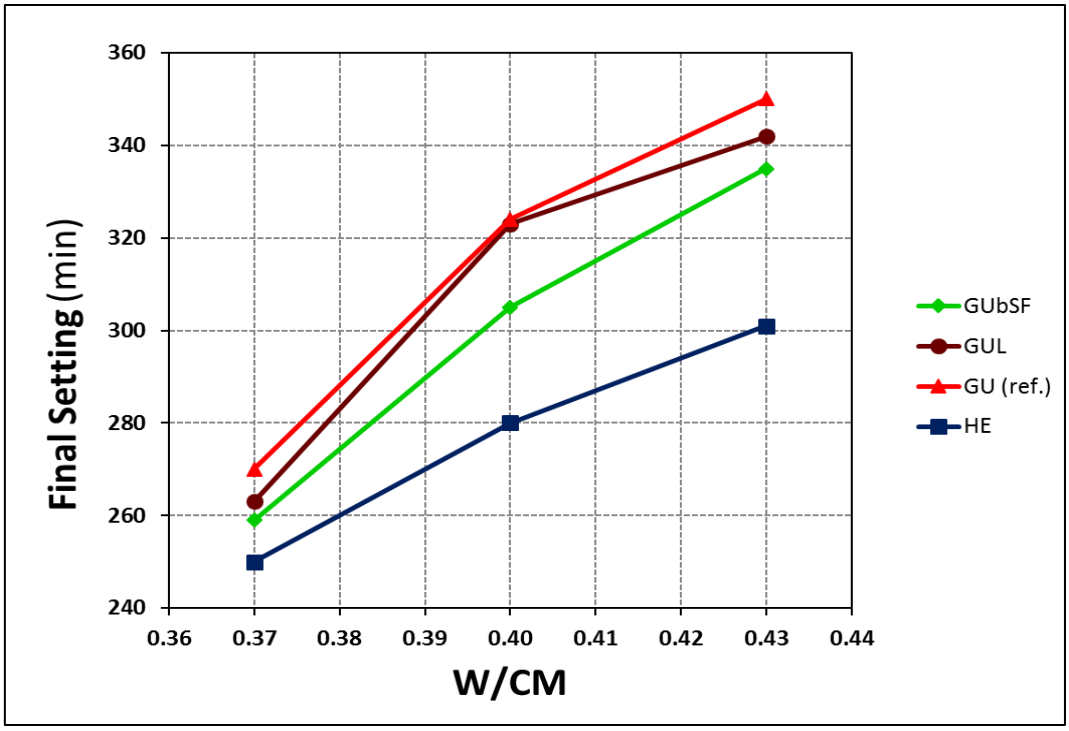


**Figure 4-41: Final setting time of cement paste mixtures**

By comparing Figure 4-40 and Figure 4-41, it can be observed that both initial and final setting times depend on the W/CM ratio. Also, the HE initial setting time at W/CM ratios greater than 0.40 is not significantly influenced by the addition of water, whereas the final setting time for these mixtures is more affected by the extra water.

Although the literature has shown than the replacement of mortar aggregate with limestone could result in earlier setting time (Bentz et al., 2016), the results presented in Figure 4-40 show that cement replacement with limestone did not affect the initial setting. However, Figure 4-41 shows the final setting time of the cement paste mixture made with GUL cement was slightly earlier than that of the paste made with GU cement.

Significant difference in the setting times of cement mixtures in Figure 4-40 and Figure 4-41 has shown the importance of having a universal method for measuring the setting.

### 4.2.5. Rheology Vane Shear

At the preliminary testing stage of this research project, all cement paste mixtures were tested for the stiffening time according to the method described in Section 3.3.3. Stiffening of the cement paste begins when its yield stress starts developing. To determine the viscosity development time, cement pastes were cast in Ø50×100 mm cylinders and tested with the Vane shear apparatus after mixing. Since the Vane shear strength may be greatly influenced by the rate at which shear occurs, the torque was applied using a motorized vane device (instead of a hand-crank manual torqueing).

Based on the results tabulated in Table 4-2, it was found that stiffening of the pastes occurs at around 120 minutes on average. This time frame of 120 minutes also meets the requirement described in CSA A23.1-14 for the maximum allowable time for pouring and finishing a cement-based batch, if the mixture temperature does not exceed the limits in Table 14 of CSA A23.1-14 (2014). This is the time a cement-based mix starts stiffening and cannot be properly placed and consolidated.

**Table 4-2: Preliminary test results of the Vane shear to determine the stiffening time**

| **Mix Design** | | **$\Delta_f - \Delta_i$ ° at the Time of Testing** (min.) | | | | | | | |
|---|---|---|---|---|---|---|---|---|---|
| **Cement Type** | **W/CM** | **30** | **60** | **90** | **100** | **110** | **120** | **130** | **140** |
| **GU** | **0.37** | 0 | 0 | 0 | 0 | 0 | 4° | NT | NT* |
| | **0.40** | 0 | 0 | 0 | 0 | 0 | 0 | 3° | NT |
| | **0.43** | 0 | 0 | 0 | 0 | 0 | 0 | 2° | NT |
| **GUL** | **0.37** | 0 | 0 | 0 | 0 | 0 | 7° | NT | NT |
| | **0.40** | 0 | 0 | 0 | 0 | 0 | 4° | NT | NT |
| | **0.43** | 0 | 0 | 0 | 0 | 0 | 2° | NT | NT |
| **GUbSF** | **0.37** | 0 | 0 | 0 | 0 | 2° | NT | NT | NT |
| | **0.40** | 0 | 0 | 0 | 0 | 2° | NT | NT | NT |
| | **0.43** | 0 | 0 | 0 | 0 | 0 | 2° | NT | NT |
| **HE** | **0.37** | 0 | 0 | 0 | 1° | NT | NT | NT | NT |
| | **0.40** | 0 | 0 | 0 | 0 | 3° | NT | NT | NT |
| | **0.43** | 0 | 0 | 0 | 0 | 2° | NT | NT | NT |

*NT= Not Tested (as the beginning of the stiffening time was determined)

From this initial observation, it was decided that the rheology properties of all cement pastes be studied at 2 hours and at initial setting. For this purpose, a Ø50×100 mm cement paste

cylinder was cast and tested according to the method described in Section 3.3.3. Figure 4-42 illustrates the Vane shear test setup.

**Figure 4-42: Vane shear test setup for cement paste cylinders at 2 hours**

The rotational strength (the Vane shear strength) of the cement paste, which can be an indicator for the pumpability in the mixture, was calculated according to the relations described in ASTM D4648, and the results are shown in Figure 4-43.

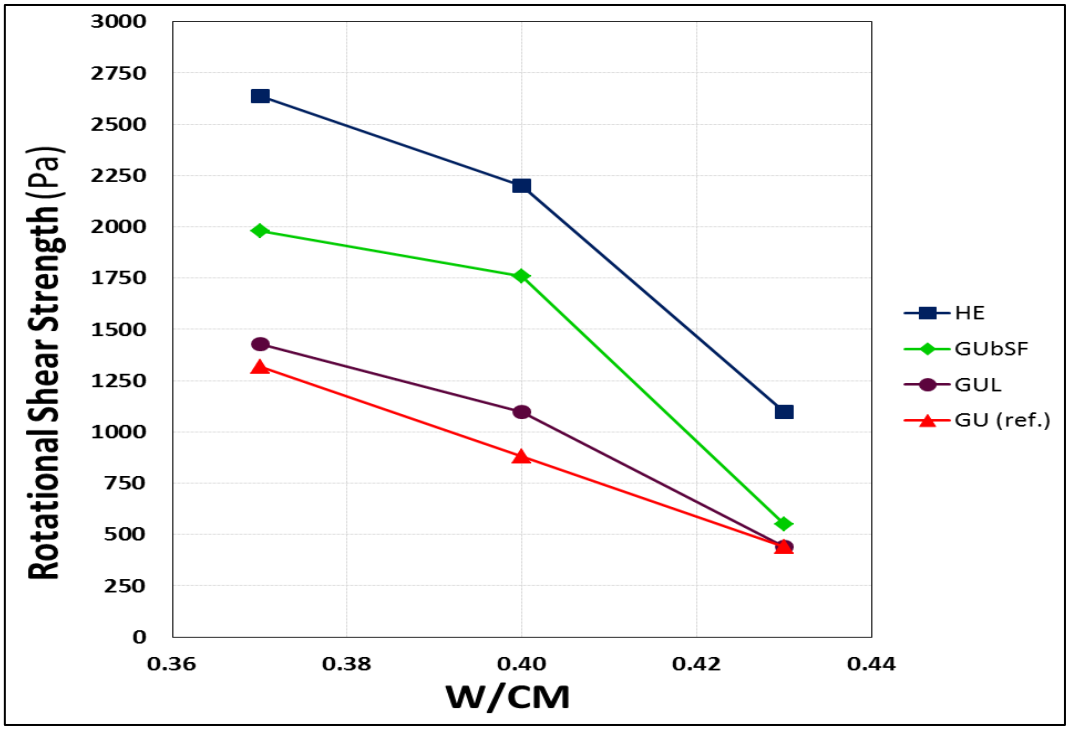


**Figure 4-43: Rotational undrained shear strength development of cement pastes at 2 hours of hydration**

Figure 4-44 illustrates the development of the Vane shear strength in cement pastes at the time of initial setting. It is important to mention that the measurement of the rotation strength beyond initial setting was not possible.

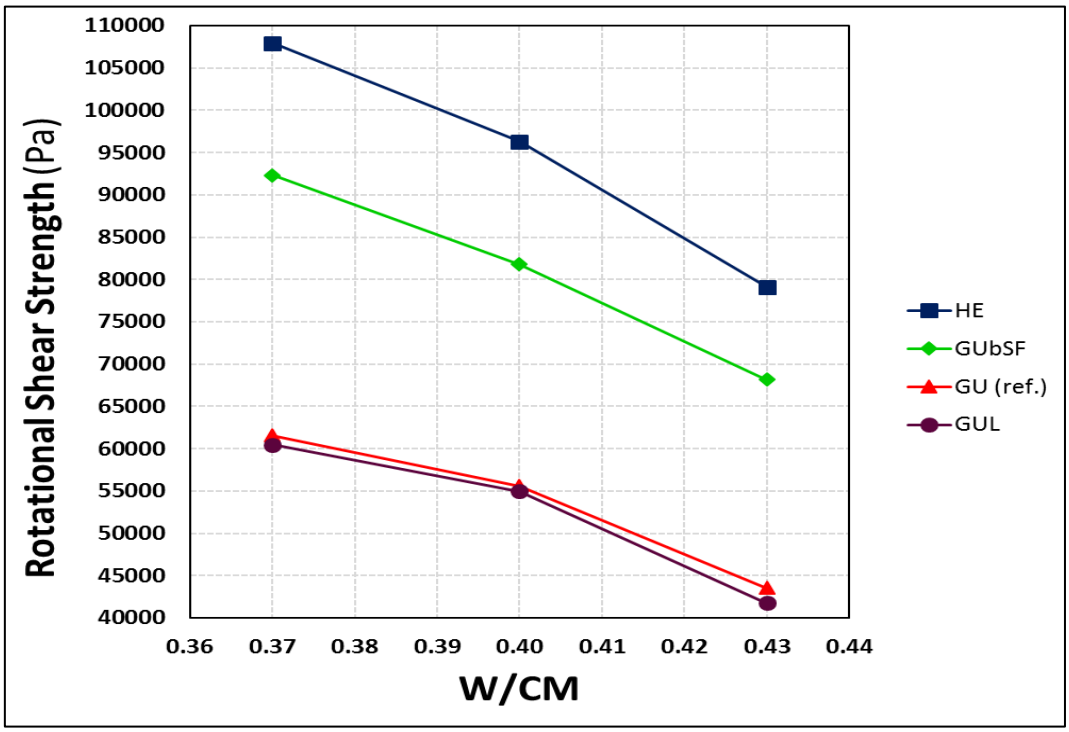


**Figure 4-44: Rotational undrained shear strength development of cement pastes at initial setting**

As the W/CM ratio increases, the shear resistance of the mixtures decreases. This reduction is significant in the HE cement paste mixture compared to the GU mixture, which is used in this study as the reference mixture. It is noted that the limestone in the GUL paste does not influence the workability of the mixture significantly, while silica fume decreases the fresh paste workability. Also, HE mixtures lost their workability faster than other mixtures.

After completing all the test results and mix designs in Figure 4-20, it has been observed that HE mixtures showed higher electrical resistivity and faster resistivity development over the first 24 hours of hydration. By considering the physical behaviour of HE mixtures at the initial setting time in Figure 4-40 and its rotational strength in Figure 4-43, it can be concluded that the higher resistivity in HE mixtures is from the faster hydration and therefore earlier cement

hydration product formation. HE cement reacts with water faster than other types of cement which results in sooner hydration product formation.

It is important to mention that during testing, the possibility of bleeding in the specimens was monitored. Since the rotational rate of the machine was chosen to avoid any moisture drainage (bleeding in cement pastes), it was necessary to monitor bleeding by visual inspection during the test. There was no bleeding in any of the samples tested, so the undrained shear strength was determined by the Vane shear technique.

### 4.2.6. Thermal Properties

The internal temperature of the mixtures was measured for 24 hours after first mixing. As described in Chapter 3, to eliminate the effect of the starting temperature difference, the mixing temperature was controlled. All the mixing materials were controlled at room temperature (22-23°C), which was assumed to be the initial temperature of the mixes.

The thermometer used with the resistance-meter measures temperature in integer numbers, while the change in the cement paste internal temperature is in decimal digits. A thermometer providing a higher-degree accuracy was used for all the mixtures until the final setting time (indicated with the second vertical black line in Figure 4-45), while the original thermometer incorporated in the resistance-meter was used for the remaining of the experiment, as shown in Figure 4-45 (for GU 0.43).

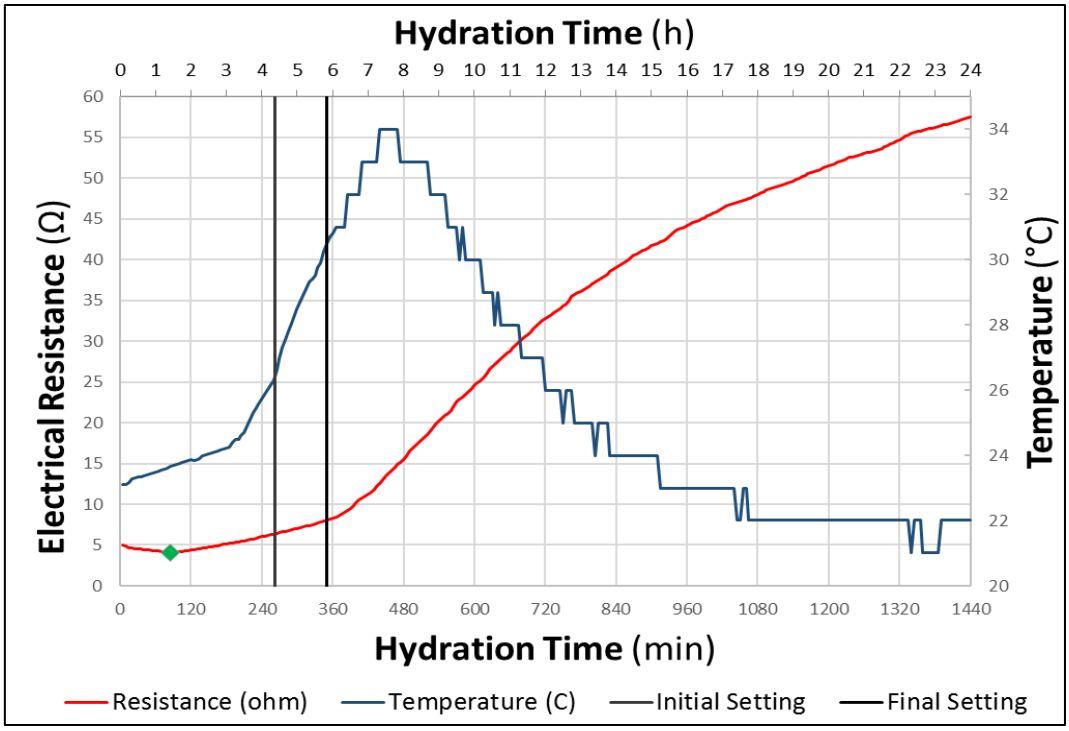


**Figure 4-45: Internal temperature development of cement a paste mixture (GU 0.43)**

It is observed that there is a rapid increase in the initial temperature of the mixture (which is controlled at room temperature) for the first 1.5-2 hours. After a short period of constant temperature (or sometimes barely reduction in temperature), it starts increasing at a faster rate, reaching to a maximum mixture temperature after a few hours from mixing (7-8 hours in Figure 4-45). Finally, the internal temperature of the mixture drops until it reaches room temperature at 24 hours.

The thermometer used failed upon reaching 50°C, as shown in Figure 4-46. This issue was observed only in mixtures with HE and GUbSF cement and low W/CM (0.37 and 0.40).

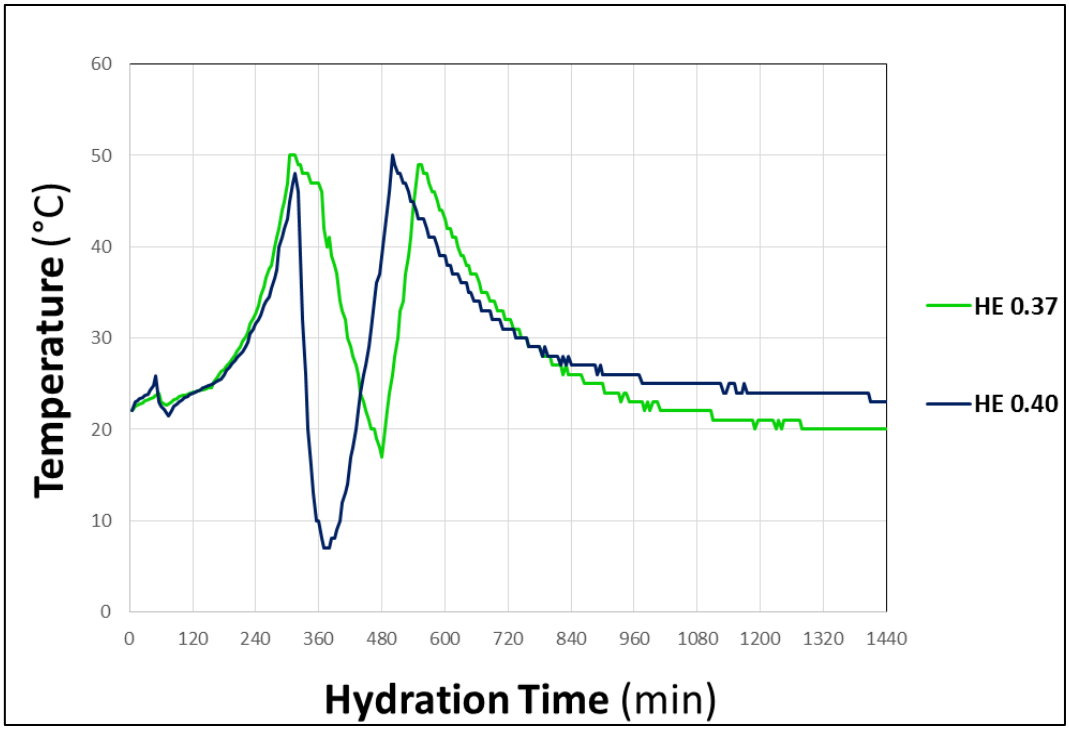


**Figure 4-46: Temperature measurement failure upon reaching 50° C in thermometers**

To overcome the limitation of the initial thermos-meter, another thermometer (Fisher Scientific Traceable 255NA) with higher maximum temperature capacity was used at the same time, as shown in Figure 4-47.

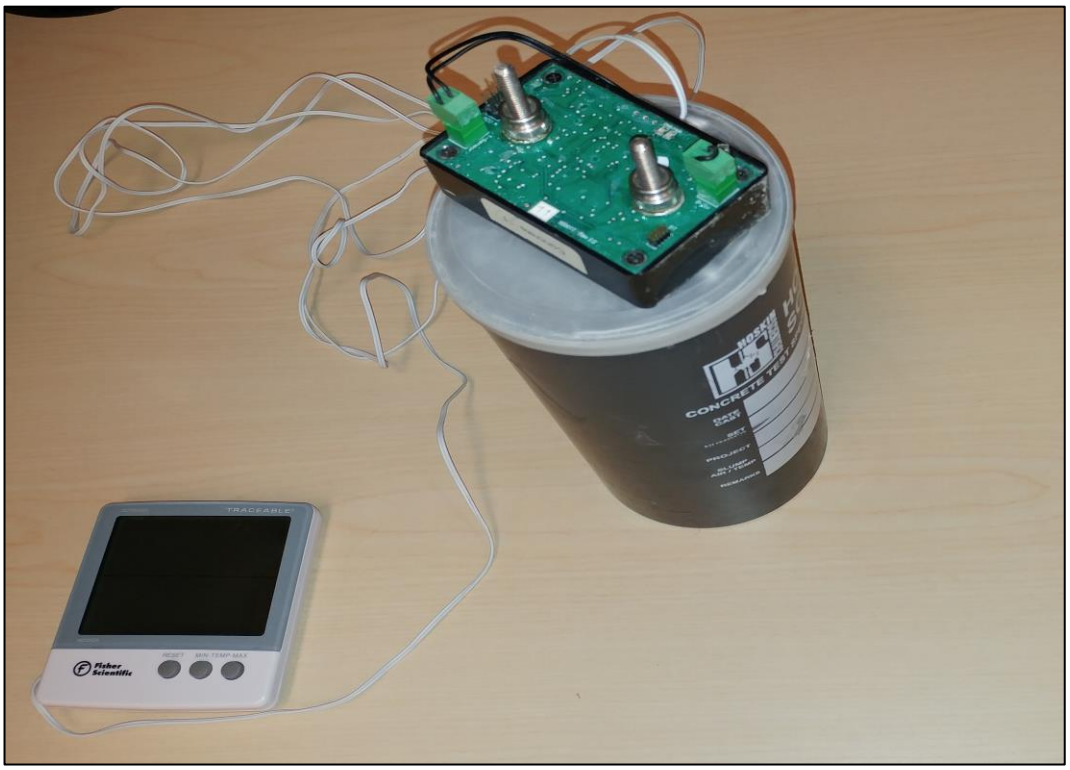


**Figure 4-47: Usage of additional thermometer for mixtures with high dormant temperature**

Since the initial temperature of all mixtures is the same (room temperature, 22-23°C) and it is assumed that there is not thermal energy transfer between the cement paste specimen and the environment (through the walls of the plastic mould), the only factor affecting the specimen temperature is the cement hydration exothermic energy. The changes in mixture temperature over the first 24 hours are illustrated in Figure 4-48.

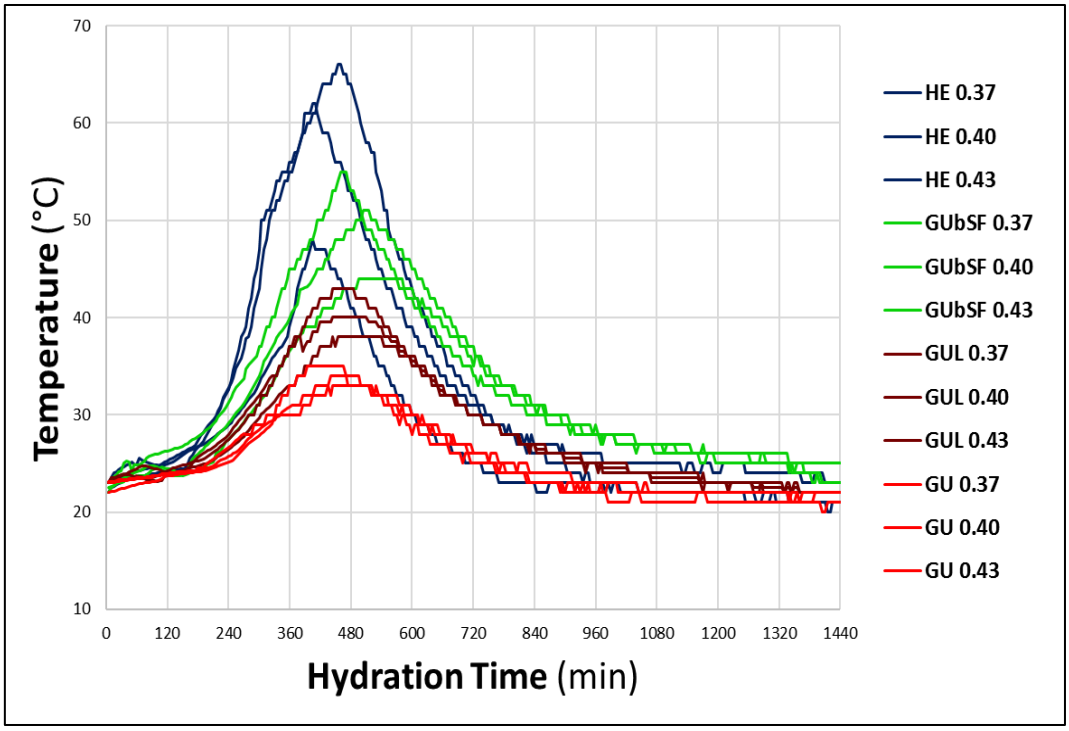


**Figure 4-48: Internal temperature of mixtures over the first 24 hours of hydration**

It is observed that the temperature of cement paste mixtures remained almost the same over the first 2-3 of hydration corresponding to the dormant period of cement hydration, in which the Portland cement hydration activity is not significant. The heat generated in this period (represented by the changes in the internal temperature of the mixture) is very little. After the dormant period, the rate of the cement hydration (and the rate of increase in the samples internal temperature) increases sharply. Close to the peak, the hydration becomes diffusion controlled, and the rate of hydration slows down. After reaching a maximum, the temperature starts decreasing due to heat dissipation.

Theoretically, the rate of cement hydration (and therefore heat generation in the mixture) is very high during the first several minutes of hydration due to the dissolution of the ions into the mixing water (the same reason for a rapid drop in the electrical resistivity of the mixture right after mixing). However, the rise in the initial temperature of the GU and GUL mixes was not observed significantly (although the first reading happened very early right after mixing, about 4 minutes). It can be concluded that the dissolution of ions in the water affects

the electrical properties of the mixture much more significantly than the rate of hydration before the dormant period.

The rate of change in adiabatic temperature (dT/dt) of the mixtures, calculated from the first derivative of the temperature with respect to time is tabulated in Table 4-3.

**Table 4-3: Rate of adiabatic temperature change over the first 24 hours of hydration**

| **Mix Design** | | **Average dT/dt** (°C/ min.) | |
|---|---|---|---|
| **Cement** | **W/CM** | **Dormant to Peak** | **Peak to Control Temperature** |
| **GU (ref.)** | **0.37** | 0.041 | -0.028 |
| | **0.40** | 0.034 | -0.024 |
| | **0.43** | 0.031 | -0.021 |
| **GUL** | **0.37** | 0.062 | -0.033 |
| | **0.40** | 0.049 | -0.028 |
| | **0.43** | 0.036 | -0.025 |
| **GUbSF** | **0.37** | 0.084 | -0.059 |
| | **0.40** | 0.071 | -0.038 |
| | **0.43** | 0.053 | -0.032 |
| **HE** | **0.37** | 0.137 | -0.085 |
| | **0.40** | 0.130 | -0.066 |
| | **0.43** | 0.091 | -0.056 |

It is observed that replacement of GU cement with limestone increases the rate of change of adiabatic temperature, and this increase is quite significant with silica fume replacement. The rate of decreasing the mixture temperature to the control temperature (room temperature) is also faster in mixtures with partial cement replacement by silica fume or limestone than that of mixtures made of GU cement. In all the mix designs, the highest rate of change (increase and decrease) was observed in mixture with Type 30 cement (HE mixtures). Since it is assumed that Adiabatic Temperature (AT) is measured, the values in Table 4-3 are indicative

of the rate of cement hydration. It can be said that the highest rate of hydration was observed in HE mixtures followed by GUbSF and GUL cement pastes.

Figure 4-49 to Figure 4-52 show the changes in the temperature of fresh cement paste mixtures over the first 24 hours. It is stated that in all the mixtures, mixtures with lower W/CM ratio resulted in higher temperatures over the first 24 hours of hydration; however, the effect of W/CM ratio on the dormant period was not significant. In addition, the peak of the Adiabatic Temperature Rise (ATR) was delayed as the W/CM ratio increased.

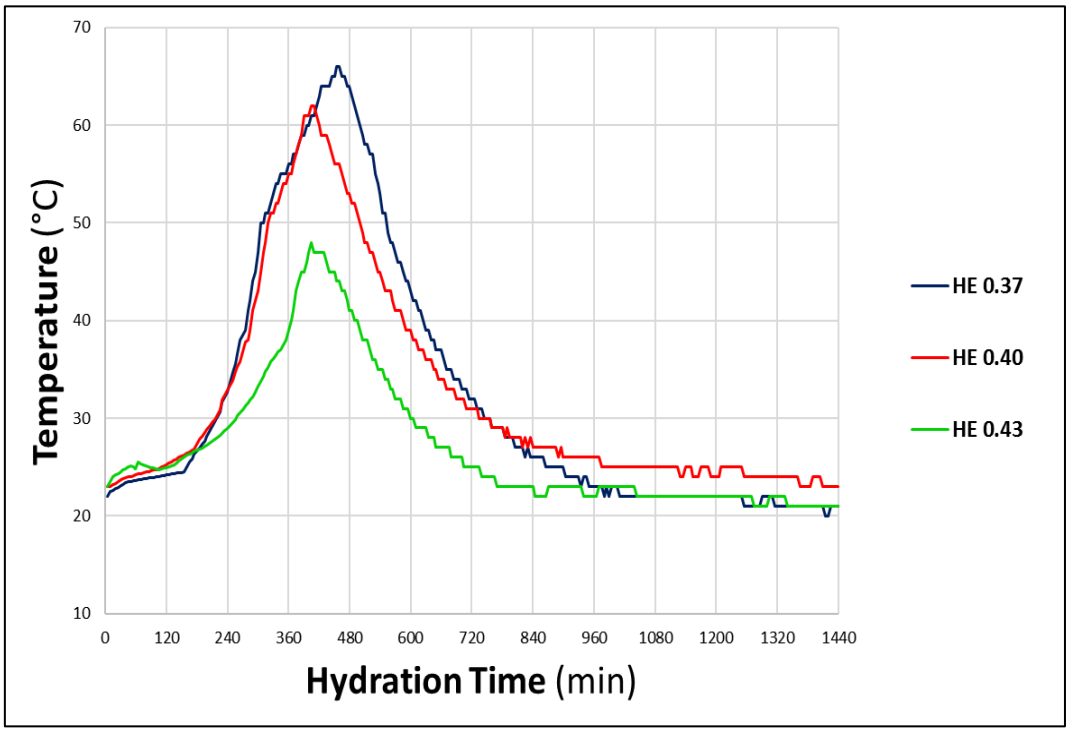


**Figure 4-49: Internal temperature of HE mixtures over the first 24 hours of hydration**

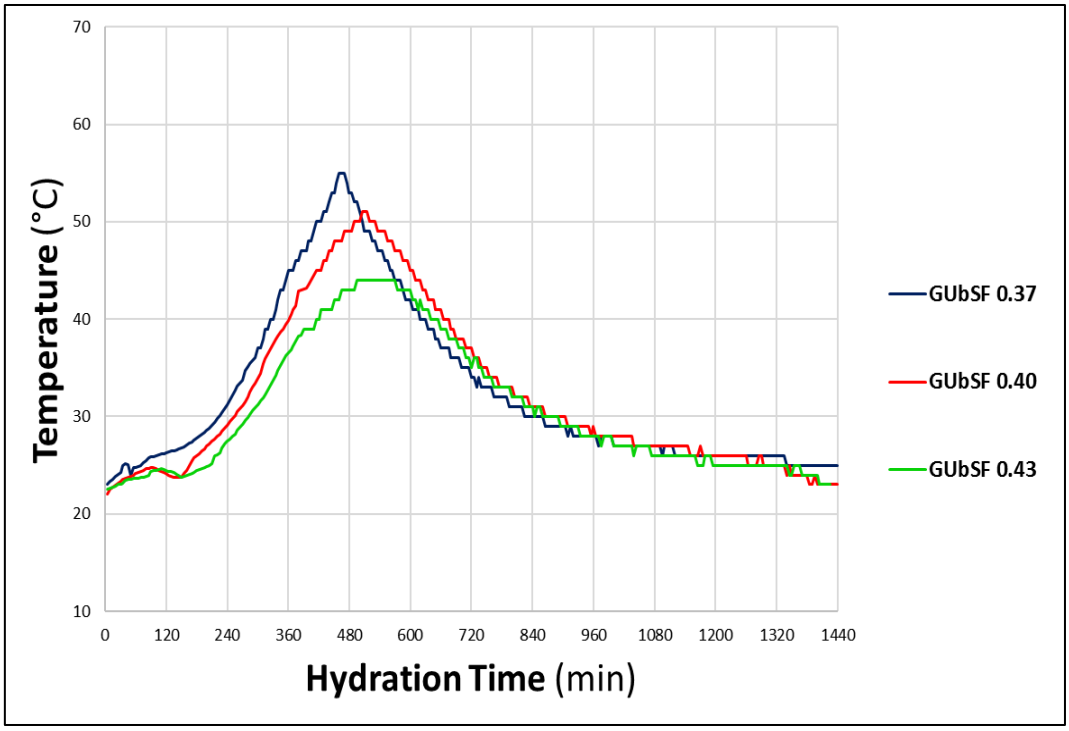


**Figure 4-50: Internal temperature of GUbSF mixtures over the first 24 hours of hydration**

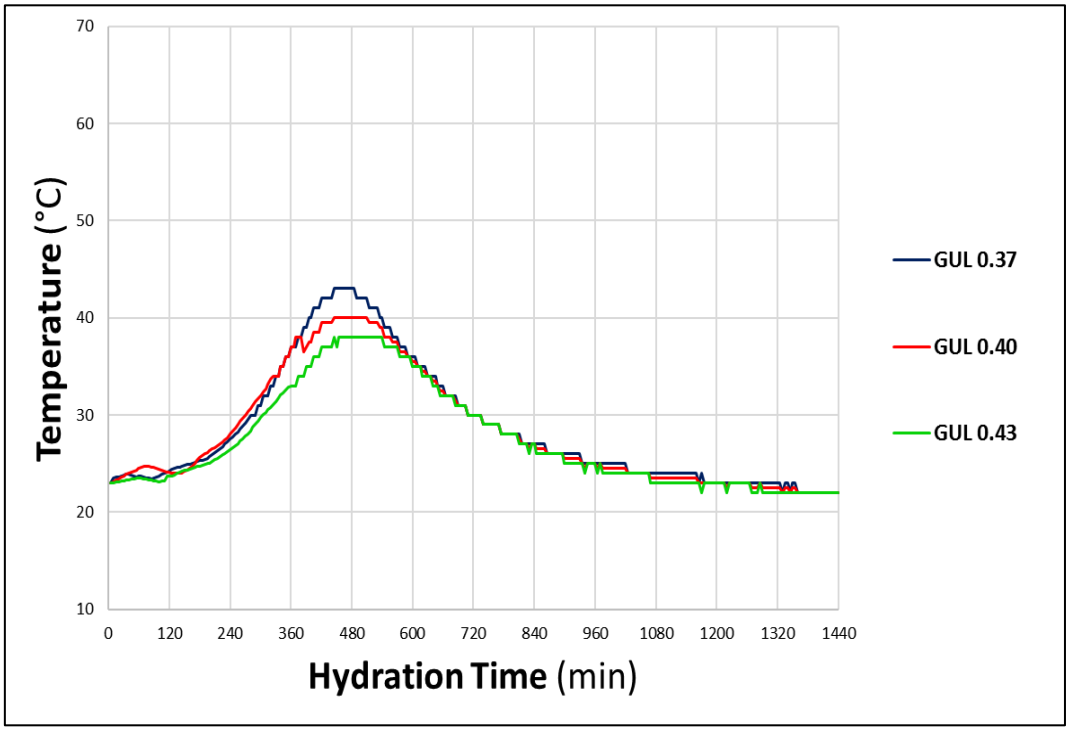


**Figure 4-51: Internal temperature of GUL mixtures over the first 24 hours of hydration**

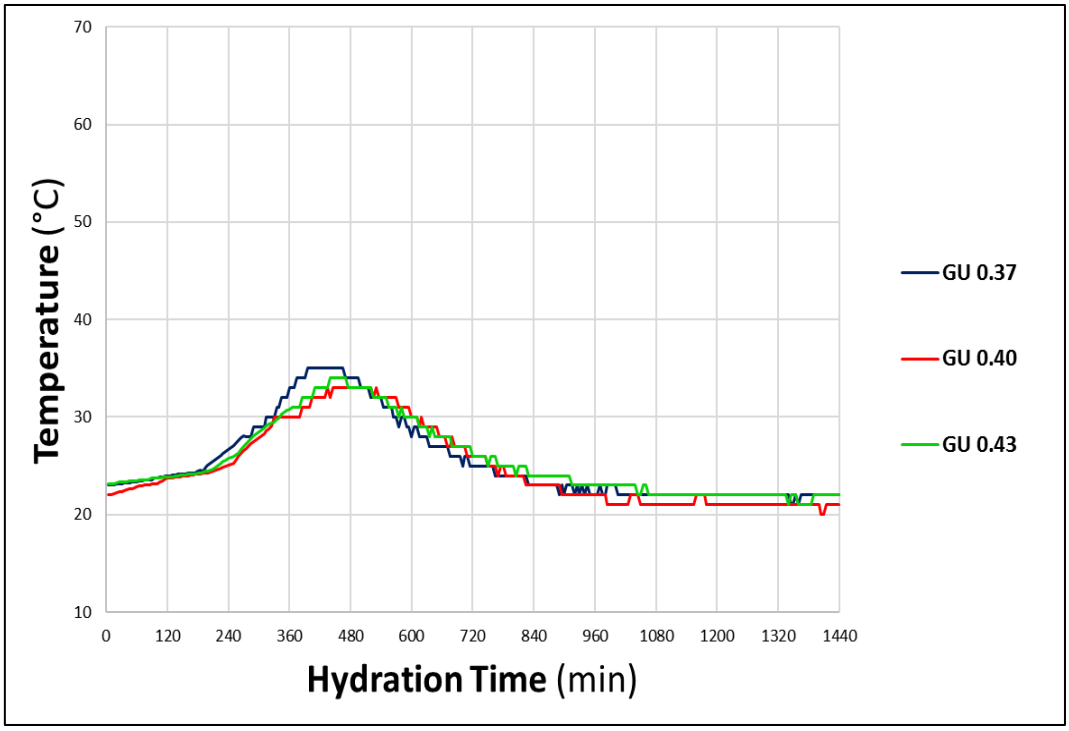


**Figure 4-52: Internal temperature of GU mixtures over the first 24 hours of hydration**

### 4.2.6.1. Cement Type Effects on Mixture Temperature

Replacement of cement with pozzolanic or other materials can affect the hydration of the mixtures. To study the effect of the cement type used on the paste mixtures hydration, the temperature of the mixtures with the same W/CM ratio during the first 24 hours is compared in Figure 4-53 to Figure 4-55.

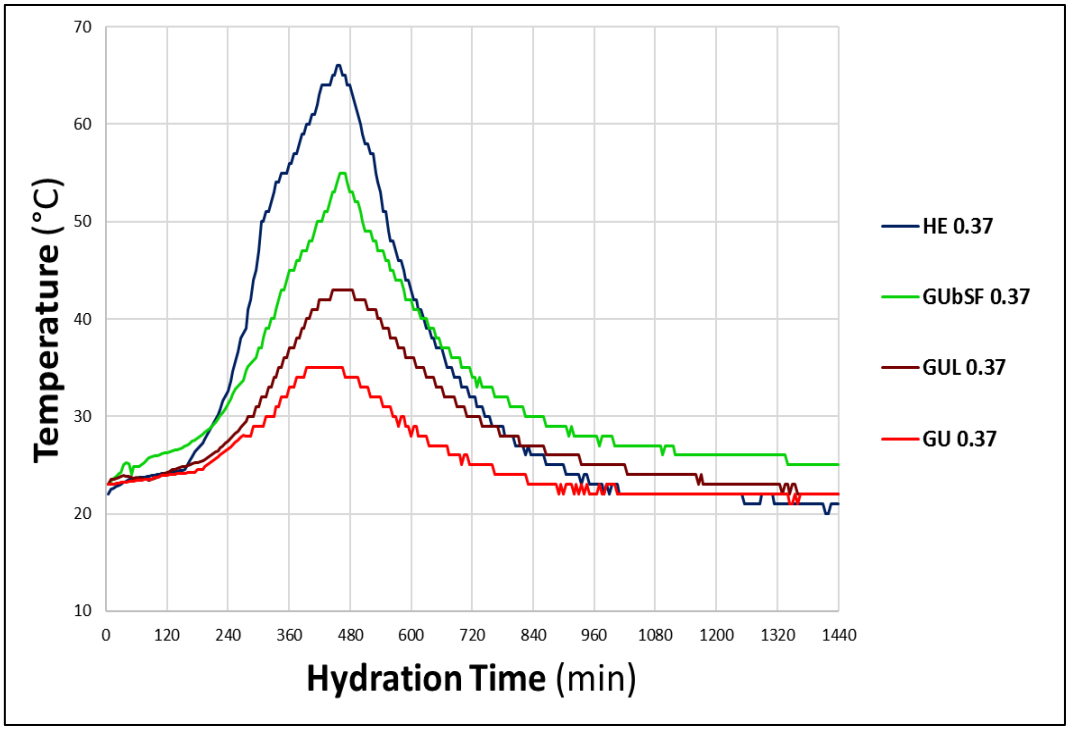


**Figure 4-53: First 24-hour temperature change of cement paste mixtures with W/CM=0.37**

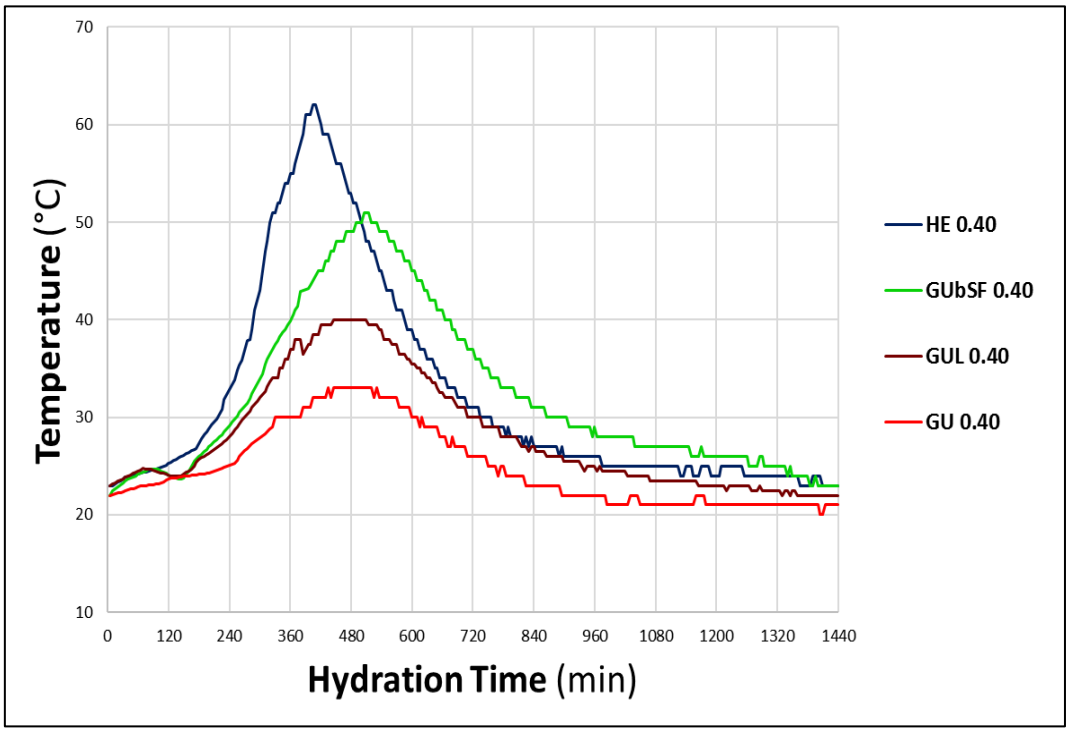


**Figure 4-54: First 24-hour temperature change of cement paste mixtures with W/CM=0.40**

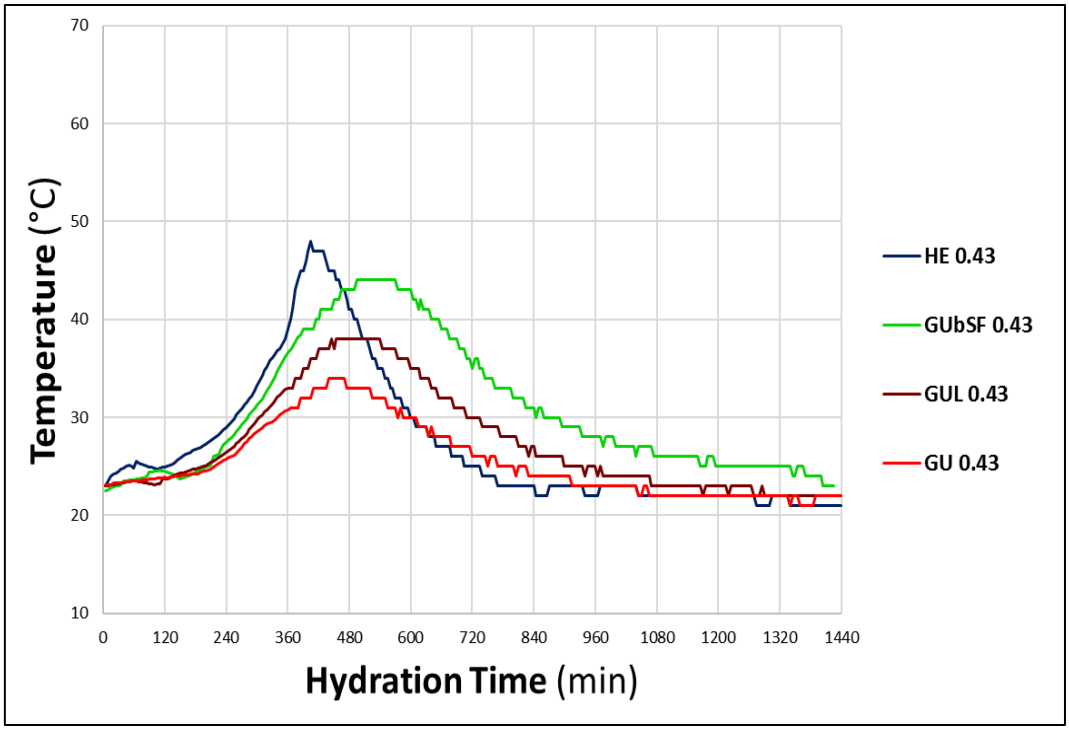


**Figure 4-55: First 24-hour temperature change of cement paste mixtures with W/CM=0.40**

The contribution of silica fume to cement hydration resulted in an increase in the mixture temperature over the first 24 hours compared to the control mixture (GU cement). Silica fume mixtures showed shorter dormant period, higher ATR all the time and higher rate of temperature increase than GU mixtures.

Furthermore, 12-15% limestone replacement of Type 10 cement in GUL cements resulted in not significantly shorter dormant period, but higher temperature of the mixtures (with similar W/CM ratio). In addition, it is observed that the replacement of cement with limestone did not postpone the dormant period.

In all W/CM ratios, mixtures with HE (Type 30) cement showed higher temperature at all times, higher maximum temperature and shortest dormant period. In these mixes, the rate of temperature change was higher than the rest of the mixtures.

#### 4.2.6.2. Temperature and Setting Time

The internal temperature of cement mortar samples at the time of setting can be used as an indicator for setting and cement hydration. The internal temperature of the cement pastes at the times of setting is tabulated in Table 4-4.

**Table 4-4: Internal temperature of specimens at setting times**

| **Mix Design** | | **Internal Temperature** (°C) | | | |
|---|---|---|---|---|---|
| **Cement** | **W/CM** | **Initial Setting Time** (min.) | **T**°C | **Final Setting Time** (min.) | **T**°C |
| **GU (ref.)** | **0.37** | 212 | 25.5 | 270 | 28.1 |
| | **0.40** | 230 | 24.9 | 324 | 29.0 |
| | **0.43** | 262 | 26.4 | 350 | 30.5 |
| **GUL** | **0.37** | 210 | 26.1 | 263 | 29.5 |
| | **0.40** | 231 | 27.5 | 323 | 33.7 |
| | **0.43** | 269 | 27.8 | 342 | 32.2 |
| **GUbSF** | **0.37** | 240 | 31.3 | 259 | 35.8 |
| | **0.40** | 269 | 31.1 | 305 | 39.9 |
| | **0.43** | 310 | 31.9 | 335 | 38.4 |
| **HE** | **0.37** | 174 | 26.3 | 250 | 38.0 |
| | **0.40** | 198 | 28.8 | 280 | 38.0 |
| | **0.43** | 204 | 27.4 | 301 | 33.3 |

In most mixtures, higher temperatures resulted in lower setting times. In other words, mixes with higher internal temperature (which is an indication of cement hydration) showed fast setting. However, the opposite was observed in the initial setting time of GUbSF mixtures. Although, the initial temperature of the mixtures containing silica fume was slightly higher from mixing until initial setting (see Figure 4-53 to Figure 4-55), the initial setting time happened later than the reference mixture (GU) or GUL mixtures. In contrast, the final setting time of GUbSF mixtures was earlier than that of GU and GUL mixtures. This can be explained

by the later contribution of silica fume to the paste hydration. From the beginning to around the initial setting time, silica fume did not contribute to the reaction, so a lower amount of Portland cement content delayed the initial setting time. Surface area is the best parameter to describe the fineness of the cement and therefore early-stage reactivity. The surface area of a cement is characterized by the Blaine air permeability test, which is described by ASTM C204. The fineness by air permeability and retained on a No. 325 mesh (size 0.044mm) is tabulated Table 4-5 (detailed test results from the supplier are provided in Appendix A).

**Table 4-5: Surface area and particle size analysis of cement powders (Source: Lafarge Canada)**

| **Cement Type** (from Lafarge Cement) | **Supplementary Cementitious Material** (% replacement) | **Fineness by air Permeability (Blaine)** | **Retained 325 Mesh** |
|---|---|---|---|
| | | ($m^2$/kg) | % |
| **General Use** *(GU-Type 10)* | <5% Limestone | 368 | 4 |
| **Limestone Cement** *(GUL)* | 12 - 15 | 484 | 1.2 |
| **Silica Fume Blended** *(GUbSF)* | 5.5 - 7.5 | 567 | 7.9 |
| **High Early** *(HE-Type 30)* | | 576 | 0.3 |

GUbSF and HE cement powder have the highest surface area as determined by ASTM C204. Therefore, the rate of hydration and the generation of the heat of hydration for those mixtures compared to GU cement pastes, as observed in Figure 4-53 to Figure 4-55. However, a higher temperature did not result in an earlier initial setting time; GUIbSF pastes set initially later than GU and GUL pastes, as reported in Table 4-4. It is observed that silica fume (and other pozzolans) acts like a calcium sink in the pore solution in the first few hours, resulting in

delays in the formation of CH and C-S-H and, initial setting times (Langan and Weng, 2002). After the initial setting time, silica fume starts contributing slowly to the hydration of cement paste which results in both a higher temperature (higher rate of hydration) and a reduction in the final setting time. In addition, it is observed that the longer the dormant period, the later the setting time occurs. In a concrete project, setting time (mainly the initial setting time) can be influenced by changing the dormant period (i.e., by changing the cement type or addition of additives). Therefore, the mixture Adiabatic Temperature (AT) can be used as an indicator of the setting time. The statistical analysis of the data for the initial and final setting time of all mix designs used in this research is presented in Table 4-6 and Table 4-7, respectively.

**Table 4-6: Average values of initial setting time and corresponding temperature of cement pastes**

| **Mix Design (W/CM= 0.37, 0.40, 0.43)** | **Average Initial Setting Time** (min.) | **Standard Deviation-σ** | **COV** (%) | **Average T** (°C) | **Standard Deviation-σ** | **COV** (%) |
|---|---|---|---|---|---|---|
| **GU (ref.)** | 235 | 25.32 | 11 | 25.6 | 0.75 | 3 |
| **GUL** | 237 | 29.91 | 13 | 27.1 | 0.90 | 3 |
| **GUbSF** | 273 | 35.17 | 13 | 31.4 | 0.42 | 1 |
| **HE** | 192 | 15.87 | 8 | 27.5 | 1.25 | 5 |

**Table 4-7: Average values of final setting time and corresponding temperature of cement pastes**

| **Mix Design (W/CM= 0.37, 0.40, 0.43)** | **Average Final Setting Time** (min.) | **Standard Deviation-σ** | **COV** (%) | **Average T** (°C) | **Standard Deviation-σ** | **COV** (%) |
|---|---|---|---|---|---|---|
| **GU (ref.)** | 315 | 40.81 | 13 | 29.2 | 1.21 | 4 |
| **GUL** | 309 | 41.23 | 13 | 31.8 | 2.13 | 7 |
| **GUbSF** | 300 | 38.28 | 13 | 38.0 | 2.07 | 5 |
| **HE** | 277 | 25.63 | 9 | 36.4 | 2.71 | 7 |

$\boldsymbol{\sigma} = \sqrt{\frac{\sum_{i=1}^{N}(X_i - \bar{X})^2}{N-1}}$ and Coefficient of Variation (COV)= $\sigma/\bar{X}$, where $\bar{X}$ is the average.

The low statistical standard deviations (σ), used to quantify the amount of variation or dispersion of initial and final setting times, and COV, a measure of relative variability, in Table 4-6 and Table 4-7 indicate that the average temperature values are close to the internal

temperatures of the cement paste mixtures. However, higher COV (or error) in calculating the average setting times have shown that the initial and final setting times were influenced by the W/CM ratio and therefore the calculated average values are not representative. In other words, the setting time of cement paste cannot be represented independently from the W/CM ratio.

Therefore, it can be concluded that the initial and final setting times happen when the internal temperature of the mixture is about 27±2°C and 33±2°C, respectively. More specifically, the setting time temperature of different cement types is tabulated in Table 4-8.

**Table 4-8: Average temperature as an indicator for setting time of cements**

| Cement Type | Average T(°C) at Initial Setting | Average T(°C) at Final Setting |
|---|---|---|
| **GU (ref.)** | 25.0±1.0 | 29.0±1.5 |
| **GUL** | 27.0±1.0 | 31.0±2.0 |
| **GUbSF** | 31.0±0.5 | 38.0±2.0 |
| **HE** | 27.0±1.5 | 36.0±3.0 |

### 4.3. Microstructure Level Test Results

The microstructure of cement pastes has been studied at various stages of the cement hydration process: at 2 hours (as it is the maximum allowable time for placing, compacting, and finishing a cement-based mixture, according to CSA A23.1), initial setting, final setting, and 24 hours. At each stage of testing, the pore solution cathodic analysis, hydration products, and microstructure crystals were studied and analyzed. The pore solution was only analyzed at 2 hours, since it is not possible to extract it from cement pastes beyond that time even when using the centrifuge technique.

### 4.3.1. Pore Solution Analysis

For each mix design and W/CM ratio, the pore solution ionic concentration/analysis, pH, density, and electrical conductivity were measured on pore solutions extracted at 2 hours of hydration. The process of solution sample extraction was described in Section 3.4.1. The process of extraction and preparation of solution samples took less than 15 minutes for every batch. In most of the cases, except HE 0.37 and HE 0.40, the vacuum suction method was used to extract the pore solution from the semi-hydrated mixture at 2 hours. For HE 0.37 and HE 0.40, the centrifuge method as described in Section 3.4.1 was employed. In that method, two samples of semi-hydrated cement paste were prepared and placed in two opposite spots of the sample holder in the centrifuge as illustrated in Figure 4-56.


**Figure 4-56: Sample set up in the centrifuge for pore solution extraction**

All extracted pore solution analyses were kept at room temperature for 24 hours and tested within a day.

#### 4.3.1.1. Pore solution density

The pore solution density, which is an indicator for solids in the extracted pore solution, for each of the cement pastes is tabulated in Table 4-9. Note the average density of distilled water was 1.003 g/cm$^3$.

**Table 4-9: Pore solution density**

| **Mix Design** | | **Density** (gr/cm$^3$) | | |
|---|---|---|---|---|
| **Cement** | **W/CM** | **Average** (3 measurements) | **Standard Deviation-σ** | **COV** (%) |
| **GU (ref.)** | **0.37** | 1.030 | 0.001 | 0.05 |
| | **0.40** | 1.027 | 0.003 | 0.27 |
| | **0.43** | 1.027 | 0.002 | 0.24 |
| **GUL** | **0.37** | 1.039 | 0.001 | 0.11 |
| | **0.40** | 1.032 | 0.001 | 0.12 |
| | **0.43** | 1.029 | 0.001 | 0.10 |
| **GUbSF** | **0.37** | 1.035 | 0.003 | 0.34 |
| | **0.40** | 1.027 | 0.003 | 0.27 |
| | **0.43** | 1.031 | 0.001 | 0.11 |
| **HE** | **0.37** | 1.039 | 0.004 | 0.34 |
| | **0.40** | 1.041 | 0.003 | 0.25 |
| | **0.43** | 1.037 | 0.002 | 0.18 |

The main purpose of conducting a density test was to control the quality of the pore solutions. In case a significant difference in the pore solution densities exists, the extracted solution was discarded, and another sample would be prepared. As reported in Table 4-9, the densities of the extracted pore solutions were acceptable; therefore, the extracted pore solutions were used for chemical analysis.

### 4.3.1.2. Pore solution chemical analysis and pH measurement

The pH of all cement mixtures was measured at the time of the solution extraction (at 2 hours) as shown in Figure 4-57.

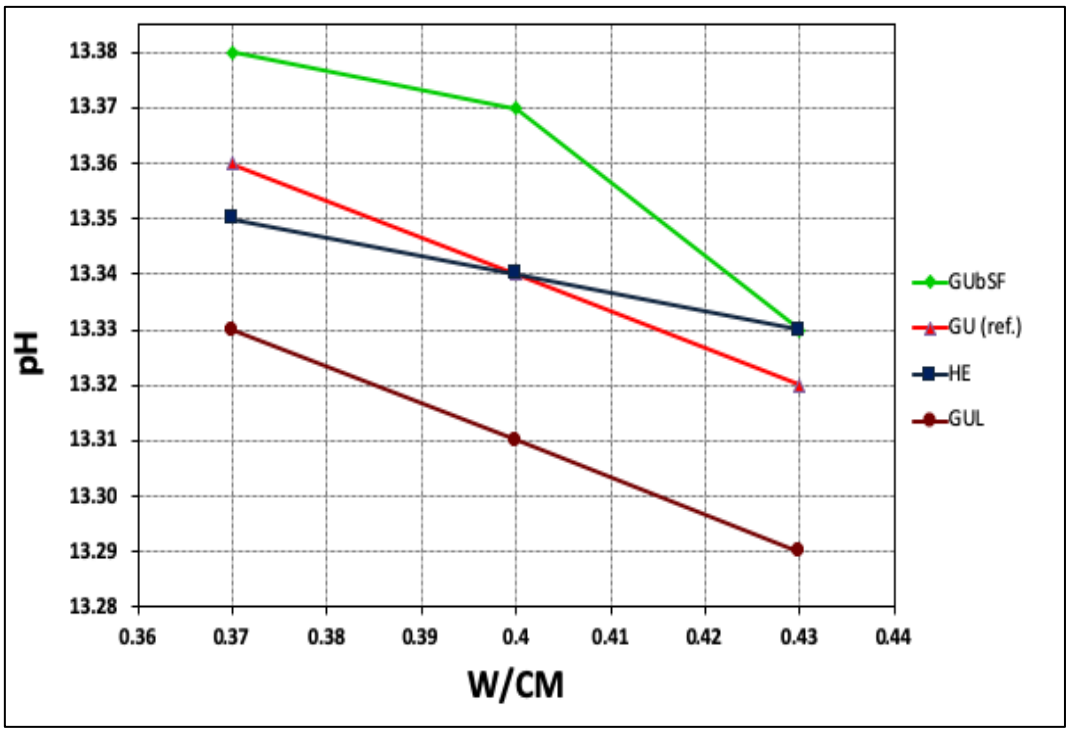


**Figure 4-57: pH determination of pore solutions extracted at 2 hours of hydration**

As explained in Section 3.4.1.1, the concentration of hydroxide ($OH^-$) can be calculated from the pH value, as tabulated in Table 4-10.

**Table 4-10: Concentration of hydroxide in 2-hour extracted pore solutions**

| Mix Design | | pH | $OH^-$ (mol/l) |
|---|---|---|---|
| **Cement** | **W/CM** | **Measured** | **Calculated** |
| **GU (ref.)** | **0.37** | 13.36 | 0.23 |
| | **0.40** | 13.34 | 0.22 |
| | **0.43** | 13.32 | 0.21 |
| **GUL** | **0.37** | 13.33 | 0.21 |
| | **0.40** | 13.31 | 0.20 |
| | **0.43** | 13.29 | 0.19 |
| **GUbSF** | **0.37** | 13.38 | 0.24 |
| | **0.40** | 13.37 | 0.23 |
| | **0.43** | 13.33 | 0.21 |
| **HE** | **0.37** | 13.35 | 0.22 |
| | **0.40** | 13.34 | 0.22 |
| | **0.43** | 13.33 | 0.21 |

When a cement powder is in contact with water, all the oxides in the powder (e.g., $SiO_2$, $Al_2O_3$, $Fe_2O_3$, CaO, MgO, $SO_3$) react with water. As a result, hydroxides are formed, as summarized below:

$$SiO_2 + H_2O \rightarrow H_2SiO_3.H_2O$$

$$Al_2O_3 + H_2O \rightarrow Al(OH)_3 + H_2$$

$$Fe_2O_3 + H_2O \rightarrow 2Fe(OH)_3$$

$$CaO + H_2O \rightarrow Ca(OH)$$

$$MgO + H_2O \rightarrow Mg(OH)_2$$

Inductively coupled plasma/optical emission spectrometry (ICP/OES) is a powerful tool for the determination of metals in a variety of different sample matrices. In this project, ICP-OES was an instrumental analytical technique that allowed the quantification of elemental traces (results of the cement hydration and leachates) into the extracted pore solution. ICP was selected in this research project for extracted pore solution ionic analysis because of its capability for efficient and reproducible vaporization, atomization, excitation, and ionization for a wide range of elements in various sample matrices, over other excitation sources (as reported and compared in the literature by Hou and Jones, 2000). This is due to the super high temperature of the plasma (up to 10,000 K). All extracted pore solutions were acidified with HCl before injecting them into the ICP-OES. As explained in Table 3-1, none of the mix designs contained slag, so acidifying was an acceptable practice to drop the pH of the solutions.

As shown in Figure 3-16, ICP-OES uses either the axial view (observation from the direction parallel to the plasma) or the radial view (observation from the direction perpendicular to the plasma) of the emission spectra to determine the elements in the solution. The instrument used in this project was the "Agilent Vista-Pro ICP-OES Simultaneous Charge Coupled Device (CCD) detector" from Varian Inc. with the radial view was used as shown in Figure 4-58.

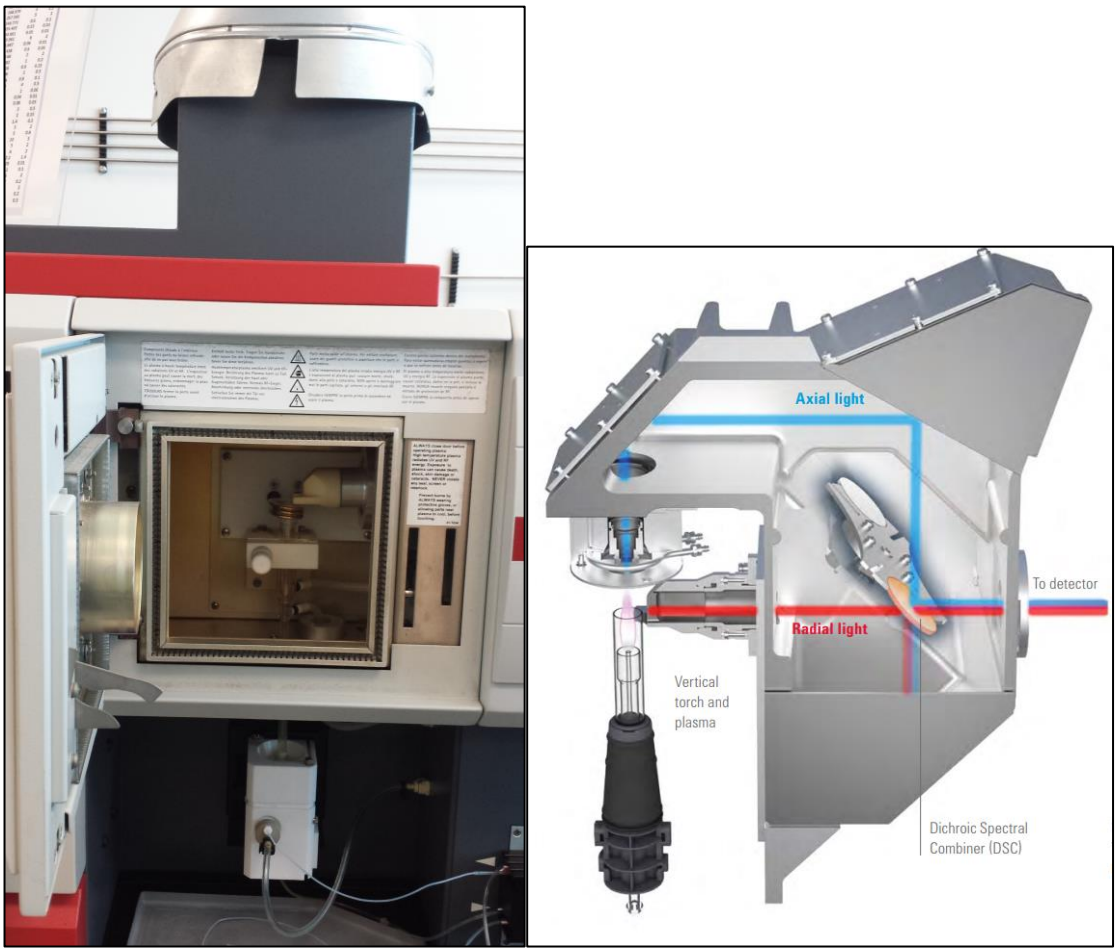


**Figure 4-58: Simultaneous CCD ICP-OES with radial view used in the project - Radial view of ICP-OES system (http://hpst.cz/sites/default/files/attachments/icp-oes-5991-8147en-ebook.pdf)**

Since there was some concern about the coexisting elements in the pore solution, the radial view was selected (the axial view is more affected by the coexisting elements in the sample). The conditions of the ICP-OES are summarized in Table 4-11. For the initial calibration solution preparation, the values provided by Kauppi et al. in Caruso et al., (2017) were used. After the first series of analysis was done and when all concentrations were not detected, the composition of the calibration solutions became adjusted to ensure that the whole range of concentration was measured.

**Table 4-11: ICP-OES instrument operating conditions**

| Item | Condition |
|---|---|
| Radio Frequency (RF) | 40 MHz |
| RF power of coil | 1150W |
| Wavelength detection range | 167–785 nm |
| Flow rate of Argon gas | 1.5L/min. in 1.5 L/min. increments |
| Flow rate of nebulizer gas | 0.65L/min. in 0.1 L/min. increments |
| Nebulizer type | Concentric glass |
| Flow rate of coolant gas | 12L/min. in 0.75 L/min. increments |
| Charge Coupled Device (CCD) resolution | 70,000 pixels |

The concentric type of nebulizer used was perfect for samples not containing possible fused silica. The extracted pore solutions were filtered since any particle that could cause clogging in the nebulizer. In this nebulizer, the sample solution was pumped and flowed through the inner capillary of the nebulizer. At a 90º angle, the argon gas is supplied into the outer tube, as shown in the setup in Figure 4-59. As the gas passed with high velocity into the tube of the pore solution sample, the stream sheared into tiny droplets.

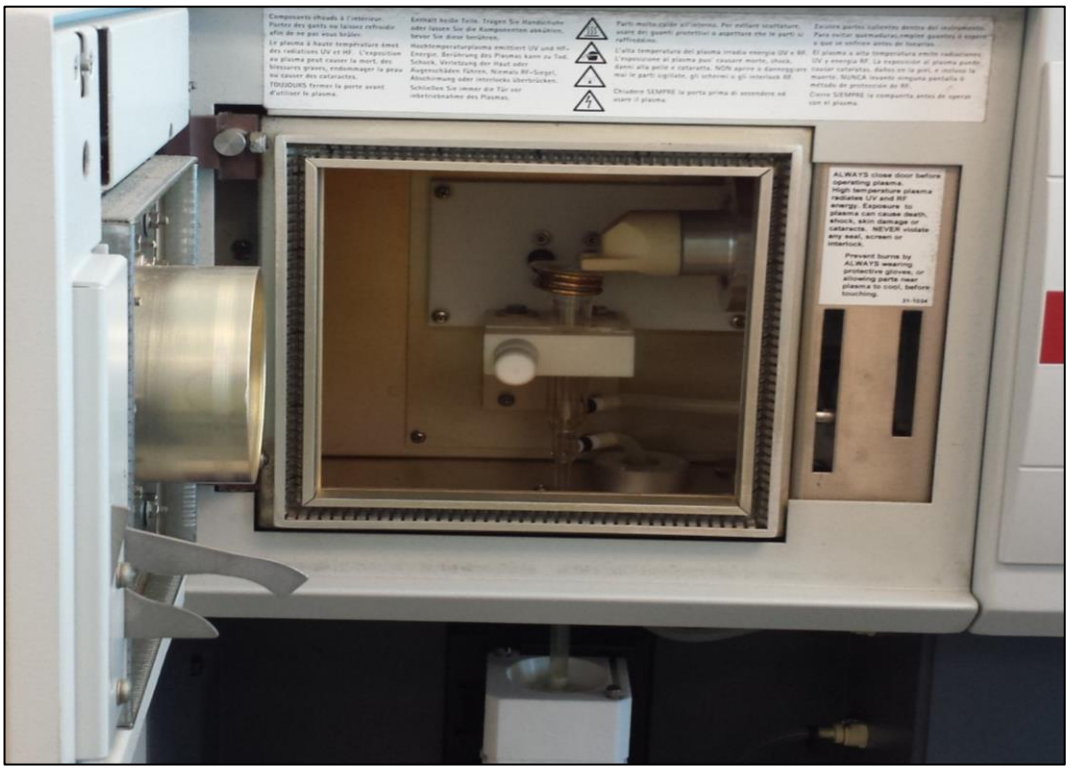


**Figure 4-59: Set up of the concentric nebulizer in the ICP-OES**

The qualitatively and quantitatively determination of the elements (ions) in the extracted pore solutions were determined by the "The Agilent MultiCal" software as the data processing system. The concentrations were calculated from the linear correspondence between the signal and the analyte concentration of the resulting signal, as summarized in Table 4-12.

**Table 4-12: Ionic concentration of pore solutions extracted from the cement pastes at 2 hours of hydration**

| Mix Design | | Cation Data (ppm) | | | | | | |
|---|---|---|---|---|---|---|---|---|
| **Cement** | **W/CM** | **$Al^{3+}$** | **$Ca^{2+}$** | **$K^{+}$** | **$Mg^{2+}$** | **$Na^{+}$** | **$S^{2-}$** | **Total** |
| **GU** (ref.) | **0.37** | 0.47 | 442.60 | 14745.60 | 0.009 | 2251.42 | 5272.26 | 22712.4 |
| | **0.40** | 0.42 | 401.77 | 14150.90 | 0.007 | 2068.30 | 4968.74 | 21590.1 |
| | **0.43** | 0.39 | 259.17 | 13696.30 | 0.014 | 1982.82 | 4761.66 | 20700.3 |
| **GUL** | **0.37** | 0.42 | 464.50 | 13993.20 | 0.048 | 2193.02 | 4675.30 | 21326.5 |
| | **0.40** | 0.38 | 611.52 | 13679.70 | 0.022 | 2015.10 | 4263.63 | 20570.4 |
| | **0.43** | 0.45 | 537.40 | 13521.00 | 0.074 | 1880.00 | 4085.94 | 20024.9 |
| **GUbSF** | **0.37** | 0.35 | 132.03 | 14450.30 | 0.024 | 3591.84 | 5736.75 | 23911.3 |
| | **0.40** | 0.34 | 96.39 | 14200.00 | 0.029 | 3239.28 | 5675.47 | 23211.5 |
| | **0.43** | 0.28 | 100.72 | 14199.00 | 0.024 | 3316.68 | 5413.98 | 23030.7 |
| **HE** | **0.37** | 4.11 | 3.93 | 16596.90 | 0.002 | 4274.04 | 7018.19 | 27897.2 |
| | **0.40** | 3.89 | 5.48 | 16456.30 | 0.001 | 3994.43 | 6690.14 | 27150.2 |
| | **0.43** | 2.69 | 16.01 | 16616.50 | 0.003 | 3663.78 | 6633.00 | 26932.0 |

The results in Table 4-12 show that ICP-OES is a perfect method to address the main challenge of element analysis in a complex matrix. A complex matrix contains elements at very high concentrations (e.g., sodium) and at very low concentrations (e.g., aluminum). This technique has shown the ability to detect and analyze elements in a wide range of concentrations. This is the advantage of this method compared to similar methods focusing on the analysis of thermodynamics and speciation aspects of cement pore solutions, as reported in previous researches.

The units of ppm reported in Table 4-12 should be converted to a unit comparable with other units of the measurement. For freshwater and other dilute aqueous solutions with density of 1.0, ppm is equal to mg/l, but the density values measured and presented in Table 4-9 show

that the density of the diluted solution is more than 1.0. Therefore, to normalize the measurements by ICP-OES, the concentration in ppm is divided by the density Table 4-13 and calculated as:

$$1.00 \text{ mg/l water} = (1.00 \text{ mg/l})\ (1 \text{ ml/density}_{relative})\ (1 \text{ l/1000 ml})(1000 \text{ mg/g})$$

**Table 4-13: Normalized ionic concentration of pore solutions extracted from the cement pastes at 2 hours of hydration**

| **Mix Design** | | **Cation Data** (mg/l) | | | | | | |
|---|---|---|---|---|---|---|---|---|
| **Cement** | **W/CM** | **$Al^{3+}$** | **$Ca^{2+}$** | **$K^{+}$** | **$Mg^{2+}$** | **$Na^{+}$** | **$S^{2-}$** | **Total** |
| **GU** (ref.) | **0.37** | 0.46 | 429.67 | 14314.98 | 0.009 | 2185.67 | 5118.29 | 22049.1 |
| | **0.40** | 0.41 | 391.03 | 13772.62 | 0.007 | 2013.01 | 4835.92 | 21013.0 |
| | **0.43** | 0.38 | 252.45 | 13341.43 | 0.014 | 1931.45 | 4638.29 | 20164.0 |
| **GUL** | **0.37** | 0.41 | 447.06 | 13467.89 | 0.046 | 2110.69 | 4499.79 | 20525.9 |
| | **0.40** | 0.36 | 592.71 | 13258.85 | 0.021 | 1953.11 | 4132.46 | 19937.5 |
| | **0.43** | 0.44 | 522.08 | 13135.45 | 0.072 | 1826.39 | 3969.43 | 19453.9 |
| **GUbSF** | **0.37** | 0.33 | 127.52 | 13956.78 | 0.023 | 3469.17 | 5540.82 | 23046.4 |
| | **0.40** | 0.33 | 93.81 | 13820.41 | 0.028 | 3152.69 | 5523.75 | 22785.7 |
| | **0.43** | 0.27 | 97.67 | 13769.29 | 0.024 | 3216.31 | 5250.13 | 22333.7 |
| **HE** | **0.37** | 3.96 | 3.78 | 15972.90 | 0.002 | 4113.35 | 6754.32 | 26848.3 |
| | **0.40** | 3.74 | 5.26 | 15802.96 | 0.001 | 3835.85 | 6424.53 | 26072.3 |
| | **0.43** | 2.60 | 15.44 | 16023.52 | 0.003 | 3533.03 | 6396.29 | 25970.9 |

As expected, the concentration of calcium in the pore solution extracted from the limestone or calcium carbonate ($CaCO_3$) cements (and then GU cements) was higher than that in other solution samples. In contrast, the percentage of CaO in the GUL powder was not significantly different from the CaO concentration in the other types of cement (refer to Appendix E). Therefore, it can be concluded that calcium is more bonded in GUbSF and HE hydration products than in GUL and GU, whereas much calcium was leached and stayed in the pore

solutions extracted from GU and GUL mixtures. Sulphur content has the second-highest concentrations in the pore solution. It is leached into the pore solution because of the addition of gypsum to the Portland cement (explained in Section 3.4.2). The leakage of it in the pore solution results in further reaction of $C_3A$ with it and further prevention of flash setting (reaction pattern was described in Section 3.4.2). As a result of that, ettringite is formed and as cement hydration continues, the concentration of sulphate ions in the pore solution decreases. As expected from high $SO_3$ percentage in HE cement (see Table 3-2), the highest amount of sulphur is noted in the pore solution extracted from HE mixtures. After HE, the GUbSF pore solution showed the highest sulphur content, while the $SO_3$ oxide percentage in GUbSF cement was the same as that in GU and GUL cements. This indicates that gypsum leached more into the pore solution of GUbSF mixtures compared to the other Portland cements.

Before analyzing the pore solution ionic concentration, it is important to mention that the oxide analysis of the cement powders (Figure A-1 to Figure A-4) has indicated that there is no significant difference between the chemical contents of the cements (except a higher percentage of $SiO_2$ in GUbSF). The 2-hour pore solution ionic concentration in the GU and GUL mixes was similar as shown in Table 4-13. The HE and GUbSF mixes showed higher ions leached into the pore solution from the cement powder particles. The highest number of ions in the pore solution corresponded to HE mixtures as illustrated in Figure 4-60. Aluminium (Al) leached into the pore solution in the HE mixtures much more than that in the other mixtures with other types of cement. On the other hand, the concentration of magnesium (Mg) in the pore solution extracted from the HE cement pastes was significantly lower than that in other pore solutions.

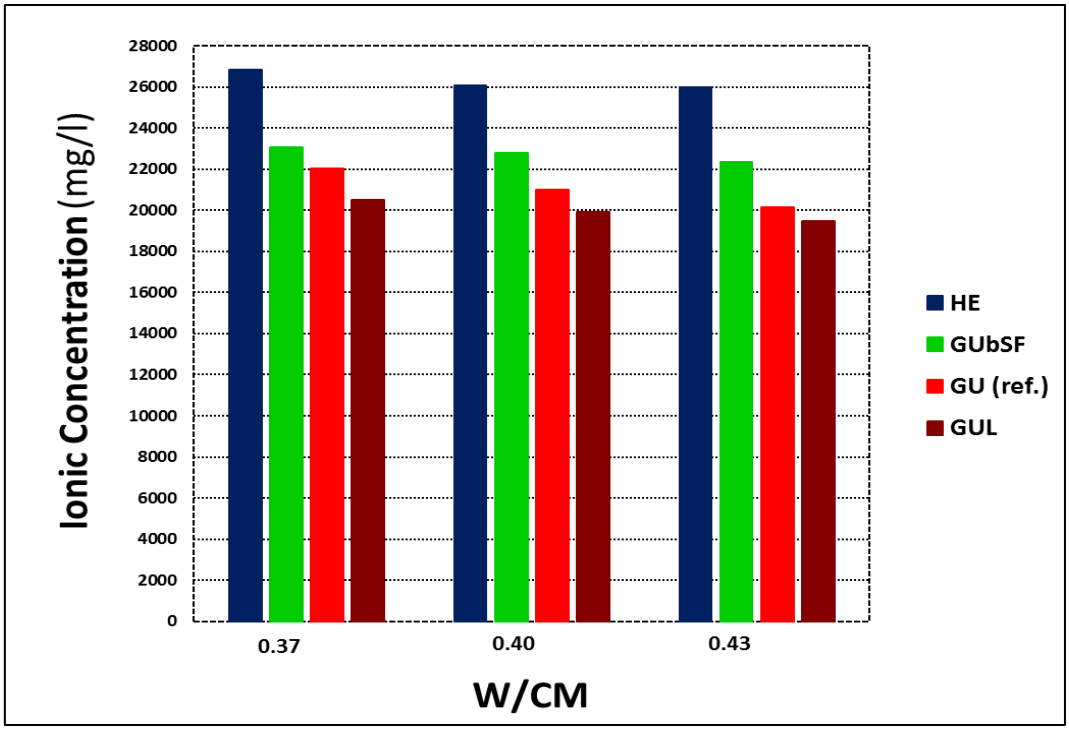


**Figure 4-60: Comparison of the ionic concentration in different cements pastes**

As illustrated in Figure 4-60, an increase in W/CM ratio resulted in a decrease in the total ionic concentration of the pore solution after 2 hours, but the effect was not significant. Also, it can be observed that the total ions leached into the pore solution was almost the same on GU and GUL mixtures during the first 2 hours of hydration (before the setting time starts).

ICP-OES has proved that it is a reliable method to detect elements in the pore solution at very high and very low concentration (such as $Al^{3+}$ and $Mg^{2+}$ in very low concentrations and others in very high concentrations as tabulated in Table 4-13).

The concentrations of hydroxides in the pore solution represent the alkalinity of the paste. As explained in Section 3.4.1.1, hydroxides are ionized in the ICP-OES instrument into ions. Therefore, the sum of alkalis (mainly sodium $Na^{+}$ and potassium $K^{+}$ as the highest concentrations) in the pore solution represents the alkalinity of the paste. The sum of alkalis of the cement paste extracted pore solutions after 2 hours of hydration is tabulated in Table 4-14.

**Table 4-14: Alkalinity of pore solution after 2 hours of hydration**

| **Mix Design** | | **Alkalis in Cement Powder*** (%) | **Sum of Alkalis** (ppm) |
|---|---|---|---|
| **Cement** | **W/CM** | **$Na_2Oe + K_2O$** | **$Na^+ + K^+$** |
| **GU** (ref.) | **0.37** | 0.60 | 16997 |
| | **0.40** | | 16219 |
| | **0.43** | | 15679 |
| **GUL** | **0.37** | 0.61 | 16186 |
| | **0.40** | | 15695 |
| | **0.43** | | 15401 |
| **GUbSF** | **0.37** | 0.86 | 18042 |
| | **0.40** | | 17439 |
| | **0.43** | | 17516 |
| **HE** | **0.37** | 0.86 | 20871 |
| | **0.40** | | 20451 |
| | **0.43** | | 20280 |

*Alkalis is Cement (eq %) = $Na_2O$ (%) + 0.658.$K_2O$ (%)

As calculated, the pore solution extracted from the HE pastes had the highest alkalis followed by GUbSF pore solution. The higher value of alkalis in the pore solution is because of that in dry cement powders. GU and GUL with similar alkalis content in dry powder showed similar alkalis in the pore solution, as well. It can be concluded that during the initial hours of hydration, $Na^+$ and $K^+$ did not contribute to the cement paste hydration and their concentration in all the mixtures stayed similar. This is opposite to the concentration of calcium $Ca^{++}$ which was leached and stayed in the pore solution (see Table 4-12) and it was higher in GUL and GU pore solutions compared to solutions from HE and GUbSF mixes, although the CaO% in all cement powders was almost equal as shown in Table 3-2. Therefore, it can be concluded that $Ca^{++}$ contributed to the early hydration in HE and GUbSF mixtures much more than in GU and GUL pastes.

#### 4.3.4.3. Pore solution electrical properties

To study the effect of the pore solution on the electrical properties of the mixture, the electrical properties of the extracted pore solution were studied. At the stages before the final setting time (fresh stage), the electrical properties of the pore solution are the most influencing factor on the electrical properties of the cement paste, as electrons transfer through the pore solution in the connected pore network. The instrument described in Section 3.4.1.3 measures the electrical conductance. To measure the electrical resistivity of the pore solutions, the extracted samples were diluted by ×1000, ×2000, and ×4000 times with water (except for GUL mixtures which were diluted for ×500, ×1000, and ×2000 times with water). Electrical conductance values (in milliSiemens-mS) presented in Table 4-15 are the "slope/1000" of the electrical conductance versus dilution linear relationship. All electrical conductance versus the dilution factor graphs are presented in Appendix F.

**Table 4-15: Electrical conductivity and resistivity of extracted pore solutions**

| **Mix Design** | | **Electrical Conductance** (mS) | **Electrical Resistance** (Ω) |
|---|---|---|---|
| **Cement** | **W/CM** | | |
| **GU** | 0.37 | 105.143 | 9.511 |
| | 0.40 | 99.800 | 10.020 |
| | 0.43 | 97.229 | 10.285 |
| **GUL** | 0.37 | 97.829 | 10.222 |
| | 0.40 | 89.671 | 11.152 |
| | 0.43 | 85.171 | 11.741 |
| **GUbSF** | 0.37 | 116.371 | 8.593 |
| | 0.40 | 109.571 | 9.126 |
| | 0.43 | 108.743 | 9.196 |
| **HE** | 0.37 | 124.657 | 8.022 |
| | 0.40 | 120.571 | 8.294 |
| | 0.43 | 116.829 | 8.560 |

Considering the fact that all pore solutions were kept at room temperature for 24 hours prior to testing, the specimens' temperature was similar and within the room temperature range. Therefore, electrical resistance normalization was not needed. Electrical resistance (or conductance) is affected by the samples' electrical properties, geometry and also the conductance-meter properties. To study the electrical properties of the extracted pore solution at 2 hours, the electrical resistivity (which is independent from samples size, shape, and measuring instrument probes) was determined. Then, the electrical resistivity of the pore solution can be compared to the electrical resistivity of the similar cement paste at 2 hours. To convert the measured electrical resistance (tabulated in Table 4-15) to electrical resistivity, the conversion factor calculated from a known solution (Sodium Chloride or NaCl with a standard conductivity of 20mS/cm at room temperature) was used. At room temperature, the NaCl solution was diluted with water by ×2000, ×4000, and ×6000 times. The electrical conductance of the NaCl solution (in micro Siemens) presented as the "slope/1000" of the electrical conductance versus the dilution linear relationship is shown in Figure 4-61.

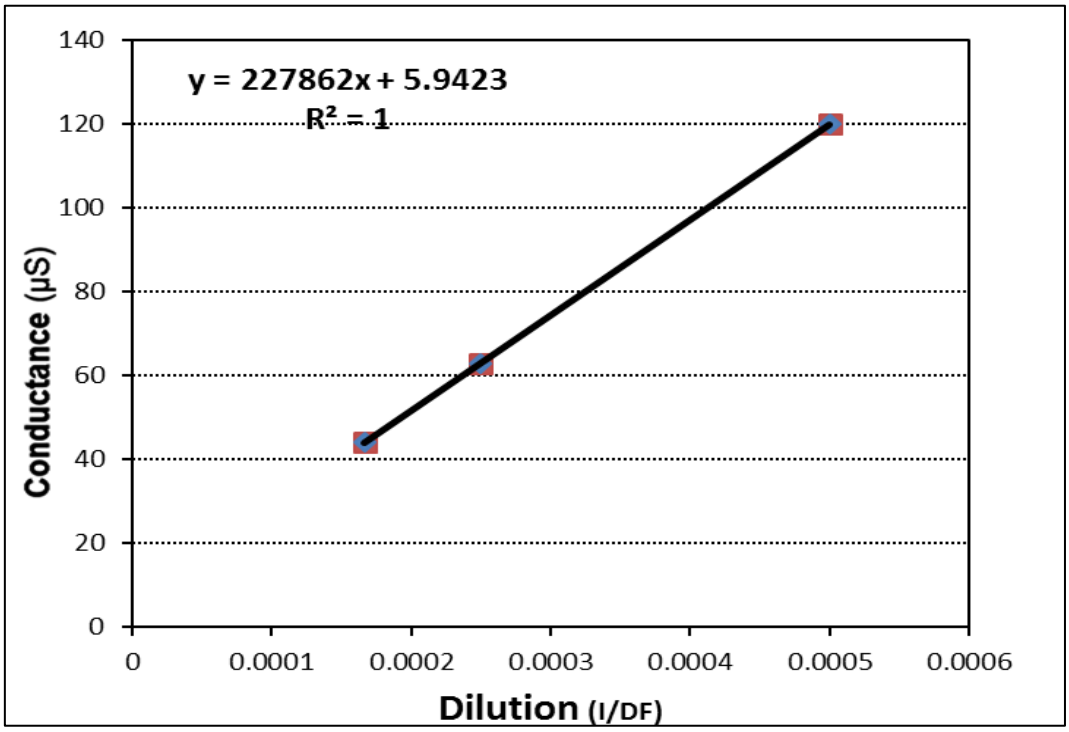


**Figure 4-61: Conductance measurement relationship with the dilution factor of the standard known solution**

The slope of the graph is the conductivity of the solution in micro Siemens per unit length. By dividing it by 100, the conductivity of the standard solution NaCl was determined as 228 mS per unit length (resistance= 4.386 Ω per unit length). As reported by the supplier (Ricca Chemical Co.), the conductivity of the standard solution at room temperature (22-23°C) is 20 mS/cm. Therefore, the resistivity of the solution is 0.05 kΩ.cm. The conversion factor for resistance to resistivity is 11.4 cm. By the help of the conversion factors, the electrical resistivity of the extracted pore solutions from the 2-hour hydrated cement pastes is calculated, and they tabulated in Table 4-16.

**Table 4-16: Electrical resistivity and conductivity of extracted pore solution at 2 hours of hydration**

| **Mix Design** | | **Electrical Conductivity** (mS/cm) | **Electrical Resistivity** (Ω.cm) |
|---|---|---|---|
| **Cement** | **W/CM** | | |
| **GU** | 0.37 | 9.23 | 108.42 |
| | 0.40 | 8.76 | 114.23 |
| | 0.43 | 8.53 | 117.25 |
| **GUL** | 0.37 | 8.59 | 116.53 |
| | 0.40 | 7.87 | 127.13 |
| | 0.43 | 7.48 | 133.85 |
| **GUbSF** | 0.37 | 10.21 | 97.96 |
| | 0.40 | 9.62 | 104.04 |
| | 0.43 | 9.54 | 104.83 |
| **HE** | 0.37 | 10.94 | 91.45 |
| | 0.40 | 10.58 | 94.55 |
| | 0.43 | 10.25 | 97.58 |

As opposed to the electrical resistivity of cement pastes, it is observed that the electrical resistance of the pore solution is directly proportional to the W/CM as illustrated in Figure 4-62.

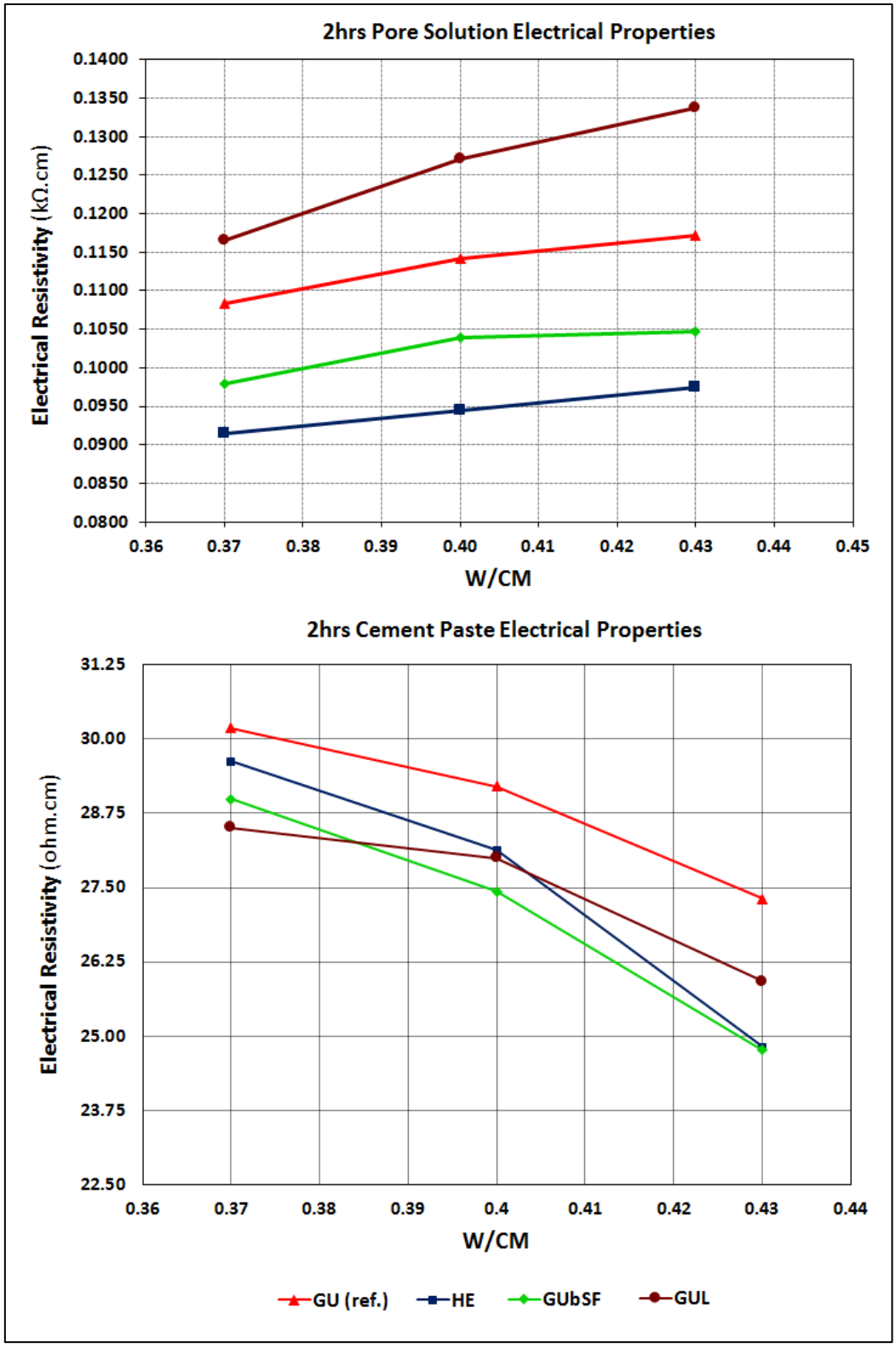


**Figure 4-62: Comparison between the 2-hour electrical resistivity of cement paste and its pore solution**

It is noted that the electrical resistivity development in the pore solution behaves oppositely to that of the cement paste. Due to the reduction in the ionic concentration in the pore solution with an increase in the water content of the mix design (shown in Figure 4-60), electrons cannot transfer through the pore solution as easily as in low W/CM mixtures. Therefore, the electrical conductivity of the pore solution decreases and its resistivity increases. However, the trends are opposite for the electrical resistivity of the cement paste at the same stage of hydration (2 hours). It shows that the electrical resistivity of the matrix even at 2 hours of hydration is influenced by the formation of the pore structure much more than by the electrical resistivity of the pore solution in the pore network. In other words, focusing on the electrical properties of the pore solution cannot provide a proper understanding of the electrical properties development of the hydrating cement matrix, even at the early ages of hydration.

It has been noted that in studying the electrical conductivity of the pore solution, the charges of ions is not important as the concentration of ions in a unit volume of the pore solution, as tabulated in Table 4-12. This is because electrons (or protons) transfer from an electrode to the other with the help of the ions, so the higher the number of ions in the pore solution, the higher is the conductivity of the pore solution (as shown in Figure 4-62).

### 4.3.2. Hydration Products Quantity

Thermos-Gravimetric Analysis (TGA) provides quantitative measurement of the mass change in materials associated with thermal degradation. In this research, all cement paste samples were analyzed by Thermos-Gravimetric Analysis (TGA) to investigate the composition of the semi-hydrated cement paste (more importantly the Calcium Hydroxide-CH) at different times. Derivatives Thermo-gravimetric Analysis (DTA) and Thermos-Gravimetric Analysis (TGA) methods were carried out on cement paste samples to study the hydration products and determine the degree of hydration at each stage of testing. All test results were analyzed with the "Universal V.4.5A TA Instruments" software as shown in the appendix C. In this project, calcium hydrate (CH) and 1000°C loss of ignition were quantified.

The samples were taken into the TGA analyser, where they were placed in a ceramic crucible and heated from room temperature to 1000°C at a heating rate of 10°C.min$^{-1}$ using Nitrogen

as a medium under static condition. TGA/DTA were done, simultaneously. The atmosphere was purged with Nitrogen to prevent oxidation or other undesired reactions. The analyzer usually consists of a high-precision balance with a pan (generally platinum) loaded with the sample to measure the changes in its weight.

Each phase is characterized by two factors:

a) Temperature range where hydration product decomposition is observed, and

b) The specific mass loss in that temperature range.

Analysis in TGA was carried out by raising the temperature gradually and plotting weight against temperature as shown in figures in Appendix B. It is important to mention that all aspects of the TGA testing, including sample loading, sample weighing (before and during testing), auto sampler movement (in case that more than one sample was placed in the carousel), furnace movement, pan unloading after the test and furnace cooling, are automated and software controlled.

It can be observed that in every TGA curve three or four significant weight loss steps are noted. The TGA/DTA results are tabulated in Table 4-17 to Table 4-28.

**Table 4-17: TGA/DTA results for GU 0.37 cement pastes**

| Mix Design | | Hydration Stage | Temperature Range (°C) | Peak Temperature (°C) | Weight Loss (%) |
|---|---|---|---|---|---|
| **Cement** | **W/CM** | | | | |
| **General Use Cement-GU (ref.)** | **0.37** | **2 hours** | **23-100** | 48.5 | 0.38 |
| | | | **100-350** | 100.9 | 0.91 |
| | | | **350-500** | 406.8 | 1.14 |
| | | | **>500** | 641.6 | 1.58 |
| | | **At Initial Setting** | **23-100** | 49.3 | 0.53 |
| | | | **100-350** | 101.8 | 1.16 |
| | | | **350-500** | 418.1 | 1.49 |
| | | | **>500** | 641.6 | 1.80 |
| | | **At Final Setting** | **23-100** | 50.1 | 0.61 |
| | | | **100-350** | 101.8 | 1.28 |
| | | | **350-500** | 416.4 | 1.78 |
| | | | **>500** | 639.9 | 1.95 |
| | | **24 hours** | **23-100** | 56.6 | 1.75 |
| | | | **100-350** | N.D. | N.D. |
| | | | **350-500** | 421.0 | 8.57 |
| | | | **>500** | 645.5 | 4.06 |

*N.D.: Not Detected*

**Table 4-18: TGA/DTA results for GU 0.40 cement pastes**

| Mix Design | | Hydration Stage | Temperature Range (°C) | Peak Temperature (°C) | Weight Loss (%) |
|---|---|---|---|---|---|
| **Cement** | **W/CM** | | | | |
| **General Use Cement-GU (ref.)** | **0.40** | **2 Hours** | **23-100** | 50.0 | 0.40 |
| | | | **100-350** | 102.0 | 0.89 |
| | | | **350-500** | 410.3 | 1.19 |
| | | | **>500** | 643.9 | 1.61 |
| | | **At Initial Setting** | **23-100** | 51.8 | 0.59 |
| | | | **100-350** | 102.1 | 1.30 |
| | | | **350-500** | 419.9 | 1.60 |
| | | | **>500** | 640.0 | 1.75 |
| | | **At Final Setting** | **23-100** | 51.8 | 0.61 |
| | | | **100-350** | 101.2 | 1.24 |
| | | | **350-500** | 418.9 | 1.86 |
| | | | **>500** | 642.0 | 1.99 |
| | | **24 Hours** | **23-100** | 40.3 | 0.98 |
| | | | **100-350** | 59.3 | 1.60 |
| | | | **350-500** | 420.2 | 8.00 |
| | | | **>500** | 649.2 | 3.40 |

**Table 4-19: TGA/DTA results for GU 0.43 cement pastes**

| Mix Design | | Hydration Stage | Temperature Range (°C) | Peak Temperature (°C) | Weight Loss (%) |
|---|---|---|---|---|---|
| **Cement** | **W/CM** | | | | |
| **General Use Cement-GU (ref.)** | **0.43** | **2 Hours** | **23-100** | 50.9 | 0.41 |
| | | | **100-350** | 102.6 | 0.88 |
| | | | **350-500** | 411.6 | 1.16 |
| | | | **>500** | 644.8 | 1.62 |
| | | **At Initial Setting** | **23-100** | 51.7 | 0.61 |
| | | | **100-350** | 101.8 | 1.32 |
| | | | **350-500** | 420.5 | 1.85 |
| | | | **>500** | 639.9 | 1.73 |
| | | **At Final Setting** | **23-100** | 52.5 | 0.57 |
| | | | **100-350** | 101.0 | 1.25 |
| | | | **350-500** | 420.5 | 1.98 |
| | | | **>500** | 642.4 | 2.01 |
| | | **24 Hours** | **23-100** | 35.6 | 0.31 |
| | | | **100-350** | 58.2 | 1.58 |
| | | | **350-500** | 418.1 | 7.23 |
| | | | **>500** | 648.8 | 3.34 |

**Table 4-20: TGA/DTA results for GUL 0.37 cement pastes**

| Mix Design | | Hydration Stage | Temperature Range (°C) | Peak Temperature (°C) | Weight Loss (%) |
|---|---|---|---|---|---|
| **Cement** | **W/CM** | | | | |
| **General Use Limestone Cement-GUL** | **0.37** | **2 Hours** | **23-100** | 49.8 | 0.70 |
| | | | **100-350** | 93.4 | 1.02 |
| | | | **350-500** | 400.7 | 1.00 |
| | | | **>500** | 681.3 | 3.88 |
| | | **At Initial Setting** | **23-100** | 47.4 | 0.79 |
| | | | **100-350** | 92.6 | 1.37 |
| | | | **350-500** | 412.8 | 1.57 |
| | | | **>500** | 663.5 | 4.32 |
| | | **At Final Setting** | **23-100** | 44.9 | 0.59 |
| | | | **100-350** | 95.9 | 1.40 |
| | | | **350-500** | 425.0 | 1.71 |
| | | | **>500** | 658.6 | 4.21 |
| | | **24 Hours** | **23-100** | NA | NA |
| | | | **100-350** | 50.6 | 1.86 |
| | | | **350-500** | 415.2 | 9.49 |
| | | | **>500** | 662.7 | 5.39 |

**Table 4-21: TGA/DTA results for GUL 0.40 cement pastes**

| Mix Design | | Hydration Stage | Temperature Range (°C) | Peak Temperature (°C) | Weight Loss (%) |
|---|---|---|---|---|---|
| **Cement** | **W/CM** | | | | |
| **General Use Limestone Cement-GUL** | **0.40** | **2 Hours** | **23-100** | 55.4 | 1.13 |
| | | | **100-350** | 95.1 | 1.41 |
| | | | **350-500** | 425.0 | 2.09 |
| | | | **>500** | 683.7 | 4.60 |
| | | **At Initial Setting** | **23-100** | 53.9 | 1.11 |
| | | | **100-350** | N.D. | N.D. |
| | | | **350-500** | 411.4 | 3.39 |
| | | | **>500** | 680.9 | 4.44 |
| | | **At Final Setting** | **23-100** | 51.9 | 0.78 |
| | | | **100-350** | 97.2 | 1.29 |
| | | | **350-500** | 406.0 | 1.60 |
| | | | **>500** | 677.6 | 4.32 |
| | | **24 Hours** | **23-100** | 63.5 | 1.86 |
| | | | **100-350** | 171.1 | 61.18 |
| | | | **350-500** | 427.7 | 52.68 |
| | | | **>500** | 689.1 | 5.71 |

*N.D.: Not Detected*

**Table 4-22: TGA/DTA results for GUL 0.43 cement pastes**

| Mix Design | | Hydration Stage | Temperature Range (°C) | Peak Temperature (°C) | Weight Loss (%) |
|---|---|---|---|---|---|
| **Cement** | **W/CM** | | | | |
| **General Use Limestone Cement-GUL** | **0.43** | **2 Hours** | **23-100** | 45.1 | 0.26 |
| | | | **100-350** | 94.5 | 0.75 |
| | | | **350-500** | 406.0 | 1.74 |
| | | | **>500** | 655.2 | 4.21 |
| | | **At Initial Setting** | **23-100** | 53.0 | 0.63 |
| | | | **100-350** | N.D. | N.D. |
| | | | **350-500** | 419.3 | 3.68 |
| | | | **>500** | 669.9 | 4.47 |
| | | **At Final Setting** | **23-100** | 51.9 | 0.40 |
| | | | **100-350** | 94.5 | 0.97 |
| | | | **350-500** | 417.5 | 1.88 |
| | | | **>500** | 672.1 | 88.95 |
| | | **24 Hours** | **23-100** | 72.5 | 2.06 |
| | | | **100-350** | 159.9 | 1.15 |
| | | | **350-500** | 400.7 | 8.12 |
| | | | **>500** | 692.1 | 5.00 |

*N.D.: Not Detected*

**Table 4-23: TGA/DTA results for GUbSF 0.37 cement pastes**

| Mix Design | | Hydration Stage | Temperature Range (°C) | Peak Temperature (°C) | Weight Loss (%) |
|---|---|---|---|---|---|
| **Cement** | **W/CM** | | | | |
| **General Use Silica Fume Cement-GUbSF** | **0.37** | **2 Hours** | **23-100** | 47.4 | 0.31 |
| | | | **100-350** | 93.3 | 0.93 |
| | | | **350-500** | 413.0 | 1.42 |
| | | | **>500** | 638.0 | 1.33 |
| | | **At Initial Setting** | **23-100** | 50.9 | 0.45 |
| | | | **100-350** | 96.0 | 1.13 |
| | | | **350-500** | 425.8 | 1.94 |
| | | | **>500** | 645.4 | 1.80 |
| | | **At Final Setting** | **23-100** | 49.3 | 0.53 |
| | | | **100-350** | 94.0 | 1.22 |
| | | | **350-500** | 409.6 | 1.88 |
| | | | **>500** | 642.7 | 1.69 |
| | | **24 Hours** | **23-100** | 54.8 | 1.73 |
| | | | **100-350** | 98.1 | 3.00 |
| | | | **350-500** | 421.1 | 6.52 |
| | | | **>500** | 644.8 | 4.03 |

**Table 4-24: TGA/DTA results for GUbSF 0.40 cement pastes**

| Mix Design | | Hydration Stage | Temperature Range (°C) | Peak Temperature (°C) | Weight Loss (%) |
|---|---|---|---|---|---|
| **Cement** | **W/CM** | | | | |
| **General Use Silica Fume Cement-GUbSF** | **0.40** | **2 Hours** | **23-100** | 49.0 | 0.58 |
| | | | **100-350** | 94.3 | 1.13 |
| | | | **350-500** | 415.2 | 1.46 |
| | | | **>500** | 643.3 | 1.33 |
| | | **At Initial Setting** | **23-100** | 47.4 | 0.71 |
| | | | **100-350** | 94.0 | 1.56 |
| | | | **350-500** | 404.2 | 1.73 |
| | | | **>500** | 640.0 | 1.61 |
| | | **At Final Setting** | **23-100** | 50.1 | 1.03 |
| | | | **100-350** | 94.7 | 2.00 |
| | | | **350-500** | 413.6 | 2.77 |
| | | | **>500** | 638.7 | 2.09 |
| | | **24 Hours** | **23-100** | 64.5 | 1.95 |
| | | | **100-350** | N.D. | N.D. |
| | | | **350-500** | 436.1 | 8.95 |
| | | | **>500** | 649.8 | 12.95 |

*N.D.: Not Detected*

**Table 4-25: TGA/DTA results for GUbSF 0.43 cement pastes**

| Mix Design | | Hydration Stage | Temperature Range (°C) | Peak Temperature (°C) | Weight Loss (%) |
|---|---|---|---|---|---|
| **Cement** | **W/CM** | | | | |
| **General Use Silica Fume Cement-GUbSF** | **0.43** | **2 Hours** | **23-100** | 46.4 | 0.24 |
| | | | **100-350** | 92.5 | 0.75 |
| | | | **350-500** | 406.0 | 1.53 |
| | | | **>500** | 634.2 | 1.38 |
| | | **At Initial Setting** | **23-100** | 47.4 | 0.43 |
| | | | **100-350** | 93.4 | 1.12 |
| | | | **350-500** | 412.8 | 2.40 |
| | | | **>500** | 637.6 | 2.10 |
| | | **At Final Setting** | **23-100** | 53.0 | 0.48 |
| | | | **100-350** | 97.5 | 1.24 |
| | | | **350-500** | 418.5 | 2.47 |
| | | | **>500** | 640.0 | 2.23 |
| | | **24 Hours** | **23-100** | 55.9 | 1.45 |
| | | | **100-350** | N.D. | N.D. |
| | | | **350-500** | 418.9 | 8.61 |
| | | | **>500** | 647.8 | 3.84 |

*N.D.: Not Detected*

**Table 4-26: TGA/DTA results for HE 0.37 cement pastes**

| Mix Design | | Hydration Stage | Temperature Range (°C) | Peak Temperature (°C) | Weight Loss (%) |
|---|---|---|---|---|---|
| **Cement** | **W/CM** | | | | |
| **High Early Cement-HE** | **0.37** | **2 Hours** | **23-100** | 53.2 | 0.18 |
| | | | **100-350** | 94.5 | 0.62 |
| | | | **350-500** | 414.1 | 1.65 |
| | | | **>500** | 632.8 | 1.69 |
| | | **At Initial Setting** | **23-100** | 53.9 | 0.24 |
| | | | **100-350** | 93.2 | 0.65 |
| | | | **350-500** | 409.4 | 1.69 |
| | | | **>500** | 636.9 | 1.80 |
| | | **At Final Setting** | **23-100** | 58.6 | 0.41 |
| | | | **100-350** | 97.2 | 0.78 |
| | | | **350-500** | 419.6 | 1.87 |
| | | | **>500** | 643.7 | 2.04 |
| | | **24 Hours** | **23-100** | 60.3 | 1.76 |
| | | | **100-350** | N.D. | N.D. |
| | | | **350-500** | 420.1 | 9.23 |
| | | | **>500** | 641.6 | 4.43 |

*N.D.: Not Detected*

**Table 4-27: TGA/DTA results for HE 0.40 cement pastes**

| Mix Design | | Hydration Stage | Temperature Range (°C) | Peak Temperature (°C) | Weight Loss (%) |
|---|---|---|---|---|---|
| **Cement** | **W/CM** | | | | |
| **High Early Cement-HE** | **0.40** | **2 Hours** | **23-100** | 45.1 | 0.30 |
| | | | **100-350** | 95.2 | 0.76 |
| | | | **350-500** | 412.8 | 1.19 |
| | | | **>500** | 629.5 | 1.12 |
| | | **At Initial Setting** | **23-100** | 48.5 | 0.69 |
| | | | **100-350** | 94.5 | 1.40 |
| | | | **350-500** | 422.9 | 1.89 |
| | | | **>500** | 636.9 | 2.01 |
| | | **At Final Setting** | **23-100** | 52.5 | 0.83 |
| | | | **100-350** | 97.9 | 1.58 |
| | | | **350-500** | 423.6 | 2.30 |
| | | | **>500** | 636.9 | 2.24 |
| | | **24 Hours** | **23-100** | 59.3 | 2.46 |
| | | | **100-350** | 121.6 | 4.32 |
| | | | **350-500** | 424.3 | 6.40 |
| | | | **>500** | 643.7 | 4.79 |

**Table 4-28: TGA/DTA results for HE 0.43 cement pastes**

| Mix Design | | Hydration Stage | Temperature Range (°C) | Peak Temperature (°C) | Weight Loss (%) |
|---|---|---|---|---|---|
| **Cement** | **W/CM** | | | | |
| **High Early Cement-HE** | **0.43** | **2 Hours** | **23-100** | 64.0 | 0.18 |
| | | | **100-350** | 97.2 | 0.54 |
| | | | **350-500** | 412.1 | 1.44 |
| | | | **>500** | 641.0 | 1.65 |
| | | **At Initial Setting** | **23-100** | 65.4 | 0.30 |
| | | | **100-350** | 97.2 | 0.59 |
| | | | **350-500** | 416.8 | 1.77 |
| | | | **>500** | 642.3 | 1.91 |
| | | **At Final Setting** | **23-100** | 68.8 | 0.75 |
| | | | **100-350** | 97.9 | 0.70 |
| | | | **350-500** | 427.7 | 2.78 |
| | | | **>500** | 644.4 | 3.64 |
| | | **24 Hours** | **23-100** | 78.9 | 2.38 |
| | | | **100-350** | N.D. | N.D. |
| | | | **350-500** | 420.9 | 8.22 |
| | | | **>500** | 643.7 | 4.07 |

*N.D.: Not Detected*

TGA/DTA graphs for each mix design at four testing times are presented in Appendix C. The graphs show four major endothermic effects during the cement hydration. The corresponding peaks overlaps in the graphs are due to the dynamic heating process. The sharp peaks in the DTA graphs account for a major part of the weight loss.

The temperature ranges up to 100°C is associated with the drying (capillary pore residual water or alcohol) and/or with the de-hydration of ettringite (at a later stage of hydration such as 1-day in this project). The weight loss at this stage increased as the hydration proceeded (more water/alcohol or ettringite content). As shown by Pane and Hansen (2004), the

chemically bound water obtained in this stage is proportional to the amount of hydration. In addition, the temperature at which the drying happened increased as the hydration proceeded. The 100°C weight loss percentage in all mixtures at different stages of hydration is illustrated in Figure 4-63 to Figure 4-66.

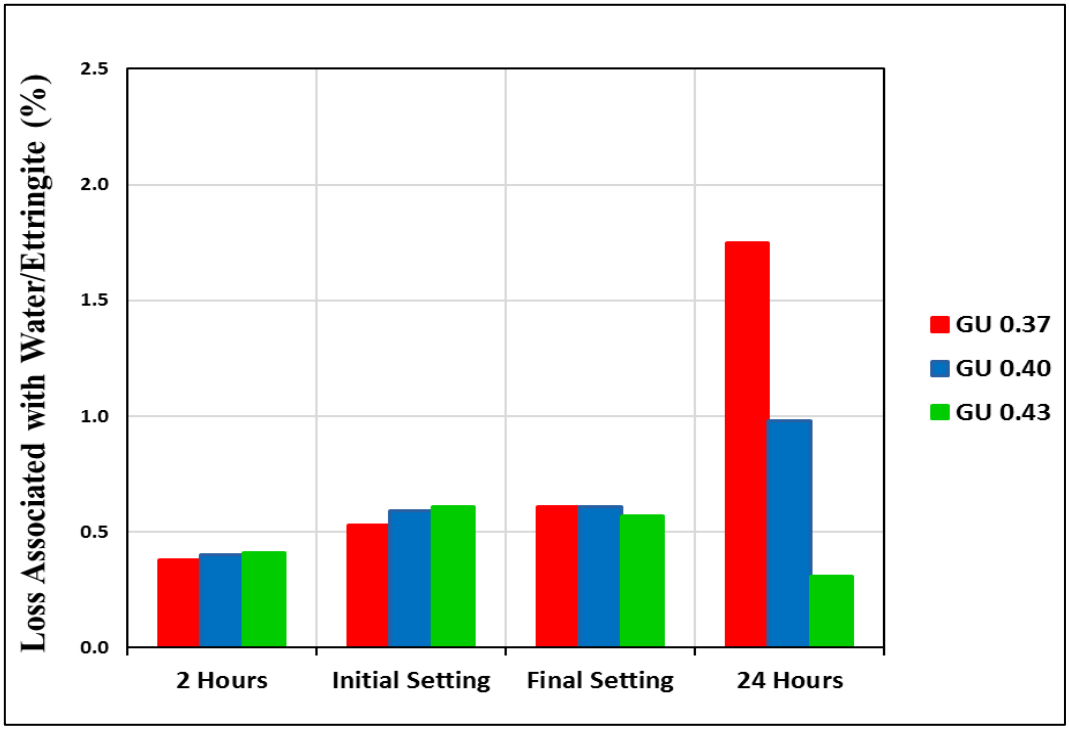


**Figure 4-63: Weight loss at 100°C in stages of hydration of GU cement pastes**

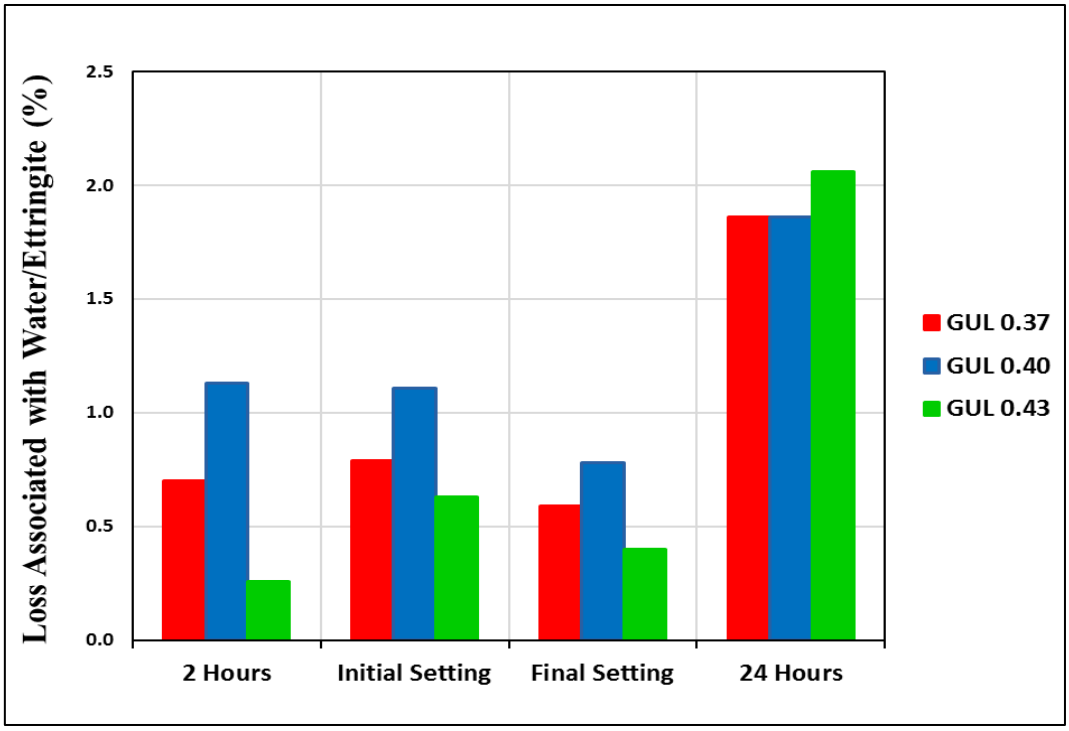


**Figure 4-64: Weight loss at 100°C in stages of hydration of GUL cement pastes**

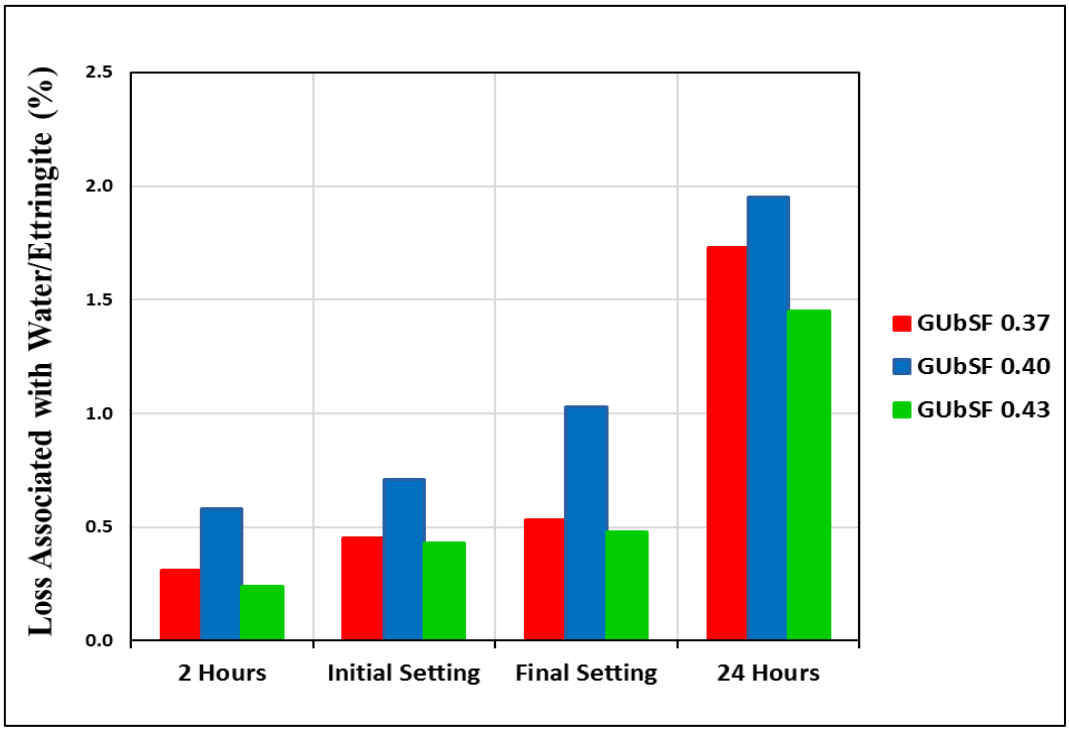


**Figure 4-65: Weight loss at 100°C in stages of hydration of GUbSF cement pastes**

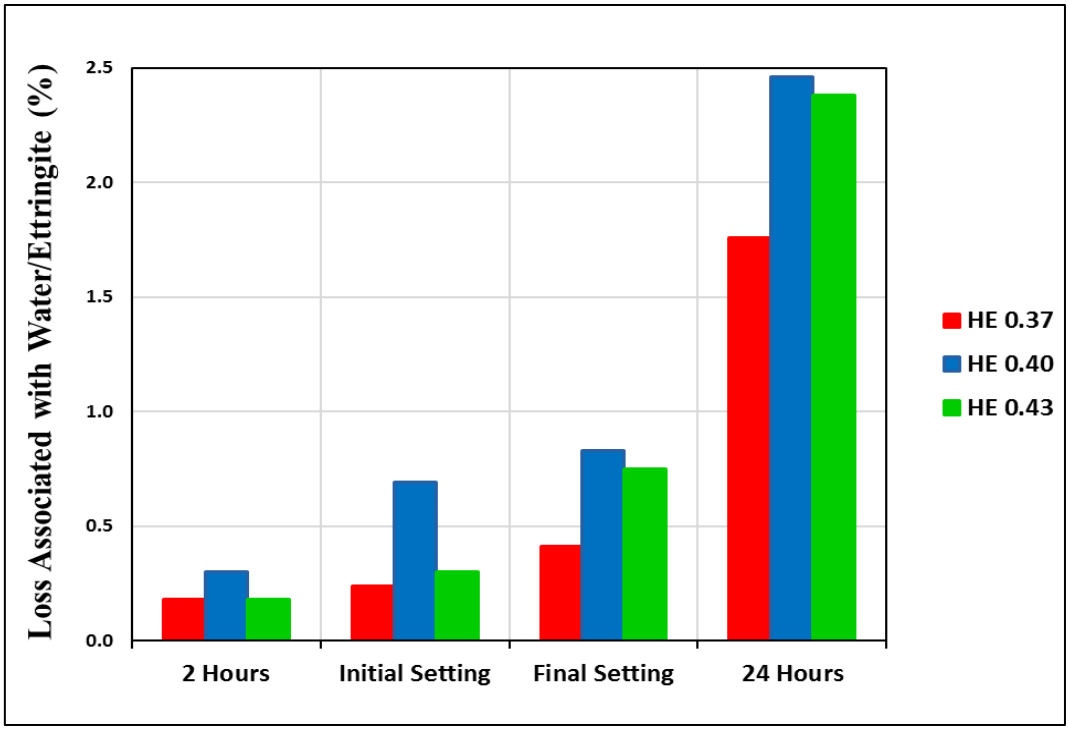


**Figure 4-66: Weight loss at 100°C in stages of hydration of HE cement pastes**

In this stage, the replacement of cement with limestone resulted in about 40-50% less loss at early ages, but almost no influence at later age loss (probably due to less ettringite formation). The same trends were observed for the GUbSF and HE mixtures TGA results in comparison to the GU (reference) mixtures.

The second stage (100-350°C) corresponds to the dehydration of C-S-H, ettringite (AFt) and mono-sulphate (AFm). Detecting C-S-H with the DTA curves analysis was not possible, as visible peaks were not observed for C-S-H in this stage. In opposite, ettringite formation could be detected by analyzing the TGA/DTA graphs in this temperature range. It was observed that in all mixtures, ettringite is decreased and converts to AFm as cement hydrates. In 1-day samples, the ettringite peak was detected at about 90-100°C, and formation of AFm was observed around 100-120°C. Among all the mixes, the loss representing ettringite and AFm is the highest in the HE mixtures followed by the GUbSF mixtures after 1 day of hydration. However, when comparing GU and GUL mixtures at 1 day, the amount of ettringite and AFm detected is almost the same.

The next temperature range of 350-500°C is associated to the de-hydration of Portlandite (CH). It can be concluded from the values in Table 4-17 to Table 4-28 that the addition of limestone (GUL mixtures) resulted in 0.5-1.0% increase in the mass loss (%) in the DTA graphs (more CH formation in the mixture) at all stages of hydration compared to GU mixtures. As the cement paste hydrated more, the amount of Portlandite detected by the TGA technique, increased. The highest amount of CH was observed in the HE mixtures followed by that in the GUbSF mixtures. It shows that HE and GUbSF mixtures had more hydration products than the reference mixture (GU cement paste). Replacement of cement with limestone resulted in more hydration products, as well.

The TGA curves were also used to calculate the amount of Portlandite, as the main by-product of cement hydration, and the change in its content, based on the formula given in Equation 3-14.

The changes in Portlandite content with W/CM ratio are shown in Figure 4-67 to Figure 4-70.

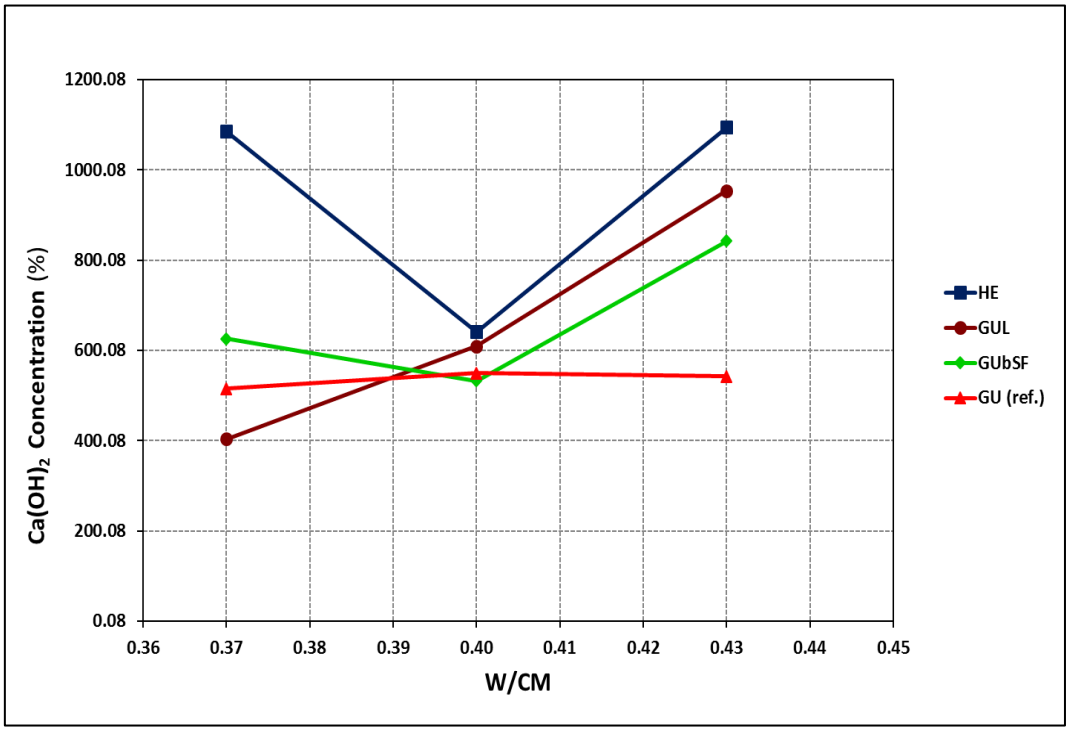


**Figure 4-67: Changes in $Ca(OH)_2$ concentration with W/CM ratio at 2 hours of hydration**

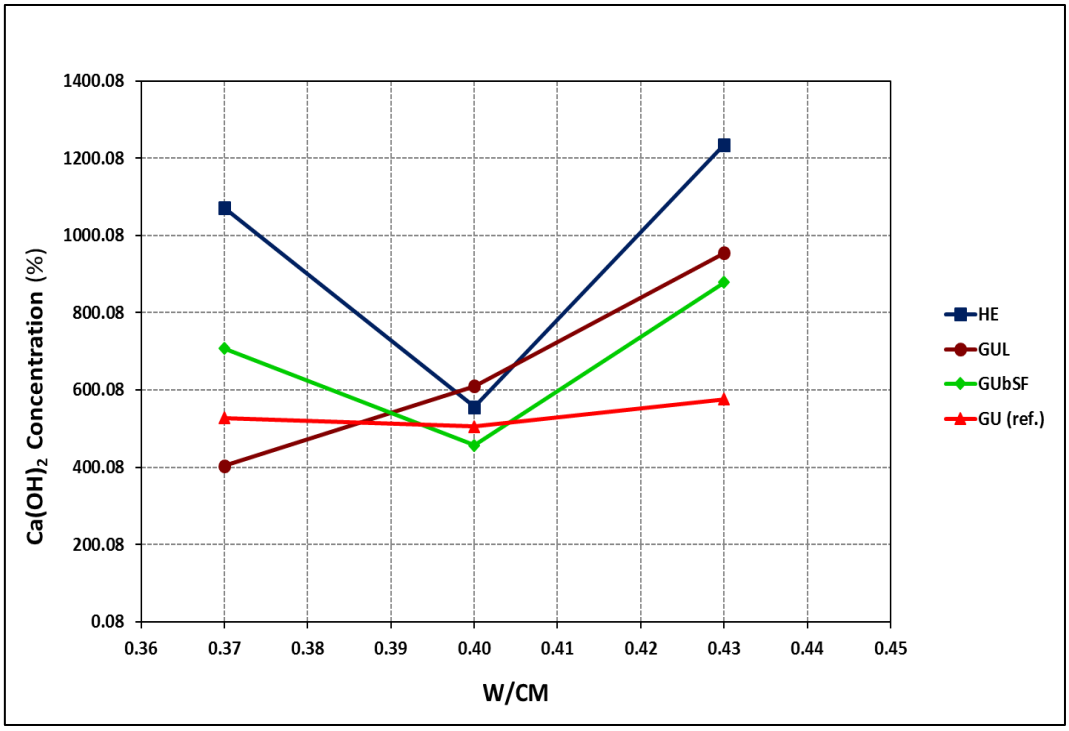


**Figure 4-68: Changes in $Ca(OH)_2$ concentration with W/CM ratio at initial setting**

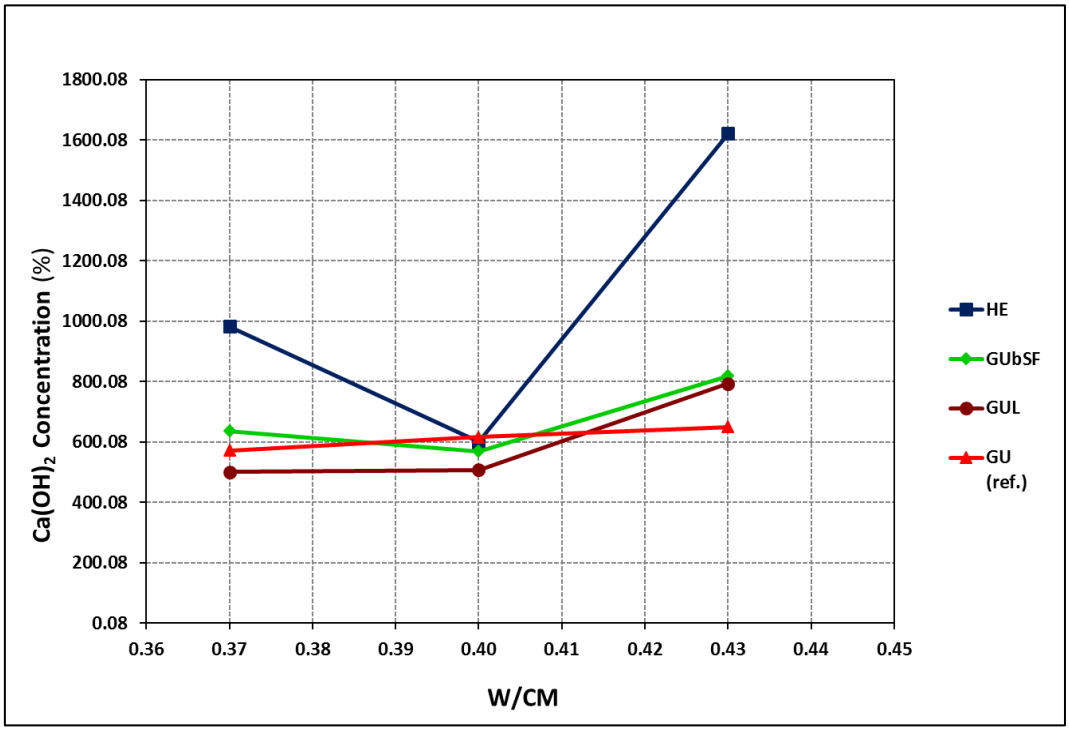


**Figure 4-69: Changes in $Ca(OH)_2$ concentration with W/CM ratio at final setting**

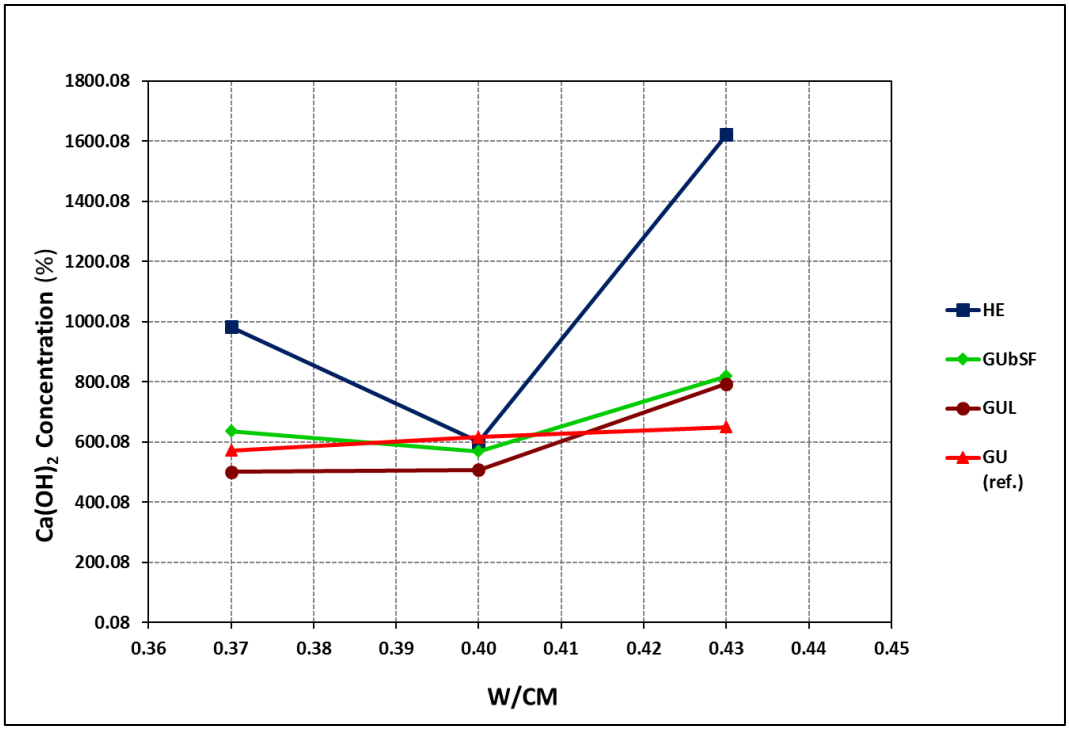


**Figure 4-70: Changes in $Ca(OH)_2$ concentration with W/CM ratio at 24 hours of hydration**

To analyze the hydration of the cement pastes by observing the formation of Portlandite, the CH percentage at each stage of hydration is plotted in Figure 4-71 to Figure 4-74 for GU, GUL, GUbSF, and HE mixtures, respectively.

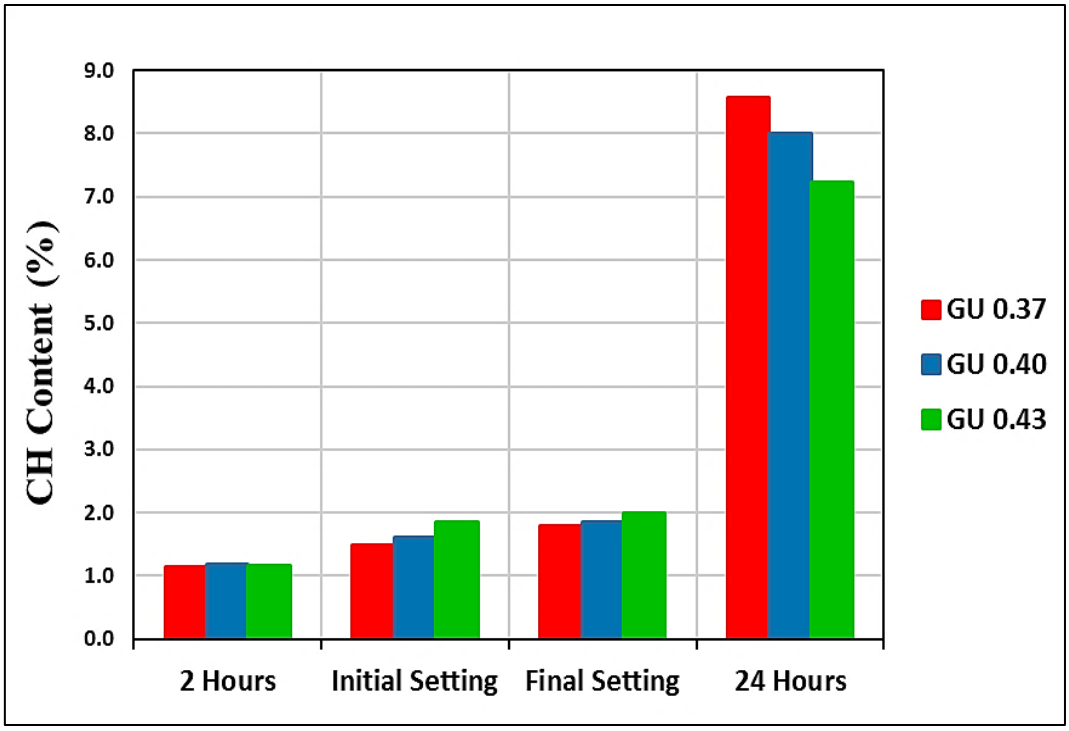


**Figure 4-71: Portlandite content in GU mixtures at different stages of hydration from TGA/DTA**

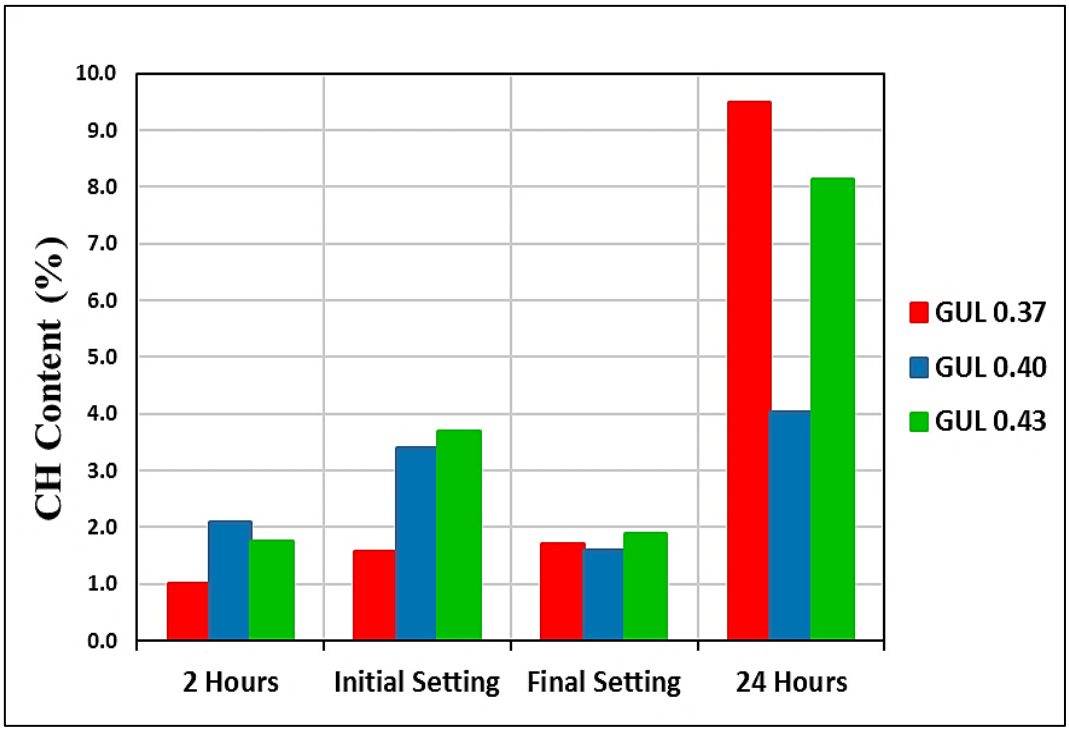


**Figure 4-72: Portlandite content in GUL mixtures at different stages of hydration from TGA/DTA**

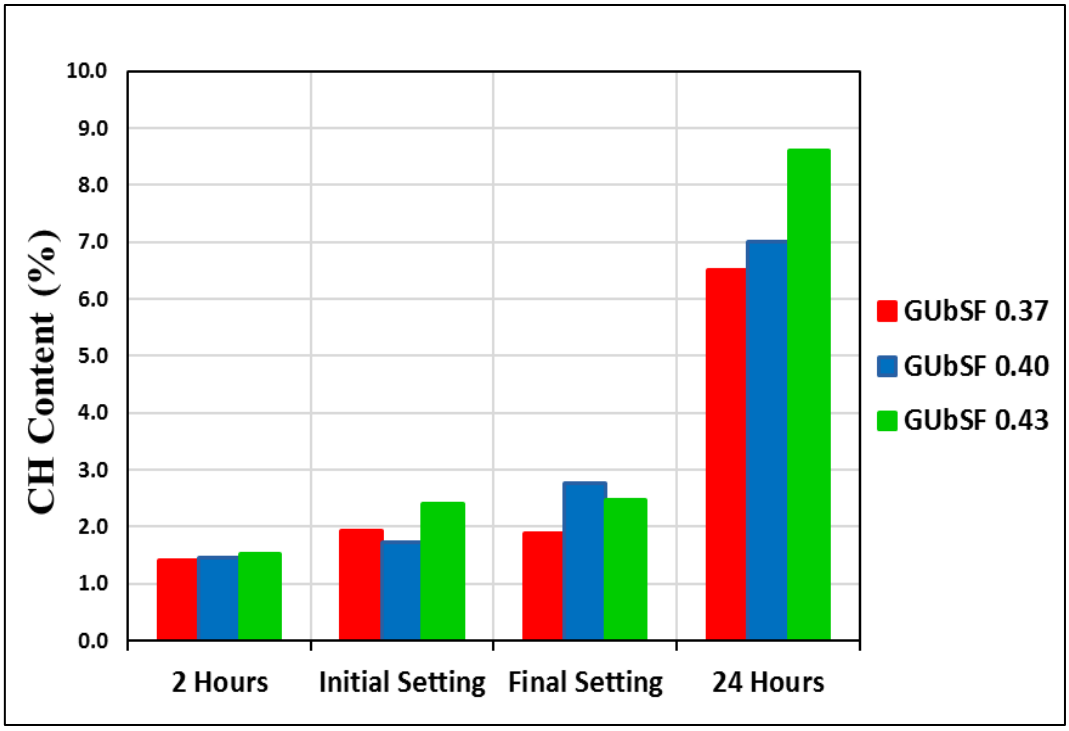


**Figure 4-73: Portlandite content in GUbSF mixtures at different stages of hydration from TGA/DTA**

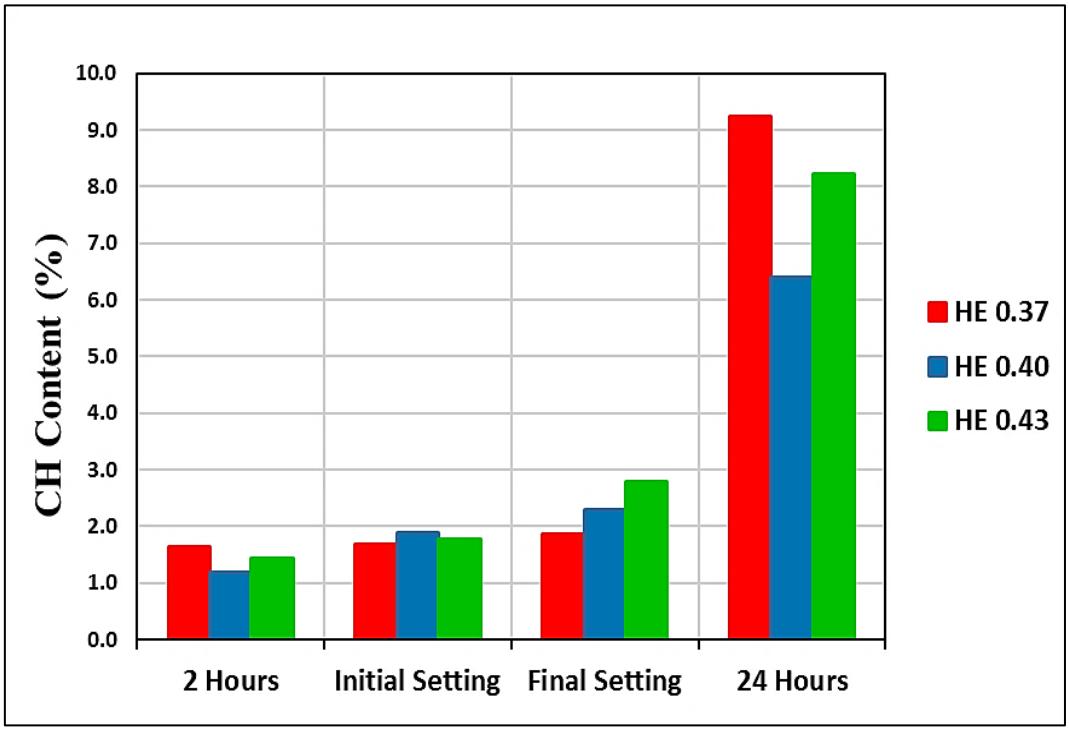


**Figure 4-74: Portlandite content in HE mixtures at different stages of hydration from TGA/DTA**

From the figures, it is observed that there is not a clear trend between the W/CM ratio and the concentration of Portlandite. It is also observed that the CH content in GU cement paste did not change significantly (see Figure 4-71), as W/CM ratio increased, while this change was more significant in the HE and GUbSF mixtures.

In opposite, the concentration of CH has more meaningful relationship with the type of cement and the length of hydration as shown in Figure 4-75 and Figure 4-76.

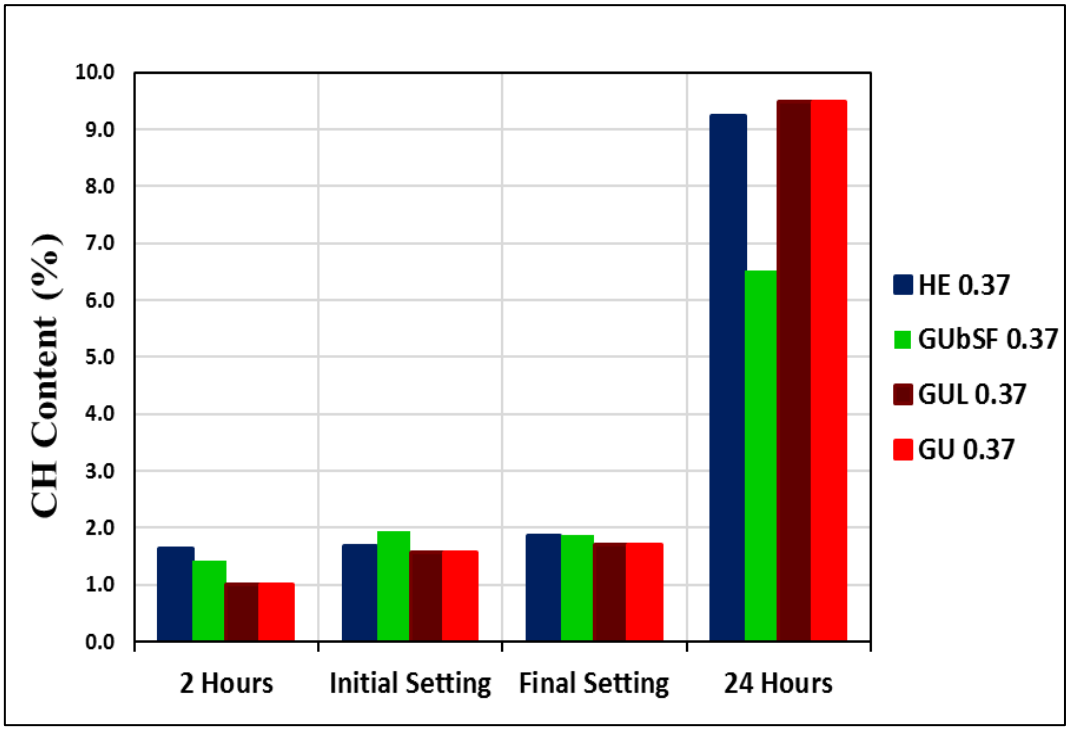


**Figure 4-75: Cement type effect on CH content over 24 hours of hydration in low W/CM ratio mixtures**

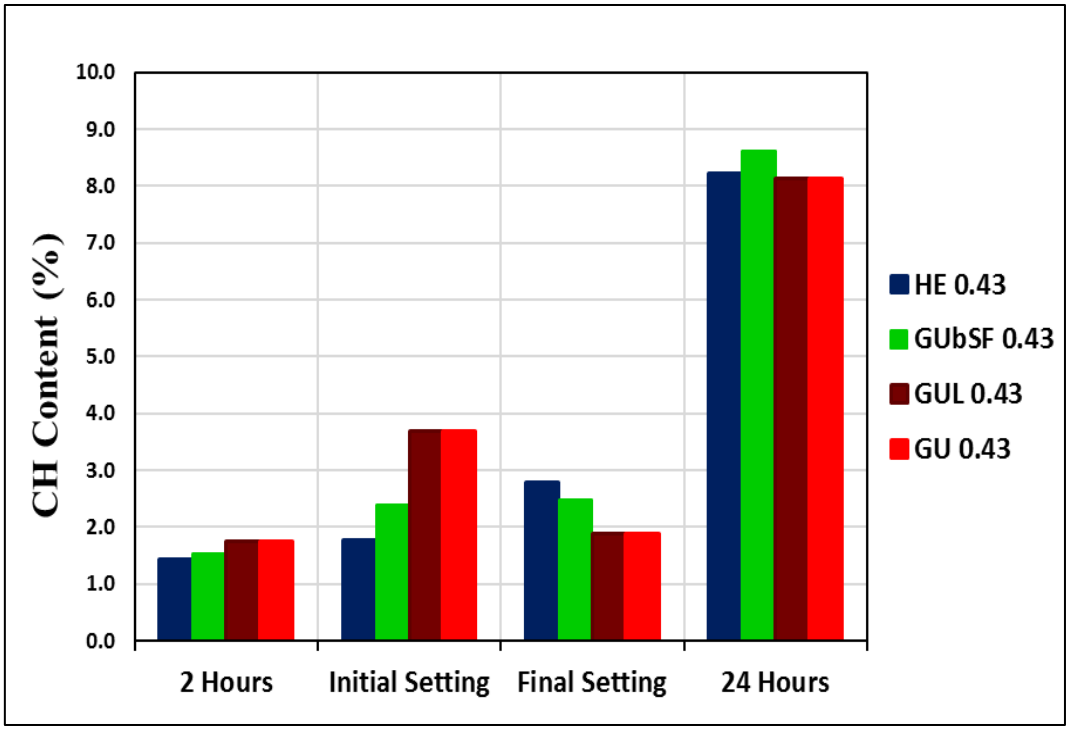


**Figure 4-76: Cement type effect on CH content over 24 hours of hydration in high W/CM ratio mixtures**

It can be observed that the contribution of Silica Fume or limestone to CH production cannot be detected over the first 24 hours with TGA technology.

De-carbonation of $CaCO_3$ (calcite) occurs at temperature greater than 500°C; and its effect can be detected in values in Table 4-17 to Table 4-26. Water is removed from this hydration biproduct via the dynamic heating process. In all mixtures, calcite content increased as the cement pastes hydrated. The highest amount of calcite was observed in GUL mixtures followed by the HE and GUbSF mixtures.

For un-hydrated cement powders, the Loss-on-Ignition or LOI (calculated by heating up a cement sample to 900 – 1000°C until a constant weight is obtained) is summarized in Table 4-29. All cement powders were tested for total weight loss with the TGA instrument before conducting any further test to make sure there were in the acceptable range indicated in CSA A3301.

**Table 4-29: Comparison between total weight loss of cement powders with TGA and ASTM D7348**

| Portland Cement Type | Total Weight Loss (measured by TGA) | Total LOI* (reported by the supplier) | Maximum Limit (CSA A3001) |
|---|---|---|---|
| **GU (ref.)** | 1.8% | 2.0% | 3.0 (if the LOI at 550°C<3.0%) |
| **GUL** | 5.7% | 5.2% | 10% |
| **GUbSF** | 0.5% | 2.3% | 3.5% |
| **HE** | 2.0% | 2.4% | 3.0% |

*According to CSA A3001, the maximum LOI is limited to 3.0% (may exceed to 3.5% if the LOI at 550°C<3.0%)

The Loss-on-Ignition (LOI) is a quality control factor. According to ASTM D7348, 2.0±0.5g of cement powder is heated up to 750°C (after removing the water at 110°C), and the weight loss associated with brining is known as the LOI. A high LOI could indicate pre-hydration and carbonation of the cement powder. As shown in Table 4-29, the total weight loss and LOI of all cement powders were in the acceptable range of CSA A3001, which indicated that cement powders were in good quality with no carbonation or pre-hydration at the time of testing in the project.

In addition to the weight loss in un-hydrated cement powders, the total weight loss of semi-hydrated cement paste samples is reported in Table 4-30 for the GU and GUL cement pastes and in Table 4-31 for the GUbSF and HE cement pastes.

**Table 4-30: Total weight loss of semi-hydrated GU and GUL cement pastes with TGA instrument**

| Mix Design | | Hydration Stage | Total Weight Loss (%) |
|---|---|---|---|
| **Cement** | **W/CM** | | |
| **GU** | **0.37** | **2 hours** | 4.7 |
| | | **Initial Setting** | 5.7 |
| | | **Final Setting** | 6.7 |
| | | **1 Day** | 16.4 |
| | **0.40** | **2 hours** | 5.1 |
| | | **Initial Setting** | 6.6 |
| | | **Final Setting** | 6.9 |
| | | **1 Day** | 13.8 |
| | **0.43** | **2 hours** | 4.7 |
| | | **Initial Setting** | 6.7 |
| | | **Final Setting** | 6.6 |
| | | **1 Day** | 14.5 |
| **GUL** | **0.37** | **2 hours** | 7.9 |
| | | **Initial Setting** | 9.7 |
| | | **Final Setting** | 9.7 |
| | | **1 Day** | 19.8 |
| | **0.40** | **2 hours** | 10.6 |
| | | **Initial Setting** | 10.5 |
| | | **Final Setting** | 9.4 |
| | | **1 Day** | 18.9 |
| | **0.43** | **2 hours** | 8.6 |
| | | **Initial Setting** | 10.6 |
| | | **Final Setting** | 9.4 |
| | | **1 Day** | 17.8 |

**Table 4-31: Total weight loss of semi-hydrated GUbSF and HE cement pastes with TGA instrument**

| Mix Design | | Hydration Stage | Total Weight Loss (%) |
|---|---|---|---|
| **Cement** | **W/CM** | | |
| **GUbSF** | **0.37** | **2 hours** | 4.5 |
| | | **Initial Setting** | 6.1 |
| | | **Final Setting** | 6.5 |
| | | **1 Day** | 17.4 |
| | **0.40** | **2 hours** | 6.3 |
| | | **Initial Setting** | 8.8 |
| | | **Final Setting** | 5.1 |
| | | **1 Day** | 16.8 |
| | **0.43** | **2 hours** | 4.2 |
| | | **Initial Setting** | 6.7 |
| | | **Final Setting** | 7.1 |
| | | **1 Day** | 15.7 |
| **HE** | **0.37** | **2 hours** | 4.6 |
| | | **Initial Setting** | 5.0 |
| | | **Final Setting** | 5.7 |
| | | **1 Day** | 17.6 |
| | **0.40** | **2 hours** | 4.0 |
| | | **Initial Setting** | 6.5 |
| | | **Final Setting** | 7.8 |
| | | **1 Day** | 20.2 |
| | **0.43** | **2 hours** | 3.7 |
| | | **Initial Setting** | 5.2 |
| | | **Final Setting** | 8.6 |
| | | **1 Day** | 16.3 |

It is observed from Table 4-30 and Table 4-31 that the W/CM ratio did not influence the total weight loss of the mixtures with the same cement powder.

As cement becomes hydrated, the total mass loss over 1000°C increased (about 50-80% from 2 hours of hydration to initial setting and from initial setting to final setting). This increase became more significant (100-200%) when cement samples became hydrated further from final setting time to beyond 24 hours of hydration. Due to cement hydration, more hydration products (C-S-H, AFm, Portlandite, and Calcite) were formed, and therefore, higher weight loss due to the TGA test heating was detected.

### 4.3.3. Hydration Products Crystal Formation

As described in Section 3.4.2.2, the Powder Diffraction File (PDF) database of X-ray powder diffraction patterns maintained by the International Center for Diffraction Data (ICDD) was used to determine I/Ic. The automated program interface automatically measures I/Ic and peak area from the quantitative analysis by cement powder diffraction patterns and their comparison with PDF.

In the presence of water, Alite ($C_3S$), which has the largest mineralogical component proportion in Portland cement powder, reacts very easily and fast. It is responsible for quick setting of cement during hydration and early-stage strength. Belite ($C_2S$), a mineralogical compound containing 3 to 4 polymorphous forms, reacts with water easily and transforms into hydrated calcium silicate; it is responsible for later setting and strengthening the cement matrix at later ages (i.e., 7 days). The hydration of these two mineralogical compounds forms most of the main cement hydration product (Calcium-Silicate-Hydrate or Tobermorite, C-S-H). The cement reactivity depends on the $C_3S/C_2S$ ratio.

Since only the first 24 hours of hydration are studied in this research project, the Alite hydration is mainly the influencing factor on cement paste properties.

As described in Chapter 3, the hydration of Celite ($C_3A$), a mineralogical component present as crystals in cement powder, is the main reason behind the flash setting of cement. To slow down the reactivity of $C_3A$ with water, clinkers are ground with gypsum ($CaSO_4.2H_2O$) which

reacts with $C_3A$ and therefore controls setting. The combination of gypsum and Celite is responsible for setting of cement. Gypsum also reacts with Brownmillerite ($C_4AF$) in the presence of water to form Calcium Hydrosulphate-ferrite to accelerate the hydration of $C_2S$ and $C_3S$. Furthermore, $C_4AF$ is responsible for the colour of cement. As a result of cement hydration, the mineralogical components of cement powders are transformed into tobermorite, Portlandite, and ettringite (Jumata and Manea, 2011).

The crystals formed at different stages of hydration were detected and analyzed by the help of the X-ray Diffraction (XRD) test results. Its measurement is completed in three steps:

> ***Step I)*** The semi-hydrated cement powders' diffraction spectrum is identified by means of the X-ray diffract meter,
>
> ***Step II)*** The interplane distances "d" are calculated with the help of Bragg's law, and the Miller indices of the diffraction planes as schematically shown in Figure 3-33, and
>
> ***Step III)*** With the data in Step II, the corresponding sheet is searched in the powder diffraction file database, and finally, the full description of the crystalline phase from the crystallographic is found and reported.

Crystal formation at the stages of testing helps analyzing the changes in physical and electrical properties of the cement paste.

Due to the limitation of the instrument, Reference Intensity Ratio (RIR) number, and the nature of the cement paste in the first 24 hours of hydration, the crystals identified and studied with XRD are introduced in Table 4-32. In the table, the Quality Mark (QM) is determined based on comparison between the experimental and calculated crystals pattern. The latest pattern is calculated based on experimentally determined crystal structures.

**Table 4-32: Phase name and chemical composition of analyzed chemicals by XRD**

| Phase name | Chemical formula | RIR | Experimental QM* |
|---|---|---|---|
| Portlandite | $Ca(OH)_2$ | 1.4 | I |
| Brownmillerite | $Ca_2(Al,Fe+3)_2O_5$ | 1.32 | S |
| Ettringite | $Ca_6Al_2(SO_4)_3(OH)_{12}(H_2O)_{26}$ | 1.67 | S |
| Gypsum | $Ca(SO_4)(H_2O)_2$ | 1.98 | I |
| Calcite | $Ca(CO_3)$ | 3.21 | I |
| Belite (Larnite) | $Ca_2(SiO_4)$ | 0.75 | S |
| Alite (Hatrurite) | $Ca_3(SiO_4)$ O | 0.78 | B |
| Hydrated Calcium Silicate (Tobermorite 9A) | $Ca_5(Si_6O_{16})(OH)_2$ | 0.51 | B |

*S: Well characterized chemically and crystallographyically
*I: Well characterized chemically
*B: Don't meet criteria for I and S

The main crystalline phases (about 85% of the phases in Portland cement) detected from the diffractograms of un-hydrated cement powders are mainly:

Alite-$Ca_3SiO_5$, in majority in the sample

Belite-$Ca_2SiO_4$

Brownmillerite-$Ca_{2(}Al,Fe+3)2O_5$

Gypsum-$CaSO_4 \cdot 2H_2O$

The phase quantities measured by the XRD for the unhydrated Portland cements tested are tabulated in Table 4-33.

**Table 4-33: Phase analysis of unhydrated Portland cements**

| Cement Type | GU | GUL | GUbSF | HE |
|---|---|---|---|---|
| **Brownmillerite-$C_4AF$** | 12.0 | 11.0 | 9.0 | 9.2 |
| **Gypsum** | 3.6 | 3.6 | 3.0 | 4.2 |
| **Alite (Hatrurite)-$C_3S$** | 56.0 | 54.0 | 59.0 | 57.0 |
| **Belite (Larnite)-$C_2S$** | 13.1 | 11.5 | 14.2 | 15.0 |
| **Portlandite-CH** | 3.0 | 2.1 | 2.0 | 2.0 |
| **Tobermorite-CSH** | 6.0 | 6.0 | 5.4 | 5.0 |
| **Calcite** | 5.4 | 10.0 | 6.1 | 6.7 |
| **Ettringite** | 1.0 | 1.3 | 1.3 | 0.9 |
| **Σ** | 100.1 | 99.5 | 100.0 | 100.0 |

The measurement profiles of the un-hydrated cement powders are presented in Appendix D. The measured minerals composition in Table 4-33 and the minerals composition reported by the cement supplier (presented in Table 3-2) match within acceptable variance (below 2%).

On the other hand, in hydrated cement powders at different stages of hydration, the following phases were identified from the XRD diffractograms:

Alite-$Ca_3SiO_5$, in majority in the sample

Portlandite-CH-$Ca(OH)_2$

Ettringite-$Ca_6Al(SO_4)_3(OH)_{12}*26H_2O$

Calcium Silicate Hydrate-CSH-$Ca_{1.5}Si_{3.5}xH_2O$

Gypsum-$CaSO_4 \cdot 2H_2O$

Haturite or Alite-$Ca_3(SiO_4)$

Larnite or Belite- $Ca_2(SiO_4)$

Brownmilerite - $Ca_2(Al,Fe)_2O_5$

The most important phase detected by XRD in hydrated cement paste is C-S-H, which was detected in most of the samples at a position around 2θ=30-31˚. Portlandite showed two diffraction halos at a position around 2θ=17-18˚ and 2θ=35-36˚ The quantitative analysis of the phases are summarized in Table 4-35 to Table 4-38. It is important to mention that the analyzing programs assumed that the combination of all phases identified accounts for 100% of the specimen. This is one of the limitations of the RIR method, as non-crystalline phases or unidentified materials are not considered in the analysis.

The quantification accuracy of cement minerals, hydrates and amorphous phases are reported in the literature (Hoshino et al., 2006). The accuracy of the measured/analyzed phases was in the acceptable range as summarized in Table 4-34.

**Table 4-34: Average accuracy percentage of XRD quantity analysis**

| **Accuracy** (% mass) | **Hydration Phase** | | | | | | | |
|---|---|---|---|---|---|---|---|---|
| | **Brownmillerite** | **Calcite** | **Ettringite** | **Gypsum** | **Alite** | **Belite** | **Portlandite** | **Tobermorite** |
| | ±2.2 | ±4.1 | ±5.3 | ±3.4 | ±3.1 | ±2.8 | ±4.9 | ±3.8 |

**Table 4-35: XRD quantitative analysis of hydrated GU cement pastes**

| Mix Design | GU 0.37 | | | | GU 0.40 | | | | GU 0.43 | | | |
|---|---|---|---|---|---|---|---|---|---|---|---|---|
| **Stage of Hydration** | **2 Hours** | **Initial Setting** | **Final Setting** | **24 Hours** | **2 Hours** | **Initial Setting** | **Final Setting** | **24 Hours** | **2 Hours** | **Initial Setting** | **Final Setting** | **24 Hours** |
| **Brownmillerite** | 15.0 | 14.0 | 13.1 | 7.9 | 15.0 | 13.0 | 11.0 | 9.1 | 13.0 | 12.1 | 11.5 | 7.6 |
| **Calcite** | 2.0 | 6.0 | 5.5 | 3.0 | 2.6 | 6.0 | 5.4 | 3.6 | 3.1 | 2.9 | 2.8 | 3.1 |
| **Ettringite** | 2.5 | 2.0 | 2.0 | 3.5 | 2.5 | 2.2 | 1.8 | 3.0 | 3.5 | 2.2 | 1.8 | 2.6 |
| **Gypsum** | 2.9 | 2.6 | 1.8 | 1.4 | 3.0 | 2.5 | 1.4 | 1.0 | 2.8 | 2.0 | 1.3 | 0.7 |
| **Alite (Haturite)** | 52.0 | 50.0 | 42.0 | 12.5 | 52.4 | 52.0 | 46.0 | 10.0 | 50.0 | 51.0 | 48.5 | 15.6 |
| **Belite (Larnite)** | 15.0 | 14.1 | 14 | 9.9 | 13.0 | 13.0 | 14.0 | 10.0 | 16.0 | 16.0 | 15.2 | 10.0 |
| **Portlandite** | 2.8 | 3.0 | 9.0 | 21.6 | 3.1 | 3.0 | 10.0 | 24.0 | 3.2 | 6.5 | 7.9 | 24.6 |
| **Tobermorite** | 9.0 | 9.0 | 12.0 | 40.0 | 8.0 | 8.5 | 10.5 | 39.0 | 8.0 | 7.7 | 11.0 | 36.8 |

**Table 4-36: XRD quantitative analysis of hydrated GUbSF cement pastes**

| Mix Design | GUbSF 0.37 | | | | GUbSF 0.40 | | | | GUbSF 0.43 | | | |
|---|---|---|---|---|---|---|---|---|---|---|---|---|
| Stage of Hydration | 2 Hours | Initial Setting | Final Setting | 24 Hours | 2 Hours | Initial Setting | Final Setting | 24 Hours | 2 Hours | Initial Setting | Final Setting | 24 Hours |
| Brownmillerite | 9.2 | 9.0 | 8.2 | 3.8 | 8.7 | 8.3 | 9.0 | 4.1 | 8.5 | 7.8 | 6.9 | 5.5 |
| Calcite | 5.5 | 4.7 | 4.2 | 2.8 | 5.0 | 3.1 | 5.5 | 3.3 | 3.0 | 6.0 | 4.7 | 3.4 |
| Ettringite | 3.2 | 2.9 | 2.5 | 2.0 | 4.6 | 3.0 | 3.2 | 4.9 | 2.9 | 2.0 | 1.7 | 3.8 |
| Gypsum | 3.0 | 2.8 | 2.5 | 0.6 | 3.2 | 2.3 | 1.8 | 0.2 | 3.1 | 2.9 | 2.3 | 0.4 |
| Alite (Haturite) | 53.0 | 46.0 | 39.0 | 10 | 50 | 48.3 | 36.4 | 11.2 | 52.0 | 45.0 | 40.3 | 13.4 |
| Belite (Larnite) | 14.0 | 13.0 | 13.5 | 9.0 | 16.0 | 14.0 | 12.8 | 9.7 | 15.3 | 13.5 | 11.4 | 10.4 |
| Portlandite | 7.0 | 13.0 | 15.0 | 20.5 | 8.0 | 9.8 | 14.8 | 22.5 | 10.2 | 15 | 20.0 | 23.6 |
| Tobermorite | 6.0 | 8.6 | 14.5 | 51.0 | 6.0 | 10.0 | 16.5 | 44.5 | 5.0 | 11.5 | 12.5 | 40.0 |

**Table 4-37: XRD quantitative analysis of hydrated GUL cement pastes**

| Mix Design | GUL 0.37 | | | | GUL0.40 | | | | GUL 0.43 | | | |
|---|---|---|---|---|---|---|---|---|---|---|---|---|
| **Stage of Hydration** | **2 Hours** | **Initial Setting** | **Final Setting** | **24 Hours** | **2 Hours** | **Initial Setting** | **Final Setting** | **24 Hours** | **2 Hours** | **Initial Setting** | **Final Setting** | **24 Hours** |
| **Brownmillerite** | 16.0 | 15.2 | 12.9 | 8.1 | 14.9 | 12.0 | 11..0 | 7.3 | 16.0 | 14.5 | 11.3 | 5.1 |
| **Calcite** | 5.5 | 4.3 | 4.0 | 7.6 | 15.0 | 11.1 | 10.9 | 8.1 | 14 | 8.3 | 8.0 | 9.0 |
| **Ettringite** | 3.9 | 3.0 | 2.9 | 3.6 | 5.0 | 4.4 | 4.2 | 4.9 | 3.0 | 2.1 | 2.6 | 2.6 |
| **Gypsum** | 2.8 | 2.2 | 1.8 | 1.8 | 2.3 | 2.0 | 1.2 | 0.9 | 2.0 | 1.5 | 0.9 | 0.5 |
| **Alite (Haturite)** | 45.0 | 40 | 35.4 | 13 | 39.5 | 37 | 36.9 | 7.6 | 40.2 | 38.0 | 35.0 | 8.0 |
| **Belite (Larnite)** | 11.0 | 10.0 | 9.5 | 7.3 | 11.0 | 11.0 | 10.0 | 7.3 | 11.5 | 11.0 | 10.0 | 7.9 |
| **Portlandite** | 4.0 | 10.0 | 14.3 | 12.0 | 4.5 | 11.0 | 9.7 | 18.1 | 4.3 | 12 | 13.9 | 22.8 |
| **Tobermorite** | 12.0 | 15.9 | 19.0 | 47.2 | 10.9 | 13.0 | 17.0 | 45.9 | 9.0 | 12.8 | 16.5 | 44.2 |

**Table 4-38: XRD quantitative analysis of hydrated HE cement pastes**

| Mix Design | HE 0.37 | | | | HE 0.40 | | | | HE 0.43 | | | |
|---|---|---|---|---|---|---|---|---|---|---|---|---|
| Stage of Hydration | 2 Hours | Initial Setting | Final Setting | 24 Hours | 2 Hours | Initial Setting | Final Setting | 24 Hours | 2 Hours | Initial Setting | Final Setting | 24 Hours |
| Brownmillerite | 14.0 | 15.0 | 12.0 | 8.0 | 13.0 | 11.0 | 10.0 | 4.0 | 13.0 | 13.0 | 12.0 | 8.2 |
| Calcite | 4.7 | 3.1 | 6.0 | 3.4 | 3.3 | 4.1 | 7.0 | 3.2 | 3.5 | 2.5 | 2.7 | 2.7 |
| Ettringite | 2.0 | 1.0 | 0.5 | 1.3 | 2.5 | 3.5 | 1.0 | 1.9 | 1.9 | 0.9 | 0.9 | 1.9 |
| Gypsum | 4.0 | 3.5 | 2.7 | 1.5 | 3.9 | 2.9 | 1.3 | 0.9 | 3.4 | 3.2 | 2.9 | 1.2 |
| Alite (Haturite) | 45 | 35.6 | 24.9 | 1.9 | 46.6 | 38 | 26 | 2.5 | 42.3 | 39.3 | 31.3 | 4.1 |
| Belite (Larnite) | 11.0 | 10.0 | 9.0 | 7.9 | 10 | 9.9 | 9.5 | 8.1 | 16.0 | 12.0 | 11.0 | 9.5 |
| Portlandite | 11.0 | 15.3 | 18.0 | 11.0 | 9.9 | 15.6 | 20.3 | 21 | 9.0 | 15.0 | 16.8 | 20.6 |
| Tobermorite | 12.0 | 16.5 | 26.9 | 65.0 | 11.0 | 15.0 | 25.0 | 59.6 | 10.9 | 16.0 | 22.4 | 52.5 |

The diffraction spectra shown in Appendix D, summarized in Table 4-35 to Table 4-38, have shown that Alite was detected in the majority of the samples. It is also observed that ettringite and Portlandite are present in all the hydration stages beyond 2 hours of hydration. Permeable (porous) Calcium Silicate Hydrate (C-S-H) crystal start forming beyond the initial setting and more significantly beyond the final setting stage. It permits diffusion of the ions in the pore solution, so more hydration of cement at the early age will happen.

To understand the values reported in Table 4-35 to Table 4-38, crystals contents at different times of hydration are presented in Figure 4-77 to Figure 4-80.

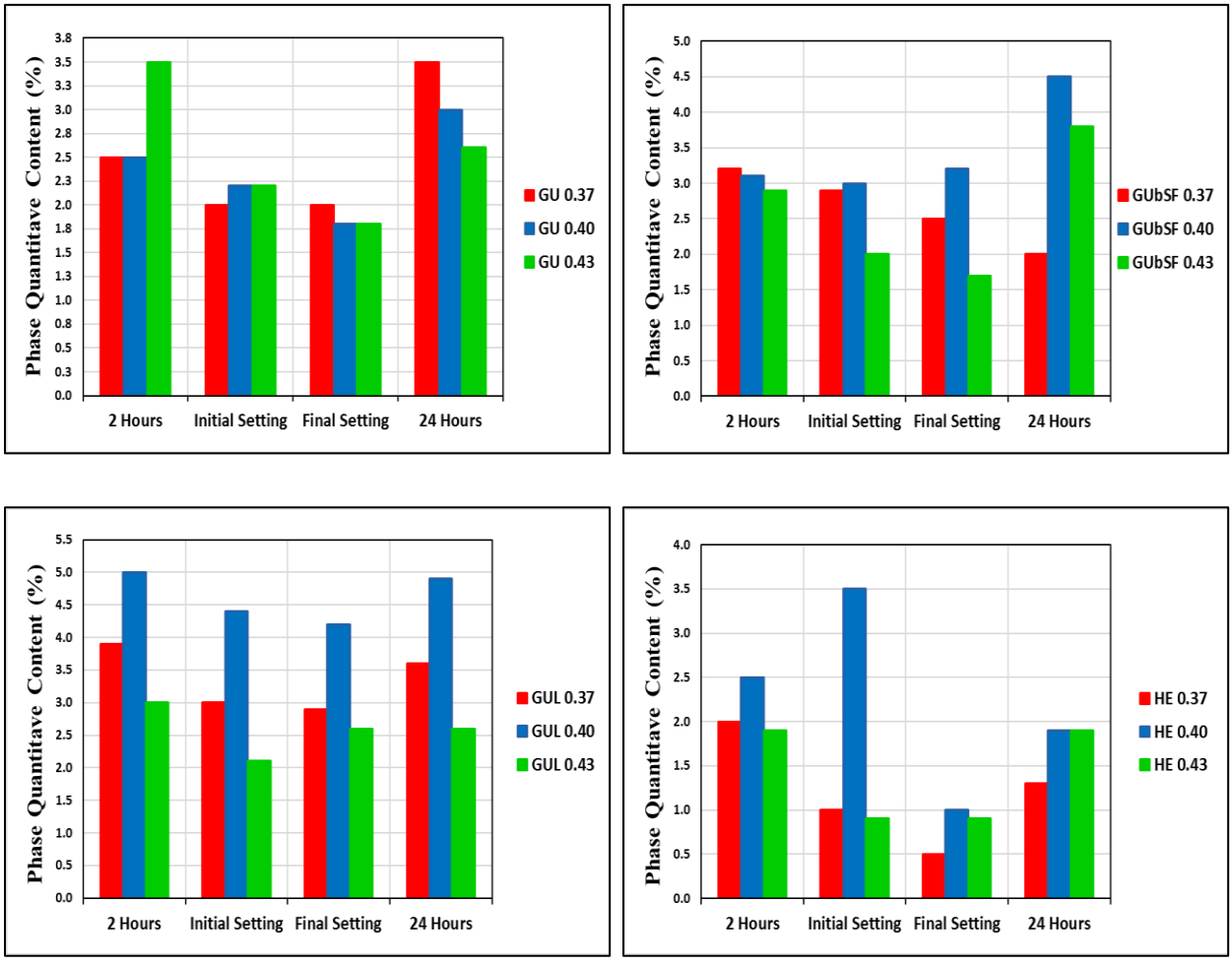


**Figure 4-77: Ettringite content in cement mixtures at different times of hydration**

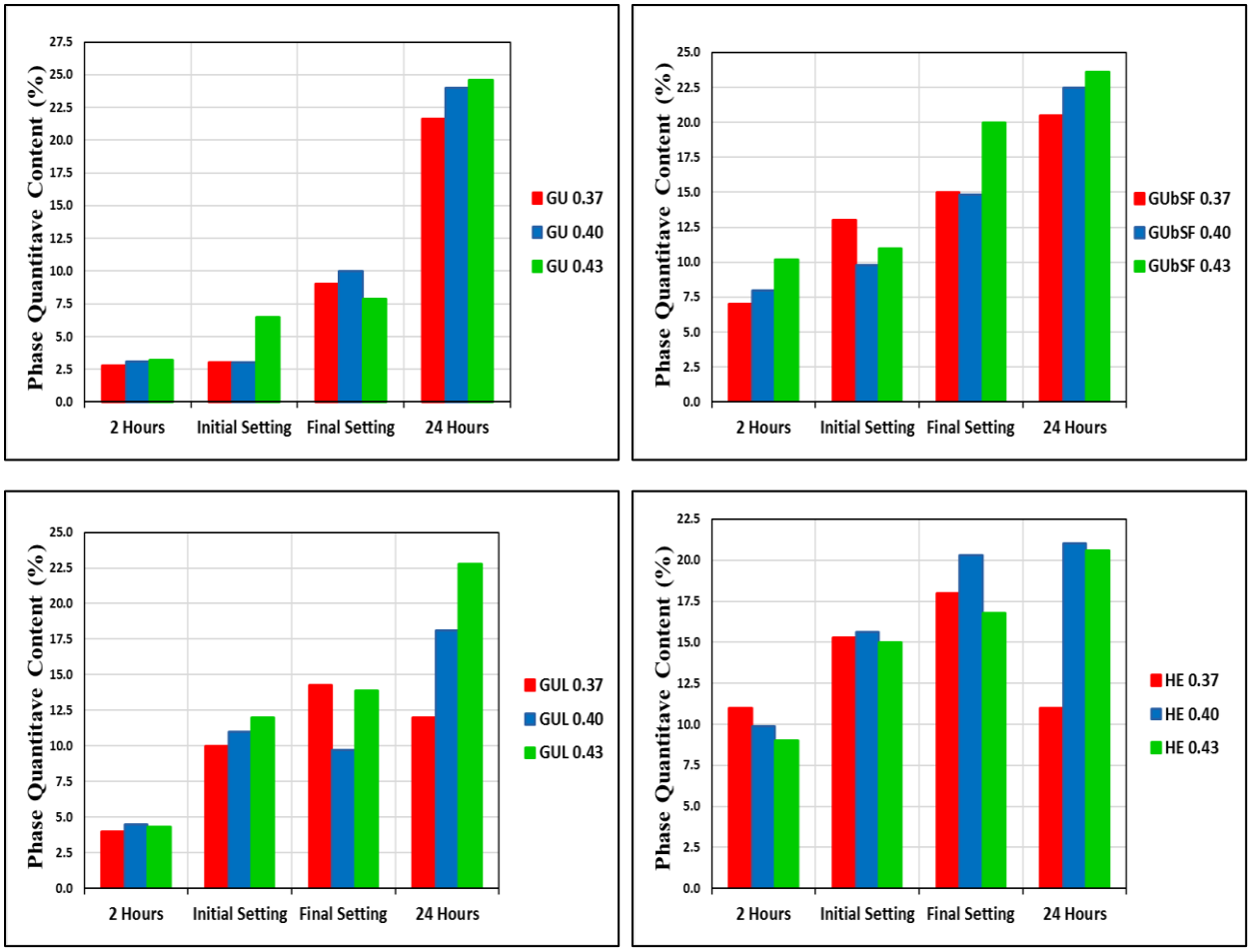


**Figure 4-78: Calcium hydroxide content in cement mixtures at different times of hydration**

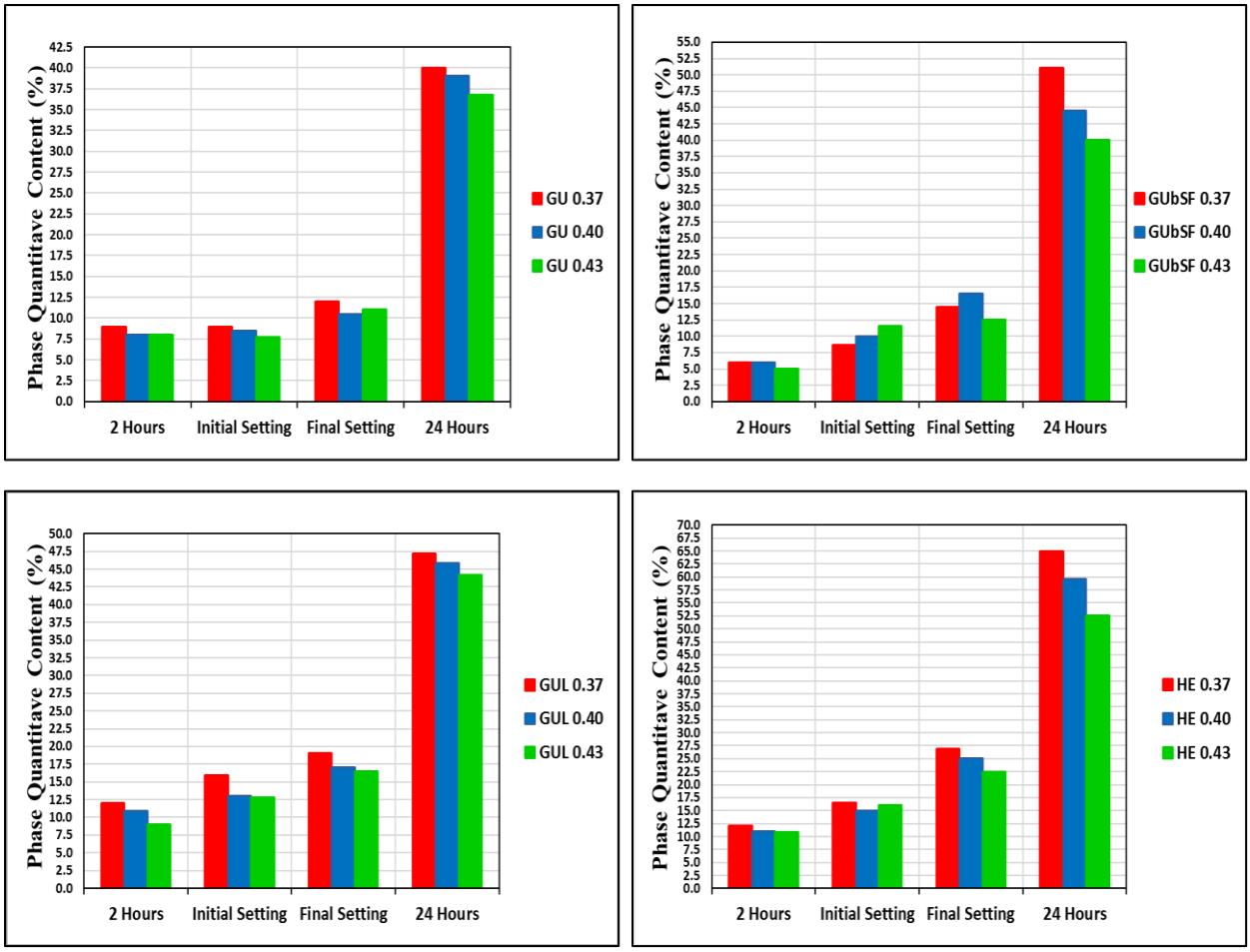


**Figure 4-79: C-S-H content in cement mixtures at different times of hydration**

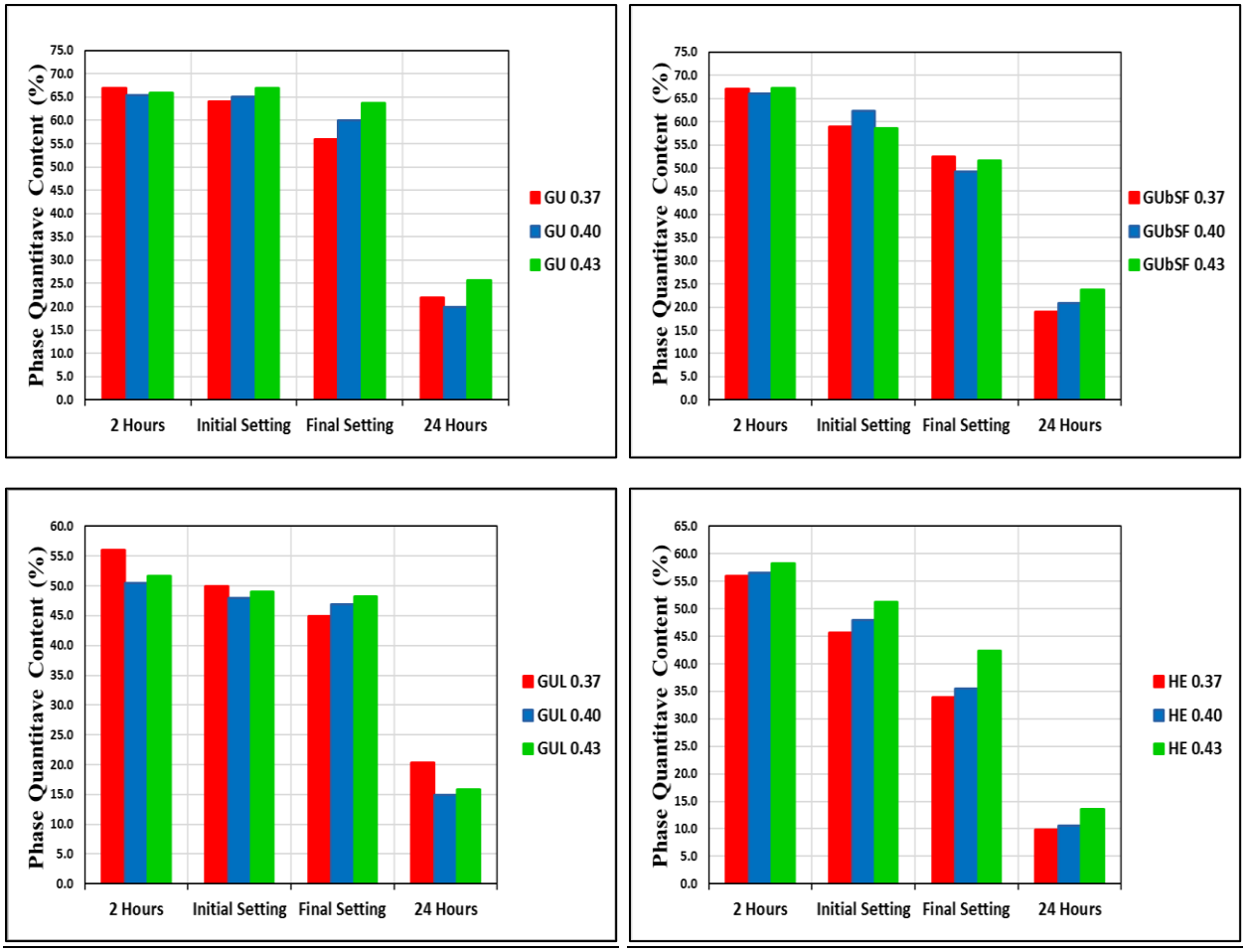


**Figure 4-80: Combination of Alite and Belite content in cement mixtures at different times of hydration**

It was noted that as Portland cement became in contact with water, $C_3A$ rapidly reacted and ettringite started forming. This conclusion was derived from comparison of the ettringite quantitative analysis after 2 hours of hydration (Figure 4-77) with the initial ettringite content in un-hydrated cement (XRD quantitative analysis in Table 4-33). Also, by comparing the values in Figure 4-77 and Figure 4-80 with that in Table 4-33 for all cements, it is observed that during the first 2 hours of hydration, the quantity of Alite ($C_3S$) and by Belite ($C_2S$) are approximately the same as the un-hydrated cement.

It was noted from Figure 4-77 that the ettringite and C-S-H content in GUbSF was lower than that in GU and GUL prior to the initial setting time. This can explain the higher consistency penetration value of GUbSF (presented in Section 4.2.1.2) and longer initial setting time (described in Section

4.2.4). However, the ettringite content of GUbSF increased by the final setting time, so a lower final setting time was achieved (as per Section 4.2.4). This dual behaviour of GUbSF can be explained by a relatively higher sulphur leakage in the pore solution of GUbSF at 2 hours (described in Section 4.3.1.2), which results in more reaction with $C_3A$ and further ettringite formation.

Beyond 2 hours, reduction in Alite and Belite due to hydration is observed. Two hours of hydration represents the time when cement starts stiffening, due to formation of ettringite. This time was measured in Section 4.2.5. Beyond this time, it is noted that Alite started hydrating and C-S-H started forming (by quantitative analyzing of the phases at 2 hours and initial setting in Figure 4-79 and Figure 4-80). This conversion was more significant in the HE mixtures. In addition, Portlandite was detected for the first time at around initial setting time. Furthermore, beyond 2 hours of hydration until initial setting, ettringite became more stable, and significant changes in its quantitative analysis results were not observed (especially in GU and GUL mixtures as tabulated in Table 4-35 and Table 4-37). From initial setting to the final setting, values reported in Table 4-35 to Table 4-38 showed $SO_4^{2-}$ consumption (reduction in gypsum). Ettringite (AFt) was converted into other phases (e.g., monosulphate and $C_4AH_{19}$) as shown in Figure 4-77. As a result, Portlandite and Tobermorite (C-S-H) were formed in all cements (see Figure 4-78 and Figure 4-79). That conversation and reactions were more significant in HE, followed by GU and GUbSF, and finally GUL mixtures.

Around 24 hours of hydration, a second reaction of $C_3A$, with a significant reduction in gypsum content as shown in Table 4-35 to Table 4-38, was observed. As a result, hydrated AFt was observed in the paste resulting from that secondary hydration (slight increase in ettringite presence in Table 4-35 to Table 4-38). At 24 hours of hydration, the components in anhydrous cement (Alite, Belite, Gypsum, but not Brownmillerite) were largely consumed, and the hydration products (C-S-H, CH, and AFt,) were formed in all the cement pastes. There were more hydration products in the HE and GU mixtures. The reaction between silica fume and biproducts of cement hydration (Portlandite or CH) did not proceed significantly even after 24 hours of hydration (comparison of CH in Table 4-36). It is expected to see less CH beyond 24 hours of hydration, as it is consumed by the secondary hydration of silica fume particles. However, it was noted in the results presented

in Section 4.2.3 that the 24-hour compressive strength of the GUbSF samples was higher than that in the reference samples, which can be due to the presence of silica fume particles acting as fillers.

At this stage of hydration, the changes in mineralogical components (where hydro-silicates and hydro-aluminates were observed in C-S-H, CH, and ettringite) were noted. Due to the reactions of $C_4AF$ after one day of hydration, which can be observed in the tables when Brownmillerite percentage reduced at 24 hours of hydration, AFm and AFt were formed.

# 5. ANALYSIS OF TEST RESULTS

## 5.1. Development of Electrical Resistivity

In this chapter, all the test results presented in Chapter 4 will be used to infer setting times from electrical resistivity measurements, as per the main objective of the research program.

By analyzing the electrical resistivity and its ROC over the first 24 hours of cement paste hydration, four major stages of hydration can be detected. These stages, shown with vertical dash and solid lines in Figure 5-1 to Figure 5-12, are:

**Stage I) Stiffening:** From the mixing time to the first turning point in the electrical resistivity (transition point from decreasing to increasing resistivity), which is shown with the first dash line in the graphs.

**Stage II) Setting:** Stage over which resistivity starts to increase slowly. This stage starts from the turning point in the electrical resistivity to final setting (second solid line in the graphs). The initial setting time, within this stage, is indicated with the first solid vertical line in the graphs.

**Stage III) Hardening:** This stage starts from the final setting time (the second solid vertical line in the graphs) to the point where $\frac{d^2\rho}{dt^2}$=0, which is shown with the second vertical dash line in the graphs.

**Stage IV) Strengthening:** From the second dash line to the end of the 24-h hydration period. In this stage, the electrical resistivity increases at a very slow rate.

Similarly, a comparison between the electrical resistivity values and the Adiabatic Temperature (AT) of the cement paste samples over the first 24 hours of hydration shows almost similar four stages of hydration, as below:

**Stage I) Change in Temperature (dormant period):** From the mixing time to almost the first 2 hours of hydration (indicated by the first vertical dash line in the graphs), the temperature of the cement paste mixtures increased by 1.0 to 1.5°C. This stage is similar to Stage I of hydration.

**Stage II) Heating:** This stage starts around 2 hours of hydration to somewhere between close to the final setting time (second vertical solid lines in the graphs). In this stage, the temperature of the cement paste mixtures increased significantly due to the hydration of cementing materials particles. This stage is similar to Stage II of hydration, but it ends earlier.

**Stage III) Momentum Reduction:** From the final setting time to the peak in internal temperature (shown with the second dash vertical line in the graphs), the temperature ROC starts to decrease; however, the AT is still increasing in its value due to the cementing materials hydration.

**Stage IV) Cooling:** From the peak of the AT to the end of the measurement (24 hours of hydration), the temperature of the cement paste samples starts to decrease. At the end of Stage IV, the AT reaches equilibrium at room temperature (22-23°C).

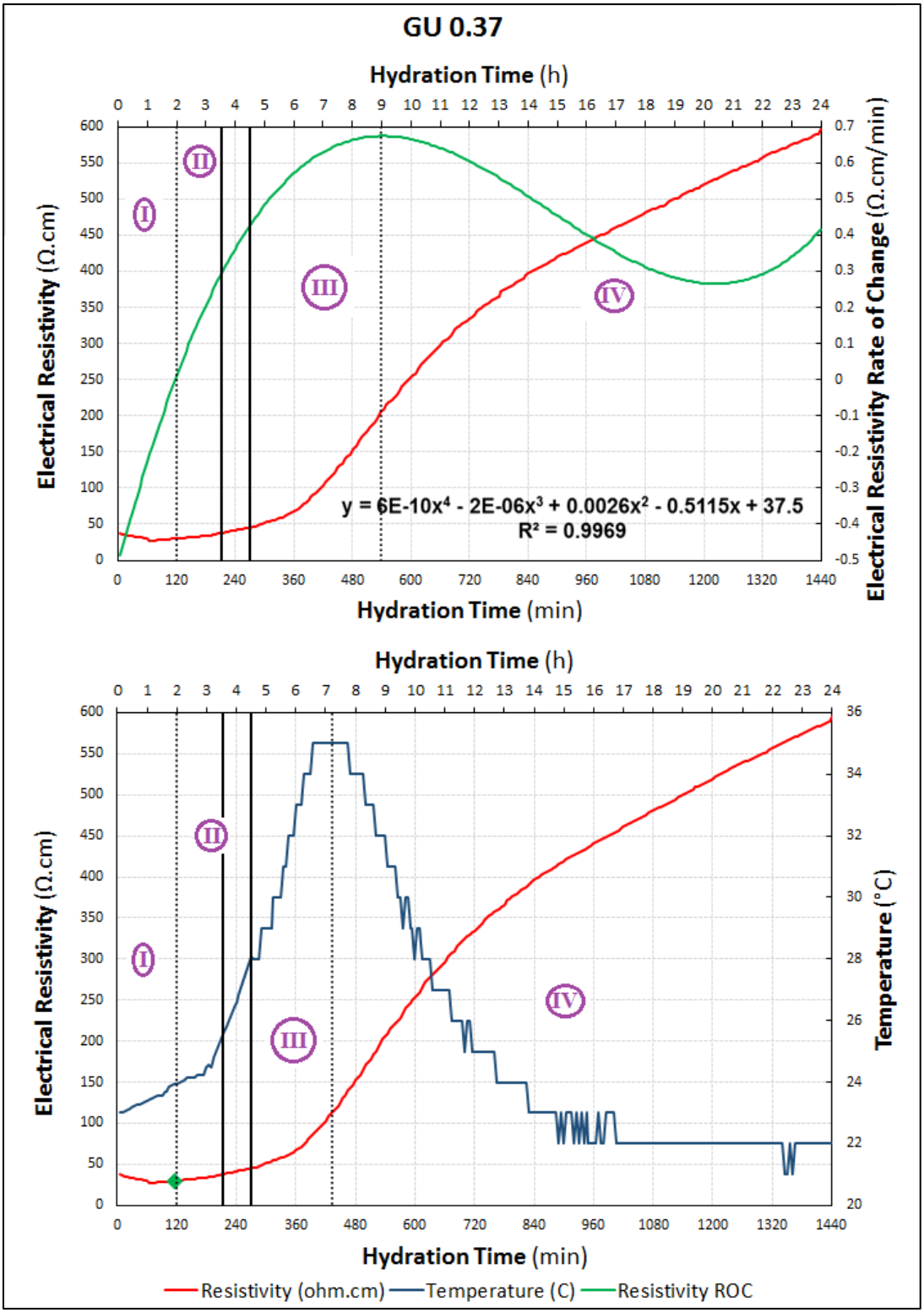


**Figure 5-1: Four stages of hydration based on the electrical resistivity ROC (top graph) and temperature development (bottom graph) of GU 0.37 paste during the first 24 hours of hydration**

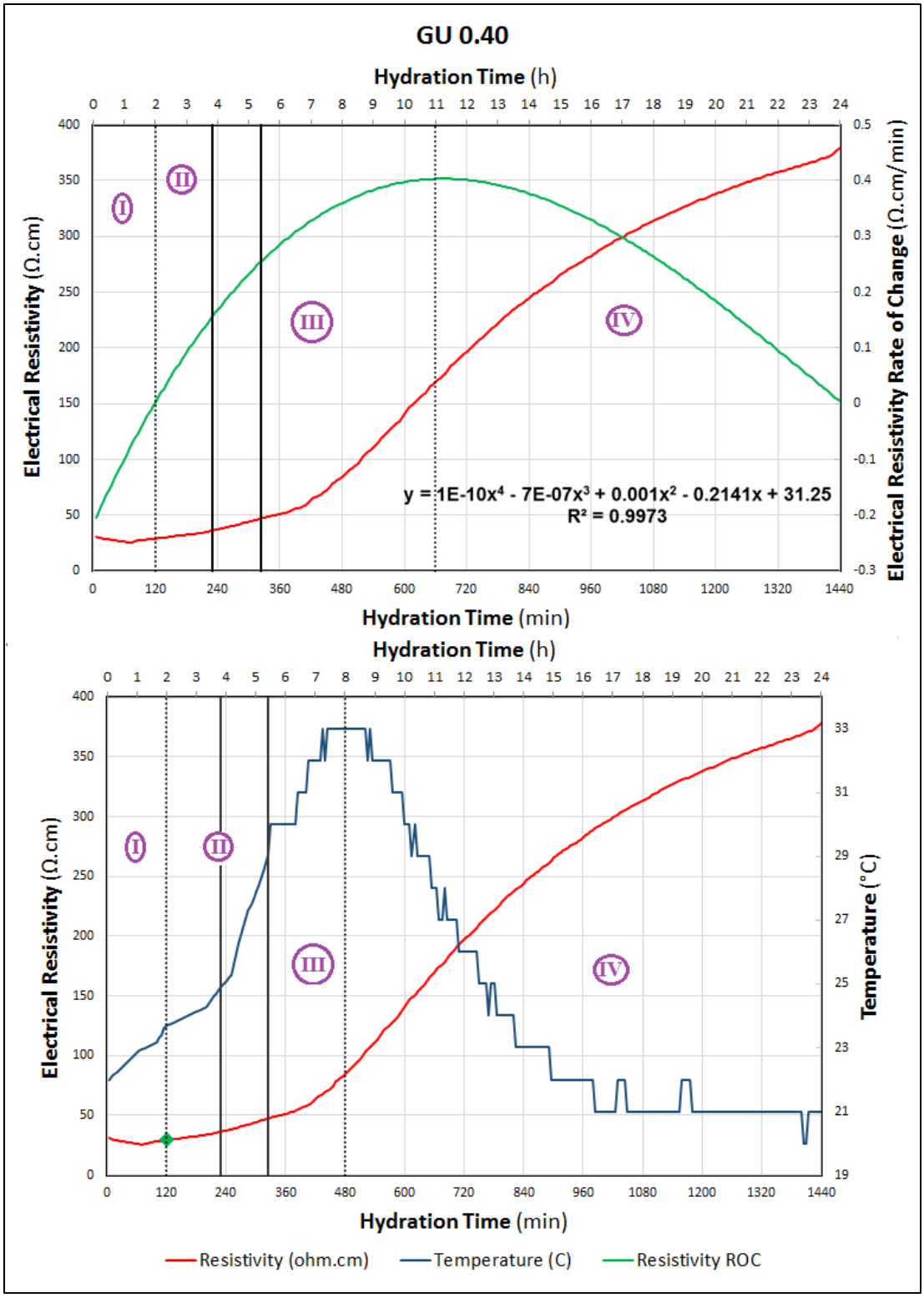


**Figure 5-2: Four stages of hydration based on the electrical resistivity ROC (top graph) and temperature development (bottom graph) of GU 0.40 paste during the first 24 hours of hydration**

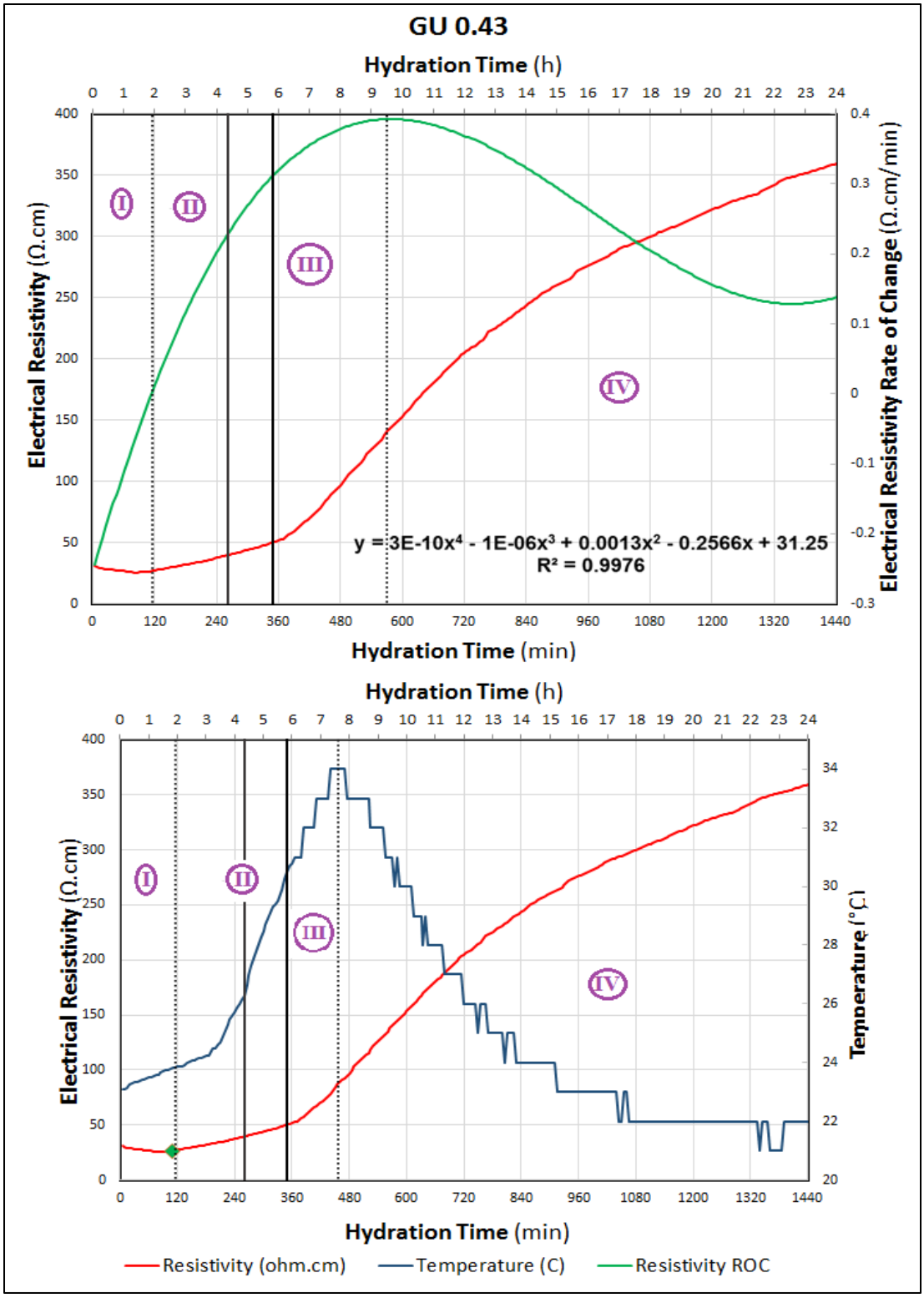


**Figure 5-3: Four stages of hydration based on the electrical resistivity ROC (top graph) and temperature development (bottom graph) of GU 0.43 paste during the first 24 hours of hydration**

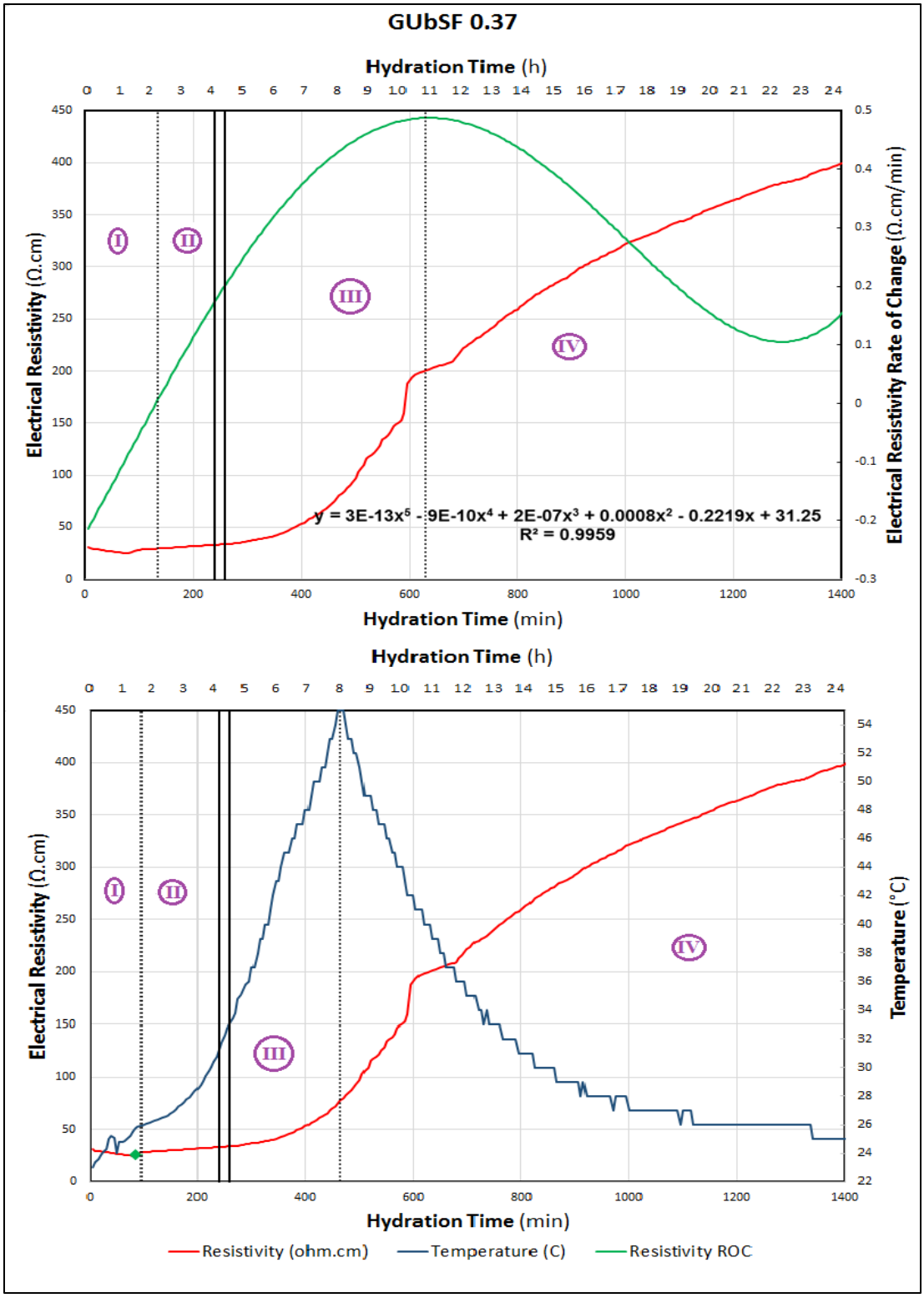


**Figure 5-4: Four stages of hydration based on the electrical resistivity ROC (top graph) and temperature development (bottom graph) of GUbSF 0.37 paste during the first 24 hours of hydration**

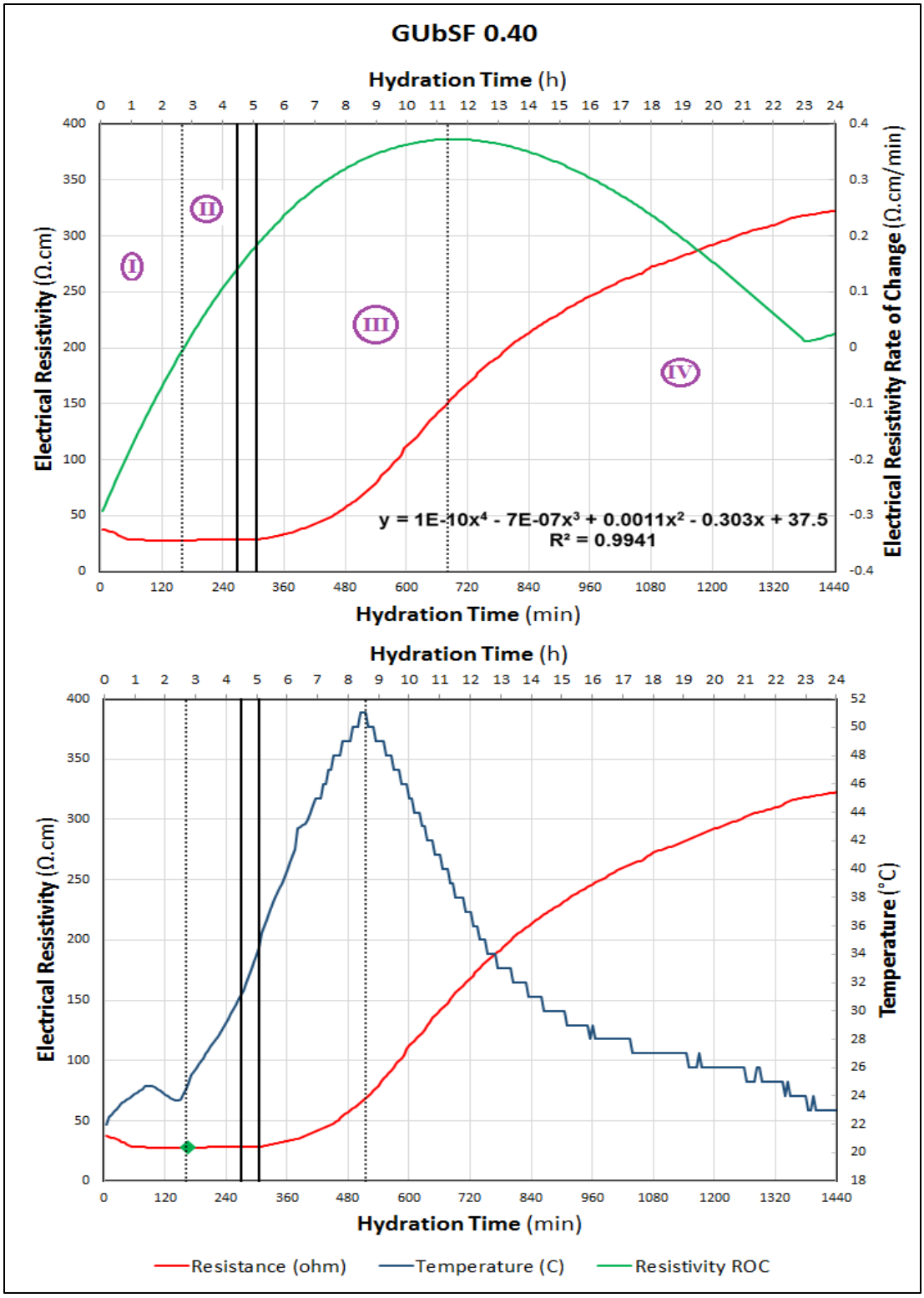


**Figure 5-5: Four stages of hydration based on the electrical resistivity ROC (top graph) and temperature development (bottom graph) of GUbSF 0.40 paste during the first 24 hours of hydration**

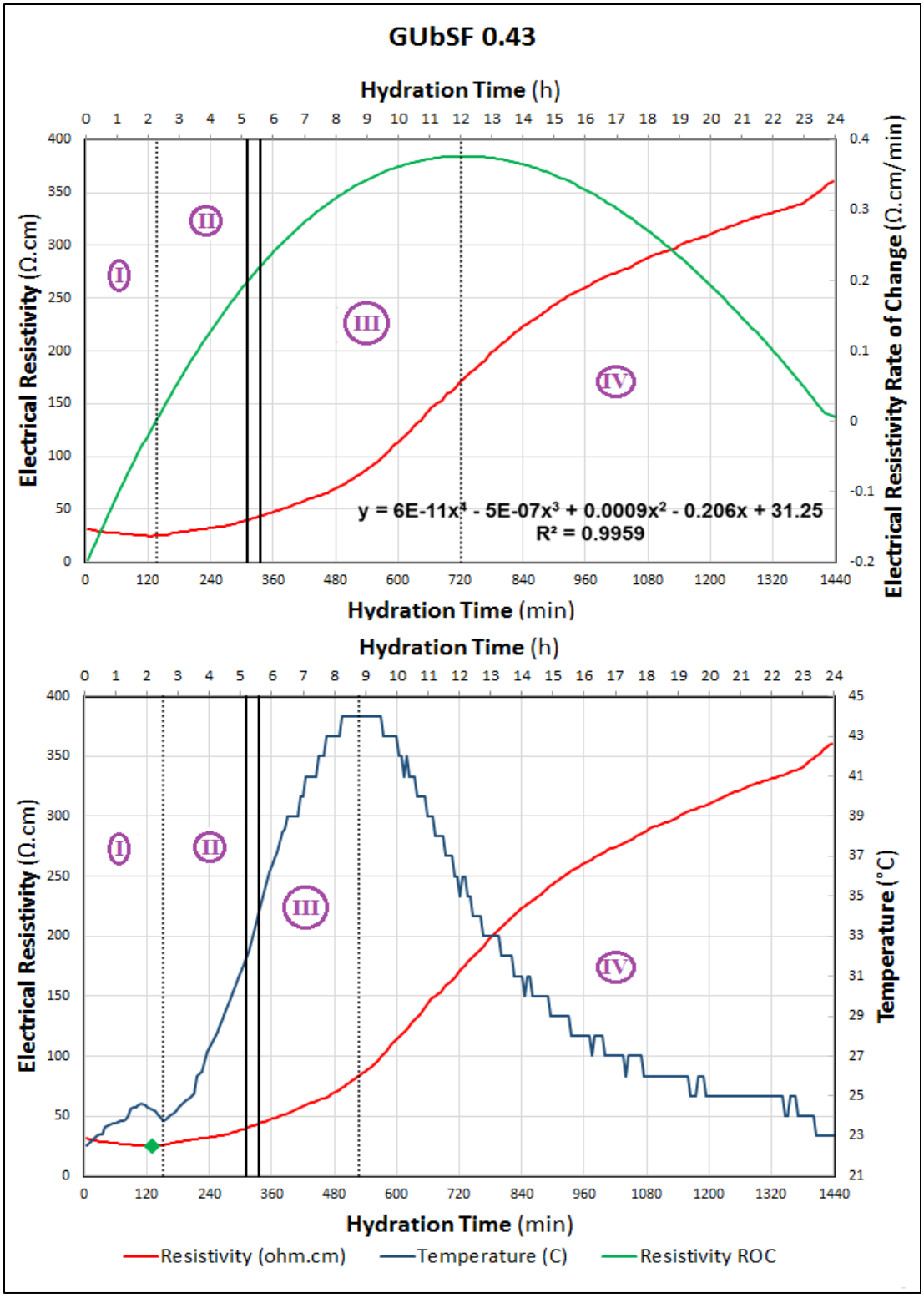


**Figure 5-6: Four stages of hydration based on the electrical resistivity ROC (top graph) and temperature development (bottom graph) of GUbSF 0.43 paste during the first 24 hours of hydration**

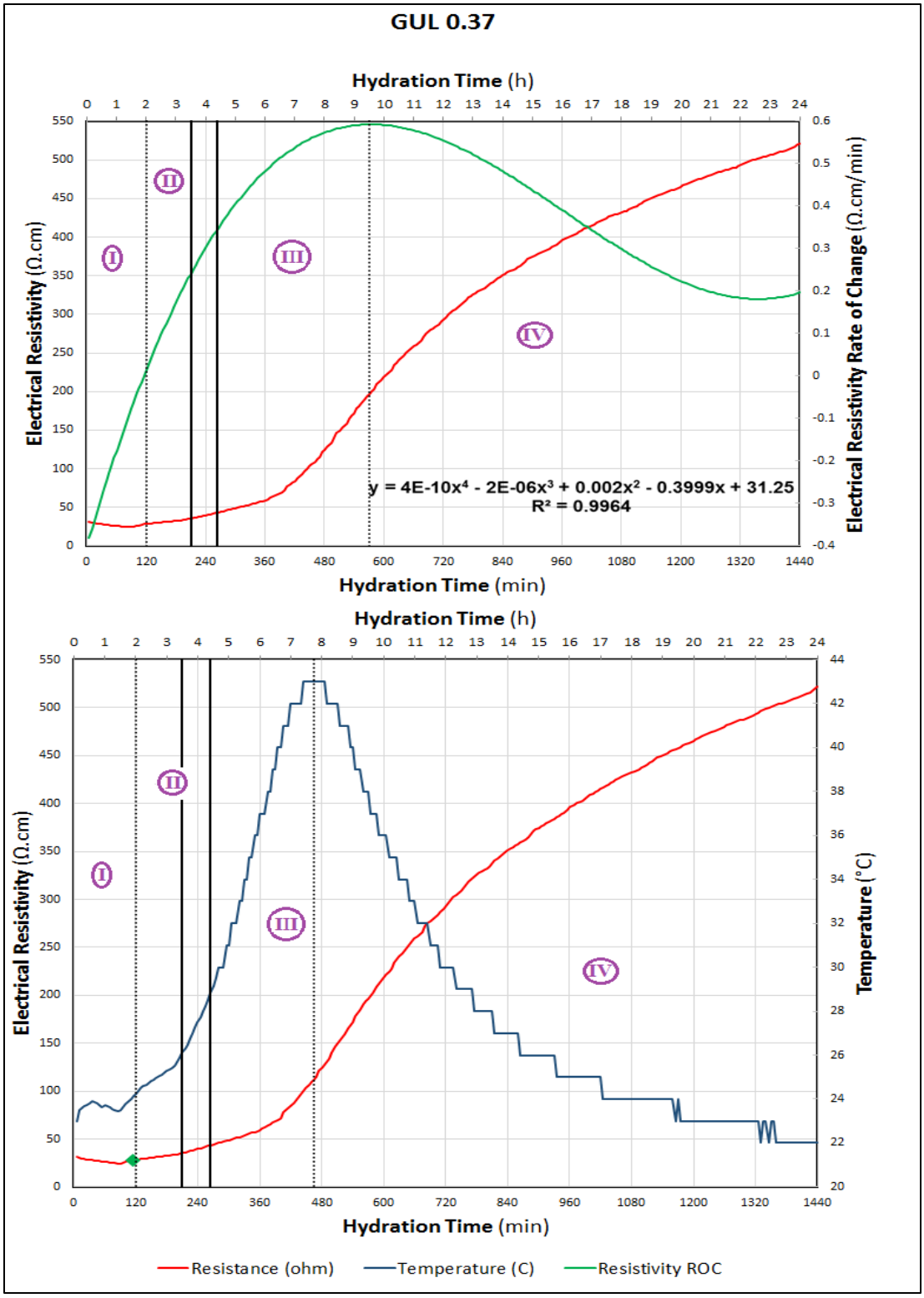


**Figure 5-7: Four stages of hydration based on the electrical resistivity ROC (top graph) and temperature development (bottom graph) of GUL 0.37 paste during the first 24 hours of hydration**

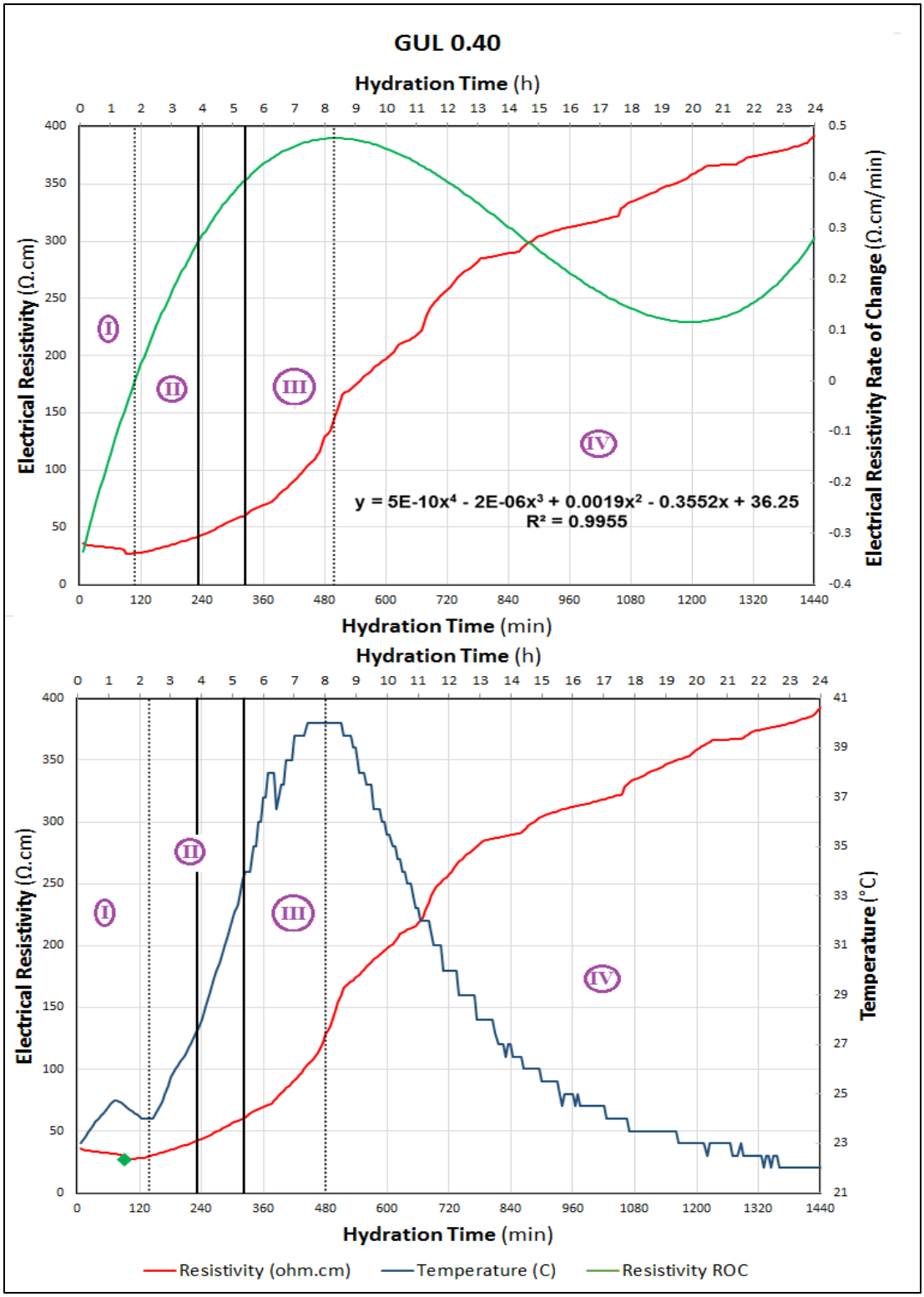


**Figure 5-8: Four stages of hydration based on the electrical resistivity ROC (top graph) and temperature development (bottom graph) of GUL 0.40 paste during the first 24 hours of hydration**

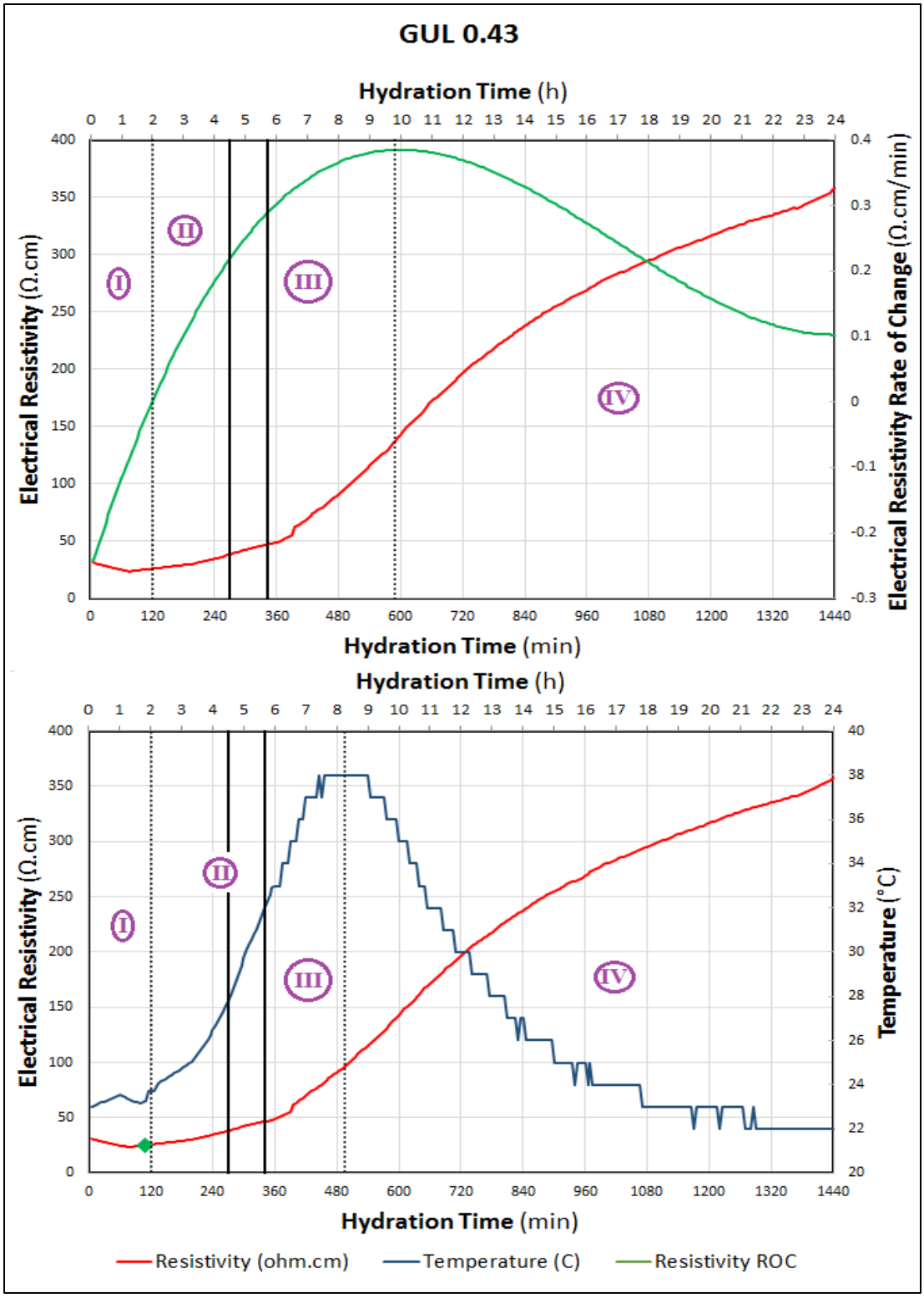


**Figure 5-9: Four stages of hydration based on the electrical resistivity ROC (top graph) and temperature development (bottom graph) of GUL 0.43 paste during the first 24 hours of hydration**

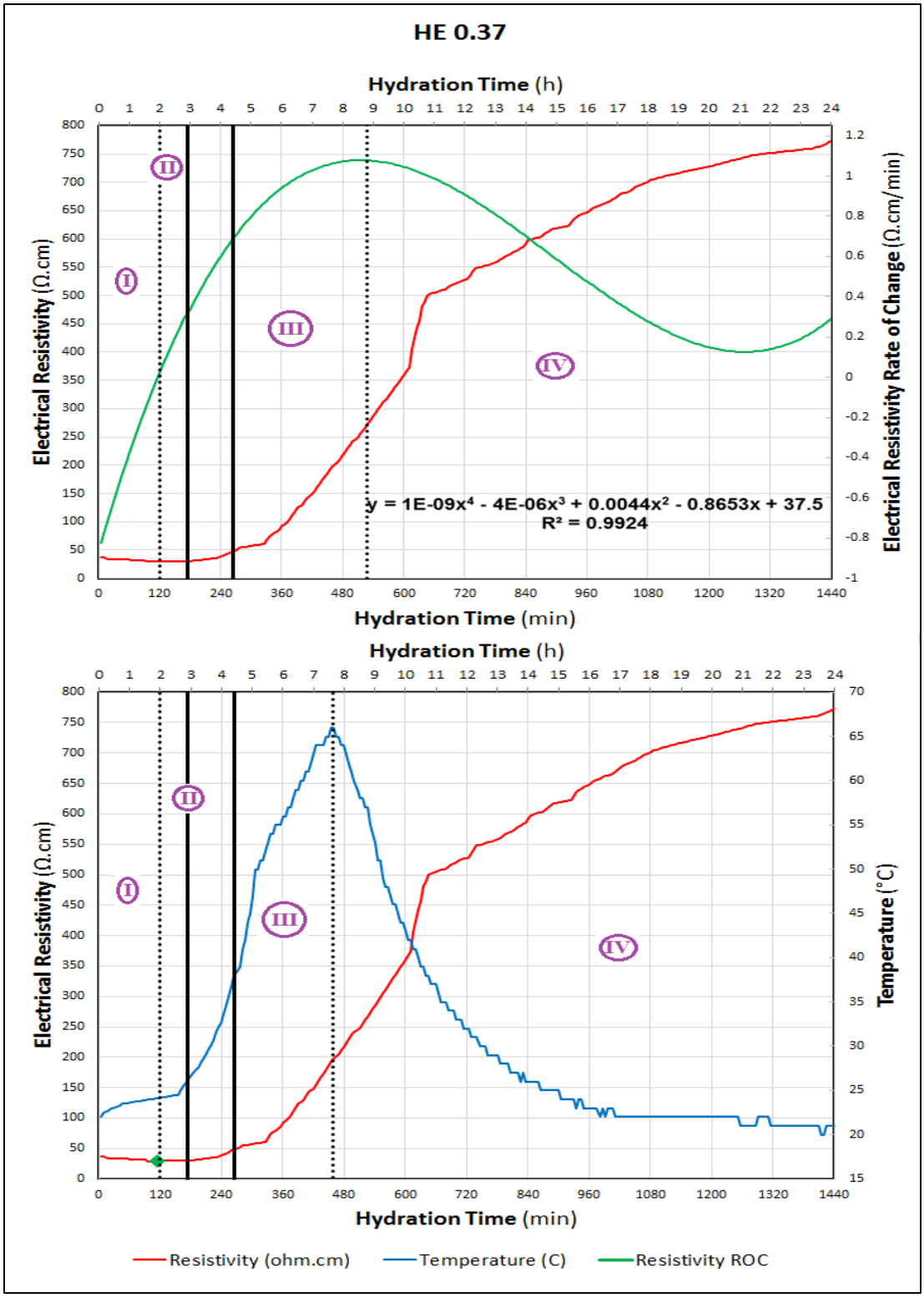


**Figure 5-10: Four stages of hydration based on the electrical resistivity ROC (top graph) and temperature development (bottom graph) of HE 0.37 paste during the first 24 hours of hydration**

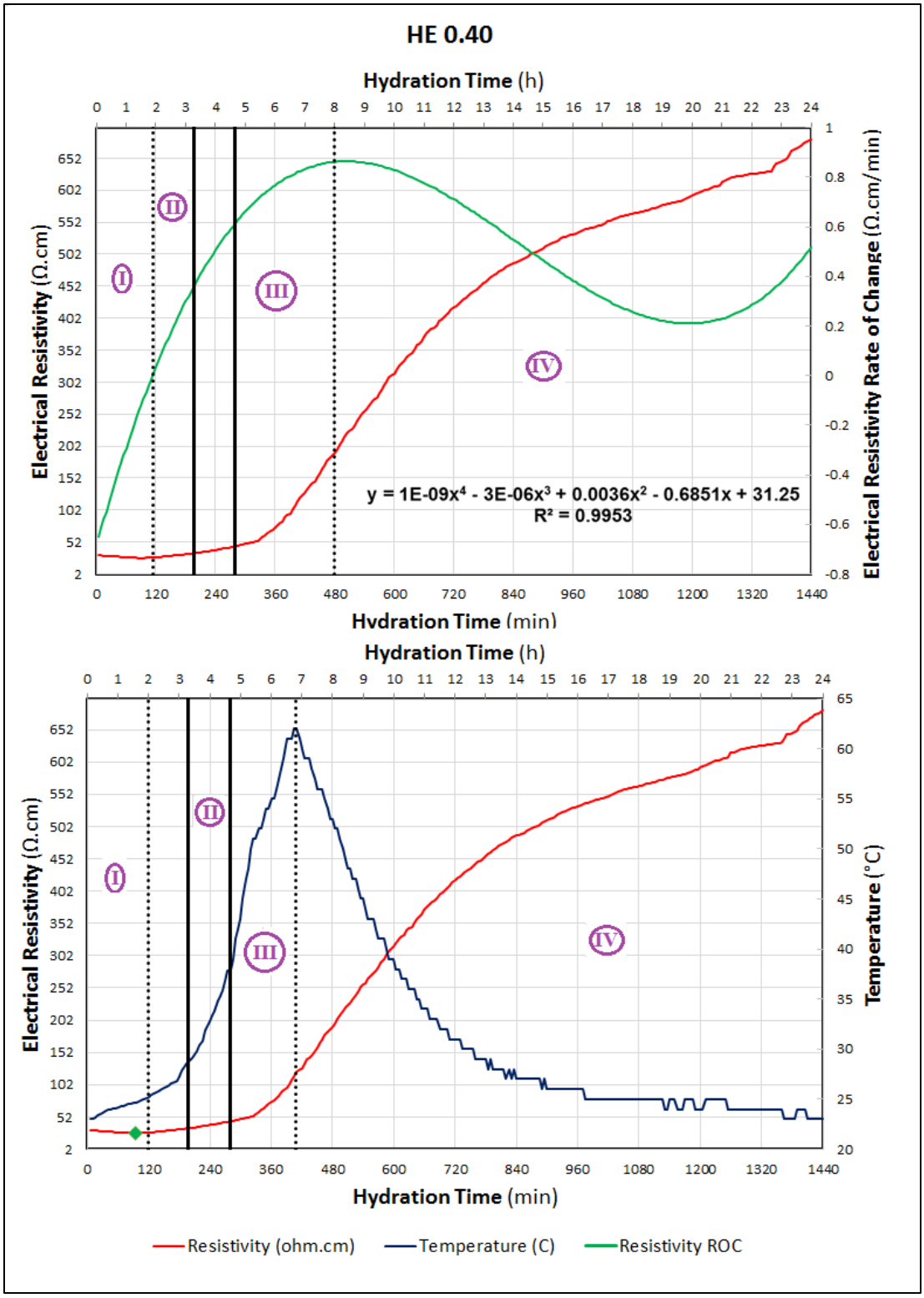


**Figure 5-11: Four stages of hydration based on the electrical resistivity ROC (top graph) and temperature development (bottom graph) of HE 0.40 paste during the first 24 hours of hydration**

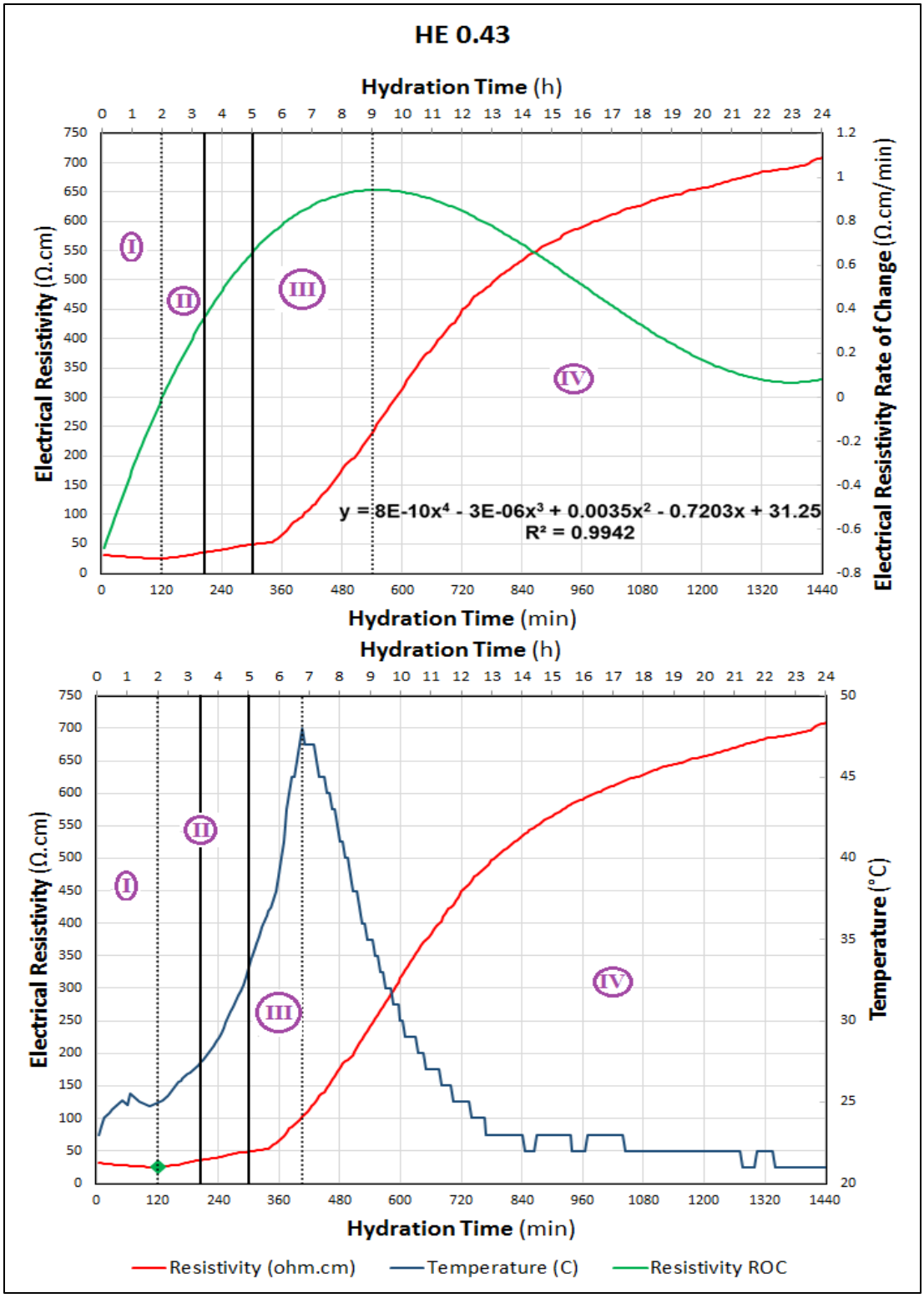


**Figure 5-12: Four stages of hydration based on the electrical resistivity ROC (top graph) and temperature development (bottom graph) of HE 0.43 paste during the first 24 hours of hydration**

The measured properties of the cement paste specimens in Chapter 4 have been used to analyze the electrical and thermal behaviour of the specimens in the different stages of hydration. In the analysis, the cements were categorized as fast (e.g., HE and GUbSF) and normal (e.g., GU and GUL) setting cements. The way cement types are categorized is based on the results illustrated in Figure 4-1 (mini-slump cone or initial consistency results) and Figure 4-4 (construction consistency results).

### 5.1.1. Stage I (Stiffening Stage)

As observed, the dissolution of cement ions in Stage I resulted in a decrease in the electrical resistivity of the cement pastes, but no significant effect was measured in the internal temperature. Therefore, it can be said that ionic dissolution can be detected accurately by monitoring the electrical properties of the cement-based samples, but it cannot be detected by monitoring the internal temperature changes.

In the GU and HE mixtures, which showed some consistency development and therefore hydration prior to 1-hour as per data in Table 4-1, it is noted that the internal temperature started increasing at a slow rate. Unlike the behaviour of HE and GU mixtures, the temperature of GUL and GUbSF mixtures did not increase prior to 1-hour (Figure 5-4 to Figure 5-9). In those mixtures, the increase in the temperature is noted between 1 hour and 2 hours prior to construction consistency development. On the other hand, the first development in the construction consistency is considered the beginning of hydration. Therefore, it can be concluded that monitoring the internal temperature can help in determining the beginning of hydration for GU and HE mixtures.

Mixtures with supplementary cementing materials and replaced Portland cement (e.g., GUbSF and GUL) have shown a drop in their internal temperature (cooling down to equilibrium), because cement exothermic hydration starts later (around 2 hours). The temperatures corresponding to the construction consistencies are tabulated in Table 5-1.

**Table 5-1: Construction consistency versus cement paste temperature**

| Cement Type | Mixture | 1 hr Consistency (mm) | Temperature (˚C) | 2 hrs Consistency (mm) | Temperature (˚C) |
|---|---|---|---|---|---|
| GUbSF | GUbSF 0.37 | 40.00 | 24.80 | 5.50 | 26.29 |
| | GUbSF 0.40 | 40.00 | 24.13 | 30.00 | 24.11 |
| | GUbSF 0.43 | 40.00 | 23.65 | 40.00 | 24.46 |
| GUL | GUL 0.37 | 40.00 | 23.70 | 16.00 | 24.25 |
| | GUL 0.40 | 40.00 | 24.48 | 38.00 | 24.07 |
| | GUL 0.43 | 40.00 | 23.52 | 40.00 | 23.70 |
| HE | HE 0.37 | 15.50 | 23.64 | 1.33 | 24.18 |
| | HE 0.40 | 34.50 | 24.19 | 2.70 | 25.26 |
| | HE 0.43 | 38.00 | 24.83 | 5.10 | 24.96 |
| GU | GU 0.37 | 38.00 | 23.39 | 5.00 | 23.96 |
| | GU 0.40 | 40.00 | 22.85 | 12.50 | 23.70 |
| | GU 0.43 | 40.00 | 23.49 | 32.00 | 23.86 |

It can be concluded that the development of consistency in the cement paste mixtures starts when the temperature of the mix has increased by approximately 1.5-2.0°C from the initial mixing temperature. However, monitoring the ROC in the electrical resistivity is shown to be a more reliable indicator. It can be observed in the data plotted in Figure 5-1 to Figure 5-12 that the ROC becomes zero around the time when the construction consistency starts to develop. Prior to the time of construction consistency development, the mixture is a combination of solid particles floating freely in a liquid medium, and no construction work (other than mixing to make contact between solid particles and the liquids) should be started. Any addition of water to a mixture beyond that time can compromise the later-age compressive strength and durability of the mixture.

The development of consistency in the stiffening stage can be due to the formation of ettringite and Portlandite. However, the 1-hour XRD and TGA results are not available. From the 2-hour XRD analysis presented in Table 4-35 to Table 4-38 and TGA test results in Table 4-17 to Table 4-28, it is noted that the HE and GUbSF mixtures had more hydration products than the reference mixture (GU cement paste). Also, the tabulated results indicate that the replacement of cement with limestone resulted in more hydration products at 2 hours. Hence, although silica fume

contributed later to the hydration (to the point that a later construction consistency and a drop in internal temperature were observed), its hydration resulted in a higher quantity of hydration products. On the contrary, replacement of Portland cement with limestone resulted in the latest development in hydration, consistency development, temperature increase, and hydration product formation.

Beyond the point of consistency, a minor decrease or slow increase in the internal temperature of the cement pastes has been observed. This trend continues until the cement mixture gains its viscosity (determined by the Vane shear test as presented in Section 4.2.5). This point corresponds to the end of Stage I (around 2 hours of hydration). The corresponding temperatures at the point of stiffening (end of Stage I of hydration) in the cement pastes are tabulated in Table 5-2.

**Table 5-2: Internal cement paste temperature at the time of viscosity development**

| Cement Type | Mixture | 2 hours | |
|---|---|---|---|
| | | Rotational Strength (kPa) | Temperature (˚C) |
| GUbSF | GUbSF 0.37 | 1.98 | 26.29 |
| | GUbSF 0.40 | 1.76 | 24.11 |
| | GUbSF 0.43 | 0.55 | 24.46 |
| GUL | GUL 0.37 | 1.43 | 24.25 |
| | GUL 0.40 | 1.10 | 24.07 |
| | GUL 0.43 | 0.44 | 23.70 |
| HE | HE 0.37 | 2.64 | 24.18 |
| | HE 0.40 | 2.20 | 25.26 |
| | HE 0.43 | 1.10 | 24.96 |
| GU | GU 0.37 | 1.32 | 23.96 |
| | GU 0.40 | 0.88 | 23.70 |
| | GU 0.43 | 0.44 | 23.86 |

It is concluded that the viscosity of the cement paste mixtures starts developing at 24.0±0.2˚C for GU and GUL cements and 25.0±0.8˚C for HE and GUbSF cements. As a general indicator, a rapid increase of approximately 10% in the internal temperature of a mixture can be used to determine the time of viscosity development. Determination of the time of viscosity development is crucial for the concrete industry, because, by this moment, all cementing material pouring and

consolidation need to be completed. Hence, the concrete industry can benefit from a more reliable indicator that monitors temperature.

### 5.1.2. Stage II (Setting Stage)

Beyond Stage I of hydration, both the internal temperature and the electrical resistivity of the mixtures are influenced by the hydration. It has been observed in Stage II of hydration, from the stiffening time until the final setting time, that stiffening, AT and electrical resistivity increased. The increase in the stiffening and corresponding temperatures are tabulated in Table 5-3.

**Table 5-3: Internal cement paste temperature at the time of viscosity development**

| Cement Type | Mixture | 2 hours | | Initial Setting | |
|---|---|---|---|---|---|
| | | Rotational Strength (kPa) | Temperature (˚C) | Rotational Strength (kPa) | Temperature (˚C) |
| GUbSF | GUbSF 0.37 | 1.98 | 26.29 | 92.32 | 31.25 |
| | GUbSF 0.40 | 1.76 | 24.11 | 81.78 | 31.13 |
| | GUbSF 0.43 | 0.55 | 24.46 | 68.14 | 31.89 |
| GUL | GUL 0.37 | 1.43 | 24.25 | 60.45 | 26.10 |
| | GUL 0.40 | 1.10 | 24.07 | 54.95 | 27.47 |
| | GUL 0.43 | 0.44 | 23.70 | 41.76 | 27.80 |
| HE | HE 0.37 | 2.64 | 24.18 | 107.93 | 26.30 |
| | HE 0.40 | 2.20 | 25.26 | 96.28 | 28.67 |
| | HE 0.43 | 1.10 | 24.96 | 79.13 | 27.41 |
| GU | GU 0.37 | 1.32 | 23.96 | 61.55 | 25.53 |
| | GU 0.40 | 0.88 | 23.70 | 55.61 | 24.89 |
| | GU 0.43 | 0.44 | 23.86 | 43.52 | 26.47 |

It is important to mention that at the final setting stage, no rotational strength was recorded, as the Vane shear apparatus was not able to perform the rotation. The order of rotational strength development at the initial setting stage in different cement pastes is due to the formation of cement hydration products detected by the TGA test method and reported in Section 4.3.2. According to the test results summarized in Table 4-17 to Table 4-28, the HE, GUbSF, GUL and finally GU cement pastes had shown highest to lowest C-S-H and CH content, respectively. This finding was

consistent with the development of rotational shear strength in the mixtures around the initial setting time.

From the microstructure analysis of the pore structure (Sections 4.3.2 and 4.3.3), ettringite starts decreasing in this stage, as it converts to monosulphate. It was observed that the main cause of cement paste setting was the formation of C-S-H, as more C-S-H was detected by XRD in the initial setting time than at 2 hours. Also, it was observed that around the setting time, the $C_2S$ and mainly $C_3S$ contents were decreased, as they were hydrated, and C-S-H was formed. By formation of C-S-H, the content of ettringite was also decreased. These reactions result in an increase in the AT. In other words, monitoring the formation of calcium silicate hydrate can lead to anticipation of the setting time of cement pastes. The increase in C-S-H content was significant at the final setting time, as shown in Table 4-35 to Table 4-38.

From the electrical resistivity point of view, Stage II (or Setting Stage) starts when the rate of change in the electrical resistivity values of the cement paste mixtures becomes zero (it was negative in Stage I). The same trend is noted in the temperature graphs, as the beginning of Stage II is the time when the temperature of the mixtures started to increase. From the data in Stage II of hydration, the electrical resistivity and corresponding temperature at the initial and final setting times are tabulated in Table 5-4.

**Table 5-4: Electrical resistivity and internal temperature values at setting times of cement pastes**

| Cement Type | Mixture | Initial Setting | | Final Setting | |
|---|---|---|---|---|---|
| | | Electrical Resistivity (Ω.cm) | Temperature (˚C) | Electrical Resistivity (Ω.cm) | Temperature (˚C) |
| GUbSF | GUbSF 0.37 | 33.16 | 31.25 | 33.85 | 33.08 |
| | GUbSF 0.40 | 28.69 | 31.13 | 28.91 | 34.47 |
| | GUbSF 0.43 | 39.93 | 31.89 | 43.75 | 34.22 |
| GUL | GUL 0.37 | 35.45 | 26.10 | 43.05 | 28.67 |
| | GUL 0.40 | 41.83 | 27.47 | 60.47 | 33.83 |
| | GUL 0.43 | 38.33 | 27.80 | 46.93 | 32.18 |
| HE | HE 0.37 | 29.75 | 26.30 | 48.50 | 38.00 |
| | HE 0.40 | 34.29 | 28.67 | 45.44 | 38.00 |
| | HE 0.43 | 35.50 | 27.41 | 48.83 | 33.30 |
| GU | GU 0.37 | 37.88 | 25.53 | 45.31 | 28.08 |
| | GU 0.40 | 36.40 | 24.89 | 47.38 | 29.04 |
| | GU 0.43 | 39.84 | 26.47 | 50.35 | 30.49 |

As can be concluded from the results in Figure 4-21 to Figure 4-24, and also from the data tabulated in Table 5-4, the electrical resistivity values in Stage II are not influenced significantly by cement hydration, despite the physical properties of the mixture (e.g., setting and stiffening) are affected. Based on the measured electrical resistivity values, an electrical resistivity of 36±4 Ω.cm and 45±8 Ω.cm can be used as the indicator for initial and final setting times, respectively. In the case that normal setting cements are specified, the average electrical resistivity values of 38±2 Ω.cm and 49 ±6 Ω.cm represent initial setting and final setting times, respectively. For GUbSF and HE cements, the average electrical resistivity values of 33±4 Ω.cm and 41±8 Ω.cm represent initial and final setting times, respectively.

It was noted that the range of electrical resistivity values to indicate the setting times was wide, which is not practical for the concrete industry. However, a more practical range of internal temperatures can be suggested to signify the setting times; according to the values reported in Table 5-4, a cement paste temperature of 28±2°C and 33±3°C can be used as the indicator for initial and final setting times, respectively. As a general indicator, an increase of 30% and 45-50%

in the internal temperature of the mixture can represent the initial setting time and final setting time, respectively.

### 5.1.3. Stage III (Hardening Stage)

The end of Stage II and beginning of Stage III corresponds to the time at which a sharp increase in the electrical resistivity is recorded. This time is around the final setting time. It is also observed in Stage III that the internal temperature of the mixtures raises significantly compared to that in Stage II. This stage is beyond the final setting time, and it can be said that the physical behaviour of the cement-based mixtures changes from setting to hardening. In Stage III, the increase in the electrical resistivity value of the mixtures becomes more significant. As observed in Figure 5-1 to Figure 5-12, the ROC in the electrical resistivity starts to increase into positive values from zero at Stage II until the end of Stage III. If the electrical resistivity development is considered as an indicator, Stage IIII ends when the momentum of the ROC becomes zero. However, it has been observed from Figure 5-1 to Figure 5-12 that the AT is a better indicator for determining the end of Stage III. Stage III ends when the internal temperature reaches a maximum, and the momentum in the temperature trend becomes zero.

During Stage III, thermal curing must be implemented to protect the concrete from experiencing a rapid temperature increase. Addition of moisture, for the purpose of curing, does not result in an increase in the mixture free water, as the mixture is beyond the setting time. From a temperature point of view, the internal temperature of the cement paste mixtures is still increasing in the hardening stage (although about 50% of Alite and Belite had been used in hydration as observed in Section 4.3.3), but with a reduced momentum to the point that the temperature ROC becomes zero at the end of this stage. It can be concluded that the increase in temperature beyond the final setting time, as seen in Figure 4-48, was because of the hydration of $C_2S$, $C_3S$, and $C_3A$.

### 5.1.4. Stage IV (Strengthening Stage)

As the ROC in the AT becomes zero, hardening is completed and strengthening begins, so partial loading is allowed. Stage IV of hydration begins when the momentum of the electrical resistivity value starts to decrease. This reduction in the ROC of the electrical resistivity of the cement paste mixtures means that the cement pastes become more electrical resistant, but at a lower rate. The

study of the microstructure of the cement pastes at 24 hours indicates that the ROC of the electrical resistivity starts to decrease due to the formation of C-S-H, which is porous at the beginning and therefore allows for diffusion of ions in the pore solution, promoting more hydration reactions. The diffusion of ions and the formation of more hydration products have opposite effects in the electrical resistivity development of the mixtures. Therefore, in this stage, although the resistivity of the cement pastes increases due to the formation of the pore structure, the rate of increase is slower due to ions diffusion in the pore solution. Among the cement types, the presence of more ettringite in the HE and GUbSF cement pastes at this stage (see Figure 4-63 to Figure 4-66) can be another factor in observing higher electrical resistivity values in those cement mixtures in comparison with those in the GU and GUL cement pastes.

From a thermal behaviour point of view, Stage IV is the stage that the ROC of the internal temperature of a cement paste becomes negative in value, as the mixture starts cooling down to room temperature. This is because of the slower rate of cement exothermic hydration. This reduction was faster in the GU cement paste, because the HE, GUbSF, and GUL cement pastes had more cement hydration products than GU at 24 hours of hydration, as per the TGA results presented in Table 4-17 to Table 4-28. This observation is important for the concrete industry as rapid internal temperature reduction must be prevented in concrete elements. Therefore, thermal protection should be started in this stage. Also, if heat or steam curing is required, it can be practiced during Stage IV of hydration. Prior to Stage IV, any heat curing can result in an internal temperature above the limit.

From a strength point of view, the formation of C-S-H (as proved by the XRD results presented in Section 4.3.3) is responsible for linking together the semi-hydrated cement particles into the 3D network of the pore structure. This is the beginning of the cement paste strengthening. It was observed that the addition of limestone resulted in a higher 1-day compressive strength in the GUL cement paste than that of the GUbSF cement paste. The limestone reaction took place earlier than the silica fume reaction. To study the effect of limestone, the C-S-H content of GUL and GUbSF mixtures at 24 hours (from the XRD analysis in Table 4-35 to Table 4-37) is compared in Figure 5-13.

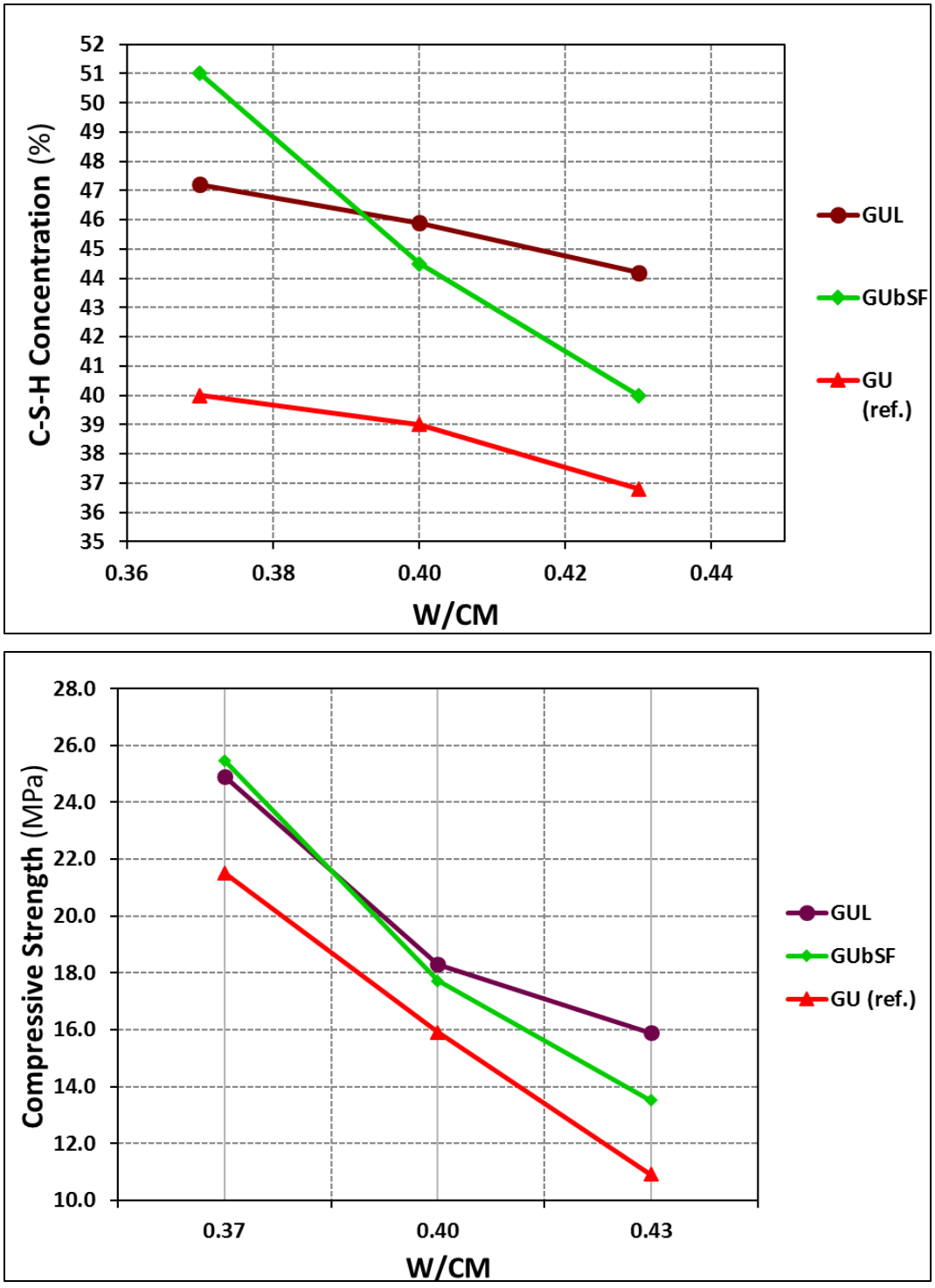


**Figure 5-13: C-S-H concentration (top) and compressive strength (bottom) of cement paste mixtures at 24 hrs**

From Figure 5-13, it is observed that regardless of the W/CM, the GUL cement paste with higher 1-day compressive strength than that of the GUbSF cement paste has a higher content of C-S-H.

For a W/CM ratio of 0.37, the GUbSF cement paste had more C-S-H percentage compared to C-S-H in the GUL cement paste, with a corresponding higher compressive strength at 24 hours. The hydration of cement paste at this stage is also confirmed by the reactivity of Alite and Belite, as illustrated in Figure 4-80, where more than 70 % of the initial $C_2S$+$C_3S$ content had been reacted by the end of Stage IV.

## 5.2. Electrical Resistivity Normalization

As described in Section 2.3.4.1, the electrical resistivity increases as the temperature of the mixture decreases for all cementing-based mixtures. The Arrhenius relationship expressed in Equation 2-14 can be employed to correct the measured electrical resistivity values for temperature effects using an activation energy of conduction if the mixture temperature is above 0˚C during the first 24 hours of hydration.

### 5.2.1. Determination of Activation Energy of Conduction

Before using Equation 2-14 for normalizing the measured electrical resistivity values, the activation energy of conduction needs to be determined. By using the method described in Section 2.3.4.1, the activation energy of conduction, $E_a$, can be determined by multiplying the slope of the conductivity (1/Ω.cm) versus 1000/($T$+273) curve by the gas constant, where $T$ is the testing temperature in °C. However, the curves representing the development of electrical resistivity for the first 24 hours of hydration for all the cement paste mixtures, presented in Figure 5-1 to Figure 5-12, have shown that the electrical resistivity changes during that period. Therefore, a constant activation energy cannot be determined since the slopes of the conductivity graphs change from every stage of hydration.

In determining the activation energy of conduction $E_a$, it was noted that the cementing-based specimens display two conductivity behaviours in Stage I of hydration, as illustrated in Figure 5-14 to Figure 5-17. In this stage of hydration, the momentum of the conductivity versus temperature graph both increases and decreases. Within the other phases of hydration, the slope of the conductivity versus temperature remains constant in that hydration phase.

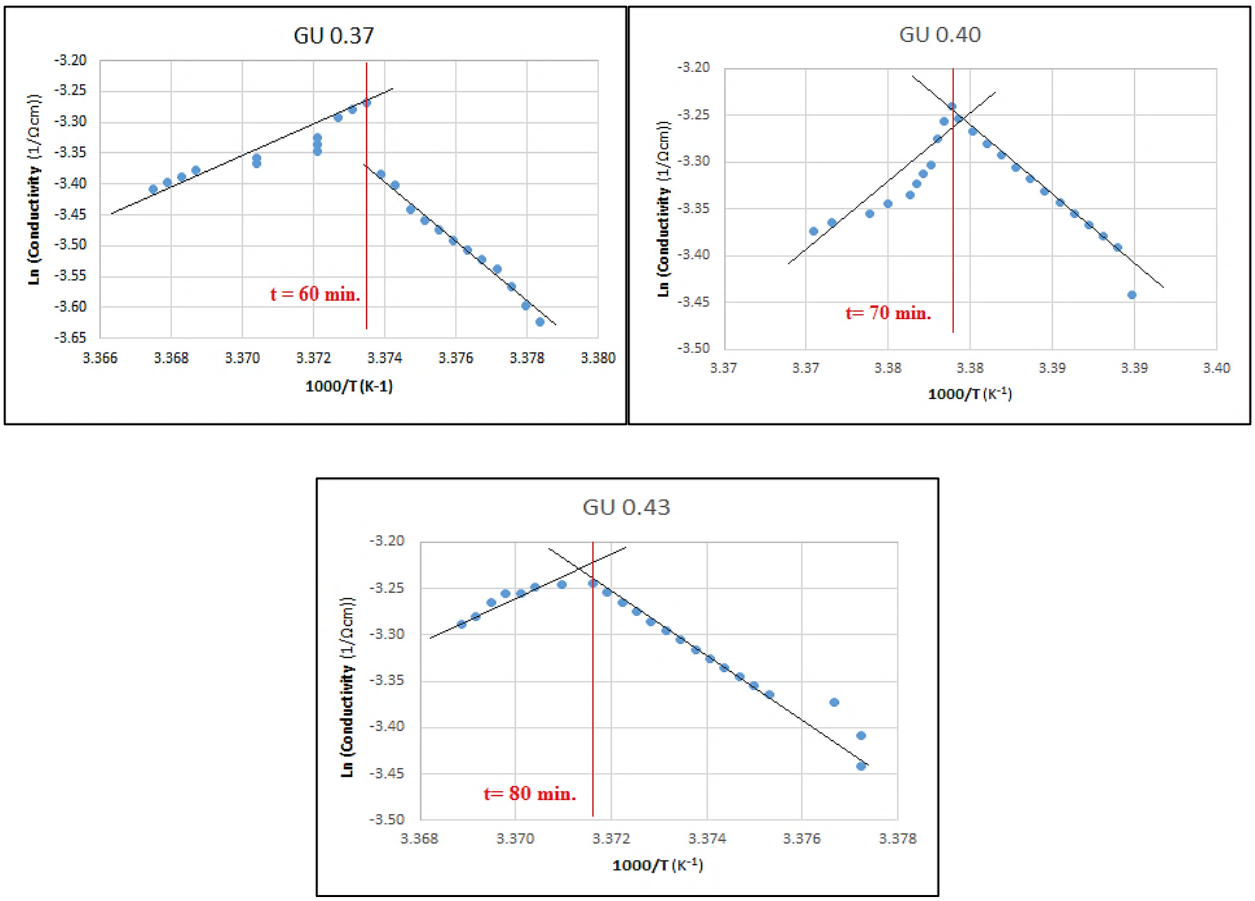


**Figure 5-14: Conductivity behaviour of GU specimens during Stage I of hydration**

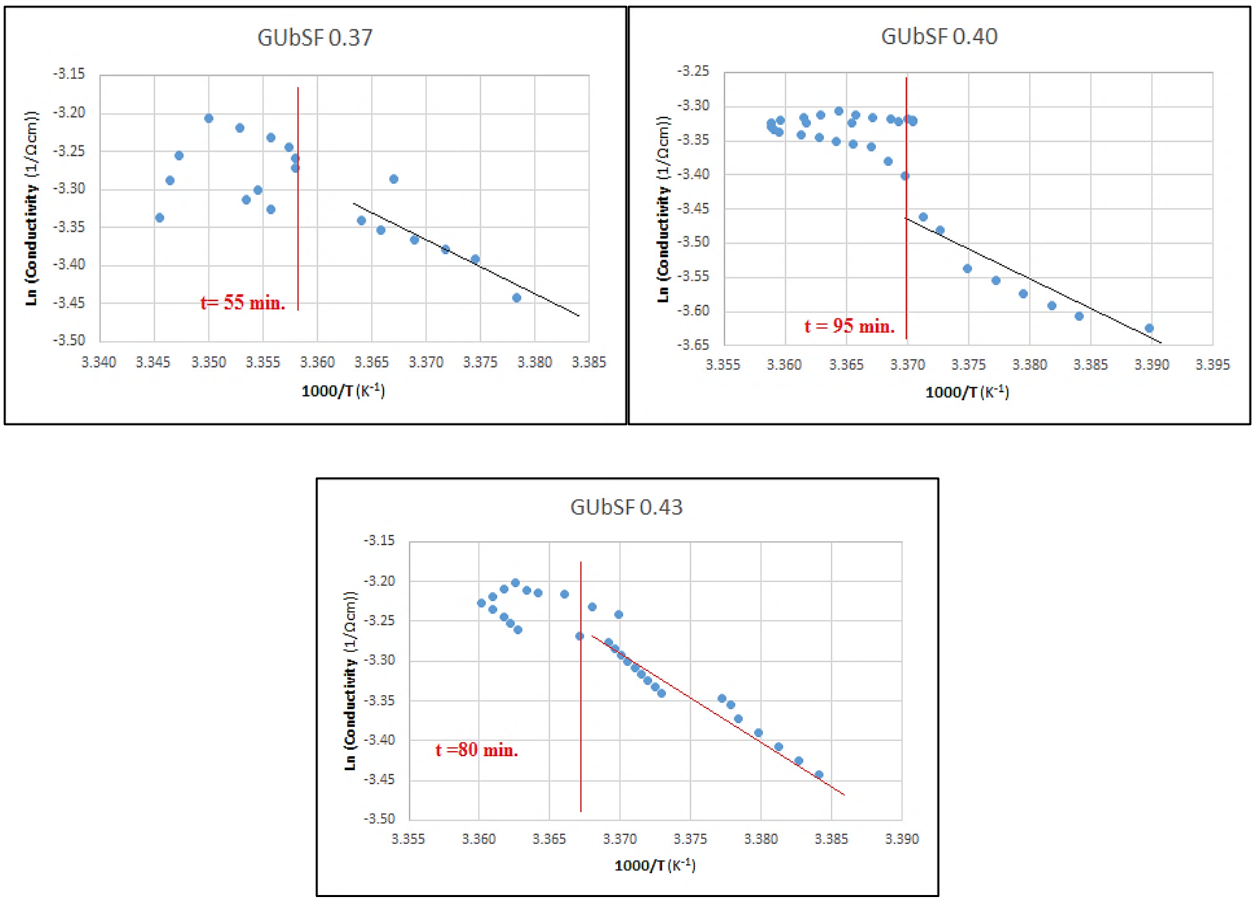


**Figure 5-15: Conductivity behaviour of GUbSF specimens during Stage I of hydration**

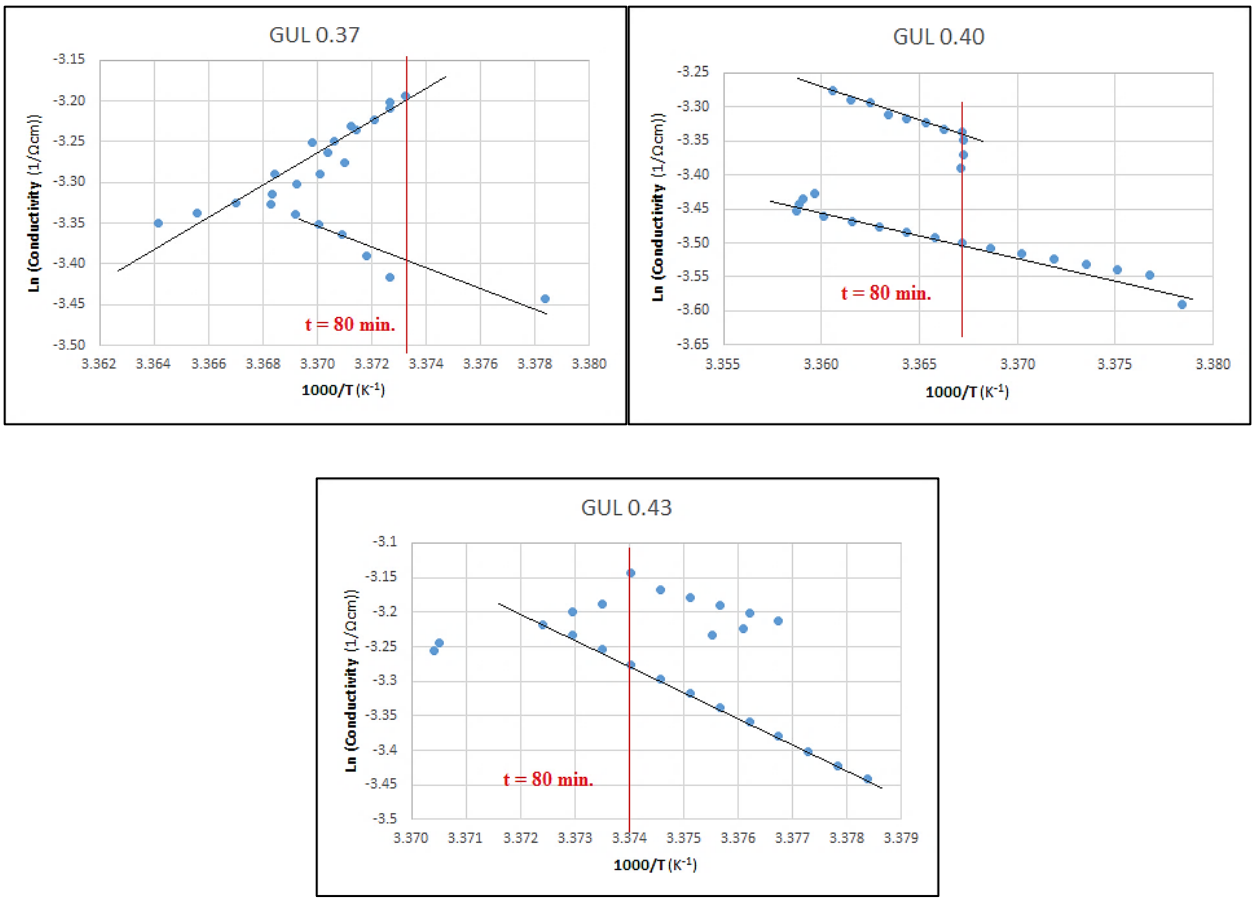


**Figure 5-16: Conductivity behaviour of GUL specimens during Stage I of hydration**

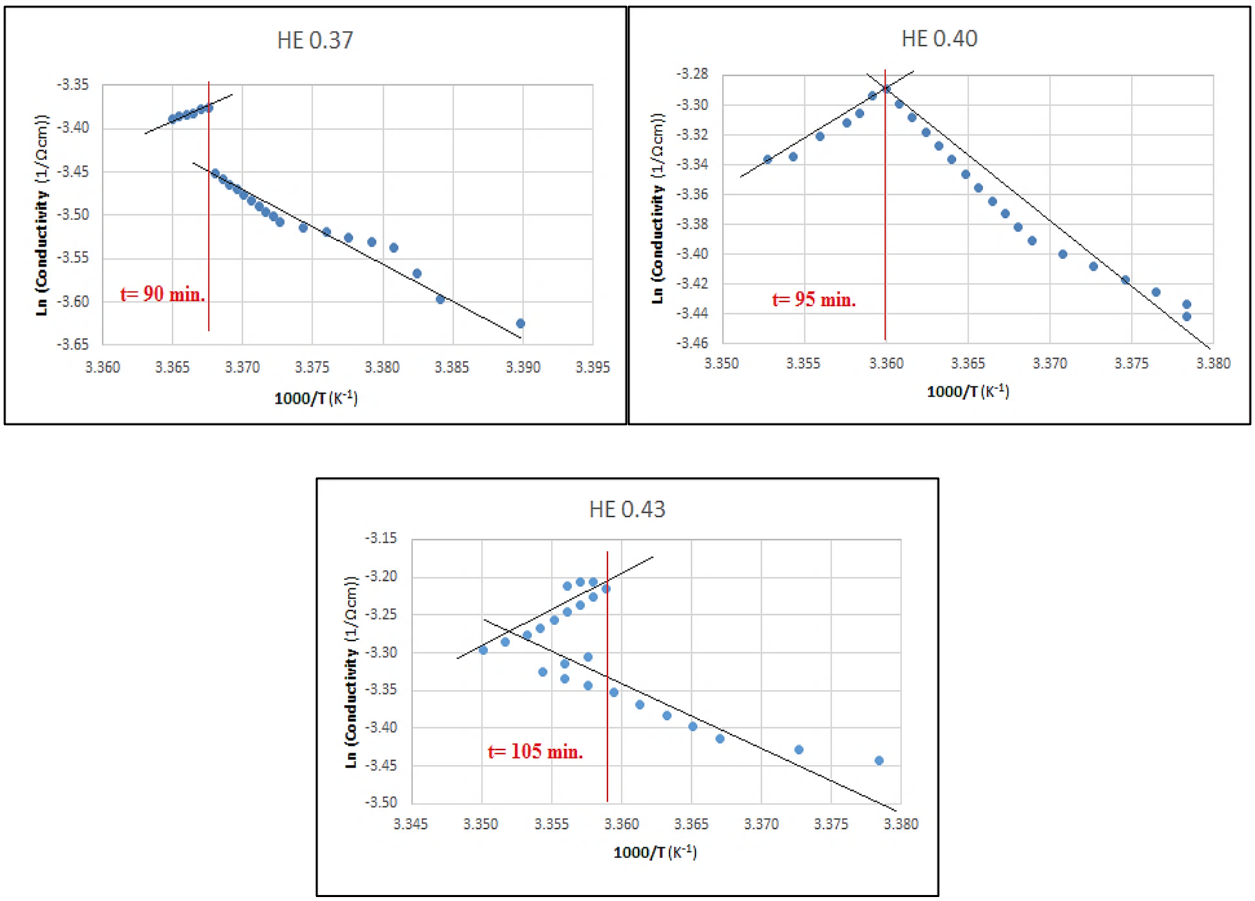


**Figure 5-17: Conductivity behaviour of HE specimens during Stage I of hydration**

The times at which the momentum of the conductivity of the mixtures' changes are tabulated in Table 5-5. The time at which the construction consistency is developed, the only other changing parameter during Stage I of hydration, is also tabulated in Table 5-5.

**Table 5-5: Time of construction consistency development and time of conductivity change in Stage I**

| Mix Design | | Construction Consistency Development (min.) | Time of change in Conductivity Momentum (min.) |
|---|---|---|---|
| **Cement Type** | **W/CM** | | |
| **GU** | **0.37** | 60 | 60 |
| | **0.40** | 70 | 70 |
| | **0.43** | 90 | 80 |
| **GUL** | **0.37** | 80 | 80 |
| | **0.40** | 100 | 80 |
| | **0.43** | 125 | 80 |
| **GUbSF** | **0.37** | 65 | 55 |
| | **0.40** | 85 | 95 |
| | **0.43** | 120 | 80 |
| **HE** | **0.37** | 45 | 90 |
| | **0.40** | 55 | 95 |
| | **0.43** | 60 | 105 |

It is noted that in most of the mixtures, the change in the slope of the conductivity versus temperature graphs happens around the time that the construction consistency of the specimens starts developing. As discussed in Section 2.3.2, the main cause for the rapid increase in measured conductivity of the mixtures at the beginning of Stage I is the diffusion of the ions in the medium. Also, it was discussed that the diffused ions can be absorbed by the cement hydration products. As concluded from the data presented in Section 4.3 and analysis in Section 5.1, the construction consistency in the mixtures develops when the physical pore structure starts forming. At that time, the ionic concentration starts decreasing because ions get absorbed in the formed pore structure. The change in the ionic concentration before and after the development of the construction consistency (and therefore pore structure formation) is the reason behind the changes in the momentum of the conductivity development in Stage I of the mixtures' hydration. Therefore, monitoring the momentum of the electrical conductivity (or resistivity) development in Stage I can lead to estimating the beginning of the construction consistency development and therefore the beginning of the pore structure formation. This can be beneficial to the concrete ready-mix industry.

In addition to the two different slopes in the linear regression of the conductivity versus temperature graphs in Stage I, the slope of the similar graphs in the other stages of hydration were also not constant. A constant value of the activation energy of conduction cannot therefore be

calculated. In this case, the constant $E_a$ value of 15.8 kJ/mol for saturated specimens is employed, as suggested by previous researchers reviewed in Section 2.3.4 (Coyle et al., 2019).

### 5.2.2. Normalizing Measured Electrical Resistivity Values

Since all the specimens in this study were kept in a controlled and sealed environment during the first 24 hours of hydration, it is considered that the mixtures were in a saturated condition during all four stages of hydration. Hence, the constant activation energy of conductance of 15.8 kJ/mol is employed for the first 24 hours of hydration of the mixtures.

By using the relationship described in Equation 2-14, the measured electrical resistivity values presented in Figure 4-6 to Figure 4-17 were normalized. The normalized electrical resistivity values are plotted in comparison with the measured values in Figure 5-18 to Figure 5-29.

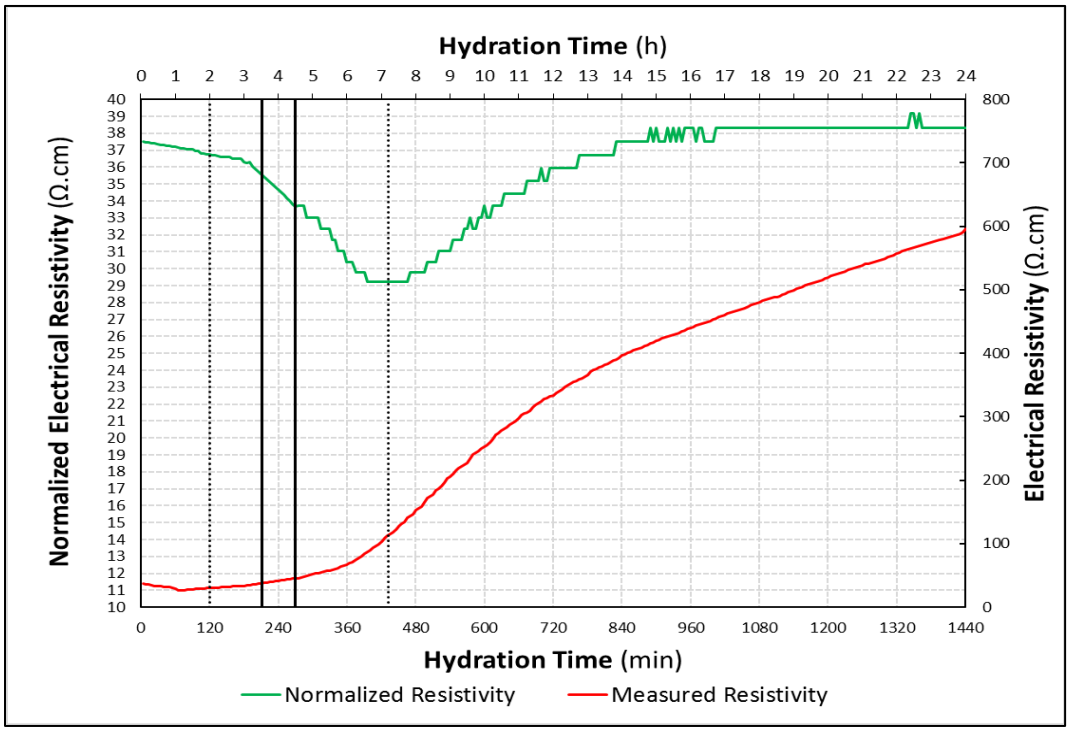


**Figure 5-18: Normalized and measured electrical resistivity development of GU 0.37 mixtures over the first 24 hours of hydration**

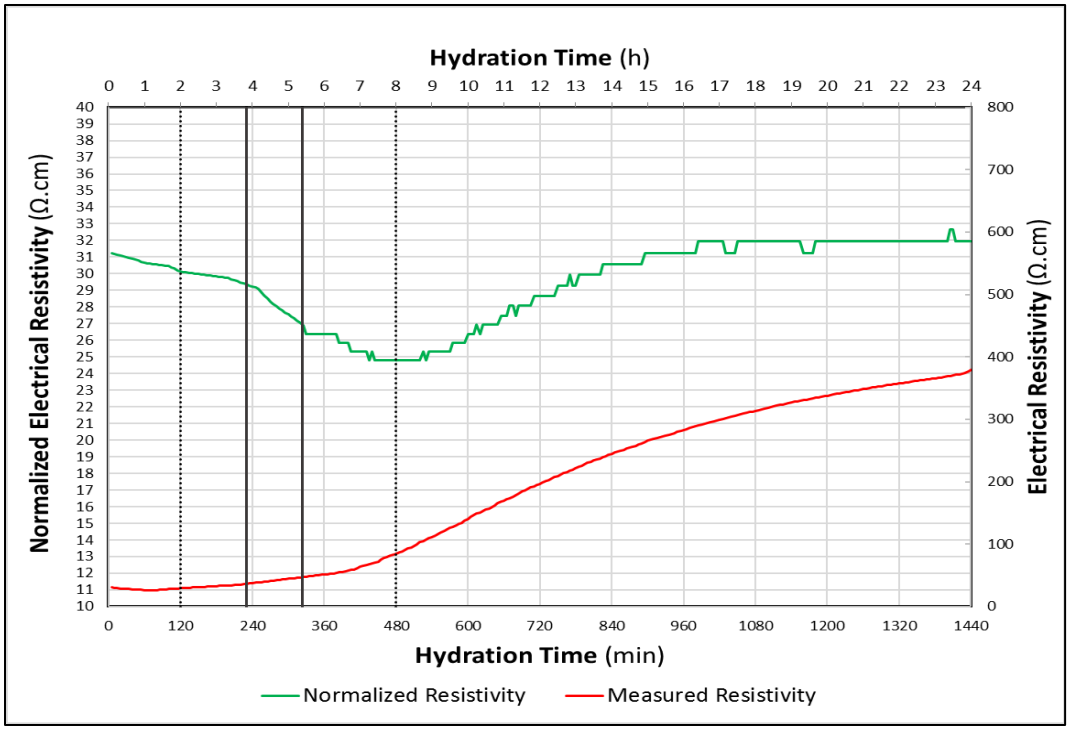


**Figure 5-19: Normalized and measured electrical resistivity development of GU 0.40 mixtures over the first 24 hours of hydration**

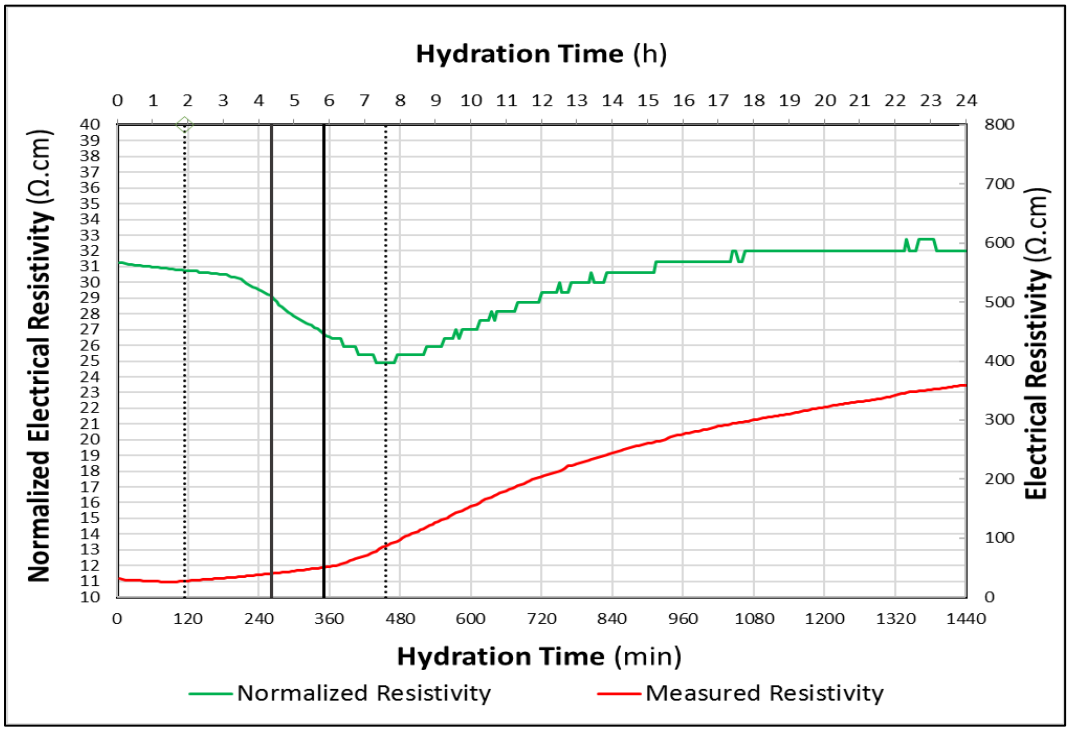


**Figure 5-20: Normalized and measured electrical resistivity development of GU 0.43 mixtures over the first 24 hours of hydration**

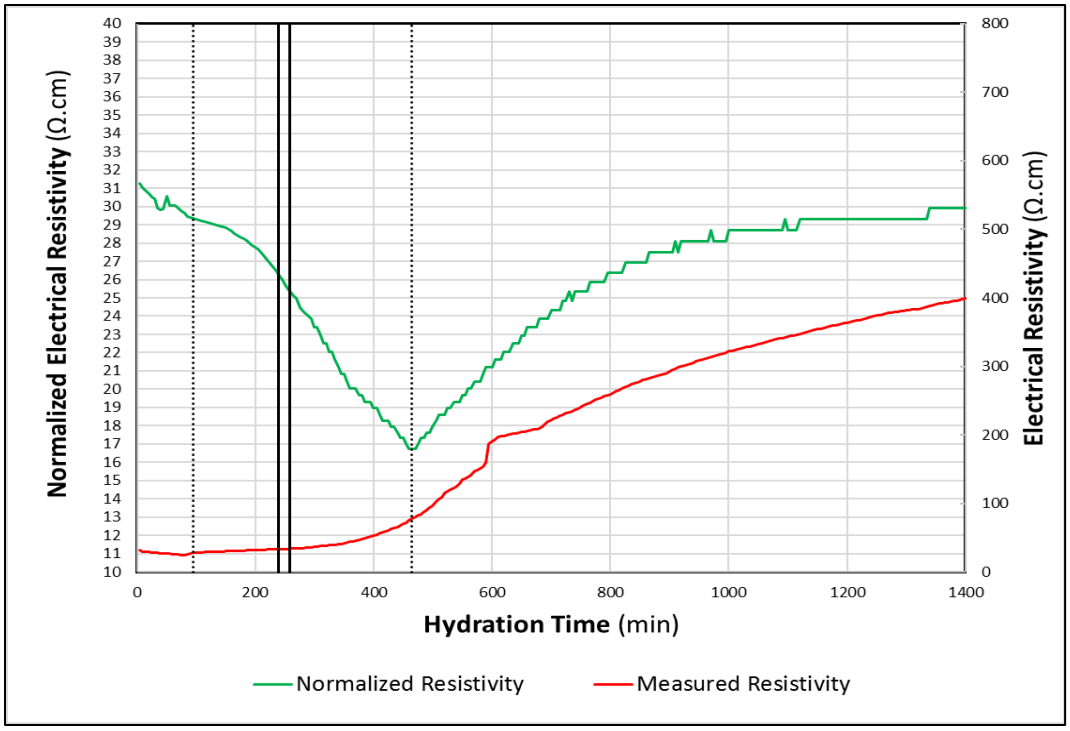


**Figure 5-21: Normalized and measured electrical resistivity development of GUbSF 0.37 mixtures over the first 24 hours of hydration**

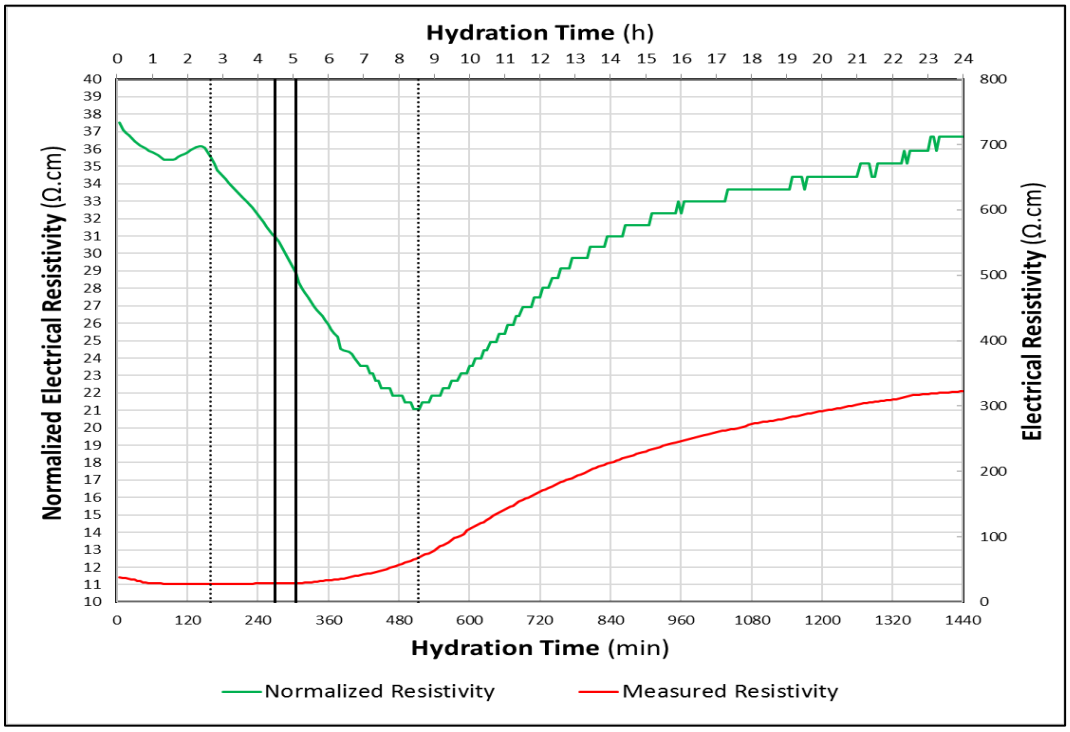


**Figure 5-22: Normalized and measured electrical resistivity development of GUbSF 0.40 mixtures over the first 24 hours of hydration**

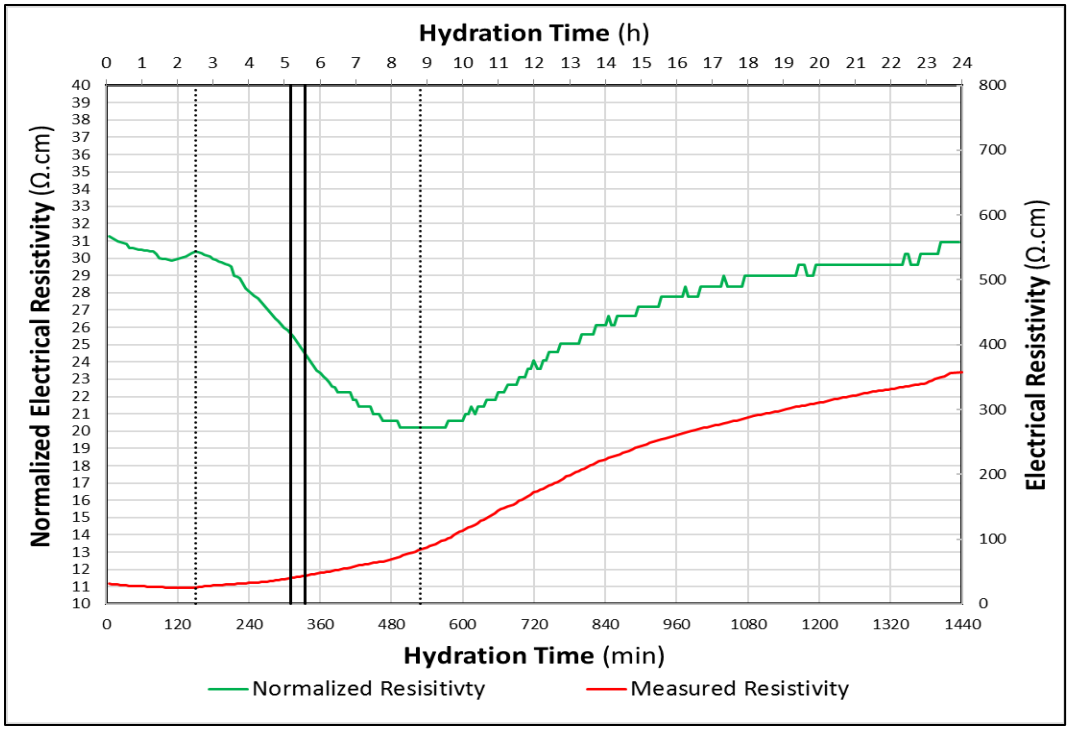


**Figure 5-23: Normalized and measured electrical resistivity development of GUbSF 0.43 mixtures over the first 24 hours of hydration**

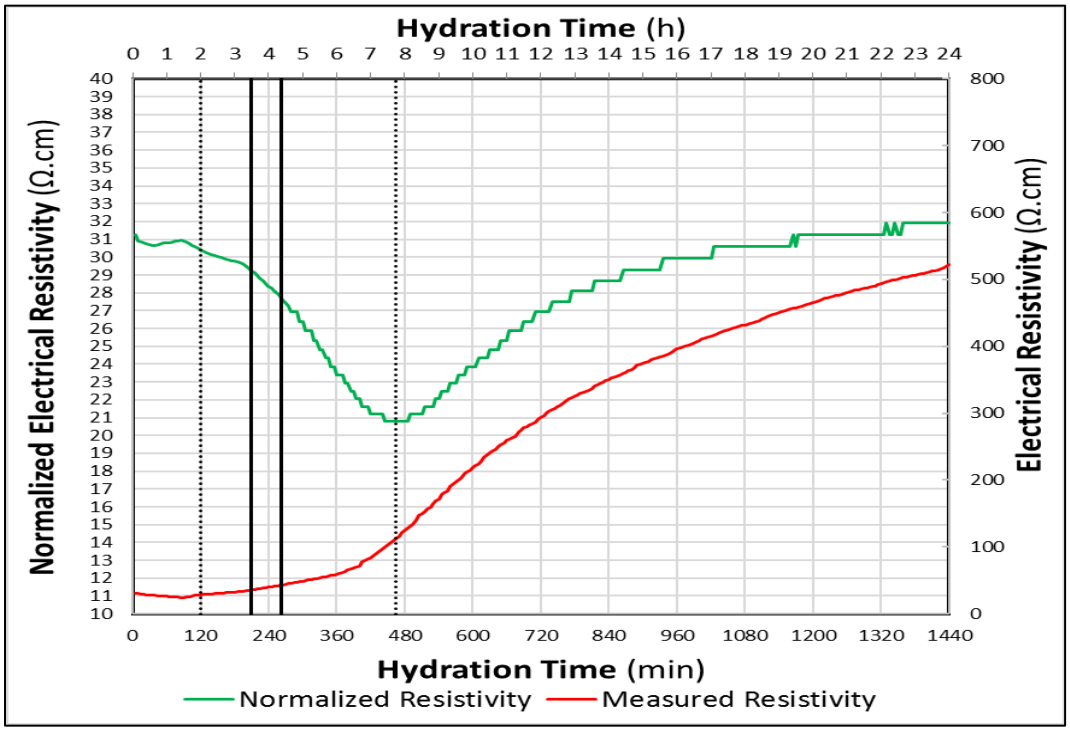


**Figure 5-24: Normalized and measured electrical resistivity development of GUL 0.37 mixtures over the first 24 hours of hydration**

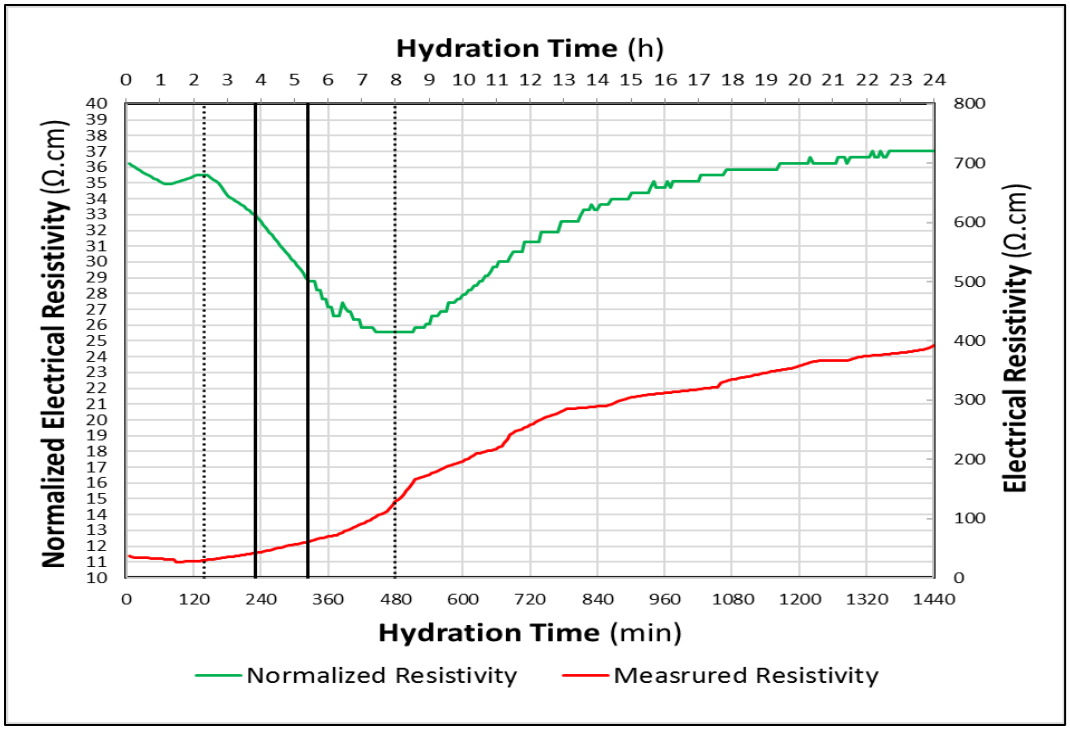


**Figure 5-25: Normalized and measured electrical resistivity development of GUL 0.40 mixtures over the first 24 hours of hydration**

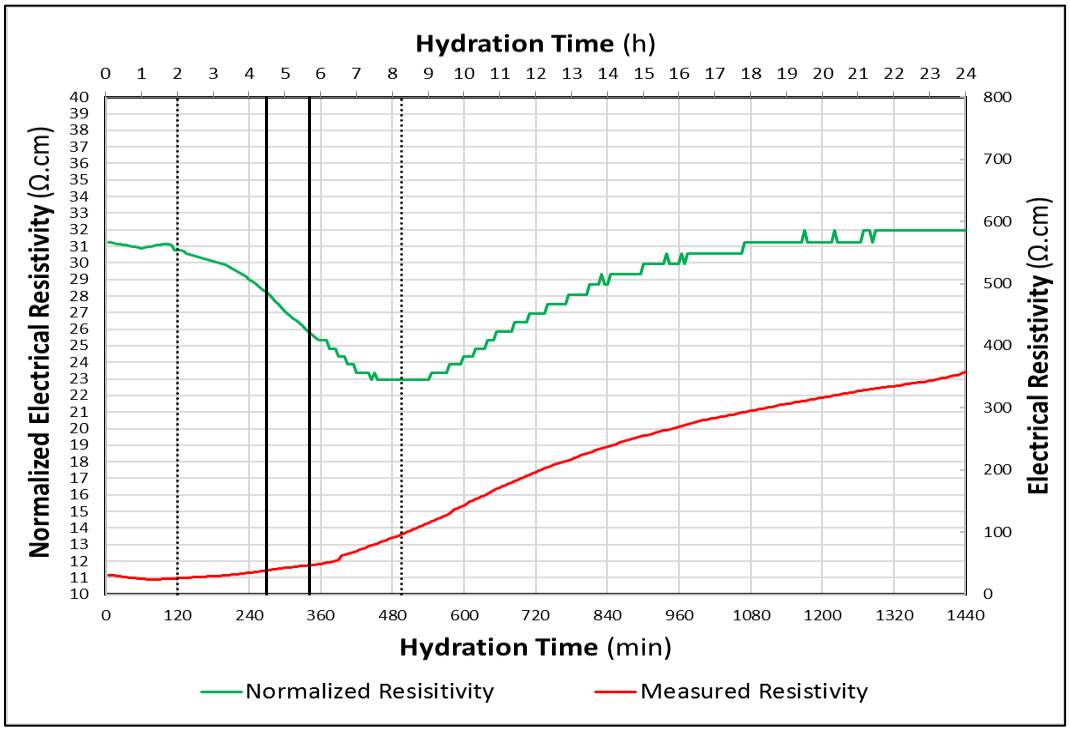


**Figure 5-26: Normalized and measured electrical resistivity development of GUL 0.43 mixtures over the first 24 hours of hydration**

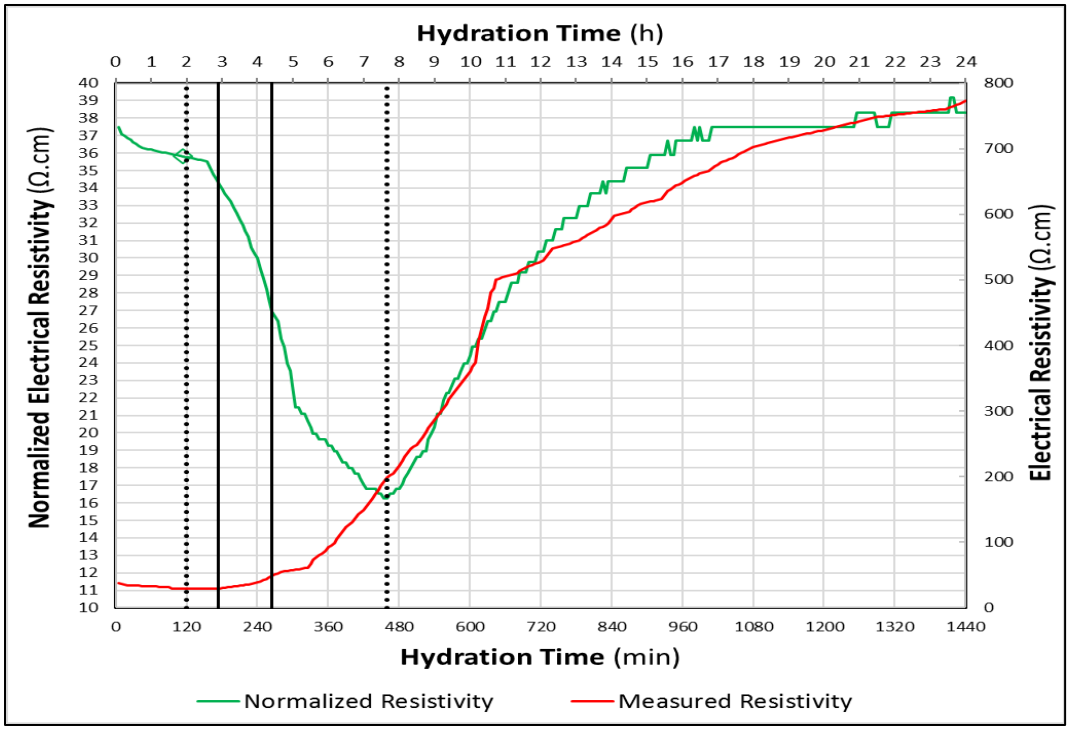


**Figure 5-27: Normalized and measured electrical resistivity development of HE 0.37 mixtures over the first 24 hours of hydration**

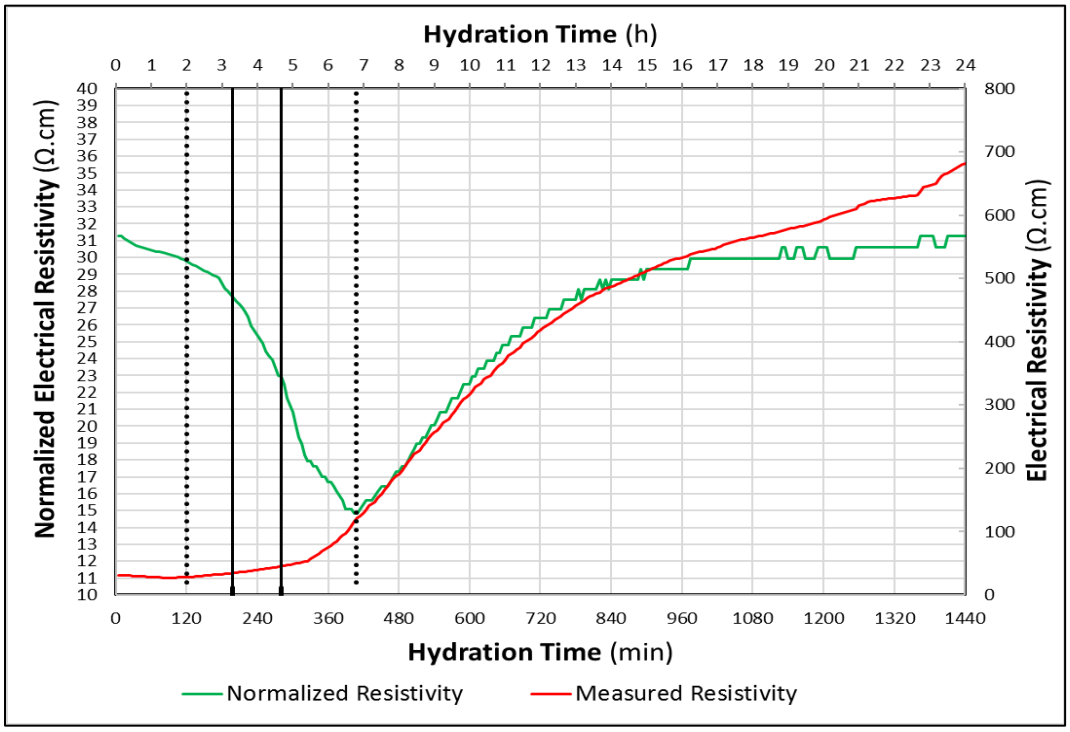


**Figure 5-28: Normalized and measured electrical resistivity development of HE 0.40 mixtures over the first 24 hours of hydration**

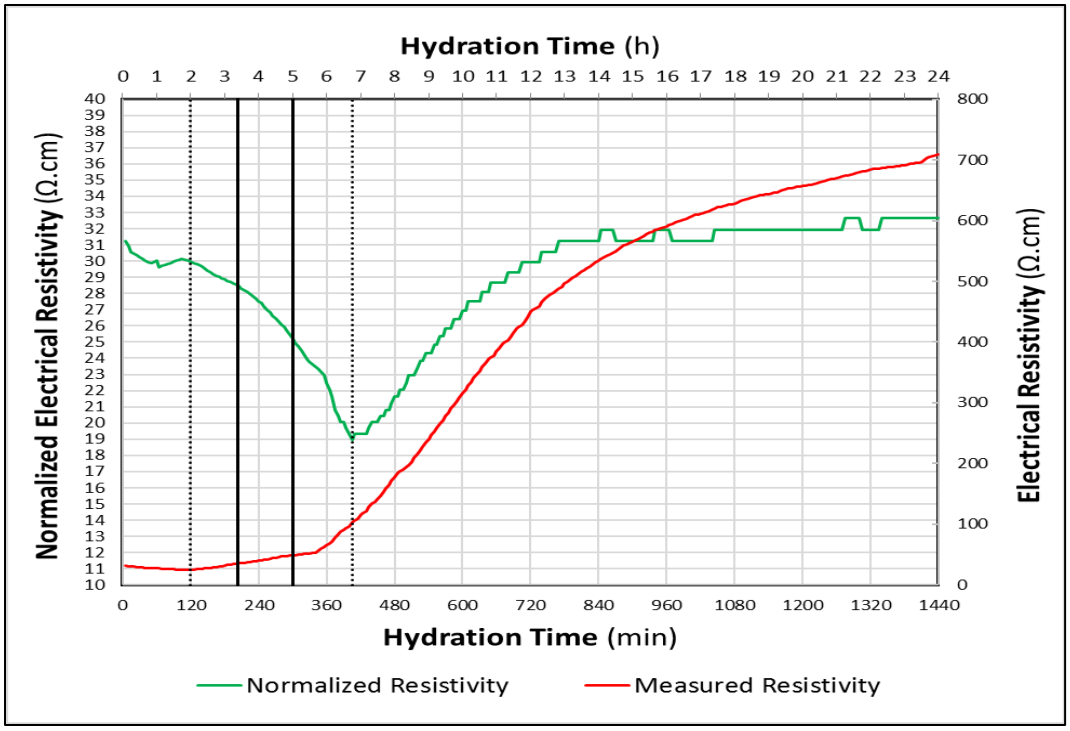


**Figure 5-29: Normalized and measured electrical resistivity development of HE 0.43 mixtures over the first 24 hours of hydration**

All four stages of hydration, discussed in Section 5.1, can be noted in the normalized electrical resistivity curves for the first 24 hours of hydration of all the mixtures. As opposed to the measured electrical resistivity, the normalized resistivity decreases in the first three stages of hydration. From the graphs plotted in Figure 5-18 to Figure 5-29, it can be noted that the initial measured electrical resistivity for all mixtures is the same, whereas the initial normalized electrical resistivity ranges from 31 to 37 (Ω.cm). The normalized values (independent from temperature effects) decrease in the first three stages of hydration, while the measured values (temperature affected resistivity values) increase. In the strengthening stage or Stage IV, both electrical resistivity values increase as hydration proceeds. The turning points at the normalized electrical resistivity graphs plotted in Figure 5-18 to Figure 5-29 can be used to signal the initiation of the strengthening stage. Prior to this point, the measured electrical resistivity values were mainly influenced by the heat of hydration in the mixtures. Although it was observed in Sections 4.3.2. and 4.2.3 that hydration products were developed in Stages I, II, and III, their development could not make the mixtures electrically resistant. This observation is probably caused by the presence of more ions in the pore

solutions in those stages, which made the mixtures electrically less resistant. This is something that could not be verified due to the challenge of extracting the pore solution beyond Stage I, and therefore its analysis was not possible, as described in Section 4.3.1. Beyond Stage III, when the mixtures specimens started cooling down to the room temperature, the measured electrical resistivity values were influenced more by the physical pore structure development than by temperature. This is the reason behind a similar trend in both the measured and normalized electrical resistivity values in Stage IV.

### 5.3. Practical Applications for the Concrete Industry

The main goal of this research program is to suggest to the concrete industry a practical application for using the electrical resistivity (measured and normalized) and internal temperature values of cementing-based mixtures to determine the setting times. During the program, it was noted that the electrical and thermal properties of the mixtures can also be used as indicators for determination of different stages of hydration.

Based on the results presented in Chapter 4 and analysis from Chapter 5, practical applications of the research outcomes are summarised and tabulated in Table 5-6.

**Table 5-6: Electrical resistivity and internal temperature values at setting times of cement pastes**

| Stage of Hydration | Concrete Property / Microstructure Analysis | Occurrence | Industrial Application | Indicator | | Indication |
|---|---|---|---|---|---|---|
| | | | | Concept | Monitoring Property | Value |
| Stage I | Construction Consistency (gypsum dissolution & hydration beginning) | Mid-stage | Beginning of Casting | Beginning of Pore Structure Formation | Momentum in Conductivity Change | Switching Between -/+ ROC |
| | Yield Stress (ettringite and AFm formation) | End of Stage (about 2 hours) | End of Concrete Pumping\Pouring | Heat of Hydration Development | Temperature | Rapid 10% increase in temperature |
| Stage II | Initial Setting (C-S-H formation/ettringite reduction) | Mid-stage | End of Concrete Work + Final Finishing | Ettringite Formation | Electrical Resistivity | 38±2 Ω.cm (GU and GUL cement) |
| | | | | | | 33±4 Ω.cm (HE and GUbSF cement) |
| | | | | Heat of Hydration | Temperature | 30% increase in temperature |
| | Final Setting (C-S-H formation/ettringite reduction) | End of Stage | Beginning of Curing | Pore Structure Formation | Electrical Resistivity | 49±6 Ω.cm (GU and GUL cement) |
| | | | | | | 41±8 Ω.cm (HE and GUbSF cement) |
| | | | | Heat of Hydration | Temperature | 45-50% increase in temperature |
| Stage III | Hardening Stage (C-S-H formation) | Mid-stage | Curing Period | Formation of C-S-H | ROC in Electrical Resistivity | Decreasing towards zero |
| | | End of Stage | | | Temperature | Achievement of Maximum Temperature |
| | | | | | ROC in Electrical Resistivity | 0 |
| Stage IV | Hardening (C-S-H and CH increase) | Beginning of Stage | Strength Development/ Loading | Reduction in the Rate of Hydration | ROC Normalized Electrical Resistivity | Switching Between -/+ ROC |

The indicating values for setting times can be used to replace the time-consuming and laboratory-based method, described in ASTM C191 (Standard Test Method for Time of Setting of Hydraulic Cement by Vicat Needle). The method proposed in this research program can be applied in the field, as indicating factors are independent from the construction site's environmental conditions.

# 6. SUMMARY AND FUTURE WORK

## 6.1. Introduction

The feasibility of using a practical and non-destructive technique to detect the actual cementing-based pastes' setting time was studied in this research project. During the program, the electrical properties of cementing-based mixtures were monitored over the first 24 hours of hydration. These properties were noted to be influenced by the cements hydration, similar to the setting time. To isolate the effect of the specimen geometry, electrical resistivity was chosen as the electrical properties' representative, which was measured by an in-house resistivity-meter setup. Since the formation of hydration products and crystallization is exothermic, the changes in the internal temperature of the mixtures were also monitored. To isolate the thermal effects on the electrical properties of the mixtures, the measured electrical resistivity values were normalized with the internal temperatures.

To develop a reliable and accurate method, the microstructure factors affecting the electrical resistivity development of fresh cement paste, which were (1) the ionic concentration and (2) the hydration products, were also studied.

Finally, reliable indicators considering not only the fresh stage ionic concentration, but also the development and changes in the physical characteristics of the microstructure were proposed to the industry, so that electrical resistivity (representing the electrical properties of the cement paste) and internal temperature measurements can be used as factors, predicting the initial and final setting times of cast in-place concrete.

## 6.2. Conclusions

1- Development of the 1-hour construction consistency is an indication for the initiation of cement hydration. Mixtures which developed 1-hour construction consistency (e.g., HE mixtures) showed an increase in the internal temperature (which is a sign of the beginning of the exothermic cement hydration process), while others showed some decrease during the first hour of hydration. However, monitoring the momentum of electrical resistivity is a more reliable indicator; it becomes zero around the time when the construction consistency starts to develop.

2- The dissolution of cement ions during Stage I of hydration can be detected by the rapid reduction in the electrical resistivity of the paste, while the temperature of the paste does not change significantly.

3- The development of the construction consistency in the cement paste mixtures, which is considered an indicator of the beginning of cement hydration, starts when the momentum in the electrical conductivity of the mixtures switches from negative to positive.

4- The maximum allowable time for a cementing material transportation, pouring, and consolidation can be determined by monitoring the beginning of stiffening. The first significant increase in the internal temperature of the mixtures is observed at the time at which the mixtures start stiffening (around 2 hours of hydration approximately). It is concluded that the viscosity of the cement paste mixtures starts developing at 24.0±0.2˚C in GU and GUL cements and at 25.0±0.8˚C in HE and GUbSF cements. Monitoring the temperature for a 10% increase is more reliable rather than setting a time indicator.

5- Among all cements, GUbSF showed longer initial setting time, due to the delayed pozzolanic reaction of silica fume. This finding can be beneficial to the concrete industry, as longer concrete work time is allowed. However, to prevent pre-mature finishing of concrete surfaces with GUbSF cement (and surface scaling and flaking later), it has to be considered that the concrete sets longer than usual.

6- Beyond the stiffening stage (Stage II of hydration), both the internal temperature and the electrical resistivity values of the cement paste are influenced by the cement hydration (both increasing). In this stage, concrete starts to set due to the increase in reactivity of Alite and Belite.

7- In the Setting stage, the cementing-based pastes electrical resistivity and internal temperature show a similar trend. The pastes' internal temperature of 28±2°C and 33±3°C can be used as the indicator for initial and final setting times, respectively. For normal setting mixtures (i.e., GU and GUL cements), the average electrical resistivity values of 38±2 Ω.cm and 49±6 Ω.cm represent initial setting and final setting times, respectively.

For GUbSF and HE cements, the average electrical resistivity values of 33±4 Ω.cm and 41±8 Ω.cm represent initial and final setting times, respectively.

8- Although electrical resistivity values can be used for determining the initial and final setting times, the internal temperatures can be more reliable indicators. An increase of 30% and 45-50% in the internal temperature of a mixture can be used as indicators for initial setting and final setting times, respectively.

9- The increase of the cement paste temperature before final setting (Stage I and Stage II) is mainly due to the reactions of Alite and Belite. However, the temperature of the mixtures kept increasing beyond final setting, although about 50% of Alite and Belite had already reacted.

10- As hydration proceeds, the setting phases transit to hardening, which is confirmed by CH and C-S-H formation in the TGA and XRD analysis. This is the beginning of Stage III, where a sharp increase in the electrical resistivity of the cement paste can be observed, which can be used as an indicator for detecting the final setting time. The formation of C-S-H and CH is the main reason behind the rapid increase in the ROC of the electrical resistivity of cement paste.

11- Stage III of hydration (Hardening stage) is crucial for the concrete industry, as moist curing can be started at this time. The ROC of the electrical resistivity of the cement paste mixtures becomes negative at the end of this stage, which means that the cement pastes become more electrical resistant, but at a lower rate. The study of the microstructure of the cement pastes through XRD analysis at the end of this stage shows that due to the formation of C-S-H, which is porous at the beginning (and therefore allows for diffusion of ions of the pore solution), the ROC of the electrical resistivity starts to reduce.

12- Stage IV of hydration (Strengthening stage) begins when the ROC in the normalized electrical resistivity becomes zero.

13- Beyond Stage IV of hydration, the electrical resistivity of the cement pastes increases due to the development of the pore structure, but at a slower rate as the ions content in the pore

solution reduces by the hydration process. Significant formation of C-S-H (as proved by the XRD results) in Stage III and beyond is responsible for linking together the semi-hydrated cement particles into the 3D network of the pore structure. This is the beginning of the cement paste hardening, which can be detected by the reduction in the rate of electrical resistivity increase of the cement paste. Concrete or cement paste moist curing can start at this time of hydration.

14- The addition of limestone did not affect the initial and the final setting time significantly; however, it resulted in higher 1-day compressive strength (even higher than that in the GUbSF cement paste).

15- The W/CM ratio did not have any meaningful influence on the reaction ratio of cement pastes (the reaction rate of Alite and Belite) at different stages of hydration according to the XRD measurements.

16- Replacement of Portland cement with silica fume results in longer initial setting time, but shorter final setting time. Delay in the leakage of sulfur into the pore solution (and therefore delayed ettringite formation) is the reason behind this dual behaviour. Understanding this behaviour is very important for the concrete industry because it leads to a shorter surface finishing time when a mixture contains GUbSF cement.

### 6.3. Future Work

Mix designs with Blast Furnace Slag (BFS) powder are commonly used in the concrete industry. It is important to study the setting time development of mixtures containing slag. It is suggested to focus on those mixtures and employ a selective dissolution method to quantify the amount of unhydrated BFS, since XRD cannot distinguish between the amorphous phases of unhydrated BFS and C-S-H.

The range of W/CM ratio in this research project covers many exposure classes in the concrete industry. For future work, studying lower W/CM ratios which are typically used for designing ultra high-performance mixtures is beneficial.

The rate of change in the electrical resistivity values has shown two turning points. The first tuning point is the beginning of Stage IV of hydration. The second turning point is prior to 24 hours. Beyond 24 hours, the pore structure permeability is the dominant factor in the electrical resistivity development of the cement mixtures, while the pore solution characteristics and the formation of the pore structure are influencing factors in the fresh stage. Studying the micros-structure and electrical resistivity development at the second turning point of the ROC in the electrical resistivity can be beneficial in determining the point beyond which the effect of the pore solution characteristics is replaced with the effect of the pore structure characteristics.

Since it was observed that the normalized electrical resistivity values, independent from the internal temperature of the mixtures, decrease during the first three stages of hydration, while the pore structure develops because of cement hydration, it is important to extend the research to the other component of the pore system (i.e., pore solution). It is recommended to develop a powerful tool to extract the pore solution in Stage II and Stage III of hydration and analyze the electrical properties and ionic concentration of the pore solution.

## REFERENCES


Artioli G. and Bullard J. W., 2013. Cement hydration: The Role of Adsorption and Crystal Growth. *Crystal Research and Technology,* 16(1), pp. 903-918.

*ASTM C204, 2016. Standard Test Methods for Fineness of Hydraulic Cement by Air-Permeability Apparatus,* Pennsylvania: American Society of Testing and Materials.

ASTM C109, 2013. *Standard Test Method for Compressive Strength of Hydraulic Cement Mortars (Using 2-in. or [50-mm] Cube Specimens),* Pennsylvania: American Society for Testing Materials.

ASTM C150, 2007. *Standard Specification for Portland Cement,* Pennsylvania: American Socity of Testing and Materials.

ASTM C187, 2011. *Standard Test Method for Amount of Water Required for Normal Consistency of Hydraulic Cement Paste,* Pennsylvania: American Society for Testing and Materials.

ASTM C191, 2012. *Standard Test Method for Time of Setting of Hydraulic Cement by Vicat Needle,* Pennsylvania: American Society of Testing and Materials.

ASTM C204, 2016. *Standard Test Methods for Fineness of Hydraulic Cement by Air-Permeability Apparatus,* Pennsylvania: American Society for Testing Materials.

ASTM C305, 2014. *Standard Practice fo rMechanical Mixing of Hydraulic Cement Pastes and Mortars of Plastic Consistency,* Pennsylvania: American Society for Testing Materials.

ASTM D4648, 2013. *Standard Test Method for Laboratory Miniature Vane Shear Test for Saturated Fine-Grained Clayey Soil,* Pennsylvania: American Society for Testing Materials.

ASTM D7348, 2008. *Standard Test Methods for Loss on Ignition (LOI) of Solid Combustion Residues,* Pennsylvania: American Society of Testing and Materials.

Bentz D. P., Jones S. Z., and Snyder K. A., 2015. Design and Performance of Ternary Blend HighVolume Fly Ash Concretes of Moderate Slump. *Constrcution and Building Materials,* Volume 84, pp. 409-415.

Bentz D. P., Zunino F., and Lootens D., 2016. Chemical vs. Physical Acceleration of Cement Hydration: CaCl2 vs. Limestone Powder. *Concrete International* , 38(11), pp. 37-44.

Caruso F., Mantellato S., Palacios M., and Flatt R. J., 2017. ICP-OES Method for the Chracterization of Cement Pore Solutions and Their Modification by polycarboxylate-based superplasticizers. *Cement and Concrete Research,* Volume 91, pp. 52-60.

Charles B. Boss and Kenneth J. Fredeen, 2004. *Concepts, Instrumentation and Techniques in Inductively Coupled Plasma Optical Emission Spectrometry.* 3rd ed. Shelton, CA, USA: PerkinElmer, Inc.

Chrisp T. M. , Starrs G., McCarter W. J. , Rouchotas E. , and Blewett J. , 2001. Temperature-Conductivity Relationships for Concrete: An Activation Energy Approach. *Journal of Materials Science Letters ,* Volume 20, pp. 1085-1087.

Coyle A. T., Spragg R. P., Suraneni P., Amirkhanian A. N., and Tsui-Chang M., 2019. Activation Energy of Conduction for Use in Temperature Corrections on Electrical Measurements of Concrete. *Advances in Civil Engineering Materials,* 8(1), pp. 158-170.

Coyle A. T., Spragg R. P., Suraneni P., Amirkhanian A. N., Tsui-Change M. and Weiss W., J. , 2019. Activation Energy of Conduction for Use in Temperature Corrections on Electrical Measurements of Concrete. *Advances in Civil Engineering Materials ,* 8(1), pp. 158-170.

CSA A23.1/2, 2014. *Concrete Materials and Methods of Concrete Construction / Test Methods and Standard Practices for Concrete,* Ottawa, Canada: Canadian Standard Association.

CSA A3000, 2013. *Cementitious Materials Compendium,* Ottawa, Canada: Canadian Standard Association.

CSA A3003, 2008. *Chemical Test Methods for Cementitious Materials for Use in Concrete and Masonry,* Ottawa, Canada: Canadian Standards Association.

El-Dieb A. S., Hooton R. D., and Thomas M. D. A., n.d. *Electrical Resistivity of Concrete Measured by Different Methods (Unpublished paper),* s.l.: University of Toronto, Department of Civil Engineering.

Ewins A. J., 1990. Resistivity Measurements in Concrete. 32(3), pp. 120-126.

Fan M and Brown R. C., 2001. Comparison of the Loss-on-Ignition and Thermogravimetric Analysis Techniques in Measuring Unburned carbon in Coal Fly Ash. *American Chemical Society ,* pp. 1414-1417.

Ferreira R. M. and Jalali S., 2010. NDT Measurements for the Prediction of 28-day Compressive Strength. *NDT & E International,* 43(2), pp. 55-61.

Gowers K. R. and Millard S. G., 1999. Measurement of Concrete Resistivity for Assessment of Corrosion Severity of Steel Using Wenner Technique. *ACI Material Journal,* 96(5), pp. 536-541.

Hansson I. L. H. and Hansson C. M., 1983. Electrical Resistivity Measurements of Portland Cement Based Materials. *Cement and Concrete Research,* 13(5), pp. 675-683.

Hoshino S., Yamada K., and Hirao H., 2006. XRD/Rietveld Analysis of the Hydration and Strength Development of Slag and Limestone Blended Cement. *Journal of Advanced Concrete Technology ,* 4(3), pp. 357-367.

Hoshino S., Y. K. a. H. H., 2006. XRD/Rietveld Analysis of the Hydration and Strength Development of Slag and Limestone Blended Cement. *Journal of Advanced Concrete Technology,* 4(3), pp. 357-367.

Hou X. and Jones B. T., 2000. Inductively Coupled Plasma/Optical Emission Spectrometry. *Encyclopedia of Analytical Chemistry,* pp. 9468–9485.

Huang M. and Hieftje G. M., 1989 . Simultaneous measurement of spatially resolved electron temperatures, electron number densities and gas temperatures by laser light scattering from the ICP. *Spectrochimica Acta Part B: Atomic Spectroscopy,* 44(8), pp. 739-749.

Jelica Z., Ugrina L., and Jozic D., 2007. *Application of Thermal Methods in the Chemistry of Cement: Kinetic Analysis of Portlandite from Non-isothermal Thermogravimetric Data.* Sinaia, Romania, The First International Proficiency Testing Conference.

Julio-Betancourt, G. A., and R. D. Hooton, 2004. Study of the Joule Effect on Rapid Chloride Permeability Values and Evaluation of Related Electrical Properties of Concretes. *Cement and Concrete Research,* 34(6), pp. 1007-1015.

Jumate E. and Manea D. L. , 2011. X-ray Diffraction Study of Hydration Processes in the Portland Cement. *Journal of Applied Engineering Sciences (JAES),* 1(14), pp. 79-86.

Kirchheim A. P., Fernandez-Altable V., Monteiro P. J. M., Dal Molin D. C. C., and Casanova I., 2009. Analysis of Cubic and Orthorhombic C3A Hydration in Presence of Gypsum and Lime. *Journal of Materials Science,* 44(8), pp. 2038–2045.

Kosmatka S. H., Kerkhoff B., Panarese W. C., MacLeod N. F., McGrath R. J., 2011. *Design and Control of Concrete Mixtures.* 8th ed. Ottawa, Canada: Cement Association of Canada.

Krstulovi R. and Dabi P., 2000. A conceptual Model of the Cement Hydration Process. *Cement and Concrete Research,* 30(5), pp. 693-698.

Langan B. W. and Weng K., 2002. Effect of Silica Fume and Fly Ash on Heat of Hydration of Portland Cement. *Cement and Concrete Reasearch ,* Volume 32, pp. 1045-1051.

Layssi H., Ghods P., Alizadeh A., and Salehi M., 2015. Electrical Resistivity of Concrete (concepts, application, and measurment techniques). *Concrete International ,* pp. 41-46.

Liu Y. and Shi X., 2012. Ionic Transport in Cementitious Materials Under an Externally Applied Electric Field: Finite Element Modeling. *Construction and Building Materials,* Volume 27, pp. 450–460.

Liu Y., and Presuel-Moreno F. J. , 2014. Normalization of Temperature Effect on Concrete Resistivity by Method Using Arrhenius Law. *ACI Materials Journal,* 111(4), pp. 433-442.

Lopez W. and Gonzalez J. A., 1993. Influence of the Degree of Pore Saturation on the Resistivity of Concrete and the Corrosion Rate of Steel Reinforcement. *Cement and Concrete Research,* 23(2), pp. 368-376.

McCarter W. J. and Brousseau R., 1990. The A.C. Response of Hardened Cement Paste. *Cement and Concrete Research,* 6(20), pp. 891-900.

McCarter W. J. and Puyrigaud P., 1996. Water Content Assessment of Fresh Concrete. *Proceedings of the Institution of Civil Engineers - Structures and Buildings,* 110(4), pp. 417-425.

McCarter W. J., Starrs G., Kandasami S., Jones R., and Chrisp M., 2009. Electrode Configuration for Resistivity Measurements on Concrete. *ACI Materials Journal,* 106(3), pp. 258-264.

Mehta Kumar P. M. and Monteiro Paulo J., 2006. *Concrete Microstructure, Properties, and Materials.* s.l.:McGraw-Hill Educations.

Mehta P. K. And Monteiro P. J. M., 2005. *Concrete, Microstructure, Properties, and Materials.* Third ed. New York: McGraw-Hill Company.

Monfore E. G., 1968. The Electrical Resistivity of Concrete. *Journal of the PCA Research Development Laboratories,* 10(2), pp. 35-48.

Morishige Y. and Kimura A., 2008. Ionization Interference in Inductively Coupled Plasma-Optical Emission Spectroscopy. *SEI Technical Review ,* Volume 66, pp. 106-111.

Musa, N. M., 2014. Thermal Analysis of Cement Paste Partially Replaced With Neem Seed Husk Ash. *International Journal of Scientific & Engineering Research,* 5(1), pp. 1101-1105.

Neville A. M., 2008. *Properties of Concrete.* Fourth ed. Essex: Pearson Education Ltd..

Nuruddeen, M. M., 2014. Thermal Analysis of Cement Paste Partially Replaced With Neem Seed Husk Ash. *International Journal of Scientific & Engineering Research,* 5(1), pp. 1101-1105.

Polder R. B., 2001. Test Methods for on Site Measurement of Resistivity of Concrete - a RILEM TC-154 Technical Recommendation. *Construction and Building Materials,* 15(2-3), pp. 125-131.

Priyadarshana T. and Dissanayake R., 2013. Importance of Consistent Cement Quality for a Sustainable Construction. *International Journal of Materials, Mechanics and Manufacturing,* 1(4), pp. 393-397.

Saha T. K. and Purkait P., 2004. Investigation of Polarization and Depolarization Current Measurements for the Assessment of Oil-paper Insulation of Aged Transformers, Dielectrics and Electrical Insulation,. *IEEE Transactions on Dielectrics and Electrical Insulation,* 11(1), pp. 144-154.

Shahroodi A., 2010. *Development of Test Methods for Assessment of Concrete Durability for Use in Performance-Based Specifications (MASc Thesis), University of Toronto,,* Toronto: University of Toronto.

Sharpley I., 2015. *The Effect of Hydration on the Microstructural Properties of Individual Phases of Ordinary Portland Cement,* s.l.: Master's Thesis, University College London.

Snyder K. A., Feng X., Keen B.D., and Mason T.O., 2003. Estimating the Electrical Conductivity of Cement Paste Pore Solutions from OH, K, and Na Concentrations. *Cement and COncrete Research,* Volume 33, pp. 793-798.

Spragg R., Villani C., Snyder K., Bentz D., Bullard J. W. , and Weiss J., 2013. Factors That Influence Electrical Resistivity Measurements in Cementitious Systems. *Journal of the Transportation Research Board,* 11(2342), pp. 90-97.

Spragg R., Villani C., Snyder K., Bentz D., Bullard J. W., and Weiss J., 2013. Factors That Influence Electrical Resistivity Measurements in Cementitious Systems. *Journal of the Transportation Research Board,* 11(2342), pp. 90-98.

Taylor H. F. W. and Tuner A. B., 1987. Reactions of Tricalcium Silicate Paste with Organic Liquids. *Cement and Concrete Research ,* Volume 17, pp. 613-623.

Tomlinson D., Moradi F., Hajiloo H., Ghods P., Alizadeh A., Green M., 2017. Early age electrical resistivity behaviour of various concrete mixtures subject to low temperature cycling. *Cement and Concrete Composites,* Volume 83, pp. 323-344.

Tomlinson, D., Moradi F., Hajiloo H., Ghods P., Alizadeh A., and Green M., , 2017. Early age electrical resistivity behaviour of various concrete mixtures subject to low temperature cycling. *Cement and Concrete Composites,* Volume 83, pp. 323-334.

Ukrainczyk N., Ukrainczyk M., Šipušić J., Matusinović T.,, 2006. *XRD and TGA Investigation of Hardened Cement Paste Degradation.* Vela Luka, 11. Conference on Materials, Processes, Friction and Wear.

Villain G., Thiery M., Platret G., 2007. Measurement methods of carbonation profiles in concrete: Thermogravimetry, chemical analysis and gammadensimetry. *Cement and Concrete Research,* Volume 37, pp. 1182-1192.

Vollpracht A., Lothenbach B., Snellings R., Haufe J., 2016. The pore solution of blended cements: a review. *Materials and Structures ,* Volume 4, pp. 3341–3367.

Wang X., Eberhardt A. B., Scrivener K., Gallucci E., 2016. Assessing Early Age Properties of Cementitious Systems by Water-Isopropanol Replacement. *Cement and Concrete Research,* Volume 84, pp. 76-84.

Wei X. and Xiao L., 2014. Kinetics Parameters of Cement Hydration by Electrical Resistivity Measurement and Calorimetry. *Advanced in Cement Research,* 26(4), pp. 187.

Wei X.S. and Li Z. J., 2005. Study on Hydration of Portland Cement with Fly Ash Using Electrical Measurement. *Materials and Structures,* 277(38), pp. 411-417.

Xiao L., Wei X., Li Z., 2008. *Concrete Hydration Based on Electrical Resistivity Measurement.* First ed. Germany: VDM Verlag Dr. Aktiengesellschaft & Company.

# APPENDICES

## A. Raw Materials Properties Analysis

LAFARGE CEMENT

### Cement Mill Test Report

| | |
|---|---|
| Plant: | Bath, Ontario |
| Product: | Portland Cement Type GU |
| Manufactured: | April 2015 |

**CSA A3001-13 Standard Requirements**

**CHEMICAL ANALYSIS**

| Item | Spec limit | Test Result |
|---|---|---|
| Rapid Method, X-Ray | | |
| SiO2 (%) | --- | 19.4 |
| Al2O3 (%) | --- | 5.0 |
| Fe2O3 (%) | --- | 3.2 |
| CaO (%) | --- | 61.9 |
| MgO (%) | 5.0 max | 2.3 |
| SO3 (%) | 3.0 max [1] | 3.9 |
| Loss on ignition @ 950 (%) | 3.0 (3.5) max [2] | 2.0 |
| Loss on ignition @ 550(%) | 3.0 max | 0.5 |
| Insoluble residue (%) | 1.5 max [3] | 0.52 |
| Equivalent Alkalis (as Sodium Oxide) | | 0.6 |
| Potential Phase Composition | | |
| C3S (%) | --- | 55 |
| C2S (%) | --- | 14 |
| C3A (%) | --- | 8 |
| C4AF (%) | --- | 10 |

**PHYSICAL ANALYSIS**

| Item | Spec limit | Test Result |
|---|---|---|
| Blaine Fineness (m2/kg) | --- | 368 |
| + 45 um (%) | 28 max | 4 |
| Autoclave expansion (%) | 1.0 max | 0.03 |
| Compressive strength (MPa) | | |
| 1 day | | |
| 3 days | 14.5 min | 28.0 |
| 7 days | 20.0 min | 36.9 |
| 28 days (Reflects previous month's data) | 26.5 min | 48.1 |
| 28 days cv | 8.0 max | 3.4 |
| Time of setting (minutes) | | |
| Vicat Initial | 45 - 375 | 99 |
| Mortar Bar Expansion C5 (%)[3] | 0.020 max | 0.009 Q4'14 |

CSA A3001-08 Optional Chemical Requirements:

[1] May exceed 3.0% SO3 maximum based on our A3004-C5 results of <0.020% expansion at 14 days.
[2] May exceed 3.0% LOI maximum based on our LOI at 550C < 3.0 %
[3] Current Production run not available - most recent provided

We certify that the above described cement, at the time of shipment, meets the chemical and physical requirements of applicable Specifications for Type GU
CSA A3001-13 STANDARD SPECIFICATIONS FOR TYPE GU CEMENT

Certified By:

[redacted]

Eastern Canada Region - Bath Plant

[redacted]

**Figure A-1: Chemical and physical analysis of General Use (GU) cement**

LAFARGE CEMENT

# Cement Mill Test Report

## Month of Issue: May 2015

| | |
|---|---|
| **Plant:** | **St-Constant, Quebec** |
| **Product:** | **Portland Cement Type HE** |
| **Silo:** | **1 and 11** |
| **Manufactured:** | **April 2015** |

### CSA A3001-13 Standard Requirements

**CHEMICAL REQUIREMENTS**

| | Spec limit | Test Result |
|---|---|---|
| Rapid Method, X-Ray *(A3003-08)* | | |
| SiO2 (%) | --- | 19,7 |
| Al2O3 (%) | --- | 4,8 |
| Fe2O3 (%) | --- | 2,2 |
| CaO (%) | --- | 61,8 |
| MgO (%) | 5.0 max | 2,7 |
| SO3 (%) | 4.5 max | 4,2 |
| Loss on ignition (%) | 3.0 max | 2,4 |
| Insoluble residue (%)* | 1.5 max | 0,57 |
| Na2O (%) | --- | 0,29 |
| K2O (%) | --- | 0,86 |
| Na2Oeq (%) | --- | 0,86 |
| Potential Phase Composition *(A3003-08)* | | |
| C3S (%) | --- | 54 |
| C2S (%) | --- | 16 |
| C3A (%) | --- | 9 |
| C4AF (%) | --- | 7 |

**PHYSICAL REQUIREMENTS**

| | Spec limit | Test Result |
|---|---|---|
| Air content of mortar (%) *(A3004-A5)* | --- | 5 |
| Fineness by air permeability (Blaine) (m2/kg) | --- | 576 |
| Retained 325 mesh (%) *(A3004-A3)* | --- | 0,3 |
| Autoclave expansion (%) *(A3004-B5)** | 1.0 max | 0,05 |
| Compressive strength (MPa) *(A3004-C2)* | | |
| 1 day | 13.5 min | 31,6 |
| 3 days | 24.0 min | 40,5 |
| 28 days* | --- | 51,7 |
| Time of setting (minutes) | | |
| Vicat Initial *(A3004-B2)* | 45 - 250 | 85 |
| Mortar Bar Expansion (%)* *(A3004-C5)* | 0.020 max | 0,007 |

* Current Production run not available - most recent provided.

We hereby certify that the cement represented by the above chemical and physical analyses meets the requirements of CSA A3001-13 including the maximum sulphate expansion limit at 14 days (CSA A3004-C5).

For additional information on this cement test report, please contact our technical representative Danielle Palardy at 514-895-1876.

ECAN BU - St-Constant Plant

[redacted]

Certified By:

[redacted]

**Figure A-2: Chemical and physical analysis of High Early (HE) cement**

LAFARGE CEMENT

# SF™ Cement Mill Test Report

## Month of Issue: May 2015

| | |
|---|---|
| Plant: | St-Constant, Quebec |
| Product: | Type GUb-8SF Cement |
| Silo: | 6 |
| Manufactured: | April 2015 |

### CSA A3001-13 Standard Requirements

**CHEMICAL REQUIREMENTS**

| | Spec limit | Test Result |
|---|---|---|
| Rapid Method, X-Ray *(A3003-08)* | | |
| SiO2 (%) | --- | 25,0 |
| Al2O3 (%) | --- | 4,3 |
| Fe2O3 (%) | --- | 2,9 |
| CaO (%) | --- | 57,1 |
| MgO (%) | --- | 2,6 |
| SO3 (%)* | 3.0 max | 3,7 |
| Loss on ignition (%) | 3.5 max | 2,3 |
| Na2Oeq (%) | --- | 0,86 |

**PHYSICAL REQUIREMENTS**

| | Spec limit | Test Result |
|---|---|---|
| Air content of mortar (%) (A3004-A5) | --- | 6,4 |
| Fineness by air permeability (Blaine) (m2/kg) | --- | 567 |
| Retained 325 mesh (%) *(A3004-A3)* | 25 | 7,9 |
| Autoclave expansion (%) *(A3004-B5)* | 0.80 max | 0,00 |
| Compressive strength (MPa) *(A3004-C2)* | | |
| 3 days | 14.5 min | 30,0 |
| 7 days | 20.0 min | 38,6 |
| 28 days ** | 26.5 min | 51,3 |
| Time of setting (minutes) | | |
| Vicat Initial *(A3004-B2)* | 45 - 480 | 140 |
| Mortar Bar Expansion (%) (A3004-C5)** | 0.020 max | 0,004 |

* If exceeds 3.0%, must comply with a maximum expansion limit of 0.020% at 14 days when tested in accordance with CSA A3004-C5.

** Current Production run not available - most recent provided.

We hereby certify that the cement represented by the above chemical and physical analyses meets the requirements of CSA A3001-13 including the maximum sulphate expansion limit at 14 days (CSA A3004-C5).

For additional information on this cement test report, please contact our technical representative Danielle Palardy at 514-895-1876.

Certified By:

ECAN BU - St-Constant Plant

[redacted]

[redacted]

**Figure A-3: Chemical and physical analysis of General Use blended with Silica Fume (GUbSF) cement**

LAFARGE CEMENT

# Cement Mill Test Report

| | |
|---|---|
| Plant: | Bath, Ontario |
| Product: | Portland-Limestone Cement Type GUL |
| Manufactured: | April 2015 |

contempra

## CSA A3001-13 Standard Requirements

### CHEMICAL ANALYSIS

| Item | Spec limit | Test Result |
|---|---|---|
| Rapid Method, X-Ray | | |
| SiO2 (%) | --- | 18.6 |
| Al2O3 (%) | --- | 4.8 |
| Fe2O3 (%) | --- | 3.0 |
| CaO (%) | --- | 60.3 |
| MgO (%) | --- | 2.2 |
| SO3 (%) | 3.0 max [1] | 3.8 |
| Loss on ignition @ 950 (%) | 10 max | 5.2 |
| Equivalent Alkalis (as Sodium Oxide) | | 0.61 |

### PHYSICAL ANALYSIS

| Item | Spec limit | Test Result |
|---|---|---|
| Blaine Fineness ($m^2/kg$) | --- | 484 |
| + 45 um (%) | 28 max | 1.2 |
| Autoclave expansion (%) | 1.0 max | 0.05 |
| Compressive strength (MPa) | | |
| 1 day | | |
| 3 days | 14.5 min | 30.4 |
| 7 days | 20.0 min | 38.8 |
| 28 days (Reflects Oct'14 data) | 26.5 min | 47.5 |
| 28 days cv | 8.0 max | n/a |
| Time of setting (minutes) | | |
| Vicat Initial | 45 - 375 | 99 |
| Mortar Bar Expansion C5 (%) | 0.020 max | 0.007 Q4'14 |

CSA A3001-08 Optional Chemical Requirements:

[1] May exceed 3.0% SO3 maximum based on our A3004-C5 results of <0.020% expansion at 14 days.

We certify that the above described cement, at the time of shipment, meets the chemical and physical requirements of applicable Specifications for Type GUL
CSA A3001-13 STANDARD SPECIFICATIONS FOR TYPE GUL CEMENT

Certified By:

[redacted]

Eastern Canada Region - Bath Plant

[redacted]

**Figure A-4: Chemical and physical analysis of General Use-Limestone (GUL) cement**

## B. TGA Instrument (G5000-IR)

As described by the TA Instrument, "the automated Q5000-IR" is the TGA best suited to meet the most demanding research applications. It outperforms all competitors in baseline flatness, sensitivity to low-level weight changes, and flexibility in both standard and high heating rate operation. Other powerful features include a 25-position integrated auto sampler with contamination-free, sealed pan-punching capability, an internal electromagnet for easy Curie Point temperature calibration, and Platinum™ software for user convenience in scheduling automatic calibration, verification, and diagnostic tests to keep the Q5000 IR constantly in top operating condition."

The detail information of the instrument is as:

**Figure B-1: Q5000-IR machine (from the TA Instrument courtesy)**

**Temperature Controlled Thermo-balance:** Included

**Weight Range:** 100 mg

**Weighing Accuracy:** +/- 0.1%

**Weighing Precision:** +/- 0.01%

**Sensitivity:** < 0.1 µg

**Baseline Dynamic Drift:** < 10 µg

**Signal Resolution:** 0.01 µg

**Furnace Heating:** Infrared

**Temperature Range:** Ambient to 1200 °C

**Isothermal Temp Accuracy:** +/- 1 °C

**Linear Heating Rate (°C/min.):** 0.1 to 500

**Furnace Cooling (Forced air / N2):** 1200 to 35 °C < 10 min.

**Vacuum:** 10-2 torr

**Temperature Calibration:** Electromagnetic Coil/Curie Point Stds

**Auto-sampler – 25 sample:** Included

**Hi-Res TGA™:** Included

**Auto Stepwise TGA:** Included

**Modulated TGA™:** Included

**TGA/MS Operation:** Option

**Platinum™ Software:** Included

**Sample Pans:**

Platinum 50, 100 µL

Ceramic 100, 250 µL

Aluminum 80 µL

Aluminum Sealed Pan 20 µL

## C. Thermos-Gravimetric Analysis (TGA) and Derivatives Thermo-gravimetric Analysis (DTA) results

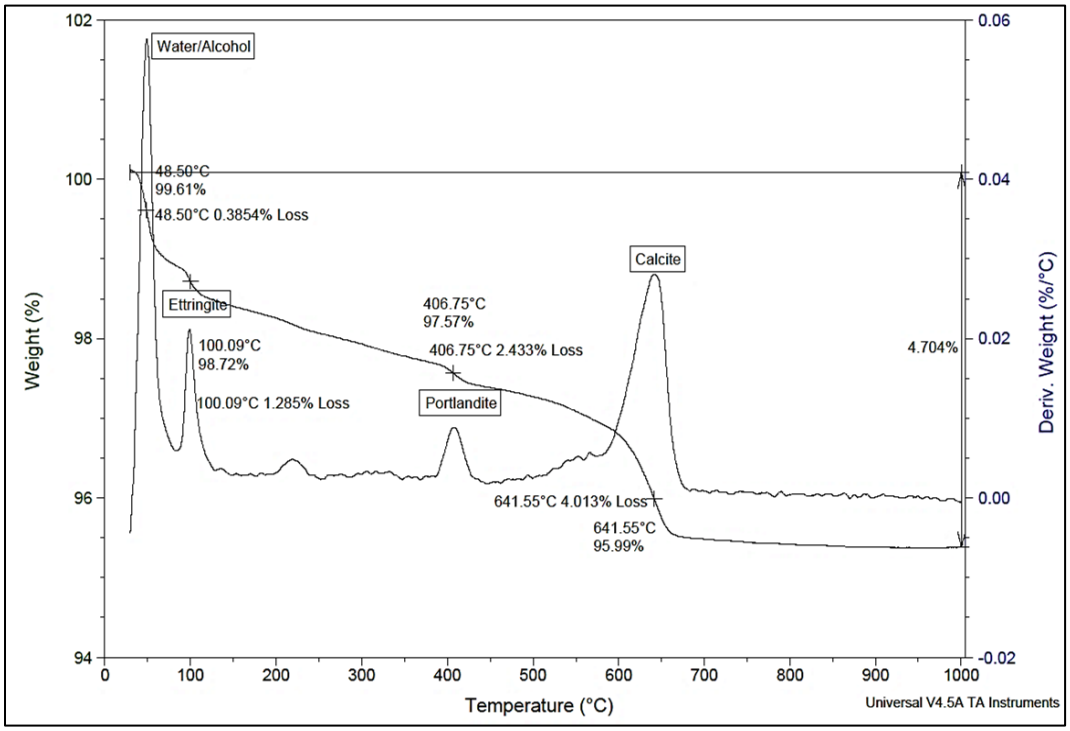


**Figure C-1: TGA/DTA graphs-analysis of GU 0.37 mixtures at 2 hours of hydration**

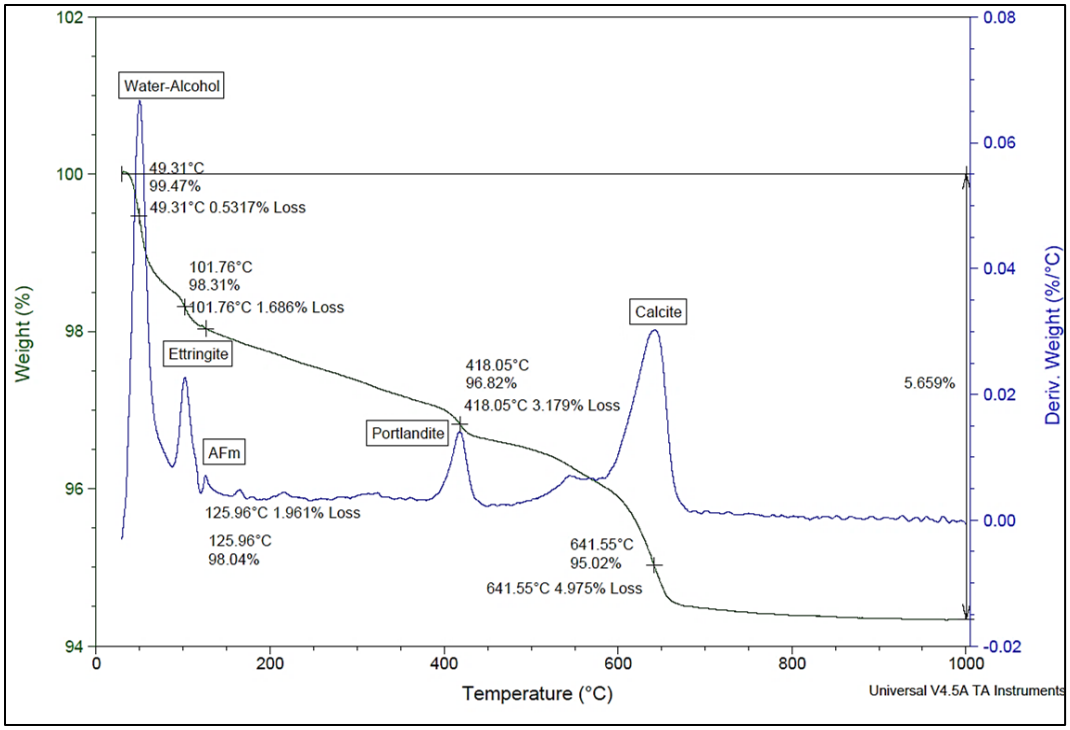


**Figure C-2: TGA/DTA graphs-analysis of GU 0.37 mixtures at initial setting**

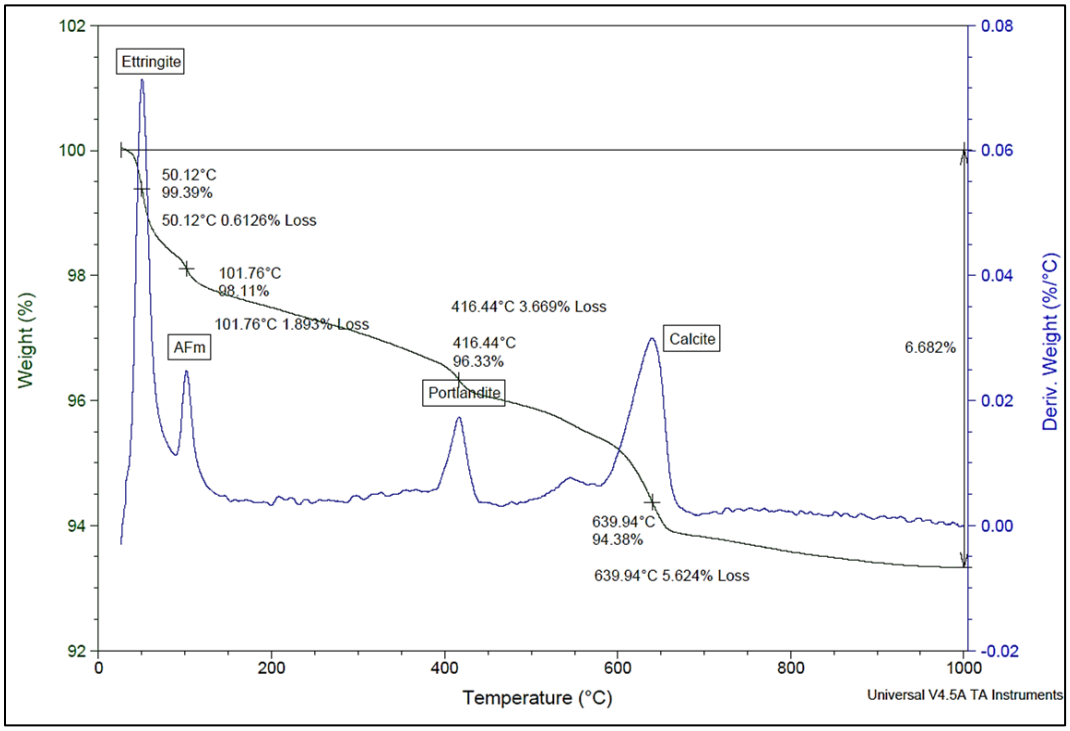


**Figure C-3: TGA/DTA graphs-analysis of GU 0.37 mixtures at final setting**

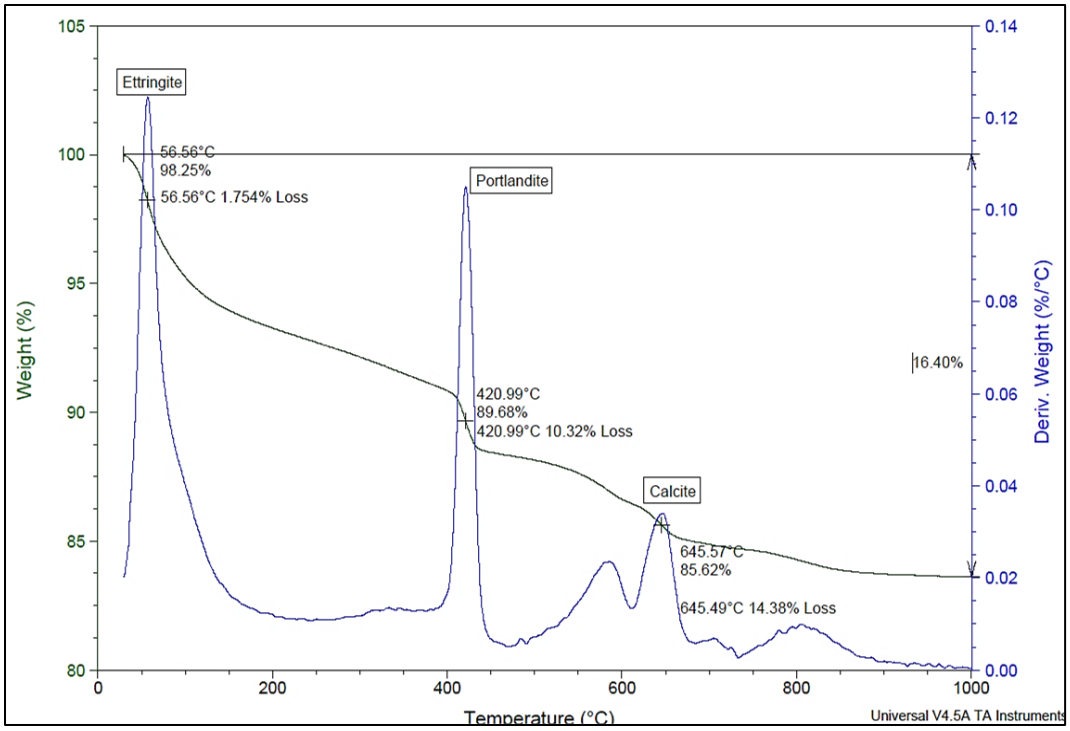


**Figure C-4: TGA/DTA graphs-analysis of GU 0.37 mixtures at 24 hours of hydration**

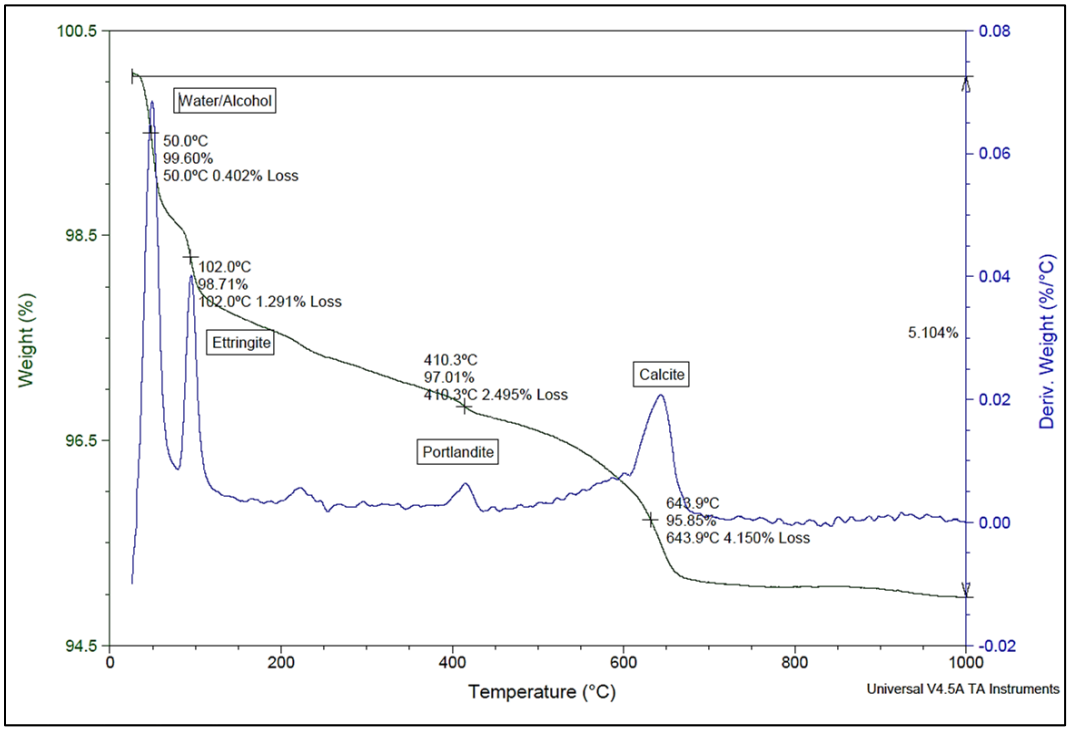


**Figure C-5: TGA/DTA graphs-analysis of GU 0.40 mixtures at 2 hours of hydration**

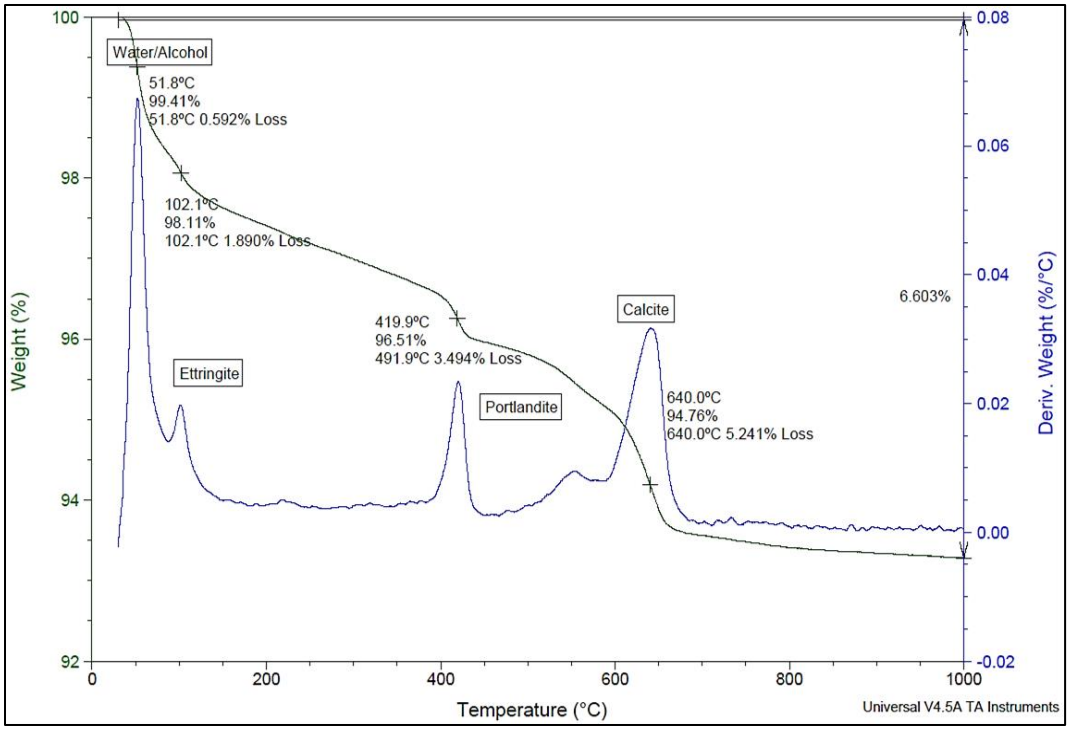


**Figure C-6: TGA/DTA graphs-analysis of GU 0.40 mixtures at initial setting**

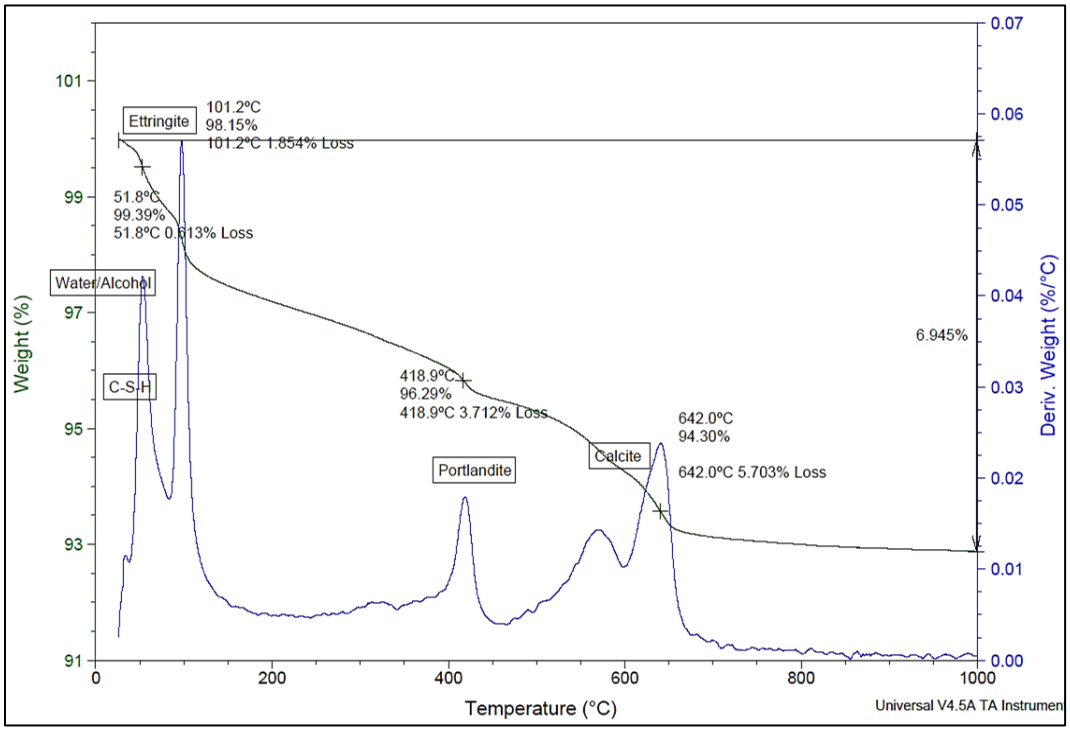


**Figure C-7: TGA/DTA graphs-analysis of GU 0.40 mixtures at final setting**

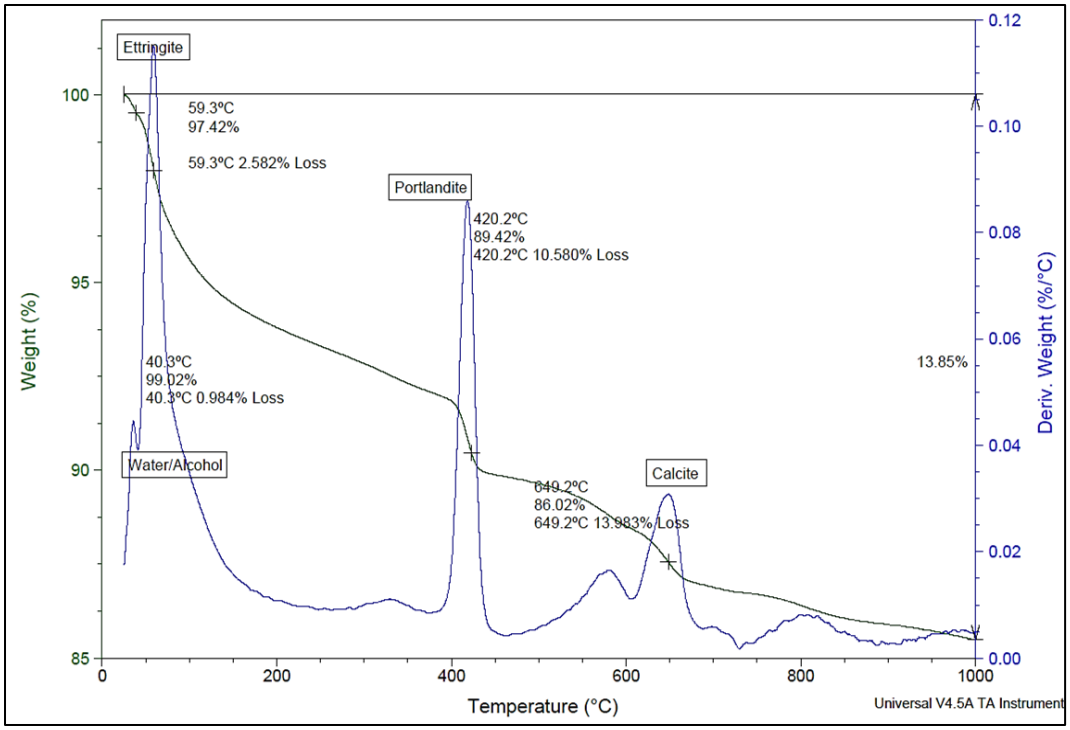


**Figure C-8: TGA/DTA graphs-analysis of GU 0.40 mixtures at 24 hours of hydration**

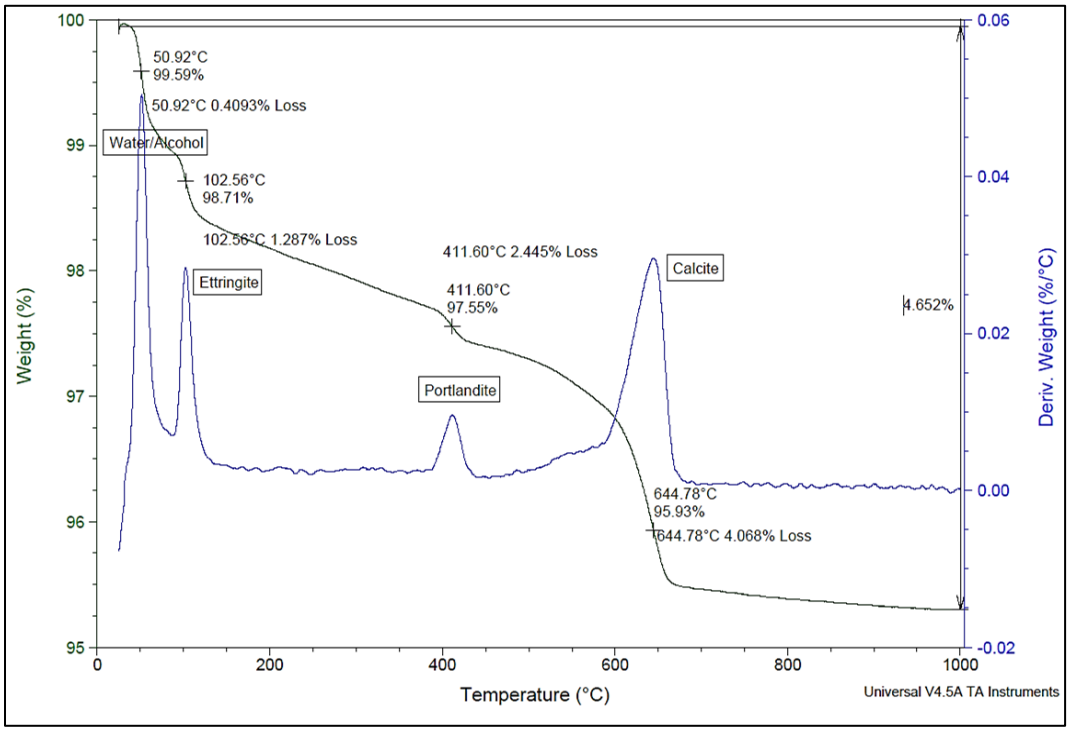


**Figure C-9: TGA/DTA graphs-analysis of GU 0.43 mixtures at 2 hours of hydration**

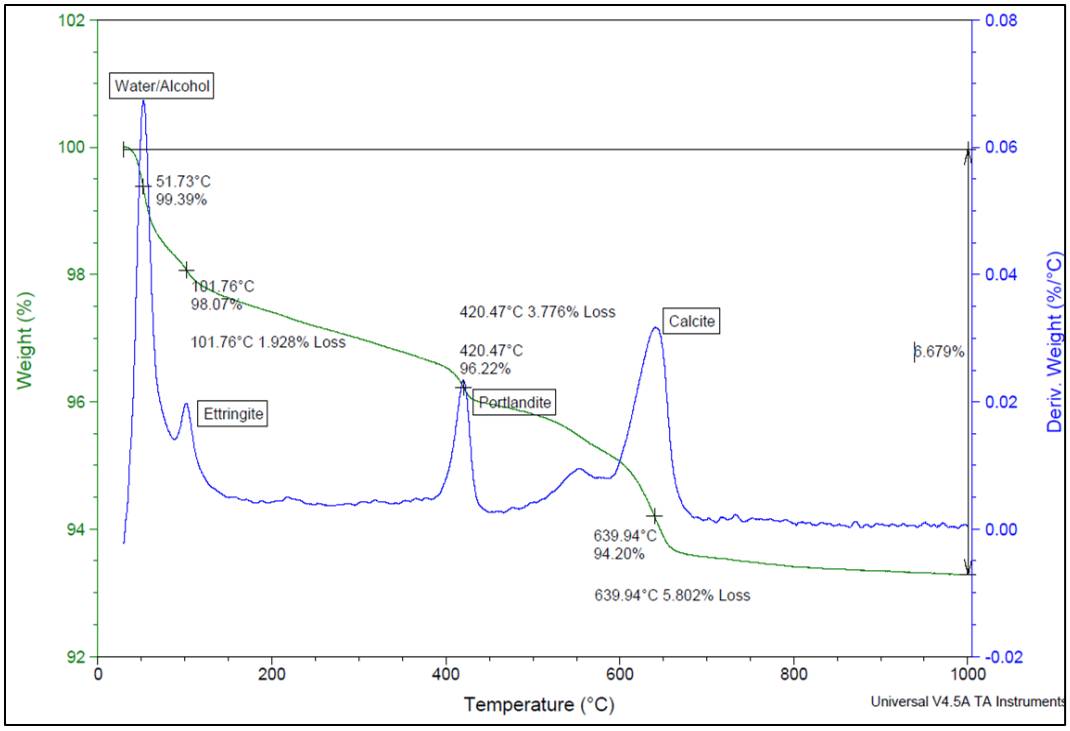


**Figure C-10: TGA/DTA graphs-analysis of GU 0.43 mixtures at initial setting**

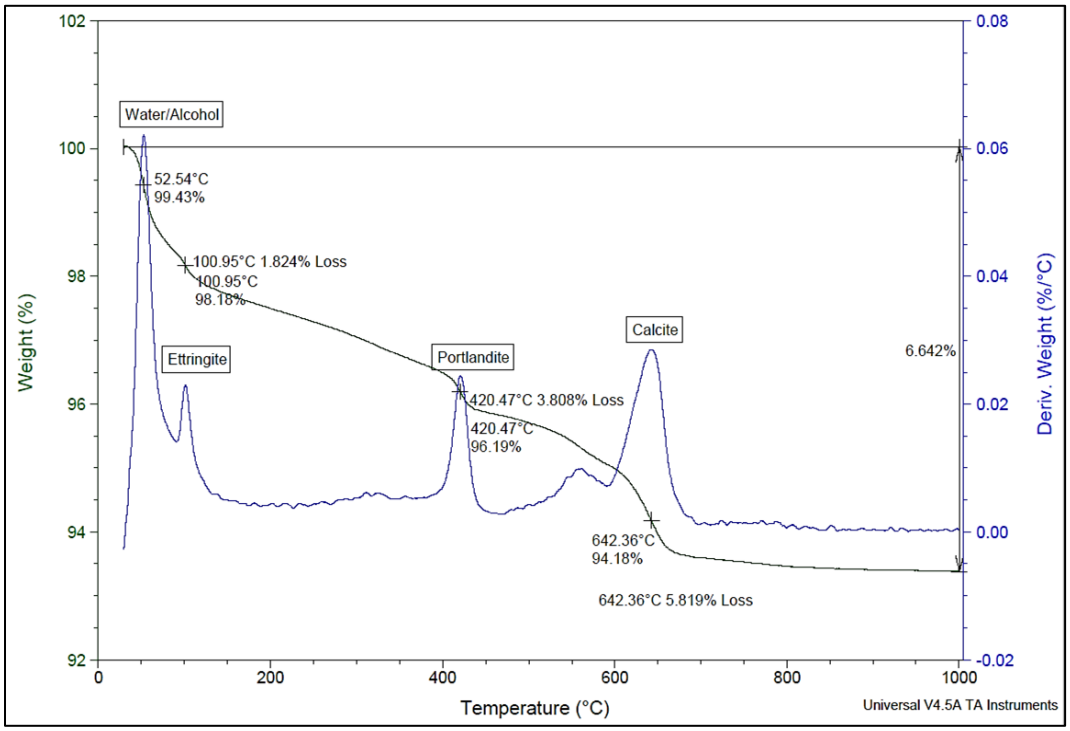


**Figure C-11: TGA/DTA graphs-analysis of GU 0.43 mixtures at final setting**

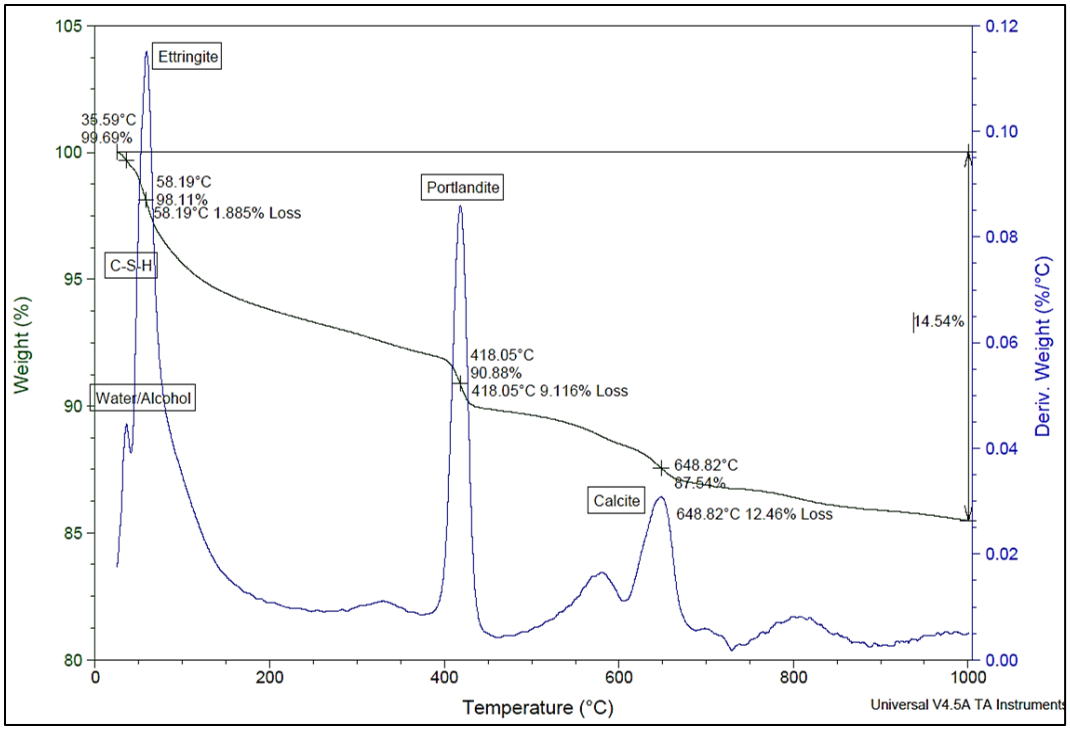


**Figure C-12: TGA/DTA graphs-analysis of GU 0.43 mixtures at 24 hours of hydration**

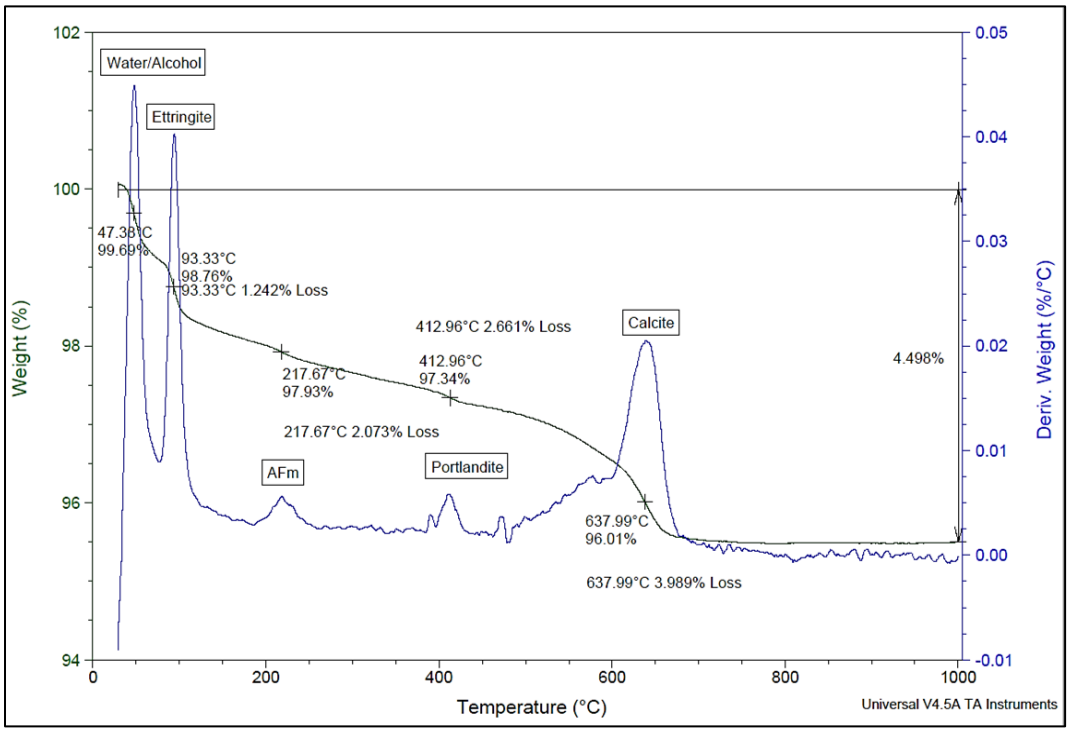


**Figure C-13: TGA/DTA graphs-analysis of GUbSF 0.37 mixtures at 2 hours of hydration**

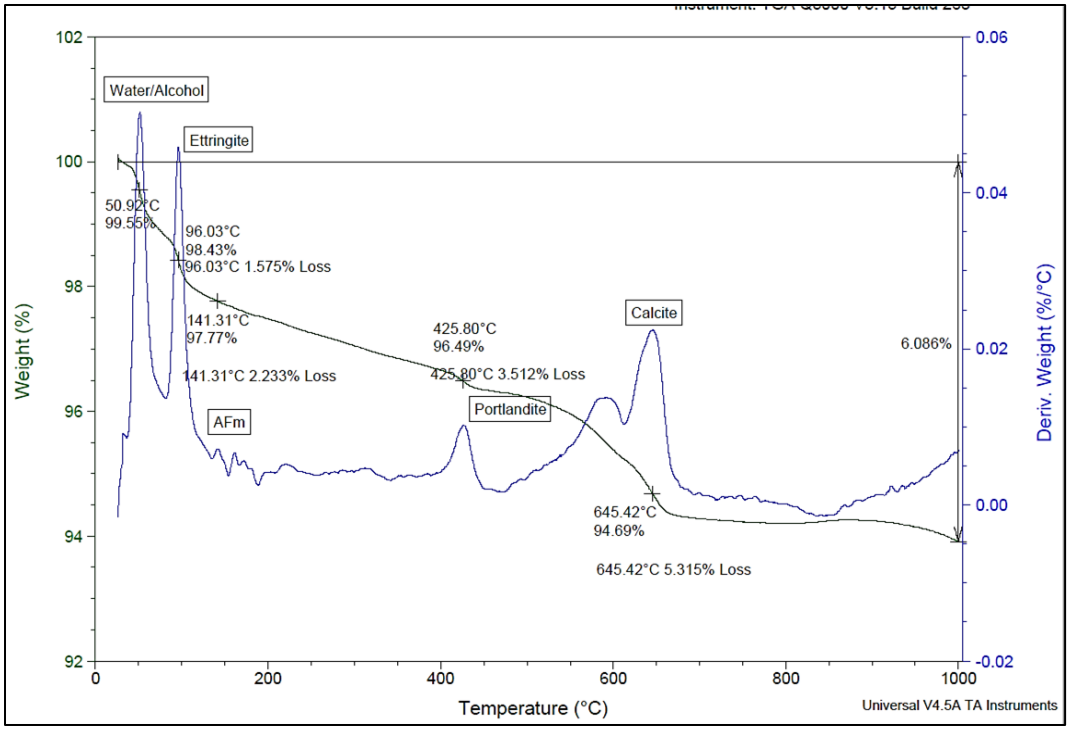


**Figure C-14: TGA/DTA graphs-analysis of GUbSF 0.37 mixtures at initial setting**

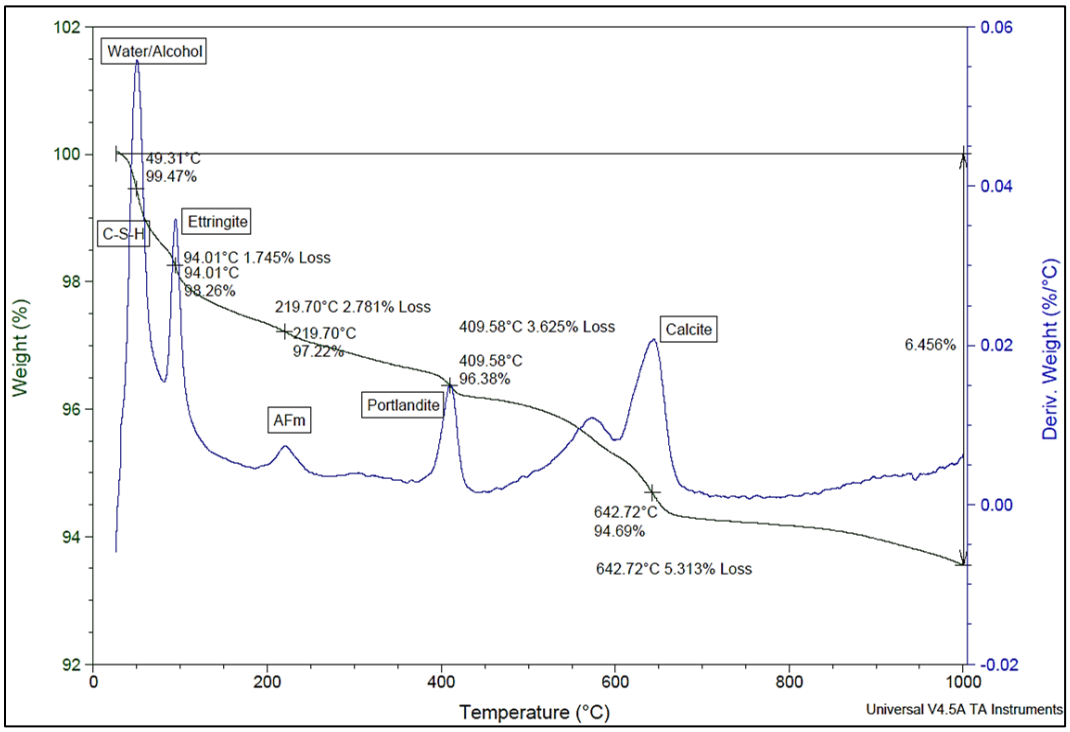


**Figure C-15: TGA/DTA graphs-analysis of GUbSF 0.37 mixtures at final setting**

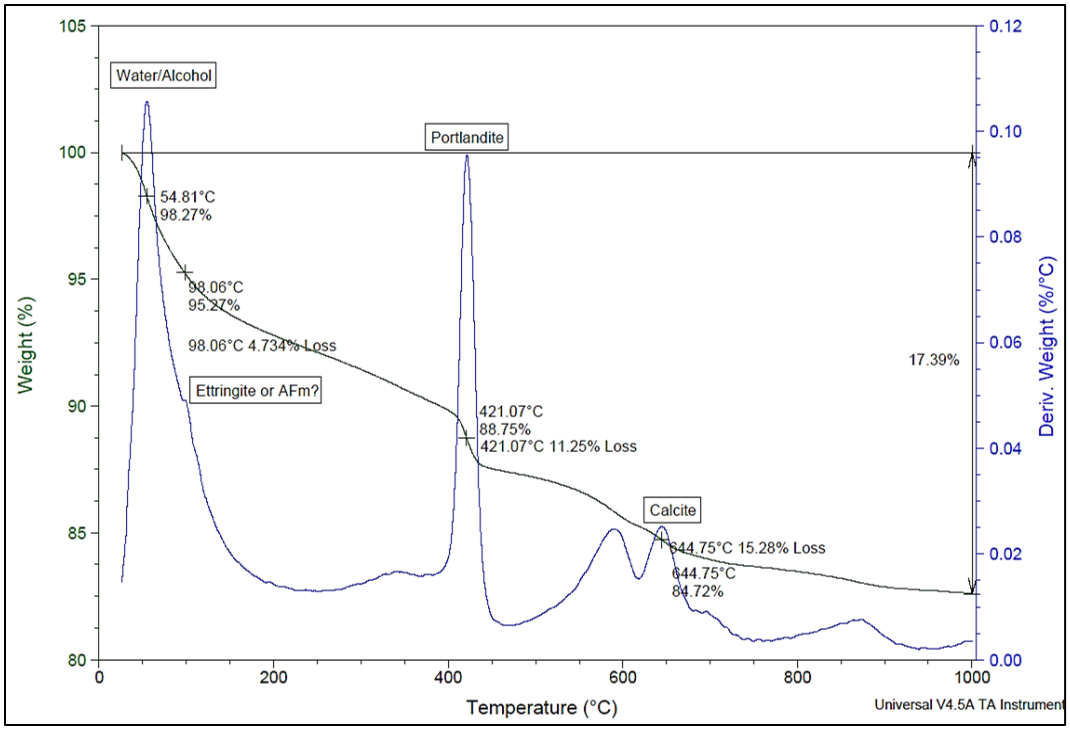


**Figure C-16: TGA/DTA graphs-analysis of GUbSF 0.37 mixtures at 24 hours of hydration**

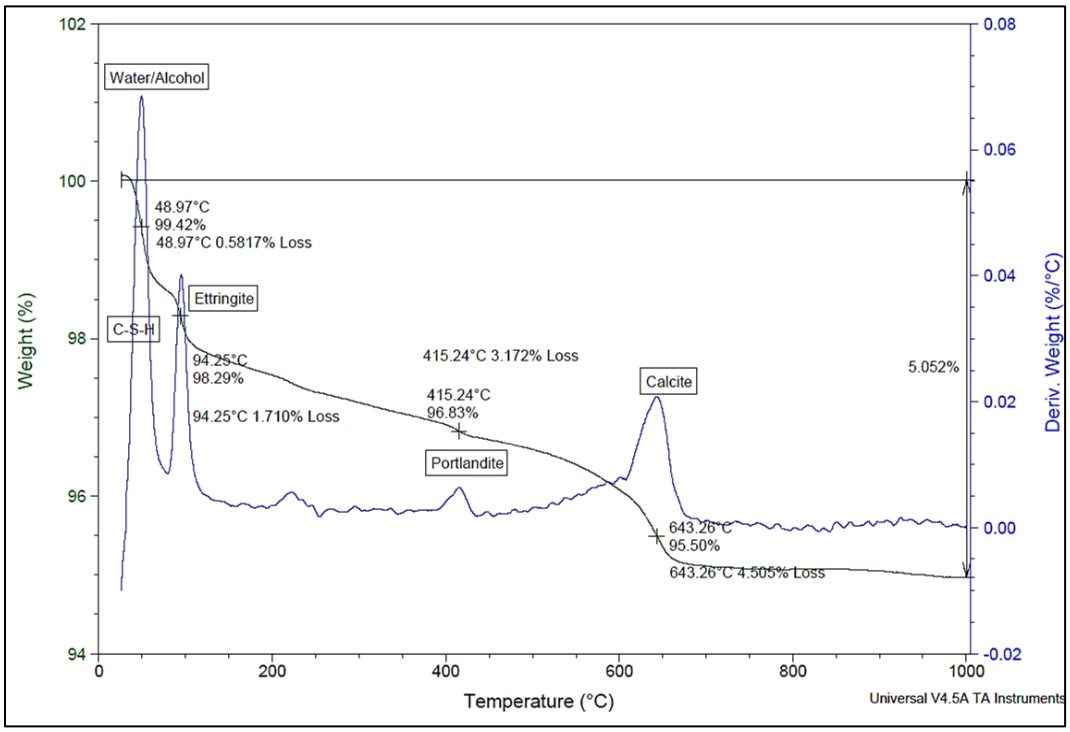


**Figure C-17: TGA/DTA graphs-analysis of GUbSF 0.40 mixtures at 2 hours of hydration**

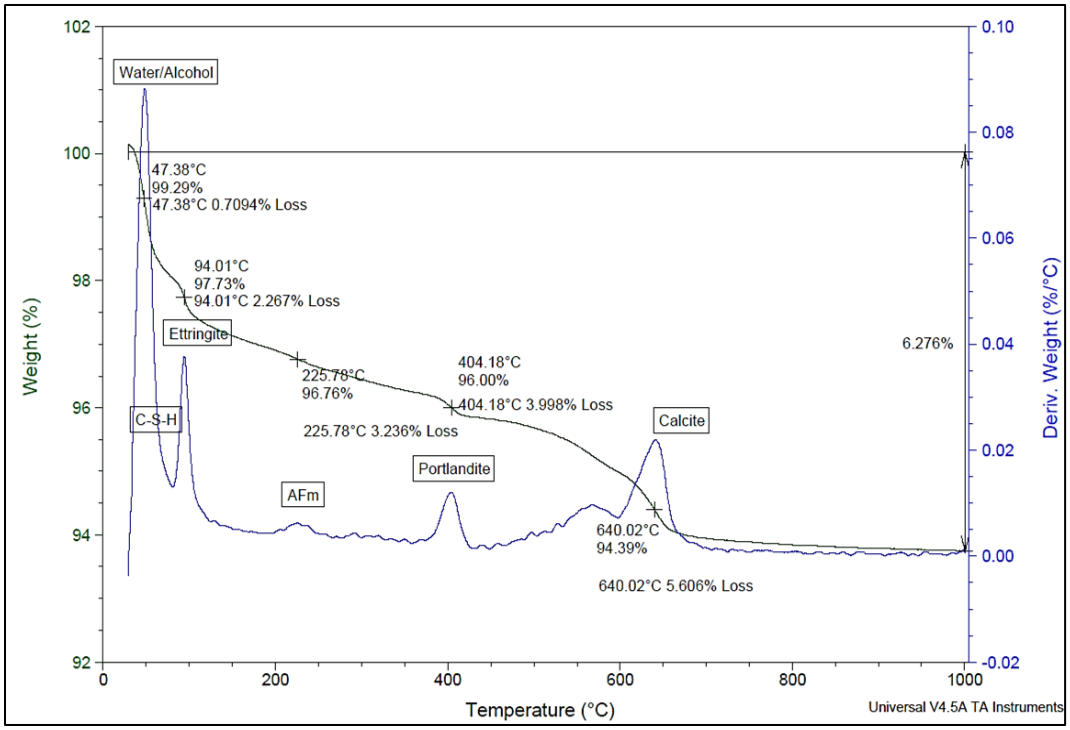


**Figure C-18: TGA/DTA graphs-analysis of GUbSF 0.40 mixtures at initial setting**

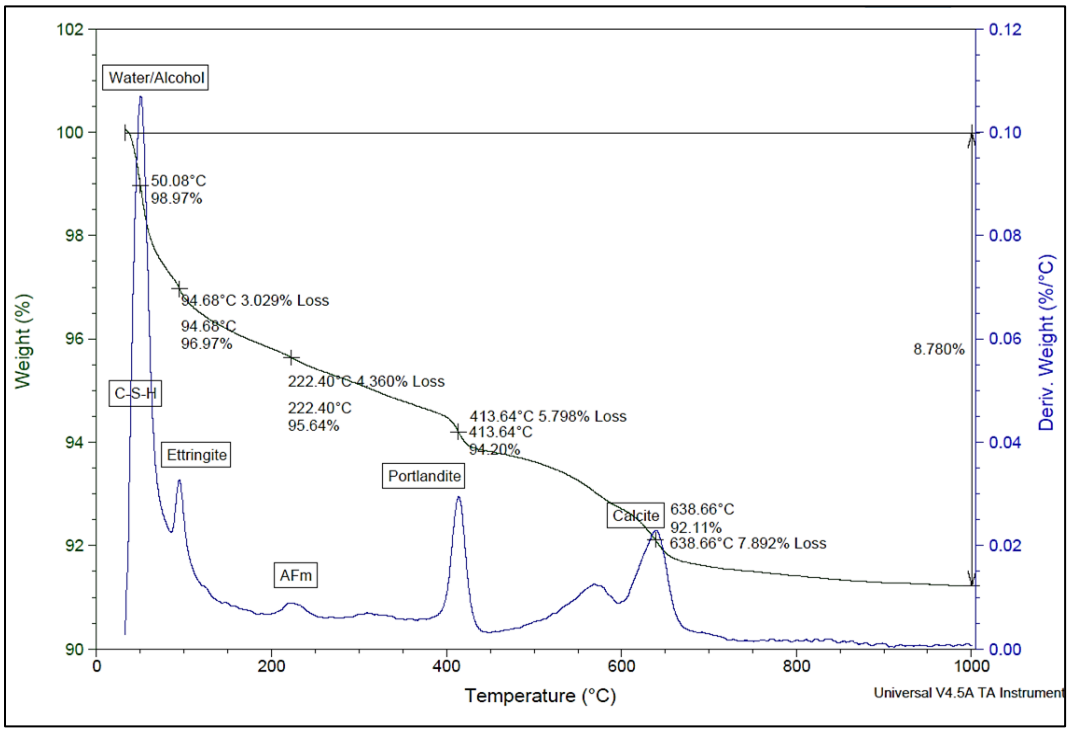


**Figure C-19: TGA/DTA graphs-analysis of GUbSF 0.40 mixtures at final setting**

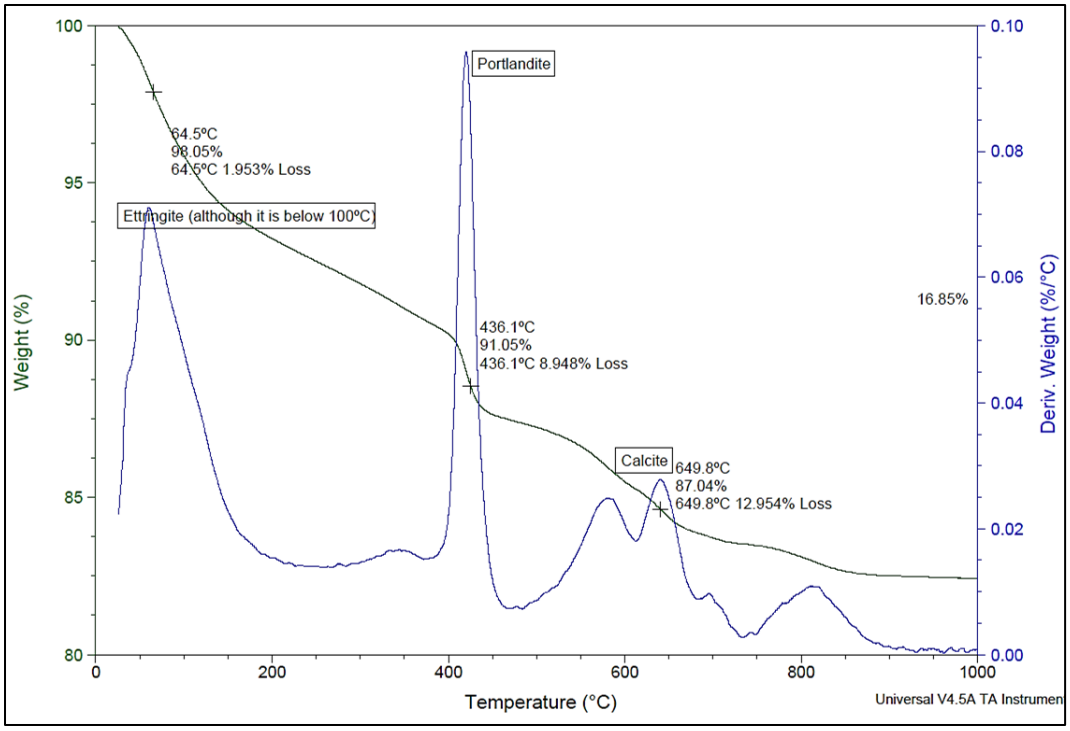


**Figure C-20: TGA/DTA graphs-analysis of GUbSF 0.40 mixtures at 24 hours of hydration**

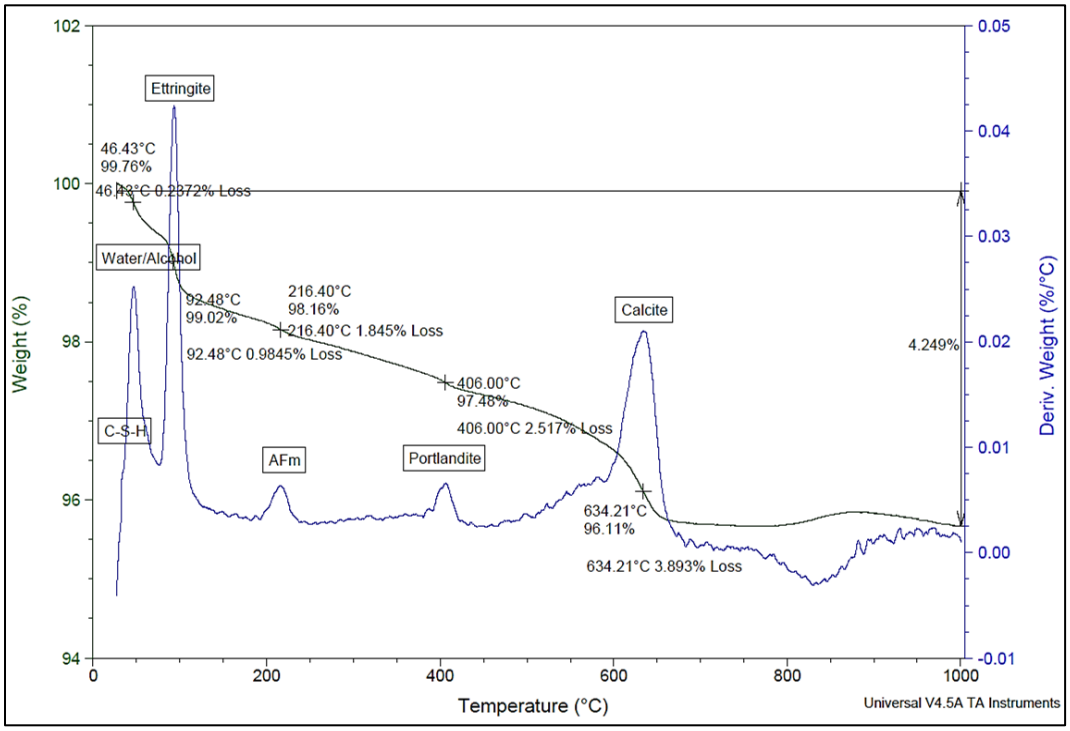


**Figure C-21: TGA/DTA graphs-analysis of GUbSF 0.43 mixtures at 2 hours of hydration**

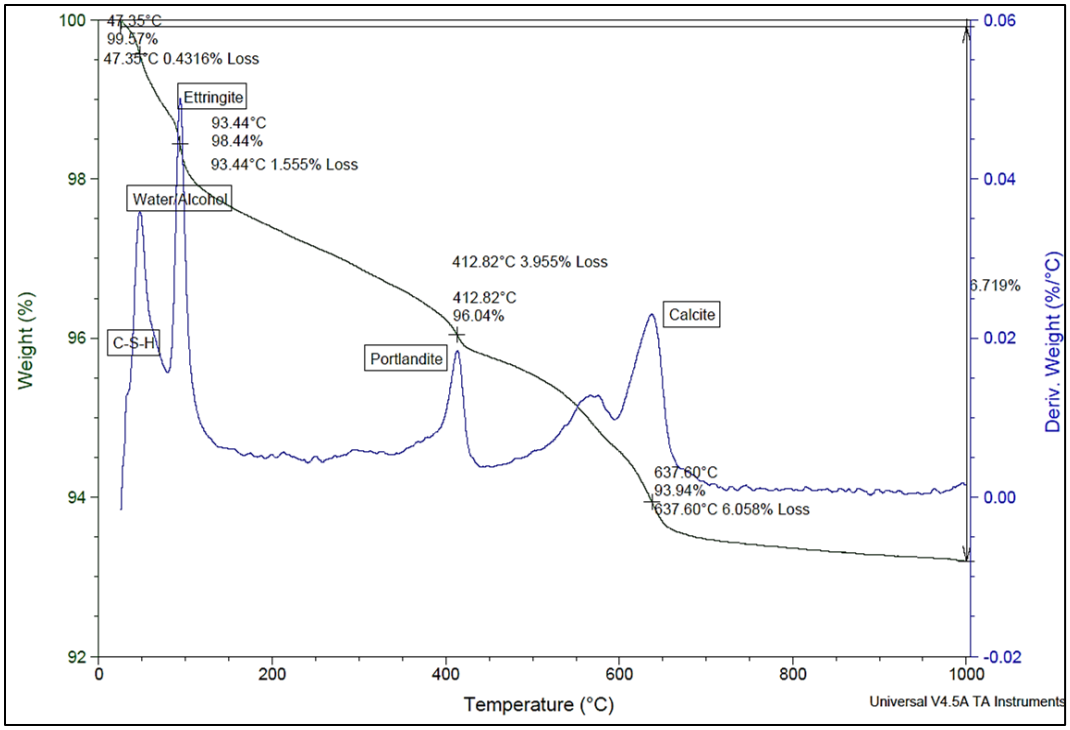


**Figure C-22: TGA/DTA graphs-analysis of GUbSF 0.43 mixtures at initial setting**

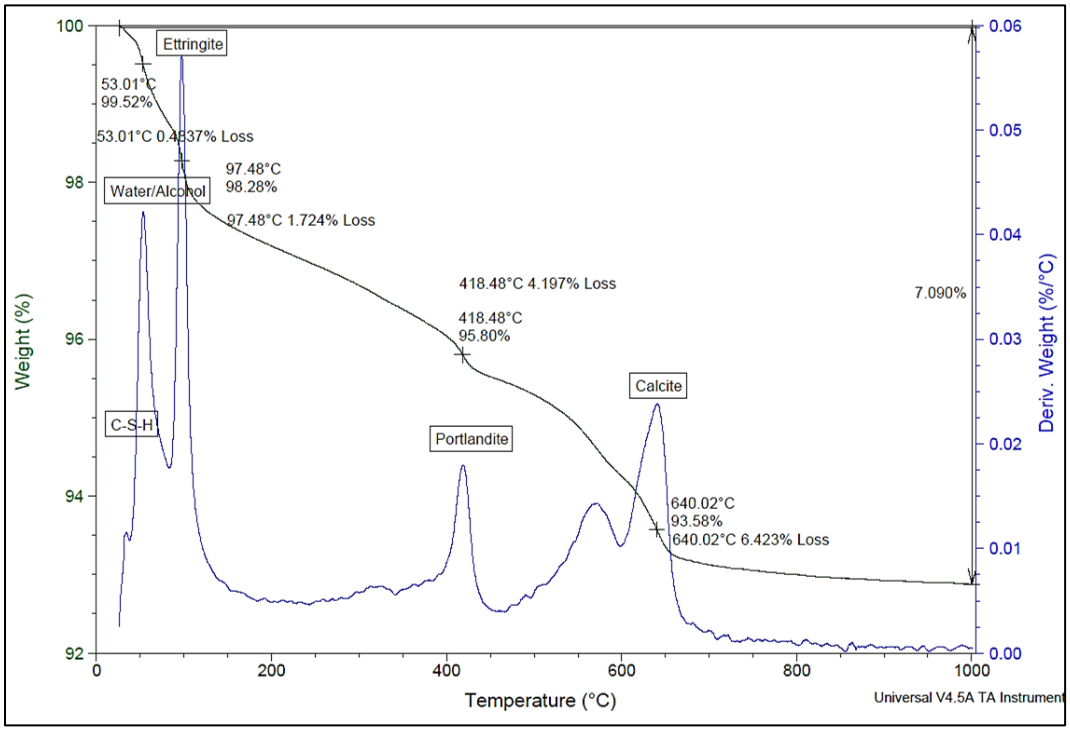


**Figure C-23: TGA/DTA graphs-analysis of GUbSF 0.43 mixtures at final setting**

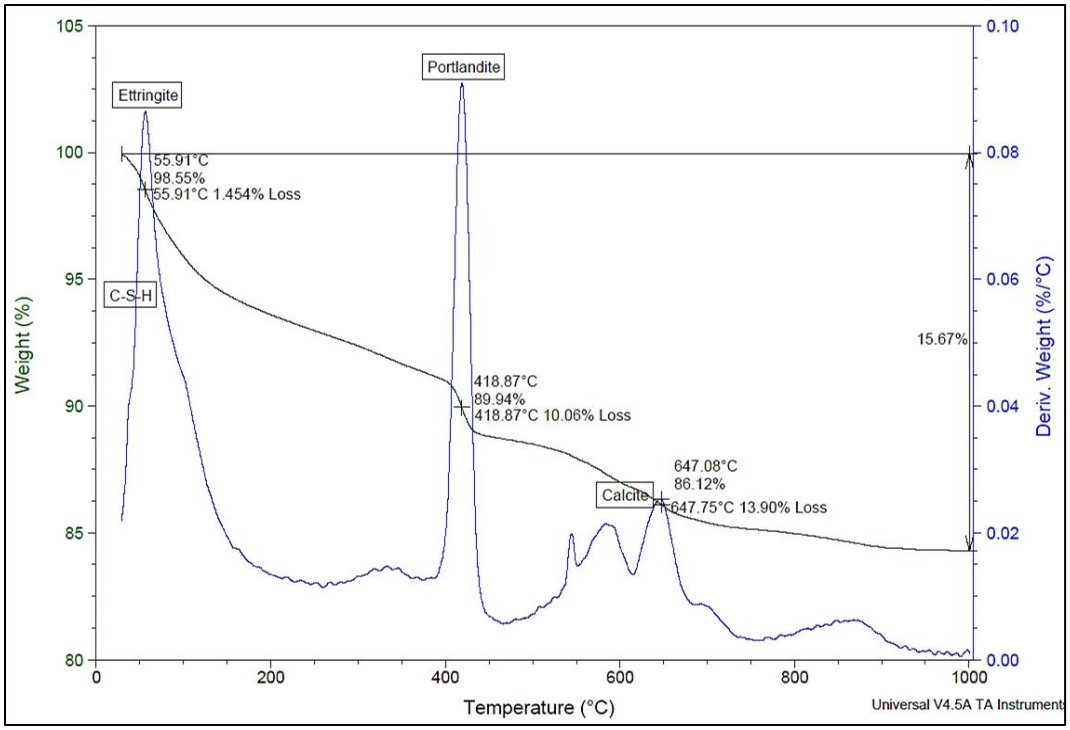


**Figure C-24: TGA/DTA graphs-analysis of GUbSF 0.43 mixtures at 24 hours of hydration**

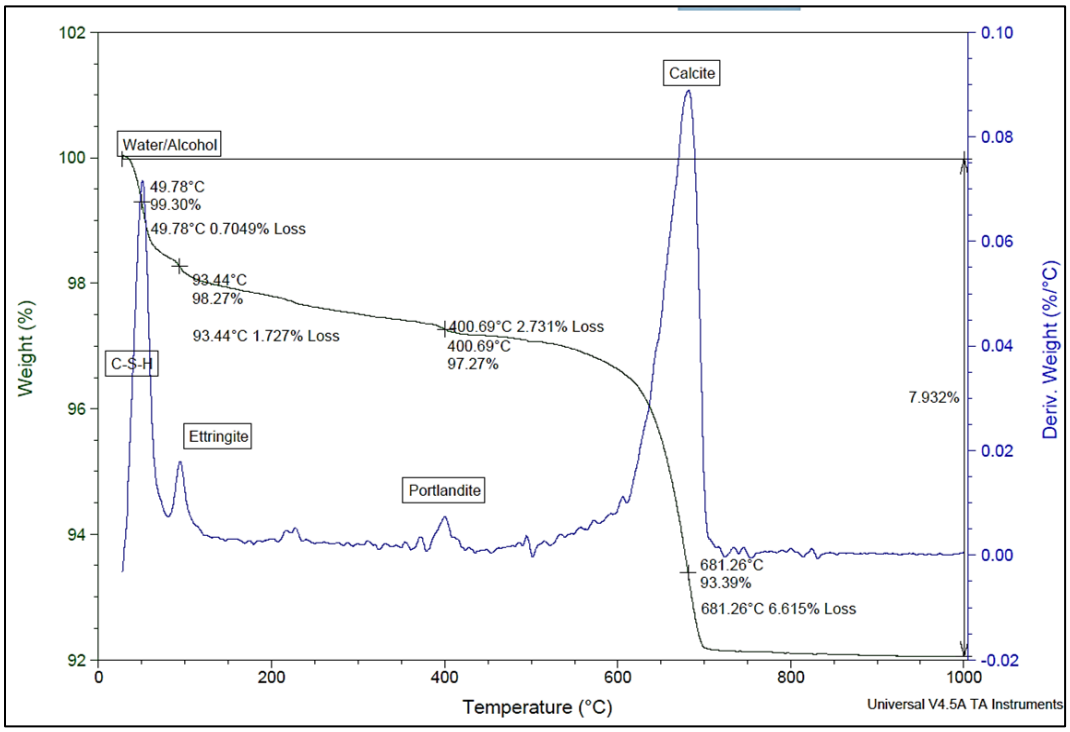


**Figure C-25: TGA/DTA graphs-analysis of GUL 0.37 mixtures at 2 hours of hydration**

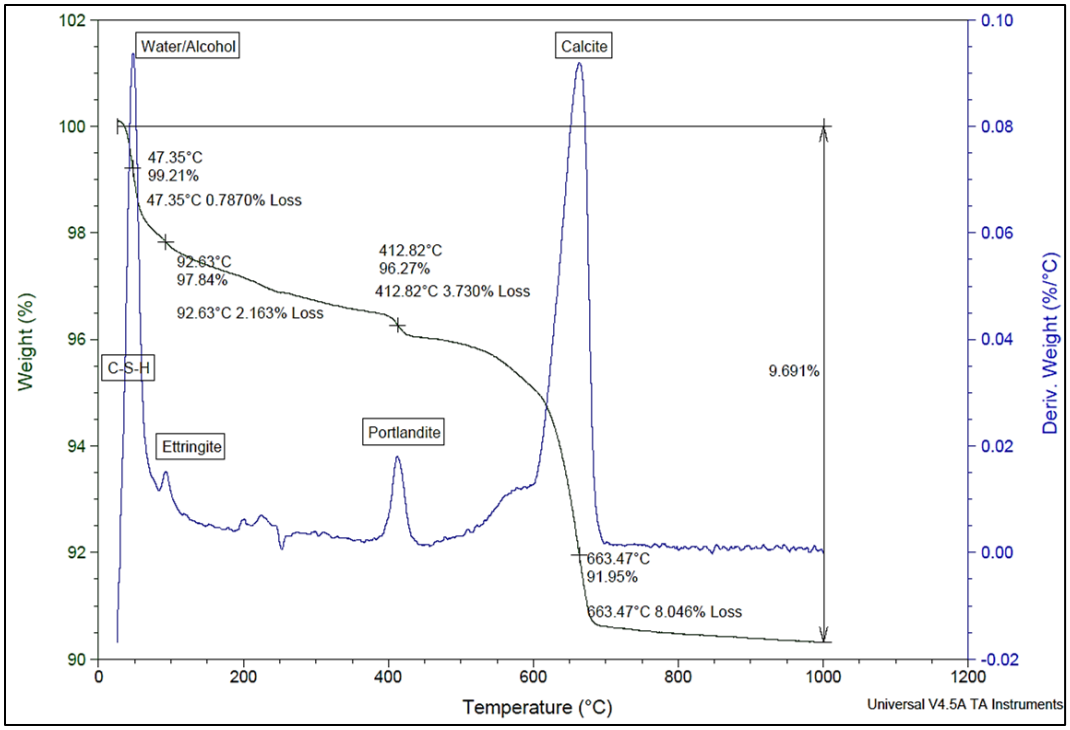


**Figure C-26: TGA/DTA graphs-analysis of GUL 0.37 mixtures at initial setting**

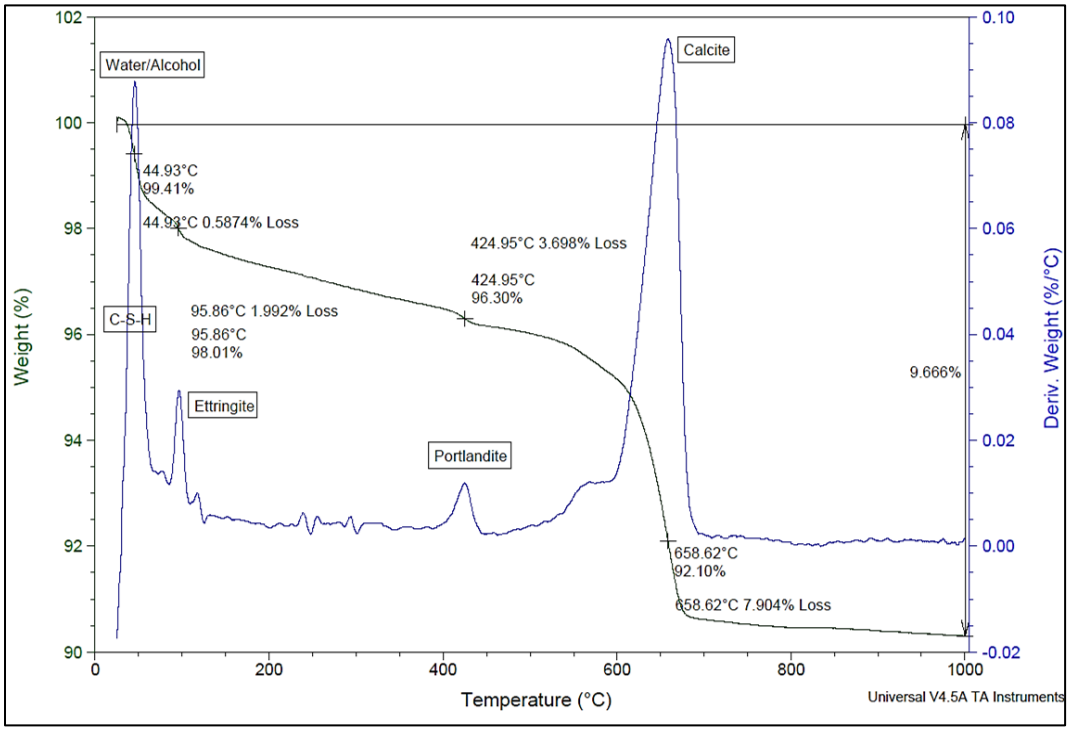


**Figure C-27: TGA/DTA graphs-analysis of GUL 0.37 mixtures at final setting**

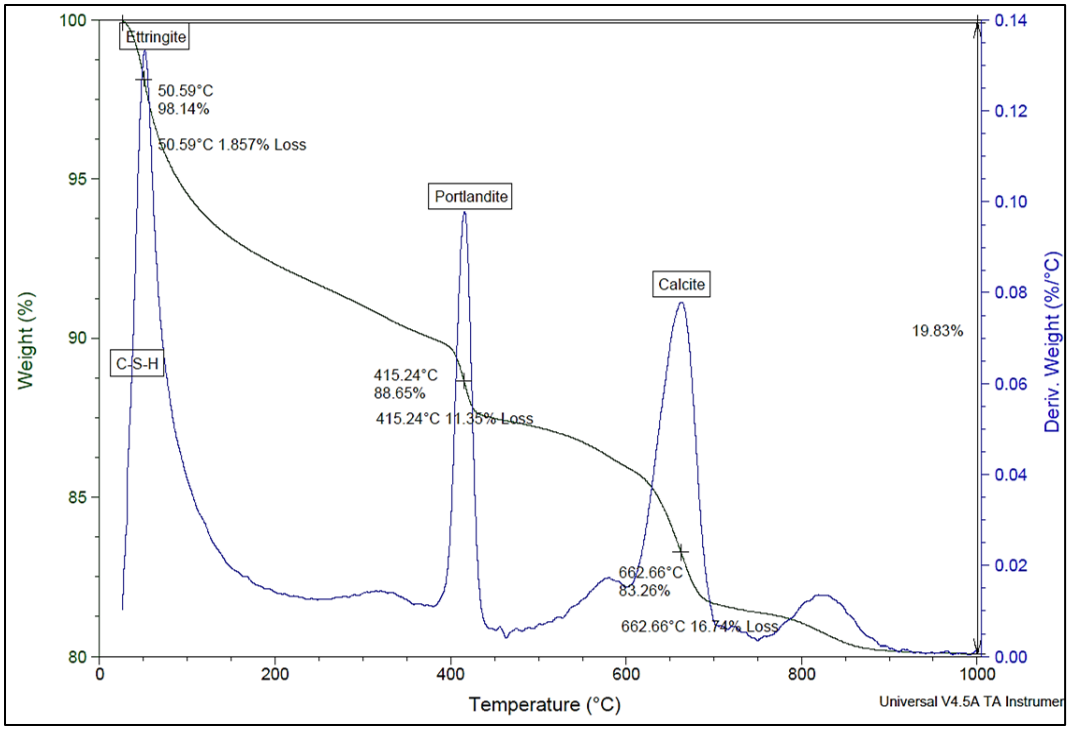


**Figure C-28: TGA/DTA graphs-analysis of GUL 0.37 mixtures at 24 hours of hydration**

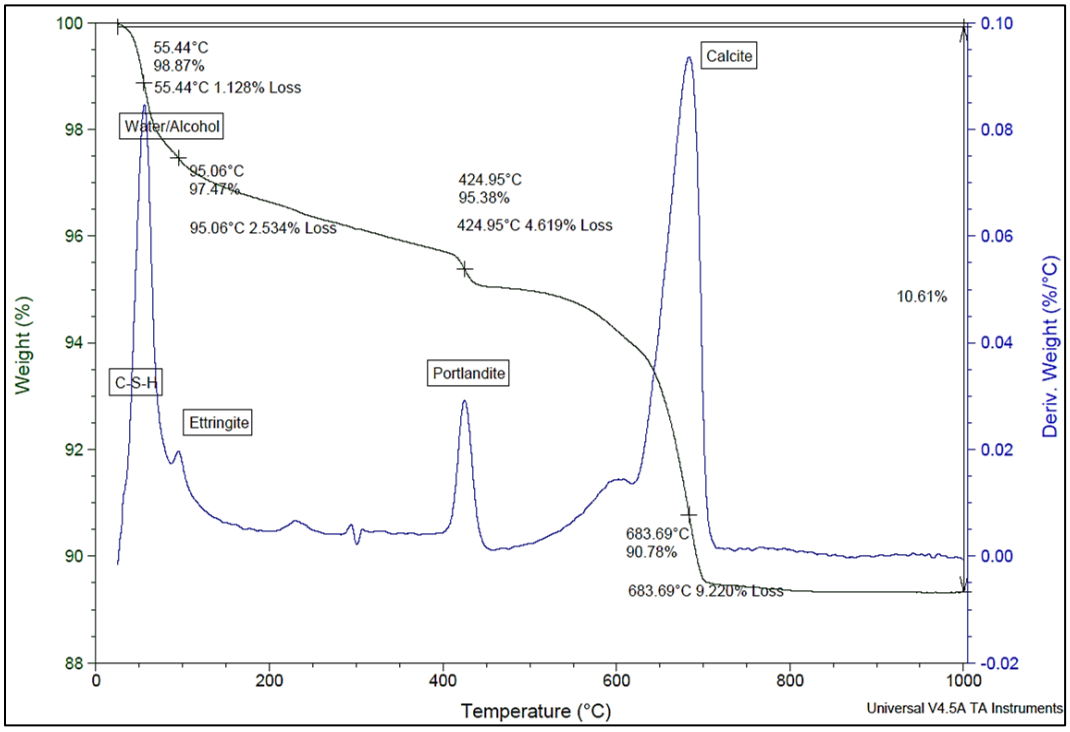


**Figure C-29: TGA/DTA graphs-analysis of GUL 0.40 mixtures at 2 hours of hydration**

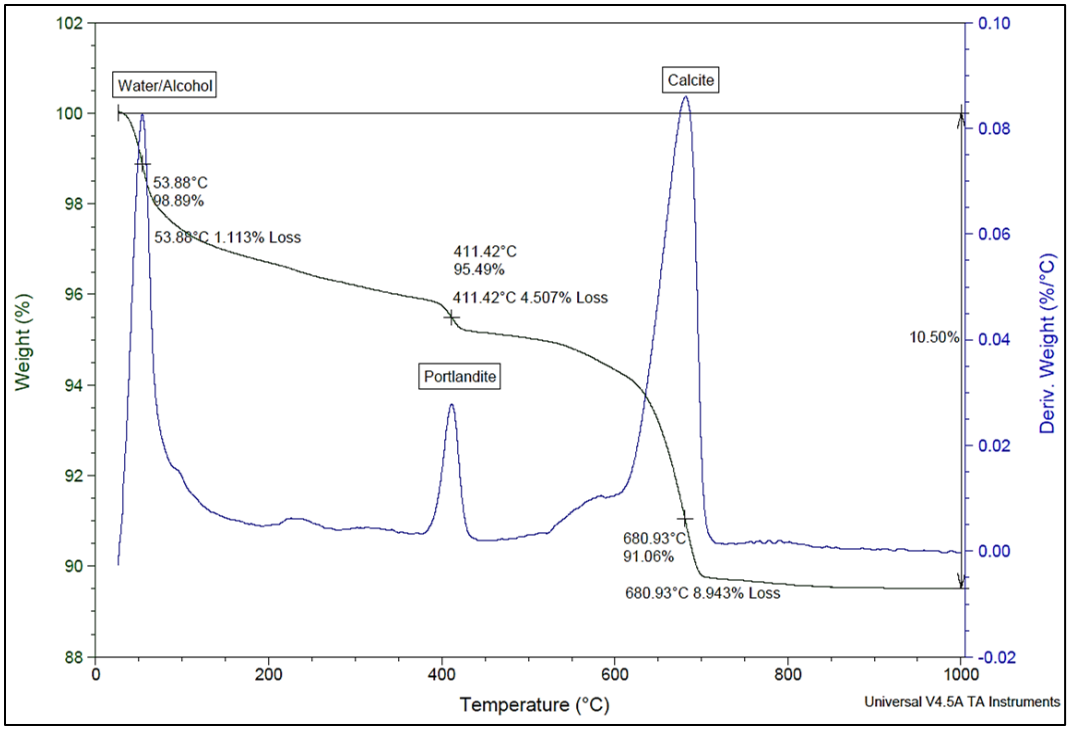


**Figure C-30: TGA/DTA graphs-analysis of GUL 0.40 mixtures at initial setting**

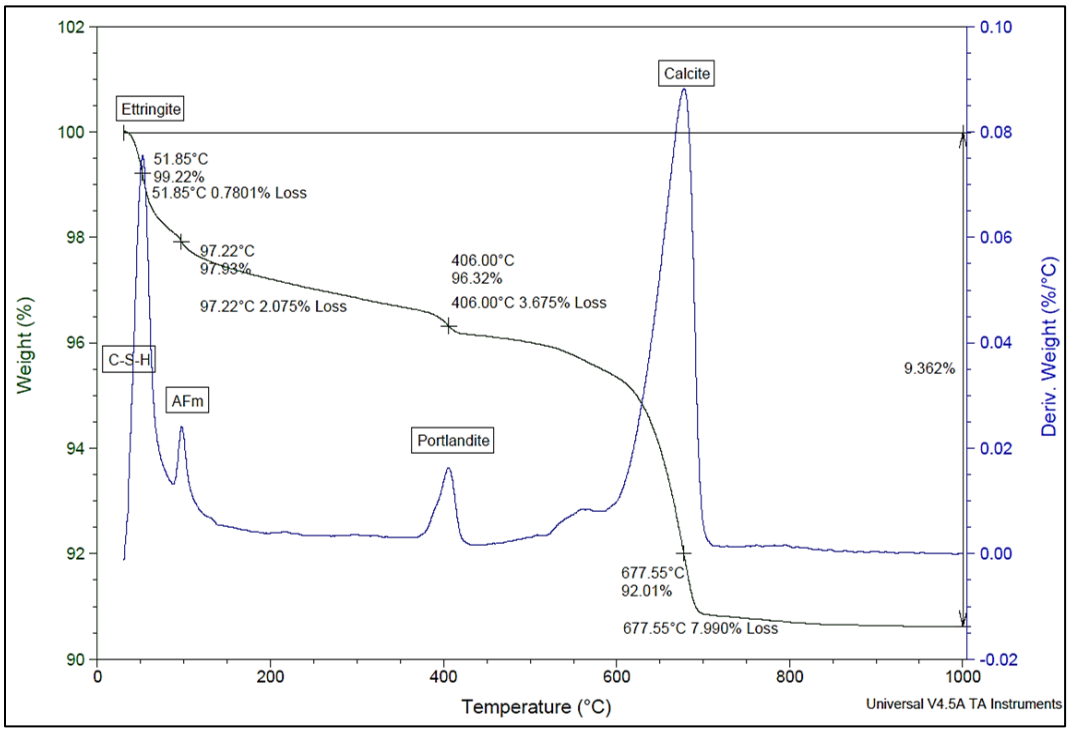


**Figure C-31: TGA/DTA graphs-analysis of GUL 0.40 mixtures at final setting**

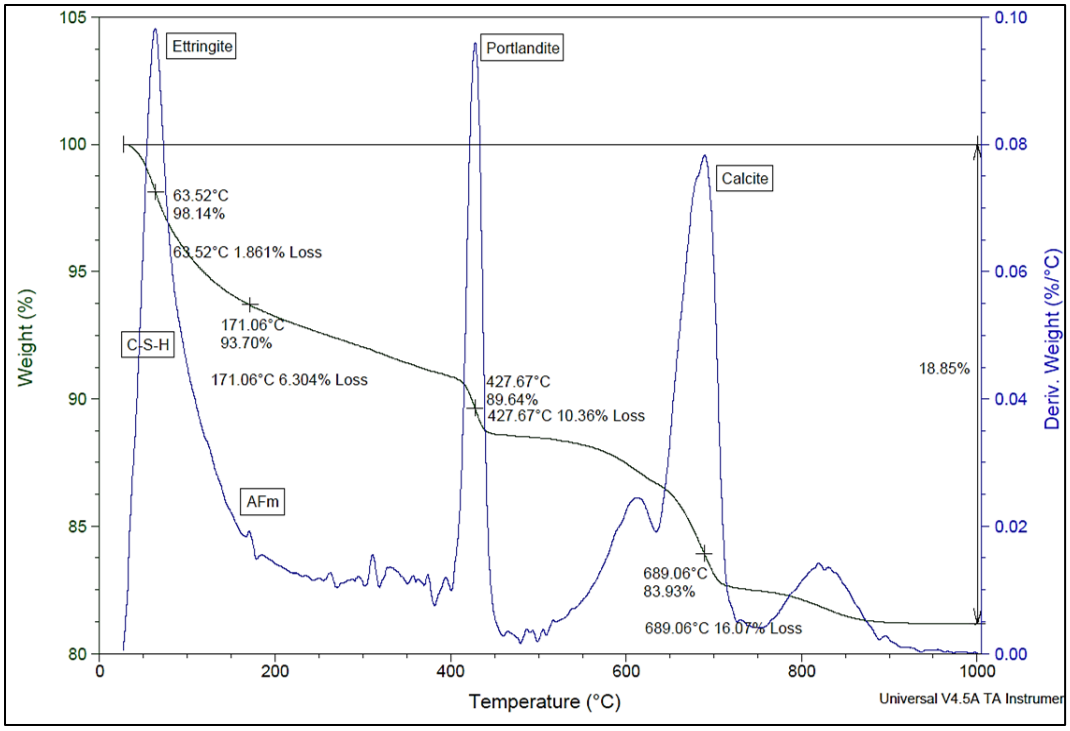


**Figure C-32: TGA/DTA graphs-analysis of GUL 0.40 mixtures at 24 hours of hydration**

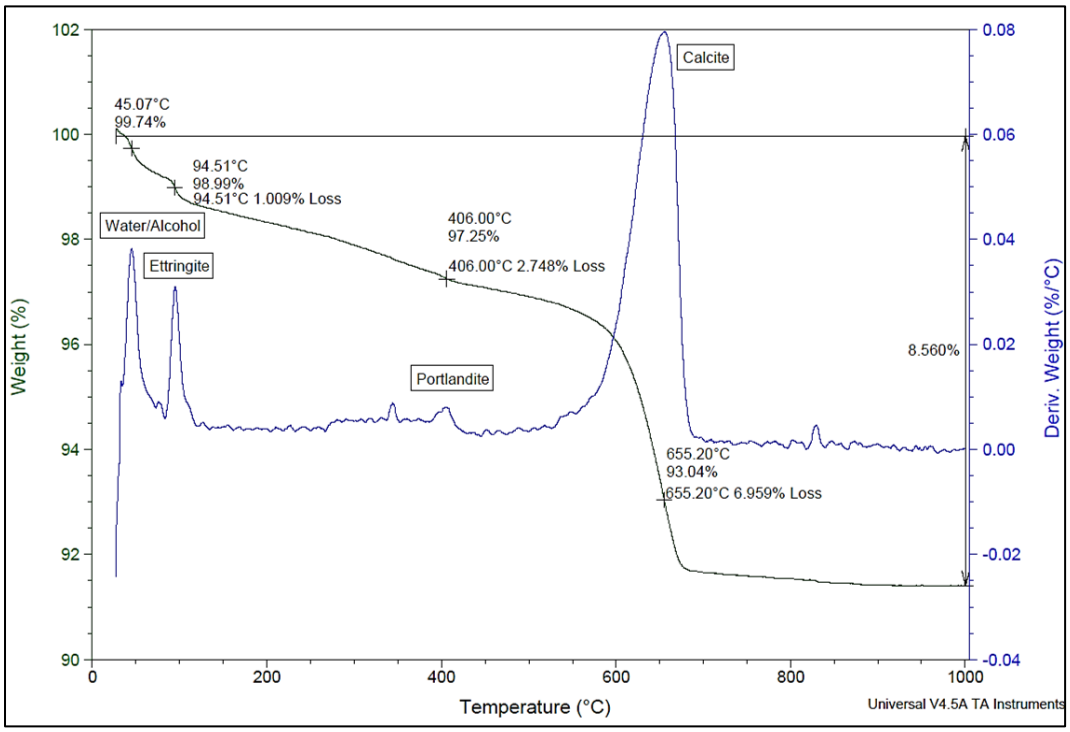


**Figure C-33: TGA/DTA graphs-analysis of GUL 0.43 mixtures at 2 hours of hydration**

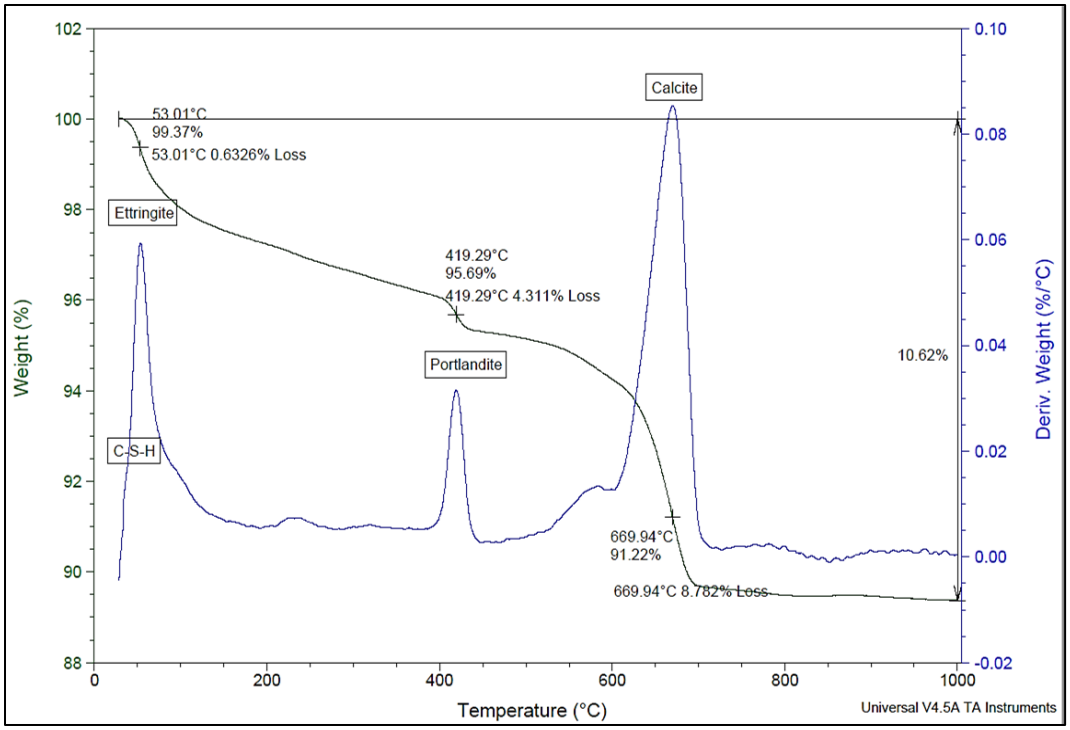


**Figure C-34: TGA/DTA graphs-analysis of GUL 0.43 mixtures at initial setting**

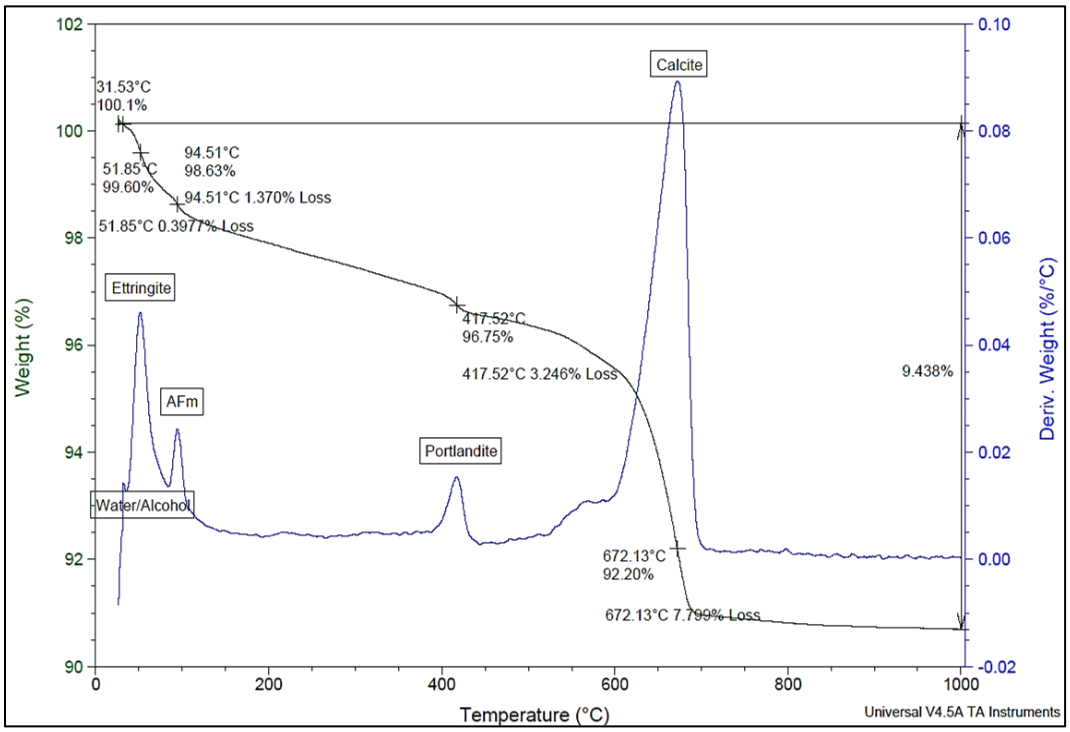


**Figure C-35: TGA/DTA graphs-analysis of GUL 0.43 mixtures at final setting**

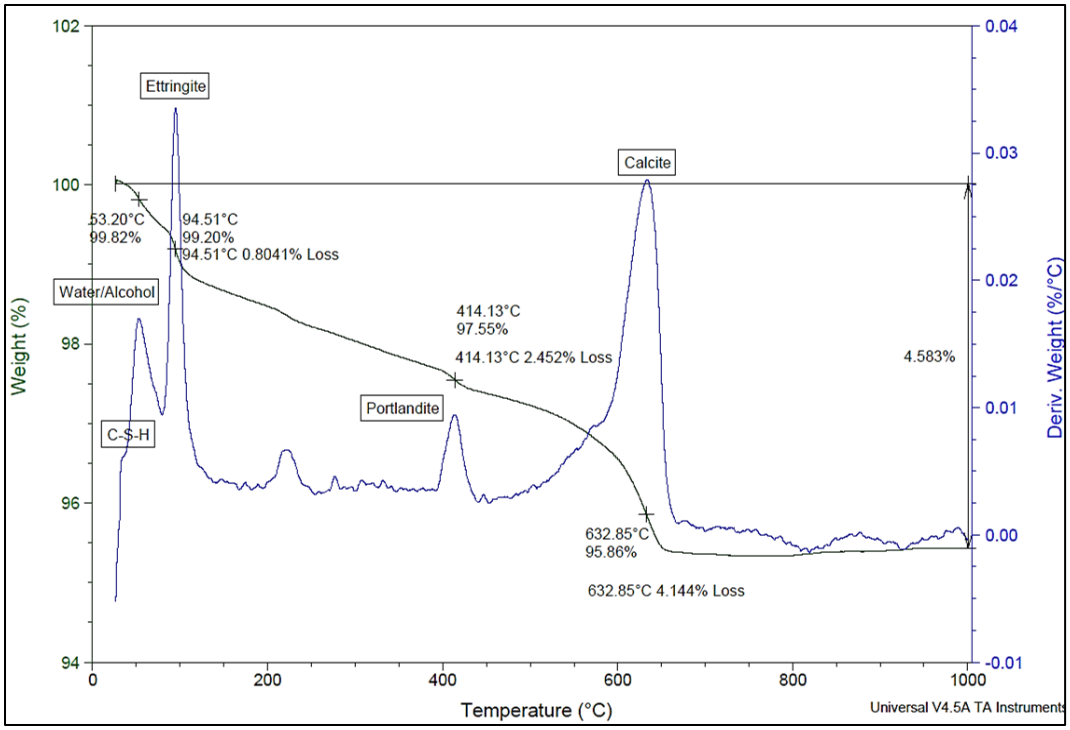


**Figure C-36: TGA/DTA graphs-analysis of HE 0.37 mixtures at 2 hours of hydration**

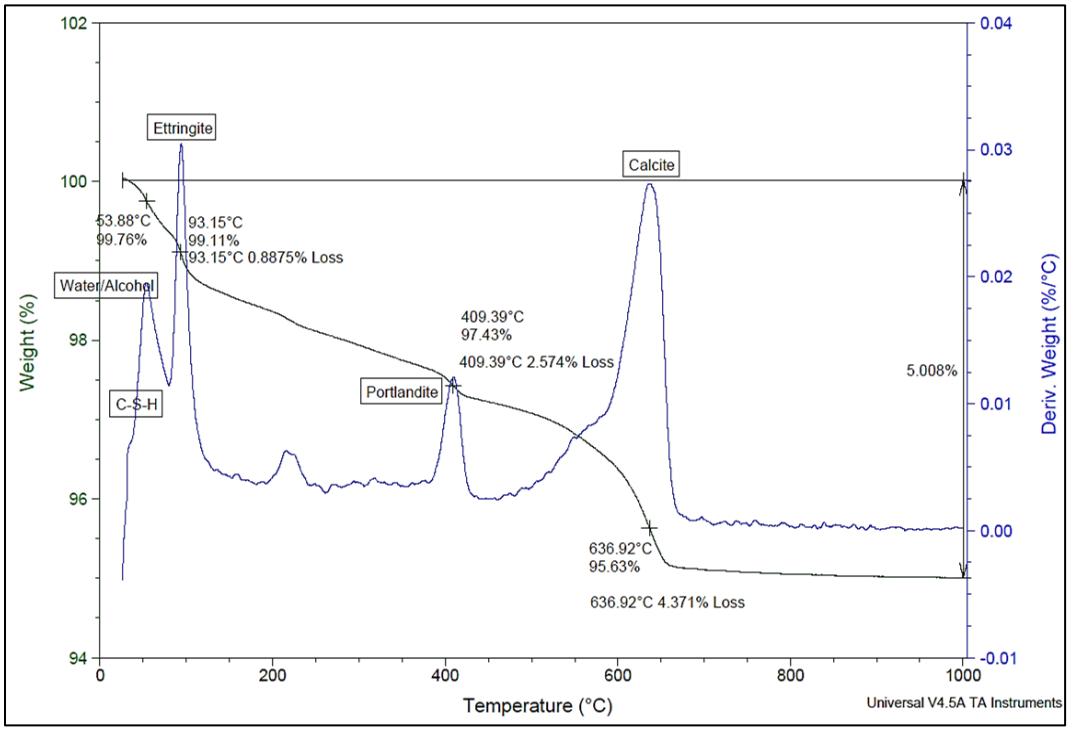


**Figure C-37: TGA/DTA graphs-analysis of HE 0.37 mixtures at initial setting**

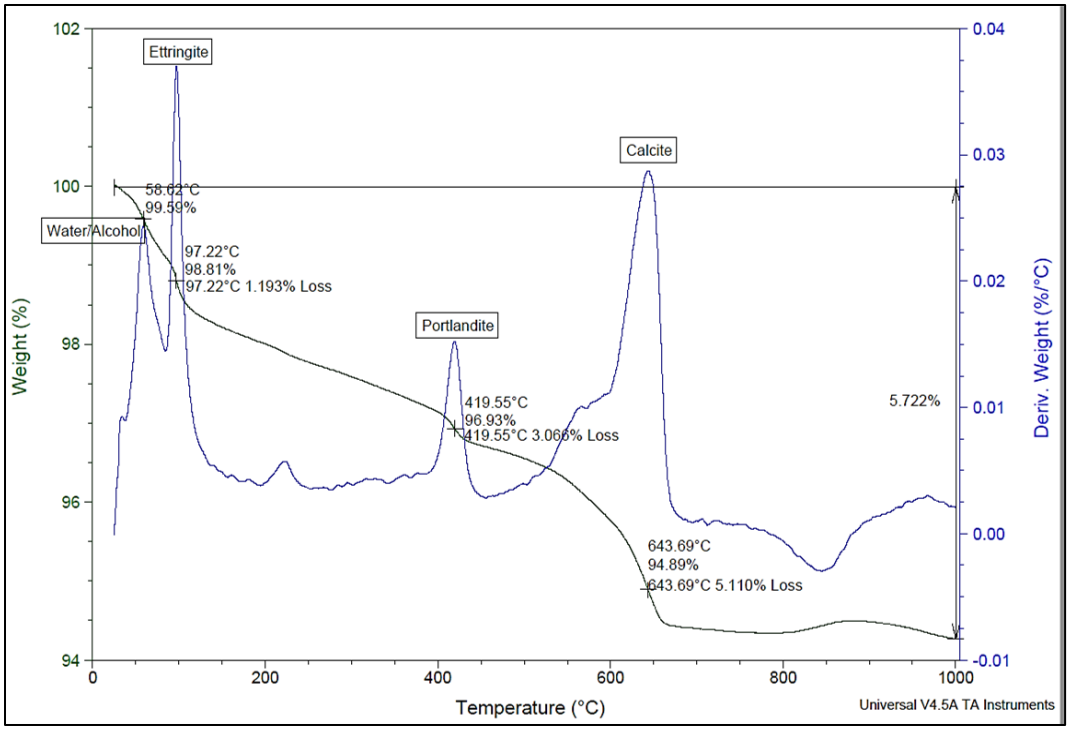


**Figure C-38: TGA/DTA graphs-analysis of HE 0.37 mixtures at final setting**

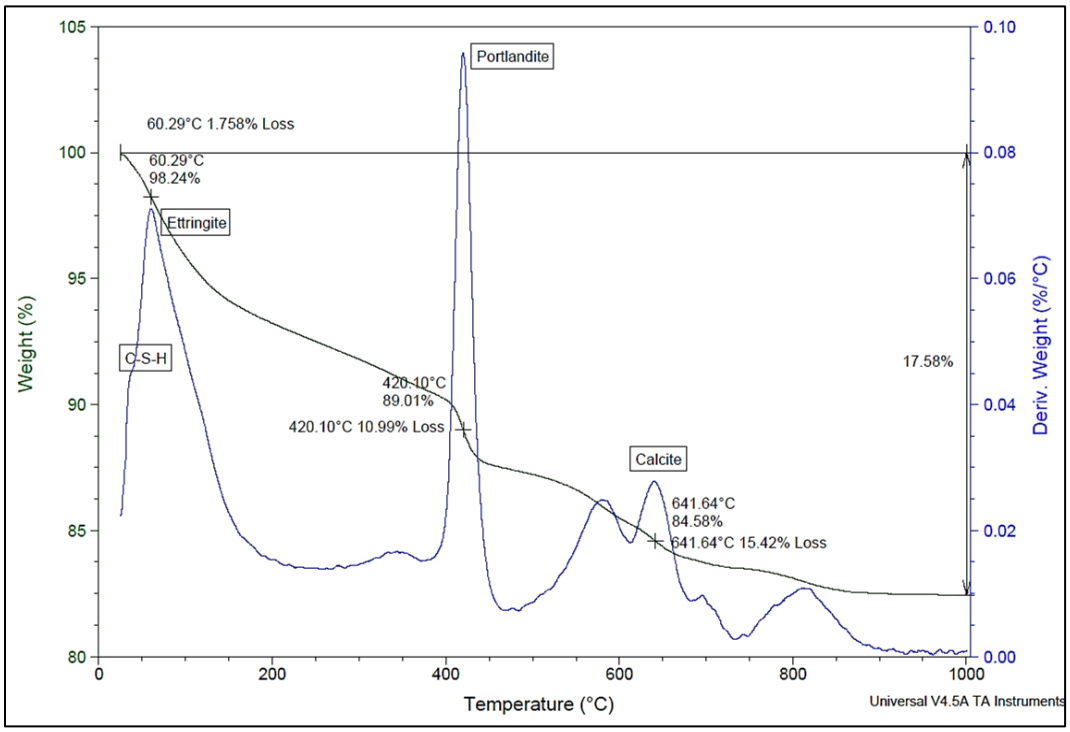


**Figure C-39: TGA/DTA graphs-analysis of HE 0.37 mixtures at 24 hours of hydration**

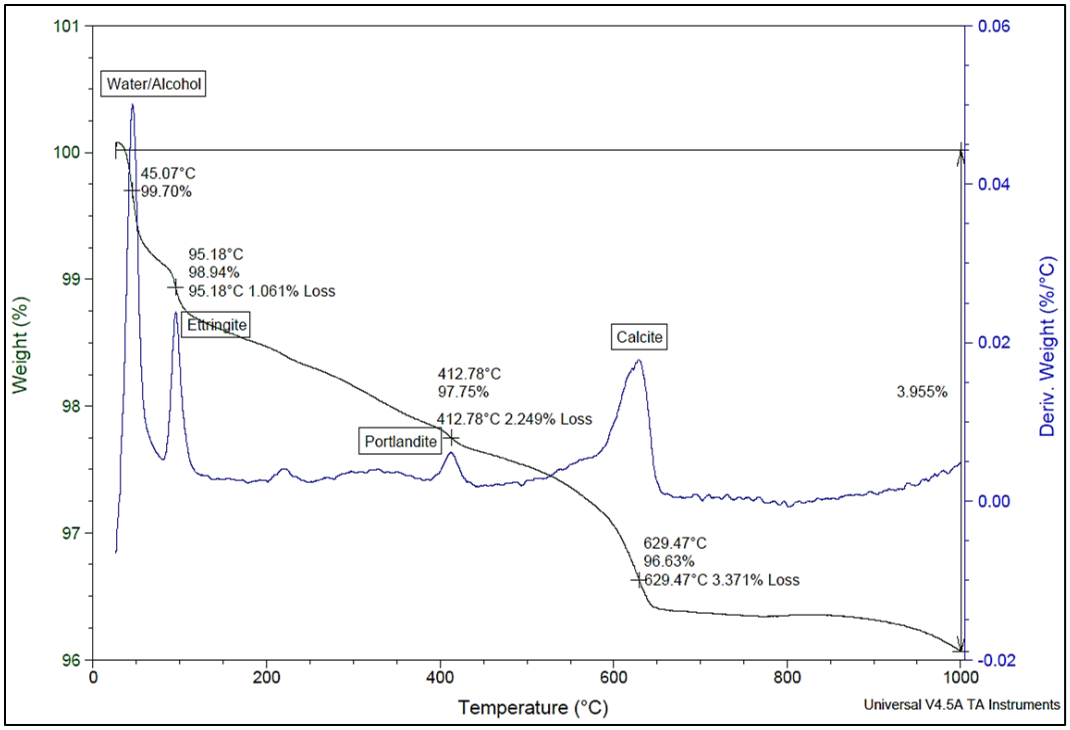


**Figure C-40: TGA/DTA graphs-analysis of HE 0.40 mixtures at 2 hours of hydration**

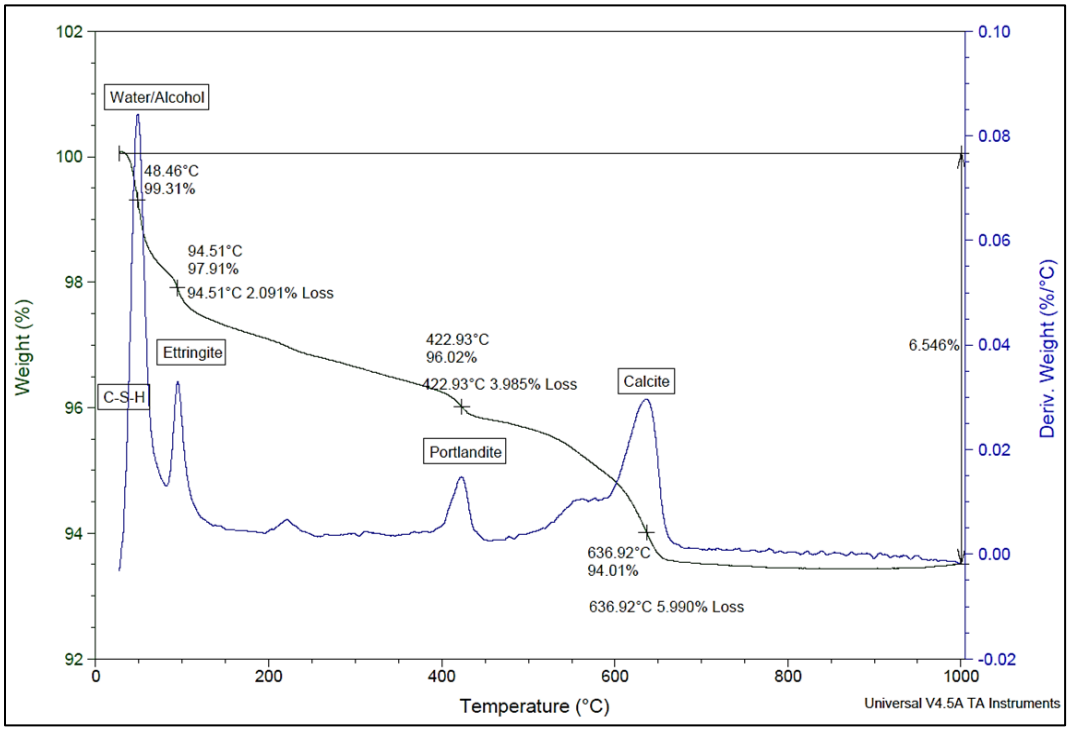


**Figure C-41: TGA/DTA graphs-analysis of HE 0.40 mixtures at initial setting**

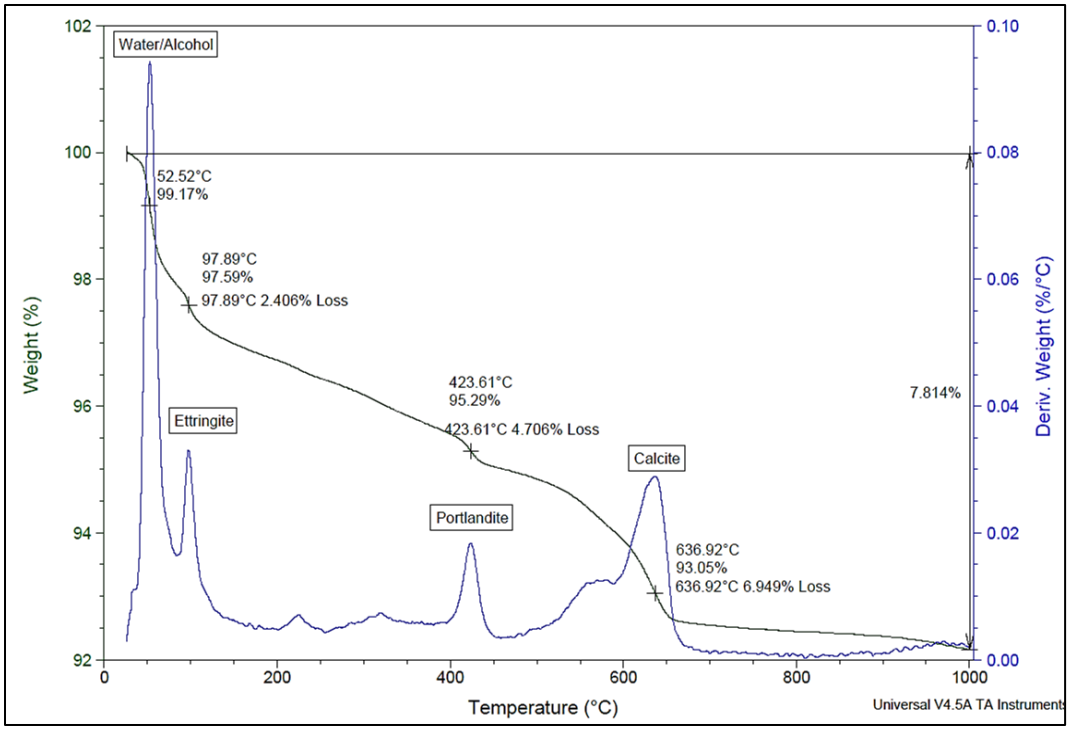


**Figure C-42: TGA/DTA graphs-analysis of HE 0.40 mixtures at final setting**

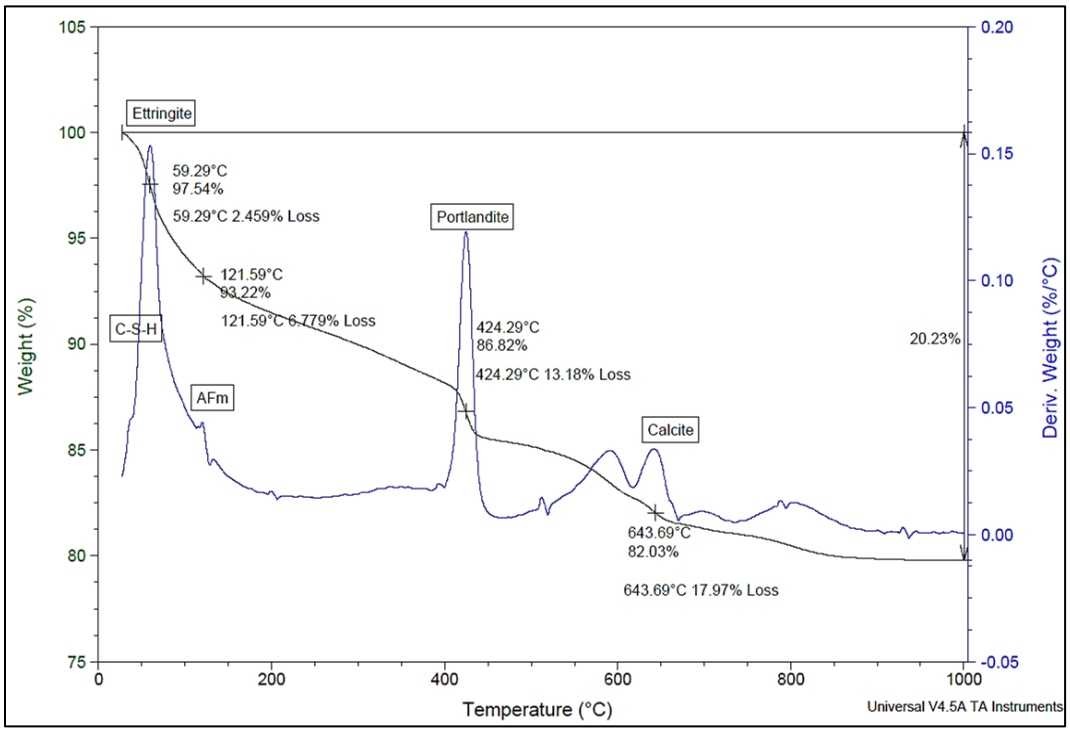


**Figure C-43: TGA/DTA graphs-analysis of HE 0.40 mixtures at 24 hours of hydration**

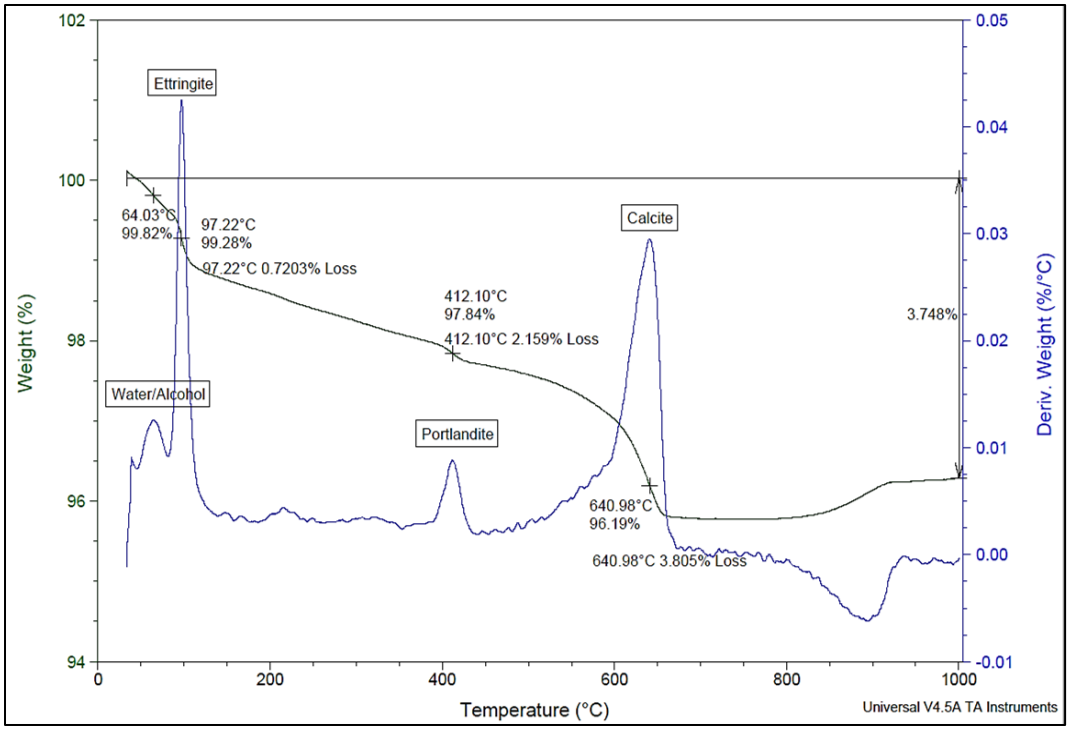


**Figure C-44: TGA/DTA graphs-analysis of HE 0.43 mixtures at 2 hours of hydration**

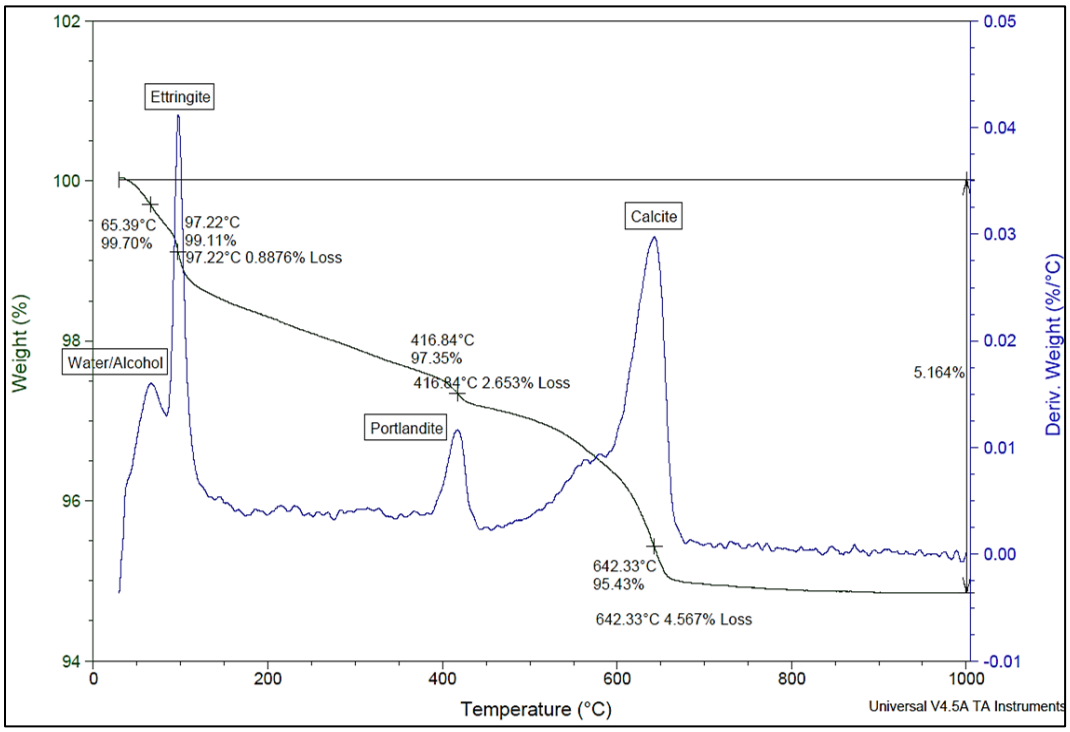


**Figure C-45: TGA/DTA graphs-analysis of HE 0.43 mixtures at initial setting**

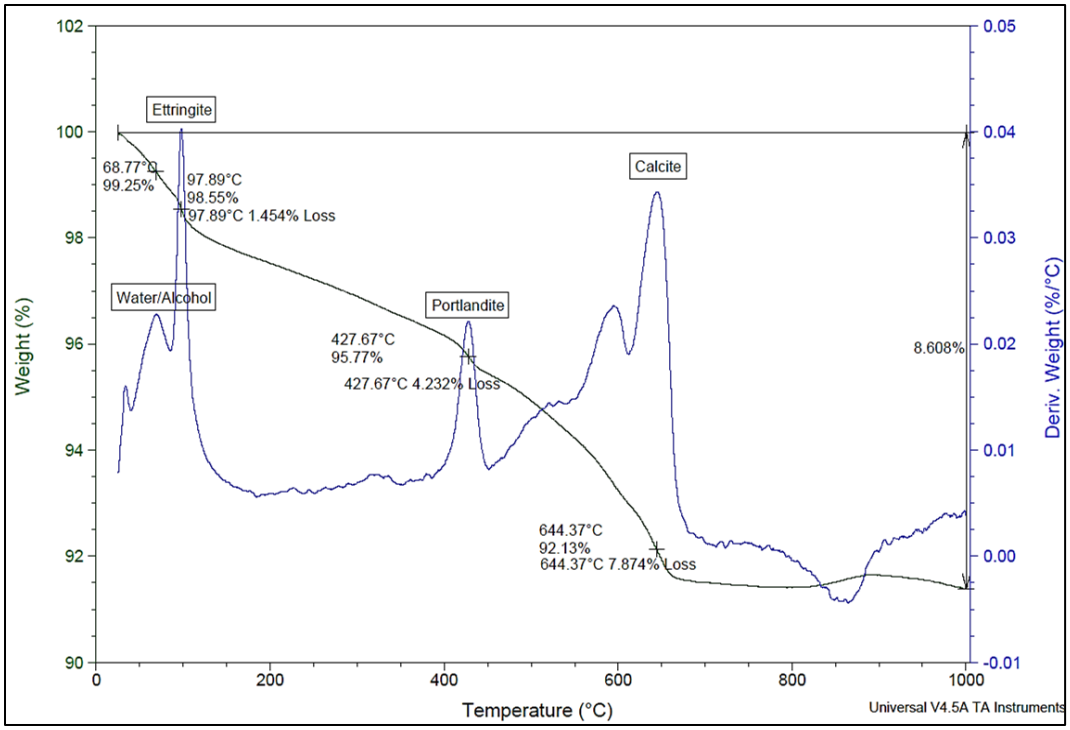


**Figure C-46: TGA/DTA graphs-analysis of HE 0.43 mixtures at final setting**

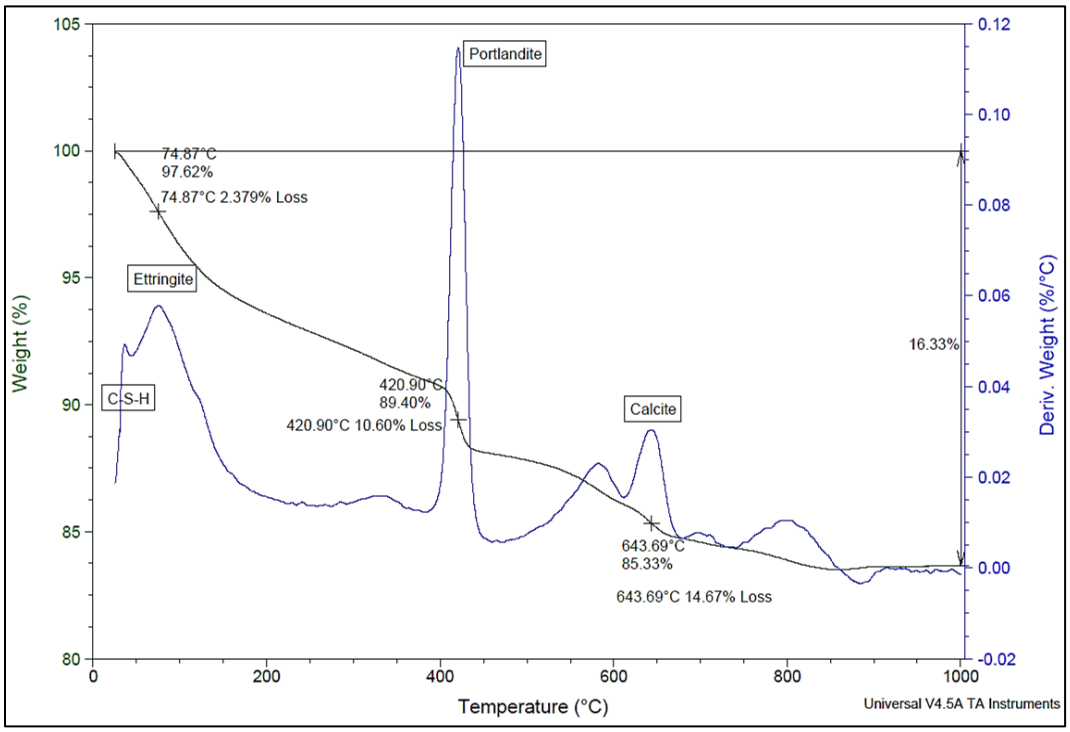


**Figure C-47: TGA/DTA graphs-analysis of HE 0.43 mixtures at 24 hours of hydration**

## D. Quantitative Analysis Results (QAR) with the help of RIR of Cement Samples

The Reference Intensity Ratio (RIR) is a method used for Quantitative Analysis. The RIR method is based upon scaling all diffraction data to the diffraction of standard reference materials.

All quantitative analyses of the cement samples are summarized in tables below. It is important to mention that for all phases; the regular detail is ICDD (PDF-2 Release 2015 RDB).

**Table D-1: QAR of GU 0.37 XRD test at 2 hours of hydration**

| **Phase name** | **Formula** | **Figure of Merit** | **DB Card Number** (PDF-2) |
|---|---|---|---|
| Brownmillerite | $Ca_2(Al,Fe)_2O_5$ | 2.856 | 00-030-0226 |
| Calcite | $CaCO_3$ | 1.507 | 01-078-3262 |
| Ettringite | $Ca_6Al_2(SO_4)_3(OH)_{12}(H_2O)_{26}$ | 3.125 | 01-075-7554 |
| Gypsum | $Ca(SO_4).(H_2O)_2$ | 3.107 | 01-076-8725 |
| Hatrurite- Alite | $Ca_3SiO_5$ | 1.571 | 01-085-1378 |
| Larnite- Belite | $Ca_2SiO_4$ | 1.426 | 01-080-8935 |
| Portlandite | $Ca(OH)_2$ | 3.090 | 00-004-0733 |
| Tobermorite | $Ca_5(Si_6O_{16})(OH)_2$ | 1.921 | 01-089-6458 |

**Table D-2: QAR of GU 0.37 XRD test at initial setting**

| **Phase name** | **Formula** | **Figure of Merit** | **DB Card Number** (PDF-2) |
|---|---|---|---|
| Brownmillerite | $Ca_2(Al,Fe)_2O_5$ | 1.493 | 00-030-0226 |
| Calcite | $CaCO_3$ | 1.732 | 01-078-3262 |
| Ettringite | $Ca_6Al_2(SO_4)_3(OH)_{12}(H_2O)_{26}$ | 1.575 | 01-075-7554 |
| Gypsum | $Ca(SO_4).(H_2O)_2$ | 1.806 | 01-076-8725 |
| Hatrurite- Alite | $Ca_3SiO_5$ | 0.813 | 01-085-1378 |
| Larnite- Belite | $Ca_2SiO_4$ | 1.325 | 01-080-8935 |
| Portlandite | $Ca(OH)_2$ | 2.897 | 00-004-0733 |
| Tobermorite | $Ca_5(Si_6O_{16})(OH)_2$ | 2.247 | 01-089-6458 |

**Table D-3: QAR of GU 0.37 XRD test at final setting**

| **Phase name** | **Formula** | **Figure of Merit** | **DB Card Number** (PDF-2) |
|---|---|---|---|
| Brownmillerite | $Ca_2(Al,Fe)_2O_5$ | 1.447 | 00-030-0226 |
| Calcite | $CaCO_3$ | 3.027 | 01-078-3262 |
| Ettringite | $Ca_6Al_2(SO_4)_3(OH)_{12}(H_2O)_{26}$ | 1.685 | 01-075-7554 |
| Gypsum | $Ca(SO_4).(H_2O)_2$ | 1.950 | 01-076-8725 |
| Hatrurite- Alite | $Ca_3SiO_5$ | 0.997 | 01-085-1378 |
| Larnite- Belite | $Ca_2SiO_4$ | 1.330 | 01-080-8935 |
| Portlandite | $Ca(OH)_2$ | 1.890 | 00-004-0733 |
| Tobermorite | $Ca_5(Si_6O_{16})(OH)_2$ | 1.828 | 01-089-6458 |

**Table D-4: QAR of GU 0.37 XRD test at 24 hours of hydration**

| **Phase name** | **Formula** | **Figure of Merit** | **DB Card Number** (PDF-2) |
|---|---|---|---|
| Brownmillerite | $Ca_2(Al,Fe)_2O_5$ | 1.612 | 00-030-0226 |
| Calcite | $CaCO_3$ | 1.309 | 01-078-3262 |
| Ettringite | $Ca_6Al_2(SO_4)_3(OH)_{12}(H_2O)_{26}$ | 0.531 | 01-075-7554 |
| Gypsum | $Ca(SO_4).(H_2O)_2$ | 2.152 | 01-076-8725 |
| Hatrurite- Alite | $Ca_3SiO_5$ | 1.356 | 01-085-1378 |
| Larnite- Belite | $Ca_2SiO_4$ | 1.168 | 01-080-8935 |
| Portlandite | $Ca(OH)_2$ | 0.895 | 00-004-0733 |
| Tobermorite | $Ca_5(Si_6O_{16})(OH)_2$ | 1.783 | 01-089-6458 |

**Table D-5: QAR of GU 0.40 XRD test at 2 hours of hydration**

| **Phase name** | **Formula** | **Figure of Merit** | **DB Card Number** (PDF-2) |
|---|---|---|---|
| Brownmillerite | $Ca_2(Al,Fe)_2O_5$ | 1.558 | 00-030-0226 |
| Calcite | $CaCO_3$ | 1.756 | 01-078-3262 |
| Ettringite | $Ca_6Al_2(SO_4)_3(OH)_{12}(H_2O)_{26}$ | 3.255 | 01-075-7554 |
| Gypsum | $Ca(SO_4).(H_2O)_2$ | 1.920 | 01-076-8725 |
| Hatrurite- Alite | $Ca_3SiO_5$ | 0.925 | 01-085-1378 |
| Larnite- Belite | $Ca_2SiO_4$ | 1.886 | 01-080-8935 |
| Portlandite | $Ca(OH)_2$ | 2.899 | 00-004-0733 |
| Tobermorite | $Ca_5(Si_6O_{16})(OH)_2$ | 1.807 | 01-089-6458 |

**Table D-6: QAR of GU 0.40 XRD test at initial setting**

| **Phase name** | **Formula** | **Figure of Merit** | **DB Card Number** (PDF-2) |
|---|---|---|---|
| Brownmillerite | $Ca_2(Al,Fe)_2O_5$ | 1.163 | 00-030-0226 |
| Calcite | $CaCO_3$ | 1.412 | 01-078-3262 |
| Ettringite | $Ca_6Al_2(SO_4)_3(OH)_{12}(H_2O)_{26}$ | 3.400 | 01-075-7554 |
| Gypsum | $Ca(SO_4).(H_2O)_2$ | 1.869 | 01-076-8725 |
| Hatrurite- Alite | $Ca_3SiO_5$ | 0.825 | 01-085-1378 |
| Larnite- Belite | $Ca_2SiO_4$ | 1.348 | 01-080-8935 |
| Portlandite | $Ca(OH)_2$ | 1.722 | 00-004-0733 |
| Tobermorite | $Ca_5(Si_6O_{16})(OH)_2$ | 3.078 | 01-089-6458 |

**Table D-7: QAR of GU 0.40 XRD test at final setting**

| **Phase name** | **Formula** | **Figure of Merit** | **DB Card Number** (PDF-2) |
|---|---|---|---|
| Brownmillerite | $Ca_2(Al,Fe)_2O_5$ | 3.078 | 00-030-0226 |
| Calcite | $CaCO_3$ | 1.499 | 01-078-3262 |
| Ettringite | $Ca_6Al_2(SO_4)_3(OH)_{12}(H_2O)_{26}$ | 3.320 | 01-075-7554 |
| Gypsum | $Ca(SO_4).(H_2O)_2$ | 3.563 | 01-076-8725 |
| Hatrurite- Alite | $Ca_3SiO_5$ | 3.143 | 01-085-1378 |
| Larnite- Belite | $Ca_2SiO_4$ | 1.695 | 01-080-8935 |
| Portlandite | $Ca(OH)_2$ | 1.818 | 00-004-0733 |
| Tobermorite | $Ca_5(Si_6O_{16})(OH)_2$ | 3.131 | 01-089-6458 |

**Table D-8: QAR of GU 0.40 XRD test at 24 hours of hydration**

| **Phase name** | **Formula** | **Figure of Merit** | **DB Card Number** (PDF-2) |
|---|---|---|---|
| Brownmillerite | $Ca_2(Al,Fe)_2O_5$ | 1.544 | 00-030-0226 |
| Calcite | $CaCO_3$ | 2.797 | 01-078-3262 |
| Ettringite | $Ca_6Al_2(SO_4)_3(OH)_{12}(H_2O)_{26}$ | 3.172 | 01-075-7554 |
| Gypsum | $Ca(SO_4).(H_2O)_2$ | 3.201 | 01-076-8725 |
| Hatrurite- Alite | $Ca_3SiO_5$ | 1.387 | 01-085-1378 |
| Larnite- Belite | $Ca_2SiO_4$ | 1.335 | 01-080-8935 |
| Portlandite | $Ca(OH)_2$ | 1.052 | 00-004-0733 |
| Tobermorite | $Ca_5(Si_6O_{16})(OH)_2$ | 2.174 | 01-089-6458 |

**Table D-9: QAR of GU 0.43 XRD test at 2 hours of hydration**

| **Phase name** | **Formula** | **Figure of Merit** | **DB Card Number** (PDF-2) |
|---|---|---|---|
| Brownmillerite | $Ca_2(Al,Fe)_2O_5$ | 1.343 | 00-030-0226 |
| Calcite | $CaCO_3$ | 1.343 | 01-078-3262 |
| Ettringite | $Ca_6Al_2(SO_4)_3(OH)_{12}(H_2O)_{26}$ | 3.157 | 01-075-7554 |
| Gypsum | $Ca(SO_4).(H_2O)_2$ | 2.929 | 01-076-8725 |
| Hatrurite- Alite | $Ca_3SiO_5$ | 1.422 | 01-085-1378 |
| Larnite- Belite | $Ca_2SiO_4$ | 1.688 | 01-080-8935 |
| Portlandite | $Ca(OH)_2$ | 3.167 | 00-004-0733 |
| Tobermorite | $Ca_5(Si_6O_{16})(OH)_2$ | 1.999 | 01-089-6458 |

**Table D-10: QAR of GU 0.43 XRD test at initial setting**

| **Phase name** | **Formula** | **Figure of Merit** | **DB Card Number** (PDF-2) |
|---|---|---|---|
| Brownmillerite | $Ca_2(Al,Fe)_2O_5$ | 1.309 | 00-030-0226 |
| Calcite | $CaCO_3$ | 1.299 | 01-078-3262 |
| Ettringite | $Ca_6Al_2(SO_4)_3(OH)_{12}(H_2O)_{26}$ | 1.887 | 01-075-7554 |
| Gypsum | $Ca(SO_4).(H_2O)_2$ | 2.963 | 01-076-8725 |
| Hatrurite- Alite | $Ca_3SiO_5$ | 1.335 | 01-085-1378 |
| Larnite- Belite | $Ca_2SiO_4$ | 1.351 | 01-080-8935 |
| Portlandite | $Ca(OH)_2$ | 1.622 | 00-004-0733 |
| Tobermorite | $Ca_5(Si_6O_{16})(OH)_2$ | 1.648 | 01-089-6458 |

**Table D-11: QAR of GU 0.43 XRD test at final setting**

| **Phase name** | **Formula** | **Figure of Merit** | **DB Card Number** (PDF-2) |
|---|---|---|---|
| Brownmillerite | $Ca_2(Al,Fe)_2O_5$ | 1.458 | 00-030-0226 |
| Calcite | $CaCO_3$ | 2.841 | 01-078-3262 |
| Ettringite | $Ca_6Al_2(SO_4)_3(OH)_{12}(H_2O)_{26}$ | 3.059 | 01-075-7554 |
| Gypsum | $Ca(SO_4).(H_2O)_2$ | 1.803 | 01-076-8725 |
| Hatrurite- Alite | $Ca_3SiO_5$ | 1.115 | 01-085-1378 |
| Larnite- Belite | $Ca_2SiO_4$ | 1.474 | 01-080-8935 |
| Portlandite | $Ca(OH)_2$ | 1.872 | 00-004-0733 |
| Tobermorite | $Ca_5(Si_6O_{16})(OH)_2$ | 1.933 | 01-089-6458 |

**Table D-12: QAR of GU 0.43 XRD test at 24 hours of hydration**

| **Phase name** | **Formula** | **Figure of Merit** | **DB Card Number** (PDF-2) |
|---|---|---|---|
| Brownmillerite | $Ca_2(Al,Fe)_2O_5$ | 1.295 | 00-030-0226 |
| Calcite | $CaCO_3$ | 2.771 | 01-078-3262 |
| Ettringite | $Ca_6Al_2(SO_4)_3(OH)_{12}(H_2O)_{26}$ | 1.691 | 01-075-7554 |
| Gypsum | $Ca(SO_4).(H_2O)_2$ | 3.160 | 01-076-8725 |
| Hatrurite- Alite | $Ca_3SiO_5$ | 1.907 | 01-085-1378 |
| Larnite- Belite | $Ca_2SiO_4$ | 1.281 | 01-080-8935 |
| Portlandite | $Ca(OH)_2$ | 1.061 | 00-004-0733 |
| Tobermorite | $Ca_5(Si_6O_{16})(OH)_2$ | 1.689 | 01-089-6458 |

**Table D-13: QAR of GUbSF 0.37 XRD test at 2 hours of hydration**

| **Phase name** | **Formula** | **Figure of Merit** | **DB Card Number** (PDF-2) |
|---|---|---|---|
| Brownmillerite | $Ca_2(Al,Fe)_2O_5$ | 1.609 | 00-030-0226 |
| Calcite | $CaCO_3$ | 1.590 | 01-078-3262 |
| Ettringite | $Ca_6Al_2(SO_4)_3(OH)_{12}(H_2O)_{26}$ | 3.237 | 01-075-7554 |
| Gypsum | $Ca(SO_4).(H_2O)_2$ | 1.397 | 01-076-8725 |
| Hatrurite- Alite | $Ca_3SiO_5$ | 0.932 | 01-085-1378 |
| Larnite- Belite | $Ca_2SiO_4$ | 1.260 | 01-080-8935 |
| Portlandite | $Ca(OH)_2$ | 2.987 | 00-004-0733 |
| Tobermorite | $Ca_5(Si_6O_{16})(OH)_2$ | 3.520 | 01-089-6458 |

**Table D-14: QAR of GUbSF 0.37 XRD test at initial setting**

| **Phase name** | **Formula** | **Figure of Merit** | **DB Card Number** (PDF-2) |
|---|---|---|---|
| Brownmillerite | $Ca_2(Al,Fe)_2O_5$ | 1.521 | 00-030-0226 |
| Calcite | $CaCO_3$ | 2.954 | 01-078-3262 |
| Ettringite | $Ca_6Al_2(SO_4)_3(OH)_{12}(H_2O)_{26}$ | 1.530 | 01-075-7554 |
| Gypsum | $Ca(SO_4).(H_2O)_2$ | 1.502 | 01-076-8725 |
| Hatrurite- Alite | $Ca_3SiO_5$ | 0.688 | 01-085-1378 |
| Larnite- Belite | $Ca_2SiO_4$ | 1.556 | 01-080-8935 |
| Portlandite | $Ca(OH)_2$ | 2.820 | 00-004-0733 |
| Tobermorite | $Ca_5(Si_6O_{16})(OH)_2$ | 1.662 | 01-089-6458 |

**Table D-15: QAR of GUbSF 0.37 XRD test at final setting**

| **Phase name** | **Formula** | **Figure of Merit** | **DB Card Number** (PDF-2) |
|---|---|---|---|
| Brownmillerite | $Ca_2(Al,Fe)_2O_5$ | 1.476 | 00-030-0226 |
| Calcite | $CaCO_3$ | 3.082 | 01-078-3262 |
| Ettringite | $Ca_6Al_2(SO_4)_3(OH)_{12}(H_2O)_{26}$ | 1.794 | 01-075-7554 |
| Gypsum | $Ca(SO_4).(H_2O)_2$ | 1.528 | 01-076-8725 |
| Hatrurite- Alite | $Ca_3SiO_5$ | 3.325 | 01-085-1378 |
| Larnite- Belite | $Ca_2SiO_4$ | 1.511 | 01-080-8935 |
| Portlandite | $Ca(OH)_2$ | 2.979 | 00-004-0733 |
| Tobermorite | $Ca_5(Si_6O_{16})(OH)_2$ | 1.789 | 01-089-6458 |

**Table D-16: QAR of GUbSF 0.37 XRD test at 24 hours of hydration**

| **Phase name** | **Formula** | **Figure of Merit** | **DB Card Number** (PDF-2) |
|---|---|---|---|
| Brownmillerite | $Ca_2(Al,Fe)_2O_5$ | 1.473 | 00-030-0226 |
| Calcite | $CaCO_3$ | 1.530 | 01-078-3262 |
| Ettringite | $Ca_6Al_2(SO_4)_3(OH)_{12}(H_2O)_{26}$ | 1.566 | 01-075-7554 |
| Gypsum | $Ca(SO_4).(H_2O)_2$ | 3.144 | 01-076-8725 |
| Hatrurite- Alite | $Ca_3SiO_5$ | 1.188 | 01-085-1378 |
| Larnite- Belite | $Ca_2SiO_4$ | 1.466 | 01-080-8935 |
| Portlandite | $Ca(OH)_2$ | 0.899 | 00-004-0733 |
| Tobermorite | $Ca_5(Si_6O_{16})(OH)_2$ | 2.083 | 01-089-6458 |

**Table D-17: QAR of GUbSF 0.40 XRD test at 2 hours of hydration**

| **Phase name** | **Formula** | **Figure of Merit** | **DB Card Number** (PDF-2) |
|---|---|---|---|
| Brownmillerite | $Ca_2(Al,Fe)_2O_5$ | 1.200 | 00-030-0226 |
| Calcite | $CaCO_3$ | 2.654 | 01-078-3262 |
| Ettringite | $Ca_6Al_2(SO_4)_3(OH)_{12}(H_2O)_{26}$ | 1.855 | 01-075-7554 |
| Gypsum | $Ca(SO_4).(H_2O)_2$ | 1.409 | 01-076-8725 |
| Hatrurite- Alite | $Ca_3SiO_5$ | 0.805 | 01-085-1378 |
| Larnite- Belite | $Ca_2SiO_4$ | 1.459 | 01-080-8935 |
| Portlandite | $Ca(OH)_2$ | 2.991 | 00-004-0733 |
| Tobermorite | $Ca_5(Si_6O_{16})(OH)_2$ | 2.094 | 01-089-6458 |

**Table D-18: QAR of GUbSF 0.40 XRD test at initial setting**

| **Phase name** | **Formula** | **Figure of Merit** | **DB Card Number** (PDF-2) |
|---|---|---|---|
| Brownmillerite | $Ca_2(Al,Fe)_2O_5$ | 1.892 | 00-030-0226 |
| Calcite | $CaCO_3$ | 1.405 | 01-078-3262 |
| Ettringite | $Ca_6Al_2(SO_4)_3(OH)_{12}(H_2O)_{26}$ | 1.954 | 01-075-7554 |
| Gypsum | $Ca(SO_4).(H_2O)_2$ | 1.447 | 01-076-8725 |
| Hatrurite- Alite | $Ca_3SiO_5$ | 1.234 | 01-085-1378 |
| Larnite- Belite | $Ca_2SiO_4$ | 1.416 | 01-080-8935 |
| Portlandite | $Ca(OH)_2$ | 1.464 | 00-004-0733 |
| Tobermorite | $Ca_5(Si_6O_{16})(OH)_2$ | 1.767 | 01-089-6458 |

**Table D-19: QAR of GUbSF 0.40 XRD test at final setting**

| **Phase name** | **Formula** | **Figure of Merit** | **DB Card Number** (PDF-2) |
|---|---|---|---|
| Brownmillerite | $Ca_2(Al,Fe)_2O_5$ | 1.420 | 00-030-0226 |
| Calcite | $CaCO_3$ | 1.490 | 01-078-3262 |
| Ettringite | $Ca_6Al_2(SO_4)_3(OH)_{12}(H_2O)_{26}$ | 1.675 | 01-075-7554 |
| Gypsum | $Ca(SO_4).(H_2O)_2$ | 3.150 | 01-076-8725 |
| Hatrurite- Alite | $Ca_3SiO_5$ | 0.958 | 01-085-1378 |
| Larnite- Belite | $Ca_2SiO_4$ | 1.803 | 01-080-8935 |
| Portlandite | $Ca(OH)_2$ | 1.603 | 00-004-0733 |
| Tobermorite | $Ca_5(Si_6O_{16})(OH)_2$ | 1.931 | 01-089-6458 |

**Table D-20: QAR of GUbSF 0.40 XRD test at 24 hours of hydration**

| **Phase name** | **Formula** | **Figure of Merit** | **DB Card Number** (PDF-2) |
|---|---|---|---|
| Brownmillerite | $Ca_2(Al,Fe)_2O_5$ | 0.949 | 00-030-0226 |
| Calcite | $CaCO_3$ | 2.750 | 01-078-3262 |
| Ettringite | $Ca_6Al_2(SO_4)_3(OH)_{12}(H_2O)_{26}$ | 0.828 | 01-075-7554 |
| Gypsum | $Ca(SO_4).(H_2O)_2$ | 0.853 | 01-076-8725 |
| Hatrurite- Alite | $Ca_3SiO_5$ | 0.929 | 01-085-1378 |
| Larnite- Belite | $Ca_2SiO_4$ | 0.859 | 01-080-8935 |
| Portlandite | $Ca(OH)_2$ | 0.793 | 00-004-0733 |
| Tobermorite | $Ca_5(Si_6O_{16})(OH)_2$ | 1.527 | 01-089-6458 |

**Table D-21: QAR of GUbSF 0.43 XRD test at 2 hours**

| **Phase name** | **Formula** | **Figure of Merit** | **DB Card Number** (PDF-2) |
|---|---|---|---|
| Brownmillerite | $Ca_2(Al,Fe)_2O_5$ | 1.387 | 00-030-0226 |
| Calcite | $CaCO_3$ | 2.727 | 01-078-3262 |
| Ettringite | $Ca_6Al_2(SO_4)_3(OH)_{12}(H_2O)_{26}$ | 2.295 | 01-075-7554 |
| Gypsum | $Ca(SO_4).(H_2O)_2$ | 1.496 | 01-076-8725 |
| Hatrurite- Alite | $Ca_3SiO_5$ | 0.775 | 01-085-1378 |
| Larnite- Belite | $Ca_2SiO_4$ | 1.488 | 01-080-8935 |
| Portlandite | $Ca(OH)_2$ | 3.033 | 00-004-0733 |
| Tobermorite | $Ca_5(Si_6O_{16})(OH)_2$ | 1.925 | 01-089-6458 |

**Table D-22: QAR of GUbSF 0.43 XRD test at initial setting**

| **Phase name** | **Formula** | **Figure of Merit** | **DB Card Number** (PDF-2) |
|---|---|---|---|
| Brownmillerite | $Ca_2(Al,Fe)_2O_5$ | 1.641 | 00-030-0226 |
| Calcite | $CaCO_3$ | 1.528 | 01-078-3262 |
| Ettringite | $Ca_6Al_2(SO_4)_3(OH)_{12}(H_2O)_{26}$ | 3.150 | 01-075-7554 |
| Gypsum | $Ca(SO_4).(H_2O)_2$ | 1.671 | 01-076-8725 |
| Hatrurite- Alite | $Ca_3SiO_5$ | 0.917 | 01-085-1378 |
| Larnite- Belite | $Ca_2SiO_4$ | 1.431 | 01-080-8935 |
| Portlandite | $Ca(OH)_2$ | 1.643 | 00-004-0733 |
| Tobermorite | $Ca_5(Si_6O_{16})(OH)_2$ | 2.003 | 01-089-6458 |

**Table D-23: QAR of GUbSF 0.43 XRD test at final setting**

| **Phase name** | **Formula** | **Figure of Merit** | **DB Card Number** (PDF-2) |
|---|---|---|---|
| Brownmillerite | $Ca_2(Al,Fe)_2O_5$ | 1.463 | 00-030-0226 |
| Calcite | $CaCO_3$ | 1.961 | 01-078-3262 |
| Ettringite | $Ca_6Al_2(SO_4)_3(OH)_{12}(H_2O)_{26}$ | 3.461 | 01-075-7554 |
| Gypsum | $Ca(SO_4).(H_2O)_2$ | 1.442 | 01-076-8725 |
| Hatrurite- Alite | $Ca_3SiO_5$ | 0.755 | 01-085-1378 |
| Larnite- Belite | $Ca_2SiO_4$ | 1.405 | 01-080-8935 |
| Portlandite | $Ca(OH)_2$ | 2.810 | 00-004-0733 |
| Tobermorite | $Ca_5(Si_6O_{16})(OH)_2$ | 1.888 | 01-089-6458 |

**Table D-24: QAR of GUbSF 0.43 XRD test at 24 hours of hydration**

| **Phase name** | **Formula** | **Figure of Merit** | **DB Card Number** (PDF-2) |
|---|---|---|---|
| Brownmillerite | $Ca_2(Al,Fe)_2O_5$ | 1.423 | 00-030-0226 |
| Calcite | $CaCO_3$ | 1.304 | 01-078-3262 |
| Ettringite | $Ca_6Al_2(SO_4)_3(OH)_{12}(H_2O)_{26}$ | 1.642 | 01-075-7554 |
| Gypsum | $Ca(SO_4).(H_2O)_2$ | 1.821 | 01-076-8725 |
| Hatrurite- Alite | $Ca_3SiO_5$ | 2.239 | 01-085-1378 |
| Larnite- Belite | $Ca_2SiO_4$ | 1.124 | 01-080-8935 |
| Portlandite | $Ca(OH)_2$ | 0.808 | 00-004-0733 |
| Tobermorite | $Ca_5(Si_6O_{16})(OH)_2$ | 1.459 | 01-089-6458 |

**Table D-25: QAR of GUL 0.37 XRD test at 2 hours of hydration**

| **Phase name** | **Formula** | **Figure of Merit** | **DB Card Number** (PDF-2) |
|---|---|---|---|
| Brownmillerite | $Ca_2(Al,Fe)_2O_5$ | 1.267 | 00-030-0226 |
| Calcite | $CaCO_3$ | 1.361 | 01-078-3262 |
| Ettringite | $Ca_6Al_2(SO_4)_3(OH)_{12}(H_2O)_{26}$ | 1.601 | 01-075-7554 |
| Gypsum | $Ca(SO_4).(H_2O)_2$ | 1.509 | 01-076-8725 |
| Hatrurite- Alite | $Ca_3SiO_5$ | 0.851 | 01-085-1378 |
| Larnite- Belite | $Ca_2SiO_4$ | 1.441 | 01-080-8935 |
| Portlandite | $Ca(OH)_2$ | 2.911 | 00-004-0733 |
| Tobermorite | $Ca_5(Si_6O_{16})(OH)_2$ | 1.666 | 01-089-6458 |

**Table D-26: QAR of GUL 0.37 XRD test at initial setting**

| **Phase name** | **Formula** | **Figure of Merit** | **DB Card Number** (PDF-2) |
|---|---|---|---|
| Brownmillerite | $Ca_2(Al,Fe)_2O_5$ | 1.414 | 00-030-0226 |
| Calcite | $CaCO_3$ | 1.078 | 01-078-3262 |
| Ettringite | $Ca_6Al_2(SO_4)_3(OH)_{12}(H_2O)_{26}$ | 1.651 | 01-075-7554 |
| Gypsum | $Ca(SO_4).(H_2O)_2$ | 1.909 | 01-076-8725 |
| Hatrurite- Alite | $Ca_3SiO_5$ | 0.849 | 01-085-1378 |
| Larnite- Belite | $Ca_2SiO_4$ | 1.312 | 01-080-8935 |
| Portlandite | $Ca(OH)_2$ | 1.505 | 00-004-0733 |
| Tobermorite | $Ca_5(Si_6O_{16})(OH)_2$ | 1.571 | 01-089-6458 |

**Table D-27: QAR of GUL 0.37 XRD test at final setting**

| **Phase name** | **Formula** | **Figure of Merit** | **DB Card Number** (PDF-2) |
|---|---|---|---|
| Brownmillerite | $Ca_2(Al,Fe)_2O_5$ | 1.275 | 00-030-0226 |
| Calcite | $CaCO_3$ | 1.314 | 01-078-3262 |
| Ettringite | $Ca_6Al_2(SO_4)_3(OH)_{12}(H_2O)_{26}$ | 1.765 | 01-075-7554 |
| Gypsum | $Ca(SO_4).(H_2O)_2$ | 1.763 | 01-076-8725 |
| Hatrurite- Alite | $Ca_3SiO_5$ | 1.028 | 01-085-1378 |
| Larnite- Belite | $Ca_2SiO_4$ | 1.427 | 01-080-8935 |
| Portlandite | $Ca(OH)_2$ | 2.836 | 00-004-0733 |
| Tobermorite | $Ca_5(Si_6O_{16})(OH)_2$ | 1.929 | 01-089-6458 |

**Table D-28: QAR of GUL 0.37 XRD test at 24 hours of hydration**

| **Phase name** | **Formula** | **Figure of Merit** | **DB Card Number** (PDF-2) |
|---|---|---|---|
| Brownmillerite | $Ca_2(Al,Fe)_2O_5$ | 1.626 | 00-030-0226 |
| Calcite | $CaCO_3$ | 1.398 | 01-078-3262 |
| Ettringite | $Ca_6Al_2(SO_4)_3(OH)_{12}(H_2O)_{26}$ | 2.951 | 01-075-7554 |
| Gypsum | $Ca(SO_4).(H_2O)_2$ | 3.215 | 01-076-8725 |
| Hatrurite- Alite | $Ca_3SiO_5$ | 1.143 | 01-085-1378 |
| Larnite- Belite | $Ca_2SiO_4$ | 2.734 | 01-080-8935 |
| Portlandite | $Ca(OH)_2$ | 1.117 | 00-004-0733 |
| Tobermorite | $Ca_5(Si_6O_{16})(OH)_2$ | 2.836 | 01-089-6458 |

**Table D-29: QAR of GUL 0.40 XRD test at 2 hours of hydration**

| **Phase name** | **Formula** | **Figure of Merit** | **DB Card Number** (PDF-2) |
|---|---|---|---|
| Brownmillerite | $Ca_2(Al,Fe)_2O_5$ | 1.669 | 00-030-0226 |
| Calcite | $CaCO_3$ | 1.263 | 01-078-3262 |
| Ettringite | $Ca_6Al_2(SO_4)_3(OH)_{12}(H_2O)_{26}$ | 1.928 | 01-075-7554 |
| Gypsum | $Ca(SO_4).(H_2O)_2$ | 3.083 | 01-076-8725 |
| Hatrurite- Alite | $Ca_3SiO_5$ | 1.900 | 01-085-1378 |
| Larnite- Belite | $Ca_2SiO_4$ | 1.565 | 01-080-8935 |
| Portlandite | $Ca(OH)_2$ | 1.386 | 00-004-0733 |
| Tobermorite | $Ca_5(Si_6O_{16})(OH)_2$ | 3.188 | 01-089-6458 |

**Table D-30: QAR of GUL 0.40 XRD test at initial setting**

| **Phase name** | **Formula** | **Figure of Merit** | **DB Card Number** (PDF-2) |
|---|---|---|---|
| Brownmillerite | $Ca_2(Al,Fe)_2O_5$ | 1.405 | 00-030-0226 |
| Calcite | $CaCO_3$ | 1.350 | 01-078-3262 |
| Ettringite | $Ca_6Al_2(SO_4)_3(OH)_{12}(H_2O)_{26}$ | 1.632 | 01-075-7554 |
| Gypsum | $Ca(SO_4).(H_2O)_2$ | 2.058 | 01-076-8725 |
| Hatrurite- Alite | $Ca_3SiO_5$ | 0.862 | 01-085-1378 |
| Larnite- Belite | $Ca_2SiO_4$ | 1.728 | 01-080-8935 |
| Portlandite | $Ca(OH)_2$ | 1.655 | 00-004-0733 |
| Tobermorite | $Ca_5(Si_6O_{16})(OH)_2$ | 1.915 | 01-089-6458 |

**Table D-31: QAR of GUL 0.40 XRD test at final setting**

| **Phase name** | **Formula** | **Figure of Merit** | **DB Card Number** (PDF-2) |
|---|---|---|---|
| Brownmillerite | $Ca_2(Al,Fe)_2O_5$ | 1.605 | 00-030-0226 |
| Calcite | $CaCO_3$ | 1.386 | 01-078-3262 |
| Ettringite | $Ca_6Al_2(SO_4)_3(OH)_{12}(H_2O)_{26}$ | 1.772 | 01-075-7554 |
| Gypsum | $Ca(SO_4).(H_2O)_2$ | 1.796 | 01-076-8725 |
| Hatrurite- Alite | $Ca_3SiO_5$ | 0.860 | 01-085-1378 |
| Larnite- Belite | $Ca_2SiO_4$ | 1.753 | 01-080-8935 |
| Portlandite | $Ca(OH)_2$ | 3.104 | 00-004-0733 |
| Tobermorite | $Ca_5(Si_6O_{16})(OH)_2$ | 1.690 | 01-089-6458 |

**Table D-32: QAR of GUL 0.40 XRD test at 24 hours of hydration**

| **Phase name** | **Formula** | **Figure of Merit** | **DB Card Number** (PDF-2) |
|---|---|---|---|
| Brownmillerite | $Ca_2(Al,Fe)_2O_5$ | 1.645 | 00-030-0226 |
| Calcite | $CaCO_3$ | 1.516 | 01-078-3262 |
| Ettringite | $Ca_6Al_2(SO_4)_3(OH)_{12}(H_2O)_{26}$ | 1.897 | 01-075-7554 |
| Gypsum | $Ca(SO_4).(H_2O)_2$ | 1.827 | 01-076-8725 |
| Hatrurite- Alite | $Ca_3SiO_5$ | 3.787 | 01-085-1378 |
| Larnite- Belite | $Ca_2SiO_4$ | 1.442 | 01-080-8935 |
| Portlandite | $Ca(OH)_2$ | 0.984 | 00-004-0733 |
| Tobermorite | $Ca_5(Si_6O_{16})(OH)_2$ | 3.068 | 01-089-6458 |

**Table D-33: QAR of GUL 0.43 XRD test at 2 hours of hydration**

| **Phase name** | **Formula** | **Figure of Merit** | **DB Card Number** (PDF-2) |
|---|---|---|---|
| Brownmillerite | $Ca_2(Al,Fe)_2O_5$ | 1.295 | 00-030-0226 |
| Calcite | $CaCO_3$ | 1.166 | 01-078-3262 |
| Ettringite | $Ca_6Al_2(SO_4)_3(OH)_{12}(H_2O)_{26}$ | 2.014 | 01-075-7554 |
| Gypsum | $Ca(SO_4).(H_2O)_2$ | 1.657 | 01-076-8725 |
| Hatrurite- Alite | $Ca_3SiO_5$ | 1.011 | 01-085-1378 |
| Larnite- Belite | $Ca_2SiO_4$ | 1.735 | 01-080-8935 |
| Portlandite | $Ca(OH)_2$ | 3.047 | 00-004-0733 |
| Tobermorite | $Ca_5(Si_6O_{16})(OH)_2$ | 1.995 | 01-089-6458 |

**Table D-34: QAR of GUL 0.43 XRD test at initial setting**

| **Phase name** | **Formula** | **Figure of Merit** | **DB Card Number** (PDF-2) |
|---|---|---|---|
| Brownmillerite | $Ca_2(Al,Fe)_2O_5$ | 1.044 | 00-030-0226 |
| Calcite | $CaCO_3$ | 3.182 | 01-078-3262 |
| Ettringite | $Ca_6Al_2(SO_4)_3(OH)_{12}(H_2O)_{26}$ | 2.110 | 01-075-7554 |
| Gypsum | $Ca(SO_4).(H_2O)_2$ | 1.661 | 01-076-8725 |
| Hatrurite- Alite | $Ca_3SiO_5$ | 1.469 | 01-085-1378 |
| Larnite- Belite | $Ca_2SiO_4$ | 1.604 | 01-080-8935 |
| Portlandite | $Ca(OH)_2$ | 1.904 | 00-004-0733 |
| Tobermorite | $Ca_5(Si_6O_{16})(OH)_2$ | 1.044 | 01-089-6458 |

**Table D-35: QAR of GUL 0.43 XRD test at final setting**

| **Phase name** | **Formula** | **Figure of Merit** | **DB Card Number** (PDF-2) |
|---|---|---|---|
| Brownmillerite | $Ca_2(Al,Fe)_2O_5$ | 1.494 | 00-030-0226 |
| Calcite | $CaCO_3$ | 1.622 | 01-078-3262 |
| Ettringite | $Ca_6Al_2(SO_4)_3(OH)_{12}(H_2O)_{26}$ | 3.232 | 01-075-7554 |
| Gypsum | $Ca(SO_4).(H_2O)_2$ | 2.931 | 01-076-8725 |
| Hatrurite- Alite | $Ca_3SiO_5$ | 1.073 | 01-085-1378 |
| Larnite- Belite | $Ca_2SiO_4$ | 3.108 | 01-080-8935 |
| Portlandite | $Ca(OH)_2$ | 2.909 | 00-004-0733 |
| Tobermorite | $Ca_5(Si_6O_{16})(OH)_2$ | 1.761 | 01-089-6458 |

**Table D-36: QAR of GUL 0.43 XRD test at 24 hours of hydration**

| **Phase name** | **Formula** | **Figure of Merit** | **DB Card Number** (PDF-2) |
|---|---|---|---|
| Brownmillerite | $Ca_2(Al,Fe)_2O_5$ | 1.405 | 00-030-0226 |
| Calcite | $CaCO_3$ | 1.166 | 01-078-3262 |
| Ettringite | $Ca_6Al_2(SO_4)_3(OH)_{12}(H_2O)_{26}$ | 3.232 | 01-075-7554 |
| Gypsum | $Ca(SO_4).(H_2O)_2$ | 2.931 | 01-076-8725 |
| Hatrurite- Alite | $Ca_3SiO_5$ | 1.073 | 01-085-1378 |
| Larnite- Belite | $Ca_2SiO_4$ | 1.604 | 01-080-8935 |
| Portlandite | $Ca(OH)_2$ | 3.047 | 00-004-0733 |
| Tobermorite | $Ca_5(Si_6O_{16})(OH)_2$ | 1.761 | 01-089-6458 |

**Table D-37: QAR of HE 0.37 XRD test at 2 hours of hydration**

| **Phase name** | **Formula** | **Figure of Merit** | **DB Card Number** (PDF-2) |
|---|---|---|---|
| Brownmillerite | $Ca_2(Al,Fe)_2O_5$ | 1.475 | 00-030-0226 |
| Calcite | $CaCO_3$ | 2.928 | 01-078-3262 |
| Ettringite | $Ca_6Al_2(SO_4)_3(OH)_{12}(H_2O)_{26}$ | 1.855 | 01-075-7554 |
| Gypsum | $Ca(SO_4).(H_2O)_2$ | 1.556 | 01-076-8725 |
| Hatrurite- Alite | $Ca_3SiO_5$ | 0.828 | 01-085-1378 |
| Larnite- Belite | $Ca_2SiO_4$ | 1.669 | 01-080-8935 |
| Portlandite | $Ca(OH)_2$ | 1.744 | 00-004-0733 |
| Tobermorite | $Ca_5(Si_6O_{16})(OH)_2$ | 2.087 | 01-089-6458 |

**Table D-38: QAR of HE 0.37 XRD test at initial setting**

| **Phase name** | **Formula** | **Figure of Merit** | **DB Card Number** (PDF-2) |
|---|---|---|---|
| Brownmillerite | $Ca_2(Al,Fe)_2O_5$ | 1.543 | 00-030-0226 |
| Calcite | $CaCO_3$ | 1.726 | 01-078-3262 |
| Ettringite | $Ca_6Al_2(SO_4)_3(OH)_{12}(H_2O)_{26}$ | 3.190 | 01-075-7554 |
| Gypsum | $Ca(SO_4).(H_2O)_2$ | 1.810 | 01-076-8725 |
| Hatrurite- Alite | $Ca_3SiO_5$ | 0.813 | 01-085-1378 |
| Larnite- Belite | $Ca_2SiO_4$ | 1.428 | 01-080-8935 |
| Portlandite | $Ca(OH)_2$ | 2.994 | 00-004-0733 |
| Tobermorite | $Ca_5(Si_6O_{16})(OH)_2$ | 1.750 | 01-089-6458 |

**Table D-39: QAR of HE 0.37 XRD test at final setting**

| **Phase name** | **Formula** | **Figure of Merit** | **DB Card Number** (PDF-2) |
|---|---|---|---|
| Brownmillerite | $Ca_2(Al,Fe)_2O_5$ | 2.772 | 00-030-0226 |
| Calcite | $CaCO_3$ | 1.601 | 01-078-3262 |
| Ettringite | $Ca_6Al_2(SO_4)_3(OH)_{12}(H_2O)_{26}$ | 3.076 | 01-075-7554 |
| Gypsum | $Ca(SO_4).(H_2O)_2$ | 1.749 | 01-076-8725 |
| Hatrurite- Alite | $Ca_3SiO_5$ | 1.560 | 01-085-1378 |
| Larnite- Belite | $Ca_2SiO_4$ | 1.640 | 01-080-8935 |
| Portlandite | $Ca(OH)_2$ | 2.822 | 00-004-0733 |
| Tobermorite | $Ca_5(Si_6O_{16})(OH)_2$ | 3.202 | 01-089-6458 |

**Table D-40: QAR of HE 0.37 XRD test at 24 hours of hydration**

| **Phase name** | **Formula** | **Figure of Merit** | **DB Card Number** (PDF-2) |
|---|---|---|---|
| Brownmillerite | $Ca_2(Al,Fe)_2O_5$ | 1.749 | 00-030-0226 |
| Calcite | $CaCO_3$ | 1.320 | 01-078-3262 |
| Ettringite | $Ca_6Al_2(SO_4)_3(OH)_{12}(H_2O)_{26}$ | 2.068 | 01-075-7554 |
| Gypsum | $Ca(SO_4).(H_2O)_2$ | 3.125 | 01-076-8725 |
| Hatrurite- Alite | $Ca_3SiO_5$ | 2.070 | 01-085-1378 |
| Larnite- Belite | $Ca_2SiO_4$ | 1.650 | 01-080-8935 |
| Portlandite | $Ca(OH)_2$ | 1.412 | 00-004-0733 |
| Tobermorite | $Ca_5(Si_6O_{16})(OH)_2$ | 1.862 | 01-089-6458 |

**Table D-41: QAR of HE 0.40 XRD test at 2 hours of hydration**

| **Phase name** | **Formula** | **Figure of Merit** | **DB Card Number** (PDF-2) |
|---|---|---|---|
| Brownmillerite | $Ca_2(Al,Fe)_2O_5$ | 1.641 | 00-030-0226 |
| Calcite | $CaCO_3$ | 2.796 | 01-078-3262 |
| Ettringite | $Ca_6Al_2(SO_4)_3(OH)_{12}(H_2O)_{26}$ | 2.126 | 01-075-7554 |
| Gypsum | $Ca(SO_4).(H_2O)_2$ | 1.626 | 01-076-8725 |
| Hatrurite- Alite | $Ca_3SiO_5$ | 1.080 | 01-085-1378 |
| Larnite- Belite | $Ca_2SiO_4$ | 1.494 | 01-080-8935 |
| Portlandite | $Ca(OH)_2$ | 2.892 | 00-004-0733 |
| Tobermorite | $Ca_5(Si_6O_{16})(OH)_2$ | 1.940 | 01-089-6458 |

**Table D-42: QAR of HE 0.40 XRD test at initial setting**

| **Phase name** | **Formula** | **Figure of Merit** | **DB Card Number** (PDF-2) |
|---|---|---|---|
| Brownmillerite | $Ca_2(Al,Fe)_2O_5$ | 1.497 | 00-030-0226 |
| Calcite | $CaCO_3$ | 2.917 | 01-078-3262 |
| Ettringite | $Ca_6Al_2(SO_4)_3(OH)_{12}(H_2O)_{26}$ | 3.011 | 01-075-7554 |
| Gypsum | $Ca(SO_4).(H_2O)_2$ | 1.669 | 01-076-8725 |
| Hatrurite- Alite | $Ca_3SiO_5$ | 0.866 | 01-085-1378 |
| Larnite- Belite | $Ca_2SiO_4$ | 1.447 | 01-080-8935 |
| Portlandite | $Ca(OH)_2$ | 2.870 | 00-004-0733 |
| Tobermorite | $Ca_5(Si_6O_{16})(OH)_2$ | 1.868 | 01-089-6458 |

**Table D-43: QAR of HE 0.40 XRD test at final setting**

| **Phase name** | **Formula** | **Figure of Merit** | **DB Card Number** (PDF-2) |
|---|---|---|---|
| Brownmillerite | $Ca_2(Al,Fe)_2O_5$ | 1.710 | 00-030-0226 |
| Calcite | $CaCO_3$ | 1.463 | 01-078-3262 |
| Ettringite | $Ca_6Al_2(SO_4)_3(OH)_{12}(H_2O)_{26}$ | 3.480 | 01-075-7554 |
| Gypsum | $Ca(SO_4).(H_2O)_2$ | 3.202 | 01-076-8725 |
| Hatrurite- Alite | $Ca_3SiO_5$ | 3.109 | 01-085-1378 |
| Larnite- Belite | $Ca_2SiO_4$ | 3.388 | 01-080-8935 |
| Portlandite | $Ca(OH)_2$ | 3.167 | 00-004-0733 |
| Tobermorite | $Ca_5(Si_6O_{16})(OH)_2$ | 2.180 | 01-089-6458 |

**Table D-44: QAR of HE 0.40 XRD test at 24 hours of hydration**

| **Phase name** | **Formula** | **Figure of Merit** | **DB Card Number** (PDF-2) |
|---|---|---|---|
| Brownmillerite | $Ca_2(Al,Fe)_2O_5$ | 1.231 | 00-030-0226 |
| Calcite | $CaCO_3$ | 1.568 | 01-078-3262 |
| Ettringite | $Ca_6Al_2(SO_4)_3(OH)_{12}(H_2O)_{26}$ | 1.663 | 01-075-7554 |
| Gypsum | $Ca(SO_4).(H_2O)_2$ | 1.917 | 01-076-8725 |
| Hatrurite- Alite | $Ca_3SiO_5$ | 1.296 | 01-085-1378 |
| Larnite- Belite | $Ca_2SiO_4$ | 1.333 | 01-080-8935 |
| Portlandite | $Ca(OH)_2$ | 0.759 | 00-004-0733 |
| Tobermorite | $Ca_5(Si_6O_{16})(OH)_2$ | 1.666 | 01-089-6458 |

**Table D-45: QAR of HE 0.43 XRD test at 2 hours of hydration**

| **Phase name** | **Formula** | **Figure of Merit** | **DB Card Number** (PDF-2) |
|---|---|---|---|
| Brownmillerite | $Ca_2(Al,Fe)_2O_5$ | 1.295 | 00-030-0226 |
| Calcite | $CaCO_3$ | 1.615 | 01-078-3262 |
| Ettringite | $Ca_6Al_2(SO_4)_3(OH)_{12}(H_2O)_{26}$ | 3.065 | 01-075-7554 |
| Gypsum | $Ca(SO_4).(H_2O)_2$ | 1.475 | 01-076-8725 |
| Hatrurite- Alite | $Ca_3SiO_5$ | 0.743 | 01-085-1378 |
| Larnite- Belite | $Ca_2SiO_4$ | 1.196 | 01-080-8935 |
| Portlandite | $Ca(OH)_2$ | 2.986 | 00-004-0733 |
| Tobermorite | $Ca_5(Si_6O_{16})(OH)_2$ | 1.959 | 01-089-6458 |

**Table D-46: QAR of HE 0.43 XRD test at initial setting**

| **Phase name** | **Formula** | **Figure of Merit** | **DB Card Number** (PDF-2) |
|---|---|---|---|
| Brownmillerite | $Ca_2(Al,Fe)_2O_5$ | 1.702 | 00-030-0226 |
| Calcite | $CaCO_3$ | 1.719 | 01-078-3262 |
| Ettringite | $Ca_6Al_2(SO_4)_3(OH)_{12}(H_2O)_{26}$ | 3.225 | 01-075-7554 |
| Gypsum | $Ca(SO_4).(H_2O)_2$ | 1.520 | 01-076-8725 |
| Hatrurite- Alite | $Ca_3SiO_5$ | 0.868 | 01-085-1378 |
| Larnite- Belite | $Ca_2SiO_4$ | 1.343 | 01-080-8935 |
| Portlandite | $Ca(OH)_2$ | 2.787 | 00-004-0733 |
| Tobermorite | $Ca_5(Si_6O_{16})(OH)_2$ | 1.975 | 01-089-6458 |

**Table D-47: QAR of HE 0.43 XRD test at final setting**

| **Phase name** | **Formula** | **Figure of Merit** | **DB Card Number** (PDF-2) |
|---|---|---|---|
| Brownmillerite | $Ca_2(Al,Fe)_2O_5$ | 1.527 | 00-030-0226 |
| Calcite | $CaCO_3$ | 1.942 | 01-078-3262 |
| Ettringite | $Ca_6Al_2(SO_4)_3(OH)_{12}(H_2O)_{26}$ | 3.232 | 01-075-7554 |
| Gypsum | $Ca(SO_4).(H_2O)_2$ | 1.675 | 01-076-8725 |
| Hatrurite- Alite | $Ca_3SiO_5$ | 0.964 | 01-085-1378 |
| Larnite- Belite | $Ca_2SiO_4$ | 1.463 | 01-080-8935 |
| Portlandite | $Ca(OH)_2$ | 3.011 | 00-004-0733 |
| Tobermorite | $Ca_5(Si_6O_{16})(OH)_2$ | 2.113 | 01-089-6458 |

**Table D-48: QAR of HE 0.43 XRD test at 24 hours of hydration**

| **Phase name** | **Formula** | **Figure of Merit** | **DB Card Number** (PDF-2) |
|---|---|---|---|
| Brownmillerite | $Ca_2(Al,Fe)_2O_5$ | 1.609 | 00-030-0226 |
| Calcite | $CaCO_3$ | 1.629 | 01-078-3262 |
| Ettringite | $Ca_6Al_2(SO_4)_3(OH)_{12}(H_2O)_{26}$ | 1.927 | 01-075-7554 |
| Gypsum | $Ca(SO_4).(H_2O)_2$ | 1.693 | 01-076-8725 |
| Hatrurite- Alite | $Ca_3SiO_5$ | 1.670 | 01-085-1378 |
| Larnite- Belite | $Ca_2SiO_4$ | 1.652 | 01-080-8935 |
| Portlandite | $Ca(OH)_2$ | 0.972 | 00-004-0733 |
| Tobermorite | $Ca_5(Si_6O_{16})(OH)_2$ | 1.692 | 01-089-6458 |

## E. X-ray Diffraction (XRD) Patterns and Crystals Analysis of Unhydrated and Hydrated Cements

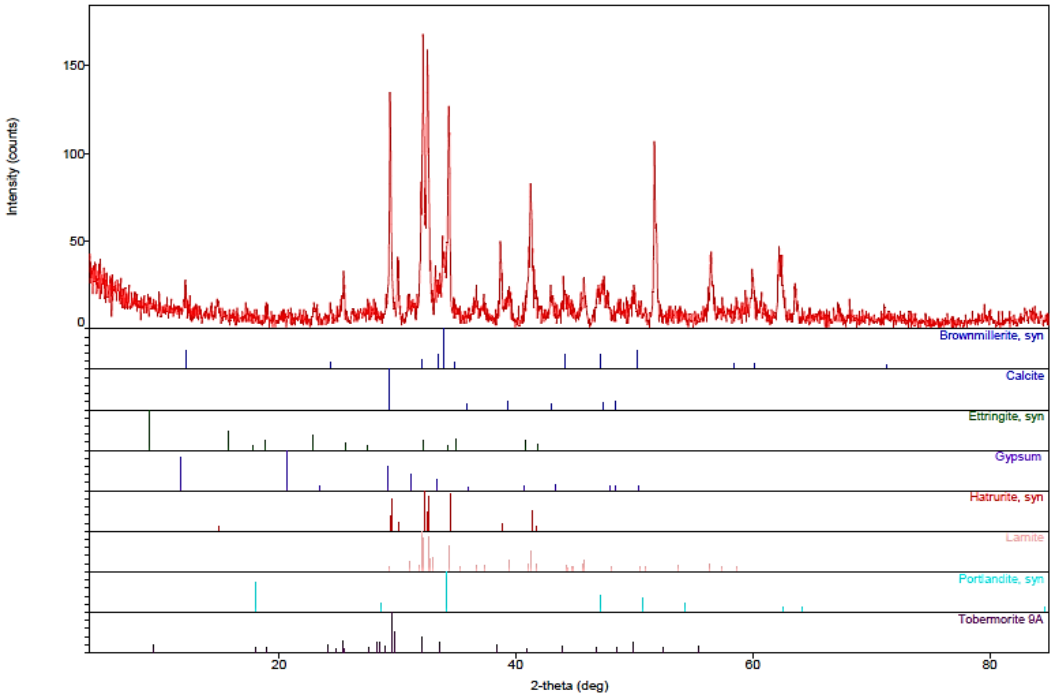


**Figure E-1: XRD pattern and crystals peak of GU cement**

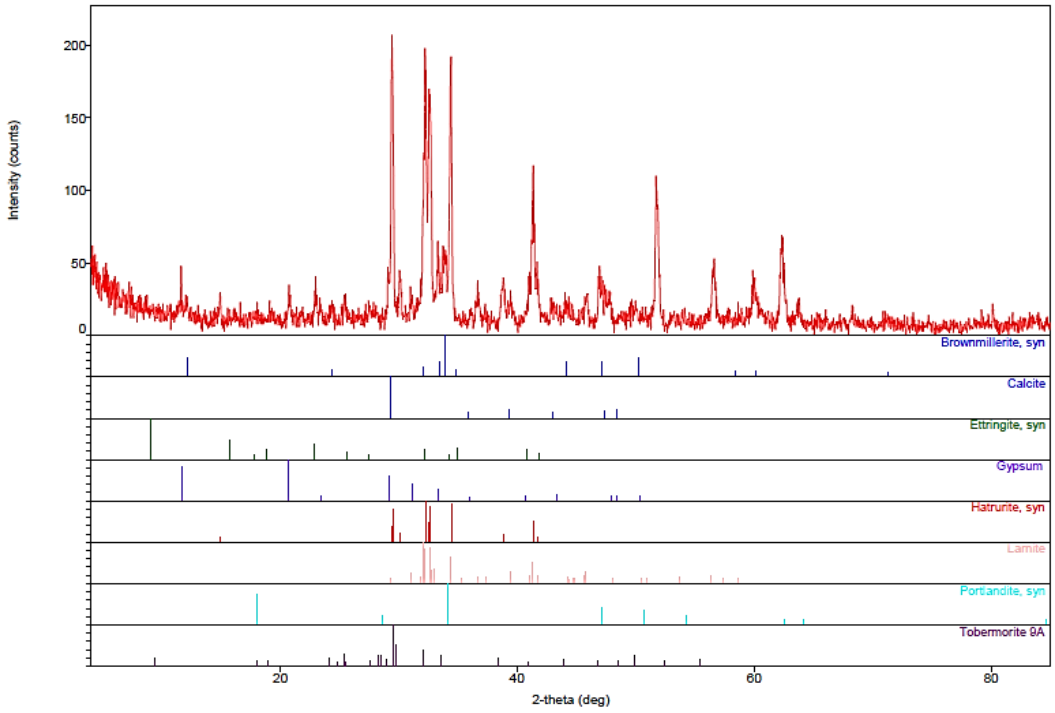


**Figure E-2: XRD pattern and crystals peak of GUbSF cement**

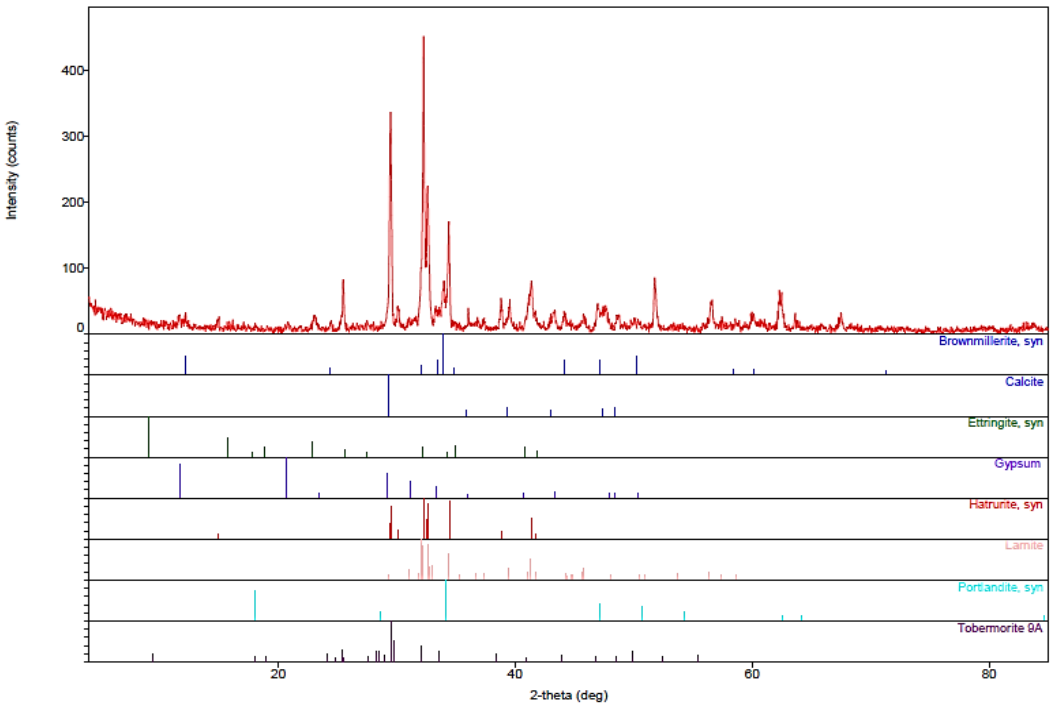


**Figure E-3: XRD pattern and crystals peak of GUL cement**

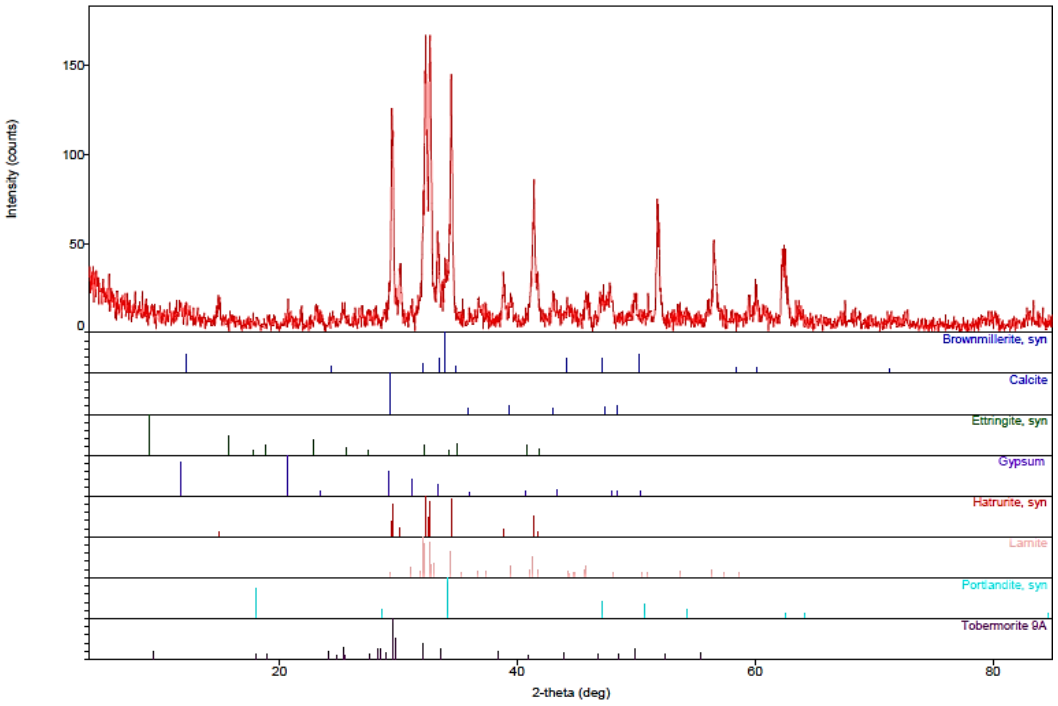


**Figure E-4: XRD pattern and crystals peak of HE cement**

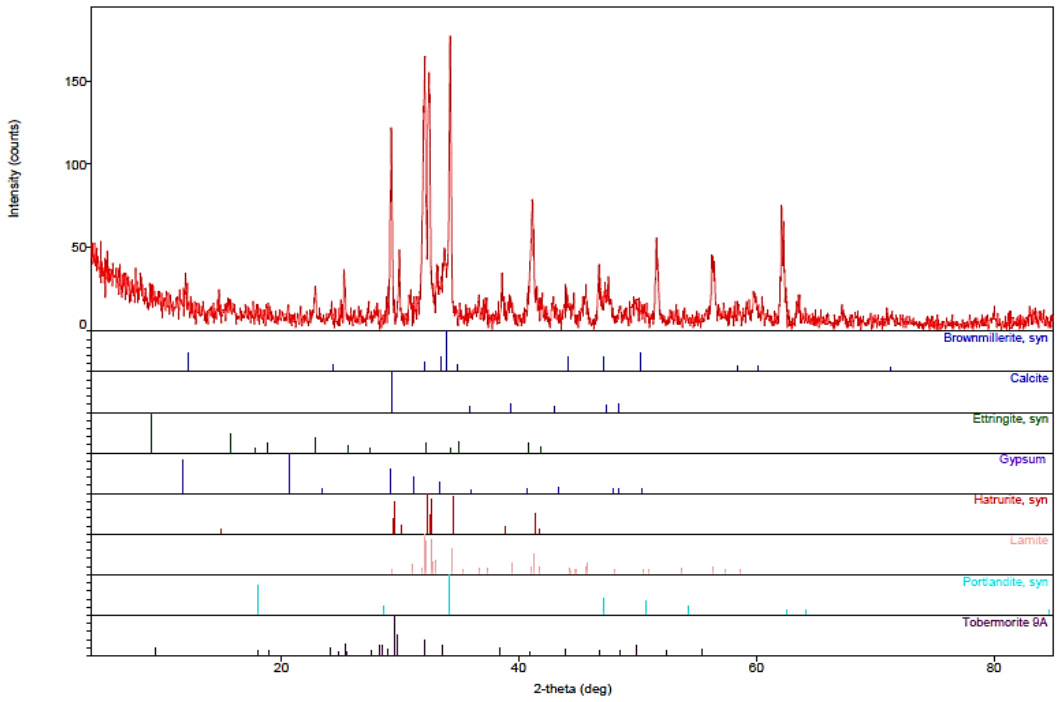


**Figure E-5: XRD pattern and crystals peak of GU 0.37 mixture at 2 hours**

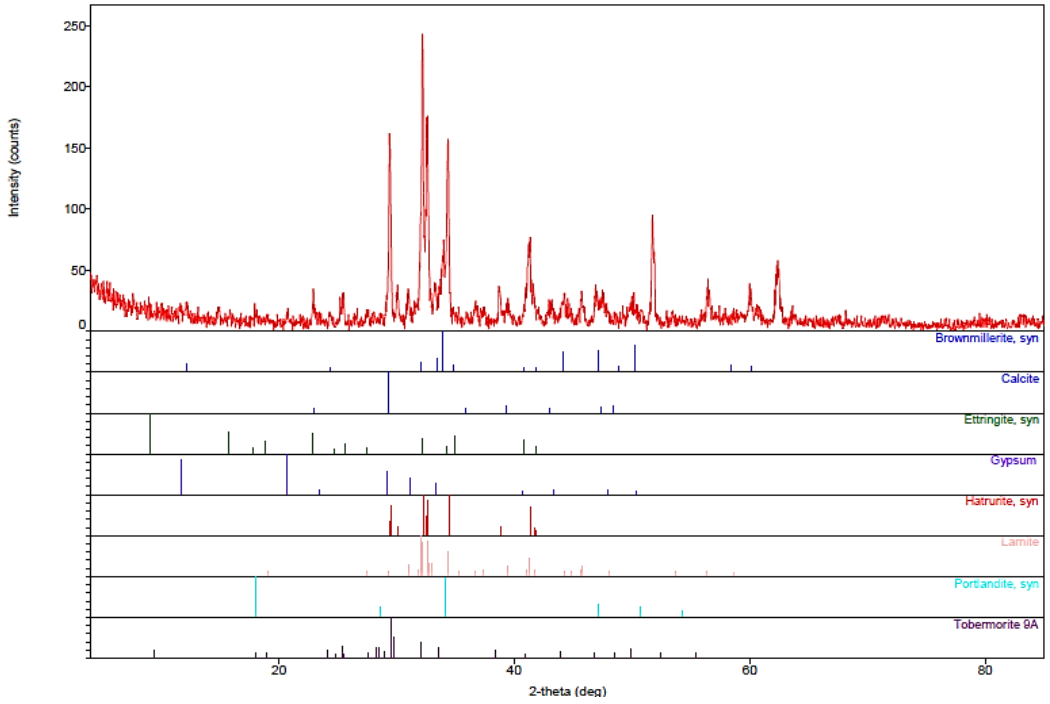


**Figure E-6: XRD pattern and crystals peak of GU 0.37 at initial setting**

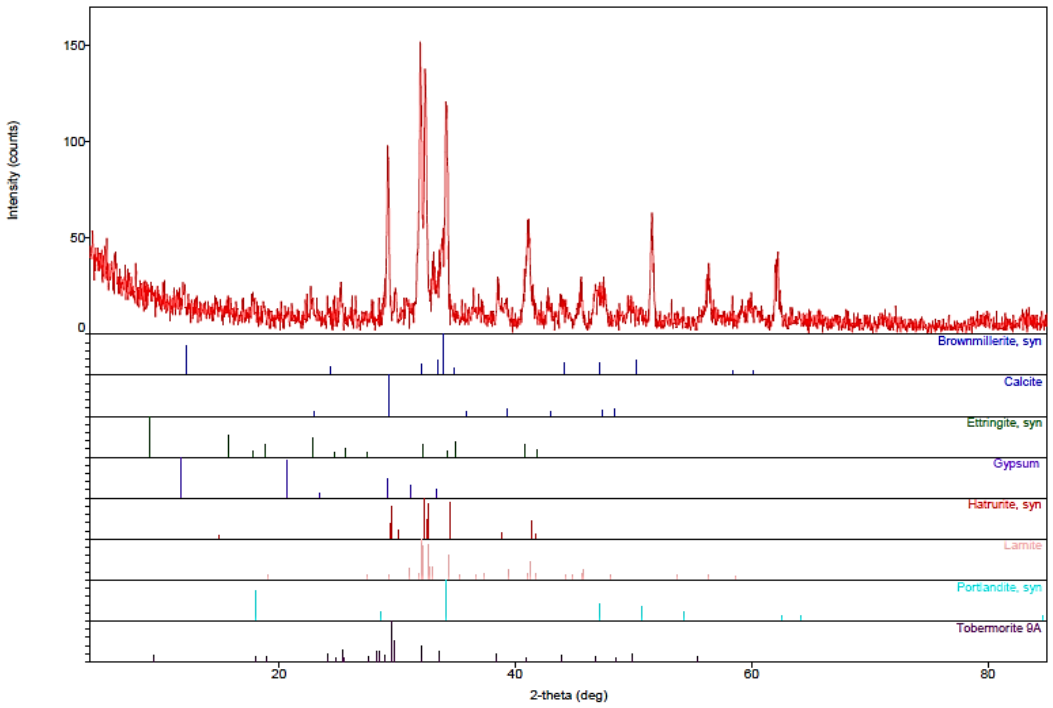


**Figure E-7: XRD pattern and crystals peak of GU 0.37 at final setting**

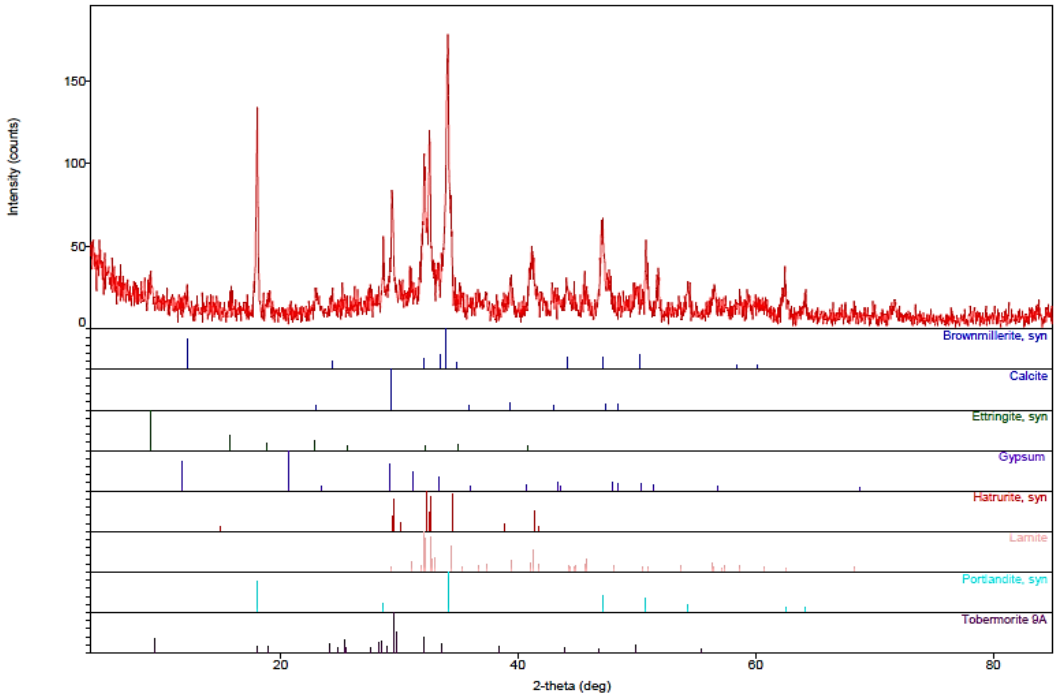


**Figure E-8: XRD pattern and crystals peak of GU 0.37 at 24 hours of hydration**

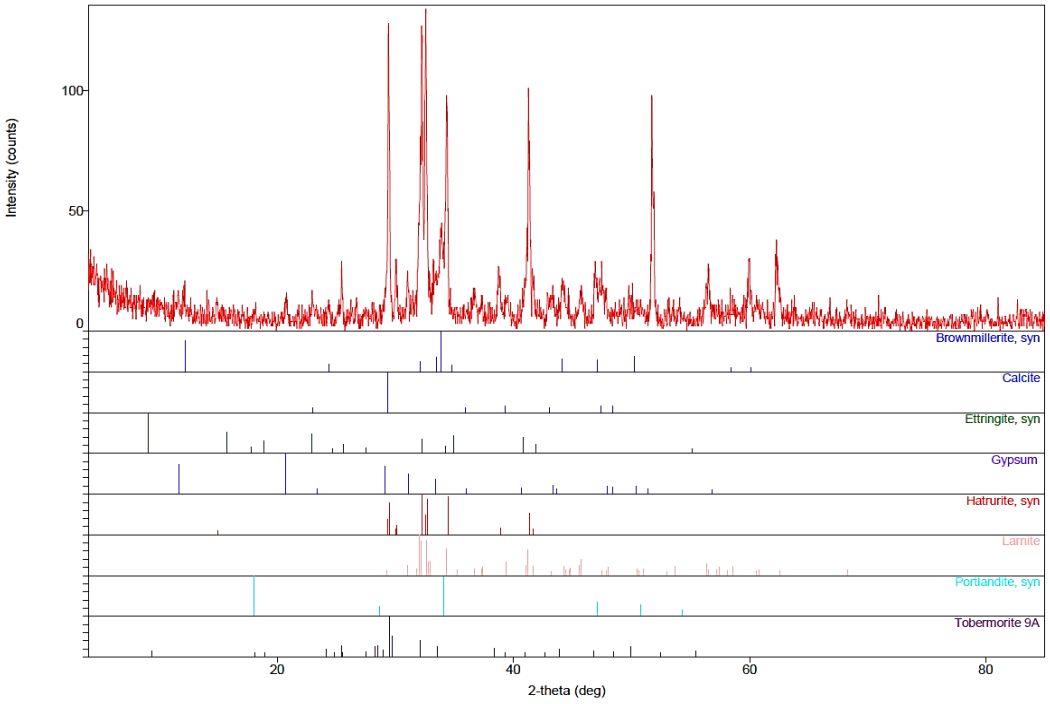


**Figure E-9: XRD pattern and crystals peak of GU 0.40 at 2 hours of hydration**

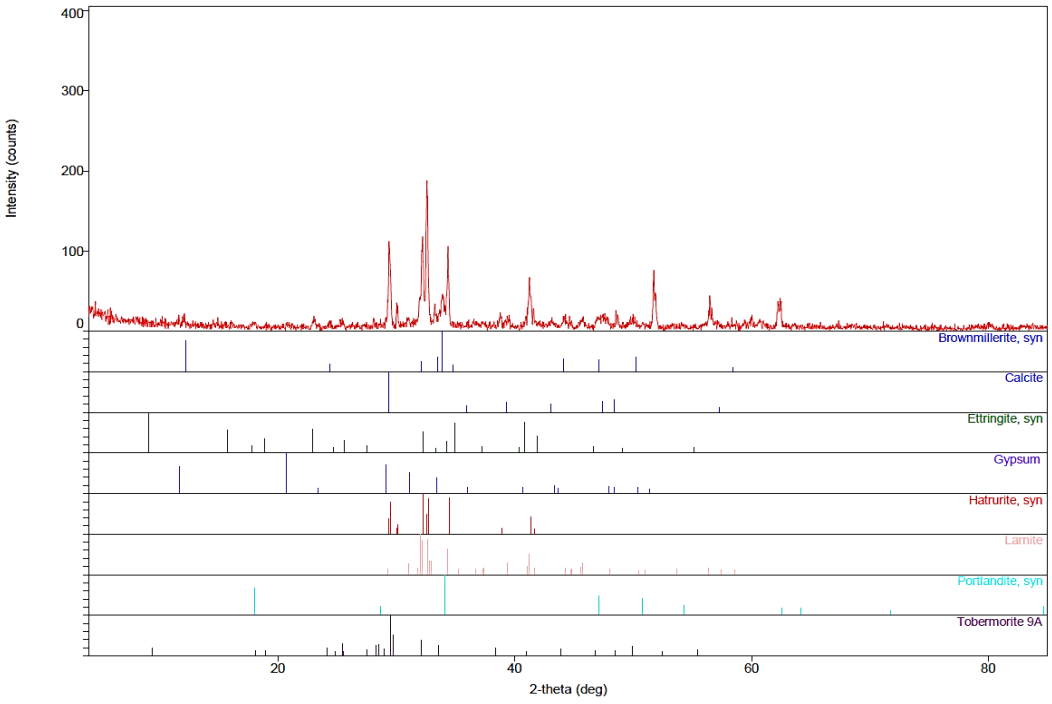


**Figure E-10: XRD pattern and crystals peak of GU 0.40 at initial setting**

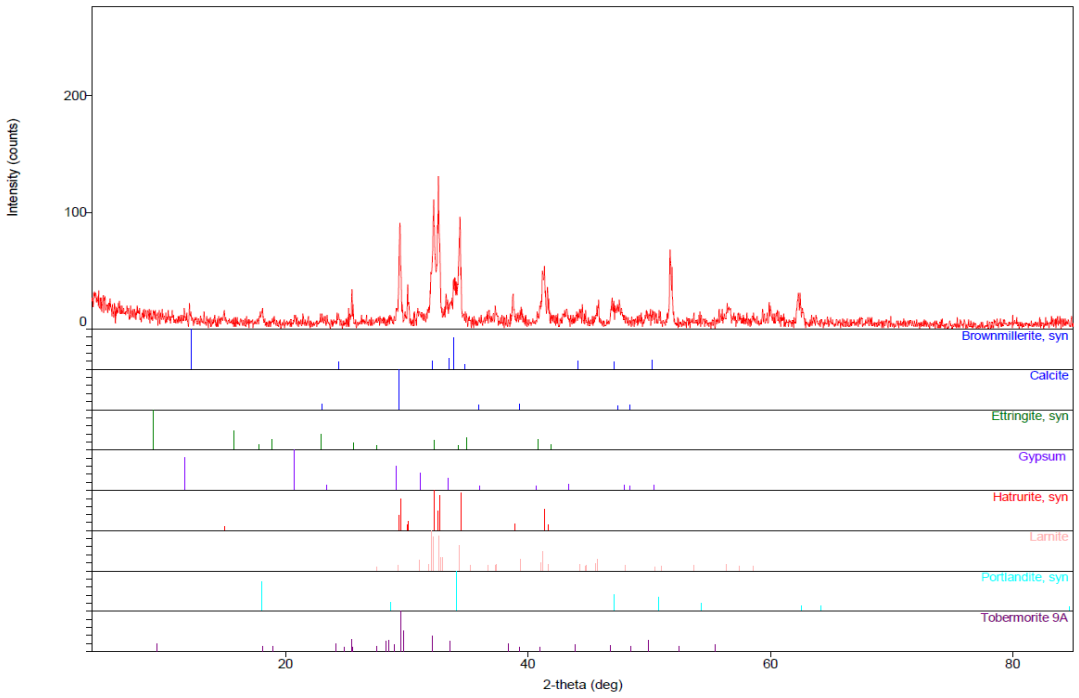


**Figure E-11: XRD pattern and crystals peak of GU 0.40 at final setting**

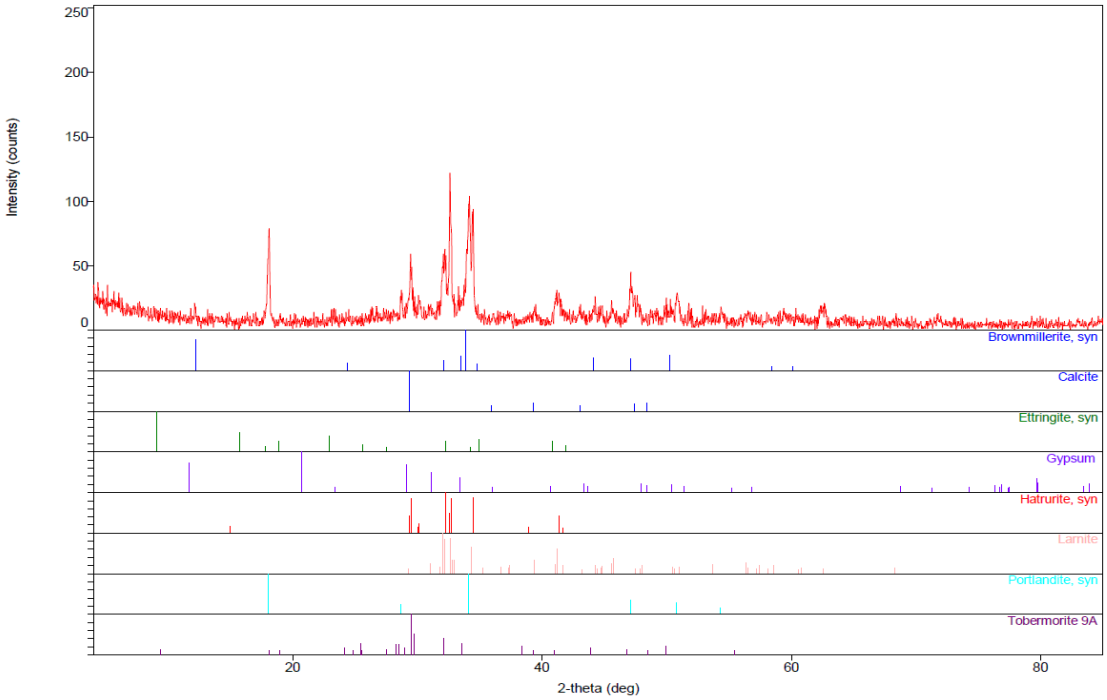


**Figure E-12: XRD pattern and crystals peak of GU 0.40 at 24 hours of hydration**

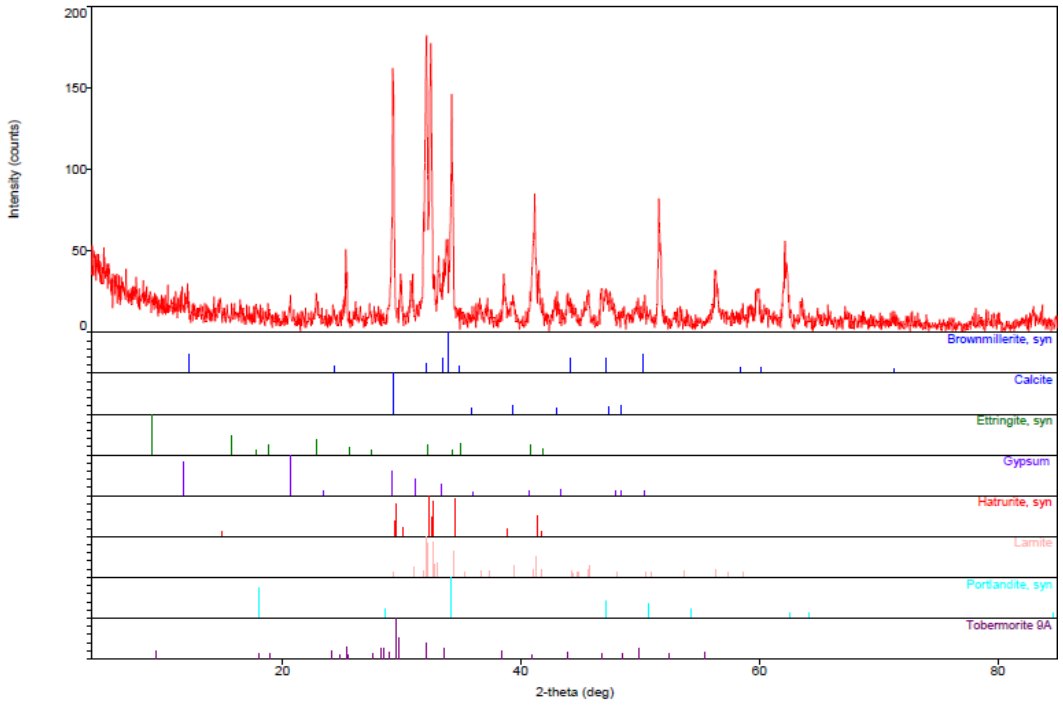


**Figure E-13: XRD pattern and crystals peak of GU 0.43 at 2 hours**

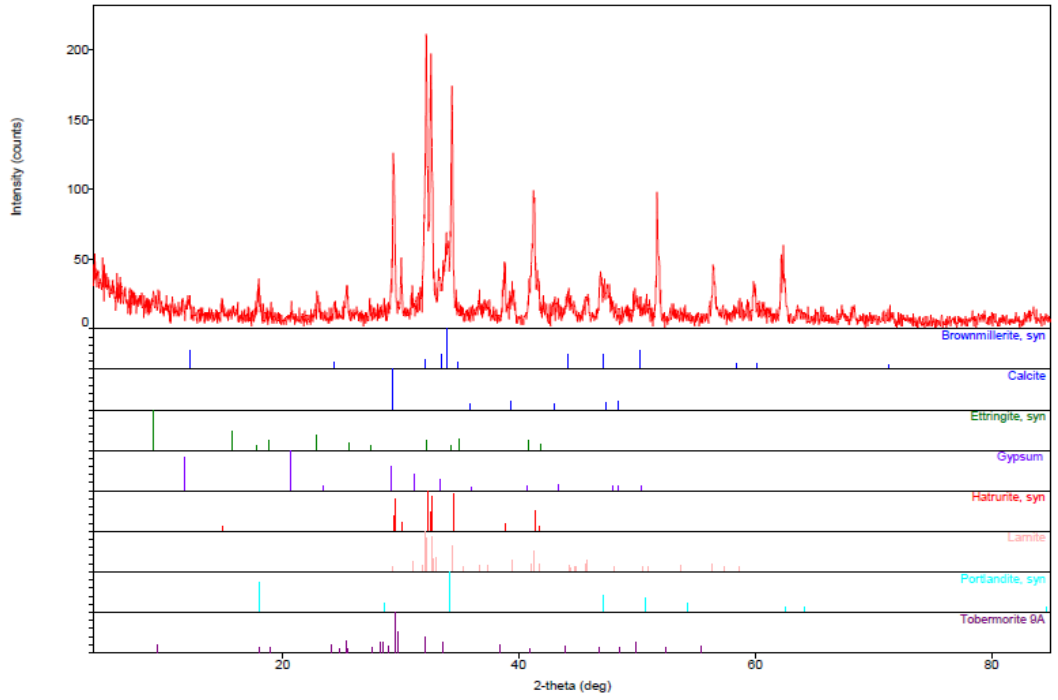


**Figure E-14: XRD pattern and crystals peak of GU 0.43 at initial setting**

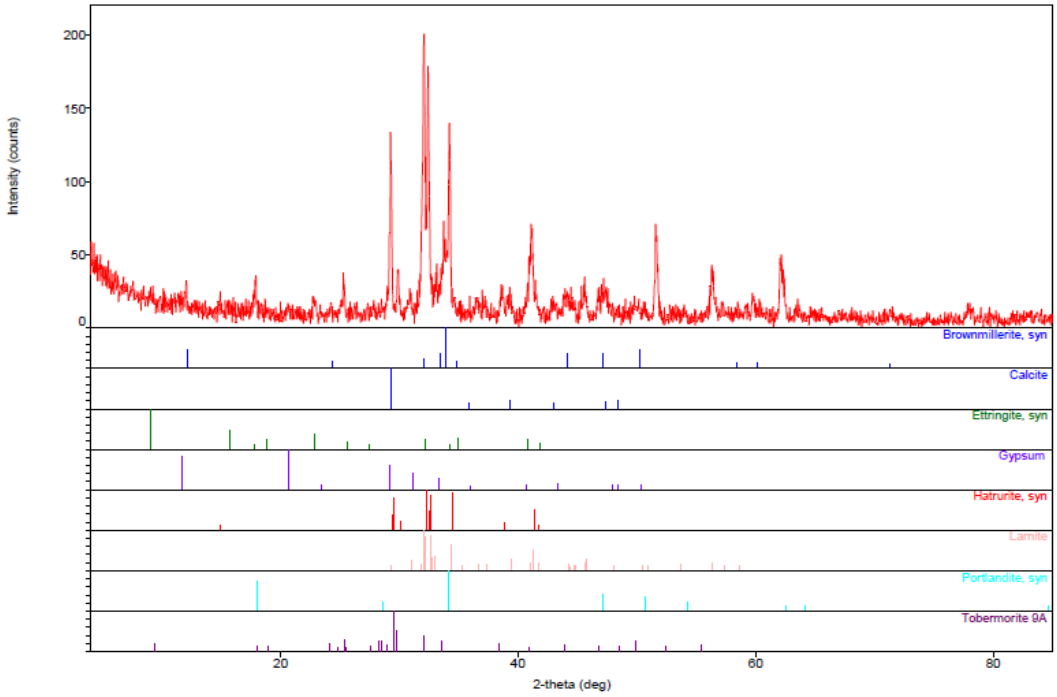


**Figure E-15: XRD pattern and crystals peak of GU 0.43 at final setting**

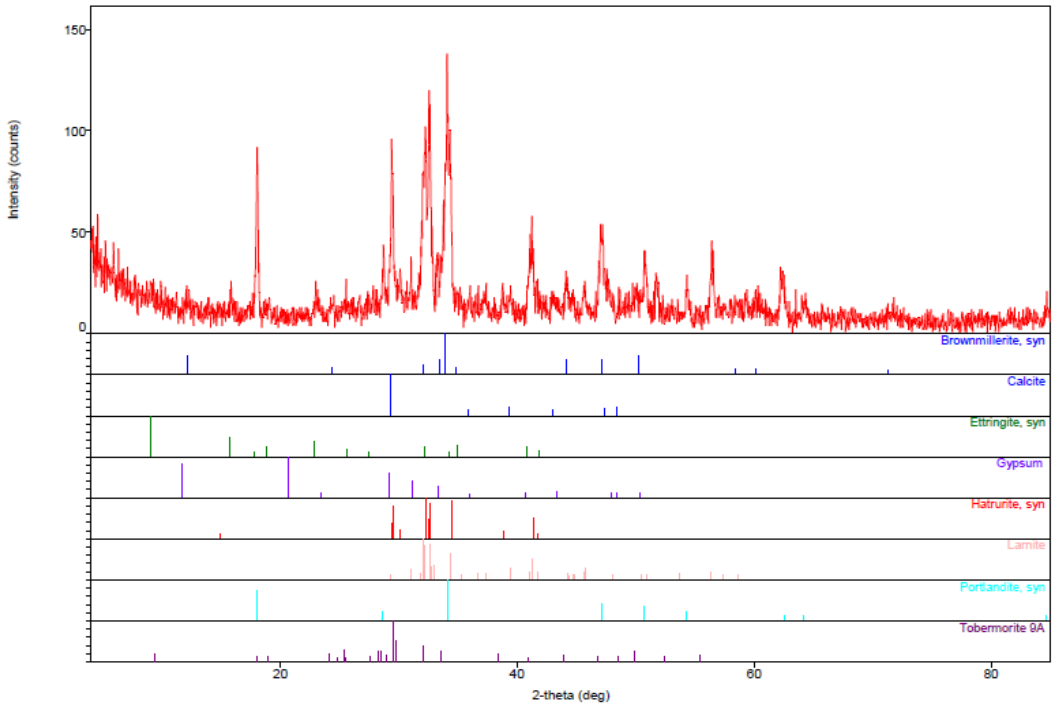


**Figure E-16: XRD pattern and crystals peak of GU 0.43 at 24 hours**

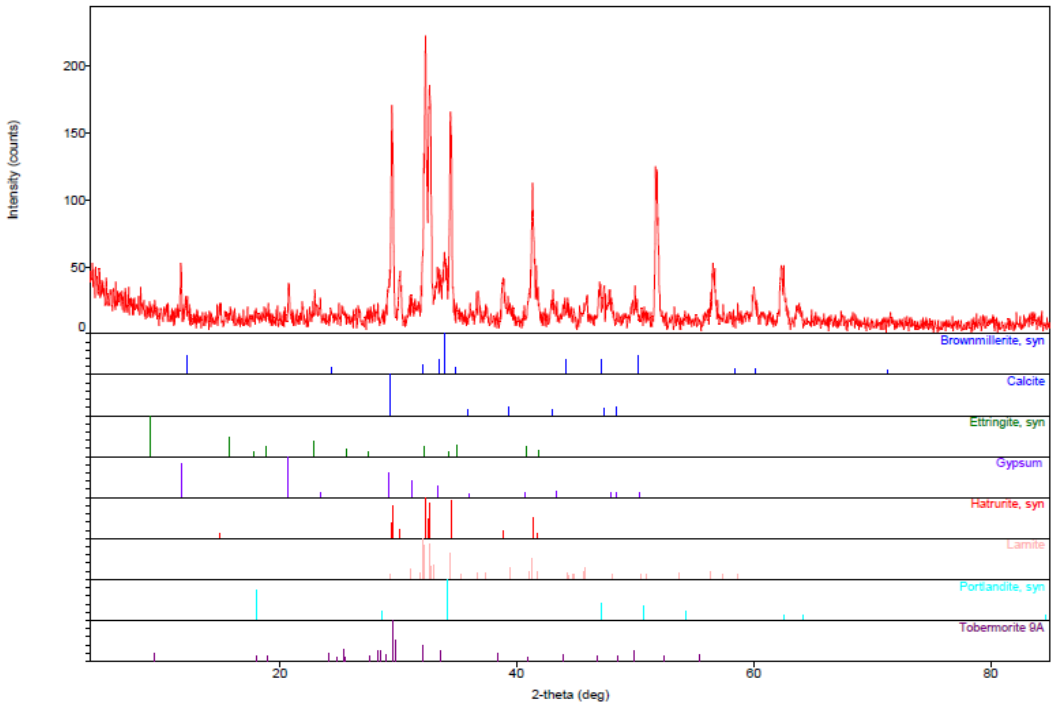


**Figure E-17: XRD pattern and crystals peak of GUbSF 0.37 at 2 hours**

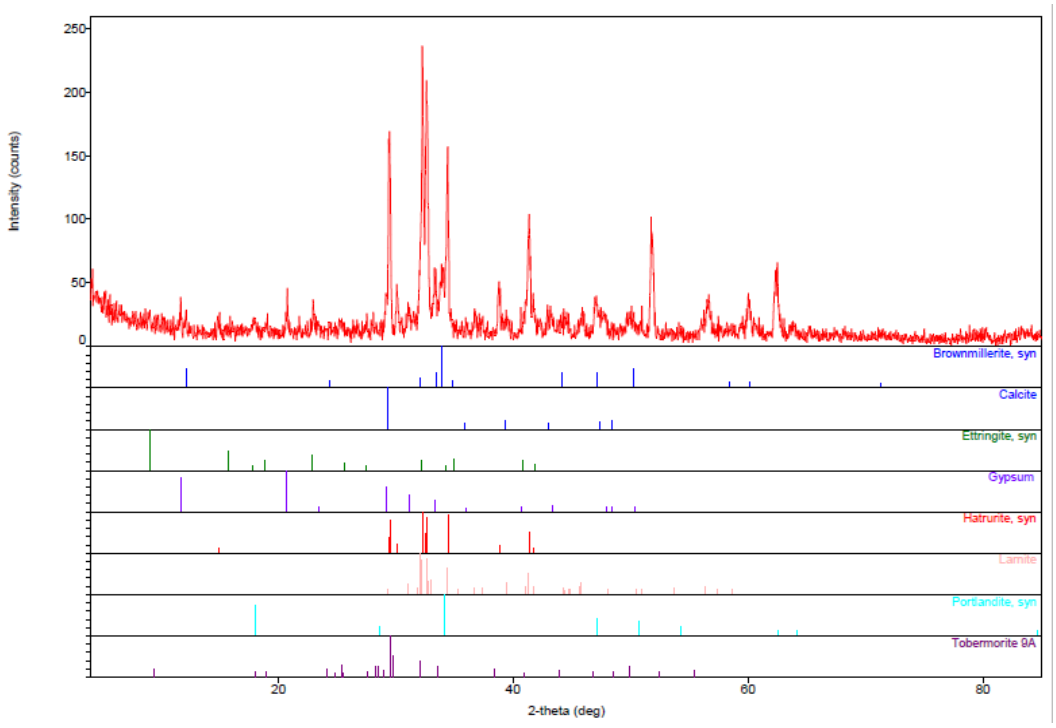


**Figure E-18: XRD pattern and crystals peak of GUbSF 0.37 at initial setting**

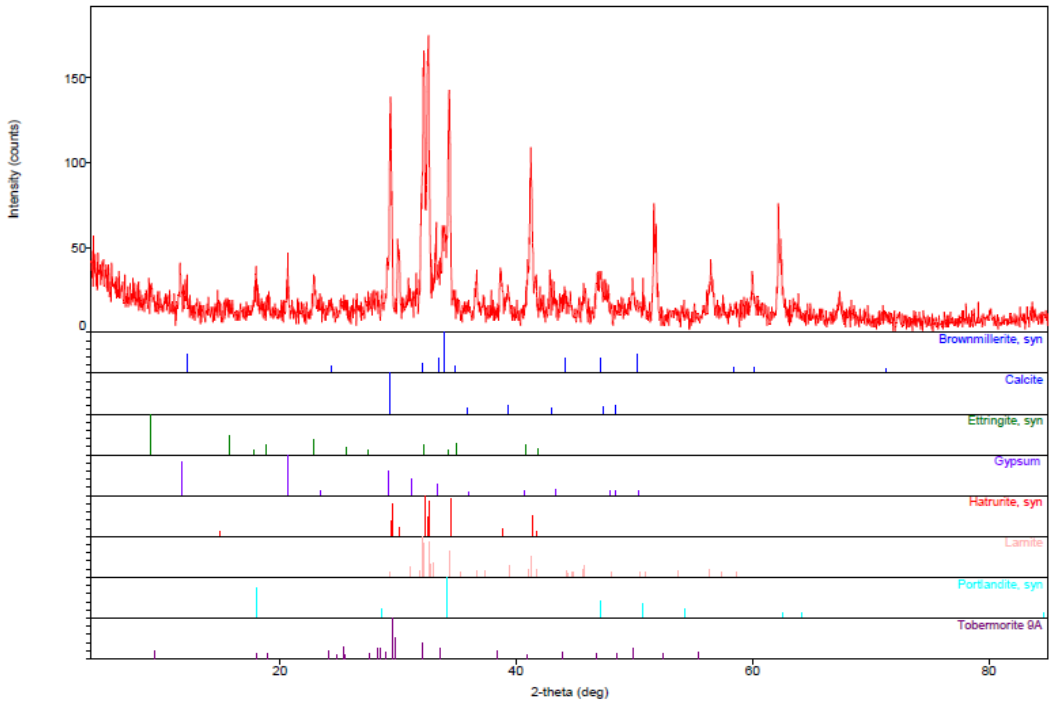


**Figure E-19: XRD pattern and crystals peak of GUbSF 0.37 at final setting**

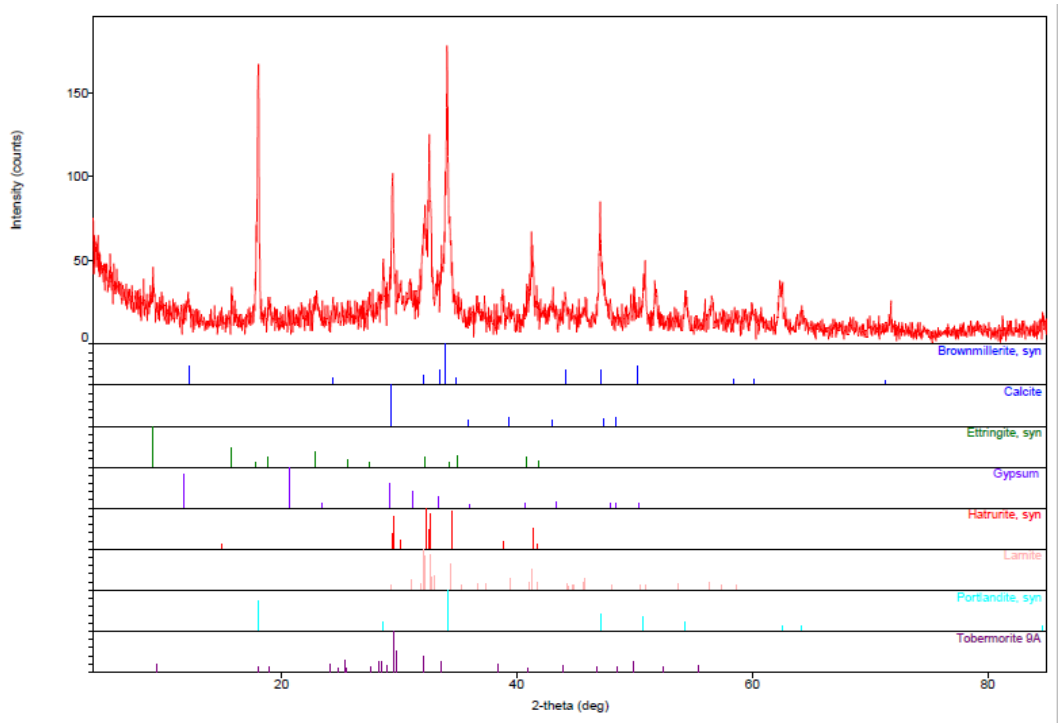


**Figure E-20: XRD pattern and crystals peak of GUbSF 0.37 at 24 hours**

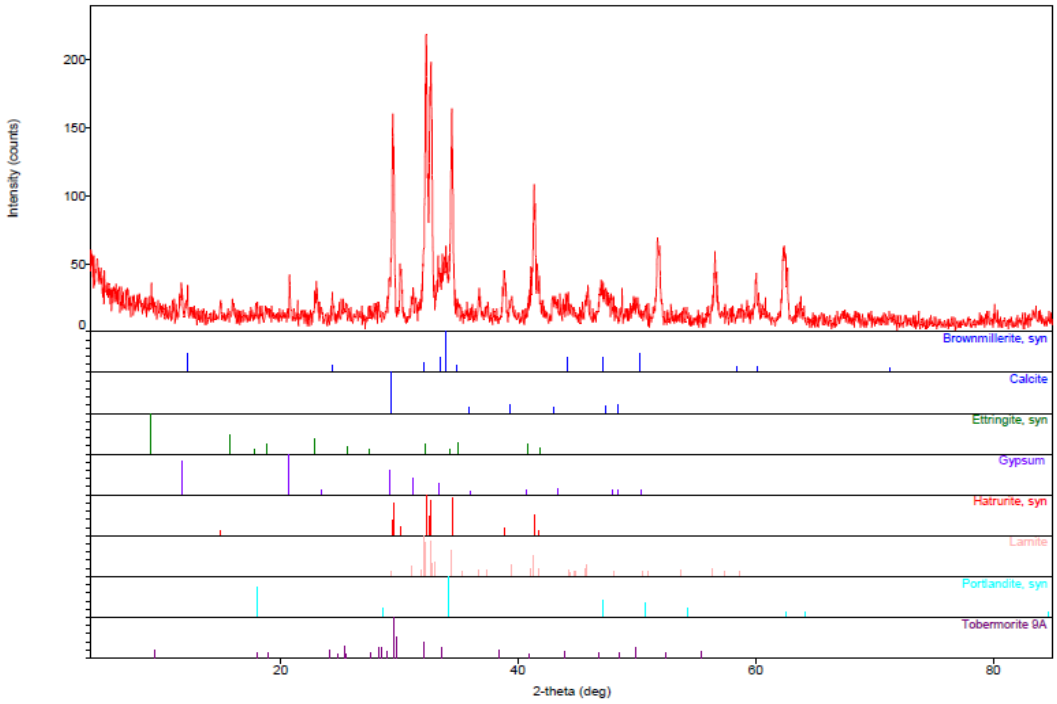


**Figure E-21: XRD pattern and crystals peak of GUbSF 0.40 at 2 hours**

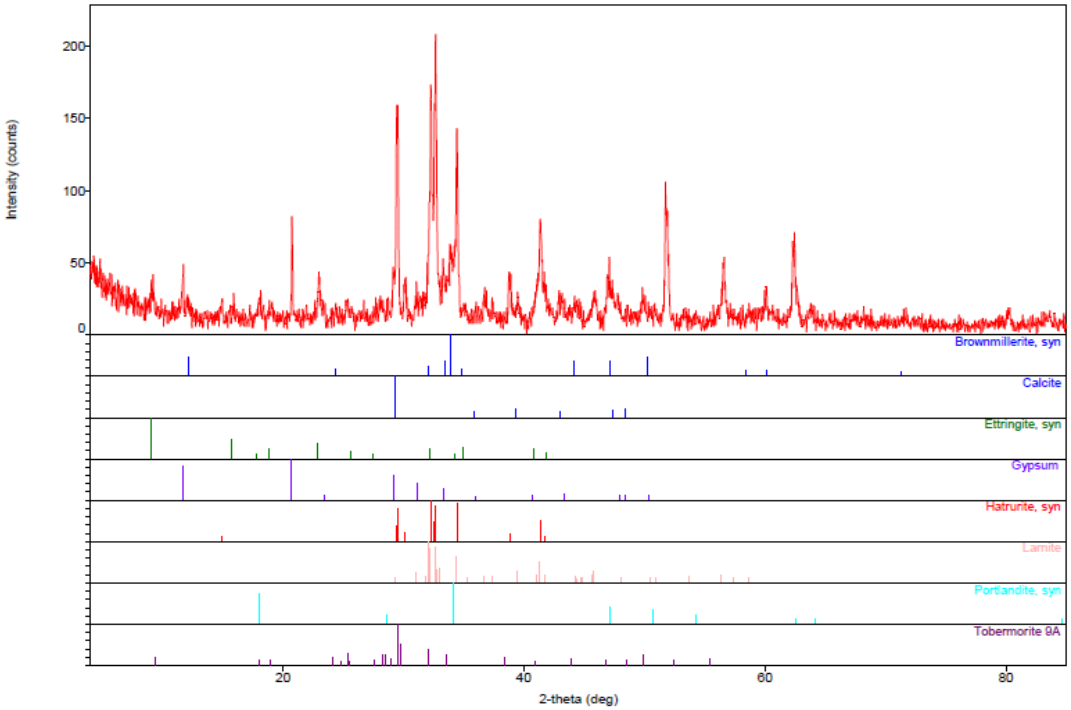


**Figure E-22: XRD pattern and crystals peak of GUbSF 0.40 at initial setting**

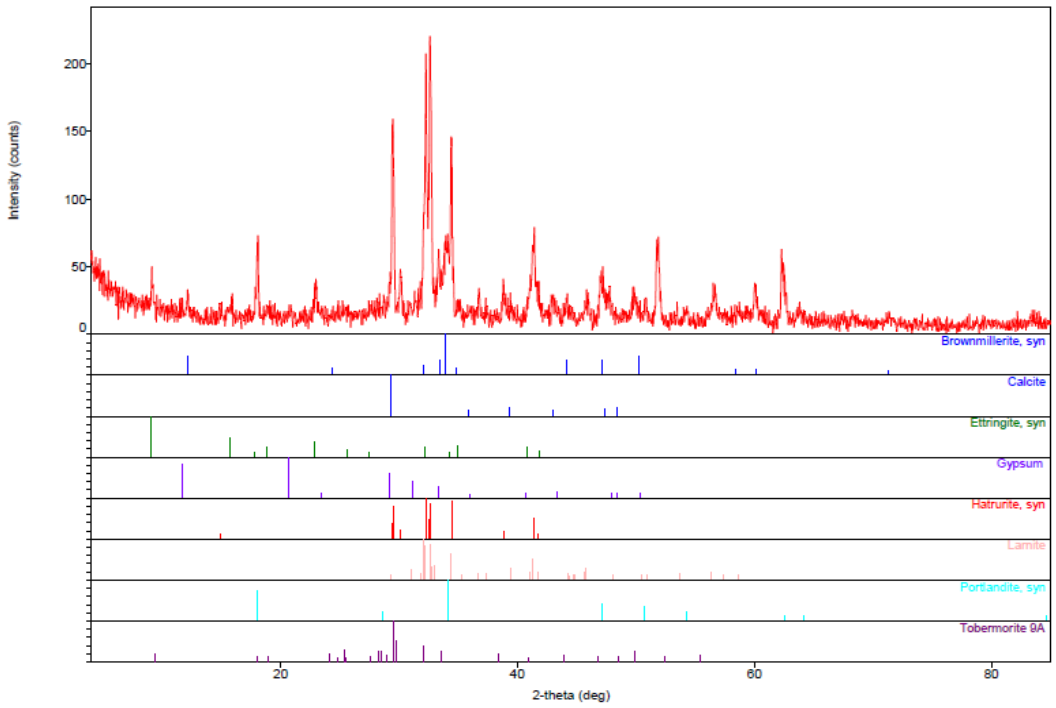


**Figure E-23: XRD pattern and crystals peak of GUbSF 0.40 at final setting**

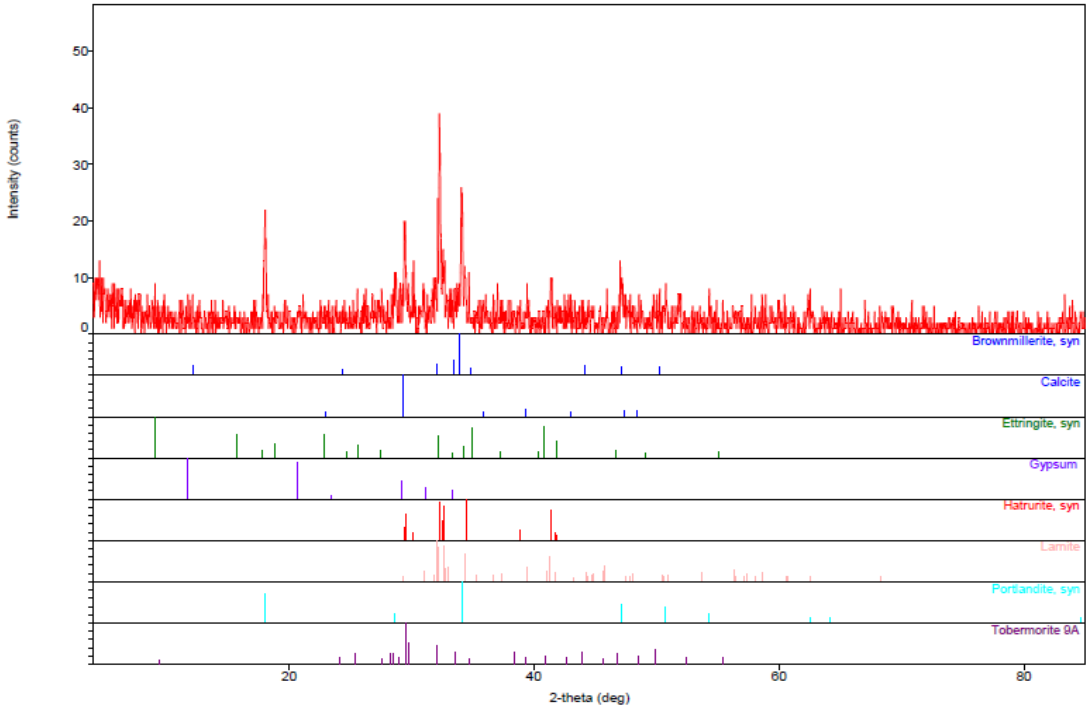


**Figure E-24: XRD pattern and crystals peak of GUbSF 0.40 at 24 hours of hydration**

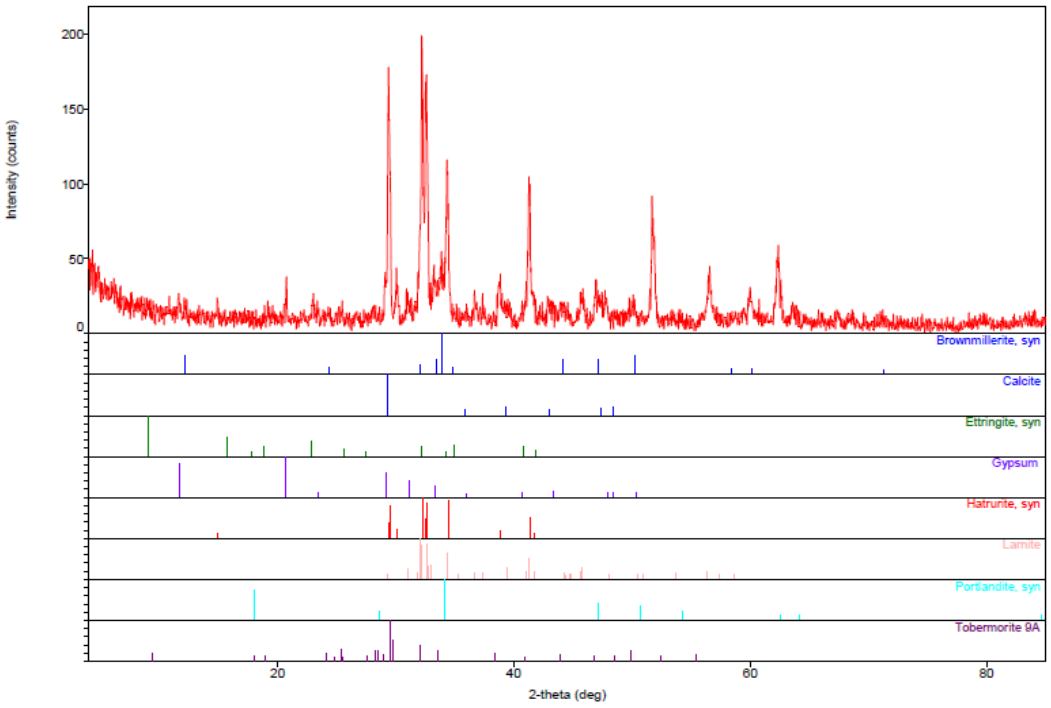


**Figure E-25: XRD pattern and crystals peak of GUbSF 0.43 at 2 hours**

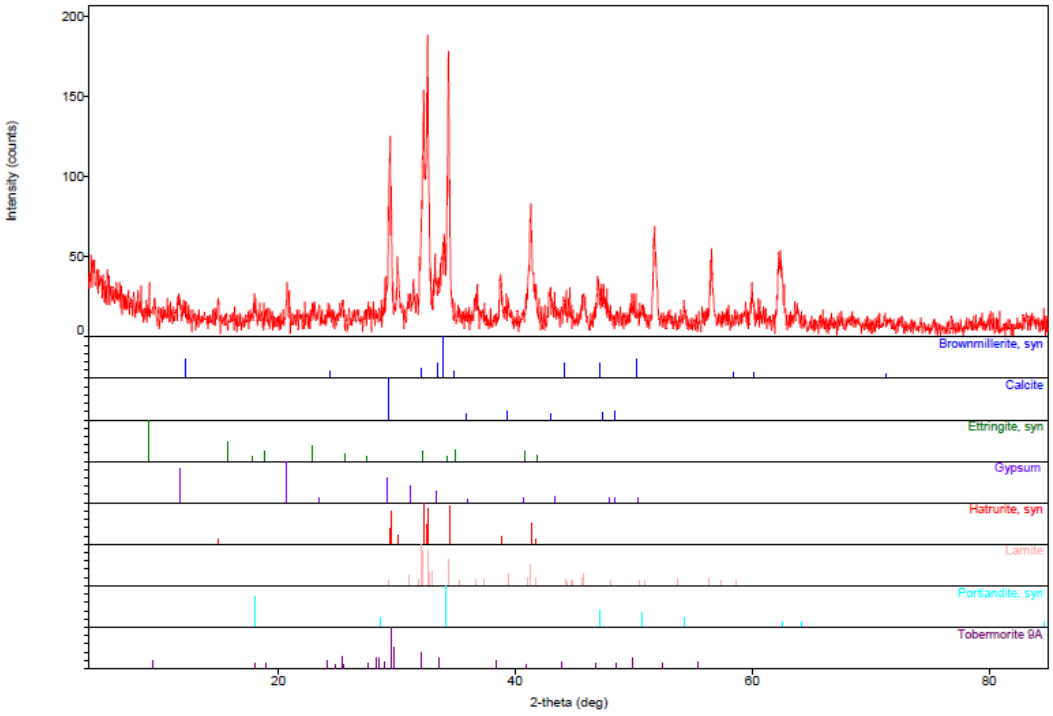


**Figure E-26: XRD pattern and crystals peak of GUbSF 0.43 at initial setting**

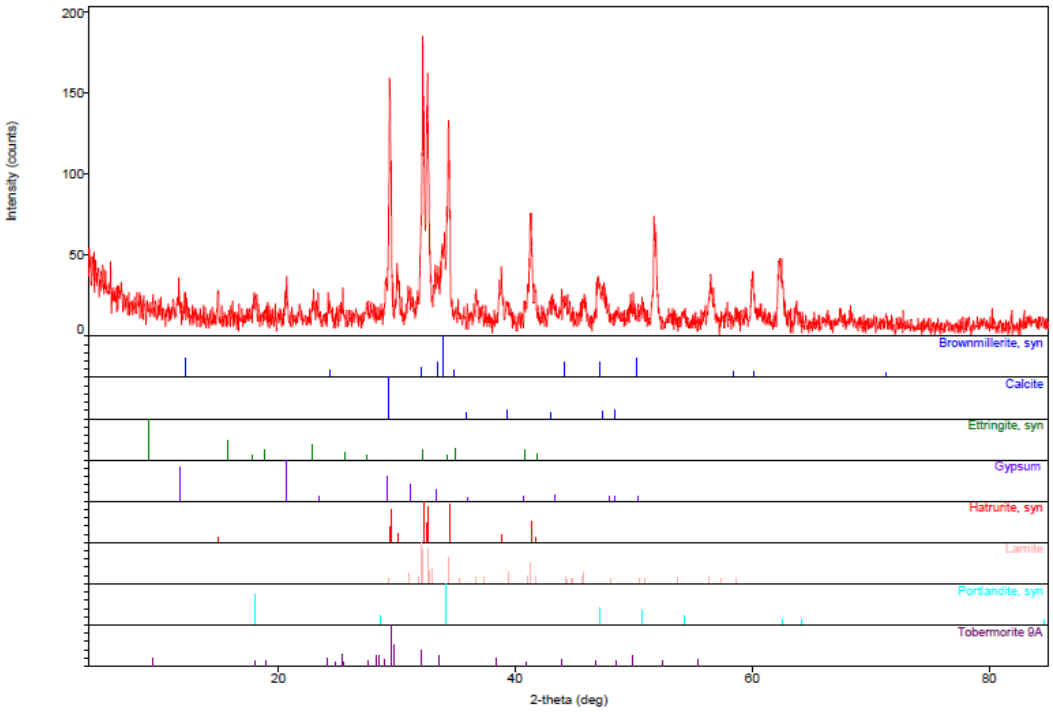


**Figure E-27: XRD pattern and crystals peak of GUbSF 0.43 at final setting**

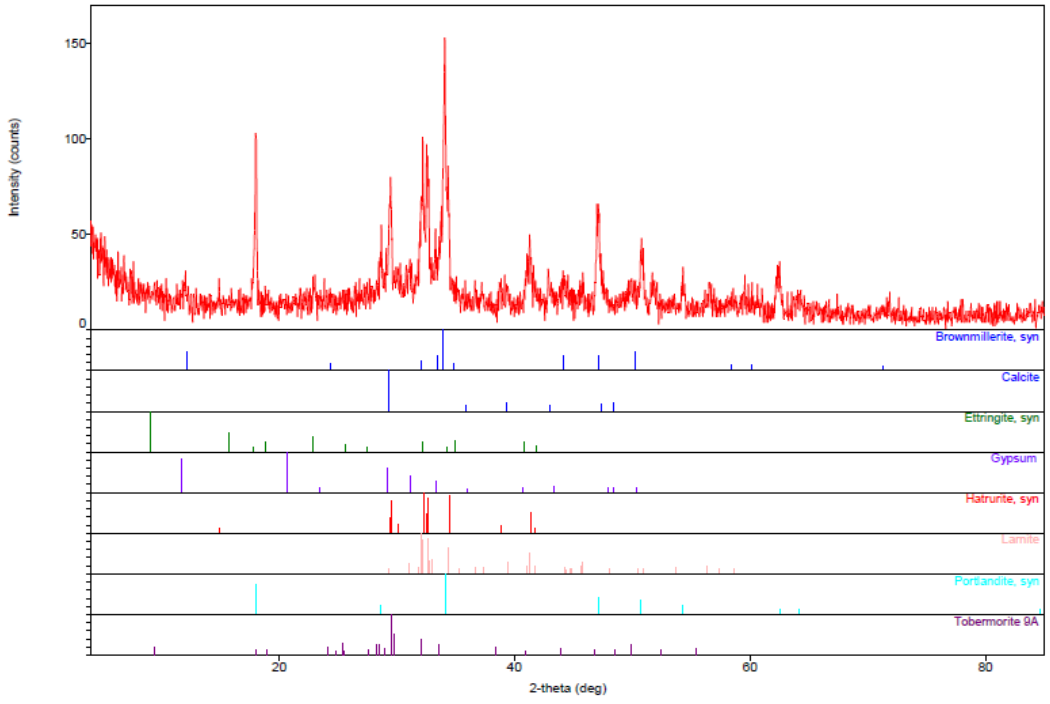


**Figure E-28: XRD pattern and crystals peak of GUbSF 0.43 at 24 hours**

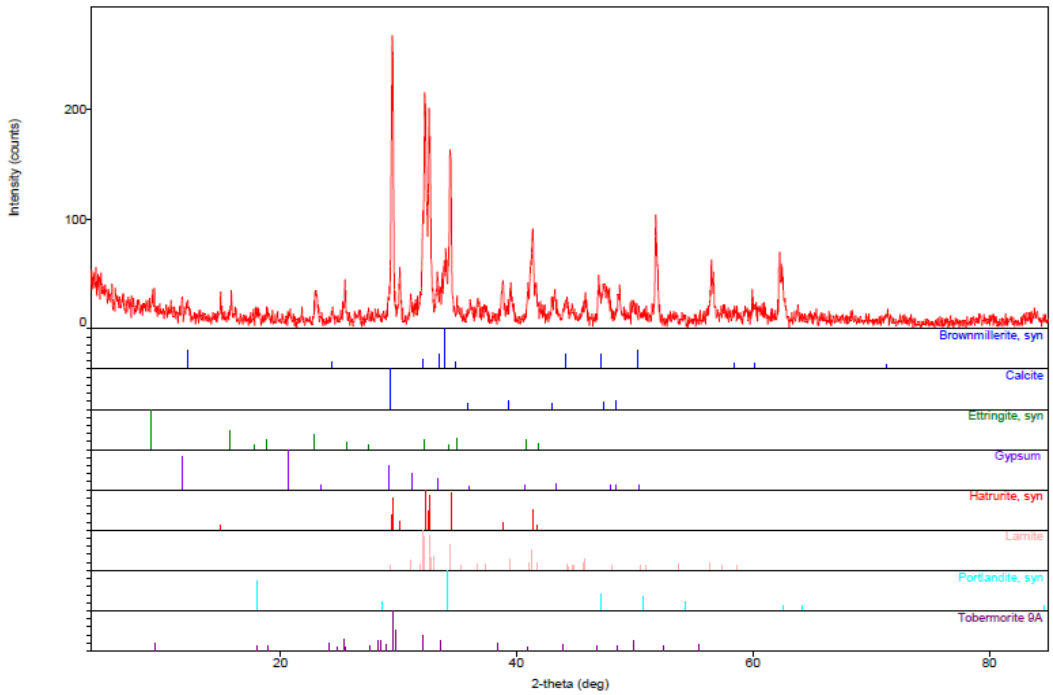


**Figure E-29: XRD pattern and crystals peak of GUL 0.37 at 2 hours**

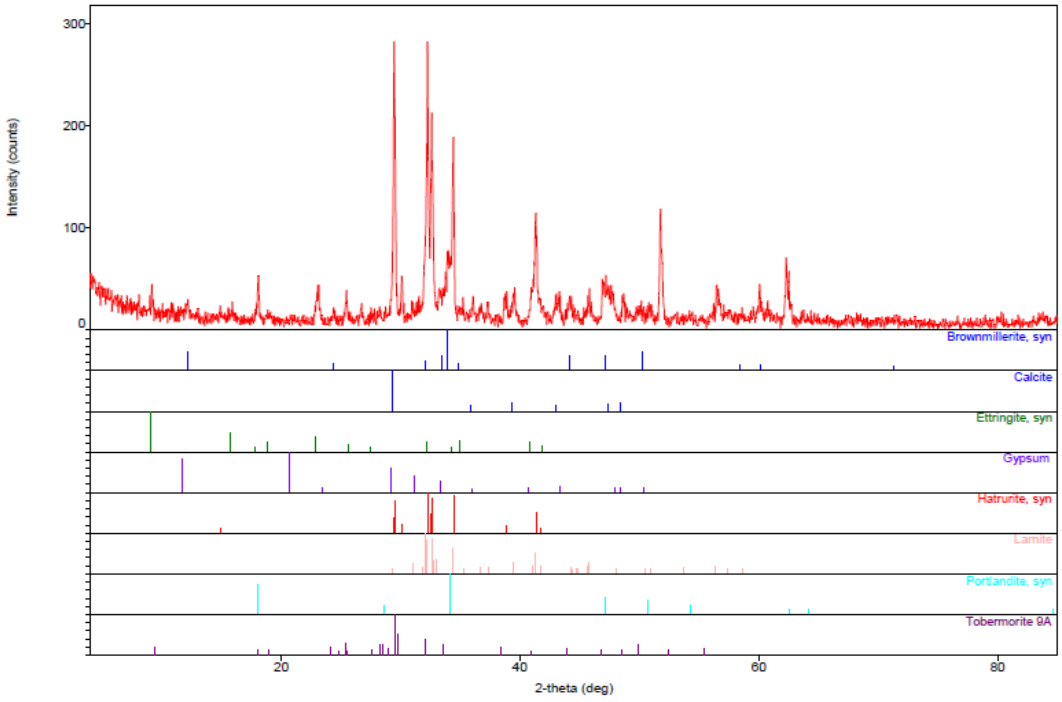


**Figure E-30: XRD pattern and crystals peak of GUL 0.37 at initial setting**

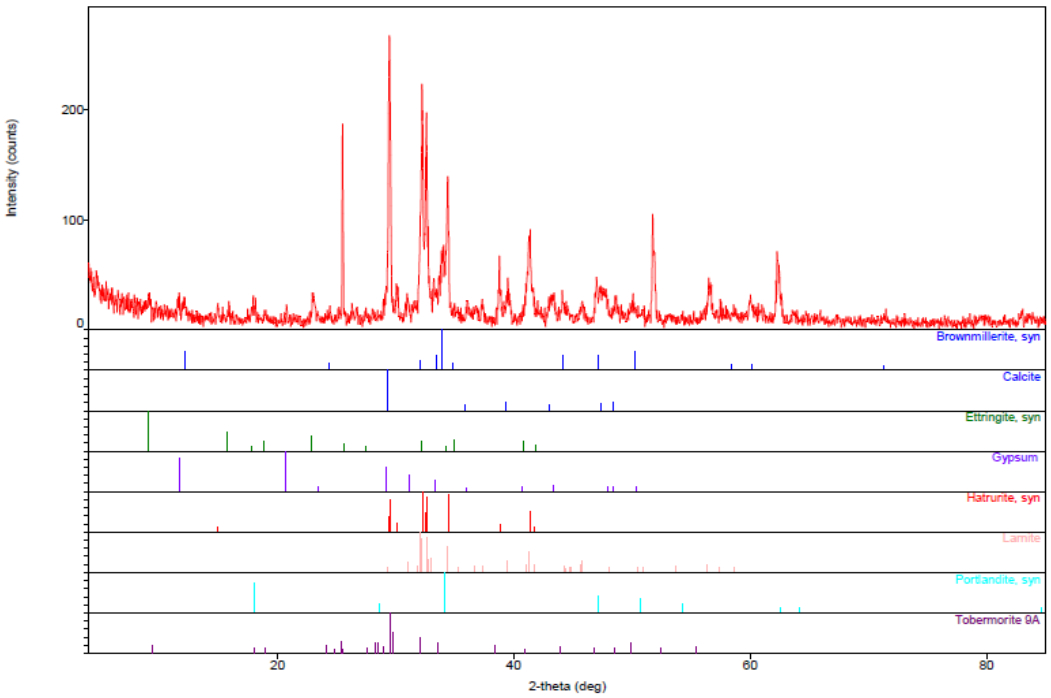


**Figure E-31: XRD pattern and crystals peak of GUL 0.37 at final setting**

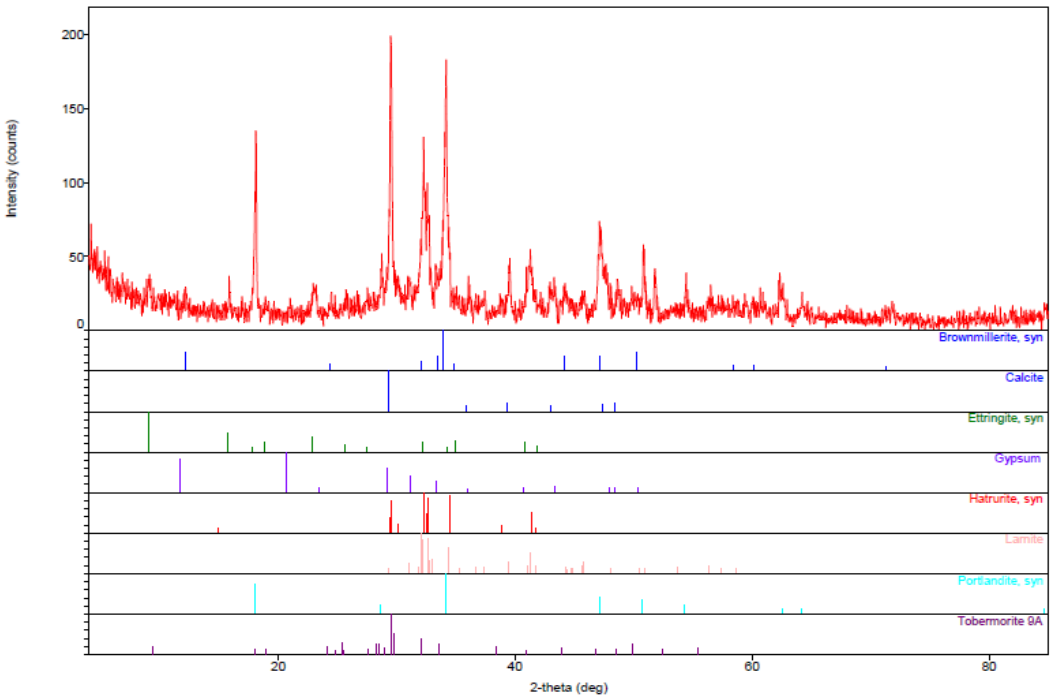


**Figure E-32: XRD pattern and crystals peak of GUL 0.37 at 24 hours**

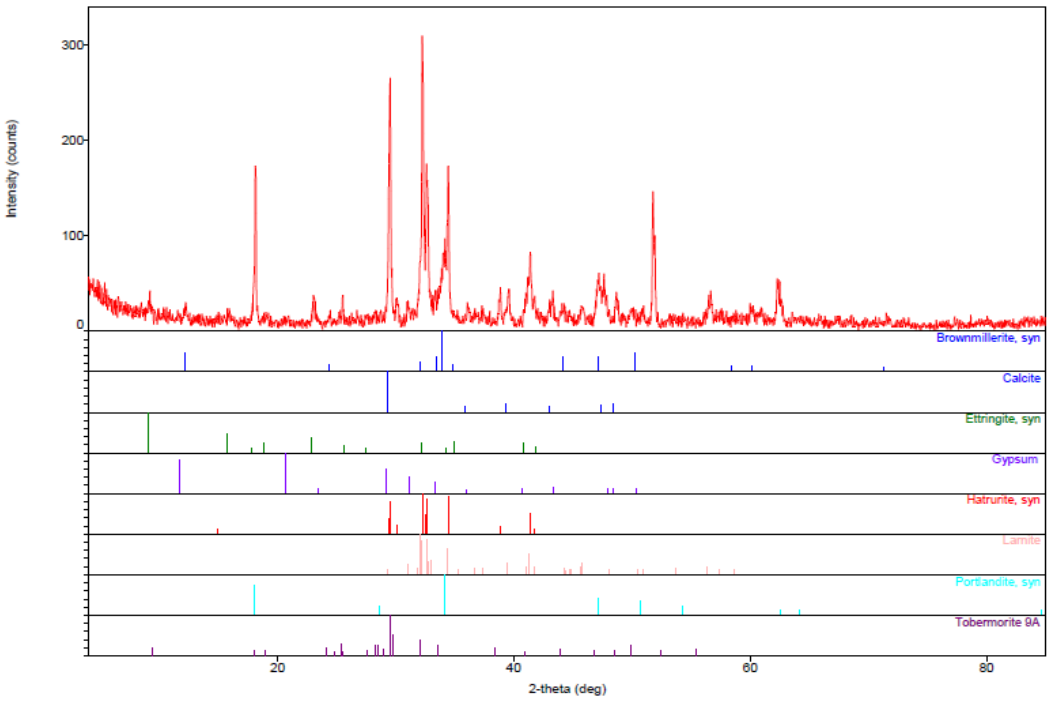


**Figure E-33: XRD pattern and crystals peak of GUL 0.40 at 2 hours**

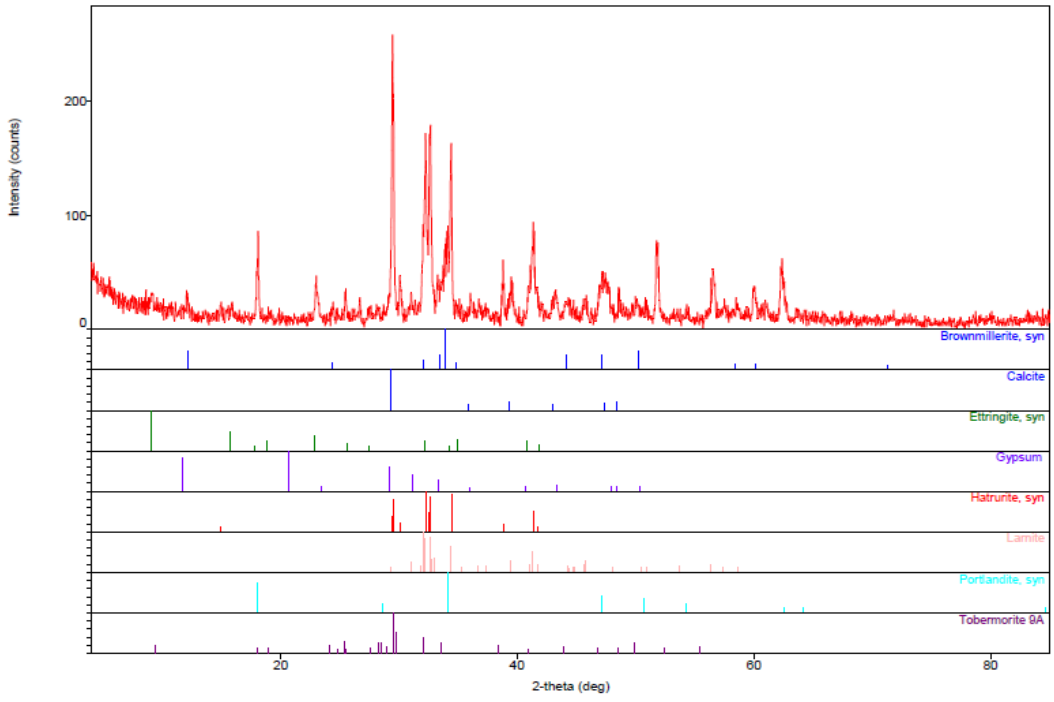


**Figure E-34: XRD pattern and crystals peak of GUL 0.40 at initial setting**

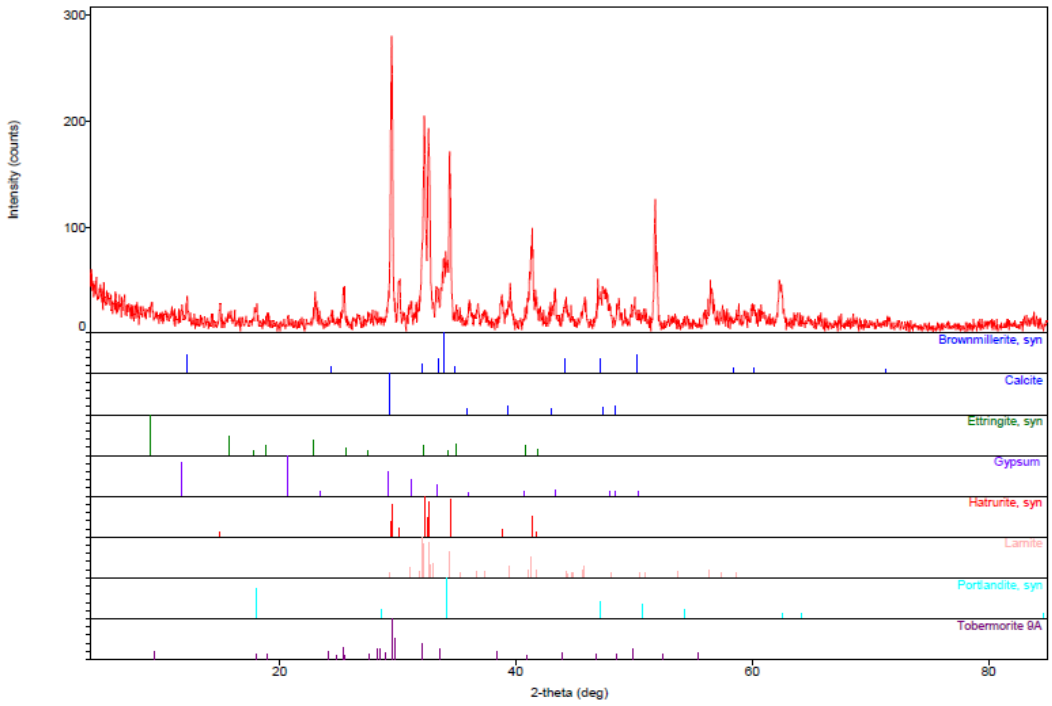


**Figure E-35: XRD pattern and crystals peak of GUL 0.40 at final setting**

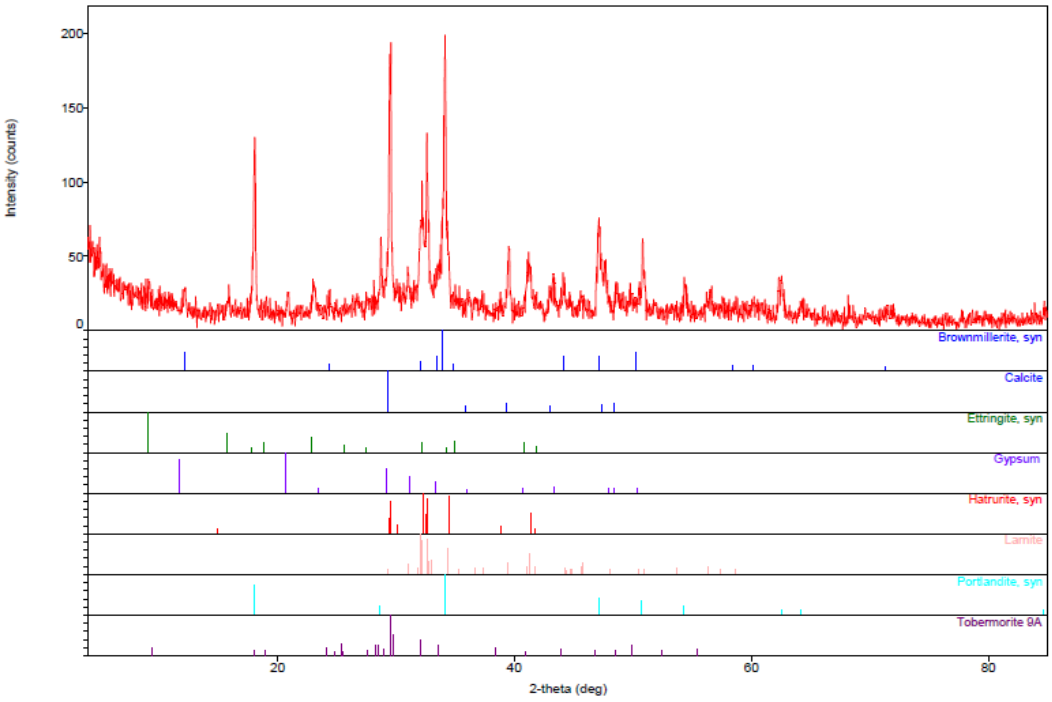


**Figure E-36: XRD pattern and crystals peak of GUL 0.40 at 24 hours of hydration**

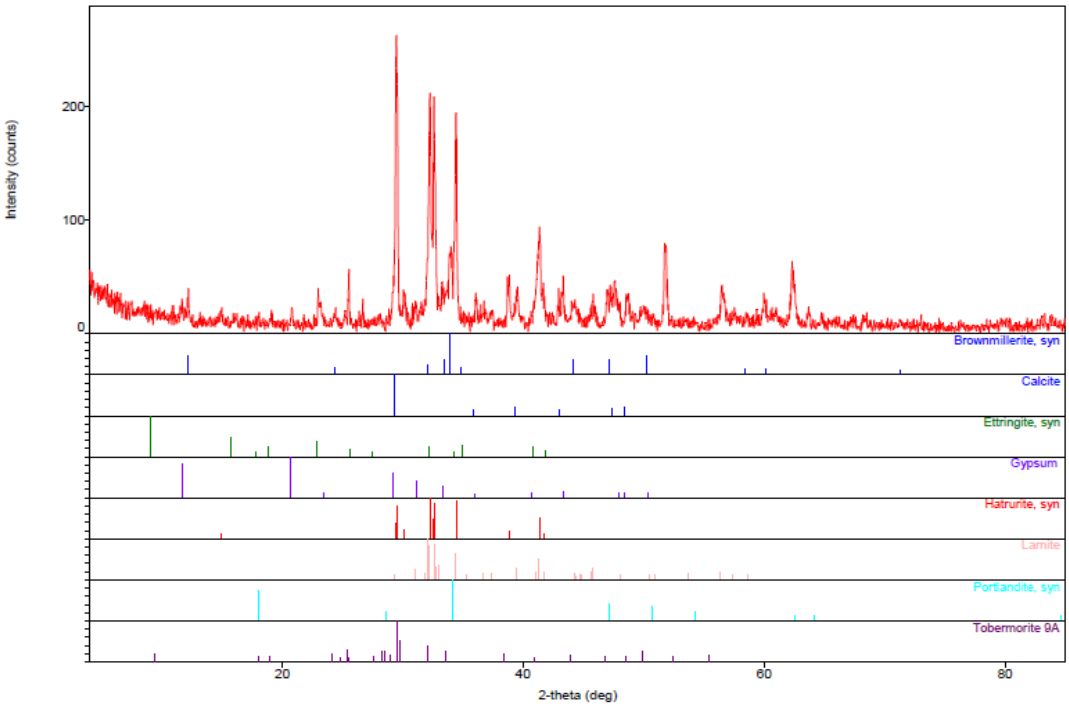


**Figure E-37: XRD pattern and crystals peak of GUL 0.43 at 2 hours of hydration**

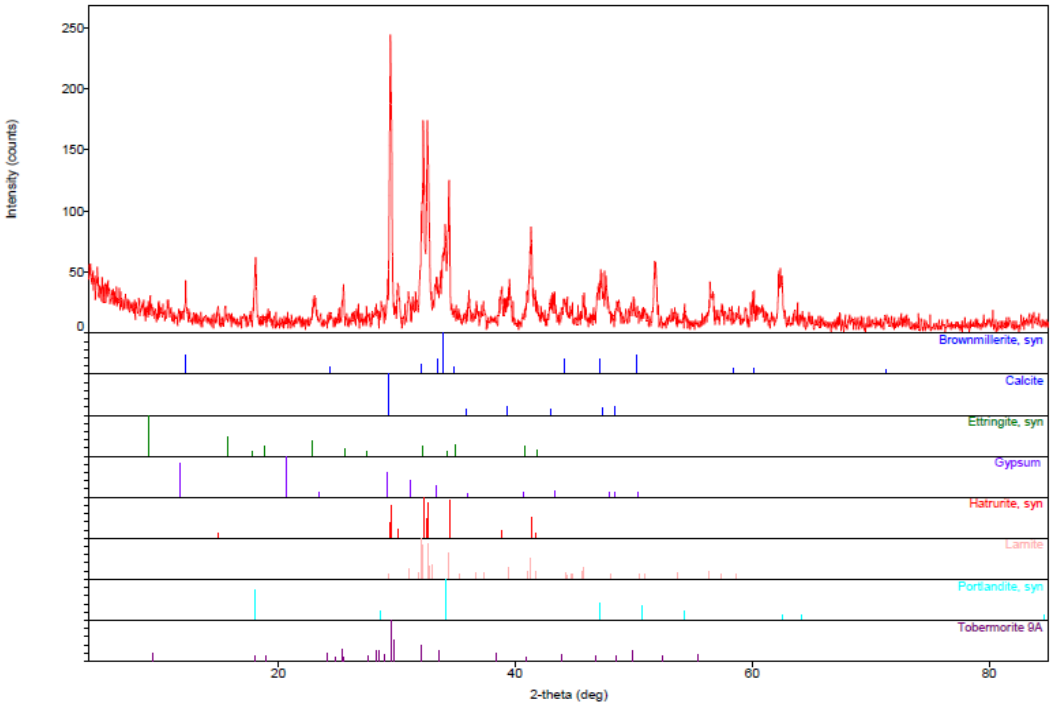


**Figure E-38: XRD pattern and crystals peak of GUL 0.43 at initial setting**

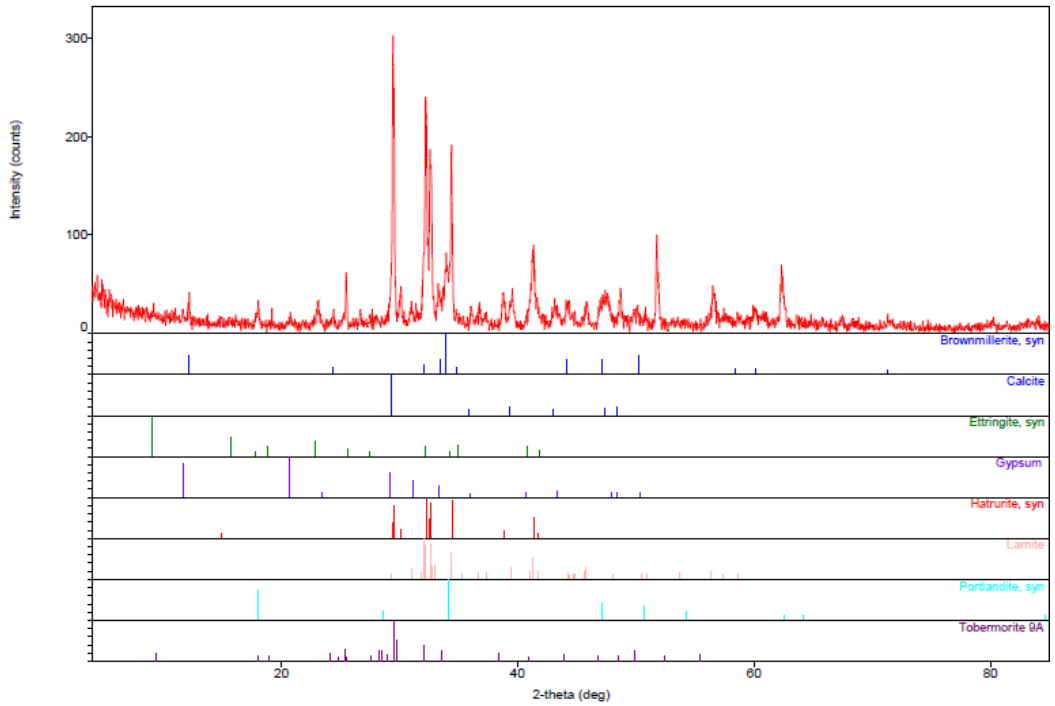


**Figure E-39: XRD pattern and crystals peak of GUL 0.43 at final setting**

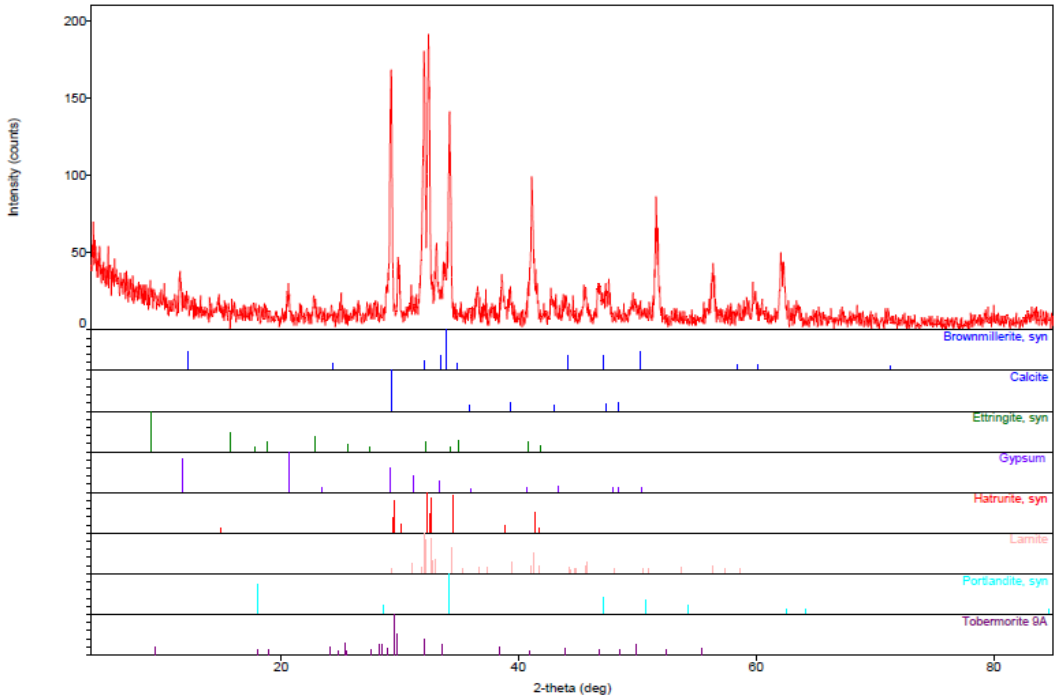


**Figure E-40: XRD pattern and crystals peak of HE 0.37 at 2 hours of hydration**

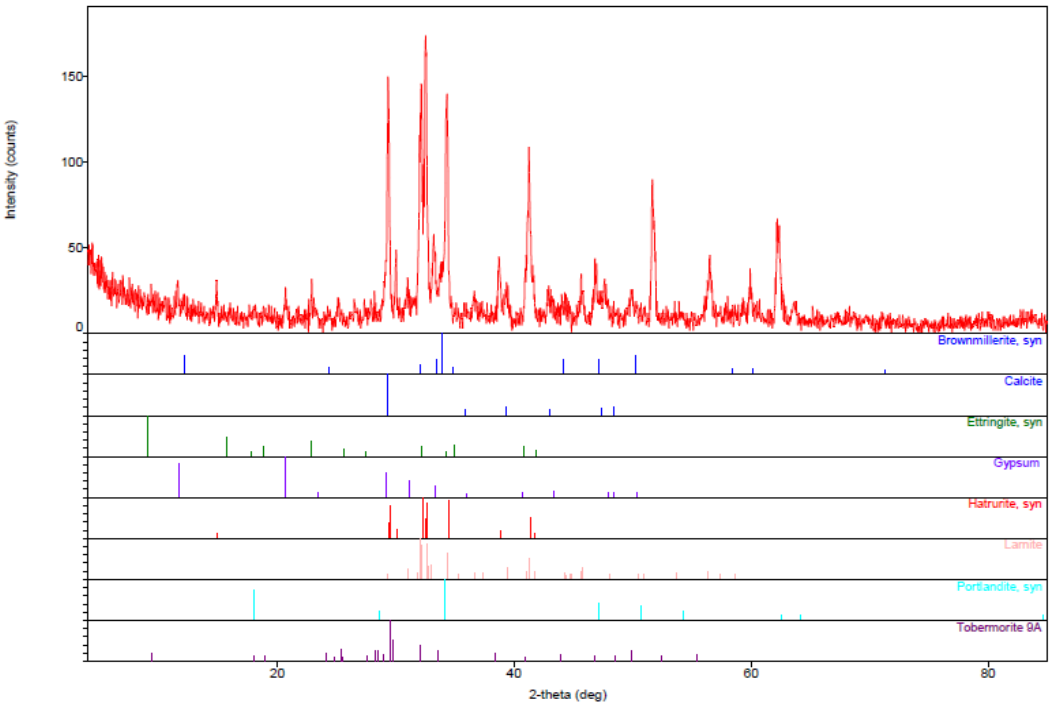


**Figure E-41: XRD pattern and crystals peak of HE 0.37 at initial setting**

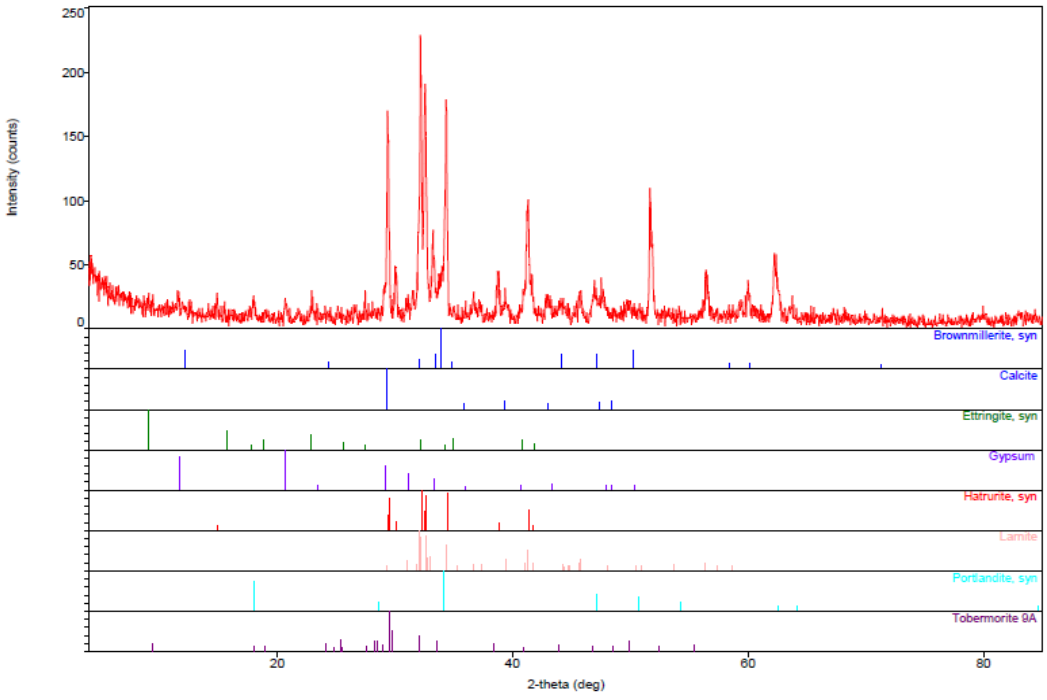


**Figure E-42: XRD pattern and crystals peak of HE 0.37 at final setting**

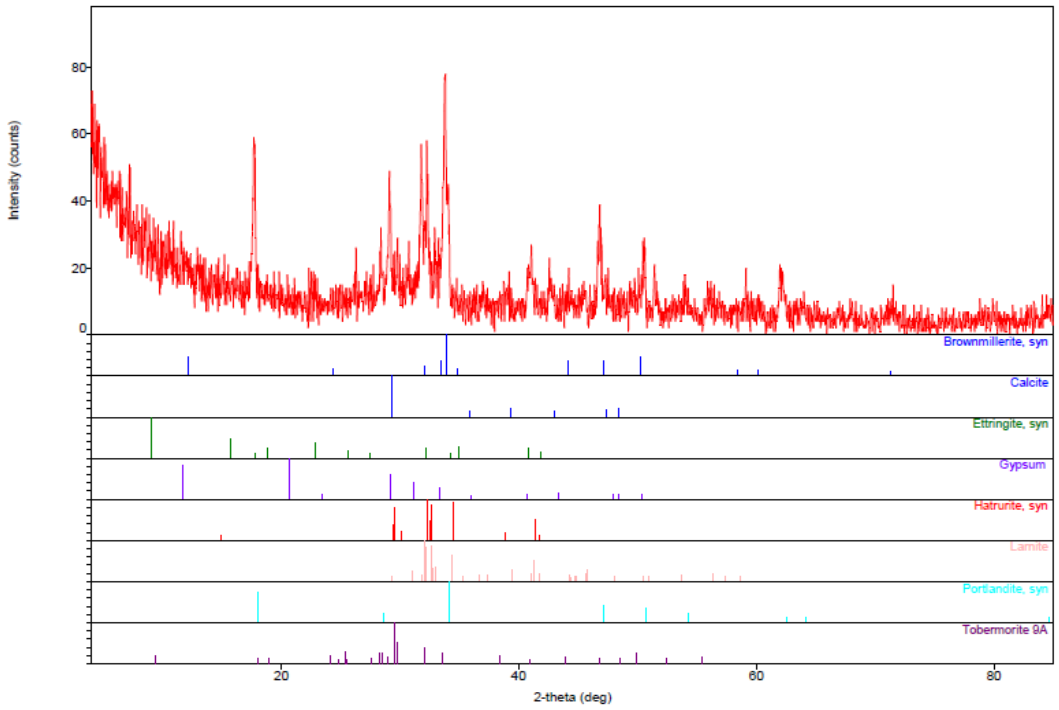


**Figure E-43: XRD pattern and crystals peak of HE 0.37 at 24 hours of hydration**

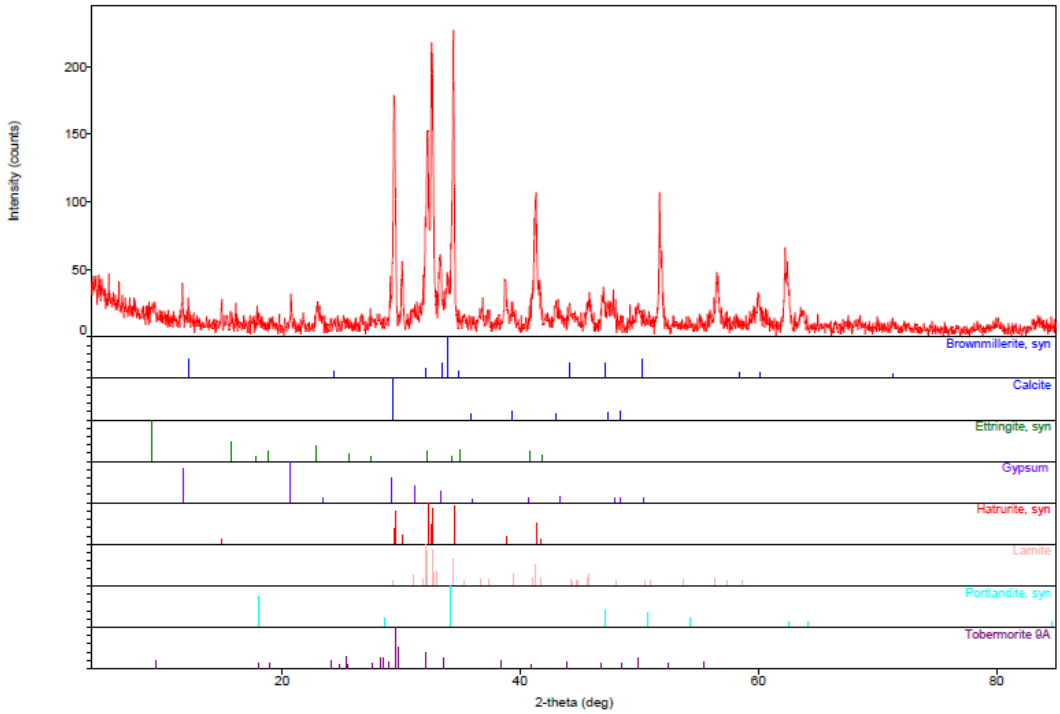


**Figure E-44: XRD pattern and crystals peak of HE 0.40 at 2 hours of hydration**

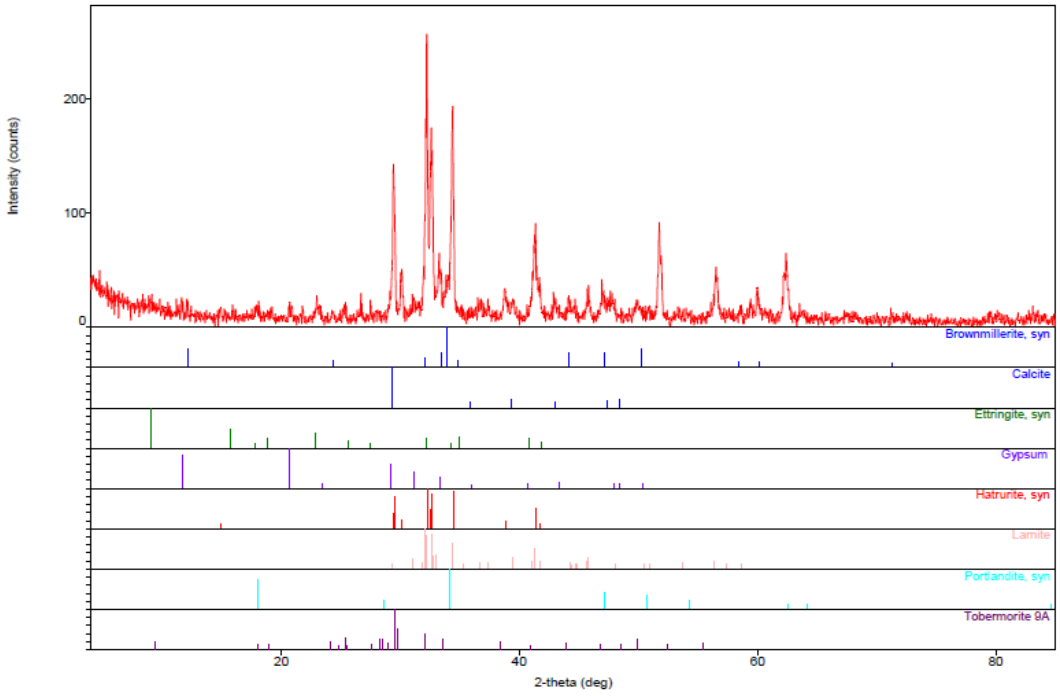


**Figure E-45: XRD pattern and crystals peak of HE 0.40 at initial setting**

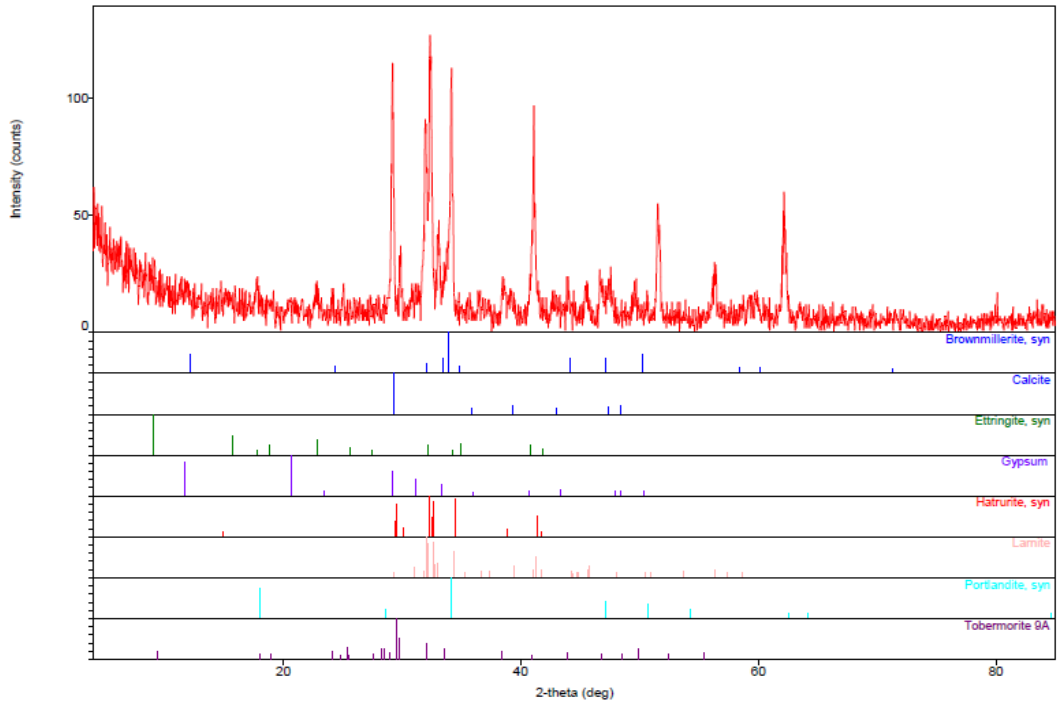


**Figure E-46: XRD pattern and crystals peak of HE 0.40 at final setting**

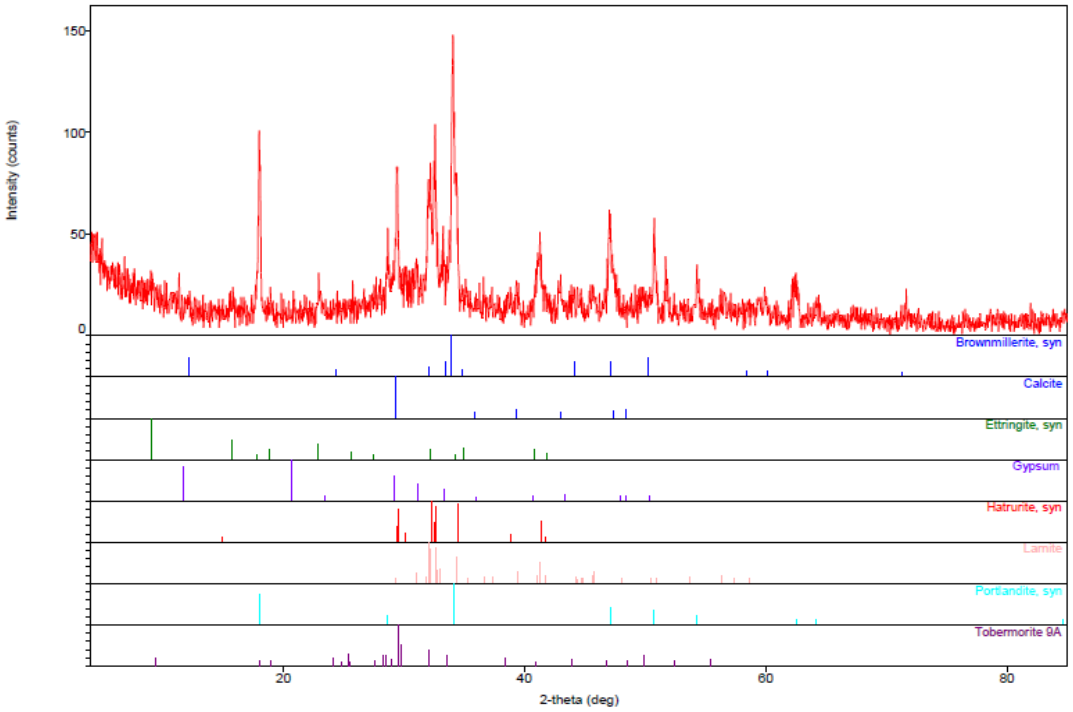


**Figure E-47: XRD pattern and crystals peak of HE 0.40 at 24 hours of hydration**

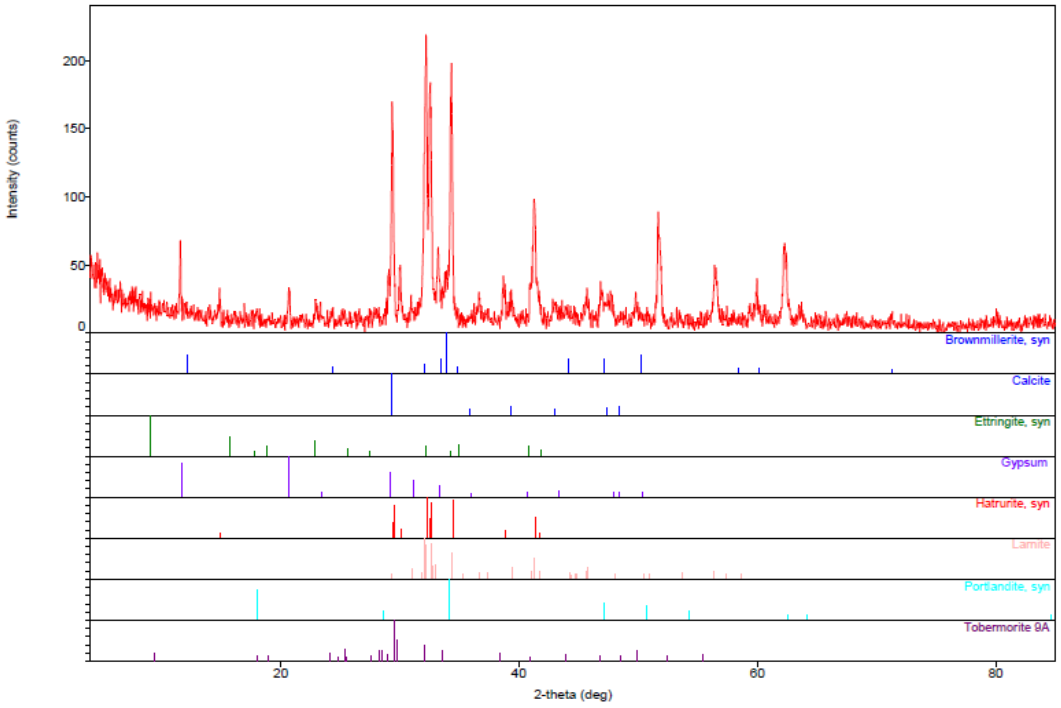


**Figure E-48: XRD pattern and crystals peak of HE 0.43 at 2 hours of hydration**

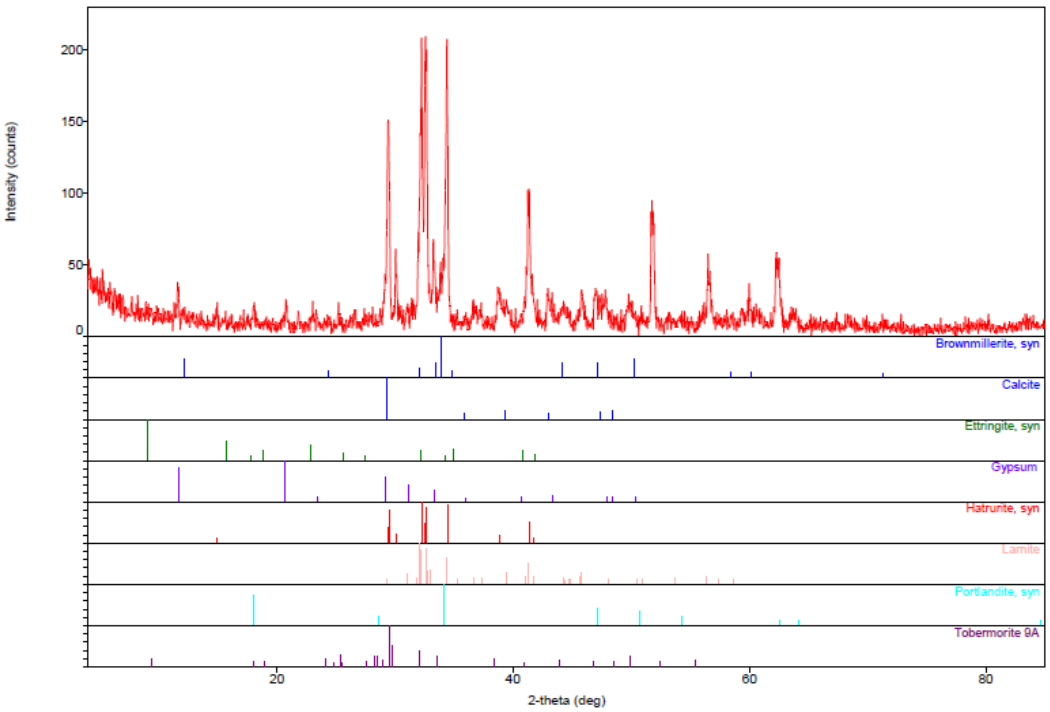


**Figure E-49: XRD pattern and crystals peak of HE 0.43 at initial setting**

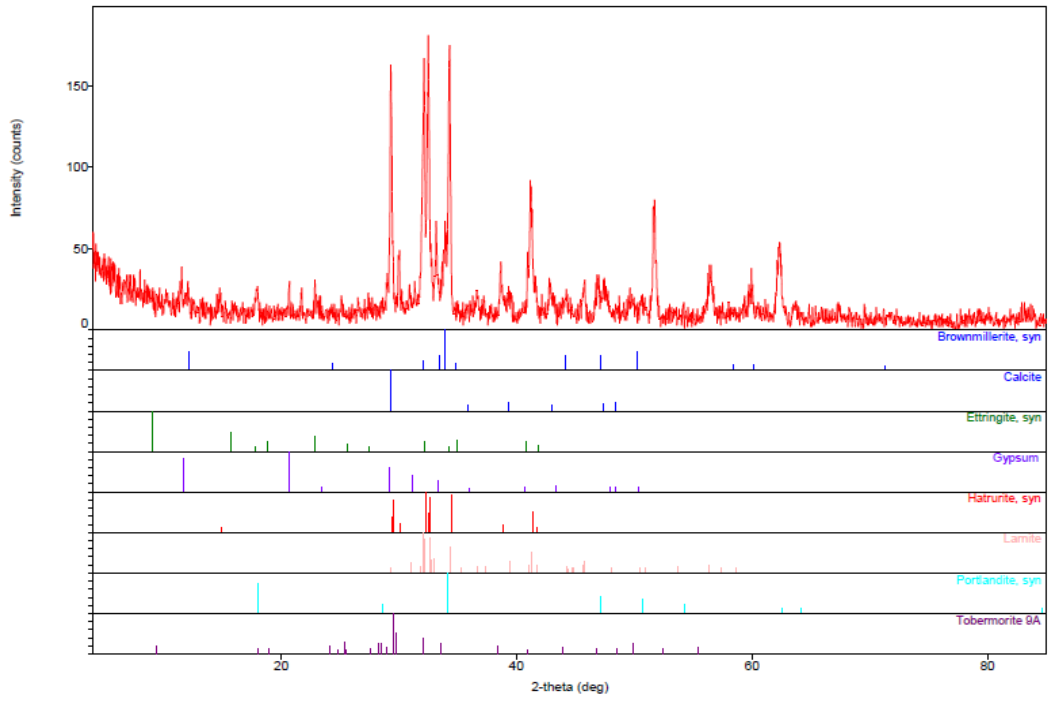


**Figure E-50: XRD pattern and crystals peak of HE 0.43 at final setting**

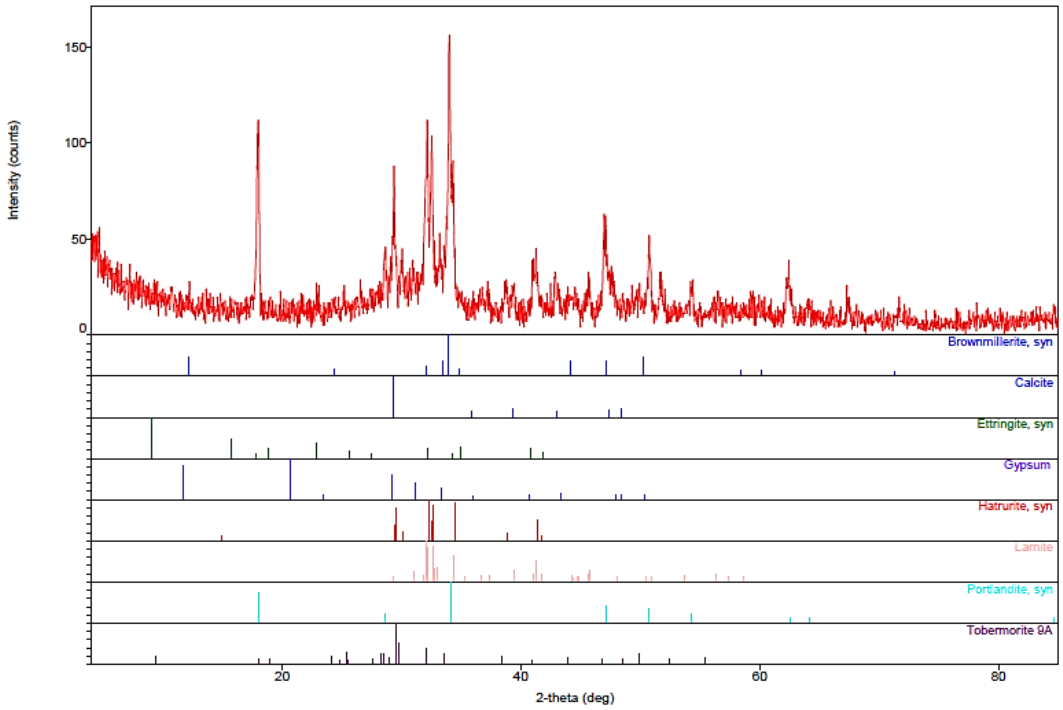


**Figure E-51: XRD pattern and crystals peak of HE 0.43 at 24 hours of hydration**

## F. Liquid Solution Conductivity-meter

(From the Oakton® Company Website)


# ECTestrs® 11 Series

### Auto-ranging for maximum resolution

**Large, easy-to-read display** – Two-line display—units, measurement status, and battery life indicators

**±1% full-scale accuracy** – The best in its class!

**Waterproof, dustproof housing** – Meets IP67 ratings, plus—it floats!

**Replaceable electrode** – Reuse same meter body over and over

**Push-button calibration** – Calibrate more precisely than trimpot adjustment—no screwdrivers needed

**Hold function** – Freezes reading until you can record it

**Auto shutoff** – Saves your batteries

**Full reading displayed** – No need to multiply the readout to obtain actual test values

**Temperature readout** – Dual display for readings at a glance; °C or °F selectable

**Automatic temperature compensation (ATC)** – Gives you accurate readings even with fluctuating temperatures

**ECTester 11+ features** – Operate as either cup-style or dip-style tester for greater flexibility

## Applications

**ECTestr 11**

**Low range:** Use for measuring conductivity (µS) in natural water. Verify reverse osmosis system operation and tap water quality. Check nutrient solution concentration in hydroponics applications.

**High range:** For measuring conductivity (µS) in salt water, wastewater, cooling tower water, and boiler condensate. Check nutrient solution concentration in hydroponics applications. Measure salinity for ponds, recirculating systems. Check saline, chemical levels in pools and spas.

**ECTestr 11+**

**Ultra-low range:** Ideal for measuring TDS or conductivity (µS) in distilled water, natural water, drinking water, and reverse osmosis systems.

**Low range:** Use for measuring TDS or conductivity (µS) in natural water. Verify reverse osmosis system operation and tap water quality. Check nutrient solution concentration in hydroponics applications.

**High range:** Use for measuring TDS or conductivity (mS) in salt water, wastewater, cooling tower water, and boiler condensate. Check nutrient solution concentration in hydroponics applications. Measure salinity in ponds and recirculating systems. Check saline and chemical levels in pools and spas.

## Specifications

ISO 9001:2000 CERTIFIED SUPPLIER CE 1 year warranty

| Model | ECTestr 11 dual-range | ECTestr 11+ multirange |
|---|---|---|
| Range | 0 to 2000 µS; 0 to 20.00 mS | 0 to 200.0 µS, 0 to 2000 µS; 0 to 20.00 mS |
| Resolution | 10 µS; 0.10 mS | 0.1 µS, 1 µS; 0.01 mS |
| Accuracy | ±1% full-scale | ±1% full-scale |
| Calibration standard range | 300 to 1990 µS; 3 to19.90 mS | 20.0 to 199.9 µS, 200 to 199.9 µS; 2.0 to 19.99 mS |
| Calibration | 2-point, manual or auto (1413 µS; 12.88 mS) | 3-point, manual or auto (84 µS, 1413 µS; 12.88 mS) |

**Temperature display:** 0 to 50°C (32 to 122°F), 0.1°C resolution, ±0.5°C accuracy

**Operating temperature:** 0 to 50°C (32 to 122°F)

**Temperature compensation:** automatic (ATC) from 0 to 50°C (32 to 122°F)

**ATC coefficient temperature:** 2% per °C, 25°C reference

**Wetted materials:** 316 stainless steel (electrodes) and Valox® housing

**Power and battery life:** four 1.5 V alkaline batteries Eveready A76 (included), 100 hrs continuous use (approx 600 tests per battery pack). Alternate replacement model LR44.

**Dimensions**

**Unit only:** 6½"L x 1½" dia (165 x 38 mm)
**Boxed:** 7¼" x 2¾" x 1⅞" (184 x 70 x 48 mm)

**Weight**

**Unit only:** 3.25 oz (90 g); **Boxed:** 6.0 oz (170 g)

## Ordering Information

| Catalog number | Description | Included |
|---|---|---|
| WD-35662-30 | ECTestr 11 dual-range | Tester, protective plastic storage case, lanyard, and batteries |
| WD-35662-35 | ECTestr 11+ multirange | |

## Accessories

**WD-35661-17 Replacement electrode** for ECTestr 11

**WD-35661-08 Replacement electrode** for ECTestr 11+

**WD-35624-45 Vinyl carrying case** with belt loop; holds one tester and solution pouches

**WD-09377-16 Replacement batteries,** 1.5 V. Pack of 6

**WD-35661-70 Deluxe calibration kit** includes two each calibration pouches (447 µS, 1413 µS, 2764 µS, 15,000 µS, and rinse water), sample jar, and foam-lined hard plastic carrying case. (Tester not included)

To measure the electrical resistivity of the pore solutions, the extracted samples became diluted for ×1000, ×2000, and ×4000 times with water (except for GUL mixtures which were diluted for ×500, ×1000, and ×2000 times with water). Electrical conductance values (in milliSiemens) presented in Table 4-15 are the "slope/1000" of the electrical conductance versus dilution linear relationship.

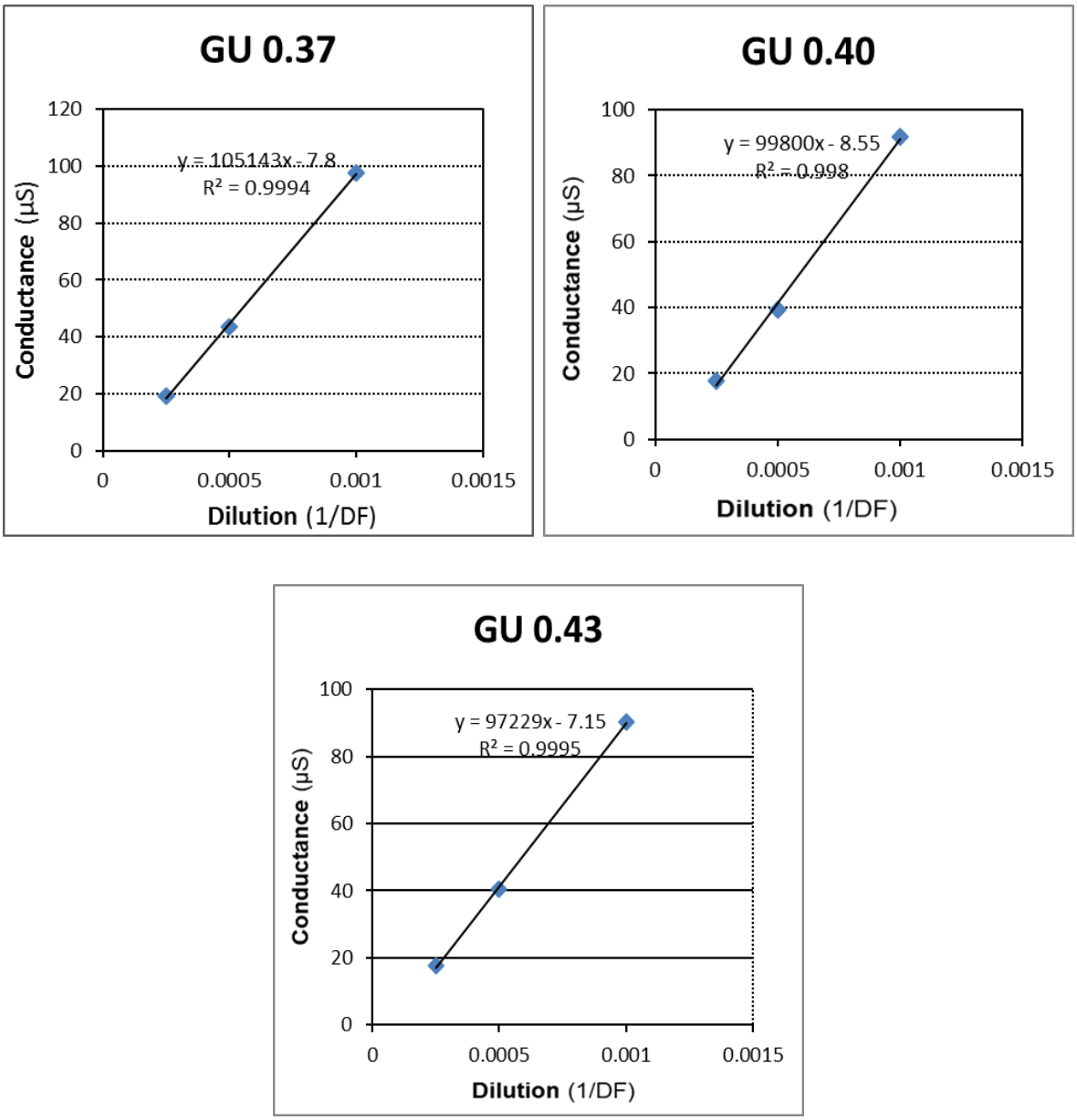


**Figure F-1: Conductance measurement relationship of extracted pore solution from GU mixtures with the Dilution Factor of the standard known solution**

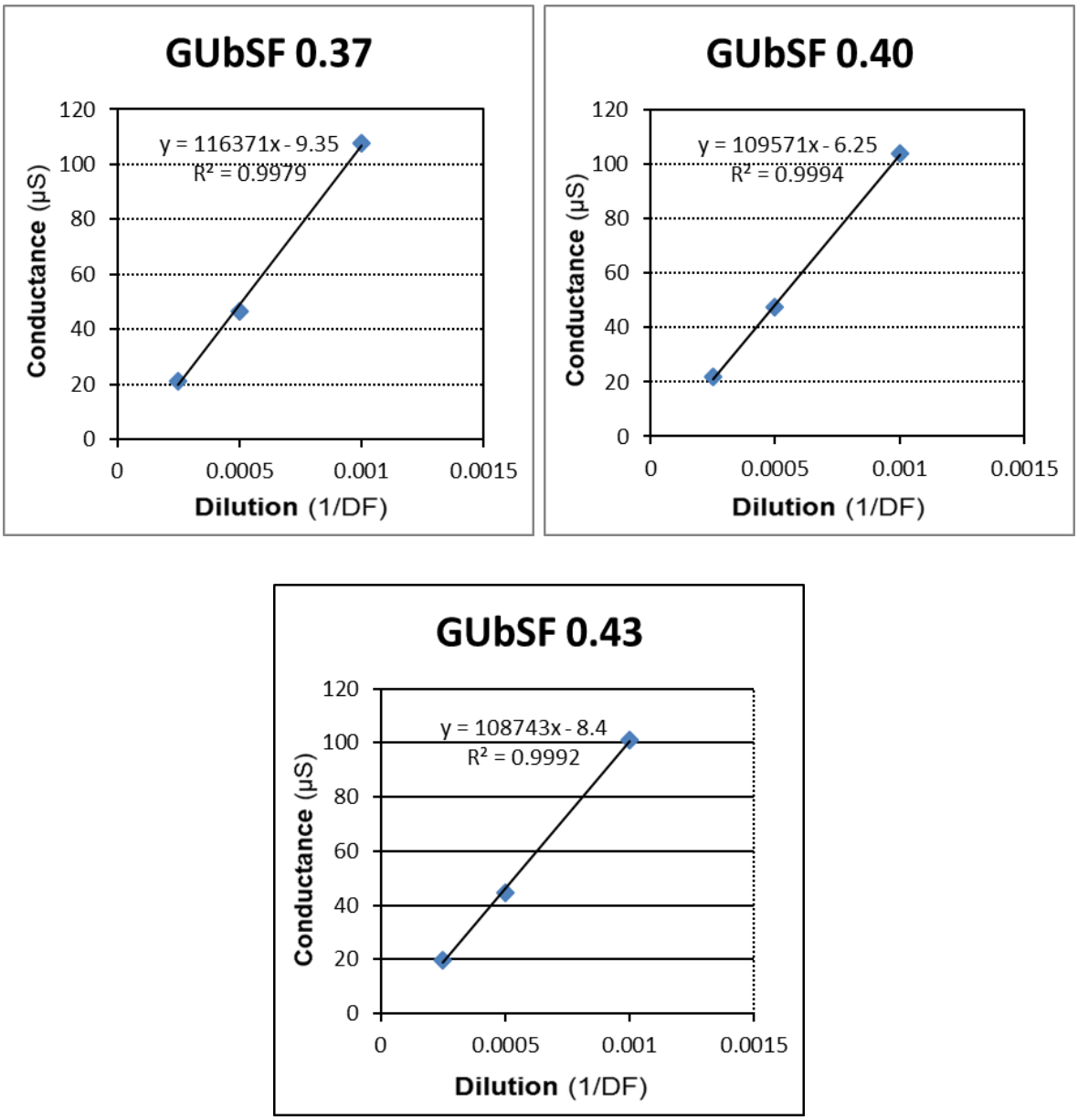


**Figure F-2: Conductance measurement relationship of extracted pore solution from GUbSF mixtures with the Dilution Factor of the standard known solution**

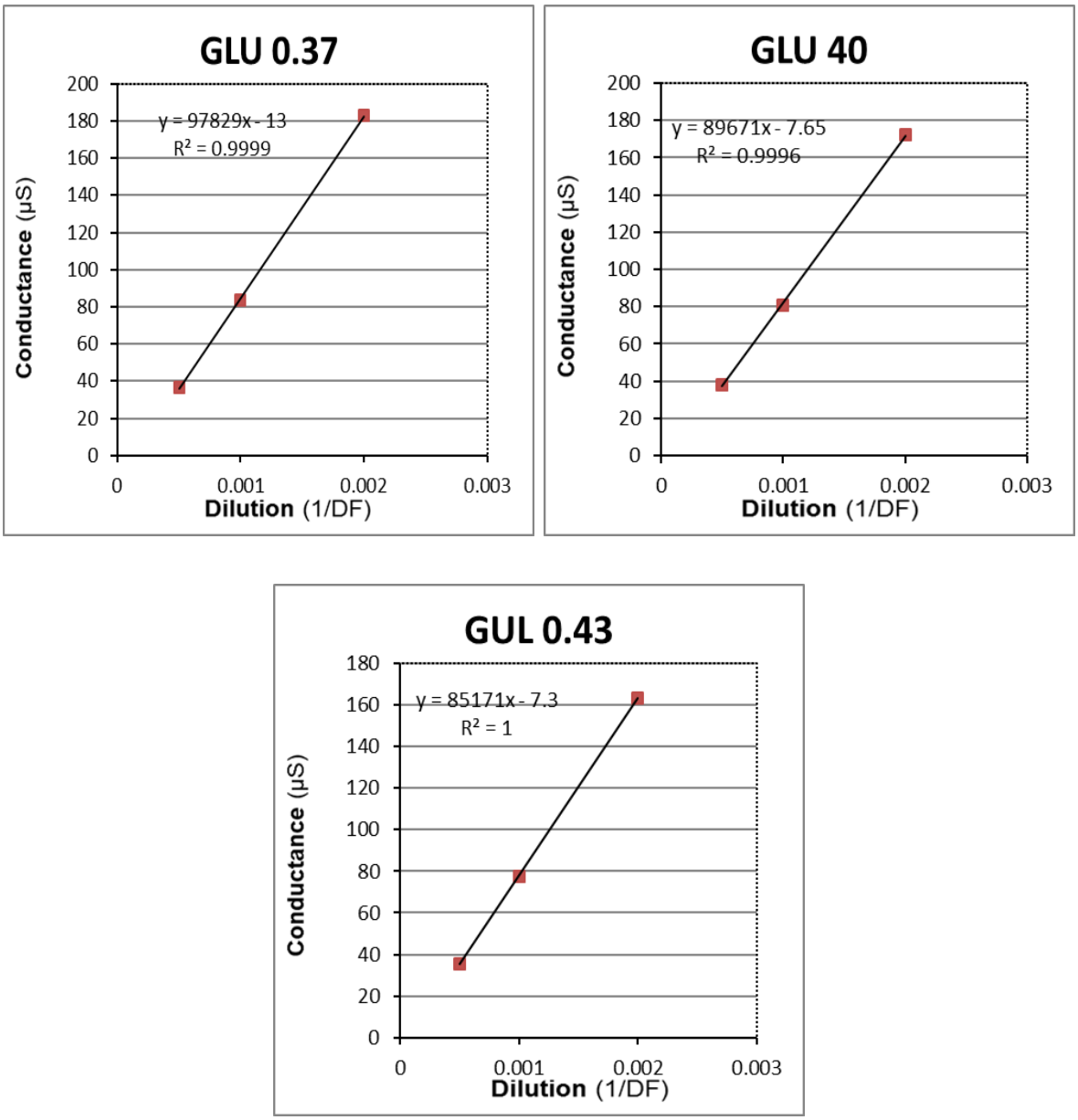


**Figure F-3: Conductance measurement relationship of extracted pore solution from GUL mixtures with the Dilution Factor of the standard known solution**

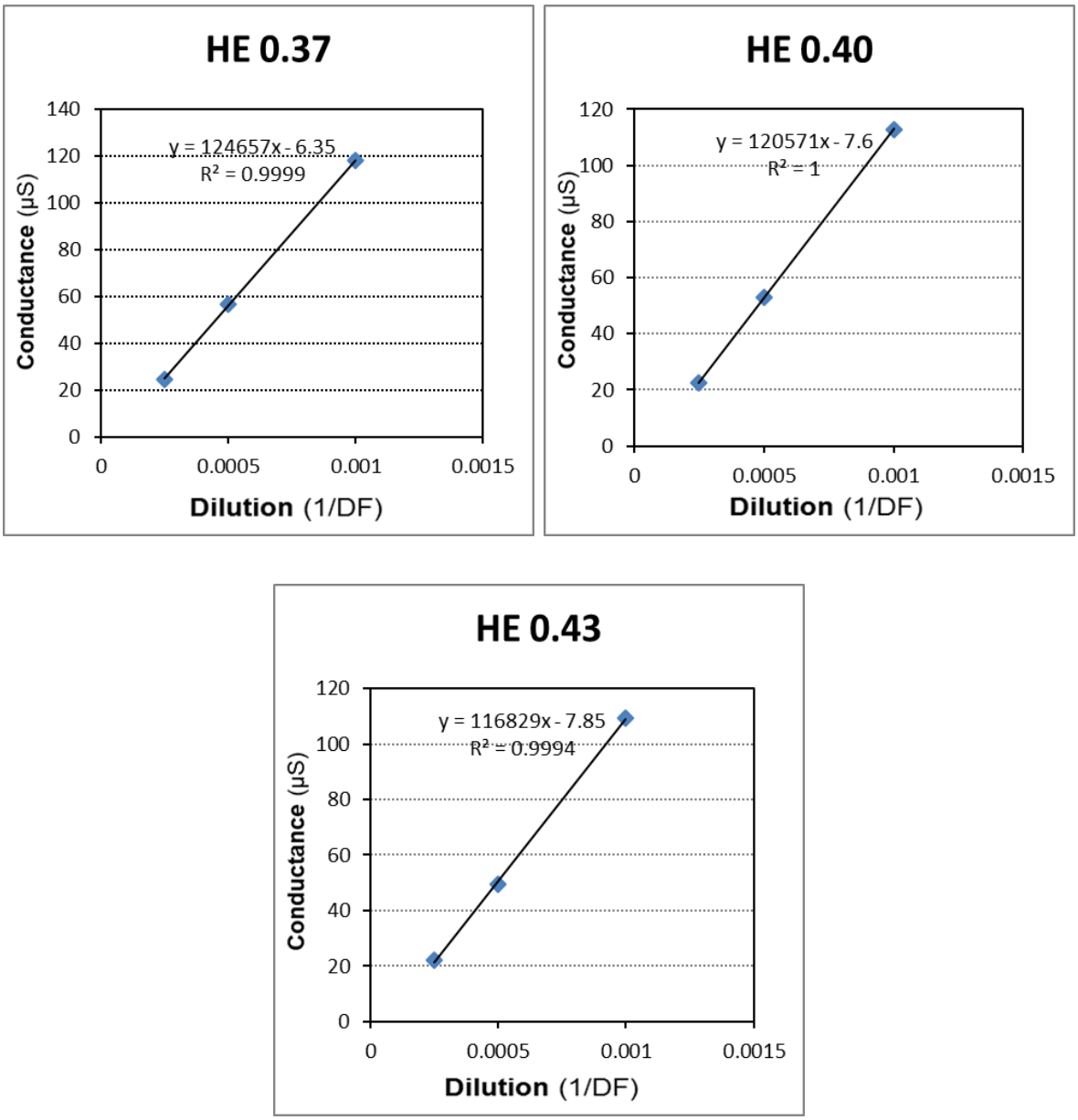


**Figure F-4: Conductance measurement relationship of extracted pore solution from HE mixtures with the Dilution Factor of the standard known solution**

## G. Detection Limits of Vista-PRO Radial and Axial Instrument

| Element | Wavelength (nm) | 3σ Detection Limits (µg/L) Vista-PRO Radial | Vista-PRO Axial |
|---|---|---|---|
| Ag | 328.068 | 1 | 0.3 |
| Al | 167.016 | 0.9 | 0.2 |
| As | 188.979 | 5 | 1.5 |
| Au | 267.595 | 5 | 1.0 |
| B | 249.773 | 0.6 | 0.1 |
| Ba | 455.403 | 0.15 | 0.03 |
| Be | 234.861 | 0.05 | 0.01 |
| Bi | 223.061 | 6 | 2 |
| Ca | 396.847 | 0.06 | 0.01 |
| Cd | 214.438 | 0.6 | 0.05 |
| Ce | 418.660 | 2 | 2 |
| Co | 238.892 | 1 | 0.2 |
| Cr | 267.716 | 0.9 | 0.15 |
| Cu | 327.396 | 1 | 0.3 |
| Fe | 259.940 | 0.8 | 0.1 |
| K | 766.490 | 4 | 0.3 |
| Li | 670.784 | 1 | 0.06 |
| Mg | 279.553 | 0.04 | 0.01 |
| Mn | 257.610 | 0.08 | 0.03 |
| Mo | 202.030 | 2 | 0.5 |
| Na | 589.592 | 2 | 0.15 |
| Ni | 231.604 | 1.4 | 0.3 |
| P | 177.432 | 5 | 2 |
| Pb | 220.353 | 5 | 0.8 |
| S | 181.971 | 10 | 5 |
| Sb | 231.147 | 5 | 2 |
| Se | 196.026 | 6 | 2 |
| Si | 251.611 | 2.2 | 1.4 |
| Sr | 407.771 | 0.05 | 0.01 |
| Ti | 334.941 | 0.2 | 0.1 |
| Tl | 190.790 | 6 | 2 |
| V | 292.402 | 0.7 | 0.2 |
| W | 207.911 | 3.5 | 2 |
| Zn | 213.856 | 0.8 | 0.2 |
| Zr | 343.823 | 0.9 | 0.3 |

## H. Compressive Strength Test Specimens and Results

| Mix Design | | Specimen | Specimen Property | | | Strength Test Results | | |
|---|---|---|---|---|---|---|---|---|
| **Cement Type** | **Mixture** | **Number** | **Weight** (gr) | **Diameter** (mm) | **Area** ($mm^2$) | **Maximum Applied Load** (kN) **@ 900 N/S** | **Strength** (MPa) | **Average Strength** (MPa) |
| **GUbSF** | GUbSF 0.37 | 1 | 393.00 | 50.86 | 2031.76 | 50.75 | 24.98 | 25.56 |
| | | 2 | 396.50 | 50.75 | 2022.78 | 52.00 | 25.71 | |
| | | 3 | 400.00 | 50.87 | 2032.16 | 52.80 | 25.98 | |
| | GUbSF 0.40 | 1 | 376.00 | 51.19 | 2057.61 | 38.89 | 18.90 | 17.70 |
| | | 2 | 380.00 | 51.00 | 2042.76 | 36.11 | 17.68 | |
| | | 3 | 382.00 | 50.80 | 2026.97 | 33.50 | 16.53 | |
| | GUbSF 0.43 | 1 | 366.50 | 50.80 | 2026.77 | 27.40 | 13.52 | 13.35 |
| | | 2 | 379.50 | 51.03 | 2045.16 | 26.65 | 13.03 | |

| | | | | | | | | |
|---|---|---|---|---|---|---|---|---|
| | | 3 | 371.50 | 50.83 | 2028.97 | 27.40 | 13.50 | |
| **GUL** | GUL 0.37 | 1 | 387.00 | 50.85 | 2030.76 | 37.57 | 18.50 | 18.12 |
| | | 2 | 389.50 | 51.29 | 2066.06 | 37.19 | 18.00 | |
| | | 3 | 394.50 | 50.85 | 2030.76 | 36.25 | 17.85 | |
| | GUL 0.40 | 1 | 368.00 | 50.00 | 1963.44 | 30.92 | 15.75 | 14.50 |
| | | 2 | 370.00 | 51.20 | 2058.81 | 27.28 | 13.25 | |
| | | 3 | 368.00 | 50.00 | 1963.44 | 28.47 | 14.50 | |
| | GUL 0.43 | 1 | 378.00 | 50.85 | 2030.76 | 22.34 | 11.00 | 11.67 |
| | | 2 | 390.50 | 51.26 | 2063.64 | 24.76 | 12.00 | |
| | | 3 | 389.50 | 52.00 | 2123.65 | 25.48 | 12.00 | |

| | | | | | | | | |
|---|---|---|---|---|---|---|---|---|
| **HE** | HE 0.37 | 1 | 387.00 | 50.78 | 2024.78 | 76.20 | 37.63 | 36.99 |
| | | 2 | 386.00 | 50.85 | 2030.76 | 74.82 | 36.84 | |
| | | 3 | 386.00 | 50.90 | 2034.96 | 74.28 | 36.50 | |
| | HE 0.40 | 1 | 381.50 | 50.85 | 2030.56 | 69.00 | 33.98 | 32.64 |
| | | 2 | 380.00 | 51.05 | 2046.77 | 67.06 | 32.76 | |
| | | 3 | 377.00 | 50.67 | 2016.41 | 62.87 | 31.18 | |
| | HE 0.43 | 1 | 375.50 | 50.78 | 2025.17 | 66.10 | 32.64 | 30.68 |
| | | 2 | 380.00 | 50.98 | 2041.16 | 62.59 | 30.66 | |
| | | 3 | 378.00 | 50.84 | 2029.76 | 58.30 | 28.72 | |
| **GU** | GU 0.37 | 1 | 391.50 | 50.89 | 2033.56 | 45.80 | 22.52 | 21.68 |

| | | | | | | | | |
|---|---|---|---|---|---|---|---|---|
| | | 2 | 392.00 | 50.70 | 2018.80 | 44.44 | 22.01 | |
| | | 3 | 397.00 | 50.83 | 2029.36 | 41.60 | 20.50 | |
| | GU 0.40 | 1 | 381.00 | 50.81 | 2027.37 | 28.40 | 14.01 | 15.91 |
| | | 2 | 383.00 | 50.10 | 1971.30 | 31.40 | 15.93 | |
| | | 3 | 384.50 | 50.04 | 1966.58 | 35.00 | 17.80 | |
| | GU 0.43 | 1 | 381.00 | 50.80 | 2026.97 | 20.74 | 10.23 | 10.93 |
| | | 2 | 382.00 | 51.56 | 2087.87 | 22.90 | 10.97 | |
| | | 3 | 376.00 | 50.82 | 2028.17 | 23.50 | 11.59 | |